QUATERNARY GLACIATION AND TECTONISM IN THE SOUTHEASTERN SIERRA NEVADA, INYO COUNTY, CALIFORNIA

Thesis by

Alan Reed Gillespie

In Partial Fulfillment of the Requirements

for the Degree of

Doctor of Philosophy

California Institute of Technology

Pasadena, California

1982

(Submitted March 23, 1982)

ACKNOWLEDGMENTS

In conducting this study, I was encouraged and assisted by numerous individuals. C.R. Allen originally suggested the field area, and provided guidance throughout the course of the project. R.P. Sharp visited critical locations and made several suggestions which were central to the progress of the research. G.J. Wasserburg sponsored the development of the new application of ^{40}Ar-^{39}Ar dating which proved to be successful in precisely dating the interglacial lavas of Sawmill Canyon. His patient efforts at developing the understanding and insight required to solve this problem are deeply appreciated. J.C. Huneke supervised my training in the use of the mass spectrometer, and helped interpret the experimental results. F. Radicati Di Brozolo assisted in this training, and T. Wen helped in chemical analysis. B. Kamb graciously allowed the unlimited use of the DynaMetric, Inc., Microseismic Timer for the relative dating of boulder deposits. R. Crook, Jr., shared in the joys of measuring the speed of acoustic waves through thousands of boulders on moraine crests from Independence to Bridgeport. K.S. Coles and C.B. Douthitt also assisted in the gathering of such data. S. Nohda accompanied me on occasion in the field. A.A. Chodos assisted with electron microprobe, X-ray, and SEM analysis. D. van Alstine and R. Crook, Jr., contributed to paleomagnetic measurements. P.O. Gillespie helped with topographic measurements.

Discussions with C. Wahrhaftig, and J.G. Moore were helpful in defining the scope of the project. The 1979 Friends of the Pleistocene field trip to the central Sierra Nevada was a valuable opportunity for consultation and discussion. In particular, P.W. Birkeland, R.B. Burke, and J. Yount were helpful. Throughout the entire study, M.M. Clark

provided advice and encouragement. K.E. Sieh likewise has helped keep the research on track.

Fellow students have listened patiently and have helped refine some of the concepts in this thesis: discussions with R.J. Weldon, K.E. Meisling, R.E. Powell, R.E. Lewis, W.S. Baldridge, and R.M. Potter were especially helpful.

Access and information were provided by personnel of the Los Angeles Water and Power Department, and also by the U.S. Forest Service at the Lone Pine, California, District Ranger's Office. D. Groves and R. Hamlin of that office especially went out of their way to help.

C.R. Allen reviewed the entire thesis. R. Crook, Jr., made corrections to Ch. 3. G.J. Wasserburg and J.C. Huneke tirelessly revised the manuscripts from which Ch. 4 was synthesized. A.V. Swatfigure and J.G. Clark typed most of the thesis. J.I. Mayne drafted many of the illustrations.

Financial support was provided by the Division of Geological and Planetary Sciences, Caltech, at critical points in the research. NSF grants EAR 78-01787 and EAR 79-19997 supported the bulk of the field and laboratory work. This project was made possible by the generous support of the National Aeronautics and Space Administration, through the Jet Propulsion Laboratory. A.B. Kahle, A.F.H. Goetz, and J.M. Soha graciously accommodated any and all changes in my work schedule at JPL as dictated by the research reported in this thesis.

My wife, Karen, tolerated this project with good humor for an excessive number of years, and without her indulgence it could not have been successfully completed.

ABSTRACT

The southeastern Sierra Nevada consists of three geographic regions. From west to east, they are: an upland region across the crest, a steep east-facing escarpment along which Owens Valley has partly subsided, and foothill blocks intermediate to the Sierra Nevada and Owens Valley. Farther east, Owens Valley is a deep graben separating the Sierra Nevada and the Inyo Range.

The main goals of this thesis were the detailed mapping of Quaternary glacial and other deposits in these regions, dating of critical events, and geomorphic analysis of the range front. The focus was on Pleistocene moraines near the range front. The motivation of this research was to improve our understanding of the chronology of Pleistocene events, to characterize details of the tectonic history of the Sierra, to infer faulting, erosion, and deposition rates, and to provide a basis for the comparison of the Quaternary geology in the southeastern Sierra and in more intensively studied regions in the central and northern Sierra and elsewhere.

The study area extended from the alluvial fans of Owens Valley west to the Sierra crest from latitude 36°45' to 37°00' N. It included the southern part of the Big Pine volcanic field, an eruptive center for basaltic lavas for most of the Pleistocene Epoch. Elevations within the study area ranged from about 1000 m (Owens Valley) to about 4000 m (peaks along the crest).

Throughout the study area the principal rocks are granodiorite and quartz monzonite of Cretaceous age. Plutons are rather small, and individual drainages generally include more than one. In the southern part of the study area, Jurassic-Triassic metavolcanic rocks are found as roof pendants. These rocks, originally ranging in composition from basalt to rhyolite, are most

common near the Sierra crest. In the northern canyons of the study area, Paleozoic metasedimentary rocks including sandy marbles and biotite schist replace the metavolcanic pendants. The foothill blocks are identical to the Sierras in composition.

Below the foothills coalescing alluvial fans grade a few km east to the alluvium and lacustrine sediments of the Owens River and Owens Lake. These sediments have been shown in geophysical studies to mask a second escarpment as high as the one of the range front, and the total bedrock relief from the Sierra crest to the floor of the graben is as much as 6 km.

During the Quaternary Period the southeastern Sierra Nevada was characterized by the down-faulting of Owens Valley along two zones, one a series of normal faults along the range front (Independence Fault) and the other a series of faults along the center of the valley (Owens Valley fault zone). This same period has seen the cutting of deep canyons through the 2-km-high escarpment. During repeated glaciations these canyons were widened and deepened. Traces of at least seven glaciations were found during this study. Moraines and other deposits left during these glaciations could be distinguished based on the degree of weathering of granitic clasts, vegetative cover, and morphologic characteristics. Absolute age limits were obtained for two of the Pleistocene glaciations by radiometric dating of basalt flows interfingered with the moraines.

Three of the recognized glaciations, probably corresponding to the Matthes, Recess Peak, and Hilgard neoglaciations found by J.H. Birman in the central Sierra Nevada, occurred during the Holocene Epoch. The youngest glaciers (Matthes glaciation) left unconsolidated and unvegetated till in stagnant rock glaciers and moraines in cirques on high peaks. Some rock glaciers are still ice-cored. Extending out from the cirques and into

the upper reaches of the canyons are moraines correlating to the Recess Peak glaciation. Till is generally consolidated and supports heavy lichen growth and bushes but few trees. The oldest Holocene glaciation (Hilgard) left few large moraines in the study area. Hilgard glaciers extended much farther down-canyon than the younger Holocene glaciers, sometimes within one or two km of the Tioga terminal moraines. Those Hilgard terminal moraines which were found have been barely breached by streams. Moraines tend to be heavily forested, and lakes are largely unsedimented. The Hilgard glaciation may have simply been the last stade of the Tioga glaciation from the evidence found in this study.

At least four Pleistocene glaciations occurred in the southeastern Sierra Nevada. All four postdate most of the significant incision of streams through the escarpment. The three youngest probably correlate with the Tioga, Tenaya, and Tahoe stages (in order of increasing age) recognized throughout the Sierra. In each case, moraine morphology has been well preserved. Tioga moraines were found down to about 2200 m elevation. Nested sets of moraines were common. The terminal moraines of the youngest of these were sometimes intact. Lakes were rare; one (Sawmill Meadow) was completely sedimented. Granitic boulders in the moraines were largely unweathered. Weathering of boulders in Tenaya moraines was similar, but a small fraction of granitic boulders were grusy. Boulders from Tahoe moraines were conspicuously weathered, and the moraines themselves were rounded and gullied.

The oldest group of moraines probably significantly predates the Tahoe glaciation. It is nevertheless post-Sherwin. Moraines in this group were found in five of the eight canyons studied. While obviously eroded, these moraines still retained their original shape. All surficial boulders were

heavily weathered, but some exposed in road cuts were fresh. No moraines of Sherwin age were identified, although Sherwin till is widespread only a few km to the north. However, on plateaus and ridges 200 to 300 m above the modern canyons near the Sierra crest were found ancient diamictons, some of which could be till. Remnants of U-shaped valleys preserved as high passes across the crest or as cols between canyons east of the crest may be testimonials to ancient glaciers of Sherwin age or older.

Radiometric dating (^{40}Ar - ^{39}Ar) of basalts interfingered with moraines in Sawmill Canyon provided a new upper limit of 0.12 my for a moraine of the Tahoe glaciation, and a range of 0.13 - 0.46 my for one pre-Tahoe glaciation. These results confirm that the Tahoe glaciation occurred during the Wisconsin stage of the continental ice age, and conclusively demonstrate the existence of pre-Wisconsin glaciers in the southern Sierra. Relative dating based on acoustic wave speeds through weathered boulders on the moraines indicates the age of the pre-Wisconsin moraine may be close to the upper limit.

Alluvial fans appear to have aggraded early in the Wisconsin glaciation (Tahoe glaciation). Subsequently, the fan heads have been incised and the locus of deposition has moved eastward down the fans. The Tenaya and Tioga glaciers during the late Wisconsin stage left outwash plains and terraces along streams cut into the older fans, but aggradation during these events was considerably less than earlier.

Three ages of fans were found. The oldest fanglomerate probably is pre-Wisconsin and is exposed in regions protected from later deposition. The heavily weathered fan deposits of this group overlie basalts which appear to be contemporaneous with dated 1.1-1.2 my-old basalts nearby. In the middle elevations of the fans, roughly 10 m of fanglomerate was

deposited over the old fanglomerate, probably during the Tahoe glaciation. Deposition rates probably are about 0.1 mm/y for the late Pleistocene Epoch. The extent and distribution of the youngest fans (Tenaya-Tioga) are variable, but they are generally found downstream from the incised Tahoe fan heads.

Faulting along the range front appears to have been dip-slip only. The offset rate along the range-front faults was determined at several canyons where the fault crossed dated moraines or lava flows. At least during the Wisconsin glaciation faulting on this zone appears to have been erratic, with rates ranging from zero to 0.5 mm/y or more. Offset moraines and terraces at Independence Creek indicated a faulting rate of 0.1 mm/y. Only a few km to the north, Tahoe moraines of both forks of Oak Creek were not offset at all, although scarps could be seen on adjacent hillsides. At Sawmill Creek an offset lava flow gave a lower limit of 0.5 mm/y. It seems that during the late Pleistocene Epoch, offset on the range front faults has been less than on the mid-valley faults east of the study area. Geodetic studies have suggested modern strain rates of 2.2 mm/y for the Owens Valley fault zone.

Basalts found in canyons through the escarpment and on terraces and ridges in the foothills to the east document stream erosion during the Pleistocene Epoch. Ridgetop basalts, dated at 1.2 my, stand at least 125 m above the modern streams through the foothills. This indicates an erosion rate of ~ 0.1 mm/y. A comparable rate of ~ 0.15 mm/y for the last 0.46 my was found for Sawmill Creek within the Sierra Nevada. Thus at least during the late Pleistocene Epoch erosion rates in the Sierra and in the foothills have been similar.

Patches of boulders and gravels atop the basalt show that some time after 1.2 my BP the foothill block was submerged by alluvial fans. Incision

may have begun in response to the inception or renewal of subsidence of the graben along the Owens Valley fault zone.

Extensive volcanism in the Big Pine Volcanic field appears to have begun at least 1.2 my ago, and has continued sporadically up to perhaps 0.05 my ago. Minor eruptions may have occurred more recently.

The eastern escarpment of the Sierra Nevada consists of two zones of truncated ridges. Within the study area, the upper zone is about 950 m high; the lower is about 750 m high. Triangular facets of the upper zone have a gradient of only ~ 24°, lower than slopes of ~ 29° in the lower zone. This could be explained if subsidence of Owens Valley along the range-front faults occurred in two great pulses.

Both absolute and relative dating methods were refined for this study. Absolute dating of the K-poor basaltic lavas was done indirectly, by ^{40}Ar-^{39}Ar analysis of K-rich granitic xenoliths found in the lava. These ancient xenoliths were partially degassed of their accumulated ^{40}Ar during heating in the magma, and it proved possible to date this heating event.

In addition to conventional relative dating methods, a new quantitative approach based on the speed of acoustic waves through individual clasts in a deposit was investigated. This method had been used only once before, on terrace deposits. The technique proved to be very useful, and was capable of discriminating moraines successfully in well-studied canyons in the central Sierra. Acoustic wave speeds may be controlled by the abundance of intergranular cracks in granitic boulders. If this is the case, then this technique relies on different processes than those exploited by conventional methods of relative dating. The successful application to moraines in this study enhances our ability to analyse glacial sequences and complements conventional semi-quantitative methods of relative dating.

TABLE OF CONTENTS

Pages

PART II: QUATERNARY GEOLOGY

List of Figures

List of Figures (continued)

List of Figures (continued)

List of Figures (continued)

List of Figures (continued)

List of Plates

List of Tables

List of Tables (continued)

CHAPTER 1

INTRODUCTION

The Sierra Nevada is one of the great geographic features of North America. Although the geology of this recently glaciated mountain range has been intensively studied by many researchers over the past century and more, and while the central Sierra Nevada has been a focus for investigations of Quaternary glaciations, many questions remain concerning the chronology of Pleistocene events and details of the Quaternary glaciations in the southern part of the range. Even the existence of glacial deposits older than the Wisconsin stage of the continental glaciations has not been conclusively demonstrated here, and the age relationships of volcanic eruptions, glaciations, and tectonic events are not well understood. With this thesis I have tried to address some of these questions. The main evidence in this investigation was the age and distribution of the glacial moraines left in the deep canyons cut through the escarpment which bounds the mountains on the east. Because of the widespread distribution and episodic nature of the advance of glaciers during the Quaternary Period, these more than other deposits serve as time markers by which the main tectonic events -- the rise of the range and subsidence of Owens Valley to the east -- may be chronicled. Thus my central effort was to map the Quaternary geology, especially glacial moraines and outwash, of a region representative of the southeastern Sierra Nevada, and to correlate glacial sequences from different canyons, and to fix the chronology to the absolute time scale. The goal of this study was to better understand the nature of the ice age in the Sierra Nevada and the late Cenozoic history of the range.

Since Pleistocene tills are difficult to date directly, the study area was chosen to include basalt flows that interfingered with moraines.

Radiometric dating of the lava could be used to establish age limits to the glaciations. Ages of moraines in nearby canyons could then be inferred from correlation of moraine sequences and weathering characteristics of the tills. The study area was also chosen far enough north that some Pleistocene glaciers descended low enough to cross the normal faults along which the Sierra escarpment was developed. The progressive offset of moraines at the range front could be used to calculate approximate long-term faulting rates, if the ages of the moraines could be determined. Finally, the location of lava flows above the bottoms of stream canyons and on alluvial fans presented the opportunity to estimate erosion and alluviation rates.

The Study Area

A 30-km-long section of the eastern escarpment of the Sierra Nevada was chosen for study (Fig. 1-1). This area lies mainly within the Mt. Pinchot Quadrangle, but extends into the Mt. Whitney, Independence, and Big Pine Quadrangles also. It satisfied the basic requirements of the proposed research: well-preserved sequences of moraines and outwash plains in several canyons crossed the range-front faults, along which scarps were evident, and lava flowing from vents within the Sierra or along the range-front faults interfingered with the moraines and outwash at three locations. Farther south, this combination of volcanic history and moraines crossing the range front is not found. To the north, the volcanic vents are somewhat east of the Sierra Nevada, so the glacial chronology cannot be readily established.

The chosen study area extended north from Independence Creek to Taboose Creek, and from the distal ends of the coalescing alluvial fans on the west side of Owens Valley to the Sierra crest. Within this area, eight canyons were selected for detailed mapping. Each of these offered some special

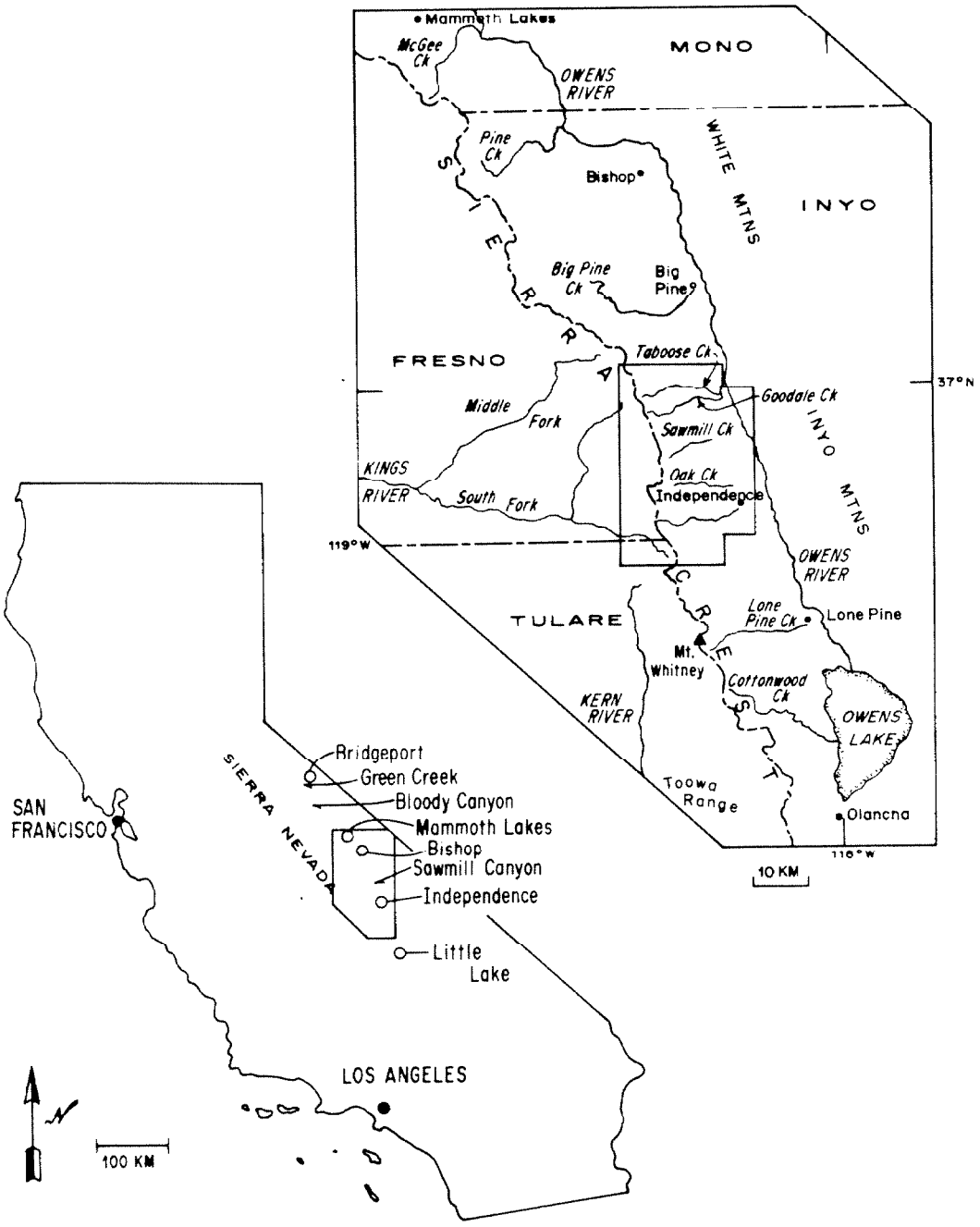

Figure 1-1. Index map of the study area.

feature which justified this effort. The southernmost canyon, Onion Valley (Independence Creek, shown in Fig. 1-1 as the creek passing through the town of Independence), has a well-preserved moraine sequence which is readily accessible by automobile. Road cuts in moraines on the north side of the canyon permit inspection of weathering profiles of tills of different ages, an opportunity unsurpassed in the southern Sierra. Most important, however, the scarp of the Independence Fault crosses moraines and outwash of various ages at the range front.

Sardine Canyon, immediately north of Onion Valley, is unique in that the late Pleistocene glaciers originated from a cirque well below the head of the canyon, which appears to be a relic from an earlier erosion cycle.

Oak Creek has two major tributaries. Moraines of the South Fork of Oak Creek are (possibly excepting the oldest) apparently unfaulted at the range front, despite the presence of old scarps on adjacent hillsides and despite the clear evidence of Holocene or latest Pleistocene faulting only a few km to the south. The moraines are perhaps even better preserved than at Independence Creek.

At the North Fork of Oak Creek are the southernmost lavas found in the study area. These are distributed at different levels in the foothills and on cut terraces above the modern stream, as well as on the alluvial fan below. The youngest lavas, at the bottom of the modern canyon, underlie and older moraine and associated outwash.

The late Pleistocene glaciers in Sawmill Canyon did not reach the range front, but lavas erupted within the Sierra underlay the largest moraine, called the Hogsback on the topographic map. Furthermore, lavas probably of the same age capped the end of an older moraine, which was covered by a thin layer of volcanic bombs and cinders. Preliminary inspection showed an

outcrop of basalt under this older moraine also, so the possibility to bracket the age of the glaciation as well as to place an upper limit on the age of the Hogsback was present.

Armstrong Canyon, immediately south of Goodale Canyon (Fig. 1-1), contained an unusually complete sequence of older moraines, possibly a consequence of the absence of a major stream. This was especially useful in assigning ages to the poorly preserved moraines of Goodale Canyon. Goodale Canyon was of interest for two reasons: the moraines and outwash at the range front overlay lava flows and possibly a cinder cone, and the cirque region contained a great depth of weathered diamicton, probably till, into which some late Pleistocene cirques were cut. This ancient diamicton resembles that of Sardine Canyon, above its cirque.

The northernmost of the eight canyons, Taboose Canyon, displayed two interesting features. The moraines at the range front were faulted, and the cirques at the crest were cut into an older and larger west-draining valley, the headwaters of the South Fork of the Kings River. During the late Pleistocene Epoch, the low divide, Taboose Pass, was obviously the site of a crest-crossing ice cap which fed glaciers on both sides of the Sierra Nevada.

Additional topics of interest in the study area are the gross geomorphic features of the escarpment, relicts of older erosion surfaces in the Sierra upland, and the depositional histories of the alluvial fans.

Physiographic Setting

The Sierra Nevada is a broad upwarp trending northwest almost 700 km from the Garlock Fault to the vicinity of Lassen Peak. The southern and central Sierra Nevada block is strongly asymmetric, a consequence of the

subsidence of a deep graben, Owens Valley, and other basins between the Sierra and the ranges to the east. The crest of the Sierra Nevada culminates in peaks 3500 m or more in height in the southern part of the range, from latitude 36°15' N 250 km to 38°15' N. It is within this region, the high Sierra, that the study area was chosen.

Many of the principal physiographic features of the study area may be seen in Fig. 1-2. The alluviated Owens Valley straddles the mid-valley fault zone along which roughly a third of the subsidence of the graben has occurred. To the west, near the town of Independence, the alluvial fans grade upwards 700 m to the normal faults at the base of the escarpment. Protruding from the fans are bedrock foothills, their stepped surfaces once part of broad erosion surfaces. Between the forks of Oak Creek, the southernmost lavas of the Big Pine volcanic field cap one of the lower surfaces. From Sawmill Creek north to Taboose Creek, basaltic cinder cones mark the range-front faults, and lava flows interfinger with the fanglomerates to the east. North of the study area (not shown in Fig. 1-2), the locus of eruptions is shifted away from the range front. The escarpment, 2 km high, is cut by deep canyons draining the Sierra uplands. The escarpment ends two or three km east of the Sierra crest. To the west, the Sierra upland consists of rows of peaks, roughly aligned with the crest and separated by east-west canyons. The crest itself is remarkably level, ranging in elevation only 500 m from the highest peaks (4000 m) to the lowest passes.

During the Cenozoic Era the Sierra Nevada was raised in several episodes, probably achieving its present elevation only in the Quaternary Period. In the Pliocene Epoch, Owens Valley began subsiding along normal faults roughly parallel to the trend of the crest. The modern Owens Valley is one of the major topographic features of the continent, and the

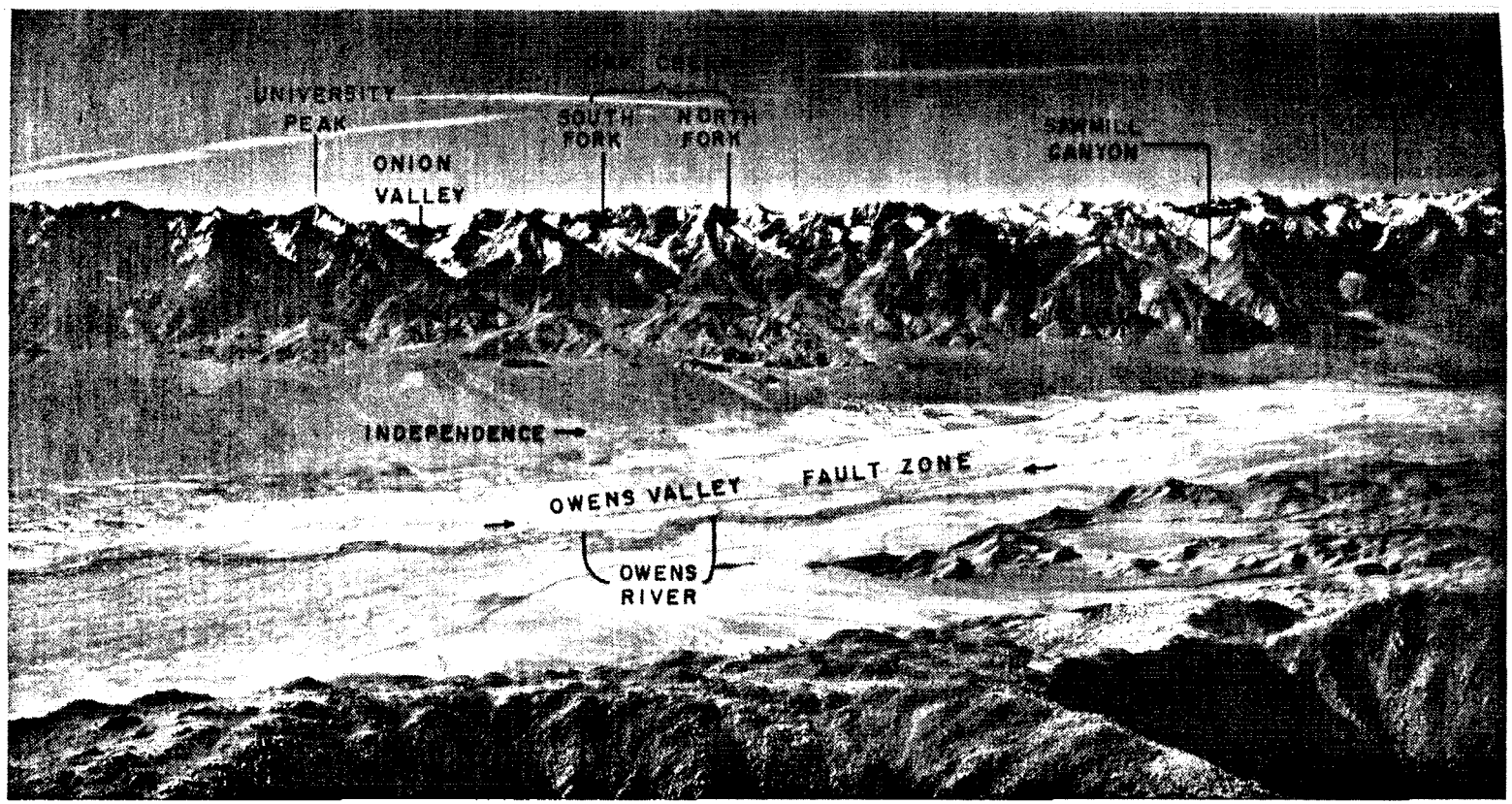

Figure 1-2. The eastern escarpment of the Sierra Nevada in the study area. The oblique aerial photograph was taken from over the Inyo Mountains looking west. About 25 km of the 2-km-high escarpment are shown. U.S. Geol. Survey photograph GS-OAI 5-1, 11-25-55.

2-km-high escarpment of the Sierra Nevada to the west is spectacular. The bedrock floor of the graben lies under a comparable depth of alluvium shed from the mountains. The range-front faults have locally served as conduits transmitting basaltic and other lavas to the surface.

The Sierra Nevada was repeatedly glaciated during the Quaternary Period. The glaciers profoundly changed the physiographic character of the range, leaving broad domelands and meadows, U-shaped canyons and valleys, and steep cliffs and sharp ridges. Most of the obvious glacially sculpted features were freshened during the last major glaciation only ten or twenty thousand years ago, but the highest regions of the Sierra were glaciated during the Holocene Epoch, and even today pocket glaciers are found in some cirques. The evidence of earlier glaciations is less obvious to the casual observer, but in most valleys multiple sets of moraines containing heavily weathered till are found well below the fresh moraines from the latest Pleistocene glaciers, and these testify to ancient and larger glaciers. Locally, the glacial moraines are offset where they cross the range-front faults. Elsewhere, moraines interfinger with lavas. Through radiometric dating of these lavas, a chronology of volcanism, glaciation, and faulting may be constructed.

Geologic Setting

For most of its length the Sierra Nevada consists of a complex core of Mesozoic plutons capped by steeply dipping older metamorphosed volcanic and sedimentary rocks. A wide range of plutonic rocks is found in the study area. This range includes ultramafic dunite and pyroxenite, gabbro and quartz diorite, and alaskite, but most of the plutonic rocks are quartz monzonite or granodiorite. Within the study area, intrusion of

the plutons occurred during the Cretaceous Period. In contrast to the Sierra Nevada west of the crest, plutons in the study area tended to be small, and generally three or more were found in each drainage. Moore (1963) identified 27 plutons in the Mt. Pinchot Quadrangle alone. This is of importance to the study of Quaternary geology because glacial and alluvial deposits may have stongly varying compositions from valley to valley, and the basis for regional correlations based on weathering information is correspondingly reduced.

Metamorphic rocks in the southern half of the study area were volcanic flows and tuffs ranging in composition from basalt to rhyolite. These were erupted during the Triassic or Jurassic Periods and metamorphosed later in the Mesozoic at the time of the emplacement of the plutons. Only in Sawmill Canyon and farther north are metasedimentary rocks found. The most prominent are marble and dark biotite schist.

Metavolcanic rocks were more resistant to weathering than granitic rocks, and the ratio of these resistates to granitic boulders at the surface of Quaternary deposits increased with the age of deposition.

During the Tertiary Period the study area was uplifted and deeply eroded, so that the granitic plutons were exposed. Remnants of erosion surfaces created during this time are scattered throughout the region. Near the end of the Tertiary and throughout the Quaternary Period, basic lavas were extruded from vents on major faults along which subsidence of Owens Valley occurred. These lavas are generally olivine basalts, typically alkalic or sub-alkalic, and contain dunite inclusions and granitic xenoliths. The dunite inclusions may reflect a deep source, possibly the upper mantle, but the granitic xenoliths may have been derived very near the surface just before eruption. Elsewhere in the Sierra Nevada volcanism began before the Pliocene

Epoch, but in the study area the oldest dated lavas (this study) were only 1.2 my old. Moore (1963) thought that some basaltic dikes might be late Pliocene in age.

The oldest unconsolidated deposits of the study area were infrequent diamictons preserved on old erosion surfaces or under ancient lavas. Most deposits were late Pleistocene fanglomerates or tills, or Holocene talus. Efforts to establish stratigraphic relationships on the eastern side of the Sierra Nevada are generally indirect, because of the lack of dissection of the alluvial fans, and this was true in the study area as well. One remarkable and puzzling aspect of the study area was the apparent absence of mid-Pleistocene tills and outwash, especially in view of their abundance farther north.

Previous Work

Local to the study area

One of the advantages of the study area was that the bedrock geology had been previously mapped, at a scale of 1:62,500. Moore (1963,1981) mapped the Mt. Pinchot Quadrangle and the Mt. Whitney Quadrangle. Bateman (1965) mapped the Big Pine Quadrangle, and Ross (1965) mapped the Independence Quadrangle, which includes the distal ends of the alluvial fans of the Sierra on its western side. However, none of these studies focused on the detailed problems of the Quaternary geology, especially the subtle distinctions among the tills and glacial outwash. No effort to subdivide the fanglomerates by age was made, although such ages may have spanned several glaciations.

Earlier researchers such as Knopf (1918), Blackwelder (1931), and Mayo (1941) studied aspects of the glacial geology and deformation history in

the study area, but as part of regional studies or surveys. Dalrymple (1964a) made a major contribution, carefully analyzing the glacial moraines of Sawmill Canyon using relative dating techniques newly refined by Sharp and Birman (1963) and Birman (1964). In this way, he was able to recognize four Pleistocene glaciations, although all seemed to be younger than the Sherwin glaciation so prominent farther north. Dalrymple's most notable contribution, however, was dating by K/Ar analysis replicates of samples of the basalt under the Hogsback, arriving at an upper age limit of 60,000 ± 100,000 (2σ) y and 90,000 ± 180,000 y for the Tahoe glaciation. The low precision, due to the low ratio of radiogenic ^{40}Ar to background ^{40}Ar present in the lava upon cooling, precluded the use of these dates as more than a rough guide to the age of the Hogsback and the Tahoe glaciation, but they demonstrated for the first time that the Tahoe glaciation was probably less than 0.1 my old. One of the chief goals of the present study was to carefully redate this lava flow to improve the precision. Dalrymple, Burke, and Birkeland (1982) have done just this, repeating the early measurements using the same techniques. They obtained a younger, more precise age of 53,000 ± 88,000 (2σ) y which they interpreted as supporting the earlier arguments of Burke and Birkeland (1979) that the Hogsback was a Tioga moraine (latest Pleistocene) rather than an older Tahoe moraine. Burke and Birkeland arrived at their conclusions during a study of relative dating of moraines in four canyons of the southern and central Sierra, of which only Sawmill Canyon was in the study area.

Both Moore (1963) and Darrow (1972) studied the lavas of the Big Pine volcanic field that are found in the study area. These studies concentrated on the petrology and stratigraphic relationships of the flows and cinder

cones, but as Darrow concluded, there was insufficient information to completely establish the volcanic chronology, at least without radiometric dating. More recently, Moore and Dodge (1980) and Dodge and Moore (1981) have included the Big Pine volcanic field in a regional study of basic lavas in the southern Sierra, but no new information was added to the chronology.

Regional

Regional studies of the Sierra Nevada and detailed studies throughout the Sierra have been well summarized in Bateman and Wahrhaftig (1966). Tectonic studies have been reported in Christensen (1966) and more recently in Huber (1981). Consequently, the list below is not comprehensive and only includes studies of particular significance to this thesis.

The only other published studies of the Quaternary geology along the eastern escarpment of the Sierra south of Long Valley appear to be those of Fleisher (1967) and Rahm (1964), although Richardson (1975) and Lubetkin (1980) have conducted studies in the Alabama Hills, in Owens Valley south of the study area. However, between them Bateman (1965) and Moore (1963,1981) have mapped the fundamental Quaternary deposits from Lone Pine to Bishop. West of the crest there has been considerable study of the Quaternary glaciations, some of which is unpublished. Matthes (1950, 1960, 1965) has studied many aspects of Quaternary geology and geomorphology in Sequoia National Park and, to the north, in the drainage of the San Joaquin River. Janda (1966) has made a careful study of the hydrology of the San Joaquin River, including a more recent inspection of the glacial geology. J.H. Birman (oral comm., 1977) has conducted extensive studies for several field seasons along the Kings River, notably near the Kings-Kern divide.

Clague, Correaga, and Birman (J.H. Birman; oral comm. 1977) have also completed a map of the glacial geology along the Kern River to the south.

Glacial geology in the central Sierra east of the crest has been well studied by numerous geologists, including in recent times Putnam (1949, 1950), Sharp (1968, 1969, 1972), Sharp and Birman (1963), Birman (1964), Curry (1966, 1968, 1971), and Burke and Birkeland (1979). Early geomorphic studies of the southern Sierra were made by Lawson (1904) and Matthes (1960). Webb (1946, 1950) described the development of the Kern basin south of Mt. Whitney, at the southern edge of the late Pleistocene glaciers. Matthes (1960, 1950) devoted considerable effort to the recognition and correlation of remnants of ancient erosion surfaces now on peaks and ridges or on benches high above modern canyons. He felt these pointed to periods of quiet separating episodic regional uplift; Wahrhaftig (1965) proposed that the correlation of these remnants was spurious, arguing that local joint spacing controlled the development of stepped surfaces in granitic terraine. Nevertheless, St. Amand and Roquemore (1979) have recently contended that the Chagoopa surface of Matthes may be correlated with a down-faulted erosion surface in the Coso Range east of the Sierra Nevada.

Geophysical surveys have defined the general configuration of bedrock below the alluviated surface of Owens Valley. Gutenberg et al. (1932) conducted early seismic surveys just south of the study area which placed lower limits on the depth of the fans near the range front, but the major contribution was the gravity survey of Pakiser, Kane, and Jackson (1964) which defined the buried bedrock escarpment along the Owens Valley fault zone.

Studies of ancient lakes east of the Sierra (e.g., Smith, 1979; Lajoie, 1968) have improved our understanding of the the climatic and pluvial history, and presumably the glacial history of the Sierra as well. Lajoie, working

with dissected lake beds and ash layers in the Mono Basin, was able to establish a detailed record of the pluvial period of the latest Pleistocene Epoch, probably correlative with the Tioga glaciation. Smith (1979) and Smith et al. (1980), working with deep cores drilled from Searles Lake, have been able to identify pluvial periods over a much longer period.

Although the gross history of late Cenozoic uplift and regional westward tilting of the Sierra Nevada envisioned by early researchers (e.g., Whitney, 1880; Ransome, 1898; and Lindgren, 1911) is widely accepted today, there have been divergent views on the elevation of the Sierra at the beginning of the Quaternary Period and the rate of uplift since then. Most studies of absolute uplift have been based on reconstructed stream profiles and erosion surfaces west of the crest (e.g., Matthes, 1930, 1960). Some control of the chronology of events is provided by radiometric dating of lava flows within the ancient canyons (e.g., Dalrymple, 1963, 1964b; Huber, 1981). Matthes (1960), Dalrymple (1964b), and Christensen (1966) agreed that the last major uplift of the Sierra probably began late in the Miocene Epoch or in the Pliocene Epoch and that the Sierra achieved its present height early in the Pleistocene Epoch. Axelrod and Ting (1960) disagreed, concluding on paleobotanical grounds that the major uplift occurred during the Pleistocene Epoch. Huber (1981) takes a middle position, arguing from reconstruction of the ancient San Joaquin River that the central Sierra was probably not high enough to support glaciation until perhaps 1.5 my ago, but that uplift began during the Pliocene and continued throughout the Pleistocene Epoch.

Some researchers feel that there may have been differential uplift, with one part of the Sierra rising first. Dalrymple (1964a) commented that uplift of the southern Sierra late in the Pleistocene Epoch, lagging uplift farther north, could explain the absence of mid-Pleistocene moraines in the south.

Christensen (1966) and Crough and Thompson (1977) argued that uplift began in the south, and this view is consistent with the tectonic interpretation of Hay (1976), who argued on theoretical grounds that the latest uplift of the Sierra Nevada began with the advent of the San Andreas fault system and accelerated about 4.5 my ago with the opening of the Gulf of California and the northward migration of the Mendocino triple junction.

From the dating of lavas on erosion surfaces near the Coso Range, the subsidence of Owens Valley appears to have begun 5-6 my ago (Giovannetti, 1979; Bacon et al., 1979); however, Matthes (1950) noted geomorphic evidence from the Sierra escarpment near Mt. Whitney that indicated the existence of a 1-km-deep Pliocene Owens Valley correlated with one of his erosion surfaces, so that subsidence may have occurred along a preexisting valley similar to that of the modern Kern River. This ancient valley itself may have resulted from an earlier episode of subsidence.

Glacial Chronology

Glacial- and time-stratigraphic nomenclature

Glacial advances are referred to as recommended by Richmond et al. (1959), except as modified by local custom. Glacial-stratigraphic units are "glaciations" and the subordinate "stades". The equivalent time-stratigraphic units are "stages" and "substages". In accepted usage, the Wisconsin, Illinoian, Nebraskan, and Kansan stages are the recognized continental glaciations in the United States. In the Sierra Nevada, glacial advances were identified and named before the correlation with the continental record was firmly established. Blackwelder (1931) identified the Tioga and Tahoe glacial advances, which would now be regarded

as substages of the Wisconsin Stage, as glacial stages in their own right. Individual advances within the Tioga or Tahoe glaciations are regarded herein as stades (or substages). The Tenaya advances (Sharp and Birman, 1963) are likewise regarded collectively as a distinct stage in the same sense, although in the end it may prove to be a stade of the Tioga glaciation.

Chronology

The overall chronology of Sierran glaciations and their probable correlation with the continental glaciations was established by early researchers, notably Matthes (1930) and Blackwelder (1931). In the ensuing years details of the glacial sequence have been added, but the major conception is unchanged. A chronology for the central and southern Sierra Nevada is presented in Table 1-1. Holocene or "neoglaciations" were restricted to high mountain ranges and have no continental equivalent. In the southern Sierra, the commonly used nomenclature has been that of Birman (1964), who established type areas of neoglacial moraines in the headwaters of Mono Creek (north of Pine Creek; Fig. 1-1). Birman and most other researchers have recognized three major advances, the last of which has been retreating during historical times. On the strength of relative weathering data, Birman argued that the oldest neoglaciation (Hilgard) postdated the Holocene altithermal, and that all Holocene glaciations occurred within the past 4000 years. Curry (1968, 1969, 1971) was able to obtain a ^{14}C date placing an older limit of about 7000 y on a Hilgard moraine near Mammoth Lakes, and largely on the strength of this date and careful lichenometric studies of neoglacial moraines at Mono Creek he proposed the neoglacial chronology shown in Table 1-1. In this conception

Table 1-1

Quaternary Glaciations

Continental Stage	Conventional Sierra Nevada Equivalent	Age	Advance, This Study
	Matthes[3]	0 - 700 y[5]	VII
	unnamed[4]	1100 y[5]	VII?
(Neoglacial)	Recess Peak[3]	2000-2700 y[5]	VI
	unnamed[4]	4000 y[5]	VI?
	Hilgard[3] *	9000-10,000 y[5]	V
late Wisconsin	Tioga[1]	10,500-25,000 y[6]	IV
mid Wisconsin	Tenaya[2]	35,000-45,000 y[6]	III
early Wisconsin	Tahoe[1]	65,000-90,000 y[6]	II
Sangamon Interglacial	-	-	-
Illinoian	Mono Basin[2]	~ 130,000 y[7]	I
Illinoian ?	Casa Diablo[4] **	~ 400,000 y[5]	I
Kansan	Sherwin[1]	0.73 my (~ 0.75 my)[8]	-
?	McGee[1]	~ 1.5 my[9] or ~ 2.7 my[5,10]	-
Nebraskan	Deadman Pass[4] †	2.8[11] - 3.2 my[12]	-

[1] Names of Blackwelder (1931)
[2] Names of Sharp and Birman, (1963)
[3] Names of Birman (1964)
[4] Names of Curry (1966, 1968)
[5] Ages follow Curry (1968, 1971)
[6] Ages follow Smith (1979)
[7] Age follows Sharp and Birman (1963) and Curry (1971)
[8] Dalrymple et al. (1965); Sharp (1968)
[9] Ages follow Huber (1981)
[10] Ages follow Dalrymple (1963)
[11] Ages follow Curry (1966)
[12] Ages follow Dalrymple (1964b)

Table 1-1 (continued)

* Birman (1964) felt that the Hilgard neoglaciation occurred about 4000 y ago.

** Bailey et al. (1976) have redated the basalts above and below the Casa Diablo till, and obtained significantly younger ages than did Curry (1968, 1971). Burke and Birkeland (1979) feel that the Casa Diablo till was deposited during the Tahoe stage. However, until the dating controversy at the Casa Diablo type area is resolved, the Casa Diablo name should probably be retained for this stage.

† Huber (1981) argues that the Deadman Pass "till" (Curry, 1966) may not have a glacial origin. Clark (1967) thought there were glaciations between the Mono Basin and Sherwin stages, and in the present study evidence is presented that a till found in Sawmill Canyon is close to its upper age limit of 463,000 y found by ^{40}Ar-^{39}Ar dating of a subjacent basalt.

Ages found by K/Ar analysis have been corrected for the new values for isotopic abundances and decay constants recommended by Steiger and Jäger (1977)

the earliest neoglaciation is not much younger than the last of the Pleistocene glaciations, and intermittent glaciations have been the rule during the last half of the Holocene Epoch, as Birman (1964) proposed.

The chronology of the late Pleistocene glaciations has been inferred largely from pluvial - interpluvial periods recorded by deposition in the lakes of the valleys and basins east of the Sierra Nevada. The chronology of Table 1-1 was reported by Smith (1979) and is based on ^{14}C dates of wood and organic carbon disseminated in the lake sediments from cores in Searles Lake (Stuiver and Smith, 1979). Searles Lake is today a playa. Glaciations are inferred to correlate at least in a general sense with pluvial periods in the lake's history. The Tioga stage and the end of the Tenaya stage were constrained by the ^{14}C dates directly. The beginning of the Tenaya stage and all of the Tahoe stage were beyond the range of ^{14}C dating, but were estimated by extrapolating sedimentation rates calibrated by the ^{14}C dates. One interesting feature of Smith's chronology is that the Tahoe glaciation in the Sierra Nevada appears to have begun about 90,000 years ago, 15,000 years before the early Wisconsin glaciation according to Goldthwaite et al. (1965) and to Frye et al. (1965). Smith interpreted the stratigraphy of Searles Lake to show more-or-less continuous deep-water deposition from 90,000 to 60,000 y BP (Tahoe stage), followed by an interpluvial period lasting until about 45,000 y BP. A brief pluvial period (Tenaya glaciation) ended about 33,000 y BP, but the following 10,000 years were characterized by short wet and dry intervals. Searles Lake was filled from 24,000 y BB to 10,000 y BP (Tioga stage). Thus the Tenaya and Tioga glaciations may not have been separated by an extended interglacial period, and the Tenaya glaciation could be regarded as an early major stade of a lengthened Tioga glaciation, instead of a glaciation in its own right.

The binary notation (glacial - interglacial) used to record glaciations in the Sierra is inadequate to describe the complexities revealed by a complete stratigraphic record.

Smith (1979) identified an earlier pluvial interval from roughly 130,000 to 110,000 y BP. This probably corresponds to a cold period around 120,000 y BP indicated by sea level fluctuations (Hopkins, 1973) and by marine stratigraphy (Ku and Broecker, 1966). Sharp and Birman (1963) and Curry (1971) felt that the Mono Basin glaciation occurred at this time.

The record of still earlier glaciations is more sketchy. Curry (1968, 1971) identified the Casa Diablo till between dated lavas which indicated an age of about 0.4 my, although this conclusion has been contested recently by Bailey et al. (1976) and by Burke and Birkeland (1979). The Sherwin till underlies the Bishop tuff (Sharp, 1968), dated at 0.73 my by K/Ar analysis of sanidine crystals (Dalrymple et al., 1965). Sharp (1968) estimated the till to be only a few tens of thousands of years older, based on its estimated degree of weathering upon burial. Easterbrook (1978) found the remnant magnetism of fine sediments from the till to be normally polarized. Mankinen and Dalrymple (1979) showed that the most probable age of the Brunhes - Matuyama reversal was about 0.73 my, so Easterbrook's findings may be taken as support for Sharp's inference.

The ancient till on McGee Mt. was thought by Huber (1981) to be no more than 1.5 my old, based on his estimates of the time the central Sierra was uplifted enough to support glaciers. Curry (1971) felt that the glaciation was similar in age to the one that left his Deadman till on the Sierra crest north of Mammoth Lakes. Dalrymple (1964b) imposed an upper age limit of 2.7 my on the McGee till by K/Ar dating of subjacent andesite. The Deadman till lies between quartz latite and andesite dated at about 2.8 my and 3.2 my,

respectively. However, Huber (1981) argued that Curry (1966, 1968, 1971) was incorrect in identifying the diamicton as a till, and that it may have been a lahar.

Pertinent Absolute Dates

Few absolute dates for the glaciations represented by moraines in the southern Sierra Nevada have been determined. Curry (1968) was able to establish an early Holocene age for the Hilgard neoglaciation, based on a ^{14}C date of 7030 ± 260 y BP (uncertainties are 2σ) for a log from a landslide covering a Hilgard moraine. Adam (1966, 1967) obtained a ^{14}C date of 9990 ± 1600 y for a tree stump from a post-Tioga swamp in the northern Sierra. Lajoie (1968) and Stuiver and Smith (1979) obtained numerous ^{14}C dates from ostracods, wood, and disseminated organic matter from late Wisconsin lake clays, but the exact relation between glaciations and high lake levels is somewhat speculative and these dates may not apply to fine detail of the glaciations. Lubetkin (1980) noted a Tioga (?) fan of Lone Pine Creek built over tufa from Owens Lake beaches. The tufa gave a ^{14}C age of about 21,000 y, consistent with the findings for Mono Lake and for Searles Lake.

Dalrymple (1964a) dated lavas (K/Ar method) between Tahoe and pre-Tahoe moraines at Sawmill Canyon, obtaining ages of 60,000 ± 100,000 y and 90,000 ± 180,000 y. Dalrymple et al. (1982) revised this date to 53,000 ± 88,000 y based on new analyses. Janda (1966) felt that quartz latite cobbles from Mammoth Mt. dated by Dalrymple (1964b) at 370,000 ± 80,000 y (K/Ar) were from a pre-Tahoe till. Curry (1971) reported K/Ar ages of 280,000 ± 134,000 y and 441,000 ± 80,000 y bracketing the Casa Diablo till, but Bailey et al. (1976) redated the same lavas, obtaining younger ages of 62,000 ± 13,000 y and 126,000 ± 25,000 y, respectively.

Other radiometric dates apply to ancient glaciations not identified in the study area.

Presentation

Research for this thesis was naturally divisible into three parts: field studies, relative dating, and radiometric dating. Presentation is arranged in the same way. Because presentation of the field research draws heavily on understanding the techniques and results of relative and absolute dating, these techniques are introduced first (Part I). The three chapters of Part I describe the conventional relative dating methods used in this study (Ch. 2), a relatively new method based on the speed of acoustic waves through weathered boulders from tills (Ch. 3), and the ^{40}Ar - ^{39}Ar dating of granitic xenoliths from basic lavas which was used to determine precise and accurate ages of eruption for the lavas (Ch. 4). In Ch. 3, the acoustic wave speed method is demonstrated for moraines from two previously studied canyons of the central Sierra, but the results for canyons in the study area are presented with the field work in Part II. In Ch. 4, the rationale of the ^{40}Ar - ^{39}Ar dating is developed and the results of all analyses are presented and discussed.

The results of the field investigations are described in Part II. Presentation is organized geographically, by canyon, from south to north, in Ch. 5. This was done because the sequence of moraines from each individual canyon rather than regional characteristics of weathered tills of each stage, was the basis for the reconstruction of the geologic history. The results are summarized in a regional format at the end of Ch. 5. Highlights and conclusions are presented in Ch. 6.

References Cited

Adam, D.P., 1966, Osgood Swamp (C-14) date A-545: Radiocarbon 8, 10.

Adam, D.P., 1967, Late Pleistocene and Recent palynology in the central Sierra Nevada: in Cushing, E.J., and Wright, H.E. Jr., eds., Quaternary Paleocology; INQUA Congress VII, Proc. 7, Yale Univ. Press, New Haven, Conn., p. 275-301.

Axelrod, D.I., and Ting, W.S., 1960, Late Pliocene floras east of the Sierra Nevada: University of California Publications in Geol. Sci. 39, 1-118.

Bacon, C.R., Giovannetti, D.M. Duffield, W.A., and Dalrymple, G.B., 1979, New constraints on the age of the Coso Formation, Inyo, County, California, [abs]: Geol. Soc. America Abstracts with Programs, 11, No. 3, p. 67.

Bailey, R.A., Dalrymple, G.B., and Lanphere, M.A., 1976, Volcanism, structure, and geochronology of Long Valley caldera, Mono County, California: Jour. Geophys. Research 81, 725-744

Bateman, P.C., 1965, Geology and Tungsten Mineralization of the Bishop District, California: U.S. Geol. Survey Prof. Paper 470, 208 p.

Bateman, P.C., and Wahrhaftig, C., 1966, Geology of the Sierra Nevada: in Bailey, E.H., ed., Geology of Northern California, California Nevada, California: Geol. Soc. America Spec. Paper 75, 80 p. Div. Mines and Geology Bull. 190, p. 107-172.

Birman, J.H., 1964, Glacial Geology Across the Crest of the Sierra California: Geol. Soc. America Spec. Paper 75, 80 p.

Blackwelder, E., 1931, Pleistocene glaciation in the Sierra Nevada and Basin ranges: Geol. Soc. America Bull. 42, 865-922.

Burke, R.M., and Birkeland, P.W., 1979, Reevaluation of multiparameter relative dating techniques and their application to the glacial sequence along the eastern escarpment of the Sierra Nevada, California: Quaternary Research 11, 21-51.

Christensen, M.N., 1966, Late Cenozoic crustal movements in the Sierra Nevada of California: Geol. Soc. America Bull. 77, 163-182.

Clark, M.M., 1967: Pleistocene Glaciation of the Drainage of the West Walker River, Sierra Nevada, California: PhD thesis, Stanford University; University Microfilms, Inc., No. 68-6401, Ann Arbor, MI., 170 p.

Crough, S.T., and Thompson, G.A., 1977, Upper mantle origin of Sierra Nevada uplift: Geology 5, 396-399.

Curry, R.R., 1966, Glaciation about 3,000,000 years ago in the Sierra Nevada, California: Science 154, 770-771.

Curry, R.R., 1968, Quaternary Climatic and Glacial History of the Sierra Nevada, California: Ph.D. thesis, Univ. of California, Berkeley, University Microfilm, Inc., No. 68-13,896, Ann Arbor, MI, 204 p.

Curry, R.R., 1969, Holocene Climatic and Glacial History of the Central Sierra Nevada, California: in Schumm, S.A. and Bradley, W.C. (eds.), United States Contributions to Quaternary Research: Geol. Soc. America Spec. Paper No. 123, 1-47.

Curry, R.R., 1971, Glacial and Pleistocene History of the Mammoth Lakes Area, California - A Geologic Guidebook: University of Montana, Dept. of Geology, Missoula, Mont., Geological Serial Publication 11, 49 p.

Dalrymple, G.B., 1963, Potassium - argon ages of some Cenozoic volcanic rocks of the Sierra Nevada, California: Geol. Soc. America Bull. 74, 379-390.

Dalrymple, G.B., 1964a, Potassium - argon dates of three interglacial basalt flows from the Sierra Nevada, California: Geol. Soc. America Bull. 75, 753 - 758.

Dalrymple, G.B., 1964b, Cenozoic chronology of the Sierra Nevada, California: University of California Publications in Geological Sciences 47, 41 p.

Dalrymple, G.B., Cox, A., and Doell, R.R., 1965, Potassium - argon age and paleomagnetism of the Bishop Tuff, California: Geol. Soc. America Bull. 76, 665-674.

Dalrymple, G.B., Burke, R.M., and Birkeland, P.W., 1982, Note concerning K-Ar dating of a basalt flow from the Tahoe-Tioga interglaciation, Sawmill Canyon, Sierra Nevada, California: Quaternary Research, in press.

Darrow, A.C., 1972, Origin of the Basalts of the Big Pine Volcanic Field, California: unpublished MS thesis, University of California, Santa Barbara, 61 p.

Dodge, F.C.W., and Moore, J.G., 1981, Late Cenozoic volcanic rocks of the southern Sierra Nevada, California: II, Geochemistry: Geol. Soc. America Bull. 92 part II, 1670-1761.

Easterbrook, D.J., 1978, Paleomagnetism of Pleistocene tills and age of Brunhes-Matuyama boundaries [abs]: Geol. Soc. America Abstracts with Programs 10, 394.

Fleisher, P.J., 1967, Glacial Geology of the Big Pine Drainage, Sierra Nevada, California: PhD thesis, Washington State University; University Microfilms, Inc., Ann Arbor MI., No. 68-695, 126 p.

Frye, J.C., Willman, H.B., and Black, R.F., 1965, Outline of glacial geology of Illinois and Wisconsin: in Wright, H.E. Jr., and Frey, D.G., eds., The Quaternary of the United States - A review for the 7th Cong. Internat. Assoc. for Quaternary Research: Princeton, N.J., Princeton Univ., p 43-62.

Giovannetti, D.M., 1979, Volcanism and sedimentation associated with the formation of southern Owens Valley, California [abs]: Geol. Soc. America Abstracts with Programs, 11, No. 3, 79.

Goldthwaite, R.P., Dreimanis, A., Forsythe, J.L., Karrow, P.F., and White, G.W., 1965, Pleistocene deposits of the Erie lobe: in Wright, H.E. Jr., and Frey, D.G., eds., The Quaternary of the United States - A review for the 7th Cong. Internat. Assoc. for Quaternary Research: Princeton, N.J., Princeton Univ., p 87-98.

Gutenberg, B., Wood, H.O., and Buwalda, J.P., 1932, Experiments testing seismographic methods for determining crustal structure: Seismo. Soc. America Bull. 22, 185-246.

Hay, E.A., 1976, Cenozoic uplifting of the Sierra Nevada in isostatic response to North American and Pacific plate interactions: Geology 4, 763-766.

Hopkins, D.M., 1973, Sea level history in Beringia during the past 250,000 years: Quaternary Research 3, 520-540.

Huber, N.K., 1981, Amount and Timing of Late Cenozoic Uplift and Tilt of the Central Sierra Nevada, California - Evidence from the Upper San Joaquin River: U.S. Geol. Survey Prof. Paper 1197, 28 p.

Janda, R.J., 1966, Pleistocene History and Hydrology of the San Joaquin River, California: Ph.D. thesis, Univ. California, Berkeley; University Microfilms, Inc., No. 67-5086, Ann Arbor MI., 425 p.

Knopf, A., 1918, A Geologic Reconnaissance of the Inyo Range and Eastern Slope of the Southern Sierra Nevada, California, with a Section on the Stratigraphy of the Inyo Range, by Edwin Kirk: U. S. Geol. Survey Prof. Paper 110, 130 p.

Ku, Teh-Lung, and Broecker, W.S., 1966, Atlantic deep-sea stratigraphy: Extension of absolute chronology to 320,000 years: Science 151, 448-450.

Lajoie, K.R., 1968, Quaternary Stratigraphy and Geologic History of Mono Basin, Eastern California: Ph.D. thesis, Univ. California, Berkeley; University Microfilms, Inc., No. 69-14,936, Ann Arbor, MI., 271 p.

Lawson, A.C., 1904, The geomorphogeny of the upper Kern basin: Univ. California Dept. Geology Bull. 3, 291-376.

Lindgren, W., 1911, The Tertiary Gravels of the Sierra Nevada of California, U.S. Geol. Survey Prof. Paper 73, 226 p.

Lubetkin, L.K., 1980, Late Quaternary Activity Along the Lone Pine Fault, Owens Valley Fault Zone, California: unpublished MS thesis, Stanford University, Stanford, Calif., 85 p.

Mankinen, E.A., and Dalrymple, G.B., 1979, Revised geomagnetic polarity time scale for the interval 0-5 my BP: Jour. Geophys. Research 84, 615-626.

Matthes, F.E., 1930, Geologic History of the Yosemite Valley: U.S. Geol. Survey Prof. Paper 160, 137 p.

Matthes, F.E., (Fryxell, F., ed.),1950, Sequoia National Park, Univ. California Press, Berkeley, 136 p.

Matthes, F.E., 1960, Reconnaissance of the Geomorphology and Glacial Geology of the San Joaquin Basin, Sierra Nevada, California: U.S. Geol. Survey Prof. Paper 329, 62 p.

Matthes, F.E., 1965, Glacial Reconnaissance of Sequoia National Park, California: U.S. Geol. Survey Prof. Paper 504-A, p. A1-A58.

Mayo, E.B., 1941, Deformation in the interval Mt. Lyell-Mt. Whitney, California: Geol. Soc. America Bull. 52, 1001-1084.

Moore, J.G., 1963, Geology of the Mount Pinchot Quadrangle, Southern Sierra Nevada, California: U.S. Geol. Survey Bull. 1130, 152 p.

Moore, J.G., 1981, Geologic map of the Mount Whitney Quadrangle, Inyo and Tulare Counties, California: U.S. Geol. Survey Map GQ-1545.

Moore, J.G., and Dodge, F.C.W., 1980, Late Cenozoic volcanic rocks of the southern Sierra Nevada, California: I, Geology and petrology: Geol. Soc. America Bull. 91 part II, 1995-2038.

Pakiser, L.C., Kane, M.F., and Jackson, W.H., 1964, Structural Geology and Volcanism of Owens Valley Region, California - a Geophysical Study: U.S. Geol. Survey Prof. Paper 438, 68 p.

Putnam, W.C., 1949, Quaternary geology of the June Lake district, California: Geol. Soc. America Bull. 60, 1281-1302.

Putnam, W.C., 1950, Moraine and shoreline relationships at Mono Lake, California: Geol. Soc. America Bull. 61, 115-122.

Rahm, D.A., 1964, Glacial geology of the Bishop area, Sierra Nevada, California [abs]: Geol. Soc. America Spec. Paper 76, 221.

Ransome, F.L., 1898, Some lava flows on the western slope of the Sierra Nevada, California: U.S. Geol. Survey Bull. 89, 71 p.

Richardson, L.K., 1975, Geology of the Alabama Hills: unpublished MS thesis, Univ. Nevada, Reno, Nevada.

Richmond, G.M., and others, 1959, Application of stratigraphic classification and nomenclature to the Quaternary: Am. Assoc. Petroleum Geologists Bull. 43, 663-675.

Ross, D.C., 1965, Geology of the Independence Quadrangle, Inyo County, California: U.S. Geol. Survey Bull. 1181-O, 64 p.

Sharp, R.P., 1968, Sherwin Till - Bishop Tuff relationship, Sierra Nevada, California: Geol. Soc. America Bull. 79, 351-364.

Sharp, R.P., 1969, Semiquantitative differentiation of glacial moraines near Convict Lake, Sierra Nevada, California: Jour. Geology 77, 68-91.

Sharp, R.P., 1972, Pleistocene glaciation, Bridgeport Basin, California: Geol. Soc. America Bull. 83, 2233-2260.

Sharp, R.P., and Birman, J.H., 1963, Additions to the classical sequence of Pleistocene glaciations, Sierra Nevada, California: Geol. Soc. America Bull. 74, 1079-1086.

Smith, G.I., 1979, Subsurface Stratigraphy and Geochemistry of Late Quaternary Evaporites, Searles Lake, California: U.S. Geol. Survey Prof. Paper 1043, 130 p.

Smith, G.I., Barczak, V.J., Moulton, G.F., and Liddicoat, J.C., 1980, Core KM-3, a Surface-to-Bedrock Record of Late Cenozoic Sedimentation in Searles Valley, California: U.S. Geol. Survey Prof. Paper (in press).

St. Amand, P., and Roquemore, G.R., 1979, Tertiary and Holocene development of the southern Sierra Nevada and Coso Range, California [abs.]: Tectonophysics 52, 409-410.

Steiger, R.H., and Jäger, E., 1977, Subcommission on Geochronology: convention on the use of decay constants in geo- and cosmochronology: Earth Planet. Sci. Lett. 36, 359-362.

Stuiver, M., and Smith, G.I., 1979, Radiocarbon ages of stratigraphic units: in Smith, G.I., 1979, Subsurface Stratigraphy and Geochemistry of Late Quaternary Evaporites, Searles Lake, California: U.S. Geol. Survey Prof. Paper 1043, p. 68-75.

Webb, R.W., 1946, Geomorphology of the middle Kern River basin, southern Sierra Nevada, California: Geol. Soc. America Bull. 57, 355-382.

Webb, R.W., 1950, Volcanic geology of Toowa Valley, southern Sierra Nevada, California: Geol. Soc. America Bull. 61, 349-357.

Wahrhaftig, C. 1965, Stepped topography of the southern Sierra Nevada: Geol. Soc. America Bull. 76, 1165-1189.

Whitney, J.D., 1880, The auriferous gravels of the Sierra Nevada of California: Harvard College Museum of Comparative Zoology Memoir, v. 6., 567 p.

PART I

TECHNIQUES OF RELATIVE AND ABSOLUTE DATING OF QUATERNARY DEPOSITS AND LAVAS

C.B. Douthitt times the propagation of acoustic waves through a weathered granodiorite boulder on the crest of a Tahoe moraine at Bloody Canyon. Wave speeds are slower through weathered boulders, and can be used as a basis for relative dating.

CHAPTER 2

CONVENTIONAL SEMI-QUANTITATIVE METHODS FOR THE RELATIVE DATING OF MORAINES

Introduction

Relative dating methods are formalized procedures for ascertaining approximate age relationships among different geologic units, or for testing the hypothesis that outcrops of similar deposits are of the same age. They are usually applied to Quaternary alluvium or clastic deposits that are difficult to date by other means. Parameters that change with time are the bases for relative age determinations. Such parameters, generally some characteristic of weathered rocks or soils, may be gathered at three levels: qualitative, "semi-quantitative", or quantitative. Qualitative estimations are useful especially for reconnaissance geology, and in recent times geologists have tended to gather data which, although judgmental in nature, could be treated statistically. This treatment generally has consisted of comparisons among deposits of the relative frequencies with which some chosen characteristic was observed (for example, clasts which were heavily weathered). These "semi-quantitative" methods are widely used because of their simplicity and efficiency. However, because they are based on subjective decisions, they have the potential for poor reproducibilty -- a potential which is realized in some cases (cf. Janda, 1966; Burke and Birkeland, 1979). Quantitative measurements -- for example, acoustic wave speeds through clasts (Crook and Kamb, 1980), the thickness of weathering rinds on clasts (Colman and Pierce, 1981), or certain characteristics of soil profiles (Burke and Birkeland, 1979) -- may provide a more reliable

basis for discrimination, but are also much more time-consuming and still do not independently provide an accurate measure of the true age of deposition. Thus semi-quantitative techniques are the most widely used, but may sometimes need to be supplemented by quantitative methods. In any case, to determine actual ages or age differences it is necessary to calibrate relative dating methods using other, direct dating techniques. The relative dating results may then be used in a limited way to infer ages where direct measurement is not possible.

The deposits of the greatest interest in the southeastern Sierra Nevada are the glacial moraines and associated outwash plains and terraces, in part because these have been faulted and can be used to calculate tectonic rates for the region.

During the Quaternary Period the Sierra Nevada were repeatedly glaciated. These glaciers reached different distances down the deep canyons which cut the eastern escarpment of the mountain range. Glaciers during one or more of the Pleistocene glaciations crossed the range front, terminating on the alluvial fans of the Owens Valley; others were restricted to the high cirques near the crest. Young extensive glaciers tended to obliterate evidence of older but less extensive glaciers, so that today only an incomplete record is preserved. The incompleteness of this record is exacerbated by the steep terrain in the canyons, allowing rapid erosion of lateral moraines or burial by talus. Thus exposure of stratigraphic relationships is rare, and a central issue in the Quaternary geology is the age relationship among various exposures of till, within a single canyon or in different canyons in the Sierra. There are three main considerations: (1) the temporal sequence of the deposits, (2) the relative ages of the deposits, and (3) the absolute ages and age differences of the deposits.

In most cases, the temporal sequence can be understood from the spatial distribution of the moraines, the younger moraines inside or upcanyon from the older. Comparison of tills from different moraines is generally based on morphologic characteristics of the moraine, on soil developement, and on weathering characteristics of the till. The systematic study of these features is the basis for relative dating.

Direct absolute dating of the younger moraines has proven difficult because of the scarcity of incorporated carbonaceous material suitable for ^{14}C dating. In most studies, dating of older moraines has relied heavily on intuition, correlation with the continental glacial sequence, and radiometric dating of rare interbedded lavas. Even where reliable absolute dates are obtained, it is necessary to use relative dating methods to correlate moraines found elsewhere to the dated sequence. Thus relative dating is one of the primary tools of the Quaternary geologist working in the Sierra Nevada. In this chapter, the relative dating methods used in the present study are presented and discussed.

Relative Dating Methods

Development

Soon after it was recognized that the Sierra Nevada owed much of their physiographic appearance to glacial corrasion (cf. Whitney, 1865), multiple glaciations had been identified (Russell, 1889; Turner, 1898, 1900). On the east side of the Sierra, Knopf (1918) distinguished bewteen Tioga and Tahoe moraines based on the obvious differences in the weathered tills. Among the first of the modern geologists, Matthes (working first in Yosemite Valley; Matthes, 1930) demonstrated three glaciations in the western Sierra,

while Blackwelder (1931) identified four different glaciations in the eastern Sierra and established a tentative correlation with the continental record. Matthes paid careful attention to geomorphic features, such as the different groups of heights of hanging canyons above the modern valleys, which pointed to multiple glaciations, and to the different degrees of weathering of glaciated bedrock or erratic boulders. Blackwelder (1931) may have been the dominant influence in the development and systematic application of relative dating methods to moraines of the Sierra Nevada.

Blackwelder based his relative age assessments on four general types of evidence: the extent of soil development; topographic relationships; the degree of erosion of moraines or other geomorphic evidence; and semi-quantitative data. In the present study area as in the regions to the north studied by Blackwelder, soil development does not appear to be a reliable indicator of age. In the southeastern Sierra Nevada this is largely because soil development is slow and because the terrain is so steep that there is significant removal of fine particles from the crests and flanks of moraines. The spatial distribution of moraines, of course, provides the temporal sequence, but no information on relative age differences. Some suggestion of relative age and age differences is provided by the degree of erosion or dissection of moraines, but these and other geomorphic data are difficult to quantify and or difficult to gather in sufficient quantities to treat statistically. Blackwelder regarded each line of evidence as complementary, and augmented the contextual and geomorphic observations with semi-quantitative data.

Blackwelder (1931) introduced the relative frequencies of boulders exposed on moraine crests and the "granite weathering ratio" as two useful semi-quantitative relative dating techniques. The first relied

on the observation that young moraines tend to be more bouldery than old ones. Blackwelder's most innovative contribution and the one he considered most reliable was the second technique, which depended on the progressive weathering of clasts in older deposits. Blackwelder grouped granitic boulders from moraine crests in three classes, according to their degree of visible weathering. Variations among moraines in the relative frequencies of boulders in the three groups was the measure of relative age. The three classes were a) almost unweathered, b) notably weathered but competent, and c) cavernous or rotten. Only boulders of "average granodiorite" were classified. Blackwelder placed about 90% of the boulders on Tioga moraines in the first category. This fraction was reduced to 30% for Tahoe moraines, with 10% in the third class.

Birman (1964) applied the granite weathering ratio (GWR) widely in his studies in the central Sierra Nevada. In doing this he eliminated one category, calling rocks either "fresh" or "weathered". "Weathered" rocks had rough surfaces that shed grains. Birman (1964) found the fraction of weathered boulders to increase from 30% to 49% to 67% from Tioga to Tenaya to Tahoe moraines. Both Blackwelder (1931) and Birman (1964) viewed the GWR method as a correlative tool for different drainages. Sharp (1965), on the other hand, emphasized the effect of lithologic differences on the GWR and restricted its use to moraines on the same side of one valley. Clark (1967) agreed with Sharp, noting the influence of vegetative cover, pre-transport weathering (cf. Richmond, 1962), wind and microtopography on weathering rates. Burke and Birkeland (1979) considered spalling of boulders during fires (Blackwelder, 1927) to cause the GWR of forested moraines to indicate an anomalously young age.

Birman (1964) and Fleisher (1967) found the GWR to be independent of

altitude. McCulloch (1963) and Janda (1966) disagreed, Janda pointing out variations with proximity to the cirque on a single lateral moraine. The variation of GWR with transport distance or altitude-related weathering rates supports Sharp's limited application of relative dating.

Birman (1964) attempted to reduce bias by using two observers, one judging the extent of weathering and the other recording the decisions. Clark (1967) commented that most observers would probably have a rough idea of the count, regardless of who kept tally. Certainly the use of two observers decreases the efficiency, since it doubles the manpower required.

Although the GWR has generally proven useful, Clark (1967) noted that it was ineffective at discriminating among Pleistocene moraines of the West Walker River, in the Sierra north of Bridgeport, California. In keeping with Blackwelder's advice, most observers have used a variety of semi-quantitative techniques to improve the chances of success.

Sharp (1965) used the ratio of areas on moraine crests covered by stones to areas covered by grus as one easily observed indication of age. Grus is generally more common on older moraines, where it is shed by disintegrating clasts. In drainages including both granitic plutons and metamorphic or other rocks more resistant to weathering, Sharp (1965) successfully used the ratio of the easily weathered granitic stones to the "resistates" as a measure of age. Clark (1967) found this ratio to be successful at discriminating moraines of the West Walker River, showing the advantage of the multi-parameter approach. He considered this method to be especially appealing because the classification of rock types is straightforward and objective.

Janda (1966) proposed using the degree of roundness of boulders rather than the degree of weathering per se as one measure of relative age.

Boulder roundness increases with age as grains are shed from the surface; thus this parameter is complementary to the GWR as a measure of weathering.

Fleisher (1967) noted that many boulders on young moraines merely rest on the surface, whereas most boulders on ancient moraines are largely buried. He introduced a parameter which he called "boulder relief", which is a measure of the degree of boulders on the crests of moraines or other deposits. Fleisher defined "boulder relief" as the ratio of the height of the top of the boulder above the ground to the horizontal diameter. This parameter is clearly affected not only by the accumulation of grus at the base of boulders, but also by the degradation of the boulder surfaces exposed to weathering. Thus boulders tend to flatten with time, or the boulder relief parameter decreases with time.

Recently, Burke and Birkeland (1979) have expanded the scope of semi-quantitative measurements in a detailed multi-parameter study of the eastern Sierra Nevada. In addition to some of the parameters introduced above, they measured the relative frequencies of: boulders with oxidized surfaces; boulders with weathering rinds; boulders with solution pits; and boulders split along joints. They also measured maximum and average depths of pits, relief of aplite dikes and diorite inclusions, and solution along joints.

Colman (1981) and Colman and Pierce (1981) have shown the utility of weathering rinds in basaltic and andesitic clasts as an age indicator. Friedman and Smith (1960) and Pierce et al. (1976) used the thickness of hydration rinds on obsidian fragments, sometimes found in tephra blanketing moraines, to the same end. These latter techniques in which measurements rather than judgements are compiled are examples of quantitative relative dating methods. The results are readily treated in a rigorous statistical manner (e.g., Colman and Pierce, 1981). However, as Miller (1980) has

shown, statistical tests may also be applied to semi-quantitative data.

Most of the above techniques work best with late Pleistocene deposits. The discrimination of age differences among Holocene moraines requires different techniques or different class definitions, more sensitive to subtle changes. For example, heavily weathered boulders in neoglacial moraines are rare, certainly less than 1% of the total. Yet because transport distances are small few boulders have glacially abraded surfaces either. Instead most surfaces are hackly, as they were when the rocks were plucked from the cirque cliffs or floors. Thus the criterion of Sharp (1965) for fresh boulders is not met. However, by subdividing the "fresh" class it is possible to record differences in boulder populations as the hackly surfaces begin to flake and spall, and in this way age differences among neoglacial moraines can be detected.

A second major tool for the relative dating of neoglacial moraines is lichenometry (cf. Beschel, 1961; Benedict, 1967). Curry (1968, 1969) has established growth curves for the central Sierra Nevada for two slow-growing yellow-green species, Acarospora chlorophana and Rhizocarpon superficiale. Similar growth curves for a third yellow-green lichen, Rhizocarpon geographicum, have also been compiled (Miller and Andrews, 1975). Lichens appear on boulders on moraines within a few tens or hundreds of years after the retreat of the glacier, and the lichen colonies (thalli) continue to grow for a few thousand years. The largest lichen colonies may be used as a measure of relative age, and through growth curves may be interpreted to give approximate absolute dates. Curry (1968) found that moraines up to 6000 years old could be dated this way.

In the present study, extensive use was made of a limited number of semi-quantitative relative dating methods. These are discussed below.

Semi-quantitative methods used in the present study

Granodiorite Weathering Ratio (GWR)...

The most useful semi-quantitative parameter in the study area was probably the granite (more properly, granodiorite) weathering ratio. As used in this study, three classes of weathered boulders were generally recorded:

1) "fresh"... some glacially abraded or polished patches were found on exposed surfaces (this is the same definition used by Sharp (1965).

2) "lightly weathered"... no abraded surfaces were preserved, but the rock was competent. Classes 1 and 2 together are probably the equivalent of the "fresh" class of Birman (1964).

3) "heavily weathered"... boulders had solution pits, case-hardened or cavernous surfaces, or were otherwise strongly weathered. Aplite dikes or diorite inclusions stood in noticeable relief to the degraded surface (one or more grain diameters). Grains could be removed from the surface by boot or hammer; some boulders were bell-shaped due to degradation where exposed above ground. Grusy boulders were generally included in this category.

On occasion, class 3 was subdivided and grusy boulders were grouped together as a fourth class, or unoxidized and oxidized grusy boulders were grouped as classes 4 and 5, respectively. For neoglacial moraines, class 1 was redefined and subdivided as discussed in the previous section.

As in previous studies, only granodiorite or quartz monzonite boulders exceeding 30 cm in diameter were counted. Counts were restricted to moraine

crests. Counts were made either of all boulders in a predetermined area, or of a predetermined number of boulders in a strip of predetermined width along the moraine crest. When possible, at least 50 boulders were counted. Fleisher (1967) found that counts of 50 boulders gave similar results to counts of 100 boulders; the extra effort was better invested in additional GWR values at different sites.

Janda (1966), Clark (1967), and Burke and Birkeland (1979) all found vegetation to influence weathering rates of boulders. Therefore, the type of vegetative cover was recorded, in three categories: sage, mountain mahogany, and pine. In general, it was possible to limit comparisons to moraines under the same vegetative cover.

Because of the small size of plutons in the study area, lithologic differences among drainages were pronounced. Therefore, the GWR method in particular and semi-quantitative methods in general were used only sparingly to attempt inter-valley correlations of moraines. Necessary correlations were generally attempted by comparing sequences of moraines inferred by relative dating methods. Gross weathering characteristics and contextual and morphologic criteria were used to correlate the first order glaciations in the sequences.

Boulder Frequency Counts (BFC)...

The abundance of boulders suitable for the GWR in a predetermined area was of limited use in the study area, because of the high variability for the parameter at different sites on a single moraine. Why the BFC in this study area had greater variablity than reported in other regions of the Sierra Nevada is open to speculation, but one possibility is that the moraines, largely confined to the steep canyons, were created under more chaotic

conditions than many of those studied farther north. These latter moraines were often east of the range front, away from the steep-walled canyons, and larger.

Boulder Relief (BR)...

As at Big Pine Creek (Fleisher, 1967), boulder burial proved to be a good indicator of relative age. In the present study, three classes were used:

1) "exposed"... the height of the boulder above the soil was more than 75% of the diameter.
2) "partly buried"... the height ranged between 25% and 75% of the diameter.
3) "deeply buried"... the height was less than 25% of the diameter.

Heights and diameters were estimated for boulders that were candidates for the GWR count.

Granodiorite/"Resistate" ratios (G/R and UGR or MGR)...

The ratio G/R of boulders suitable for the GWR count to metavolcanic, aplitic, or other slow-weathering rocks was a good measure of relative age for early Wisconsin and pre-Wisconsin moraines in some canyons of this study. In Onion Valley (Independence Creek) and elsewhere, ultramafic rocks (pyroxenites and dunites) and gabbro boulders were found in moraines. These weathered rapidly, and grusy pyroxenites could be seen in road cuts of late Wisconsin till. The relative frequency of these ultramafic (U) or mafic (M) boulders to granitic and resistant boulders was therefore measured where possible, although the additional category did not prove very useful in improving age discrimination.

Roundness...

The fraction of angular boulders on the surface of a moraine or other

deposit decreases with time, and so the degree of roundness may be used as an indicator of relative age, provided transport distances are similar for all moraines to be compared. This measure was put to limited use in this study. Four categories -- angular, subangular, subrounded, and rounded -- were established. The chief advantage of this method is its simplicity. Even though the categories were completely subjective, it may be easier to judge shape swiftly than degree of weathering, and in any case the use of both parameters probably increases the reliability of relative dating.

Oxidized vs. unoxidized and pitted vs. unpitted boulders...

Discolored boulders are more frequent in older moraines, and the relative frequency can be used as another measure of weathering. Boulders from ancient deposits tend to have stained or discolored surfaces. Boulders that qualified for the GWR count were classified according to their surface color. "Oxidized" boulders had unmistakably tan or reddish surfaces; "unoxidized" boulders were neutral or gray. Obviously, some surficial staining of even fresh rocks can occur, but this was rare and not accounted for during data acquisition.

Solution pits are also abundant in boulders exposed on old moraines. Burke and Birkeland (1979) used the depth of such pits as one measure of weathering. For the present study, the relative frequency of pitted boulders was used instead. The oxidized vs. unoxidized and pitted vs. unpitted counts are probably less subject to errors of classification than the GWR or similar parameters which require more difficult judgements. For this reason, these new parameters are a useful addition to the arsenal of relative dating techniques.

Other approaches to relative dating

In addition to the semi-quantitative relative dating techniques discussed above, various subjective and quantitative observations were also used. The major quantitative approach relied on the reduction of acoustic wave speeds in aged or weathered boulders, and is discussed at length in Ch. 3. The other methods are discussed below.

Lichenometry...

Relative ages among neoglacial moraines were determined in part with the aid of lichenometry. Because neoglaciations were peripheral to the emphasis of this study, no serious effort was made to identify lichens by species, or to calibrate their growth curves against those of Curry (1968) for the central Sierra Nevada. Furthermore, estimates of lichen colony sizes were based on only a few measurements after several minutes of visual inspection, rather than on carefully compiled statistics. Thus as used, this method was only semi-quantitative.

Two measurements were made: (1) the fraction of boulders on moraine crests supporting any kind of lichen was determined, and (2) the largest minor axis of colonies or thalli of yellow-green lichens were estimated as described above. These lichens were assumed to be the same ones used by other researchers mentioned earlier in this chapter. The minor axis was used to avoid anomalously large diameters caused by coalescing colonies. Caution had to be exercised not to count lichens in unusually sheltered or moist locations, or in cracks where their growth was artificially constrained. For this reason, even careful measurements would have to be regarded as deceptively precise. Despite these problems, which in my view preclude the lichenometric data gathered in this study for absolute

dating via Curry's growth curves, in a given cirque lichen sizes probably did reveal relative ages of moraines -- at least, the results were generally consistent with estimates made by other means.

Other indicators...

Other indicators of relative age included morphologic features reflecting erosion, such as the absence of terminal and recessional moraines, the depth of gullies cut into moraines, or the exposure of bedrock knobs through the till. The extent and thickness of forest cover was of use in discriminating latest Pleistocene and Holocene moraines. Soil colors and clay coatings of cobbles from shallow soil pits were of limited use; because of the steep terraine, the transport of fine material from most sites was probably significant. However, estimated clay content from soil pits in protected locations did show a strong tendency to increase with the age of the moraine. Soil colors were probably more useful in studying road cuts, but these opportunities were infrequent. The degree of weathering of subsurface boulders (both B and C horizons) exposed in these road cuts appeared to be a sensitive measure of age.

Bedrock incision and weathering were primarily useful in this study for recognizing the lower limit of the Tioga glaciers. In the steep sections of the canyons where most of the earlier glaciers terminated, the gradient rather than the passage of time probably controlled the incision. Near the fan heads, the gradient was reduced, but aggrading fans, lava flows, and outwash terraces generally mantled bedrock.

Again because of the steep terrain, lakes were not numerous except in cirque regions. However, the few ancient lakes found behind Tioga moraines had been filled by sediment. In contrast, most lakes in terrain last

covered by Hilgard glaciers were not filled. Exceptions tended to be lakes at confluences of two or more streams, which received an unusually high load of sediment.

Testing of Relative Dating Techniques in Other Areas

Relative dating methods used in this study were calibrated by application in other, previously studied canyons of the eastern Sierra Nevada. The only drainage near the study area which had been studied at length was Big Pine Canyon (Bateman, 1965; Fleisher, 1967). The GWR and BFC counts were checked here, and were sufficient to resolve differences between Sherwin and Tahoe moraines, and between Tahoe and Tenaya moraines. Differences between Tenaya and Tioga moraines were not pronounced, but may have been obscured because of proximity to the Tioga terminal moraine. Birman (1964) suspected that relative dating methods yielded anomalously high ages when applied to terminal moraines. The BFC method, which did not prove useful in the study area, was easily capable of separating Tenaya and Tahoe moraines at Big Pine Creek.

All semi-quantitative methods were tested along with the acoustic wave speed method at Bloody Canyon and at Green Creek, in the central Sierra Nevada. These results are reported in Ch. 3.

Lumpers and Splitters

Burke and Birkeland (1979) note that by disposition Quaternary geologists appear to be divided into those who classify marginally different moraines together ("lumpers") and those who place each moraine or group of moraines in a distinct named glaciation ("splitters"). They

draw this distinction because some observers (e.g., Sharp and Birman, 1963) recognize four glaciations (Tioga, Tenaya, Tahoe, and Mono Basin) where Burke and Birkeland see only two (Tioga and Tahoe). Burke and Birkeland correctly point out that splitting can result in different moraine sequences in every valley -- sequences that cannot be satisfactorily correlated. The argument against lumpers must be that from other data (cf. Smith, 1979) the glacial record seems to be even more complex than presently recognized from the incomplete sequences of moraines studied in the Sierras. Hence regardless of whether we classify well or poorly, lumping certainly gives us an over-simplified view. Furthermore, lumping does not eliminate classification errors, merely increases the magnitude of their effect. Individual moraines must be assigned to fewer glaciations, but glaciations more widely separated in time. Thus the problem of poor correlation is not truly reduced by lumping.

In the present study, an effort has been made to assign moraines to separate glaciations or to stades of a glaciation based on the statistical separability of the data, as discussed in Ch. 3. However, for clarity and consistency with the literature, the Tenaya moraines, not clearly separable from older Tioga moraines, were assigned to a separate glaciation, when in fact it seemed possible that the Tenaya could best be regarded as a very early stade of the Tioga glaciation. This was done since the stade was widely recognized, and was distinct by the methods of this study at Bloody Canyon and at Green Creek.

Ultimately, the problem of assignments will fade into insignificance if direct dating techniques for moraines are ever devised. The actual record of glacial advances and retreats is probably only poorly described by a simple classification system of glaciations and stades, and in any

event it should be emphasized that relative dating of incomplete sequences of moraines is probably not the way to resolve this controversy.

Summary

Relative dating methods have been applied to moraines in areas scattered throughout the Sierra Nevada by numerous geologists over a span of many decades. These studies have enjoyed various degrees of success. This pattern was repeated in the present study, but in general the CWR was capable of resolving at least first-order glaciations, and the GWR of subsurface boulders exposed in road cuts was even more sensitive. However, because of the recognized problems with conventional methods of relative dating, a new technique was developed and applied as required. This technique, based on the speed of acoustic waves through individual clasts, is described in Ch. 3. In combination, semi-quantitative and other relative dating methods were probably adequate to recognize major Holocene and Pleistocene glaciations, but were probably not consistently able to discriminate stades.

References Cited

Bateman, P.C., 1965, Geology and Tungsten Mineralization of the Bishop District, California: U.S. Geol. Survey Prof. Paper 470, 208 p.

Benedict, J.B., 1967, Recent glacial history of an alpine area in the Colorado Front Range, U.S.A., Part I. Establishing a lichen growth curve: Jour. Glaciology 6, 817-832.

Beschel, R.E., 1961, Dating rock surfaces by lichen growth and its application to glaciology and physiology (lichenometry): p. 1044-1062 in Raasch, G.O., ed., Geology of the Arctic, v II (Proc. First Internat. Symposium on Arctic Geol.), Univ. Toronto Press, 461 p.

Birman, J.H., 1964, Glacial geology across the crest of the Sierra Nevada, California: Geol. Soc. America Spec. Paper 75, 80 p.

Blackwelder, E., 1927, Fire as an agent in rock weathering: Jour. Geology 35, 134-140.

Blackwelder, E., 1931, Pleistocene glaciation in the Sierra Nevada and Basin ranges: Geol. Soc. America Bull. 42, 865-922.

Burke, R.M., and Birkeland, P.W., 1979, Reevaluation of multiparameter relative dating techniques and their application to the glacial sequence along the eastern escarpment of the Sierra Nevada, California: Quaternary Research 11, 21-51.

Clark, M.M., 1967: Pleistocene Glaciation of the Drainage of the West Walker River, Sierra Nevada, California: PhD thesis, Stanford University; University Microfilms, Inc., No. 68-6401, Ann Arbor, MI., 170 p.

Colman, S.M., 1981, Rock weathering as a function of time: Quaternary Research 15, 250-264.

Colman, S.M., and Pierce, K.L., 1981, Weathering Rinds on Andesitic and Basaltic Stones as a Quaternary Age Indicator, Western United States: U.S. Geol. Survey Prof. Paper 1210, 56 p.

Crook, R. Jr., and Kamb, B., 1980, A new method of alluvial age dating based on progressive weathering, with application to the time-history of fault activity in Southern California: Final Report, U.S. Geol. Survey Contract No. 14-08-0001-17760, 41 p.

Curry, R.R., 1968, Quaternary Climatic and Glacial History of the Sierra Nevada, California: PhD thesis, Univ. California, Berkeley; University Microfilms, Inc., No. 68-13,896, 204 p.

Curry, R.R., 1969, Holocene climatic and glacial history of the central Sierra Nevada: in Schumm, S.A., and Bradley, W.C., eds., United States Contributions to Quaternary Research: Geol. Soc. America Spec. Paper 123, 1-49.

Fleisher, P.J., 1967, Glacial Geology of the Big Pine Drainage, Sierra Nevada, California: PhD thesis, Washington State University; University Microfilms, Inc., Ann Arbor MI., No. 68-695, 126 p.

Friedman, I. and Smith, R.L., 1960, A new dating method using obsidian - Part I, the development of the method: American Antiquity 25, 476-522.

Janda, R.J., 1966, Pleistocene History and Hydrology of the Upper San Joaquin River, California: PhD thesis, University of California, Berkeley; University Microfilms, Inc., Ann Arbor, MI., No. 67-5086, 425 p.

Knopf, A., 1918, A Geologic Reconnaissance of the Inyo Range and Eastern Slope of the Southern Sierra Nevada, California, with a Section on the Stratigraphy of the Inyo Range, by Edwin Kirk: U. S. Geol. Survey Prof. Paper 110, 130 p.

Matthes, F.E., 1930, Geologic History of the Yosemite Valley: U.S. Geol. Survey Prof. Paper 160, 137 p.

McCulloch, D.S., 1963, Late Cenozoic Erosional History of Huerfano Park, Colorado: PhD thesis, Univ. of Michigan; University Microfilms, Inc., No. 63-6922, Ann Arbor, MI., 158 p.

Miller, C.D., 1980, A statistical method for relative-age dating of moraines in the Sawatch Range, Colorado: Geol. Soc. America Bull. 90, Part I, 1153-1164.

Miller, G.H., and Andrews, J.T., 1972, Quaternary history of Northern Cumberland Peninsula, East Baffin Island, N.W.T., Canada, Part IV: Preliminary lichen growth curve for Rhizocarpon geographicum: Geol. Soc. America Bull. 83, 1133-1138.

Pierce, K.L., Obradovich, J.D., and Friedman, I., 1976, Obsidian hydration dating and correlation of Bull Lake and Pinedale Glaciations near West Yellowstone, Montana: Geol. Soc. America Bull. 87, 703-710.

Richmond, G.M., 1962, Quaternary stratigraphy of the LaSalle Mountains, Utah: U.S. Geol. Survey Prof. Paper 324, 135 p.

Russell, I.C., 1889, The Quaternary history of Mono Valley, California: U.S. Geol. Survey Ann. Report 8, 261-394.

Sharp, R.P., 1965, Sonora Pass Junction to Bloody Canyon: in Wahrhaftig, C.A., and Sharp, R.P. (eds.), Guidebook for Field Conference I, Northern Great Basin and California: INQUA (Internat. Assoc. Quaternary Research), 7th Cong., 1965, p. 74-84.

Sharp, R.P., and Birman, J.H., 1963, Additions to the classical sequence of Pleistocene glaciations, Sierra Nevada, California: Geol. Soc. America Bull. 74, 1079-1086.

Smith, G.I., 1979, Subsurface Stratigraphy and Geochemistry of Late Quaternary Evaporites, Searles Lake, California: U.S. Geol. Survey Prof. Paper 1043, 130 p.

Turner, H.W., 1898, Origin of Yosemite Valley [abs]: Science, new series, v. 7, 358-359.

Turner, H.W., 1900, The Pleistocene geology of the south central Sierra Nevada with especial reference to the origin of Yosemite Valley: California Academy of Science, Proc., 3d ser., Geology 1, 262-321.

Whitney, J.D., 1865, Geological Survey of California, Report of progress and synopsis of the field work from 1860 to 1864: California Geol. Survey, Geology 1, 498 p.

CHAPTER 3

RELATIVE DATING OF MORAINES USING ACOUSTIC WAVE SPEEDS IN BOULDERS

3.0 INTRODUCTION

In the five decades since Blackwelder (1931) enumerated relative weathering criteria which could be used to identify tills of different ages, various researchers have applied these relative dating methods to numerous moraine sequences throughout the Sierra Nevada. During this time concepts used in relative dating have evolved considerably along the lines discussed in Chapter 2, the most notable improvement being the introduction of the "semi-quantitative" approach of Sharp and Birman (1963) and Birman (1964). Despite these and other refinements of technique and repeated studies of moraines in the same Sierra valleys by different workers, there remains disagreement over age assignments of important glacial deposits (e.g., Sharp and Birman, 1963; Sharp, 1972; Curry, 1968, 1971; Dalrymple, 1964; and Burke and Birkeland, 1979).

There seem to be two problems with conventional approaches to relative dating: either (1) they are somewhat subjective ("semi-quantitative") and result in nominal data, which are not a satisfactory base for statistical comparisons; or (2) they are excessively time consuming, so that extensive data cannot be gathered. The hazard of the first approach, typified by the collection of granodiorite weathering ratios, is that the results are not always repeatable, and that the degree of error is hard to assess. The hazard of the second approach, typified by the detailed chemical and other analyses of soils from pits about 1 m deep dug into moraine crests by Burke and Birkeland (1979), is that the few study sites must be presciently

chosen to sample completely all glacial deposits present. This can be critical because, as pointed out by R.P. Sharp (oral comm., 1978), even moraines of simple morphology may be composite, formed by superposed till deposited during two or more distinct glacial advances. If too few sites are studied, or if the sites are distributed poorly, this complexity may not be detected.

In an effort to solve these problems, I have applied a new relative dating method which is objective and quantitative and which yields reproducible results, but which is not so time-consuming as to preclude extensive coverage of a study area in a reasonable amount of time. This method was first developed by Crook and Kamb (1980). It consists of measuring the speed of acoustic waves through the surface layers of different granitic boulders in a deposit. This speed is reduced as the boulders weather, from about 4 km/s for fresh clasts to about 0.3 km/s for disintegrating ones. Relative age estimates are based on mean speeds for groups of boulders to reduce the chance of error. As long as the extent of weathering is a monotonic function of time, the speed of acoustic waves appears to be a valid basis for age comparisons.

Glacial moraines in the Sierra Nevada typically contain numerous granitic boulders suitable for the measurement of acoustic wave speeds. Thus relative dating by this new method appears feasible.

Crook and Kamb (1980) applied this method to terrace deposits of Pleistocene and Holocene age from the San Gabriel Mountains, Los Angeles County, California. They restricted measurements to clasts from a single pluton, the Mt. Lowe granodiorite, a widespread and easily recognized rock. In this way they hoped to minimize variability in weathering rates of boulders in the sampled populations. Throughout much of the Sierra

Nevada, this is not possible. Many plutons are contained entirely within one or two drainages, and relative age comparisons among glacial deposits in adjacent valleys must often be based on rocks from different plutons. Also, rocks from different plutons may be similar in appearance. Especially when weathered, these may not be readily distinguished in the field. Thus the problem faced in the Sierra Nevada was potentially more complex than that of Crook and Kamb (1980). If comparisons among moraines of several valleys were to be made, measurements could be restricted only to granodiorites and quartz monzonites (for example), and not to rocks from a single pluton. For this reason, additional variability among measured clasts deposited contemporaneously should be expected in the Sierra Nevada moraines.

This increased variability requires larger differences in mean speeds before distinction can be made between sites. It therefore reduces the sensitivity of the method. On the other hand, at least in theory, boulders of the same rock type in a single glacial deposit should all have about the same apparent age. Most boulders are plucked from fresh bedrock and even weathered boulders are abraded by the glacier at about the same time, *before* deposition. In terrace deposits, rocks are generally weathered to various degrees before washing into streams, and abraded less thoroughly before deposition. Thus boulders in river terraces might be expected to show greater variability in acoustic wave speeds than the same boulders in glacial moraines. Which of the contrary tendencies controls the standard deviation of the wave-speed distribution may vary from valley to valley.

To test the use of acoustic wave speeds as a way to relatively date moraines, R. Crook and I applied the method to glacial tills in two valleys which had previously been studied by Sharp (1972), Sharp and Birman (1963),

and Burke and Birkeland (1979). These valleys, Bloody Canyon and Green Creek (Fig. 3-1), cut the eastern escarpment of the Sierra Nevada north of my study area in Inyo County. This work was intended not only to test the new relative dating method, but to help resolve the disagreement over age assignments of glacial deposits in these valleys.

In the discussion which follows, five topics are addressed: 1) the measurement of acoustic wave speeds; (2) simple models to describe the loss of speed as weathering progresses; (3) characteristics of the data; (4) treatment of the data; and (5) application of the method to the moraines of Bloody Canyon and Green Creek.

3.1 MEASUREMENT OF ACOUSTIC WAVE SPEEDS

There are three distinct aspects to collecting data for relative dating by acoustic wave speeds. First, the boulders to be measured must be representative of the population that they are intended to represent. Second, the wave speed must be determined for each boulder in the sample. Third, obvious errors must be edited from the recorded data before the data can be subjected to appropriate statistical tests and analyzed.

Sampling Strategy

In this study, sampling consisted of measuring wave speeds (V_p) in each acceptable boulder encountered on a portion of a moraine crest until a predetermined number of boulders had been measured. Typically, 25 or 30 boulders were measured at each site, which was typically an area 3 m wide by 10 m long. Only granodiorite or quartz monzonite boulders that could be

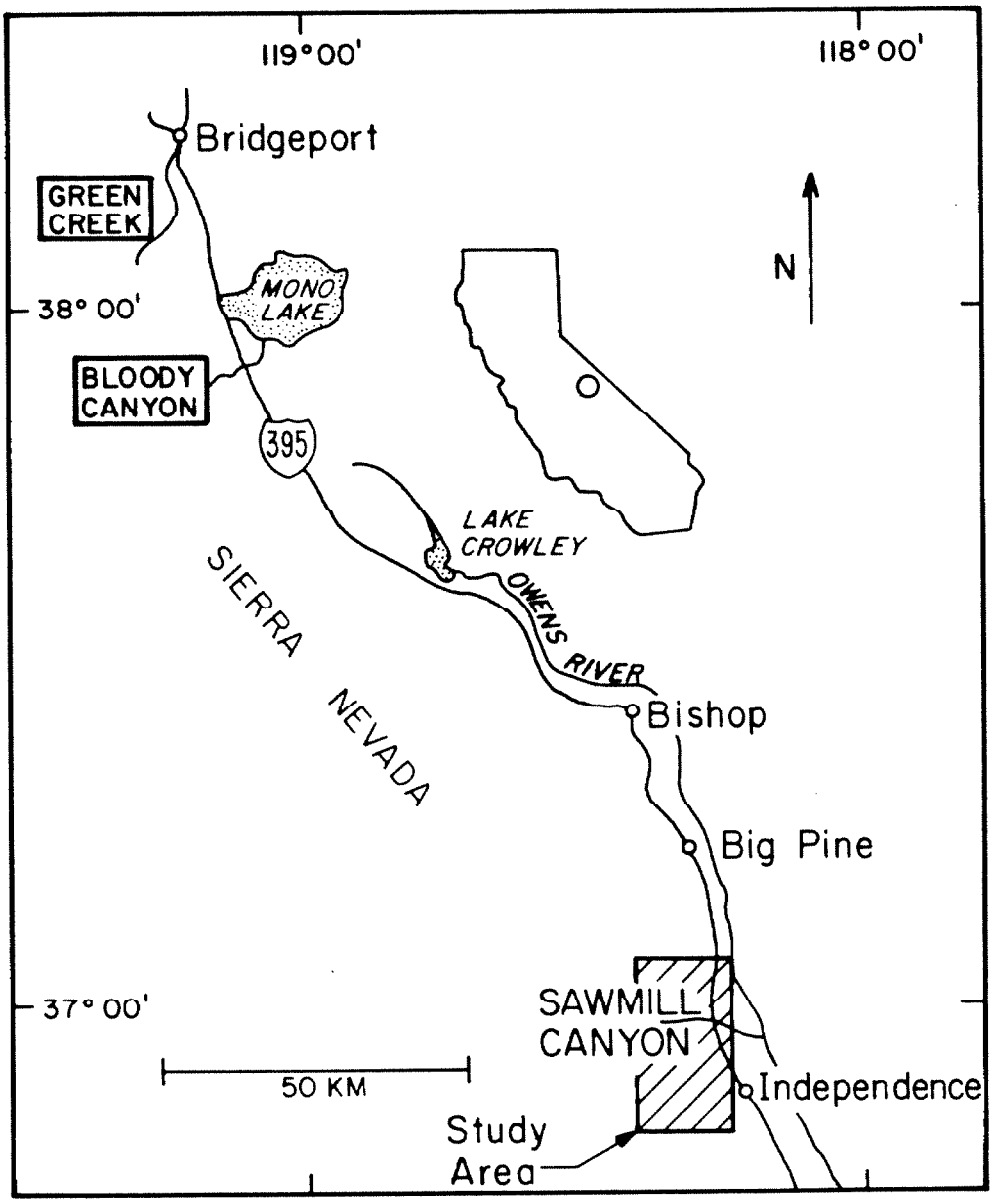

Fig. 3-1. Map showing locations of moraines at Bloody Canyon and Green Creek used to test the acoustic wave speed relative dating technique. Location of the principal study area for which the technique was intended is shown for reference.

used for granodiorite weathering ratio counts (cf. Chapter 2) were measured. The minimum diameter was 25 cm; the diameter parallel to the wave path exceeded 30 cm. Measurements were made on what appeared to be the original surface of the boulder, not on recent surfaces created by splitting of the boulder along joint planes. Regions of the boulder with gross defects such as cracks or exfoliation shells were avoided.

Thill et al. (1969) showed that the elastic properties of the Salisbury granite were anisotropic, and that compressional wave speeds varied with direction by about 13%. Crook and Kamb (1980) calculated that for the Mt. Lowe granodiorite clast anisotropy contributed only 35% of the total variance of speeds for each of three groups of clasts. Thus speeds determined for 2n clasts would define the population of speeds better than speeds for two different measurements on each of n clasts. In this study, granitic rocks had no strongly directional fabrics, and wave speeds were measured in one direction only.

Sites were distributed along moraine crests in a pattern designed to test homogeneity of the wave-speed distributions for the sampled groups of boulders. Thus sites were not selected randomly, but were located either at roughly equal intervals along the crest or where overlap of the moraine by younger tills seemed likely. Sites were established only on moraine crests to minimize the variations in the weathering history and conditions of the boulders. The moraines studied at Bloody Canyon and at Green Creek were all well away from the mountains and from sources of talus, which might have a different weathering age than the till. Sites on end moraines were avoided except in special instances, because earlier researchers (Janda, 1966; McCulloch, 1963; Sharp, 1969, 1972) have maintained that relative weathering data are more variable there than on lateral moraines.

Measurement Technique

Ideally, the speed of acoustic waves in individual boulders is calculated from the travel times of compressional (P) waves arriving at a fixed detector from a source placed at different points on a line on the surface of the boulder. The detector is a transducer attached to the boulder by a putty compound. Waves are transmitted from the rock to the transducer via a metal stylus, and the wave is introduced into the rock by a hammer blow to a steel ball held against the rock. When the hammer hits the ball an electric circuit is closed which starts a high-speed clock, called a Microseismic Timer (DynaMetric, Inc.). Detection of the wave at the sensing transducer stops the clock, and the elapsed time in microseconds is displayed. The lowest repeatable value in a consecutive series of travel times with the same instrument configuration is chosen as the first arrival of the P wave.

Crook and Kamb (1980) generally measured travel times for four to six impact locations and found the speed from the slopes of the regression line fit to the travel time profile. In this study, only three travel times were measured per boulder. This enabled the determination of more wave speeds. The source was placed 50 mm (d_1), 150 mm (d_2), and 250 mm (d_3) from the detector. The wave speed (km/s) was taken to be

$$Vp = \frac{1}{2}\left(\frac{d_2 - d_1}{t_2 - t_1} + \frac{d_3 - d_1}{t_3 - t_1}\right) \qquad (1)$$

where t_1, t_2, and t_3 are the respective travel times in μs. The use of travel-time differences to calculate the speeds was required because each measured travel time included an unknown delay time (usually of about 20 μs), resulting chiefly from the detection mechanism in the

Microseismic Timer that recognizes the P wave. The use of only three points reduced measurement time to about three minutes per boulder, but still provided two speed determinations. Large inconsistencies in these two speeds generally revealed operator error in reading the elapsed times or the presence of gross physical defects in the wave path.

Reproducibility

Crook and Kamb (1980) found that under laboratory conditions speeds for individual boulders of Mt. Lowe granodiorite were reproducible with a standard deviation of less than 0.05 km/s. A standard deviation of 0.07 km/s was achieved for a quartz monzonite boulder from Onion Valley, south of Sawmill Canyon in the Sierra Nevada (Fig. 3-1). Some error is to be expected from the uncertainty in the impact location, which is determined by the size of the steel ball in contact with the rock. Scars left by this ball after repeated blows with the hammer are about 2 mm in radius, and were a measure of the uncertainty of the point at which the waves were introduced into the rock. Additionally, the location of the impact target was only measured to within 1 mm. For the impact point geometry used in this study, the measurement uncertainty from these sources together was about 1.5%. The average repeatability of about ± 0.05 km/s was determined for boulders with wave speeds of about 2 km/s. Thus the actual uncertainty was about 2.5%, slightly larger than the uncertainty from geometric factors. For this study, 0.05 km/s was taken to represent the precision of the technique and was assumed to apply to all speeds.

Crook and Kamb (1980) found that the mean speed for a group of 19 boulders was reproducible within 1%, which is compatible with the measurement

precision. Six impact points were used to determine each wave speed. They concluded that the reduced precision resulting from using fewer impact points would be small compared to the variation in speeds among boulders. By measuring fewer travel times per boulders, more boulders could be included in the sample at each site, and thus the population could be better represented.

Characteristics of the Measured Signal and Data Editing

When the hammer is struck against the boulder, a complicated train of waves is generated. Typical waves sensed by the transducer were recorded on an oscilloscope by Crook and Kamb (1980) and are duplicated in Fig. 3-2a. Two types of waves are readily distinguished: first to arrive are low-amplitude waves which are replaced after about 0.4 ms by waves with amplitudes an order of magnitude larger. Figure 3-2b is a histogram of the peak-to-peak time difference for wavelets in Fig. 3-2a; it shows there are two characteristic frequencies centered at 11 khz and at 3.3 khz. The lower-amplitude waves have the higher frequency. These are probably P waves. The 3.3-khz waves are probably S and surface waves (although the transducer is directionally sensitive, and hence should suppress response to transverse waves).

The Microseismic Timer accepts as the time of first arrival the moment when the amplitude of the wave first becomes less than a specified negative level (Crook, oral comm., 1981). For a simple sinusoid, the times thus indicated are probably good approximations to the actual travel times. On the other hand, if two or more sinusoids make up the signal, this need not be the case. Such a situation is illustrated in

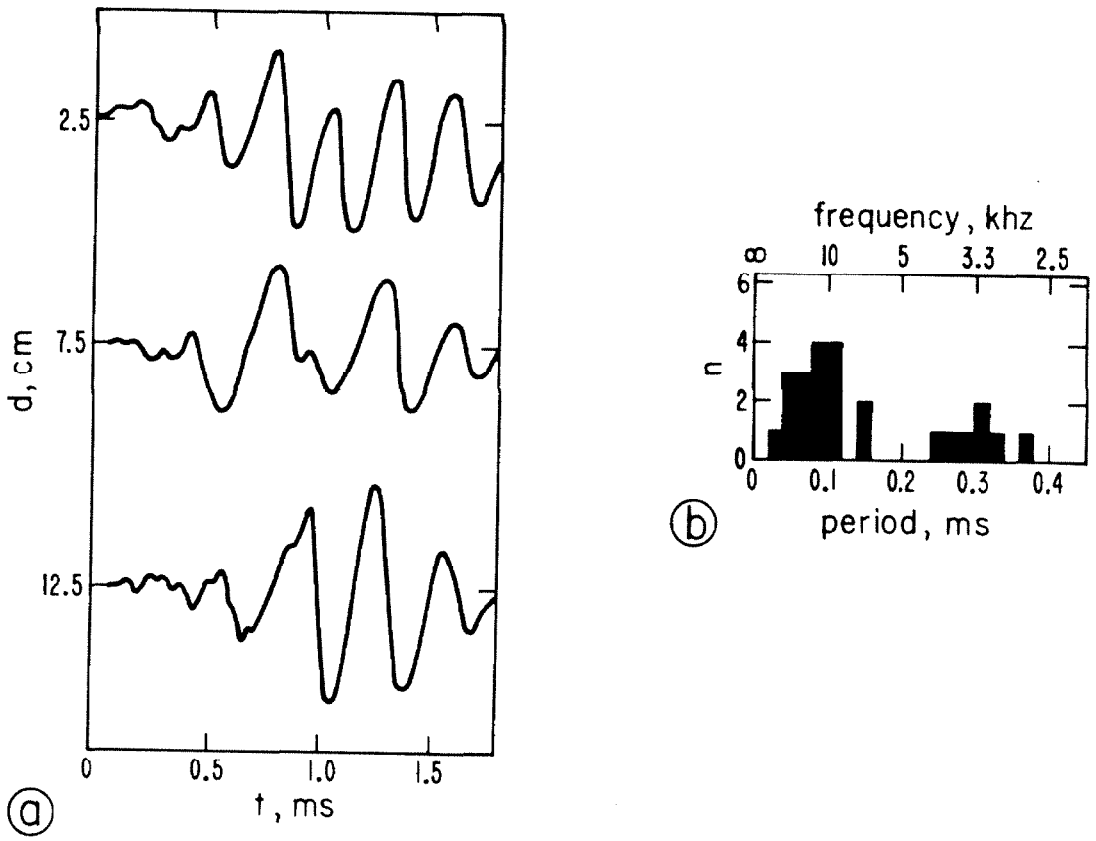

Fig. 3-2. Typical waves detected by the sensing transducer of the Microseismic Timer.

a) Oscilloscope tracing of waves from three impact points at three different distances d. Abscissa shows time. (After Crook and Kamb, 1980).

b) Spectrum of waves shown in (a). Ordinate shows n, the number of wave crest pairs found at each frequency. Spectrum shows clearly the bimodality of the waves sensed by the detector. The P waves form the mode centered near 11 khz; the large amplitude S or surface waves form the mode near 3.3 khz.

Fig. 3-3. The wave train is taken to consist of two sinusoids with frequencies of 11 khz and 3.3 khz respectively. If the 11-khz wave is a P wave and the 3.3-khz wave is an S wave, then the ratio of their speeds is $1/\sqrt{3}$ if Poisson's ratio is 0.25 (cf. Bullen, 1965). In Fig. 3-3 the speed of the P wave is assumed to be 2.0 km/s, and the speed of the 3.3-khz wave is taken to be 1.15 km/s. The amplitude of the 3.3-khz wave is only that of the component to which the transducer is sensitive. If the wave is an S wave, that component is probably a small fraction of the actual amplitude. Because of the very small distances between the impact point and the transducer, there is little dispersion and the waves interfere. Figure 3-3 shows that the arrival time measured by the Microseismic Timer may be controlled by the phase of the 3.3-khz wave. If the first oscillations of both components are positive (as shown), then the measured arrivals (shown by ▣) of the composite wave (heavy solid lines) are delayed by 0.09 ms or more compared to the arrival times (shown by ●) of the simple 11-khz wave. If the first oscillations of the two constituent waves are opposite, then the measured arrivals (shown by o) of the composite wave (heavy dashed line) are advanced. The waves just described would thus give different apparent speeds of 0.6 km/s, 2.0 km/s, and and 1.7 km/s, respectively.

Inspection of the actual wave trains in Fig. 3-2a shows that the early-arriving 11-khz waves do appear to be modulated by a wave of lower frequency. This is best seen in the wave train recorded at a distance 12.5 cm from the impact point. The frequency of the carrier wave seems to be about 3 khz, and it is probably the same wave which dominates the end of the record. The reason wave interference does not significantly affect this relative dating technique is that, unlike the model in Fig. 3-3, the amplitude of

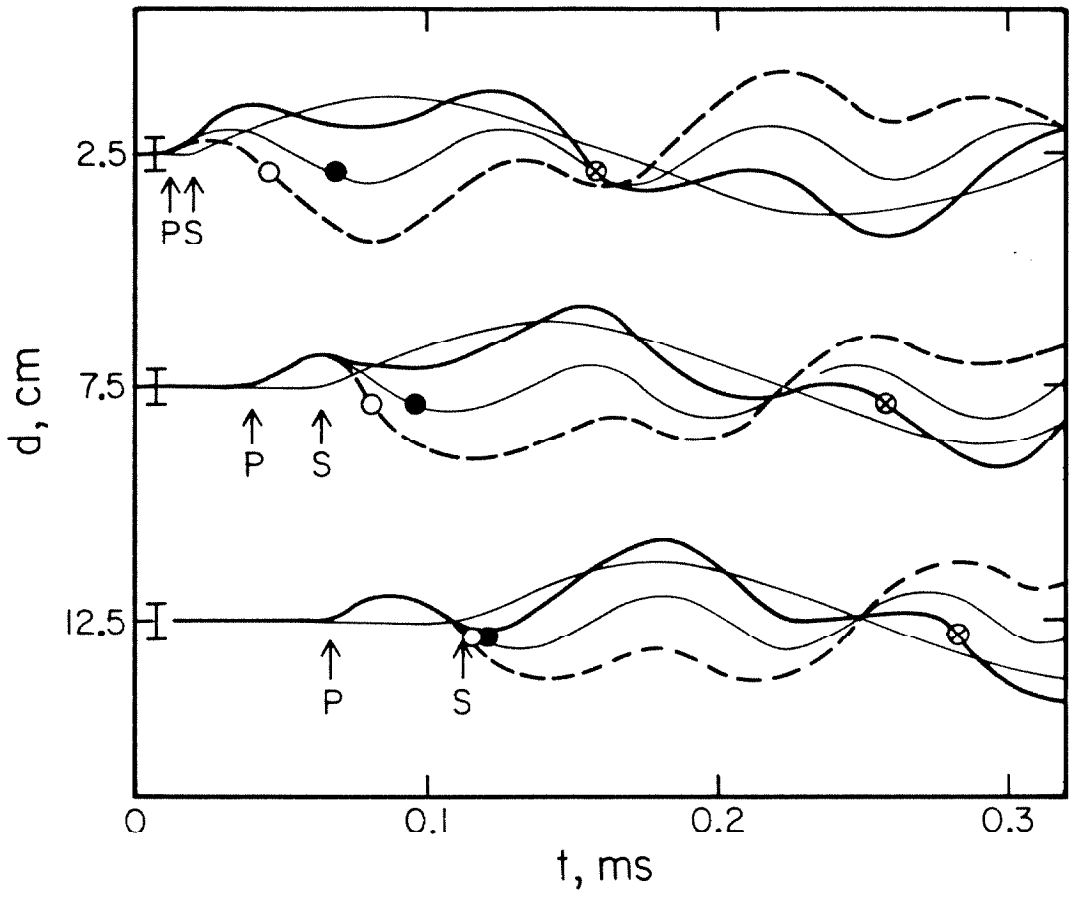

Fig. 3-3. Interference of P and S or surface waves may affect the apparent arrival time measured by the Microseismic Timer. Synthetic wave trains are shown for three different source distances d. Time t is shown on the abscissa. P and S waves are represented by simple sinusoids (light lines). The sum of the two amplitudes is shown by the heavy solid line; the difference is shown by the heavy dashed line. The threshold amplitude of the Microseismic Timer is shown by the vertical bars on the wave trains near the ordinate. Apparent arrival times are marked by filled circles (P waves) and by open circles or circles with crosses (composite waves). Actual first arrivals are shown by arrows. Filled circles define a travel-time line giving the correct P-wave speed; apparent travel times for composite waves give anomalously low speeds.

the low-frequency wave appears to build slowly with time, so that its effect during the first cycle of the P wave is probably negligible. It also seems likely that the amplitude of the low-frequency wave varies with each hammer blow; thus the grossly defective travel times (e.g., those marked by ⊠) can be edited in the field by picking the lowest repeated travel times.

A second difficulty in picking meaningful travel time arises because of attenuation of the P waves with distance travelled. As Fig. 3-4 shows, the first wave may not exceed the chosen amplitude threshold and the clock may not be stopped until a larger wave arrives. This will generally be the second oscillation. If the first wave stops the clock when the impact point is close to the transducer but not when it is far away, an artifactual travel-time curve will result. In Fig. 3-4, the incoming wave is an amplitude-modulated 10-khz P wave travelling at 2 km/s. At an impact distance of 5 cm, the first wave trough (a_1) exceeds the amplitude threshold (shaded) and stops the clock at 0.085 ms. At impact distances of 10 cm and 15 cm, the wave is attenuated and the first troughs (a_2 and a_3, respectively) do not exceed the threshold; instead the larger second troughs (b_2 and b_3) stop the clock, resulting in an artifactual travel time vs. distance curve (heavy line).

The number of artifactual travel times measured in the field can be minimized by reducing the threshold so that the first troughs a_2 and a_3 do stop the clock (dashed travel-time curve in Fig. 3-4). If this is not done, the affected data must be edited. If six points are determined for each travel-time curve this is relatively easy. An affected curve would consist of two parallel segments offset by about 0.1 ms. If only three points are determined (as in this study), diagnosis can not be so

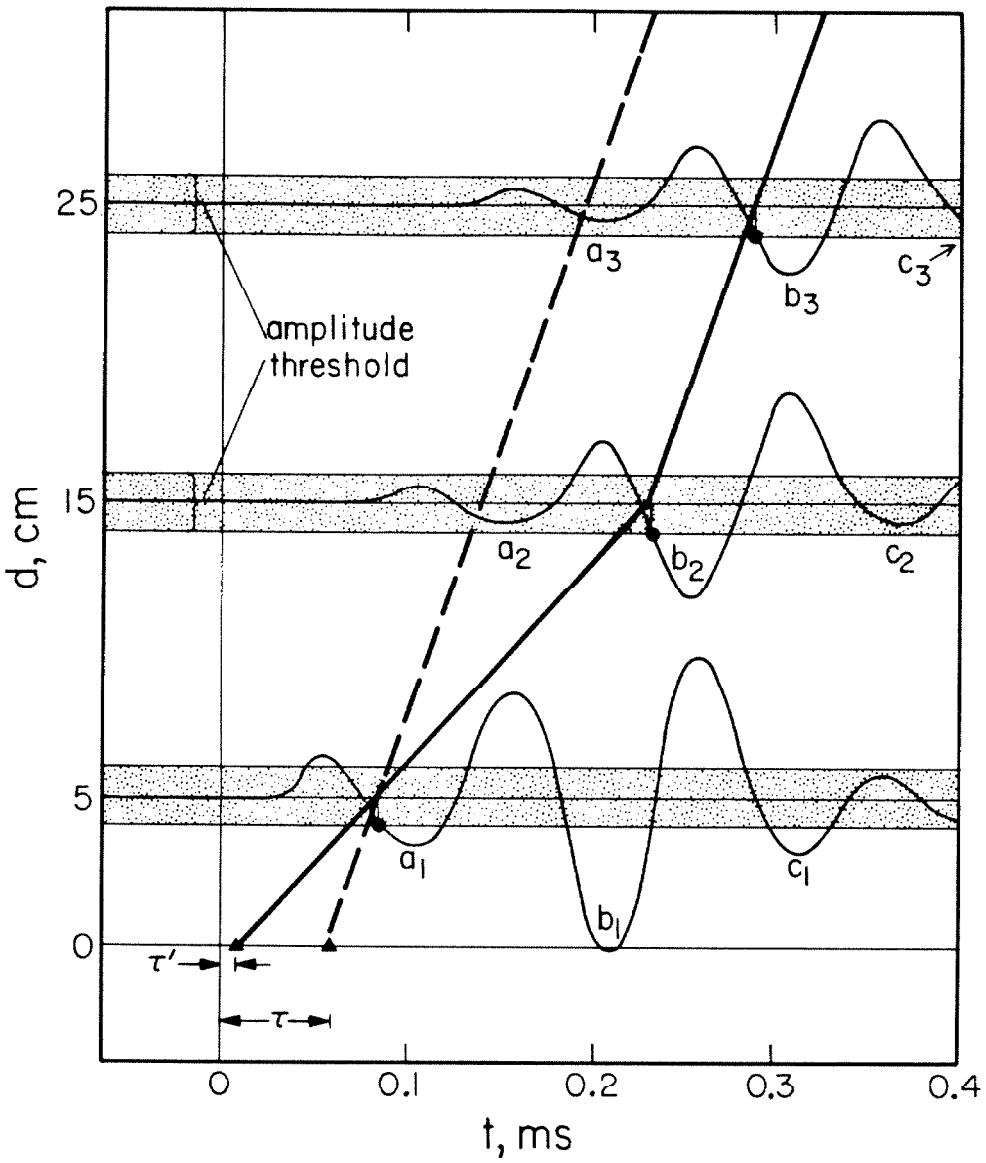

Fig. 3-4. Schematic representation of 11-khz amplitude-modulated P waves from impact points at distances d = 5 cm, 15 cm, and 25 cm from the Microseismic Timer detector. The abscissa is time, t. The shaded zone for each wave train is an amplitude threshold. When the negative amplitude of the wave first exceeds this limit, the Microseismic Timer senses the arrival of the wave. In the illustration, the waves from impact points 15 cm and 25 cm from the detector have been attenuated so that the first trough (a_1, a_2, a_3) is not sensed. Filled circles show the arrival times times measured by the Microseismic Timer for each wave. The Microseismic Timer detects the first trough (a_1) for d = 5 cm, but the second troughs (b_2 and b_3) at d = 15 cm and 25 cm. The solid line is the apparent travel-time curve and yields an artifactual apparent speed because the true first arrivals are not detected. In most cases, such V_p will be too small.

Erroneous travel-time curves may be detected because their abscissa intercepts (τ') may be less than perhaps 0.025 ms. In the example shown, the true first arrivals would be detected if the instrument gain was increased (or the threshold lowered). The travel-time curve in this case is shown by the dashed line: it intersects the abscissa at $\tau \approx 0.06$ ms and its slope gives a correct wave speed of about 2.2 km/s.

certain. The unaffected travel-time curve will generally intersect the abscissa at 0.03 ms to 0.07 ms. This intersection describes a delay time, τ, which mainly reflects the time required after the "true" first arrival of the wave for its amplitude to exceed the threshold value.

If trough a_1 stops the clock when the impact distance is 5 cm, b_2 when it is 15 cm, and c_3 when it is 25 cm, then the apparent delay time τ' (Fig. 3-4) will be much smaller than the actual delay time τ. It may even be negative. A travel time curve giving a small or negative τ' is clearly artifactual and must be edited. The travel time curve of Fig. 3-4 is not so readily identified as artifactual, because the apparent delay time found from all three travel times is not as small as τ'. If not edited, artifactual speeds caused by wave attenuation would reduce the mean speed for the sample and would increase the standard deviation.

It should be recalled that the wave train may lose its pure spectral character rapidly as the low-frequency component increases in amplitude. Thus actual travel-time curves could be more difficult to interpret than the ones discussed above.

Despite myriad potential difficulties in using the Microseismic Timer to determine wave speed, two facts stand out: (1) Crook and Kamb (1980) observed that average wave speeds determined by inspection of oscilloscope records agreed with those found using the Microseismic Timer; and (2) they found that measured wave speeds, real or apparent, did form a repeatable basis for successfully discriminating terrace deposits of different Quaternary ages.

3.2 SIMPLE MODELS OF WEATHERING OF BOULDERS AND THE DECREASE OF ACOUSTIC WAVE SPEEDS

Simple models can be used to describe the gross features of boulder weathering from the viewpoint of acoustic wave transmission. There are two topics of interest for the use of wave speeds as an indicator of relative age: (1) the mechanism which slows waves as weathering processes; and (2) changes with age in the distribution of wave speeds in boulders of a single well-mixed till.

Wave-Speed Retardation with Weathering

Two obvious changes occur in granitic rock weathering at the surface of the earth: the rock is chemically altered, and intergranular cracks develop. These processes are probably related. For instance, as grains are altered they may expand, which promotes cracking; pervasive cracks promote the circulation of water through the rock, which hastens alteration. Heavily weathered granitic boulders in the mountains and deserts of eastern California may show effects of both intense chemical weathering and granular disintegration. Boulders from ancient deposits are typically oxidized, exhibiting strong surface discoloration, and are grusy. Biotite flakes in such rocks may be altered and discolored. Feldspars may appear chalky in hand samples. Conversely, boulders in some locations develop resistant rinds or case-hardened crusts in which grains of the parent boulder are cemented together to form a resistant shell.

Presumably one or more of the above processes controls the speed of acoustic waves through weathering boulders. Crook and Kamb (1980) found that even for stream deposits less than 1000 years old, wave speeds

averaged only 2.1 km/s for granitic boulders (Mt. Lowe granodiorite). This is considerably lower than the 4-km/s speed characteristic of freshly quarried granite (Quincy granite; Birch, 1937). Clasts from the stream deposits were not visibly weathered, and chemical alteration could have been incipient only. If reductions of wave speed perhaps exceeding 45% are unaccompanied by chemical alteration, then the formation of intergranular cracks must be the controlling factor.

There is some evidence for this contention. Noting that Birch (1960) found that for granites the wave speed V* was proportional to pressure, Nur and Simmons (1969) showed that this effect was greatly reduced if the granite was saturated with water. V for wet samples was about 50% larger than V for dry samples, at 1 atm pressure. They attributed the reduction to the presence of "microcracks" much smaller than the wavelength of the P waves, and less than the grain diameter. The presence of microcracks appeared to strongly increase the compressibility (k^{-1}) of the rock, thereby decreasing V even though cracks and pores occupied less than 1% of the volume of the rock. The abundance of microcracks was correlated to the difference between wave speeds for the wet and dry samples.

In a subsequent paper, Nur and Simmons (1970) reported microcracking to be especially pronounced in quartz-bearing rocks. Noting the high value of the coefficient of thermal expansion and the high compressibility of quartz compared to other rock-forming minerals, they argued that this

---

*In this discussion V is the actual P wave speed, or the speed found by conventional means: $V = \sqrt{(k + (4/3)\mu)/\rho}$, where k is the bulk modulus, μ is the shear modulus or rigidity, and ρ is the density of the rock. V_p is the P wave speed found using the Microseismic Timer and Eq. (1).

might lead to high local stresses resulting in cracking as the rock, which crystallized at high pressures and temperatures, was cooled and exhumed by erosion. If this were true, further cracking might be expected in granitic clasts after they were plucked from bedrock. Such cracking might be promoted by diurnal or seasonal temperature fluctuations, which in the Sierra Nevada may sometimes exceed 50°C. Ide (1937) demonstrated by measuring V before and after heating fresh Quincy granite at 1 atm pressure that microcracking could be induced by thermal changes. No reduction was noted at 100° C, but V was reduced from 3.72 km/s to 2.75 km/s at 250° C and to 0.78 km/s at 500° C. These changes were irreversible. Although grains appeared unaltered in thin sections made of the cooled rock, the rock itself was friable after heating. Thus the creation of microcracks seemed to be the controlling factor in the reduction of acoustic wave speeds with age.

Cracking could be spontaneous or induced by fluctuations in temperature, as discussed above. It could also result from frost riving or from chemical weathering, especially of micas which expand as they are altered. If cracking is largely spontaneous or the result of thermal fluctuations, it may be proportional to the fraction R of uncracked rock remaining. If $\eta = 1-R$ is the fractional crack porosity of the rock and $\dot{R} = -\lambda R$, then $\dot{\eta} = -\dot{R}$ and $\eta = 1-\exp(-\lambda t)$, where λ is a constant and t is the time since exposure of the rock at the earth's surface. Nur and Simmons (1970) observed that the reduction of V between dry and wet granites was linearly proportional to the crack porosity. Thus a simple model of the reduction of V with age might be

$$V_p(\eta(t)) = a - b \exp(-\lambda t) \qquad (2)$$

where a, b, and λ are constants. Ide (1937) found for the Quincy granite

that V = 0.78 km/s when the rock had been cracked to the point of disintegration. If for the Mt. Lowe granodiorite a = 0.78 km/s, then b = 0.20 and λ = 1.52 may be found by linear regression from the V_p data and age estimates of Crook and Kamb (1980). The correlation coefficient r exceeds 0.99, and may be increased if the estimate of a is reduced. Physically, a must have a minimum value of about 0.34 km/s, the speed of sound in air.

Certainly $\dot{\eta}(t)$ need not be the function described above, but to fit observed values of V_p and t, it must be a decreasing function of t. For example, if $\dot{\eta}(t) = \lambda\ (1 + t)^{-1}$, then $\eta(t) = \lambda\ \ln(1 + t)$ or

$$V_p\ (\eta(t)) = c + d\ \ln(1 + t) \qquad (3)$$

This function has been used to describe the thickness of weathering rinds on clasts from deposits of different ages by Colman (1981), who also discussed a variety of similar functions which had previously been used to the same end. For Eq. (3), the data of Crook and Kamb (1980) gave r = 0.998, c = 2.20 km/s, and d = 0.17. While the V_p data appear to be best fit by a logarithmic function of time, the actual function cannot be deduced from the limited data available. Furthermore, while chemical weathering and cracking appear to be similar functions of time, cracking caused by chemical weathering may proceed at a different rate than cracking from induced thermal stress. Finally, chemical weathering may become sufficiently pronounced that the weathering products themselves and not just resultant cracking may affect the elasticity of the rock. Long term climatic changes might introduce or remove frost riving as a factor, or change chemical weathering rates. Some or all of these factors may simply change the value of the coefficients of Eq. (2), so

that a,b,c,d, and λ are themselves functions of time, but the functional form of V(t) may also change. For instance, case-hardening may actually cause V to increase with the passage of time. This is because the pores and cracks in the weathered rind (the top few cm of the clast) may fill with clay or cement (e.g., Conca, 1982, has found calcite filling cracks in crusts developed in rocks of the Aztec Sandstone in Nevada). The effect of cementing the cracks should be the same as filling them with water: to decrease to compressibility and thus to increase V.

As the effects of chemical weathering and crust formation become pronounced, V should begin to vary radially in the boulder. If no crust is present, V will increase with depth. The waves actually measured are constrained by the sensor configuration to travel mainly through the upper few cm of the rock. Thus the speeds actually measured will be close to the minimum for the clast. Crook and Kamb (1980) demonstrated this by comparing values of V_p found as described in §3.1 to wave speeds found by placing the transducer on the face opposite the impact point. Waves passing through the clasts were about 25% faster than those traveling through only the outer part of the clasts.

If a crust has developed on a weathered boulder, then the radial profile of V may not be monotonic: high values may be found near the clast surface, a minimum just beneath the crust, and a high value near the clast center. The measured wave will be confined to the crust, and may have the maximum speed for the clast. Thus, case-hardening may invalidate the fundamental assumption in the use of wave speeds as a measure of relative age: that V_p decreases montonically with time.

The Behavior of Populations of V_p with Increasing Age of Deposition

Discussion in the previous section focused on the change with age of V for a single boulder. In this section the change in populations of measured speeds (V_p) is addressed.

Several factors must be considered: the initial distribution or probability density function (PDF) of wave speeds in the population of boulders; the functional dependence of V on t; dispersion in the values of V for identical boulders; and removal of boulders from the measurable population by granular disintegration. For the purpose of this discussion it will be assumed that $V_p = V$.

If Eq. (3) is used to describe the change in V_p with time, then V_p is controlled by three variables: t, c, and d. Of these, c and d are properties of the rock. Because of variability of the rock, the initial distribution of $V_p(t,c,d)$ will not be an impulse but will show some scatter in the (c, d) plane. As mentioned in the previous section, although Eq. (3) may adequately describe V_p for an interval of time, it may be that c and d vary with time, or even that Eq. (3) is supplanted by a different relationship after $\dot{n}$ has become small and chemical weathering has become significant. The dispersive term may reflect spatial changes in weathering conditions or characterisitics of the rock other than c and d which may influence weathering. By the time granular disintegration begins, V_p will be low. For this discussion disintegration will be assumed to coincide with the reduction of V_p to some threshold.

A model for the temporal change in the PDF of V_p is thus given by:

$$\mathrm{PDF}[V_p(t_n,c,d)] = \Big(\mathrm{PDF}[V_p(0,c,d)] * [V_p(t_n,c,d) - V_p(0,c,d)] * \mathrm{FT}\Big\{ \prod_{i=1}^{n} \mathrm{FT}\{D(c,d)\} \Big\} \Big) \, G(V_p) \qquad (4)$$

where c and d are independent of t, * denotes convolution along the V_p axis, FT denotes the Fourier transformation, D is a dispersion function, and G is the probability that granular disintegration will remove the rock from the measurable population. Changes in V_p are assumed to occur at small increments of time, and t_n is the time after the nth increment.

This model states that the PDF of wave speeds is offset to lower values of V_p as the deposit ages. The amount of the offset may be specified by Eq. (2), Eq. (3), or some other function. The dispersion function, D, serves to broaden the PDF with time by adding small random increments to V_p for each "boulder" in the population. D, here assumed to be independent of time, basically is a description of random factors which might make identical boulders weather at different rates. An example of such a factor might be shading by adjacent boulders.

As weathering progresses, boulders eventually will become grusy. As loose grains are shed, the boulder diameter is reduced until V_p can no longer be measured with the Microseismic Timer. $G(V_p)$ is a description of the probabilty of this happening as a function of wave speed. $G(V_p)$ is zero for $V_p < 0.34$ km/s, unity for high values of V_p (e.g., > 1 km/s), and has intermediate values for the remaining range of V_p.

The above model states that the mode V_p will decrease with age, and that the PDF will broaden. As boulders begin to disintegrate the population of measurable boulders will lose members. These will have the lowest values of V_p. Ultimately, the original shape of the PDF (e.g., a normal distribution) will be unrecognizable.

Equation (4) may be generalized to allow for variation of coefficients c and d and the dispersion function D with time:

$$\mathrm{PDF}[V_p(t_n,c(t_n),d(t_n)] = \{\ \mathrm{PDF}[V_p(0,c(0),d(0)] *$$

$$\mathrm{FT}\{\prod_{i=1}^{n} \mathrm{FT}\{\ (V_p(t_i,c(t_i),d(t_i)) -$$

$$V_p(t_{i-1},c(t_{i-1}),d(t_{i-1}))) * D_i(c(0),d(0))\}\}\ G(V_p) \qquad (5)$$

In Eq. (5) the dispersion function is assumed to vary with t and with initial values of c(t) and d(t) only.

Equation (5) is illustrated schematically in Fig. 3-5 for the special case where V_p varies only with t and some single measure of weathering susceptibility w instead of with both c(0) and d(0). The uppermost plane (A) gives the initial PDF of $V_p(0,w)$. Most rocks have high values of V_p, but rocks which are highly susceptible to cracking already have lower values at t = 0. The group of planes below A (group B) pictures the incremental loss of V_p at different steps j, j+1, j+2, and n. These values of $\Delta V_p = (V_p(t_i,w) - V_p(t_{i-1},w))$ may be found using Eq. (3) or some other appropriate function. For the functions shown, the change in V_p will increase with weathering susceptibility. Planes in group C depict the dispersion function D(t,w), here shown as a gaussian function which is narrower for rocks of low weathering susceptibility. Plane D shows the function $G(V_p)$, which is independent of t and w, and planes of group E show $V_p(t,w)$ for $t = t_j$, t_{j+1}, t_{j+2}, and t_n. Conceptually, these functions are found by first convolving corresponding planes of groups C and D, and then successively convolving the initial distribution (A) with each new function at time t_1, t_2, ..., t_n to find the PDF of $V_p(t_n,w)$. Convolution is performed only along the V_p axis. The final step consists of multiplying $\mathrm{PDF}(V_p(t_n,w))$ by $G(V_p)$ (plane D) to remove grusy rocks from the population.

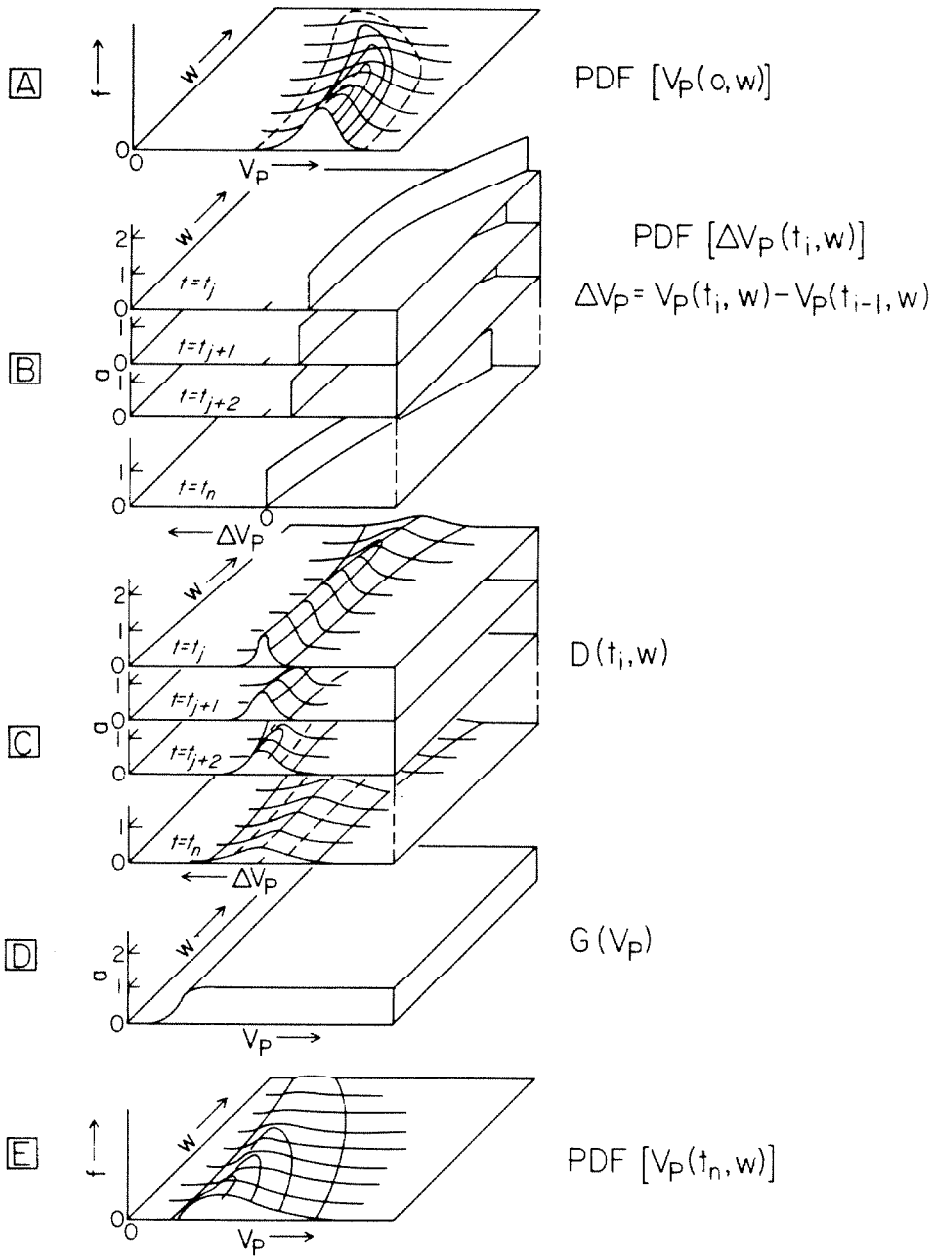

Fig. 3-5. Schematic representation of the model of changes in a population of waves speeds as a deposit ages.

Fig. 3-5 (continued)

Schematic representation of the model of changes in a population of waves speeds as a deposit ages (eq. 5). For all graphs, the abscissa is V_p or ΔV_p. Other axes are w, some measure of weathering susceptibility of a boulder, and f (frequency or probability density) or a (amplitude). The figure shows the modification of the PDF of wave speeds in a youthful deposit with the passage of time.

Plane A shows the initial PDF. Most boulders, except those which are highly susceptible to weathering, have high wave speeds. Plane E shows the PDF for the same deposit, now aged. Most wave speeds are low and the PDF is broadened by dispersion. The distribution is strongly skewed because the most weathered boulders have disintegrated.

Group B shows the ideal loss of V_p for time increments at times t_j, t_{j+1}, t_{j+2},... , and t_n. The functions are impulses of unit amplitude. ΔV_p is negative and decreases with increasing w. ΔV_p for a given w decreases with time. Convolution of the ΔV_p function and the initial PDF would result in a new PDF of identical shape, but offset towards the origin.

Group C shows dispersion functions D at times t_j, t_{j+1}, t_{j+2},..., and t_n. These describe random deviations from the ideal reduction of V_p for the population of boulders. The functions shown disperse V_p increasingly with w and with t.

Plane D shows the function $G(V_p)$, which describes the probability that a boulder will disintegrate and be removed from the population when its speed has a given value.

Using this model, the behavior of even complicated populations consisting of rocks from different plutons weathering under changing climatic conditions can be described. For purposes of the present study, it is sufficient to examine the simpler question of the variation in PDF(V_p(t,w) with time, assuming that for all rocks w = w_o. Representative distributions of V_p are shown for different times in Fig 3-6. I have assumed that V_p is given by Eq. (3), that D is independent of t, and that $G(V_p) = 0$ if $V_p < V_p'$ and $G(V_p) = 1$ if $V_p \geq V_p'$. The top profile (a) shows PDF(V_p) just after deposition. At later times ((b), (c), and (d)) the average value of V_p is reduced but the standard deviation is only slightly larger. At the time of (d), some boulders are becoming grusy. At the time of (e), the average value of V_p has been lowered further, and a fraction of the population has disintegrated. The last profile (f) shows the distribution of V_p after the mode value has been lowered below the threshold V_p'. In this simple scheme the mean V_p is reduced monotonically as weathering progresses, while the standard deviation about the mean increases in proportion to the amount of dispersion. Disintegration of weathered boulders causes the mean V_p to decrease more slowly and the standard deviation to decrease. The distribution becomes markedly flattened and asymmetric. However these trends may be masked if weathering rinds are formed.

If the model discussed above is valid, then relative age discrimination based on V_p distributions will be greatest for the youngest deposits. As deposits age, discrimination will become increasingly difficult, especially if there has been significant dispersion. Ultimately, discrimination may be so poor that the technique will be of little practical use. It may prove possible, however, to extend the range of ages which can be

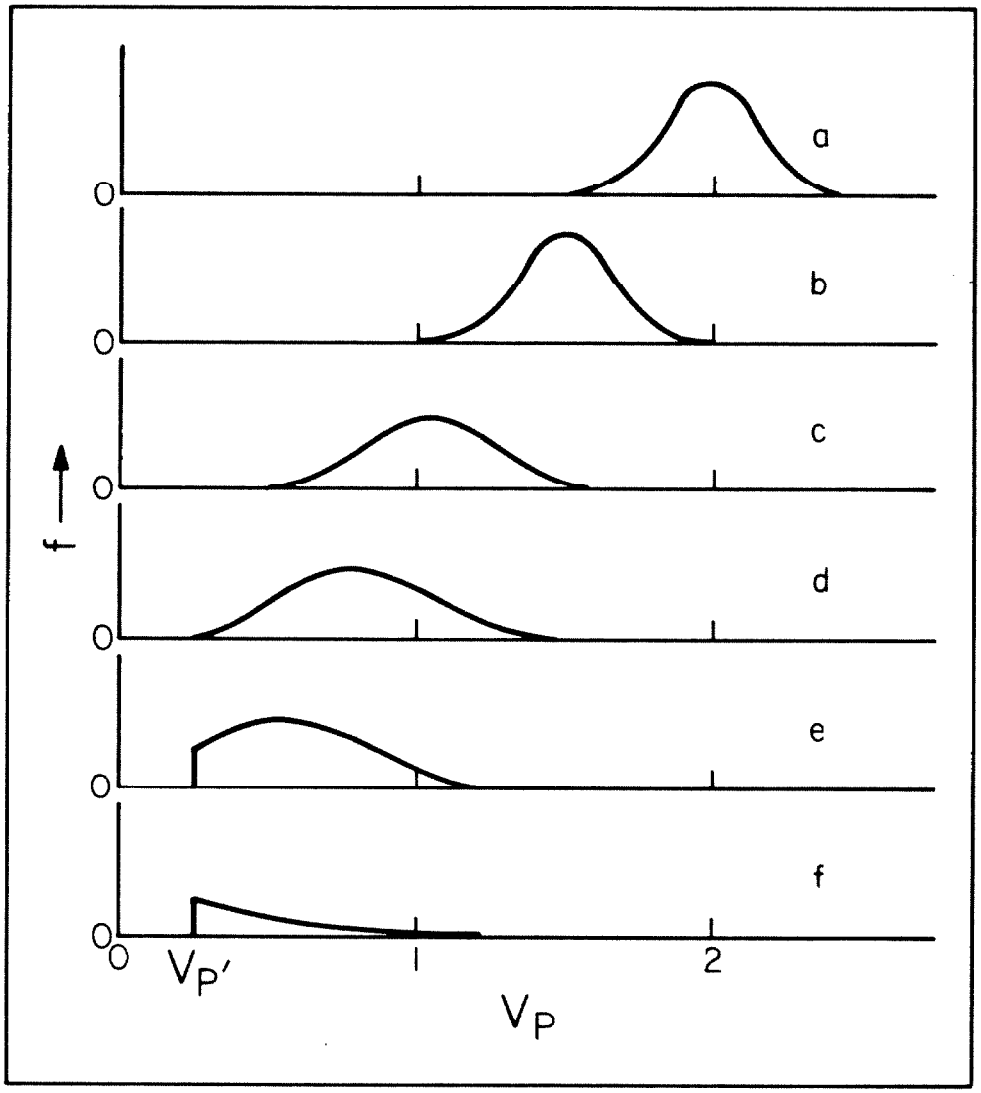

Fig 3-6. Schematic representation of a sequence of six PDF's shows the reduction of V_p with time. The abscissa shows wave speed, V_p; the ordinate shows the probability density or frequency with which a given value of V_p is encountered in the population.

Curve a represents the PDF for a young deposit. Average values of V_p are about 2 km/s. As the deposit ages this value drops to 1.5 km/s (b) and to 1.0 km/s (c), and the PDF broadens.

For this illustration, $G(V_p) = 0$ for $V_p < 0.35$ km/s and $G(V_p) = 1$ for $V_p > 0.35$ km/s. In c, values of V_p for most weathered boulders are approaching this limit. In e, about a third of the boulders have disintegrated. The PDF is strongly skewed. Ultimately, only the high-V_p tail of the original distribution remains (curve f).

studied by measuring wave speeds through rocks which weather more slowly than granodiorites.

3.3 SOME CHARACTERISTICS OF V_P DATA

In the following discussion several aspects of wave speeds measured for individual boulders and groups of boulders are addressed. These include: travel time vs. distance between the impact point and the sensor; changes in V_p with the gain setting on the Microseismic Timer; convergence of the mean V_p and the standard deviation as additional boulders are measured; and the independence of determinations of V_p for different boulders.

Figure 3-7 presents selected data and calculated variables for a single large outcrop of granodiorite in Green Creek that was glacially polished about 11,000 years ago. Impact points were distributed along an 80-cm line. Travel times for waves from these impact points are plotted in Fig. 3-7a as a function of the distance travelled. A line fit to these twelve measurements gives a wave speed of 2.4 km/s, while V_p calculated from the three travel times (indicated by X in the figure) of waves from impact points at 5, 15, and 25 cm is 2.5 km/s. This latter value would be the one found by the method used in this study.

Although the travel-time curve is basically linear, two features are worth noting. First, the travel time at d = 35 cm lies perhaps 0.03 ms below the general trend. An error of this size in reading the travel time is unlikely, and this pattern probably reflects some heterogeneity in the rock itself. The second feature is the distinct curvature of the travel-time line for impact distances of 15 cm or less. This curvature

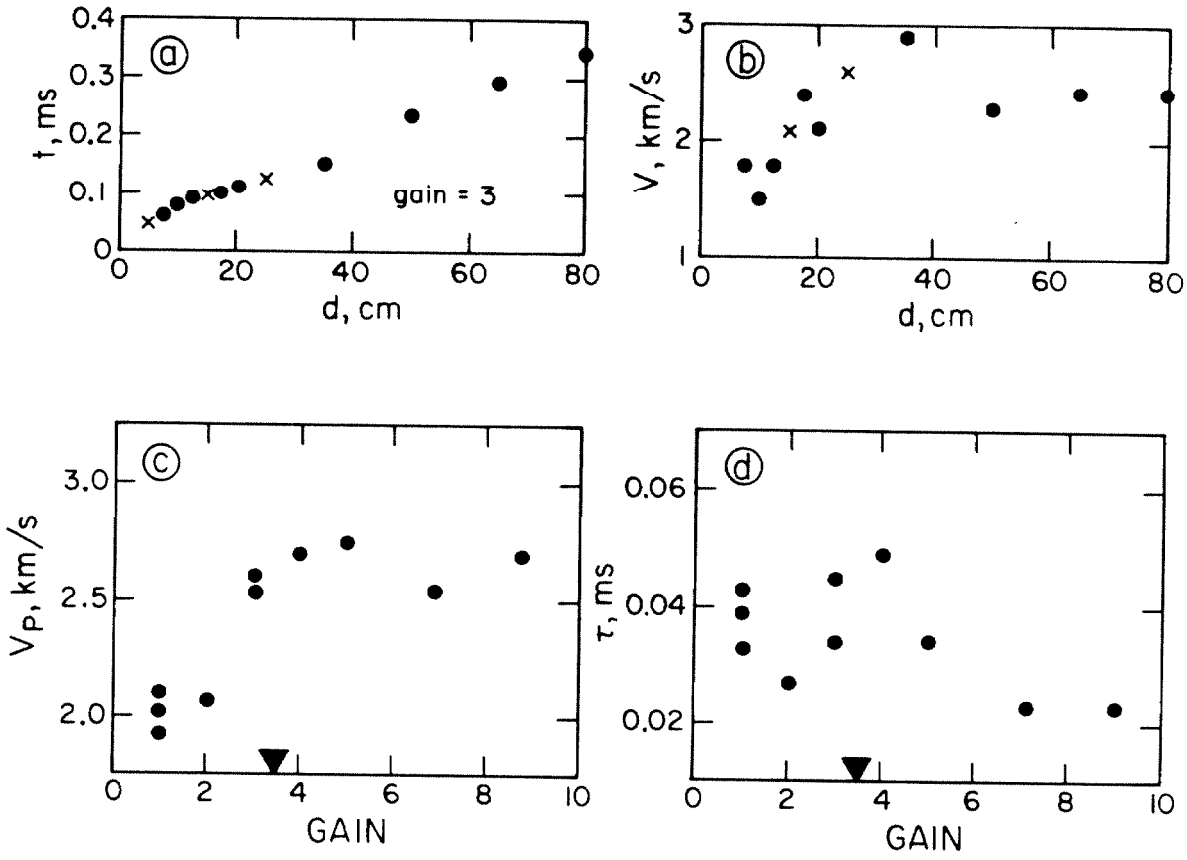

Fig. 3-7. Characteristics of V_p data gathered from granodiorite bedrock at site 13, Green Creek.

Fig. 3-7 (continued)

Characteristics of V_p data gathered from granodiorite bedrock at site 13, Green Creek.

a) Travel times (t) for waves from twelve different impact points at distances (d) of 5 cm to 80 cm from the detector define an approximately linear array. Travel times for the three impact points at distances of 5, 15, and 25 cm are marked by x. The slope of a line fit to the twelve points is about 2.4 km/s. V_p calculated according to Eq. (1) is about 2.5 km/s.

b) Speeds V calculated from the difference in travel times and impact distances for eleven pairs of data. The first point (d = 5 cm) was a member of each pair. Speeds show a tendency to increase with distance from the detector to about d = 30 cm. Speeds of waves from greater distances are probably constant. This pattern can be explained if the upper few cm of the boulder are more weathered than the core.

c) There appears to be a bimodal distribution of V_p with the gain of the Microseismic Timer. As predicted in Fig. 3-4, when the gain is low (high threshold) V_p is lower than when the gain is high. For gain settings less than 3 (arbitrary units), V_p is about 2 km/s. For higher gain settings, V_p is about 2.5 km/s. The gain setting used in this study, 3.5, is marked by a filled triangle.

d) The abscissa intercept times τ show a slight tendency to be smaller for the greater impact point distances. None was less than 0.2 ms. The observed variation is probably best attributed to spatial variations of elastic properties of the rock rather than to artifacts of the measurement technique in view of the linearity of the travel-time curve in graph a.

corresponds to an increase of the wave speed as the impact distance is increased. This could be caused by a weathering zone no more than a few cm thick. Waves from close impact points would travel entirely within the zone, but waves from more distant points would travel largely through the less weathered rock deeper in the boulder. This increase in speed V with the distance of the impact point is shown in Fig. 3-7b. For this illustration, V was taken to be $0.01(d_i-5)/(t_i-0.049)$ km/s where t_i and d_i are the travel time and distance measured for the ith impact point, and where 0.049 ms and 5 cm are the travel time and distance for the first point. Presumably as the boulder ages, the distance over which there is curvature in the travel-time line will increase. In Fig. 3-7c are displayed values of V_p determined for the same impact points (at 5, 15, and 25 cm) using the Microseismic Timer with different gain settings. High gain settings (e.g., gain = 10) correspond to a large amplification of the signal or a relatively low threshold level. At low gain settings the threshold may exceed the amplitude of the first waves to arrive. The gain setting adopted in this study (gain = 3.5) is indicated by the arrow in Fig. 3-7c.

V_p appears to be insensitive to gain as long as the gain is 3 or greater. As predicted in §3.1, V_p is significantly lower for low gains. The stability of V_p over a large range of gains is important because it suggests that V_p is also insensitive to wave amplitude, as long as it is larger than the threshold level.

In Fig. 3-7d are shown the ordinate intersections (τ) of regression lines fit to twelve values of t and d measure at different gains. τ is the delay between the actual and measured arrival times. The data show that τ is reduced at high gains to about 0.023 ms from about 0.038 ms

at gains of 5 or less. This could be explained by a 60° shift in the phase of the 11-khz wave at which the travel time is measured. This is to be expected when the wave amplitude greatly exceeds the threshold, and its observation lends credence to the interpretation presented in §3.1.

As data are measured for increasing numbers of boulders (n) from a deposit, the distribution of calculated values of V_p increasingly resembles the population of V_p for the whole deposit. The sample distribution may generally be described by its mean, $\overline{V_p}$, and its standard deviation about the mean, s. As the sample size increases, the values of these parameters converge to values characteristic of the population. The number of boulders which must be measured before convergence is achieved obviously varies with the heterogeneity of the deposit, but as shown in Fig. 3-8 for two sites, V_p and s changed little after about twenty boulders had been measured. Fig. 3-8a shows the convergence of $\overline{V_p}$ with increasing n. The error bars are the uncertainty of the mean and are given by $s/\sqrt{n}$. At site 8, little was gained by measuring the final ten boulders, and at site 28 the mean changed insignificantly after n = 10. However, the standard deviation s for site 8 (Fig. 3-8b) increased from 0.3 km/s at n = 10 to 0.5 km/s at n = 25. While 25 boulders seemed to be an adequate sample size, generally 30 boulders were measured to insure against unexpected heterogeneity or random concentrations of similar boulders in the deposit.

Actual travel-time curves for 15 boulders from each of three sites are shown in Fig. 3-9. These data are intended to illustrate the typical linearity of travel-time curves and the consistency among boulders from the same site. Where the three travel times are not colinear in these diagrams, the curve is generally convex, as seen in Fig. 3-7a. This

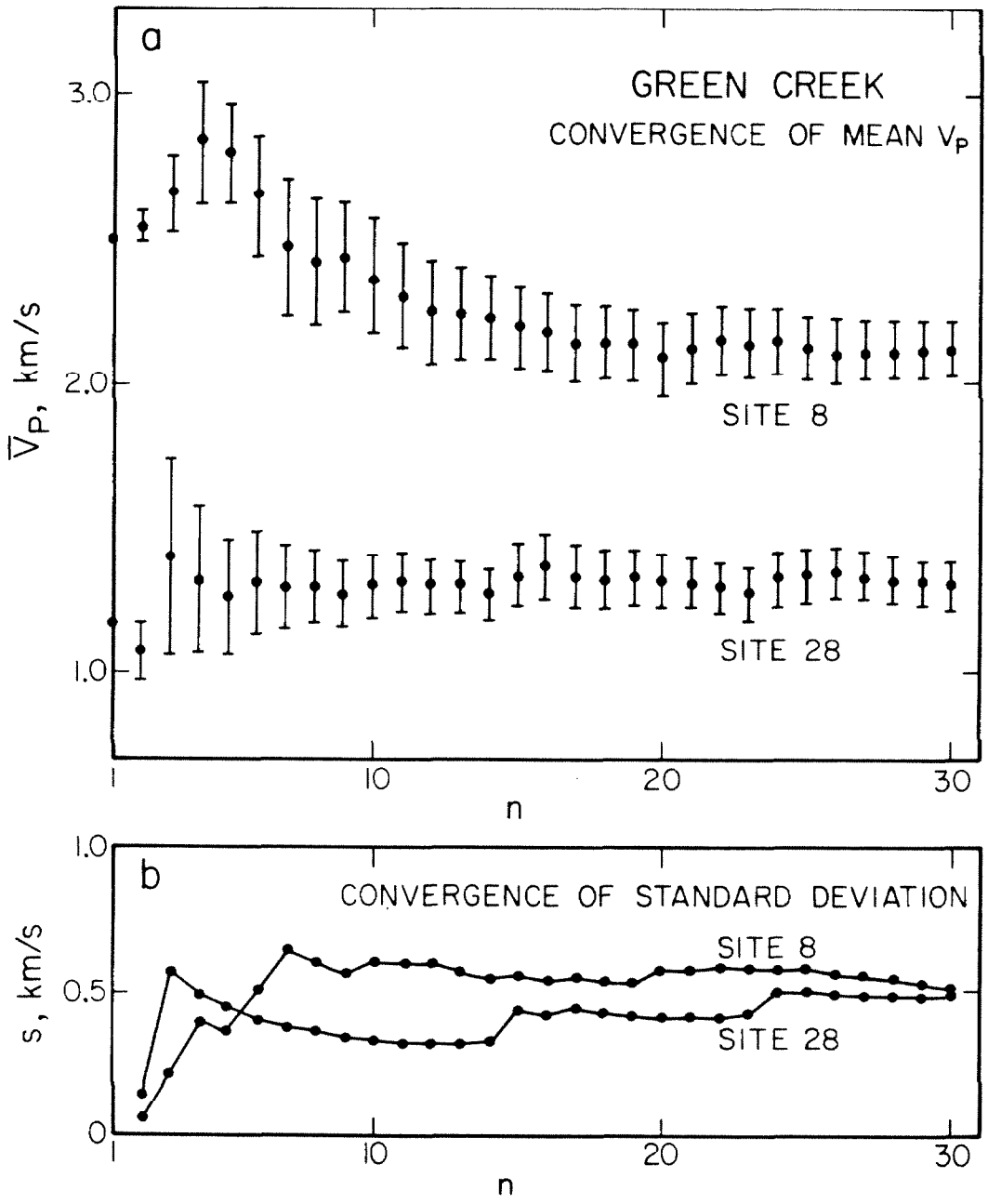

Fig. 3-8. Running mean wave speeds ($\overline{V_p}$) and standard deviations (s) of distributions of V_p from the two sites are shown in graphs a and b. Abscissas are the number of boulders measured. Error bars in graph a show the standard deviation of the mean V_p, not the standard deviation s of the distribution of V_p shown in graph b. Both $\overline{V_p}$ and s appear to converge to stable values after about 15 boulders have been measured.

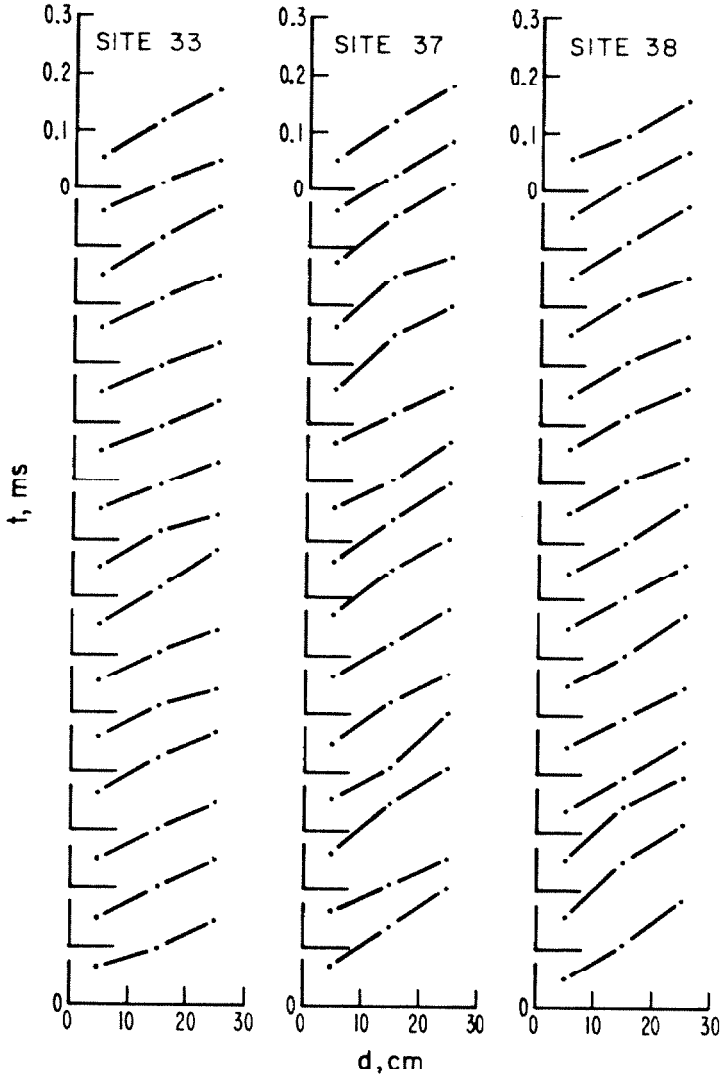

Fig. 3-9. Actual travel times (t) for 15 boulders from each of three sites at Green Creek are plotted as a function of the impact point distance (d) from the detector.

pattern is explainable by a weathered zone on the surface of the boulder. However, in a few instances (notably the fourth curve from the bottom, site 37) the travel-time curve is concave; such a pattern means the wave is slower at greater distances from the sensor. This may be due to variable elastic properties over the surface of the rock, or simply to the presence of gross defects such as cracks which can impede the progress of the wave.

The general colinearity of (t,d) pairs for a given boulder supports the interpretation of V_p as a property of the rock itself rather than the measurement process (i.e., an artifact). If this is the case, then speeds V_1 and V_2 calculated from the impact points at 5 cm and 15 cm, and at 5 cm and 25 cm, respectively, should be strongly correlated. In particular, V_2 should appear to be dependent on V_1 (or vice versa). This can be demonstrated by a transition matrix (cf. Harbaugh and Merriam, 1968), which is a frequency distribution of (V_1, V_2) pairs. A contour map of such a distribution is given in Fig. 3-10a. In this presentation, correlated or dependent variables are revealed by alignment of data near the diagonal line $(V_1 = V_2)$, while uncorrelated data are dispersed in a normal distribution and are revealed by circular contour lines. Clearly, V_2 and V_1 in Fig. 3-10a are strongly correlated, and in fact for the data shown there is less than one chance in a thousand that these variables are independent*.

In contrast, a similar transition matrix (Fig. 3-10b) relating V_p measured on successive boulders shows roughly circular contours indicating an absence of correlation. From this distribution there seems to be less than one chance in a hundred that determinations of V_p are dependent on previous measurements.

---

*The probability is estimated by testing for the Markov property (cf. Till, 1974).

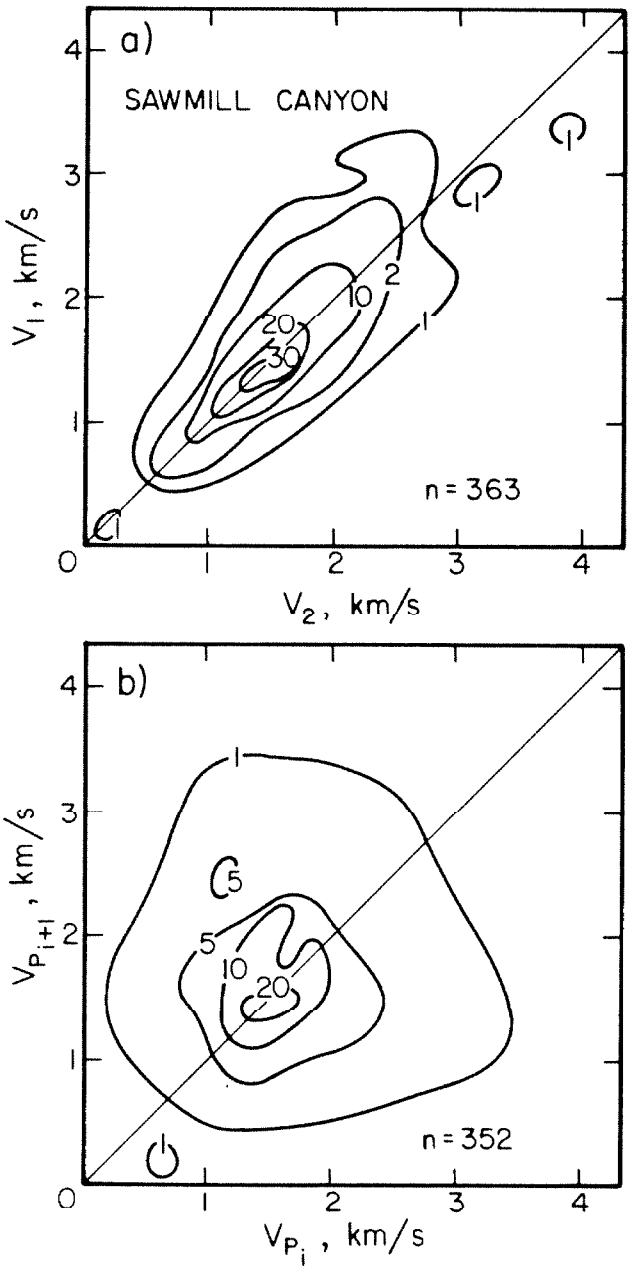

Fig. 3-10. Contour maps of wave-speed data from Sawmill Canyon, Inyo County.

a) V_1 is the speed calculated from travel times for waves from impact points at d = 5 cm and d = 15 cm; V_2 is the speed for d = 5 cm and d = 25 cm. Transition matrices or variation diagrams show that V_1 and V_2 are strongly correlated.

b) Variation diagram comparing successive measurements of V_p on different boulders shows no correlation. Presence of a correlation would indicate that sampling was not random. Absence of correlation shows that measurements are independent, a necessary condition for the statistical tests used.

Independence of successive determinations of V_p may seem to be an obvious attribute which need not be belabored. However, dependence could arise in a number of ways, among them unconscious operator bias in measurement or in boulder selection. Absence of any evidence for this is therefore encouraging, and serves to contrast the wave-speed method of relative dating to the subjective methods (Chapter 2) for which such independence can not be taken for granted. For example, it is not at all clear that an operator's classification of weathered boulders is unaffected by previous classifications. Memory in an operator must lead to some inconsistencies in classification and hence to inaccuracies in relative dating.

Summary of Data Characteristics

In summary, data from the three impact points used in this study give similar estimations of V_p compared to data from longer lines with more impact points. Data are insensitive to small changes in instrument gain or wave amplitude. Sample sizes of 25 or 30 boulders appear to be adequate to estimate population characteristics. Finally, data from a single line of impact points are strongly correlated, but there is no discernible sign of dependence between V_p found for boulders measured successively. V_p data thus appear to form an acceptable basis for relative age discrimination.

3.4 STATISTICAL TESTS

The purpose of gathering V_p data is to enable meaningful comparisons among moraines to establish relative ages of deposition. This is best accomplished using statistical tests. There are two categories of tests

which are useful: 1) tests of the hypothesis (H_o) that two different samples are drawn from the same population; and (2) tests of the hypothesis that all of several samples are drawn from the same population. In the first category are Student's t-test and the Kolmogorov-Smirnov two-sample test (cf. Bradley, 1968). In the second category are analyses of variance such as Fisher's F-test (cf. Griffiths, 1967). The two-sample t-test is a specific case of the F-test. The use of these tests in this study is discussed below.

Comparisons Between Two Samples

Student's t-test

If it can be shown that values of V_p constituting a sample are randomly drawn from a normally distributed population, then the mean and standard deviation are adequate to characterize the sample and Student's t-test may be used to compare it to other samples. The t-statistic is calculated from the difference of the sample means normalized by the pooled variance according to

$$t = \left(\frac{n_1 + n_2 - 2}{n_1 + n_2} \quad \frac{n_1 n_2}{(n_1-1)s_1^2 + (n_2-1)s_2^2} \right)^{-1/2} (\overline{V_{p_1}} - \overline{V_{p_2}}) \qquad (6)$$

where $s_i^2 = (n_i-1)^{-1} \sum_{j=1}^{n_i} (V_{p_{ji}} - \overline{V_{p_i}})^2$ is the variance of sample i and n_i is the number of measurements for sample i (cf. Griffiths 1967). The confidence with which the tested hypothesis may be rejected is widely tabulated, as a function of t and of the degrees of freedom $n_1 + n_2 - 2$. The test is sensitive chiefly to differences in the mean speeds: the greater the difference in the means, the greater the value of t and the higher the confidence with which the hypothesis that the samples were from the same

population may be rejected. On the other hand, if the means from two samples were the same, the t-test would indicate that the two samples were drawn from the same population even if the variances were so different that this was clearly not the case. This must be kept in mind when interpreting the results of testing.

Because t is dependent on the sample variances, the discrimination using the t-test decreases with decreasing measurement precision. This is because s is compounded from the intrinsic variability of the population and the measurement uncertainty. Generally, this is not a serious problem because most measurements are precise compared to the scatter of the data. In determining V_p this is not always the case. As discussed in §3.1, measurement uncertainty (p) appears to be ± 0.05 km/s (1σ). This may be a significant fraction of the standard deviation of the measured values of V_p, which may be as low as 0.2 km/s. Because the measurement uncertainty is known, it is possible to estimate the standard deviation of a sample of hypothetical perfectly precise wave speeds from their actual measured values. The expression for t may be rewritten to refer to these measured wave speeds:

$$t = \left(\frac{n_1 + n_2 - 2}{n_1 + n_2} \; \frac{n_1 \, n_2}{(n_1-1)s_1^2 + (n_2-1)s_2^2 - (n_1 + n_2)p^2} \right)^{-1/2} (\overline{V_{p_1}} - \overline{V_{p_2}}) \quad (7)$$

where p is the precision of measurement. If s_1 and s_2 were 0.2 km/s, for sample sizes in the range of interest this could lead to an increase of about 3% in the value of t.

While an increase in t would increase the confidence with which the hypothesis H_o could be rejected, the change would be virtually unnoticed against the background of large uncertainties of t due to chance in

sampling. This is easily demonstrated by a simple Monte Carlo experiment in which data from a specified normal population are repetitively drawn to form samples, using a random number generator. To each datum random noise from a second normal population representing measurement uncertainty is added. The statistic t is calculated for pairs of samples before and after the addition of the measurement uncertainty.

A contour map of the resulting matrix built up by 1000 iterations is shown in Fig. 3-11. It was calculated assuming the measurement precision p to be a quarter the size of the standard deviation s of the "measurements". Sample size was set at 25. Although groups of values of t found for samples with and without the addition of random noise are highly correlated, nevertheless there is considerable scatter about the dashed line which describes the predicted relationship of the mean values. Thus this line is a poor predictor of the actual ratio of any individual pair of t's (with and without noise). Furthermore, the ratio $p/s = 0.25$ was chosen as the worst realistic case. If p/s were reduced, the dashed line would rotate about the origin until for $p/s = 0$ it would coincide with the solid diagonal line t (without noise) = t (with noise). Thus Fig. 3-11 demonstrates that the performance of t-test based on actual imprecise measurements is not noticeably worse than the performance based on perfectly precise measurements, as long as p/s is reasonably small.

The t-test cannot be applied if the sampled population is not normally distributed. This is generally verified using a χ^2 test, but it is somewhat unsatisfactory because the results depend on the way in which the data are partitioned into cells. Lilliefors (1967) has adapted the one-sample Kolmogorov-Smirnov test for use when the population is unknown, and finds this test superior to the χ^2 test. Its use is elaborated in App. 3-A.

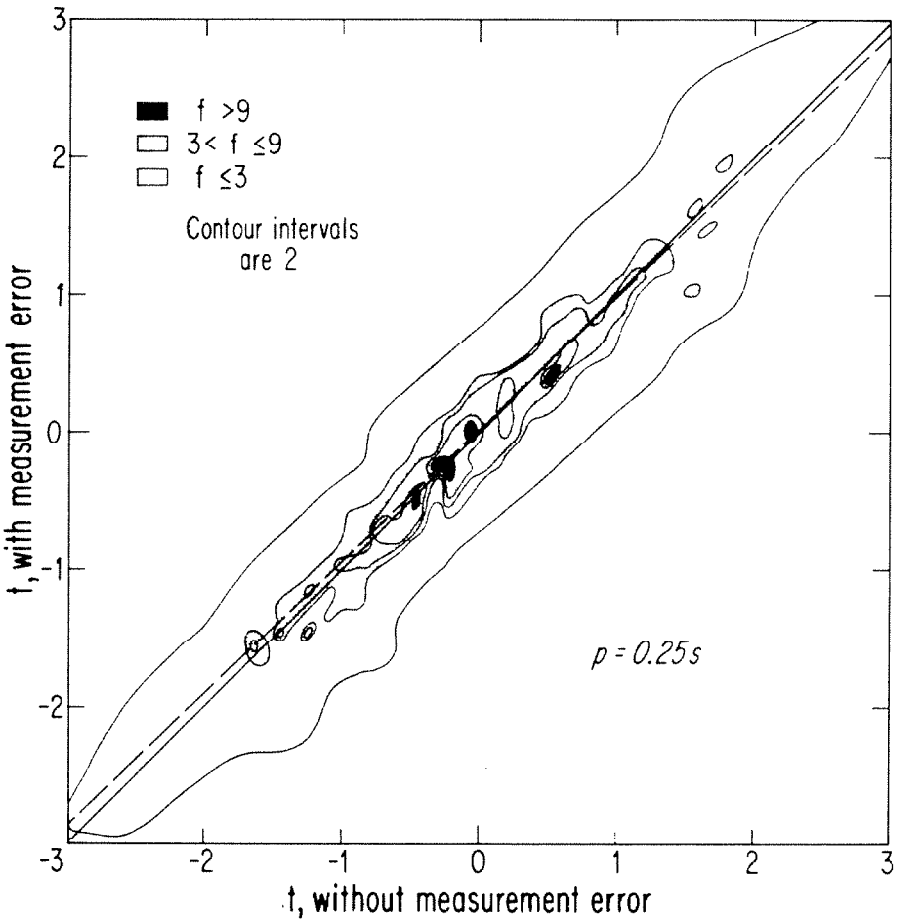

Fig. 3-11. Contour map of a transition matrix relating t-statistics calculated for 1000 synthetic data with and without added random noise simulating measurement error. The contoured variable, f, is the frequency with which a given pair of t-statistics occurred over a 0.1 x 0.1 unit square. The standard deviation of the "measurement error" (p) is taken to be 25% of the standard deviation of the data without added noise.

A regression line fit to the data is dashed in the illustration. Divergence of the dashed line from the solid diagonal reference line results from the increase of the standard deviation of data with noise added. This systematic effect is minor compared to the scatter of the data within the cluster.

The Kolmogorov-Smirnov two-sample test

If data cannot be shown to come from normal populations, then non-parametric tests (which make no assumptions of the distribution of the population) must be used. Of a large number of such tests, the Kolmogorov-Smirnov two-sample test seems best suited for application to V_p data. For a one-tailed test the test statistic is the maximum (or minimum) ordinate difference D_+ (or D_-) between the cumulative distribution functions of the two samples. For a two-tailed test the test statistic is the maximum absolute value D_{max} of the difference function. The probability that a given D_{max} or D_+ would result from testing two samples of the same population may be found from comparison with the distribution of these statistics for other samples of the same sizes randomly drawn from a population. These distributions are tabulated for small sample sizes, but if either n_1 or n_1 exceeds 40 then $4D_+^2\ n_1n_2/(n_1 + n_2)$ is distributed as χ^2 with two degrees of freedom (cf. Till, 1974). For confidences greater than 90%, tests based on D_{max} are approximately two-tailed versions of tests based on D_+, and confidences may be found by doubling those found for D_+ (cf. Bradley, 1968).

The Kolmogorov-Smirnov test basically gives a measure of the goodness-of-fit of one sample to the other. As such it is sensitive not only to differences between the means but also to differences between the shapes of the distributions. Thus for two samples having the same means but different standard deviations, the t-test would indicate the same parentage while the Kolmogorov-Smirnov test would not. In App. 3-B a more detailed comparison of the relative performance of the two tests is presented. One conclusion is that although the t-test is clearly inappropriate for non-normal samples and although the Kolmogorov-Smirnov test is less

capable than the t-test of resolving differences of normally distributed samples, there is no clear-cut point at which one test or the other should be abandoned. In this study, the t-test is considered inappropriate if one of the samples appears to be non-normal at more than 90% confidence. Since many samples were taken in a given series of moraines, a single test was chosen for a group of samples based on the distribution of confidences of normality found for the individual samples. This procedure reduces the risk of choosing the wrong test.

Effect of measurement uncertainty on the Kolmogorov-Smirnov test

Measurement uncertainties which are significant compared to the standard deviation of the population of V_p may reduce the test statistic D_+ or D_{max} by some amount. This may be visualized if it is recalled that slope of a cumulative distribution function is inversely proportional to the standard deviation of the probability density function. This is pictured in Fig. 3-12a for two normal and infinite populations of V_p whose means differ by 0.1 km/s but whose standard deviations (s) are the same. The cumulative distributions are plotted on probability paper so that they appear as straight lines. As random noise with a mean of 0.0 and a standard deviation of p is added to the measurements, s is increased and D_{max} or D_+ is decreased. Because of the non-linearity of the probability scale (ordinate), D_{max} or D_+ is also dependent on the absolute value of difference of the means, Δ.

The reduction of D_+ as s is increased or Δ is decreased is shown in Fig. 3-12b. If either s or Δ is large enough or small enough, D_+ is insensitive to small changes in the population parameters so that addition of random noise to the populations has a negligible impact. The distribution

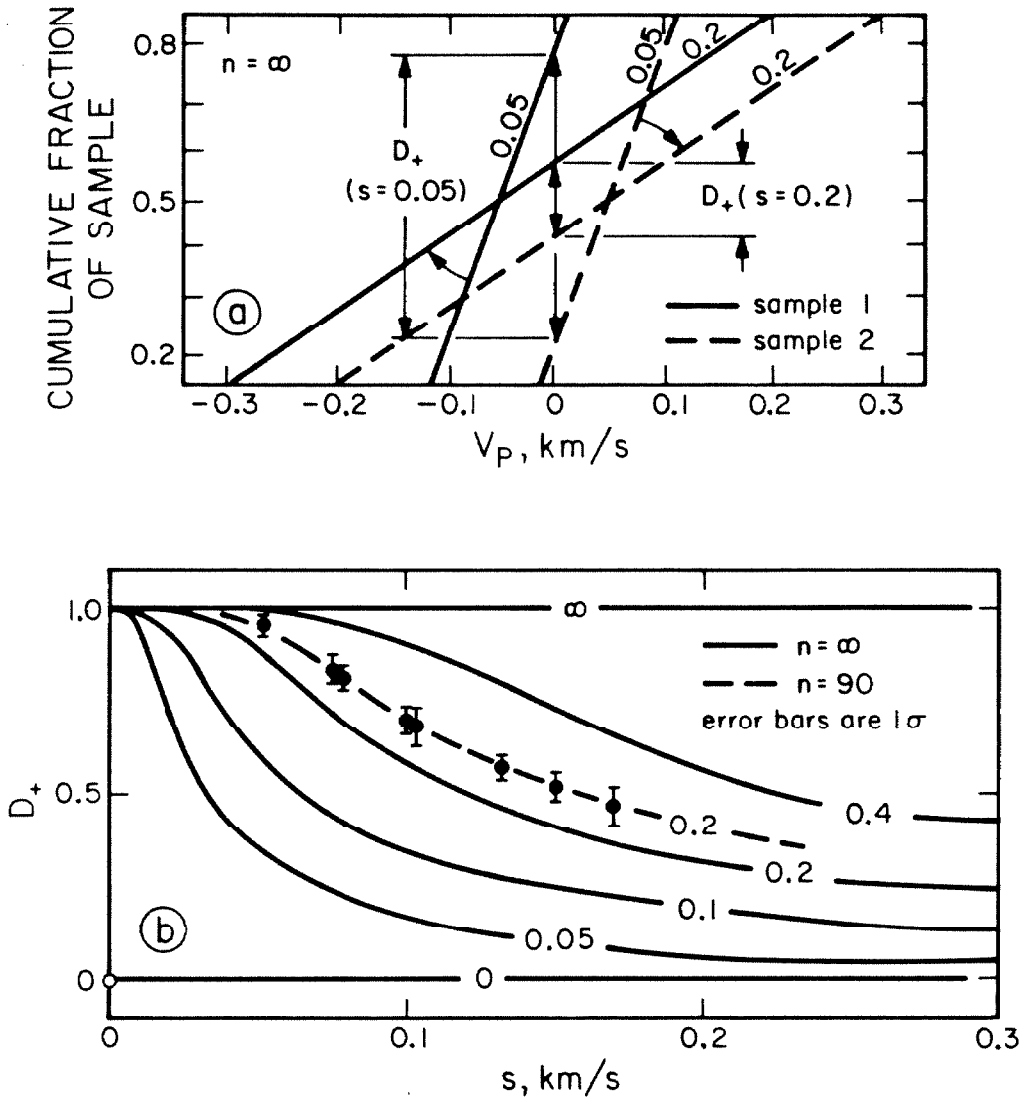

Fig. 3-12. Effects of measurement errors on the one-sample Kolmogorov-Smirnov test.

a) Cumulative distribution functions for two normal populations having means of -0.05 km/s (sample 1) and 0.05 km/s (sample 2). Both have standard deviations s of 0.05 km/s. Functions are plotted on probability grid (ordinate) so that they are straight lines. Numbers on lines are the standard deviations. Maximum difference D_+ between functions is nearly 0.6. Adding sufficient random measurement errors to increase the standard deviation of the data to 0.2 km/s reduces the slope of the cumulative distribution functions, and also reduces the maximum difference between them to less than 0.2. The Kolmogorov-Smirnov test is thus less likely to distinguish between "noisy" data from different populations than between error-free data from the same populations.

b) Curves show the decrease in D_+ with increasing s for different values of $(\overline{V_{p2}}-\overline{V_{p1}})$ (numbers on curves). Results from Monte Carlo experiments for samples of 90 "measurements" are shown as data points with error bars. D_+ is most sensitive to changes in s if s<0.2 km/s, but for most real data s>0.2 km/s. Thus for reasonable values of measurement precision (e.g., 0.05 km/s) and s, D_+ is relatively insensitive to random measurement errors.

of $-\partial D_+/\partial s$ with s is markedly skewed towards small values of s, and the mode occurs at about $s/\Delta = 0.3$. However, $(-\partial D_+/\partial s)_{max}$ decreases with increasing s and only for $s < 0.125$ does it exceed about 5 s/km. $\partial D_+/\partial \Lambda$ has a similar distribution, but for a given Λ, $\partial D_+/\partial \Lambda_{max}$ is found at greater values of s than $(-\partial D_+/\partial s)_{max}$.

For most populations of V_p in granodiorite boulders studied to date, s ranges between about 0.2 km/s and 0.6 km/s. This limits expected maxima of $\partial D_+/\partial \Delta$ to about 2.5 s/km, and maxima of $-\partial D_+/\partial \Delta$ to about 2 s/km. For infinite populations, random measurement errors will not change $\overline{V_p}$ and D_+ is thus sensitive only to changes in s. For V_p measurements, measurement precision p is about 0.05 km/s; thus D_+ for the ideal case where $p = 0$ is no more than 0.012 less than the value of D_+ for actual measurements. However, for finite samples measurement errors introduce an uncertainty in $\overline{V_p}$ of $\pm p/\sqrt{n}$, where n is the number of measurements. For typical samples tested in this study, n might range from 15 to 150. Thus for any sample, V_p will be within $\pm$ 0.013 km/s of the true value for the sample more than 68% of the time. This will result in an uncertainty in D_+ of as much as $\pm$ 0.045, more than three times the decrease due to $\partial D_+/\partial s$.

In Fig. 3-12b, the distributions of 100 values of D_+ found for several different values of s are shown for pairs of samples of 90 measurements each. The loss of D_+ with increasing s parallels the curves for infinite populations, but the values of D_+ are slightly higher. The 1σ error bars are 0.018 for $s = 0.05$ and range from 0.034 to 0.040 for other values of s. For $n_1 = n_2 = 90$, the uncertainty in D_+ from variation of the mean if $s = 0.05$ should be about $\pm$ 0.011; the uncertainty from variability in the value of s itself should be about $\pm$ 0.18. For higher values of s the relative contributions change but the expected total variabilities for

values of s from 0.05 to 0.2 lie within the observed range. Thus actual uncertainties in D_+ can be predicted from the discussion above.

If Δ is 0.4 km/s or less and s is 0.2 km/s or less before the addition of measurement error, then the variability in D_+ caused by the addition of random error of p = 0.05 km/s will be about $\pm$ 0.019 if n_1 and n_2 are 90. For two samples of the same size drawn randomly from the same population, tabulations of the distribution of D_+ show that 68% of the time D_+ will be less than 0.114, and 95% of the time D_+ will be less than 0.182 (0.203 for D_{max}). Thus the variability of D_+ or D_{max} which may be attributed to measurement error if p = 0.05 km/s is only about 20% or less of the variability expected for perfectly precise measurements (p = 0).

Although for small samples and small values of Δ the statistics D_{max} and D_+ are not the same, their behavior in general terms is similar and the results of the above analysis apply in a general way to D_{max}. This was demonstrated by Monte Carlo additions of random noise (p = 0.05 km/s) to actual V_p samples containing 19 to 160 measurements from Bloody Canyon. Values of Δ and s for the samples ranged from 0.0 to 0.37 km/s and from 0.29 to 0.47 km/s respectively. The simulated measurement errors added to 11 pairs of samples (100 iterations for each) resulted in changes in D_{max} averaging -0.006 and changes in D_+ averaging 0.003. Standard deviations of D_{max} and D_+ averaged 0.019 and 0.015 respectively but were proportional to the size of the samples according to $0.026-0.00020\ n_1n_2/(n_1+n_2)$, with a correlation coefficient of -0.827. There was no significant difference between the distributions of D_{max} and D_+, so they seemed to be similarly affected. This relationship predicts that the standard deviation for D_+ if p = 0.05 and $n_1 = n_2 = 90$ would be

0.017, which is within and close to the limit of 0.019 deduced for the same situation above.

It may be concluded that sensitivity of the test statistic to measurement precision is similar for the Student t-test and the Kolmogorov-Smirnov test. In each case, for realistic ratios of p and s, fractional changes in the test statistics t, D_+, and D_{max} are similar and are minor compared to the variability caused by idosynsyncratic differences in random samples of data from the same population. Thus the statistics based on the measured V_p data are probably representative of those based on hypothetical perfectly precise data. For the purposes of this study age discrimination of geologic deposits will be based on tests of measurements uncompensated for random measurement errors.

Use of Student's t-test on groups of samples

If sufficient samples are available, it is reasonable to test the distributions of the sample means rather than the distributions of the grouped samples. The central limit theorem states that the means, even of non-normal distributions, will themselves be normally distributed. Thus Student's t-test may be used with groups in circumstances when it may not be used with individual samples. However, before applying Student's t-test it is necessary to establish that the samples composing each group are themselves from the same population. This is done by analysis of variance, which is the topic of the next section.

Analysis of Variance

The analysis of variance commonly employed is Fisher's F-test (cf. Griffiths, 1967). This test makes three assumptions: (1) sampling

is random; (2) the sampled populations are normal; and (3) the variances of the populations are equal. I have used a sampling scheme in which sites are not random but in which boulders within sites are selected without bias with respect to their weathering characteristics. Testing showed that the Markov property, which should accompany certain kinds of bias, was absent. The other two assumptions must be verified by testing. Normality testing has been described in the previous section. Two tests are used to verify homogeneity of variance (cf. Till, 1974): These are Hartley's maximum-F test, which explores the hypothesis that the variances of the sampled populations are the same; and Cochran's test, which is designed to guard against one population variance being much larger than the others. If the above tests are satisfied, the F-test may be applied. If one or more tests cannot be satisfied, then a non-parametric analysis of variance must be employed.

In this study, Fisher's Method of Randomization was used when the F-test was inappropriate. In this method, data are grouped by sample into columns and ordered within the column according to the sequence in which they were measured. Several columns constitute a matrix, and if the samples truly represent the same population then all the data within a row may be be reordered randomly without greatly changing the value of a statistic:

$$F^{*} = \frac{\sum_{i=1}^{c} n_i(\bar{x}_i - \bar{\bar{x}})^2}{(c-1)} \left(\frac{\sum_{i=1}^{c} \sum_{j=1}^{n_i} (x_{ij} - \bar{x}_i)^2}{\sum_{i=1}^{c} (n_i - 1)} \right)^{-1} \qquad (8)$$

where c is the number of columns, n_i is the measurements in sample i, $\bar{x}_i$ is the mean of the measurements in sample i, $\bar{\bar{x}}$ is the grand mean, and x_{ij} is the jth measurement in sample i (cf. Bradley, 1968). The statistic

F calculated for the data as originally ordered is compared to a distribution of values of F^* found for different random rearrangements of the data within rows. If F^* is larger than 90% of the values found for the randomized matrix, then with that confidence the set of samples can be assumed to be from different populations. Any non-random structure within the matrix will lead to a large value of F^* compared to values for the randomized data.

This method is elegant and simple, provided there is access to a computer. In this study, 500 randomizations were used to generate the baseline distribution. This must be done anew for each test of different samples.

3.5 APPLICATION OF THE ACOUSTIC WAVE-SPEED RELATIVE DATING TECHNIQUE IN TWO TEST AREAS

To demonstrate the effectiveness of acoustic wave speeds as a basis for relative dating, the technique was tested on glacial moraines from two valleys in the northern Sierra Nevada (Fig. 3-1). These valleys were chosen because they had been previously mapped by Quaternary geologists (Sharp and Birman, 1963; Sharp, 1972; Burke and Birkeland; 1979) and appeared to be well understood. In each valley, the moraines protruded well beyond the mountain front. Sample sites on these moraines were free from rockfalls which might result in contamination of the sample by boulders of different degrees of weathering. Also, microclimatological variations among the sites of one valley were minimized by working away from the steep gradients and deep canyons of the mountains themselves. Thus conditions seemed favorable to testing the acoustic wave-speed relative dating technique.

Acoustic wave speeds were measured in 1406 boulders distributed among 59 sites. This large number of sites was chosen to allow tests for homogeneity of data within groups of sites from a single moraine to contrast with differences found among different groups. Four or five sites of twenty or thirty boulders each can be measured in a day; thus this test took about two weeks.

In addition to acoustic wave speeds, several conventional relative weathering parameters were measured, as discussed in Chapter 2. Because these data were redundant with those published by earlier researchers, they are not reproduced in their entirety here and are cited only when they substantially clarify some aspect of the geology or some characteristic of the V_p data.

Bloody Canyon

Bloody Canyon is the drainage of Walker Creek, whose headwaters are just east of Mono Pass on the crest of the Sierra Nevada. Walker Creek emerges from the mountain at about 2450 m and empties into Mono Lake. The bedrock geology was mapped by Kistler (1966); discussions and maps of the Quaternary geology are found in McGee (1885), Russell (1889), Kesseli (1941), Putnam (1949), Sharp and Birman (1963), and Burke and Birkeland (1979). Among the intrusive rocks in the canyon, only the quartz monzonite of Lee Vining Canyon is widely exposed (Fig. 3-13). A major aplitic zone within this pluton is found on the floor of the canyon and on its northern wall. This quartz monzonite was the only rock measured in this study. A large moraine complex containing boulders of the quartz monzonite is found east of the Sierra Nevada but above 2130 m elevation. The most

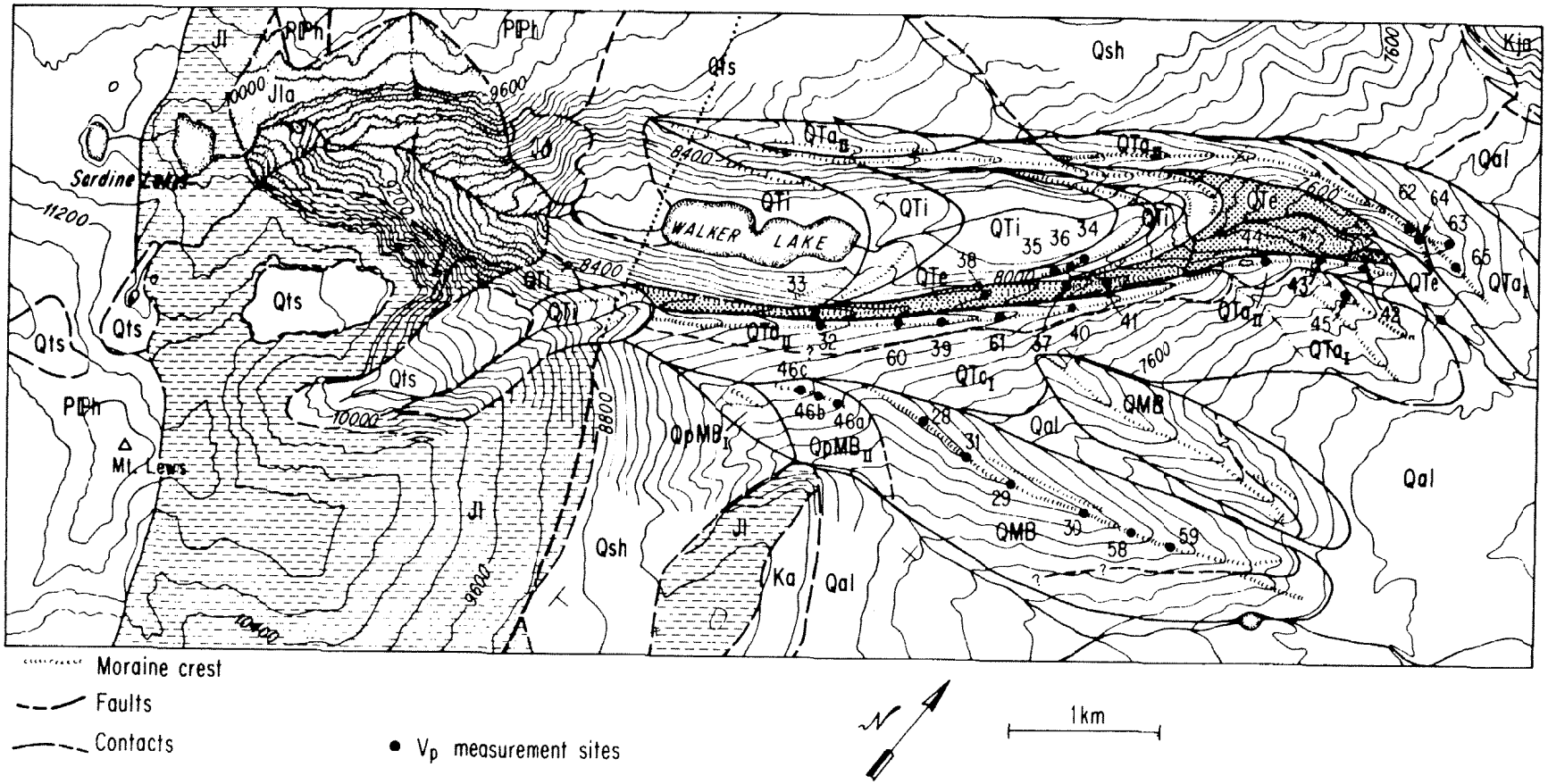

Fig. 3-13. Geologic map of Bloody Canyon, showing the V_p sites. Bedrock geology is after Kistler (1966). Quaternary geology of the glacial moraines is modified from Sharp and Birman (1963). For an explanation of the geological units, see next page.

Fig. 3-13 (continued) Geology of Bloody Canyon.

Quaternary deposits:

Qal..... alluvium (Holocene and late Pleistocene)
Qts..... talus, slopewash, and undifferentiated till (largely Holocene)
QTi..... Tioga till
QTe..... Tenaya till
QTa_{II}..... Tahoe till
QTa_{I}..... older Tahoe or Mono Basin till
QMB..... Mono Basin till
$QpMB_{II}$.... younger pre-Mono Basin till
$QpMB_{I}$..... older pre-Mono Basin till
Qsh..... Sherwin till

Mesozoic plutonic rocks:

Ka..... quartz monzonite of aeolian buttes (Cretaceous)
KJa..... alaskite of Wiliam's Butte (Cretaceous? or Jurassic?)
Jl..... quartz monzonite of Lee Vining Canyon (Jurassic)
Jla..... garnet-bearing aplite (Jurassic)
Jd..... diorite of Bloody Canyon

Paleozoic metamorphic rocks:

P Ph..... quartzo-feldspathic hornfels, calc-silicate hornfels, and carbonaceous marble (Pennsylvanian? or Permian?)
SOm..... marble and calc-silicate hornfels (Silurian? or Ordivician?)
SOq..... biotite-bearing quartzite (Silurian? or Ordivician?)

distinctive feature of the moraine complex is the ancient pair of lateral moraines protruding obliquely from under the younger moraines. The trough of the ancient glacier between these moraines is called Sawmill Canyon (not to be confused with Sawmill Canyon in Inyo County). This is the type location of the Mono Basin till. Sharp and Birman (1963) concluded that because of the weathering characteristics of the boulders, the subdued character of the broad, rounded moraines, and the different paths of the glaciers, the Mono Basin till significantly predated the early Wisconsin (Tahoe) till which buries it.

Clark (1972) attributed to normal faulting the 60-m difference in the elevations of the crests of the Tahoe and Mono Basin moraines, and argued that such an offset required a long time between glaciations.

Burke and Birkeland (1979) felt that relative weathering data did not justify separating the Mono Basin from the Tahoe moraines. They pointed out that the change in course of the glacier did not require a retreat of the glacier to the cirques, and that it could have occurred within a single glacial period. They speculated that the weathering differences between the Mono Basin and Tahoe moraines arose because of vegetative differences. (The Mono Basin moraines are covered by sage with some mahogany; the main crest of the Tahoe moraine is covered by pines and mahogany.) In particular, they identified spalling of weathered rinds during forest fires as a mechanism for selectively "freshening" boulders from the forested Tahoe moraine. Near the snout of the Tahoe moraine, sage covers the till; here the weathering characteristics were indistinguishable from those on the Mono Basin moraine. Geologic interpretations of these moraines by Sharp and Birman (1963) and by Burke and Birkeland (1979) are contrasted in Fig. 3-14.

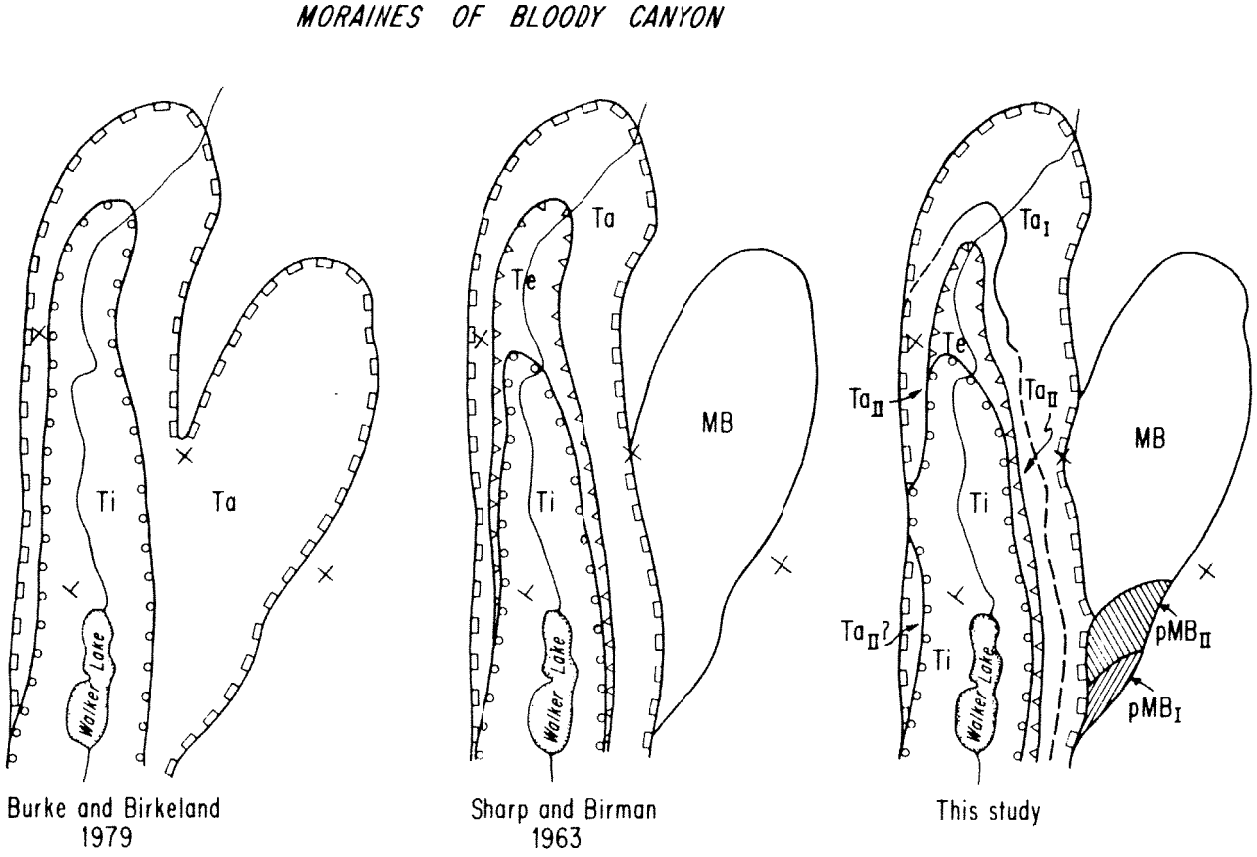

Fig. 3-14. Comparison of different interpretations of the glacial advances represented by moraines at Bloody Canyon. Burke and Birkeland recognized only two ages: Tioga (Ti) and Tahoe (Ta). The Tenaya (Te) moraines of Sharp and Birman were included with the Tioga moraines. In this study, the basic interpretation of Sharp and Birman was supported. Additionally, the Tahoe glaciation was divided into two advances, and two ancient pre-Mono Basin moraines (pMB_I and pMB_{II}) were recognized.

Burke and Birkeland (1979) felt that relative weathering data gathered at Bloody Canyon and elsewhere in the Sierra Nevada were insufficent to discriminate reliably more than two post-Sherwin glaciations; these they identified as the Tahoe and Tioga advances of the Wisconsin glaciation. In Bloody Canyon they assigned the moraines mapped as Tenaya in age by Sharp and Birman to the Tioga advance.

In preparation for gathering V_p data, I reexamined the moraines of Bloody Canyon. The entire crests of all moraines south of Walker Creek were walked. Traverses normal to the crests were made at intervals. Crests of the left-lateral moraines were walked as far west as the terminus of the Tioga moraines of Sharp and Birman (1963). The remainder of the left-lateral moraines were studied on aerial photographs only. The goal of this effort was to establish sites in an efficient manner to test the interpretations of the earlier researchers.

A generalized map of the moraines is shown in Fig. 3-14, along with the equivalent maps of Sharp and Birman (1963) and of Burke and Birkeland (1979). It is basically the same as the map of Sharp and Birman, with four exceptions: (1) the left-lateral Tioga moraine overlaps the Tahoe moraine at one point; (2) the Tenaya terminal moraine is farther west than mapped by Sharp and Birman; (3) the main moraine consists of two recognizable ages of till, called here Tahoe I and Tahoe II; and (4) remnants of two different pre-Mono Basin moraines were found south of the right-lateral Mono Basin moraine. The overlap of the left-lateral Tioga moraines was seen on aerial photographs only; it was not verified in the field. Because no sites were established this far west on the left-lateral moraine, this discrepancy is of little importance to the testing of V_p data. The other three differences are important and are discussed below.

The Tenaya terminal moraine

The eastern end of the main (Tahoe) right-lateral moraine is clearly buried by younger till. The outer flanks of the moraine are deeply gullied. The major ravine is not through-going, its head having been buried by the younger till. The older moraine is sandy and has few exposed boulders, but those which are found generally have more highly developed case-hardened surfaces then boulders found on the main crest. At about 2340 m (7680 ft) elevation, the overlapping crests of the two moraines diverge. Sharp and Birman mapped the younger moraine as Tenaya in age; Burke and Birkeland felt it was Tioga in age. From my studies it seems to be neither. The contact between the two tills on the outer flank of the moraine is found along the entire length of the moraine, not just near its eastern end. The Tenaya moraine of Sharp and Birman is separated from the Tahoe moraine by a deep fosse over most of this distance. Thus the till capping the Tahoe moraine is from an earlier and previously unrecognized Tenaya glacial advance, or it was left by a late Tahoe glacier.

Weathering data support this latter alternative. Figure 3-15a shows the distribution of granodiorite weathering ratios (GWR) and boulder relief ratios for the sites of Bloody Canyon. The fraction of boulders which were heavily weathered is displayed on the abscissa; the fraction which were deeply buried is displayed on the ordinate. The data form two clusters. Data from Tahoe and pre-Tahoe moraines are readily separated from data from Tenaya and Tioga moraines. As expected, older tills appear to contain more heavily weathered and deeply buried boulders than younger tills. Sites 40, 42, 43, and 44 lie on the disputed moraine (Fig. 3-13). Boulders from these sites appear to be more heavily weathered and deeply buried than boulders from the Tenaya moraine (sites 33, 37, 38, and 41), and thus appear to be

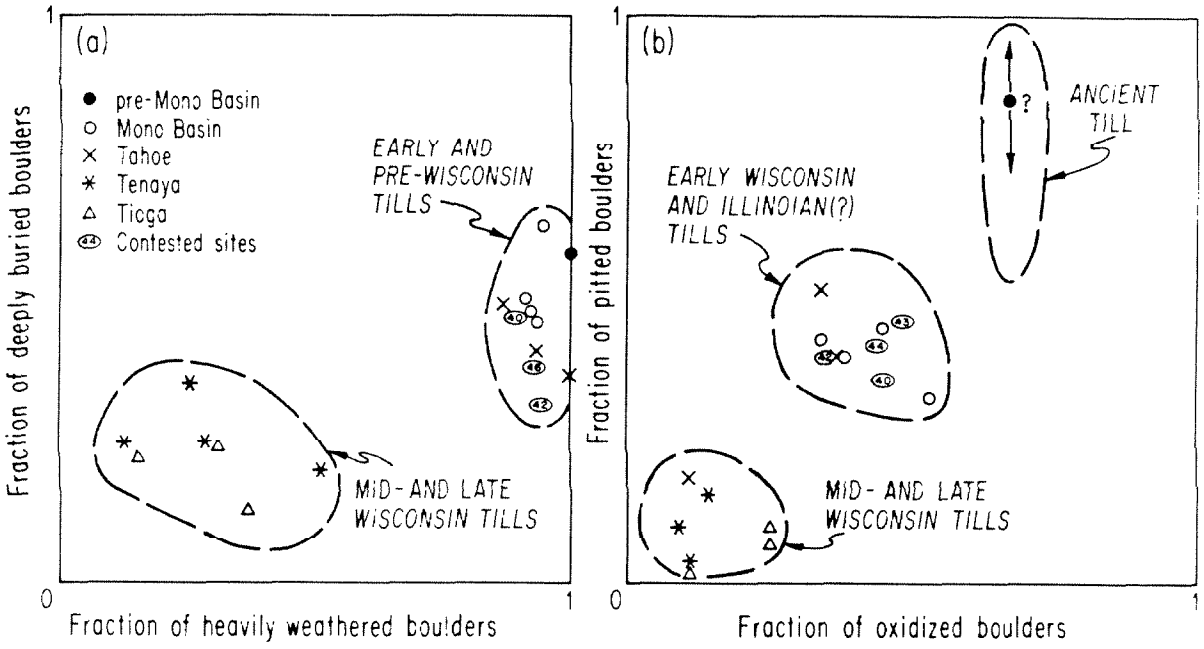

Fig. 3-15. Summary of some conventional relative weathering data for tills of Bloody Canyon. Site numbers are those of Fig. 3-13. Age designations are those of this study.

a) In old tills (early Wisconsin and pre-Wisconsin) a high fraction of boulders are heavily weathered (GWR class 3; see Ch. 2). About half the boulders on crests of the old moraines are deeply buried, so that they protrude above the surface less than a quarter of their diameters (BR class 3; see Ch. 2). Crests of young moraines are characterized by unweathered boulders which are less deeply buried. In the figure, data show an orderly progression away from the origin with increasing age of the moraine. Tioga and Tenaya moraines appear to be of similar age, based on these two weathering characteristics. All older tills plot in a second distinct cluster. Contested sites plot within this cluster and thus are probably Tahoe rather than Tenaya in age.

b) Different weathering characteristics - the fraction of boulders which have pitted surfaces and the fraction which have surfaces discolored by oxidation - also support the grouping of Tioga and Tenaya tills. As in (a), young tills should plot near the origin and old tills should plot away from the origin. One Tahoe site (32) plotted in the Tioga-Tenaya cluster. This sites was anomalous on other grounds. As in (a), the contested sites seemed to be too weathered to be considered Tenaya in age. The pre-Mono Basin site appeared to be distinct in this diagram.

older. They cannot be separated from the sites on the uncontested Tahoe moraine (sites 32, 39, and 45) and thus seem to be of equivalent age. In Fig. 3-15b the the ratios of oxidized vs. non-oxidized and pitted vs. non-pitted boulders (as defined in Chapter 2) are displayed for sites in Bloody Canyon. Both oxidation and pitting of boulders are expected to become more common as a deposit ages. The data clearly fall into three non-overlapping classes. In the first class are sites from the Tenaya and Tioga moraines (mid- and late-Wisconsin tills). Few boulders from these sites were either pitted or oxidized. In the second class are sites from the Tahoe and Mono Basin moraines (early Wisconsin and Illinoian (?) tills). About one third of the boulders from these sites are oxidized or pitted or both. The third class consists of a single site from the pre-Mono Basin moraine. About two thirds of the boulders were oxidized. Counts of pitting were not made, but by estimate in the field more than half of the boulders were pitted.

Data from all four sites on the contested moraine (Tenaya or Tahoe) plotted in the second cluster. Boulders from one site (32) on the main Tahoe moraine were exceptionally unoxidized and unpitted; data from this site plotted in the late Wisconsin cluster, and it is possible that this single site had an anomalous history. However, no data from young moraines plotted near the second cluster, and it must be concluded that till sampled at the contested sites was significantly more weathered than till of Tenaya age.

The data presented above suggest that the terminal moraine of the Tenaya sequence of Sharp and Birman (1963) is best assigned to the Tahoe glaciation.

Two ages of Tahoe till

The extensive contact between tills of two different weathering characteristics found on the outer flank of the Tahoe moraine shows that this moraine is composite. However, it was probably built in its entirety after the Mono Basin moraines were deposited. This does not rule out the possibility that especially the older Tahoe till was deposited only shortly after the Mono Basin moraine, and indeed the obvious character of the contact within the main Tahoe moraine does suggest a long time between deposition of the two tills of the Tahoe moraine. In this study, both are regarded as Tahoe in age, but this contention was one of the main hypotheses to be tested by the V_p method of relative dating.

Pre-Mono Basin moraines

Remnants of two ancient moraines are found south of the right-lateral Mono Basin moraine, near its junction with the Tahoe moraine. Shallow swales separate these moraines from each other and from the larger Mono Basin moraine. The outermost moraine is largely devoid of exposed boulders (BR class 1), and it was not possible to establish a V_p site there. The absence of boulders indicates great age, and certainly this moraine is pre-Wisconsin. The younger of the two moraines contains exposed boulders, but these are heavily weathered and oxidized (Fig. 3-15b). Furthermore, the fraction of boulders which were aplitic was 0.69, over twice the largest fraction found on the Mono Basin moraine (0.29). This alone suggests the significant passage of time between deposition of the two tills.

Acoustic wave-speed data

V_p data were taken to test the geologic interpretation presented in Fig. 3-13. Twenty-seven sites were distributed over the moraines as shown

in Fig. 3-13. All but four were south of Walker Creek. At two additional sites (42 and 44) relative weathering data but no V_p data were taken.

Measured wave speeds are summarized in Table 3-1. The vegetative cover is identified by the dominant community. In the pine forests the underbrush is generally sparse. Mahogany is interspersed with sage and pinõn pines. Areas identified as sage-covered were free of trees. Wave speeds were measured for 603 boulders at the 27 sites. Sample sizes ranged from 15 to 30 boulders. Running mean speeds and standard deviations converged to stable values within 15 boulders, and sample sizes were reduced during the course of field work so that additional sites could be included. Wave speeds are summarized by their means ($\overline{V_p}$) and standard deviations (s). Values of $\overline{V_p}$ varied from 1.09 km/s to 2.26 km/s and values of s ranged from 0.17 km/s to 0.54 km/s. $\overline{V_p}$ decreased with the age of the moraine, but s showed no obvious trends.

The V_p data were tested to determine whether samples were from normal populations. The Kolmogorov-Smirnov statistic D_{max} for each sample and the confidence C_{NL} with which the hypothesis H_o (that normal populations were sampled) may be rejected are given in Table 3-1 for each site. At least one sample from each age group had a value of C_{NL} greater than 90%, and a disproportionate number of samples seemed to have high values of C_{NL}. This is illustrated in Fig. 3-16, which compares the actual cumulative distribution of C_{NL} to the ideal for an infinite number of samples from a normal population. The actual cumulative distribution is the step function in Fig. 3-16; the ideal cumulative distribution is the line ("n = ∞"). Limits which will enclose 90% and 99% of the cumulative distributions of C_{NL} for groups of 27 samples of normal populations are also shown, as light lines parallel to the ideal distribution. The

Table 3-1

Summary of Acoustic Wave-Speed Data for Moraines of Bloody Canyon

Site[1]	Glacial Advance[2] This Study	Sharp & Birman 1963	Burke and Birkeland 1979	Vegetation[3]	$\overline{V_p}$ km/s	s km/s	No. of Boulders	D_{max}[4]	C_{NL}[5] %
34	Ti	Ti	Ti	M	2.261	0.433	15	0.180	76
35	Ti	Ti	Ti	M	2.120	0.539	18	0.231	99
36	Ti	Ti	Ti	M	2.017	0.398	16	0.116	20
33	Te	Te	Ti	M	1.894	0.324	21	0.149	74
37	Te	Te	Ti	M,P,S	1.636	0.349	17	0.214	95
38	Te	Te	Ti	M	1.817	0.275	15	0.256	98
41	Te	Te	Ti	M	1.749	0.243	16	0.187	88
32	Ta_{II}	Ta	Ta	P	1.406	0.279	20	0.137	61
60	Ta_{II}	Ta	Ta	P	1.520	0.479	30	0.083	15
39	Ta_{II}	Ta	Ta	M,S	1.772	0.473	20	0.125	54
61	Ta_{II}	Ta	Ta	M,S	1.673	0.525	30	0.108	52
40	Ta_{II}	Te	Ti	M,P,S	1.655	0.319	21	0.124	45
43	Ta_{II}	Te	Ti	M,S	1.623	0.430	20	0.167	86
62-L	Ta_{II}	Ta	Ta	S	1.549	0.444	29	0.101	38
64-L	Ta_{II}	Ta	Ta	S	1.628	0.492	28	0.093	28
63-L	Ta_{I}	Ta	Ta	S	1.511	0.406	30	0.120	68
65-L	Ta_{I}	Ta	Ta	S	1.441	0.420	30	0.082	8
45	Ta_{I}	Ta	Ta	S	1.384	0.412	19	0.125	44
28	MB	MB	Ta	S	1.305	0.443	29	0.162	95
29	MB	MB	Ta	S	1.164	0.467	20	0.250	>99
30	MB	MB	Ta	S	1.482	0.389	21	0.150	75
31	MB	MB	Ta	M	1.313	0.413	20	0.132	55
58	MB	MB	Ta	S	1.512	0.459	29	0.142	88
59	MB	MB	Ta	S	1.461	0.497	30	0.181	>99
46a	pMB	MB	Ta	S	1.229	0.289	20	0.154	77
46b	pMB	MB	Ta	S	1.113	0.355	19	0.178	91
46c	pMB	MB	Ta	S	1.086	0.169	20	0.137	61

1 Locations of sites are shown in Fig. 3-3. "L" denotes a site on a left-lateral moraine

2 Ti denotes the Tioga advance
Te denotes the Tenaya advance
Ta_I *and* Ta_{II} *denote early and late stades of the Tahoe glaciation*
MB denotes the Mono Basin advance (Sharp and Birman, 1963)
pMB denotes a pre-Mono Basin glacial advance

3 S... sage; M... mountain mohogany; P... pines

4 Kolmogorov-Smirnov statistic comparing sample to a normal population having the same mean wave speed $\overline{V_p}$ and standard deviation s.

5 C_{NL} is the confidence that the sampled population could not have been normally distributed.

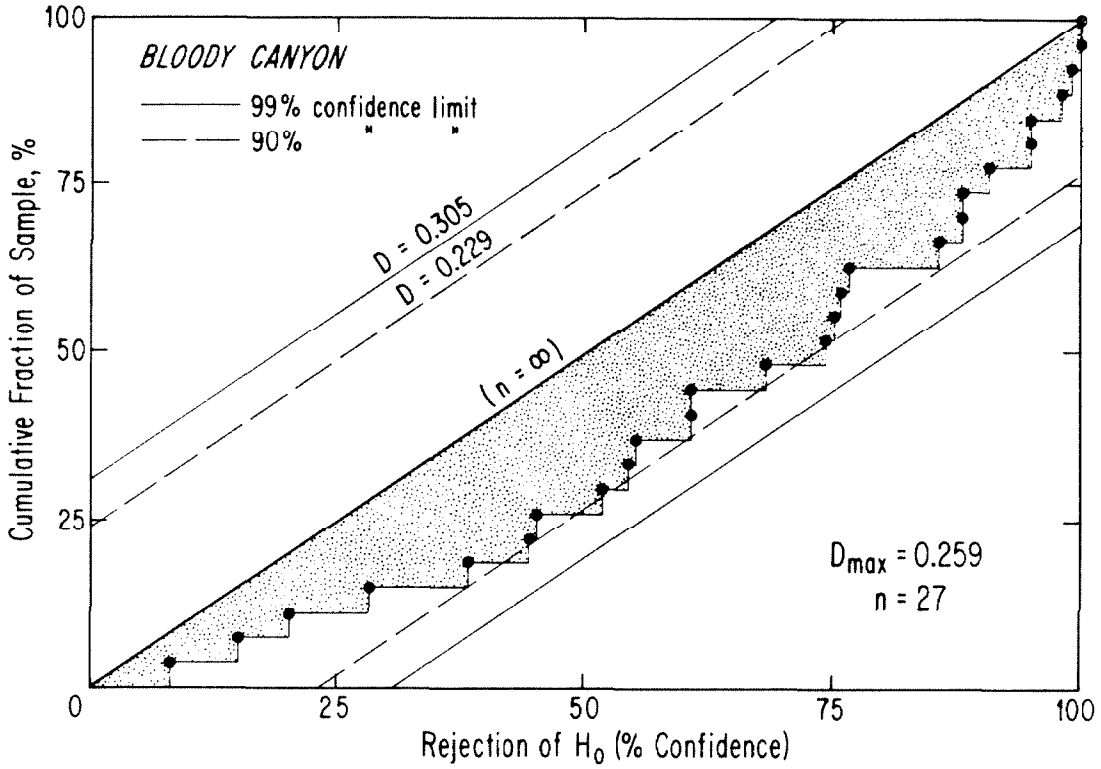

Fig. 3-16. The cumulative distribution of values of C_{NL} (the confidence with which H_0 can be rejected) for 27 sites of V_p measurements on moraines at Bloody Canyon. A disproportionate number of sites have high values of C_{NL}. By definition, the probability density for an infinite number of samples from a normal population is constant and independent of C_{NL}. The cumulative function is thus a straight line as shown ("n = ∞") if the ordinate scale is linear. For finite numbers of samples, the cumulative distribution will deviate from this ideal. Tolerances within which will lie 90% or 99% of the cumulative distribution functions of all groups of 27 samples are shown by light dashed and solid lines, respectively. The actual cumulative distribution function for Bloody Canyon sites is marked by filled circles; the difference between this function and the ideal line (stippled) equals or exceeds the 90% limit at eight locations. D_{max}, 0.259, corresponds to a confidence of about 94% that the sampled populations were not normally distributed.

ordinate-wise difference between the actual and ideal cumulative distributions equals or exceeds the 90% confidence limit at eight points. The maximum difference (D_{max}) is 0.259 and allows us to reject H_o with about 95% confidence. Consequently, acoustic wave speeds from Bloody Canyon do not appear to be normally distributed.

Inspection of Table 3-1 shows that most of the high values of C_{NL} were found for the sites on the pre-Wisconsin moraines. For only two of these nine sites was C_{NL} less than 75%, but by chance six or seven such sites should have been found. If sites on the pre-Wisconsin and the Wisconsin moraines are tested separately, D_{max} of 0.527 (9 sites) and 0.162 (18 sites) are found, respectively. These correspond to values of C_{NL} of more than 99% and much less than 90%, respectively. Thus only the samples from the older moraines are not from normal populations.

Two conclusions follow from the above discussion: (1) non-parametric tests of similarity and analysis of variance must be used on data for the pre-Wisconsin moraines; and (2) there is some fundamental difference between the older and younger populations of boulders. The most reasonable explanation of the second conclusion is that weathering somehow acts to exaggerate or create differences in V_p for different boulders. This possibility will be discussed later.

Grouping of sites . . .

Data were gathered at several sites distributed over each moraine to enable comparison between differences in V_p within individual tills and differences among tills. V_p data were then grouped according to the major age subdivisions of moraines. The cumulative distribution functions for these groups are shown in Fig. 3-17a. These are drawn on a probability

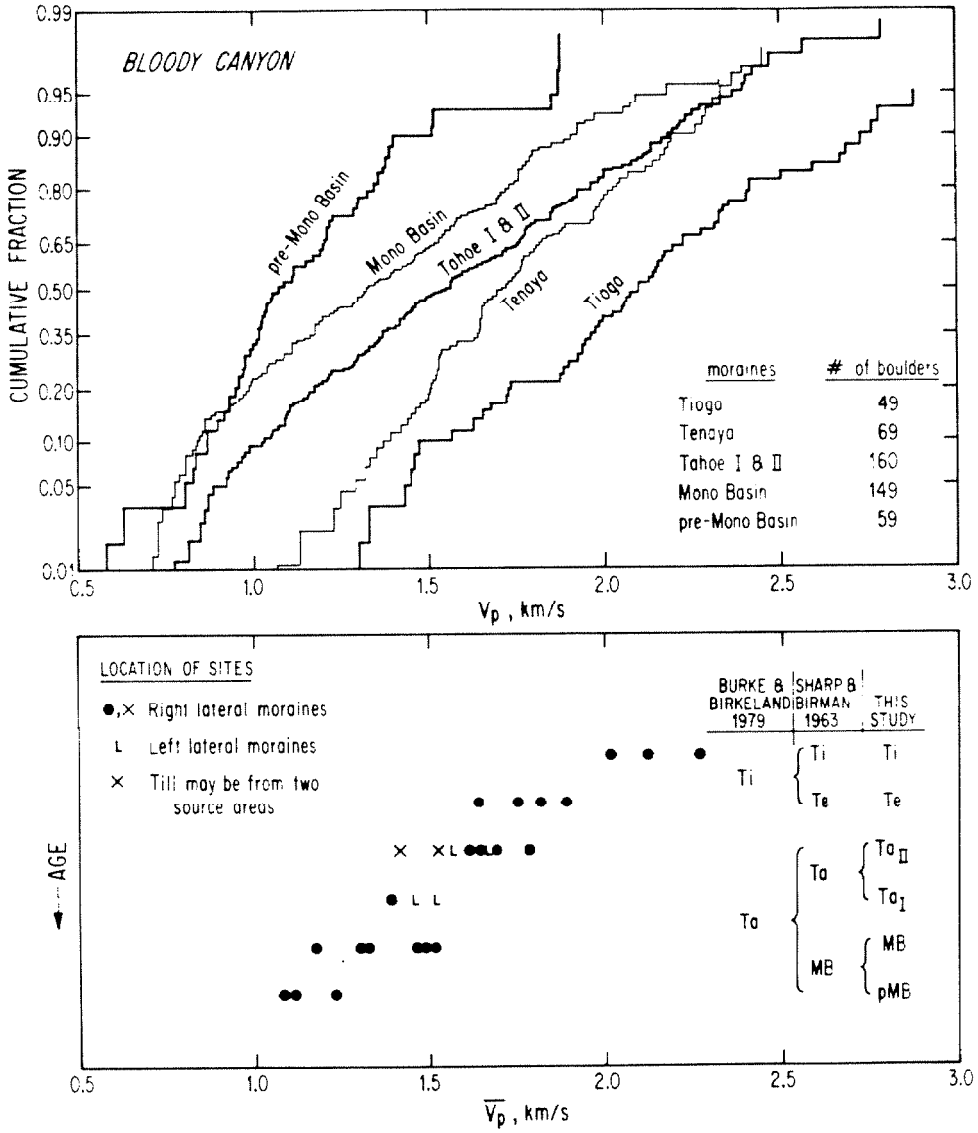

Fig. 3-17. Grouped V_p data for moraines of Bloody Canyon.

a) Cumulative distribution functions for V_p data from sites on right lateral moraines, grouped according to the age interpretations of this study. Tahoe I and Tahoe II groups were combined. The ordinate is non-linear (probability grid) so that cumulative distributions of normal populations are straight lines. In general, V_p decreases with increasing age. Oldest groups appear to have non-linear distributions and are non-normal.

b) Mean wave speeds $\overline{V_p}$ for all sites are shown as a function of their assigned ages. Although there is considerable overlap between groups, the group distributions are in general separable by statistical tests.

grid so that the cumulative distributions of normal populations plot as straight lines. Two observations are significant: (1) in general the values of V_p are lowest for boulders from the older tills; and (2) the cumulative functions for the three oldest tills are decidedly non-linear. In all three cases the curves are steeper for low values of V_p and, especially for the pre-Mono Basin data, the cumulative distribution seems to consist of two linear segments. This would be consistent with a bimodal population of V_p or with an asymmetric population skewed towards low values of V_p.

Although the cumulative distributions of the pre-Mono Basin and the Mono Basin data overlap for low values of V_p, the distributions are visually separable because the highest values of V_p for the older till are much less than the highest values for the Mono Basin till. This tendency is sufficient to reduce $\overline{V_p}$ for the pre-Mono Basin till compared to $\overline{V_p}$ for the Mono Basin till.

Values of $\overline{V_p}$ for each site are plotted in Fig. 3-17b, grouped according to the interpretation of moraine ages used in this study. The corresponding age assignments of Sharp and Birman (1963) and Burke and Birkeland (1979) are shown for reference. Although the values of $\overline{V_p}$ overlap considerably between groups, there is nevertheless a pronounced decrease in $\overline{V_p}$ with assigned age, which may be taken to show an increase in weathering. These data are amplified in Table 3-2, in which they are grouped according to the age assignments of: (a) this study; (b) Sharp and Birman (1963); and (c) Burke and Birkeland (1979). The means and standard deviations ($\overline{V_p}$ and and s) of the grouped speeds (V_p) are reported, along with the means and and standard deviations ($\overline{\overline{V_p}}$ and $s(\overline{V_p})$ of the mean speeds ($\overline{V_p}$) for sites within the groups. In each of the three groups, the group mean speeds $\overline{V_p}$ and $\overline{\overline{V_p}}$ decrease with age. Clearly the two groups of Burke and Birkeland are readily discriminated, but the consistent trend in $\overline{V_p}$ or $\overline{\overline{V_p}}$ for finer

Table 3-2

Summary of Acoustic Wave-Speed Data for Right-Lateral Moraines of Bloody Canyon

a) Sites grouped according to this study

Group	No. of Sites	No. of Boulders	Distribution of V_p		Distribution of $\overline{V_p}$	
			$\overline{V_p}$ km/s	s km/s	$\overline{\overline{V_p}}$ km/s	$s(\overline{V_p})$ km/s
Tioga	3	49	2.130	0.466	-	-
Tenaya	4	69	1.780	0.313	1.775	0.107
Tahoe II	6	141	1.607	0.445	1.608	0.128
Tahoe I	1	19	1.384	0.412	-	-
Mono Basin	6	149	1.384	0.458	1.373	0.135
pre-Mono Basin	3	59	1.144	0.283	-	-

b) Sites grouped according to Sharp and Birman (1963)

Group	No. of Sites	No. of Boulders	Distribution of V_p		Distribution of $\overline{V_p}$	
			$\overline{V_p}$ km/s	s km/s	$\overline{\overline{V_p}}$ km/s	$s(\overline{V_p})$ km/s
Tioga	3	49	2.130	0.466	-	-
Tenaya	6	110	1.728	0.340	1.729	0.110
Tahoe	5	119	1.560	0.467	1.551	0.169
Mono Basin	9	208	1.316	0.429	1.296	0.161

c) Sites grouped according to Burke and Birkeland (1979)

Group	No. of Sites	No. of Boulders	Distribution of V_p		Distribution of $\overline{V_p}$	
			$\overline{V_p}$ km/s	s km/s	$\overline{\overline{V_p}}$ km/s	$s(\overline{V_p})$ km/s
Tioga	9	159	1.851	0.425	1.864	0.228
Tahoe	14	327	1.406	0.460	1.387	0.202

subdivisions of data suggests that they have grouped data which are truly separable. The extent to which the smaller differences among the groups of this study (or of Sharp and Birman) are significant must be established by statistical testing.

Statistical testing of V_p data from Bloody Canyon . . .

The first step in statistical testing was to determine whether grouped data were drawn from the same population. If this cannot be demonstrated, then there is no basis for comparison between groups of data, and comparisons must be made on a site-to-site level. Because samples from the older tills were not from normally distributed populations, Fisher's method of randomization was used in the analysis of variance. For groups of data from younger tills, this was augmented by the conventional F-test.

If grouped samples were from the same normally distributed population, then Student's t-test could be used to compare groups. If samples were not from normally distributed populations, or if grouped data were not demonstrably from the same population, it was necessary to regroup data or to test the grouped data for normality before using the t-test. If normality for the grouped data could not be demonstrated, groups were compared with the nonparametric Kolmogorov-Smirnov test.

Results of analyses of variance using Fisher's method of randomization are shown in Fig. 3-18. The distributions of values of the test statistic F* found by randomizing the data 500 times are shown as lines; values of F* for the data as acquired are shown by crosses. The fraction of randomizations yielding values of F* which were less than F^* for the data as acquired is read from the abscissa.

Curves in Fig. 3-18a refer to data grouped as in Fig. 3-16. Samples

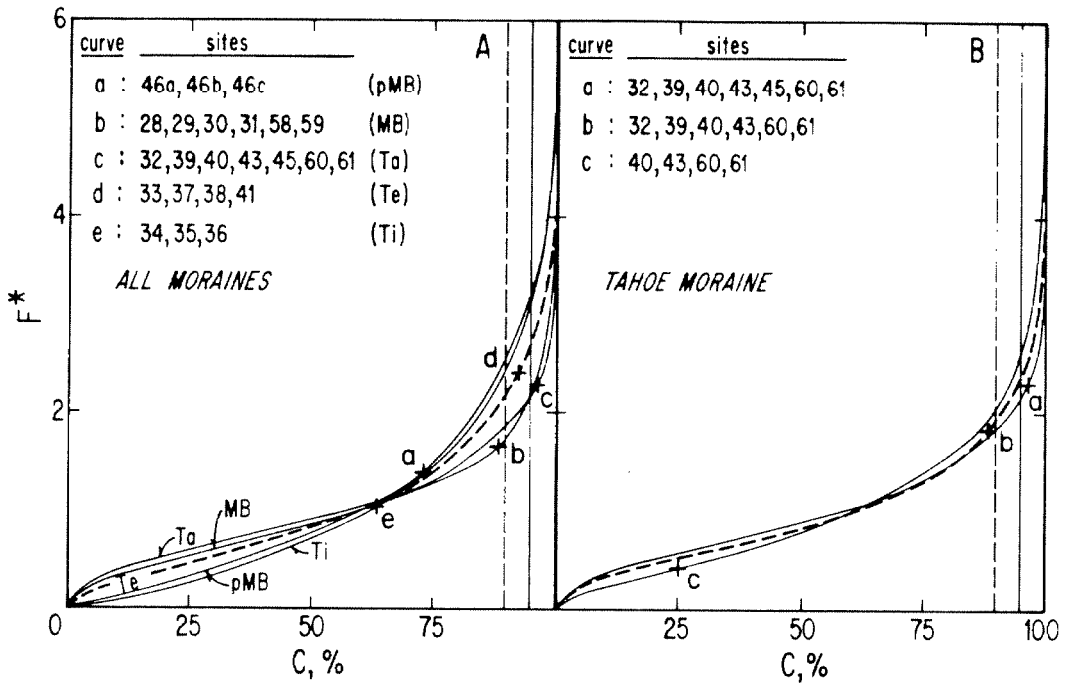

Fig. 3-18. Distributions of the F*-statistic found by Fisher's method of randomization for groups of samples of V_p data from right-lateral moraines of Bloody Canyon. Values of F* calculated for data as acquired are marked by "+". Abscissa is the confidence C with which the null hypothesis H_o may be rejected. H_o states that all samples were drawn from the same population. 90% and 95% confidence limits are marked by vertical light dashed and solid lines, respectively.

a) Pre-Mono Basin (pMB), Mono Basin (MB), and Tioga (Ti) groups appear to be homogeneous. H_o cannot be rejected with 90% confidence or more. The Tenaya (Te) group is probably heterogeneous, and there is a 96% chance that the Tahoe group is.

b) Removal of site 45, the only site from the Tahoe I moraine, reduces C to less than 90% for the Tahoe group. The remaining six sites are from the Tahoe II moraine, which may be homogeneous. Removal of two sites (32 and 39) thought to be anomalous further reduces C to 25%.

from the Tioga moraine are probably drawn from the same population; the hypothesis that they are can be rejected with only 63% confidence. Samples from the pre-Mono Basin moraine were likewise homogeneous. However, samples from the Mono Basin moraine gave an F* greater than 88% of the randomized values, and F* for data from the Tenaya moraine exceeded 90% of the randomized values. In this study, 90% was used as a cut-off level, so by this criterion the Mono Basin sites would be considered homogeneous while the Tenaya sites would be considered heterogeneous. Samples from the Tahoe moraine were heterogeneous at greater than 96% confidence.

For the analysis of variance test, site 45 from the older Tahoe moraine (Tahoe I) was included with the six sites from the younger right-lateral Tahoe moraine (Tahoe II). This could be a cause of heterogeneity. In Fig. 3-18b, the removal of site 45 from the Tahoe group is shown to reduce the confidence that the samples were from different populations, from over 96% (a)to 88% (b). Thus the Tahoe II sites are as homogeneous as (for example) the Mono Basin sites.

There is some independent evidence to suggest that the Tahoe II sites are not truly homogeneous. In Fig. 3-15b site 32 plotted within the cluster of later Wisconsin sites and was well-separated from other Tahoe sites, based on the fractions of oxidized and pitted boulders. In Table 3-1 the value of $\overline{V_p}$ for site 32 is seen to be much lower than other Tahoe II sites. These two observations are apparently contradictory, because in the first instance the rocks appear too young, while in the second they appear too old. This topic will be returned to later, but for now it is sufficient to mark the site as anomalous.

Site 32 was different from the other Tahoe II sites in that it was the closest to the mountains, and was located in a dense pine forest. A

second site (60) was established in the same pine forest between site 32 and site 39, which was located in mahogany and sage, to determine if the low $\overline{V_p}$ at site 32 was repeatable. The value of $\overline{V_p}$ was found to be intermediate to $\overline{V_p}$ at site 32 and at site 60, but still lower than $\overline{V_p}$ at other Tahoe II sites. Thus the anomalously low values of $\overline{V_p}$ seem to be localized geographically, either as a consequence of vegetative cover or, more probably, some other factor. If sites 32 and 60 are deleted from the Tahoe II group (case c in Fig. 3-18b) the value of F* is strikingly reduced such that only 25% of the values calculated for the randomized data are smaller.

Because inclusion of sites 32 and 60 in the Tahoe II group did not result in rejection (at 90% confidence or more) of the hypothesis that the samples were drawn from the same population, exclusion of these sites for inter-group comparisons is probably unwarranted.

Conventional analysis of variance using the F-test was attempted on groups of data from Wisconsin moraines. Results from these texts are summarized in Table 3-3. The data from sites on the Tioga moraine fulfilled the requirements for application of the F-test described in §3.4. The value of the F statistic was only 1.08, considerably less than the limit (F = 3.20) corresponding to 95% confidence that the samples were from different populations. Thus the F-test confirms the conclusion from Fisher's method of randomization.

The F-test applied to data from the Tenaya moraine indicated that these samples also were homogeneous. However, three of the four samples comprising the group appeared to be drawn from non-normal populations (Table 3-1), so the test may not be strictly applicable. Data from the Tahoe II group appeared to have greater differences among variances for the individual samples than expected (Hartley's test). Consequently,

Table 3-3

Analysis of Variance Using the F-Test for V_p Data From Bloody Canyon

Group	Sites	No. of Sites	No. of Boulders	Hartley's Test[1]	Cochran's Test[1]	Degrees of Freedom[2]	F-Test[3]
Tioga	34,35,36	3	49	1.83(3.25)	0.46(0.54)	16	F(2,46) = 1.08(3.20)
Tenaya	33,37,38,41	4	69	2.06(3.40)	0.34(0.41)	17	F(3,65) = 2.40(2.75)
Tahoe II	39,61,40,43	4	91	2.76(2.75)	0.35(0.37)	25	F(3,87) = 0.40(2.71)

1 95% confidence limits are shown in parentheses. If test statistic is less than this value, the group appears to be homoscedastic.

2 For Hartley's and Cochran's tests, the average number of measurements per site may be used for the degrees of freedom (cf. Till,1974).

3 The degrees of freedom are shown in parentheses following F (e.g., "F(2,46)"). The critical value of F for 95% confidence is shown in parentheses following the value of F (e.g., 1.08(3.20). If F is less than this limit, the samples tested appear to come from the same population.

Table 3-4

Tests for Normality of Groups of V_p from Bloody Canyon

				Chi-Square Test			Kolmogorov - Smirnov Test[1]	
Group	Sites	No. of Sites	No. of Boulders	χ^2	Degrees of Freedom	$C_{NL}{}^2$ %	D_{max}	$C_{NL}{}^2$ %
Tioga	34,35,36	3	49	5.6	6	53	0.077	30
Tenaya	33,37,38,41	4	69	17.1	10	93	0.124	>99
Tahoe	45,32,60,39, 61,40,43	7	160	30.9	28	65	0.056	-
Tahoe II	32,60,39,61, 40,43	6	141	28.8	24	75	0.070	-
Tahoe II	39,61,40,43	4	91	17.5	15	70	0.069	63
Mono Basin	28,29,30,31 58,59	6	149	32.1	26	81	0.065	-
pre-Mono Basin	46a,b,c	3	59	14.3	8	93	0.117	>95

1 Values of C_{NL} as a function of D_{max} were calculated for samples of up to 100 measurements (App. 3-A). For larger samples, χ^2 seems to be independent of cell boundaries and the χ^2 test is used in place of the Kolmogorov - Smirnov test.

2 C_{NL} is the confidence with which the hypothesis that the data were drawn from a normally distributed population may be rejected.

the F-test may not be applicable for this group, either. However, the F-statistic did not lead to a different conclusion than the method of randomization.

It should be concluded that at the 95% confidence level the hypothesis that samples within a group were drawn from the same population could not be rejected for any of the groups listed in Table 3-2a, although the group of all sites from the right-lateral Tahoe moraine (both Tahoe I and Tahoe II) did appear to be heterogeneous. The Tenaya group appeared to be heterogeneous with more than 90% confidence.

Were samples within a group drawn from a single normal population, the distribution of V_p for the grouped samples would necessarily be normal also. Since this condition was not clearly met for all groups, the group distributions were themselves tested for normality. Results from the Kolmogorov-Smirnov test are compared to results from the χ^2 test in Table 3-4. Only the Tenaya group and pre-Mono Basin group are drawn from mixed populations or were otherwise non-normal at more than 90% confidence. This rules out the use of Student's t-test in comparisons involving two groups.

Differences between groups of V_p data . . .

Differences between grouped V_p data were tested in three ways: (1) using the two-sample Kolmogorov - Smirnov test; (2) using Student's t-test; and (3) using Student's t-test on distributions of $\overline{V_p}$ for grouped samples rather than on distributions of V_p. As noted above, the t-test was inappropriate for comparisons involving distributions of V_p for the Tenaya or pre-Mono Basin groups.

Results of these tests for data grouped according to the age assignments of this study are presented in Table 3-5. Because the sequence of

Table 3-5

Differences Among V_p Data from Bloody Canyon Grouped According to This Study

Group	Tioga			Tenaya			Tahoe II(a)			Tahoe II(b)			Mono Basin			pre-Mono Basin			Tahoe I (left lateral)	
	K-S	$t(V_p)$	$t(\bar{V}_p)$	K-S	$t(V_p)$	$t(\bar{V}_p)$	K-S	$t(V_p)$	$t(\bar{V}_p)$	K-S	$t(V_p)$	$t(\bar{V}_p)$	K-S	$t(V_p)$	$t(\bar{V}_p)$	K-S	$t(V_p)$	$t(\bar{V}_p)$	K-S	$t(V_p)$
Tioga	D_+=0.44 D'=22.4 C >99%	t=4.84 df=116 C*>99%	t=4.03 df=5 C >99%	-	-	-	-	-	-	-	-	-	-	-	-	-	-	-	-	-
Tenaya	-	-	-	-	t=2.88 df=208 C*>99%	t=1.93 df=8 C=95%	D_+=0.20 D'=13.5 C >99%	t=1.57 df=158 C*=94%	t=1.52 df=6 C=91%	-	-	-	-	-	-	-	-	-	-	-
Tahoe (all)	-	t=-3.37 df=227 C*>99%	t=-2.39 df=9 C >99%	-	-	-	-	-	-	D_+=0.209 D'=10.5 C >99%	t=3.78 df=307 C>99%	t=2.40 df=11 C=98%	-	-	-	-	-	-	-	-
Tahoe I	-	-	-	D_-=0.238 D'=3.79 C =84%	t=-2.07 df=158 C=98%	-	D_-=0.304 D'=5.81 C =95%	t=-2.65 df=110 C>99%	-	D_-=0.119 D'=0.95 C =36%	t=0 df=166 C=50%	-	-	-	-	-	-	-	t=-.84 df=77 C**=60%
Tahoe II (b)	-	-	-	-	-	-	-	-	-	D_+=0.227 D'=14.9 C >99%	t=4.19 df=288 C>99%	t=3.09 df=10 C>99%	-	-	-	-	-	-	-	-
Mono Basin	-	-	-	-	-	-	-	-	-	-	-	-	D_+=0.341 D'=19.7 C >99%	t=3.73 df=204 C*>99%	t=2.69 df=7 C=98	-	-	-	-	-
Tahoe II (left lateral)	-	-	-	-	t=-.27 df=196 C**=21%	-	-	-	t=1.20 df=146 C**=77%	-	-	-	-	-	-	-	-	-	D_+=0.148 D'=2.56 C =71%	t=1.36 df=115 C=91%

Group	Sites
Tioga	34, 35, 36
Tenaya	33, 37, 38, 41
Tahoe (all)	45, 32, 60, 39, 61, 40, 43
Tahoe I	45
Tahoe II(a)	32, 60, 39, 61, 40, 43
Tahoe II(b)	39, 61, 40, 43
Tahoe I (left lateral)	63, 65
Mono Basin	28, 29, 30, 31, 58, 59
pre-Mono Basin	46a, 46b, 46c

K-S: Kolmogorov-Smirnov test (one-tailed). First row gives $D_+ = (\text{CDF(column)} - \text{CDF(row)})_{max}$ or $D_- = (\text{CDF(column)} - \text{CDF(row)})_{min}$, where CDF(column) is the cumulative V_p distribution for the group cited for the column and CDF(row) is the cumulative V_p distribution for the group cited for the row. The second parameter listed under "K-S" is $D' = 4D_+^2 n_1 n_2/(n_1 + n_2)$ or $D' = 4D_-^2 n_1 n_2/(n_1 + n_2)$ where n_1 and n_2 are the number of measurements in the two groups tested. For the one-tailed test, D' is distributed as χ^2 with two degrees of freedom. The third parameter C is the confidence with which the hypothesis that values of V_p for the row population (if D_+ is listed) or the column population (if D_- is listed) are not the greater may be rejected.

t: Student's t-test ($t(V_p)$. . . test of distributions of V_p; $t(\bar{V}_p)$. . . test of distributions of $\bar{V}_p$). Difference of mean speeds is the mean of the group cited in the column subtracted from the mean of the group cited in the row. The second parameter is the degrees of freedom, $df = n_1 + n_2 - 2$. The third parameter, C, is the confidence with which the hypothesis that the mean speed of the row population was not greater than that of the column population could be rejected. For those tests with negative values of t, the hypothesis tested was that the mean of the row population was not less than the mean of the column population.

* One or both populations were not normally distributed (at the 90% confidence level).
** C refers to the two-tailed test of H_o (the population means were the same).

the ages of the tills was known from the moraine morphology, it was possible to use one-tailed tests in most cases. For the t-test, the statistic t is the same for both the one-tailed and two-tailed tests, but for the Kolmogorov-Smirnov test the test statistics are different; accordingly, the D_+ (or D_-) statistic is given in Table 3-5. As long as one of the tested samples contains more than 40 measurements, a parameter D' ($D' = 4D_+^2\, n_1n_2/(n_1+n_2)$ or $D' = 4D_-^2\, n_1n_2/(n_1+n_2)$, where n_1 and n_2 are the sample sizes) is distributed as χ^2 with two degrees of freedom (cf. Till, 1974). This condition was met for all tests in Table 3-5, and D' is reported for each test. If the test statistic is D_+, the hypothesis tested was that the population represented by the group listed for the row in the matrix of Table 3-5 did not have higher values of V_p than the population of the group listed for the column. If the D_- statistic is listed, the hypothesis was that the row group did not have lower values of V_p than the column group. The confidence C with which the tested hypothesis could be rejected is also given. Values of C were found by interpolation of tabulated values for the χ^2 distribution.

Student's t-test was applied to distributions of V_p data and also to distributions of $\overline{V_p}$ found for each site in a group. In each case the t-statistic was calculated for ($\overline{V_p}$ (row) - $\overline{V_p}$ (column)), where "row" and "column" refer to the groups listed in the rows and columns of the Table. For negative values of t, the hypothesis tested was that $\overline{V_p}$ (or $\overline{\overline{V_p}}$) for the population of the column group was not less than $\overline{V_p}$ (or $\overline{\overline{V_p}}$) for the population of the row group; for positive values of t, the hypothesis tested was that $\overline{V_p}$ (or $\overline{\overline{V_p}}$) for the population of the row group was not less than $\overline{V_p}$ (or $\overline{\overline{V_p}}$) for the population of the column group. If both groups had the same relative age, the two-tailed test was used instead. This is a

test for difference only, and is based on $|t|$.

Test results confirmed that most of the groups recognized in this study were separable by V_p data. All three tests (Kolmogorov - Smirnov, the t-test on V_p, and the t-test on $\overline{V_p}$) indicated that, with more than 99% confidence, V_p for boulders from Tioga till were greater than those for boulders from Tenaya till. The t-test on V_p was probably inappropriate, because the distribution of V_p for the Tenaya group was strongly non-normal. However, as shown in App. 3-B the consequence of violation of this condition seems to be that C is underestimated. Thus, the t-test on V_p can be taken to support the results of the Kolmogorov-Smirnov test. The t-test on $\overline{V_p}$ led to the same conclusion, but when one group contains only three or four sites the validity of this test is questionable.

The Tenaya group was readily separated from the group of all sites on the right-lateral Tahoe moraine, using the t-tests. However, the same cautions listed above apply to the interpretation of the test results. Inclusion of the Tahoe I sites (45) in the Tahoe group was responsible for most of the separability; if the Tenaya group was tested against only the Tahoe II sites the separability was reduced. The most unfavorable comparison for discrimination of the Tenaya and Tahoe II tills was the one in which the "anomalous" sites 32 and 60 were excluded from the Tahoe II group. Even for this test, the values of $\overline{V_p}$ for boulders from sites on the Tenaya moraine were the greater, at the 90% confidence level or better. Clearly the Tenaya data constitute a group which, although not itself homogeneous, is distinct from the Tioga and Tahoe data.

The Tahoe II group appeared to have greater values of V_p than the single right-lateral Tahoe I site at confidences ranging from 84% to more than 99%, depending on the test used and the choice of sites for

the Tahoe II group. The conservative test for difference is the one for which the anomalous sites (32 and 60, which have low values of V_p) are included in the Tahoe II group. The Kolmogorov-Smirnov test was unable to separate these data (84% confidence), but the t-test on V_p gave a confidence of 98% that V_p for Tahoe II was truly greater than V_p for Tahoe I. Because the data are unquestionably normally distributed (Table 3-1; Table 3-4) the t-test results may be relied upon. Thus the right-lateral Tahoe moraine is confirmed to be composite.

V_p data are sufficient to discriminate the Tahoe from the Mono Basin till with 98% confidence or more (one-tailed test). If the Tahoe data are divided into the Tahoe I and Tahoe II groups, $\overline{V_p}$ for the Mono Basin group is seen to be lower than $\overline{V_p}$ for the Tahoe II group with more than 99% confidence. However, there is no significant difference between the Mono Basin data and the Tahoe I data (for the right-lateral moraine). This is consistent with the findings of Burke and Birkeland (1979), who used other relative dating methods. They did not recognize the composite nature of the Tahoe moraine, but attributed the difference in weathering to differences in the vegetation covering the different sites and to the effects of fire.

It was to test the contention of Burke and Birkeland that vegetation and fire could so strikingly affect the extent of weathering that V_p measurements were made on the left-lateral Tahoe moraine. Here both Tahoe I and Tahoe II till supported only sage. The results of the one-tailed Kolmogorov-Smirnov and Student's t-tests are similar to the results for the left-lateral groups, despite the absence of vegetation differences. However, the confidence with which the left-lateral groups could be separated was reduced for both tests compared to the confidence for the right-lateral groups.

As a further test, the right- and left-lateral Tahoe I groups and the right- and left-lateral Tahoe II groups were compared. Such comparisons may be difficult to interpret because of changes in provenance for tills on different sides of a valley. However, in this case there appear to have been no gross changes in V_p across the valley for deposits of the same age. Student's t-test was able to distinguish between neither the Tahoe I V_p data nor the Tahoe II data at more than 60% confidence (two-tailed tests), unless the anomalous sites were removed from the right-lateral Tahoe II group. Even if this was done, the confidence of separability was increased only to 77%. Thus vegetative differences do not appear to account for the differences in $\overline{V_p}$ for Tahoe I and Tahoe II tills, and it may be concluded that Tahoe I and Tahoe II tills are of different age.

Finally, the Mono Basin data were compared to data from the remnants of pre-Mono Basin moraines. The V_p values for the Mono Basin sites were significantly greater than those for the pre-Mono Basin sites, at the 98% confidence level or more. Thus the moraines appear to be of different ages.

In summary, all the groups which could be recognized using conventional mapping or relative dating methods could be confidently separated using acoustic wave speeds as a measure of weathering, with the single exception of the Tahoe I and Mono Basin moraines. This may suggest that the Tahoe I advance should be more properly included with the pre-Wisconsin Mono Basin advance, or at least that it was much closer in age to the Mono Basin than to the Tahoe II advance.

Discussion

Discussion focuses on several different topics. These include: (1) the calculation of model ages from V_p data; (2) the correlation of V_p and visual estimates of boulder weathering; (3) the increase of V_p in

rocks with case-hardened surfaces; (4) a possible source for the observed heterogeneity of data from the same moraine; and (5) points of disagreement with the interpretation of Burke and Birkeland (1979).

Model ages of moraines in Bloody Canyon . . .

If V_p is related to time in some simple way, and if the ages of two or more moraines are known independently, model ages for other moraines may be calculated. In Bloody Canyon, the age assignments of the Tioga moraine and the Tahoe II moraine are probably the least controversial. If we assume: (1) that the ages of the glaciations are those given in Ch. 1; (2) that the Tioga moraine was deposited at the glacial maximum about 18,000 y ago; (3) that the Tahoe II moraine was deposited 65,000 y ago; and (4) that $V_p = a + b \log_{10}(1+t)$ where t is the age of the moraine in years; then coefficients of a and b may be calculated and ages for the other moraines may be estimated from their values of V_p. Figure 3-19 shows that if the above conditions are met and if the estimates of V_p for the Tioga and Tahoe II moraines are the correct ones for the populations, then the calculated age of the Tenaya moraine is about 43,000 y, which is within the accepted range of 35,000 y to 45,000 y. The model age of the Mono Basin moraine is 100,000 y to 125,000 y, which is consistent with its identification with a pre-Wisconsin glacial advance. The pre-Mono Basin moraine (II) has an apparent age of about 200,000 y. The data displayed in Fig. 3-19 do not permit discrimination between an early Wisconsin or a pre-Wisconsin age for the "Tahoe I" till. Data from the left-lateral moraine suggest a Wisconsin age; data from the right-lateral moraine suggest an earlier age.

For simplicity, uncertainties in both V_p and ages for the Tioga and Tahoe moraines have been ignored in constructing Fig. 3-19. The error

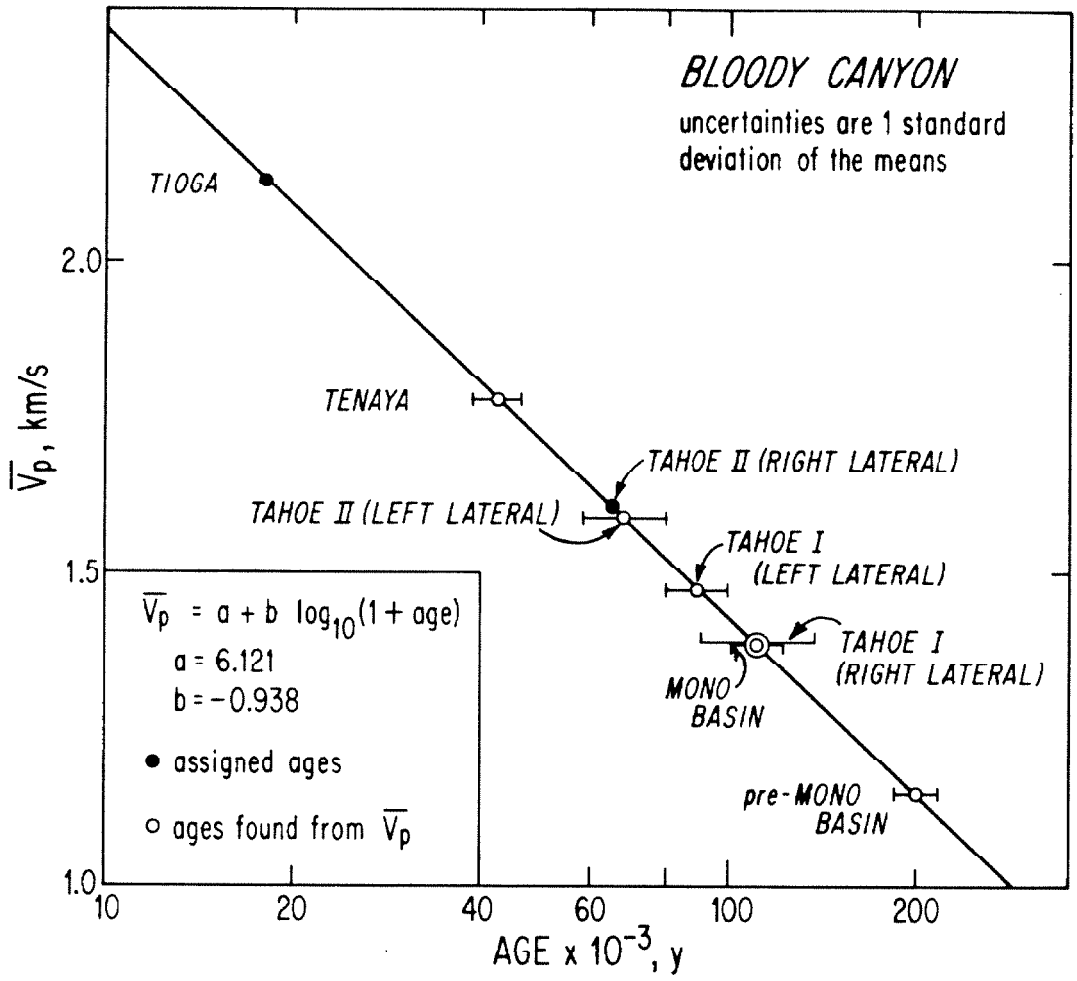

Fig. 3-19. $\overline{V_p}$ for groups of data from moraines of Bloody Canyon plotted as a function of the logarithm of their ages. Ages of the Tioga and right lateral Tahoe II groups were assumed to be 18,000 y and 65,000 y, respectively. Ages for other groups were found assuming $\overline{V_p}$ was proportional to the logarithm of the age. The function specified by the above assumptions is represented by the solid diagonal line. Ages found from $\overline{V_p}$ are model ages only. Model ages for all groups assigned to different glacial advances are separable except for the Tahoe I and Mono Basin groups.

bars for the apparent ages of the other moraines reflect only the uncertainties in the estimates of $\overline{V_p}$ for those groups of data. Because errors introduced by uncertainties in $\overline{V_p}$ for the reference tills are significant, and because the ages assigned to these tills were somewhat arbitrary, the model ages can easily be over-interpreted. It is necessary to regard them only as relative ages until independent determinations of ages of reference moraines are available and until the functional dependence of $\overline{V_p}$ on age can be firmly established.

As a cautionary example, even if the functional relationship of V_p and age is correct, by assuming extreme (2σ) values for V_p and extreme ages for the Tioga and Tahoe II tills, the apparent age of the Mono Basin moraine may be made as low as 80,000 y or as high as 400,000 y. However, under no circumstance does the age of the pre-Mono Basin till appear to be less than 100,000 y. Furthermore, as discussed in the first part of this chapter, as a deposit ages and rocks begin to disintegrate, the mean speed may decrease more slowly than anticipated because the most heavily weathered rocks can no longer be measured. Case-hardening may further slow the decrease of $\overline{V_p}$. Thus the apparent age for the pre-Mono Basin till is probably a minimum age, for both case-hardening of surfaces and reduction in the numbers of boulders exposed at the surface were observed. Regardless of the model age given the Mono Basin till, therefore, there is strong evidence for the presence of a pre-Wisconsin glacial advance at Bloody Canyon.

The correlation of V_p and visual estimates of boulder weathering . . .

Visual estimates of the degree of surface weathering of a boulder and V_p measurements are both sensitive to the length of time the boulder has been weathering. However, they are at least to some extent controlled

by different processes. For example, in rocks exposed at the surface less than a few thousand years visual inspection reveals only subtle indications of weathering. During this same time invisible microfractures may develop which act to slow acoustic waves.

Figure 3-20 is a variation diagram relating visual estimates of weathering to values of V_p measured for the same 141 boulders from Wisconsin moraines in Bloody Canyon. The mean and the minimum values of V_p for each group decrease with increasing degree of weathering. However, except for grusy rocks, all categories of weathered rocks have similar maximum values of V_p, and the spread of measured data in each class (except grusy rocks, which had only two members) was considerable. Thus while visual estimates and V_p measurements are correlated, visual estimates are poor predictors of V_p for individual boulders. One consequence of this is that unconscious bias of V_p data by selective measurement of rocks from a favored category may not have any effects on the V_p distribution which are obvious in the field. Perhaps this serves to minimize such undesired sampling errors.

V_p in rocks with case-hardened surfaces . . .

Data compiled in Fig. 3-20 were from Wisconsin moraines in which there were relatively few boulders with case-hardened surfaces. Most of these were found in the Tahoe moraine. In earlier discussions case-hardening was identified as a mechanism by which the decrease of V_p with time might be slowed, stopped, or even reversed.

In Table 3-6 the increase in the fraction of rocks with case-hardening in older moraines is documented. Rocks were characterized as having no case-hardened crust, a fragmentary or incipient crust, or a well-developed crust. The fraction of rocks with at least some evidence

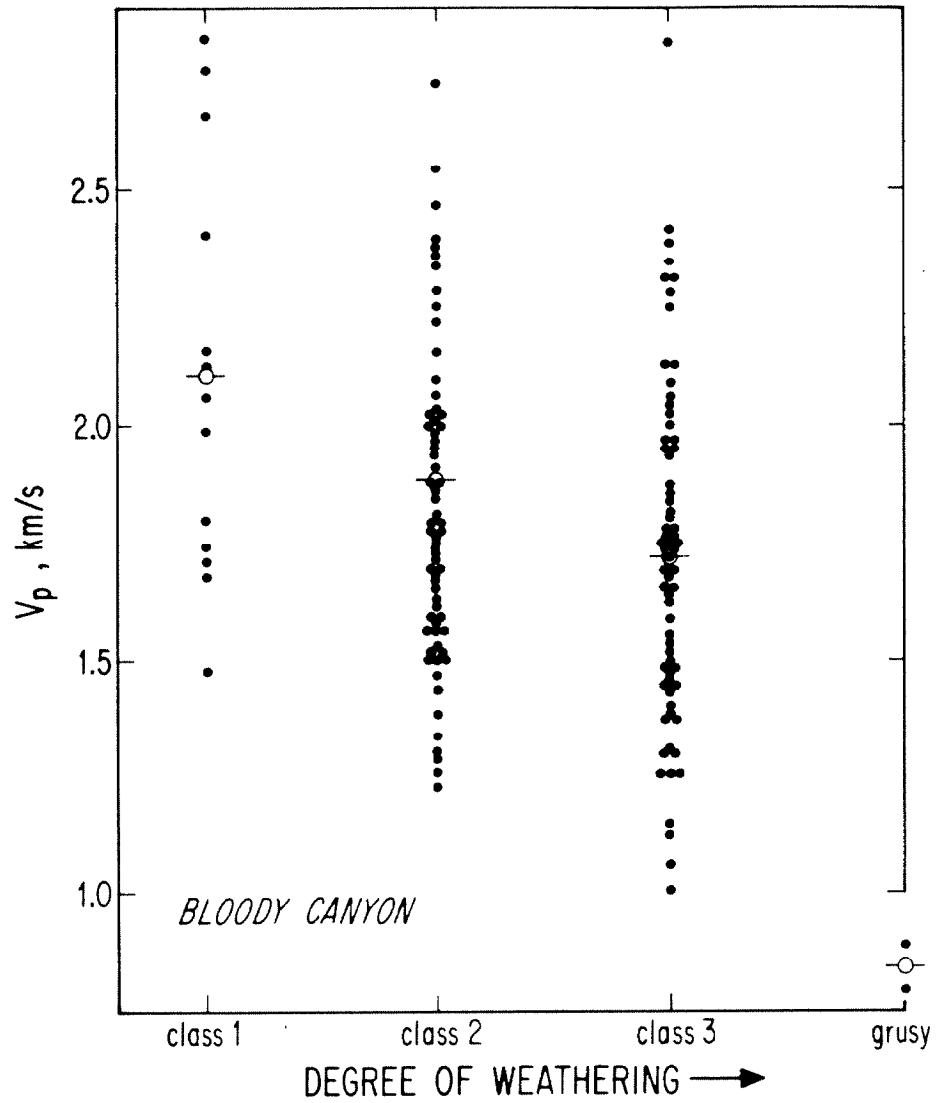

Fig. 3-20. The variation of $\overline{V_p}$ with visual estimates of the degree of weathering for 148 boulders from Wisconsin moraines of Bloody Canyon. Weathering classes are those used for granodiorite weathering ratio (GWR) estimates (Ch. 2). Filled circles show individual measurements; open circles show the means for each class. Despite the high scatter of the data, class means and minimum $\overline{V_p}$ values both decrease with increasing degree of weathering estimated visually.

Table 3-6

Variation of $\overline{V_p}$ with Age and Development of Case-Hardening of Boulder Surfaces at Bloody Canyon

Age of Moraine	No. of Boulders	Condition of Boulder Surface	Fraction of Sample	$\overline{V_p}$ km/s	s km/s
Tahoe II	72	extensive crust	0.03	2.61	-
		partial crust	0.50	1.69	0.48
		no crust	0.47	1.43	0.49
Mono Basin	90	extensive crust	0.31	1.73	0.50
		partial crust	0.50	1.43	0.39
		no crust	0.19	1.10	0.21

of case-hardening rose from 0.53 in the right-lateral Tahoe II moraine to 0.81 in the Mono Basin moraine. V_p data gathered for these rocks are also summarized in the table.

Measurements were consistently made on those portions of the surface of the boulder least affected by case-hardening; nevertheless, two trends in in the data are evident. First, $\overline{V_p}$ did indeed increase in proportion to the extent of case-hardening. Differences in $\overline{V_p}$ between categories for both the Tahoe II and Mono Basin boulders were significant at the 95% confidence level or greater (Student's t-test). Second, for boulders in a given category, $\overline{V_p}$ decreased with age. The differences between values for the Tahoe II and Mono Basin data were also significant at the 95% confidence level or greater. This second tendency is encouraging because it suggests that the acoustic wave-speed method of relative dating may be applicable even if crusts are present, at least in some instances. This may considerably extend the range for which the technique is useful.

Heterogeneity in V_p data from individual moraines . . .

Data from sites on the same moraine did not always appear to be drawn from the same population. This was especially true for the right-lateral Tahoe and Tenaya moraines. Part of the heterogeneity of the Tahoe data may be explained by the composite nature of the moraine, but no such explanation may be invoked for the Tenaya data, and even the Tahoe II data were somewhat heterogeneous.

Heterogeneity in tills of the same age could reflect local variations in weathering conditions or uneven mixing of rocks of different weathering susceptibilities. As discussed above the remaining heterogeneity of the Tahoe data did not seem to be attributable to differences

in vegetative cover, and the vegetation on the Tenaya moraine was very uniform. However, there was an obvious difference in the character of the granitic rocks from the main canyon and rocks from either the south wall or southern tributaries to Walker Creek. An aplitic zone of the Lee Vining pluton cropped out only in the floor and northern wall of Bloody Canyon. The fine-grained aplitic clasts are the dominate boulders on the surfaces of the oldest moraines, and seem to weather much more slowly than the coarser-grained quartz monzonite. Variations in the abundance of aplitic boulders among tills upon deposition could thus result in variations in boulder weathering characteristics, even among tills of the same age.

A small glacier from a cirque on the northeastern face of Mt. Lewis joined the Bloody Canyon glacier from the south. Today, Tioga moraines from this glacier overlie the right-lateral Tahoe II and Tenaya moraines (Fig. 3-13). Clearly, during the Tahoe and Tenaya glaciations this tributary must have contributed till to the large lateral moraines. This till was depleted in the slow-weathering aplitic boulders compared to till derived from Bloody Canyon. Thus the addition of till by the tributary glacier may have served to reduce wave speeds for boulders from the right-lateral moraines. If this till were poorly mixed with till from the main canyon, both the observed heterogeneity and the reduced $\overline{V_p}$ for sites 32 and 60 on the Tahoe II moraine could be explained.

Mixing of tills from different sources could also explain the non-linear cumulative distribution functions of V_p as plotted on a probability grid in Fig. 3-17a. Especially for the pre-Mono Basin data, the cumulative distribution function appears to consist of two segments which are linear when plotted on probability paper. This situation can arise in different

ways, but the most obvious is mixing of two normal populations of different means and standard deviations. Of the distributions plotted in Fig. 3-17a, only the one for the Tioga group of data did not have this kinked appearance to some degree. This was the youngest group, and it may be that differences in weathering susceptability require more than 25,000 y (the maximum age for the Tioga glaciation) to become manifest as differences in V_p.

The possibility that boulders from the same pluton and found on the same lateral moraines may weather at measurably different rates is a critical consideration in planning relative dating experiments.

Points of disagreement with Burke and Birkeland (1979) . . .

The two important differences between the maps of this study and of Sharp and Birman (1963) and the map of Burke and Birkeland (Fig. 3-14) are: (1) Burke and Birkeland grouped the Tenaya and Tioga moraines together; and (2) they grouped the Tahoe and Mono Basin moraines together. The conventional relative weathering data reported for this study (Fig. 3-15) tend to support their conclusion. However, the V_p data show: (1) that the Tenaya moraine is differently weathered than either the younger Tioga or the older Tahoe moraine; and (2) that if only two age categories are to be used, then the "Tenaya" moraine belongs with the Tahoe moraine rather than with the Tioga moraines.

The V_p data also lead to the conclusion that the Mono Basin till is distinct from the Tahoe II till, although the data do not prove that the Mono Basin till is pre-Wisconsin in age. Burke and Birkeland failed to distinguish between Tahoe I and Tahoe II moraines, and this led directly to their mistaken grouping of Mono Basin till with all Tahoe till.

V_p data show that the older Tahoe I till is indeed very similar to the Mono Basin till, but that a significant difference exists between the Tahoe II and Tahoe I tills.

Burke and Birkeland noticed pronounced differences in weathering characterisitics of tills from their single Tahoe moraine also, but attributed them to differences in weathering rates under local control. They envisioned two mechanisms: (1) influences of vegetative cover; and (2) effects of fire. Burke and Birkeland thus argued that the Tahoe II moraine (in the terminology of this study) appeared less weathered than the Tahoe I moraine solely because it was covered by pine forests rather than sage. Sage also covers the Mono Basin moraine. They argued that weathering conditions on the surface of the moraines might be affected by the depth and type of vegetation, and that periodic fires in the pine forests could lead to spalling of the weathered rinds of boulders, thus leaving fresher cores which would make the deposit appear to be younger.

V_p sites were selected to test this idea. Site 31 was established at the only location on the Mono Basin moraines where mahogany rather than sage was dominant. The distribution of V_p data was not different from distributions found at adjacent sites under sage. Tahoe II and Tahoe I sites were separable even if pine-covered sites were excluded, or even if only sage-covered sites (left-lateral moraines) were compared. Finally, from the study of Ide (1937) it is to be expected that severe heating of boulders would irrecoverably and strongly reduce V_p. This would result in apparent excess age as a consequence of forest fires, in contrast to the anomalous youth inferred from visual estimates of weathering.

In fact, just such a pattern was seen at site 32 on the Tahoe II moraine, although I have suggested a plausible alternative for the

observed reduction in V_p. Even if this pattern was due to fires at site 32, the same pattern was not observed at the four left-lateral sites (under sage and mahogany, with scattered pines). Thus vegetation did not seem to exert a dominant influence on V_p data. The one site at which observations fit predictions could be explained by other means and in any case was insufficient to justify grouping the Tahoe II and Tahoe I moraines together.

Other lines of evidence argue against vegetative control of weathering at Bloody Canyon: (1) the contact between Tahoe I and Tahoe II tills can be followed across vegetation boundaries; (2) only one arcuate fragment such as might be spalled from boulders during a fire was actually found, despite repeated searches; and (3) Colman and Pierce (1981) found no significant differences attributable to vegetative cover in rind thicknesses on basaltic and andesitic boulders from moraines at various locations. Thus it appears unlikely that vegetation is a significant factor in the weathering of boulders on moraines at Bloody Canyon and possibly elsewhere in the eastern Sierra Nevada. Finally, it seems that Burke and Birkeland were too conservative in the division of glacial deposits into only two groups, of early and late Wisconsin age. The seven recognizable moraines as old or older than the maximum Tioga moraine can be confidently separated into six age groups, and at least two and probably three are pre-Wisconsin in age. On the other hand, one of the important conclusions of Burke and Birkeland - - that the Bloody Canyon glacier may have changed course during the advance which left the Mono Basin tills rather than after it - - could not be confidently refuted.

Green Creek

Green Creek drains the eastern side of the Sierra Nevada about 25 km north of Bloody Canyon. It empties into the Bridgeport basin, about 100 m higher in elevation than Mono Lake. Green Creek is mapped on the Matterhorn Peak and the Bodie topographic quadrangles. The general geology of the Matterhorn Peak Quadrangle was mapped by Chesterman (1975). The Bodie Quadrangle was mapped by Chesterman and Gray (1975).

The canyon of Green Creek is cut largely into the quartz monzonite of Mono Dome. This quartz monzonite was the only rock measured in this study. It contains some aplitic and fine-grained facies and also has a tendency to case-harden in the weathering environment of the Bridgeport basin. A large set of moraines extends over 10 km from the mountain front along Green Creek, with the lowest end moraines encountered at 2075 m elevation. Glaciations of a wide range of ages spanning most of the Pleistocene are represented here. As at Bloody Canyon, the presence of moraines outside the confines of the steep-walled canyon is an advantage for relative dating, because the possibility of contamination of till by rockfall is removed. The prevalence of case-hardened boulder surfaces presents an undesirable complexity, however.

Sharp (1972) studied and mapped the Quaternary glacial deposits in the Bridgeport basin. Burke and Birkeland (1979) reexamined the moraines of Green Creek and presented a different interpretation from that of Sharp. These interpretations are shown in Fig. 3-21. They differ chiefly in that Burke and Birkeland recognize only two Wisconsin glaciations (Tioga and Tahoe), whereas Sharp reported three (Tioga, Tenaya, and Tahoe). Burke and Birkeland did not study the pre-Wisconsin moraines at Green Creek;

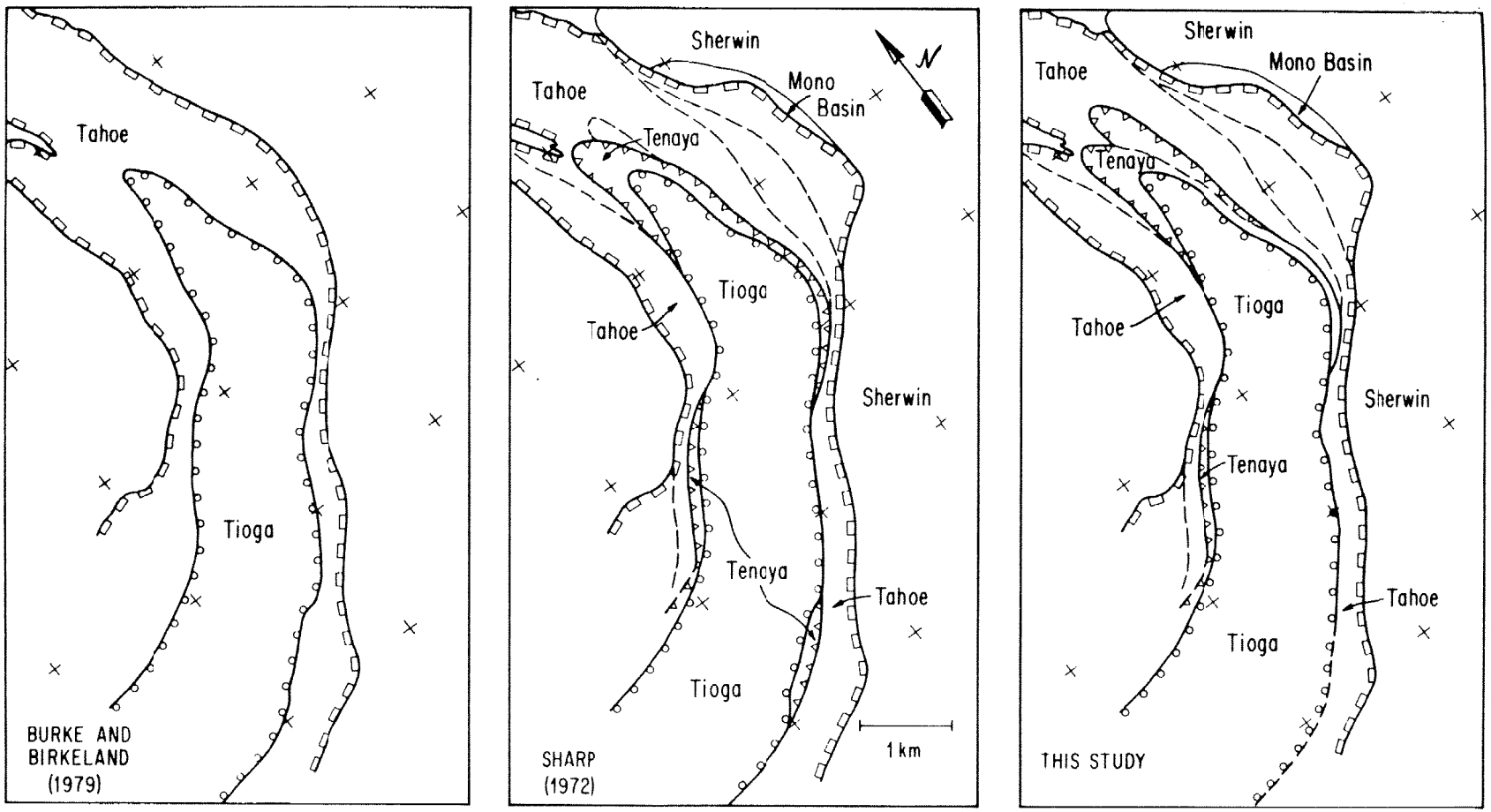

Fig. 3-21. Contrasting interpretations of the ages of glacial moraines at Green Creek by Burke and Birkeland (1979), Sharp (1972), and this study. Burke and Birkeland recognized only two ages: Tioga and Tahoe. They concluded that the Tenaya till of Sharp was indistinguishable from till of Tahoe age. The interpretation of this study differs from that of Sharp only in two minor ways: (1) an end moraine buried by the large Tenaya end moraine is considered to be of Tenaya rather than of Tahoe age; and (2) a small right-lateral moraine 6 km southwest of the Tenaya terminal moraine is considered to be of Tioga rather than Tenaya age.

Sharp identified Mono Basin and Sherwin tills from that period.

For this study the right-lateral moraines were again reexamined. Most of the crests were walked and remapped, with reliance on aerial photographs to help delineate subtle geomorphic details. As at Bloody Canyon, this new map was used to verify and modify the map of Sharp (1972). The resulting interpretation (also shown in Fig. 3-21) was used to guide the collection of V_p data. The chief differences between the maps of this study and of Sharp (1972) are: (1) the presence of a second and older Tenaya end moraine (this study); and (2) the identification (in this study) of a remnant right-lateral moraine inside the large moraine as Tioga rather than Tenaya.

The older "Tenaya" end moraine was recognized by Sharp, who designated it as Tahoe in age. On the strength of aerial photographs it was remapped somewhat larger than shown by Sharp. The assignment of the moraine to the Tenaya advance was based on inspection of road cuts near Dynamo Pond (Fig. 3-22) and on its similar appearance to the younger Tenaya end moraine.

The main right-lateral (Tahoe) moraine is unusual in that for about 3 km the Tahoe till which probably comprises the bulk of the moraine is overridden by youthful Tioga till. The contact is generally no more than a few m south (outside) of the physiographic crest. It is possible that within this overlap zone the age of the till on the crest alternates among Tahoe, Tenaya, and Tioga ages, or even that the boulders exposed on the crest represent a mixture of ages.

The interpretation of the left-lateral moraines of this study is taken directly from Sharp (1972), although contacts were verified by inspection of aerial photographs.

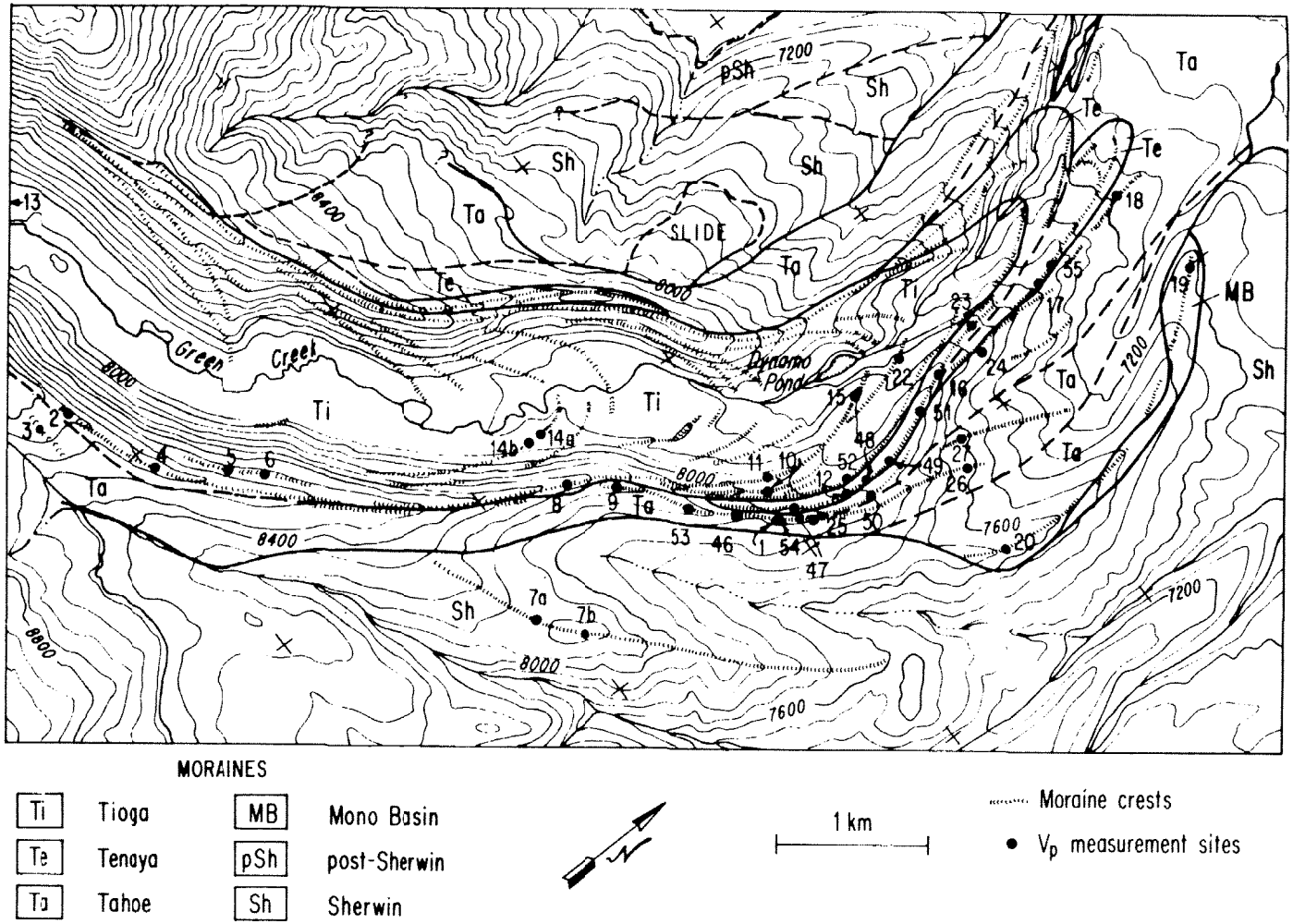

Fig. 3-22. Geologic map of the moraines of Green Creek. V_p measurement sites and other relative age dating sites are marked by filled circles and are numbered. Only at sites 22, 23, 24, 26, and 27 were no V_p measurements made. Geologic interpretation is modified from Sharp (1972). Topographic data is from the U.S. Geological Survey: Matterhorn Peak Quadrangle and Bodie Quadrangle (1:62,500). Contour intervals are 80 ft.

The central difference between the maps of Burke and Birkeland and of Sharp was that Burke and Birkeland grouped the "Tenaya" tills together with the "Tahoe" tills as an undifferentiated unit. Figure 3-23 shows that this grouping of Tenaya and Tahoe moraines was not unreasonable. In Fig. 3-23a the fraction of lightly weathered boulders (GWR class 2) is plotted against the fraction of deeply buried boulders (BR class 3) for 25 sites on the surfaces of different moraines. The locations of these and other sites are shown in Fig. 3-22. The data from sites on pre-Tioga moraines form a continuum. For the oldest sites, no boulders are only lightly weathered, and over half are deeply buried such that they protrude from the surface of the moraine less than a quarter of their diameters. For the youngest sites in the continuum, as many as one quarter of the boulders are only lightly weathered, while a similar number are deeply buried. Data from sites on the Tenaya moraines define one end of the continuum. In Fig. 3-23a the continuum is divided into overlapping clusters of Tahoe data and Tenaya data. In contrast, the cluster enclosing Tioga data is distinct from the continuum.

Data from several sites were anomalous in that they did not fit in the scheme described above. These sites are identified by number in the figure. Site 17 was from the older Tenaya moraine of this study. About twice as many deeply buried boulders were found as at sites on the younger Tenaya moraine. These data suggest that the moraine was Tahoe in age, as Sharp concluded. Equivalent weathering data for the adjacent site 55 on the same moraine were not gathered.

Site 9 was on the Tahoe moraine. Although numerous boulders from this site had case-hardened surfaces and showed effects of wind polish, more lightly weathered boulders were found than at other Tahoe sites.

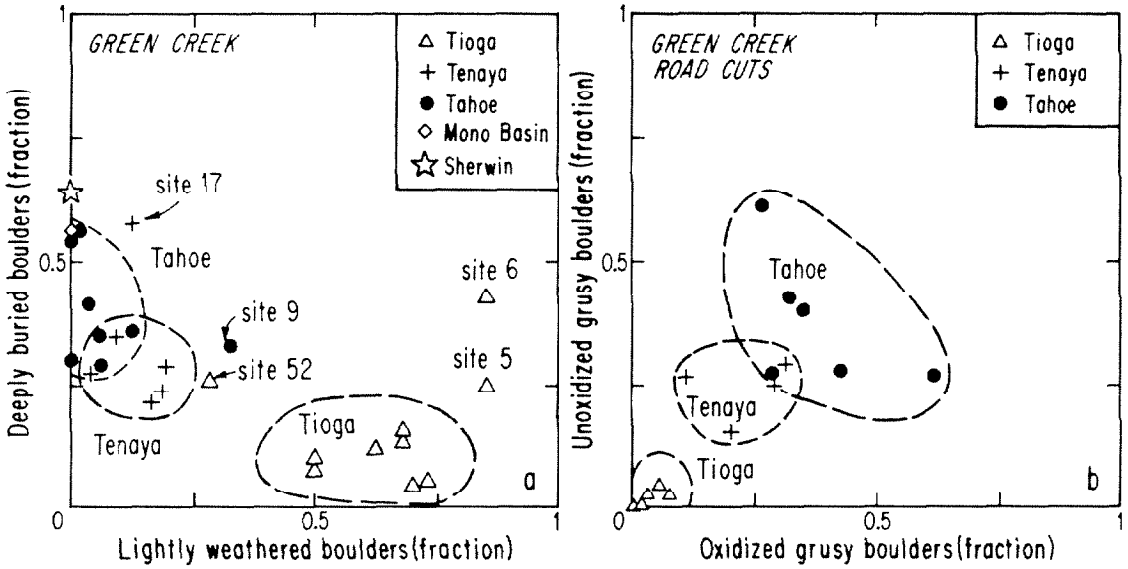

Fig. 3-23. Relative weathering data for sites on moraines of Green Creek. Sites which plot outside of clusters are identified by number. Age classifications are those of this study.

a) The fraction of boulders which are only lightly weathered (GWR class 2) decreases with age, and the fraction of boulders which are deeply buried (BR class 1) increases with age. Data plot in two distinct clusters: Tioga and pre-Tioga. Subdivision of the pre-Tioga cluster results in overlapping clusters.

b) The fractions of all boulders exposed in road cuts which are both oxidized and grusy, and which are unoxidized but grusy, both increase with age. As in (a), Tioga data form a cluster distinct from overlapping clusters of Tenaya and Tahoe data. Although the Tenaya data do not form a separate cluster, the data do show that weathering is consistently less than for Tahoe moraines.

(This site was also found to be unusual in other respects, most notably in the V_p distribution.) There is no obvious explanation.

Site 52 was from a Tioga moraine which was on the side of a larger Tenaya moraine. No fosse separated the two, and it is possible that downslope movement of boulders from the Tenaya moraine acted to "contaminate" the younger till. The weathering data shown in Fig. 3-23a are consistent with the hypothesis that mixing occurred.

Sites 5 and 6 had the highest fraction of lightly weathered boulders of any sites. In this respect they resemble Tioga sites more closely than older sites, and this is taken as support for the interpretation of the moraine on which they were located as Tioga. This moraine was thought by Sharp to be Tenaya, and indeed the fraction of deeply buried boulders is consistent with Sharp's interpretation. However, data from sites 2 and 4 on the crest above (Fig. 3-22) plotted within the Tioga cluster in Fig. 3-23a, and if these sites are on a Tioga moraine then the moraine of sites 5 and 6, which is nested inside, must be Tioga also.

Road cuts near Dynamo Pond afford an excellent opportunity to collect weathering data for subsurface boulders. Some of these data, gathered at sites 22, 23, 24, 26, and 27, are summarized in Fig. 3-23b. This figure is a variation diagram relating the fraction of boulders which were both oxidized and grusy to the fraction of boulders which were not oxidized but were grusy. Both fractions should increase with age, but the fraction of unoxidized grusy boulders must eventually decrease as the entire population becomes oxidized and grusy. Thus boulder populations of increasing age might define a crudely parabolic trajectory in this diagram, with young deposits clustered near the origin, deposits of intermediate age distributed near the center of the figure, and ancient deposits clustered

near the lower right-hand corner.

Data from the roadcuts through the Wisconsin moraines could lie along the first part of such a trajectory. Data were gathered from different depths in the roadcuts: (1) within 1.5 m of the surface; (2) from 1.5 m to 4 m depth; and (3) below 4 m. Data showed little variation with depth compared to variation among moraines, so they were grouped together for display in Fig. 3-23b. As was the case for the data from the moraine crests, clusters enclosing Tenaya and Tahoe data overlapped while Tioga data were distinct.

The confidence with which Tenaya and Tahoe tills may be distinguished must be established by statistical testing. This was not attempted in this study for conventional weathering data. Thus the conclusions that Tioga tills were distinctly less weathered than others, and that Tenaya and Tahoe tills had different but overlapping characteristics, are subjective only.

Acoustic wave-speed data

V_p data were measured for 803 boulders at 32 sites distributed over the the right lateral moraines along Green Creek. Sites are shown in Fig. 3-22. Data are summarized in Table 3-7. Mean wave speeds ranged from 1.45 km/s to 2.37 km/s, and standard deviations ranged from 0.31 km/s to 0.94 km/s. In general, $\overline{V_p}$ decreased with increasing age of the deposit. However, the lowest values of $\overline{V_p}$ were considerably greater than those for Bloody Canyon, and the standard deviations were also greater.

V_p data for each site were tested for normality, using the Kolmogorov-Smirnov test. Values of D_{max} are reported in Table 3-7. Four samples out of 32 were non-normal at the 98% confidence level or greater. This

Table 3-7

Summary of Acoustic Wave-Speed Data for Moraines of Green Creek

Site	Glacial Advance[1] This Study	Sharp, 1972	Burke and Birkeland, 1979	No. of Boulders	$\overline{V_p}$ km/s	s km/s	D_{max}[2]	C_{NL}[3] %
14a*	Ti	Ti	Ti	20	2.265	0.456	0.116	32
14b*	Ti	Ti	Ti	20	2.367	0.432	0.100	15
8	Ti	Ti	Ti	30	2.140	0.516	0.113	61
52	Ti	Ti	Ti	30	1.934	0.338	0.146	92
10	Ti	Ti	Ti	20	2.144	0.495	0.152	76
11	Ti	Ti	Ti	20	2.164	0.304	0.162	84
15	Ti	Ti	Ti	20	2.067	0.480	0.163	85
5	Ti	Te	Ta	20	2.020	0.356	0.095	11
6	Ti	Te	Ta	20	2.085	0.312	0.132	55
2	Ti	Ta?	Ta	20	2.107	0.343	0.090	9
4	Ti	Ta?	Ta	20	2.122	0.387	0.145	70
47	Te	Te	Ta	30	2.177	0.635	0.125	75
12	Te	Te	Ta	20	1.988	0.414	0.171	88
48	Te	Te	Ta	44	1.968	0.559	0.085	40
49	Te	Te	Ta	30	1.782	0.409	0.141	89
51	Te	Te	Ta	30	1.760	0.379	0.121	69
16	Te	Te	Ta	19	1.971	0.548	0.136	57
17	Te	Ta	Ta	30	2.214	0.719	0.189	>99
55	Te	Ta	Ta	28	1.642	0.461	0.150	92
20	Ta	Ta	Ta	30	1.889	0.657	0.121	69
3	Ta	Ta	Ta	20	1.882	0.585	0.107	21
18	Ta	Ta	Ta	29	1.871	0.678	0.133	81
9	Ta	Ta	Ta	20	2.217	0.519	0.148	73
53	Ta	Ta	Ta	30	1.452	0.501	0.177	>99
46	Ta	Ta	Ta	30	1.767	0.941	0.128	80
1	Ta	Ta	Ta	29	1.846	0.631	0.068	2
54**	Ta	Ta	Ta	30	1.958	0.615	0.164	98
25	Ta	Ta	Ta	20	1.837	0.676	0.126	45
50	Ta	Ta	Ta	30	1.720	0.562	0.121	69
19	MB	MB	-	30	1.690	0.668	0.190	>99
7a	Sh	Sh	-	19	1.780	0.549	0.133	54
7b	Sh	Sh	-	15	1.741	0.513	0.108	9

* Sites are near an end moraine
** 25 boulders are shared with site 1

1 Ti... Tioga
Te... Tenaya
Ta... Tahoe
MB... Mono Basin
Sh... Sherwin

2 Kolmogorov-Smirnov statistic comparing the sample to a normal population having the same $\overline{V_p}$ and s.

3 C_{NL} is the confidence that the sampled population could not have been normally distributed.

is a much greater fraction than expected, and if the cumulative distribution of values of C_{NL} for the 32 samples is plotted (Fig. 3-24) it is seen that the populations from which the samples were drawn could not have been normally distributed, with 99% confidence. Thus non-parametric tests must be used to compare sites.

Age assignments for tills at each site are listed in Table 3-7. Values of $\overline{V_p}$ range from 1.45 km/s to 2.37 km/s and are generally highest for sites on the youngest moraines. However, this tendency is not as pronounced as at Bloody Canyon. The standard deviations range from 0.30 km/s to 0.94 km/s, and seem to increase with age. In contrast, standard deviations for V_p data from Bloody Canyon generally appeared to be unaffected by the age of the till.

Data grouped according to the age assignments of this study are summarized in Table 3-8a. Mean wave speeds for grouped sites are shown in Fig. 3-25a. Although group mean speeds show a decrease with increasing age of the till, mean speeds for sites within the groups are scattered widely. Furthermore, wave speeds for boulders from Sherwin moraines are actually greater than wave speeds for boulders from the Mono Basin moraine. Thus it appears that the data are not so well-behaved as those from Bloody Canyon.

In an effort to reduce the standard deviation of the mean speeds, $s(\overline{V_p})$, new groups were established for Wisconsin moraines using only sites from the vicinity of Dynamo Pond, and the Tioga sites were split between two groups. The rationale for this was to minimize possible environmental changes by using sites from only a small section of the 10-km-long moraine complex. As seen from Fig. 3-25b and Table 3-8b, this effort was at least partially successful. Nevertheless, V_p for sites on Tahoe and Tenaya moraines were

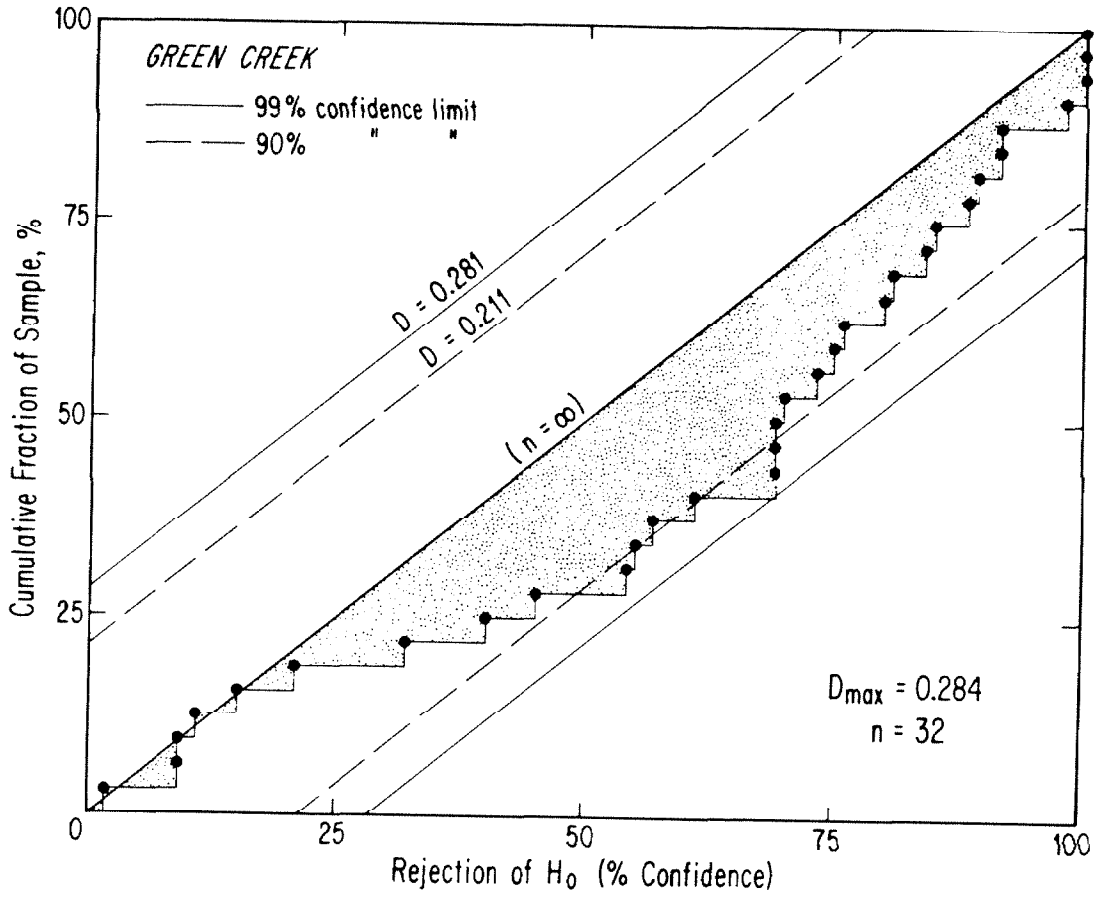

Fig. 3-24. The cumulative distribution of values of C_{NL} for 32 sites of V_p measurements on moraines at Green Creek. C_{NL} is the confidence with which hypothesis H_o (samples are from normal populations) may be rejected. A disproportionate number of sites have high values of C_{NL}. The cumulative distribution function for an infinite number of samples from a normal population is the straight line marked "n = ∞". For finite numbers of samples, the cumulative distribution will deviate from this ideal. Tolerances within which will lie 90% or 99% of the cumulative distributions of all groups of 32 samples are shown by light dashed and solid lines, respectively. The actual cumulative distribution for Green Creek sites is marked by filled circles; the maximum difference (0.284) between this step function and the ideal line exceeds the 99% limit. Thus the sampled populations were not normally distributed.

Table 3-8

Summary of Grouped Acoustic Wave-Speed Data for Moraines of Green Creek

a) All sites, grouped according to this study

Group	No. of Sites	No. of Boulders	Distribution of V_p: $\overline{V_p}$ km/s	Distribution of V_p: s km/s	Distribution of $\overline{V_p}$: $\overline{\overline{V_p}}$ km/s	Distribution of $\overline{V_p}$: $s(\overline{V_p})$ km/s
Tioga	11	240	2.121	0.418	2.129	0.115
Tenaya	8	231	1.936	0.559	1.938	0.201
Tahoe	10	268	1.829	0.665	1.844	0.192
Mono Basin	1	30	1.690	0.668	-	-
Sherwin	2	34	1.762	0.529	-	-

b) Sites on Wisconsin moraines near Dynamo Pond, grouped according to this study

Group	No. of Sites	No. of Boulders	Distribution of V_p: $\overline{V_p}$ km/s	Distribution of V_p: s km/s	Distribution of $\overline{V_p}$: $\overline{\overline{V_p}}$ km/s	Distribution of $\overline{V_p}$: $s(\overline{V_p})$ km/s
Tioga II[1]	2	40	2.316	0.441	-	-
Tioga I[2]	5	120	2.081	0.438	2.090	0.095
Tenaya[3]	6	173	1.939	0.517	1.941	0.153
Tahoe[4]	6	160	1.800	0.687	1.825	0.255

c) Sites near the range front

Group	No. of Sites	No. of Boulders	Distribution of V_p: $\overline{V_p}$ km/s	Distribution of V_p: s km/s	Distribution of $\overline{V_p}$: $\overline{\overline{V_p}}$ km/s	Distribution of $\overline{V_p}$: $s(\overline{V_p})$ km/s
Tioga ?[5]	4	80	2.083	0.347	2.084	0.045

1 Sites 14a, b
2 Sites 8, 10, 11, 15, and 52
3 Sites 47, 12, 48, 49, 51, and 16
4 Sites 9, 53, 46, 54, 25, and 50
5 Sites 2, 4, 5, and 6

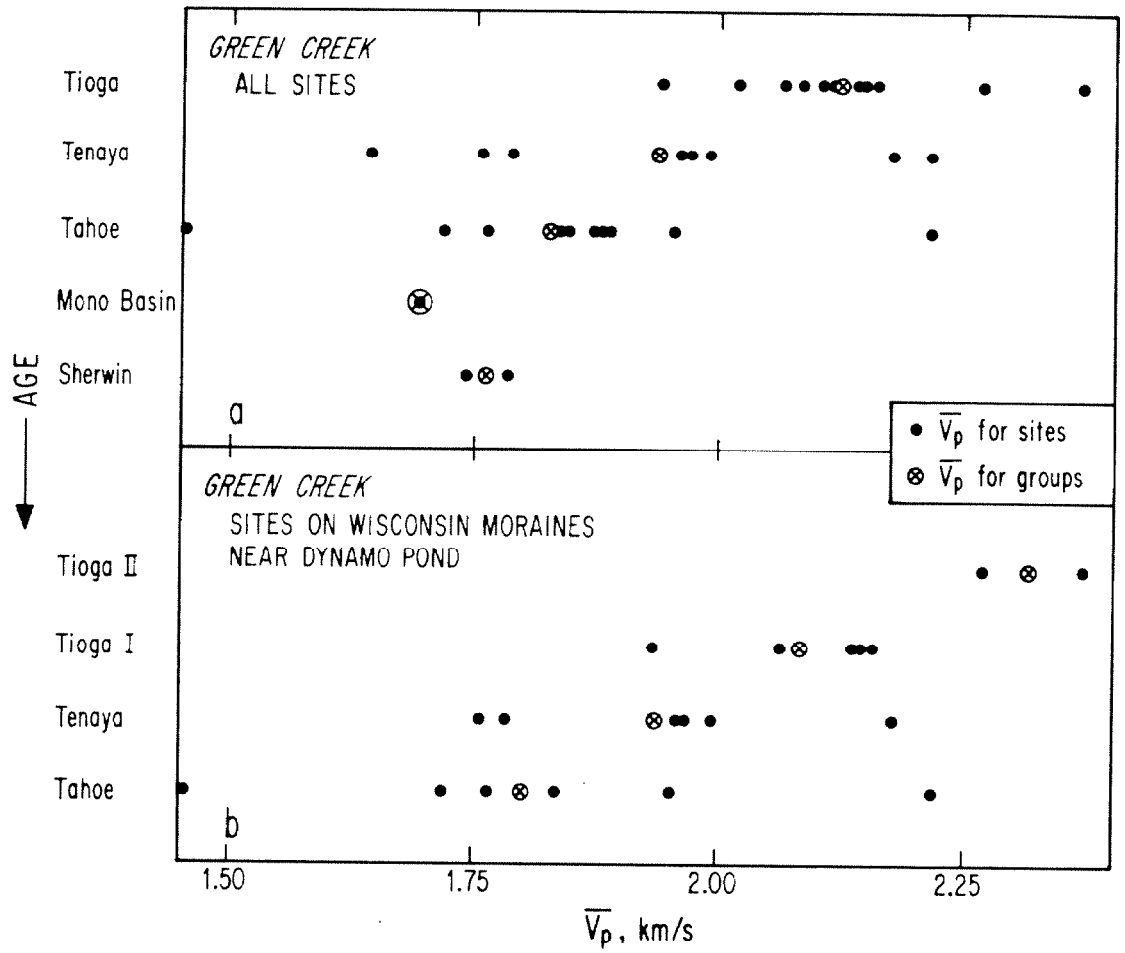

Fig. 3-25. Mean values of V_p for sites and groups of sites on moraines of Green Creek show a tendency to decrease with increasing relative age. Ordinate scale is not quantitative. Mean speeds for sites are widely scattered and groups overlap, but the distributions of means are nevertheless statistically distinct.

a) All sites are grouped according to the geologic map of Fig. 3-22.

b) Scatter is reduced somewhat by examining only sites near Dynamo Pond and by subdividing the "Tioga" group of (a).

still not tightly clustered about the group means. It should be noted that the two extreme values of $\overline{V_p}$ for the Tahoe group were from adjacent sites sites 9 and 53. There appeared to be no depositional complexities in the vicinity of these two sites, and it must be concluded that at least much of the variability of V_p data from sites near Dynamo Pond was intrinsic.

Table 3-9 gives the results of analysis of variance for the groups of Table 3-8. Analysis of variance was done using the conventional F-test and Fisher's method of randomization. Of the groups in Table 3-9a, only "Tioga" and "Sherwin" may be analyzed with the F-test, because only for these two groups can the hypotheses that the samples are normally distributed and "homoscedastic" (variances are similar) be rejected with less than 95% confidence. The F statistic (1.79) for the Tioga group was considerably smaller than the critical value at 95% confidence ($F_{10,239} = 2.25$) and thus the samples comprising the group do not appear to be from different populations at that confidence level. The F statistic for the Sherwin group (0.04) was two orders of magnitude smaller than the critical value ($F_{1,32} = 4.15$) and thus the two samples in that group are almost certainly from the same population.

Fisher's method of randomization confirms the results of the F-test for the Tioga and Sherwin groups. However, for the Tioga group the null hypothesis (that samples were from the same population) could be rejected with more than 90% confidence.

For the Tenaya group, F* was larger than all values of the statistic calculated for the randomized data, and it was obvious that there was significant heterogeneity among sites. On the other hand, heterogeneity could not be demonstrated for the Tahoe group, despite the considerable scatter of mean speeds seen in Fig. 3-25a. This scatter was probably a

Table 3-9

Analysis of Variance of V_p Data from Green Creek

a) All sites, grouped according to this study

Group	No. of Sites	Average No. of Boulders per Site	C_{NL} %	F-Test: Hartley's Test	F-Test: Cochran's Test	F-Test: F	F-Test: C,%	Fisher's Method of Randomization: F^*	Fisher's Method of Randomization: C,%
Tioga	11	22	92	2.88 (3.8)	0.15 (0.15)	$F_{10,239} = 1.79$	<95	1.80	94
Tenaya	8	29	>99	3.60 (2.3)	0.23 (0.20)	$F_{7,223} = 4.99$	>99.9	4.44	>99
Tahoe	10	27	>99	3.53 (2.8)	0.21 (0.15)	$F_{9,258} = 2.13$	>95	1.59	88
Mono Basin	1	30	>99	-	-	-	-	-	-
Sherwin	2	17	54	1.15 (3.0)	0.53 (0.71)	$F_{1,32} = 0.04$	<<95	0.07	22

b) Sites on Wisconsin moraines near Dynamo Pond, grouped according to this study

Group	No. of Sites	Average No. of Boulders per Site	C_{NL} %	F-Test: Hartley's Test	F-Test: Cochran's Test	F-Test: F	F-Test: C,%	Fisher's Method of Randomization: F^*	Fisher's Method of Randomization: C,%
Tioga II[1]	2	20	32	1.11 (2.5)	0.53 (0.71)	$F_{1,38} = 0.54$	<<95	0.52	49
Tioga I[2]	5	24	92	2.88 (3.0)	0.28 (0.30)	$F_{4,115} = 1.27$	<<95	1.29	69
Tenaya[3]	6	29	89	2.81 (2.2)	0.27 (0.19)	$F_{5,167} = 2.51$	>95	2.70	98
Tahoe[4]	6	27	>99	3.53 (2.6)	0.35 (0.21)	$F_{5,154} = 3.71$	>99	1.92	89

c) Sites near the range front

Group	No. of Sites	Average No. of Boulders per Site	C_{NL} %	F-Test: Hartley's Test	F-Test: Cochran's Test	F-Test: F	F-Test: C,%	Fisher's Method of Randomization: F^*	Fisher's Method of Randomization: C,%
Tioga?[5]	4	20	60	1.54 (3.2)	0.31 (0.40)	$F_{3,76} = 0.57$	<<95	0.33	18

1 Sites 14a and 14b
2 Sites 8, 10, 11, 15, and 52
3 Sites 47, 12, 48, 49, 51, and 16
4 Sites 9, 53, 46, 54, 25, and 50
5 Sites 2, 4, 5, and 6

C_{NL} is the confidence with which normality of the group PDF may be rejected.

F-Test: The 95% confidence limits for Hartley's and Cochran's tests are shown in parentheses following the actual values of the test statistics. The degrees of freedom for the F-tests are subscripted to F. C is the confidence with which the hypothesis of homogeneity may be rejected by the F-test.

Fisher's Method of Randomization: The test statistic F^* is proportional to heterogeneity. C is the confidence with which the hypothesis of homogeneity may be rejected.

consequence of the larger standard deviations for the distributions of V_p.

Table 3-9b shows the results of analysis of variance of groups of sites from the vicinity of Dynamo Pond only. The Tioga group was divided into two new groups, Tioga I and Tioga II. Tioga II consists of two sites on a recessional moraine upstream from Dynamo Pond. The Tioga I group did not include the sites (2, 4, 5, and 6) from moraines thought by Sharp (1972) to be Tenaya . The Tenaya group excluded the two sites (17 and 55) from the older moraine thought by Sharp (1972) to be Tahoe. The Tahoe group excluded sites 1 and 3 from the largest moraine, and also sites 18 and 20 from older moraines. Site 1 was excluded because many of the same boulders were included in the overlapping site 54.

"Tioga II" and "Tioga I" were found to be homogeneous by both tests. Because the group of sites 2, 4, 5, and 6 excluded from "Tioga I" had a very similar distribution of V_p (Table 3-8), it is likely that the heterogeneity of the group of all Tioga sites discussed above reflects a difference in age between tills at sites in the Tioga II and Tioga I groups.

"Tenaya" sites were signficantly heterogeneous, even though they were all on the same moraine. The reason for this does not seem to be mixing of tills of different ages, because mapping of the moraine failed to demonstrate a composite structure. The F-test supported the analysis of variance by randomization, but this conclusion may be invalid because the samples were not homoscedastic.

The F-test was not applicable to the "Tahoe" group. Randomization led to the conclusion that the samples were not demonstrably from different populations, at the same level of confidence found for the extended group. Thus the excluded sites were not sources of heterogeneity.

The group of sites from the contested Tioga moraine satisfied the

requirements for the F-test (Table 3-9c). The F statistic (0.57) was much smaller than the 95% critical value ($F_{3,76} = 2.73$), and the group appeared to be homogeneous.

Because not all groups were homogeneous, it was necessary to test the grouped distributions of V_p for normality to determine if Student's t-test could be used to compare groups. The results of χ^2 and Kolmogorov-Smirnov tests are shown in Table 3-10. Only distributions of V_p for the Sherwin and the Tioga groups ("Tioga", "Tioga II", and "Tioga?") appeared to be normally distributed, confirming that in general nonparametric tests had to be used.

Comparisons of grouped data are presented in Table 3-11. Because the relative ages of moraines were known from their locations, one-tailed tests were used. The Kolmogorov-Smirnov test distinguished among the "Tioga", "Tenaya", and "Tahoe" groups (category a: no sites excluded) with confidences exceeding 99%. Student's t-test on distributions of V_p was inapplicable because the distributions were non-normal. The results, shown for comparison, support the conclusions from the Kolmogorov-Smirnov test. The t-test applied to distributions of $\overline{V_p}$ may have been inappropriate because the Tenaya group was heterogeneous and therefore the distribution of $\overline{V_p}$ need not have been normal. Tests on distributions of $\overline{V_p}$ resolved the Tioga and Tenaya groups but failed to distinguish between the Tenaya and Tahoe groups.

The Kolmogorov-Smirnov test was able to distinguish between the Tahoe data and the Mono Basin data (with 92% confidence), but failed to confirm that boulders from the Mono Basin moraine were less weathered than those from the Sherwin moraine; indeed the opposite hypothesis would have been confirmed with more than 99% confidence.

Test results summarized in Table 3-11b show that V_p data from the

Table 3-10

Normality of Distributions of V_p for Groups of Samples, Green Creek

a) All sites, grouped according to this study

		χ^2 test			Kolmogorov-Smirnov test	
Group	No. of Boulders	χ^2	Degrees of Freedom	C_{NL},%	D_{max}	C_{NL},%
Tioga	240	33.1	43	14	0.052	-
Tenaya	231	89.1	42	>99.9	0.074	-
Tahoe	268	107.6	49	>99.9	0.053	-
Mono Basin	30	10.2	3	98	0.190	>99
Sherwin	34	2.6	3	54	0.095	40

b) Sites on Wisconsin Moraines near Dynamo Pond, grouped according to this study

		χ^2 test			Kolmogorov-Smirnov test	
Group	No. of Boulders	χ^2	Degrees of Freedom	C_{NL},%	D_{max}	C_{NL},%
Tioga II[1]	40	5.1	5	64	0.085	30
Tioga I[2]	120	20.0	20	54	0.076	-
Tenaya[3]	173	51.7	31	99	0.071	-
Tahoe[4]	160	70.4	28	>99.9	0.064	-

c) Sites near the range front, grouped according to this study

		χ^2 test			Kolmogorov-Smirnov test	
Group	No. of Boulders	χ^2	Degrees of Freedom	C_{NL},%	D_{max}	C_{NL},%
Tioga?[5]	80	12.8	12	60	0.072	60

1 Sites 14a and 14b
2 Sites 8, 10, 11, 15, and 52
3 Sites 47, 12, 48, 49, 51, and 16
4 Sites 9, 53, 46, 54, 25, and 50
5 Sites 2, 4, 5, and 6

Table 3-11

Results from One-Tailed Test of Differences Between Groups of V_p Data from Green Creek

a) All sites, grouped according to this study

	Kolmogorov-Smirnov Test			Student's t-Test on Distributions of V_p			Student's t-Test on Distributions of $\overline{V_p}$		
Groups	D_+	D'	C,%	t	Degrees of Freedom	C,%	t	Degrees of Freedom	C,%
Tioga vs. Tenaya	0.256	30.86	>99	4.08	469	>99	2.63	17	>99
Tenaya vs. Tahoe	0.175	15.20	>99	1.93	497	97	1.01	16	83
Tahoe vs. Mono Basin	0.217	5.08	92	-	-	-	-	-	-
Mono Basin vs. Sherwin	0.057	0.19	8	-	-	-	-	-	-

b) Sites on Wisconsin moraines near Dynamo Pond, grouped according to this study

	Kolmogorov-Smirnov Test			Student's t-Test on Distributions of V_p			Student's t-Test on Distributions of $\overline{V_p}$		
Groups	D_+	D'	C,%	t	Degrees of Freedom	C,%	t	Degrees of Freedom	C,%
Tioga II[1] vs. Tioga I[2]	0.358	15.38	>99	2.93	158	>99	-	-	-
Tioga I[2] vs. Tenaya[3]	0.228	14.73	>99	2.46	291	>99	1.89	9	96
Tenaya[3] vs. Tahoe[4]	0.210	14.66	>99	2.10	331	98	0.96	10	81

c) Sites near the range front

	Kolmogorov-Smirnov Test			Student's t-Test on Distributions of V_p			Student's t-Test on Distributions of $\overline{V_p}$		
Groups	D_+	D'	C,%	t	Degrees of Freedom	C,%	t	Degrees of Freedom	C,%
Tioga I[2] vs. Tioga?[5]	0.088	1.49	53	-0.05	198	50	0.12	7	55
Tioga?[5] vs. Tenaya[3]	0.277	16.79	>99	2.28	251	>99	1.79	8	94

1 Sites 14a and 14b
2 Sites 8, 10, 11, 15, and 52
3 Sites 47, 12, 48, 49, 51, and 16
4 Sites 9, 53, 46, 54, 25, and 50
5 Sites 2, 4, 5, and 6

Tioga recessional moraine ("Tioga II") were greater than those from the Tioga moraines closer to Dynamo Pond with more than 99% confidence. The older Tioga I moraines were separable from the adjacent Tenaya moraine with a similar confidence.

Student's t-test on distributions of V_p was strictly inapplicable to pairs of groups including the "Tenaya" or the "Tahoe" data, because these data were not normally distributed. As mentioned above, the test is likely to be too conservative (it will fail to discriminate truly different groups) under these conditions. However, the t-test gave essentially the same results as the Kolmogorov-Smirnov test: the Tenaya group was distinct from both the Tioga I and Tahoe groups with high confidence (98% or more). Tests on the distributions of $\overline{V_p}$ gave the same results as for the groups of Table 3-11a: "Tioga I" $\overline{V_p}$ were greater than "Tenaya" $\overline{V_p}$ with high confidence, but the "Tenaya" $\overline{V_p}$ could not be shown to be greater than the "Tahoe" $\overline{V_p}$.

The four samples from sites 2, 4, 5, and 6 were grouped and compared to data from Tioga I sites and Tenaya sites from near Dynamo Pond to determine the apparent age of the moraine. The test results are summarized in Table 3-11c. They show that the unknown group is inseparable from the Tioga I group, but that values of V_p are significantly greater than values of V_p for the Tenaya group. These conclusions are the same regardless of which test was used.

Discussion

Acoustic wave speeds in boulders from Green Creek appeared in general to decrease as the length of time the boulder had been exposed to weathering increased, as was observed at Bloody Canyon and in terraces of the San Gabriel Mountains (Crook and Kamb, 1980). However, the range of

measured speeds was lower at Green Creek. Two other important differences were observed: (1) data from adjacent sites on the same moraine appeared to be drawn from different populations; and (2) $\overline{V_p}$ did not decrease from the Mono Basin moraine to the Sherwin moraine. These topics and a comparison of the three interpretations of the age relationships of the glacial moraines of Green Creek (Fig. 3-21) are addressed below. A discussion of the repeatability of measurements is also included.

Heterogeneity of V_p data within groups . . .

Boulders from the same moraines seemed to be more variable in their values of V_p than observed elsewhere. This was reflected in large standard deviations at sites and in large variations in $\overline{V_p}$ among sites on the same moraine. For the Tahoe moraines, most sites had standard deviations less than 0.7 km/s. On the average, 25 or more boulders were measured at each site. Thus the standard deviation of $\overline{V_p}$ should have been less than 0.14 km/s. Instead, it was found to be 0.19 km/s or more. The excess scatter is best explained as heterogeneity within the moraine, as indicated by the analyses of variance tests. Both the standard deviations of V_p and the heterogeneity increase with age, although too few pre-Wisconsin sites were studied to verify these trends in the oldest moraines. No evidence is found to suggest that this scatter can be explained by composite moraines containing tills of different ages, and it seems likely that it arises as a consequence of weathering itself. An obvious source is the increasing abundance of boulders with case-hardened surfaces in older tills.

Visual inspection showed that the abundance of boulders with case-hardened crusts varied along the crests of individual moraines. Table 3-12 shows that at a single site on a Tahoe moraine, the variation in V_p

Table 3-12

Variation of V_p with the Development of Case-Hardened Surfaces for 30 Boulders from Site 55, Green Creek

Classification of Surface	Fraction of Sample	$\overline{V_p}$, km/s	s, km/s
Extensive Crust	0.20	1.91	0.21
Partial Crust	0.23	1.62	0.55
No Crust	0.57	1.24	0.28

$\overline{V_p}$ is the mean P-wave speed measured by the Microseismic Timer.
s is the standard deviation of the sample of wave speeds.

as a function of the extent of such crusts exceeded the range of V_p for the groups of different ages. Boulders with extensive crusts transmitted P waves at an average of 1.9 km/s, only slightly slower than fresh boulders (with no crusts) from much younger Tioga tills. Boulders without visible crusts transmitted P waves at only 1.2 km/s, slower than the mean speed for any site of any age.

An effort was consistently made to measure V_p on the part of the exposed boulder surface least affected by case-hardening. Aplitic boulders were avoided. However, at some sites on Tahoe moraines and at all sites on pre-Wisconsin moraines, all boulders had at least some visible crust and on many it was not possible to measure wave speeds on unaffected surfaces. Thus the heterogeneity of V_p data within groups, the reduced range of $\overline{V_p}$ compared to Bloody Canyon, and the absence of any decrease in $\overline{V_p}$ in Sherwin sites sites compared to the Mono Basin sites may all be attributable to the presence of case-hardened surfaces on measured boulders. If this is true, it implies that observed differences in $\overline{V_p}$ among Wisconsin moraines were minima.

Relative ages of moraines from Green Creek . . .

Regardless of the way in which V_p data were grouped, most of the stratigraphic units recognized by Sharp (1972) could be confidently discriminated using the Kolmogorov-Smirnov test. Additionally, the Tioga till of Sharp appeared to be divisible into two distinct ages based on V_p data. The confidence with which the Tioga group was divided into the Tioga I and Tioga II groups was similar to the confidence with which the Tenaya group could be separated from the Tioga I and Tahoe groups.

Figure 3-26 shows the variations of values of $\overline{V_p}$ with the estimated

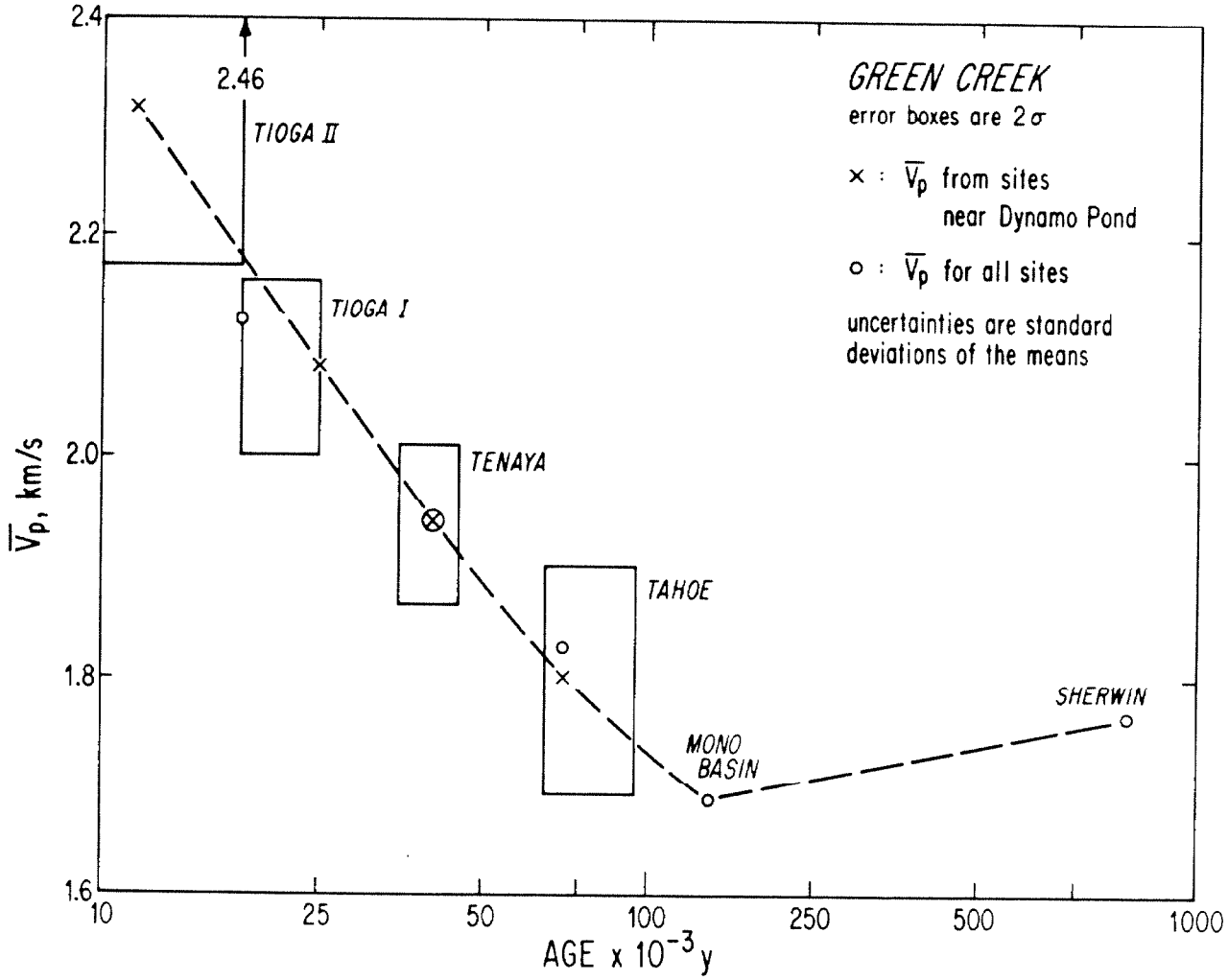

Fig. 3-26. $\overline{V_p}$ for groups of data from moraines of Green Creek plotted as a function of the logarithm of their estimated ages. All ages were assigned from literature values (Chapter 1). $\overline{V_p}$ is approximately a simple logarithmic function of age for ages less than about 0.1 my. $\overline{V_p}$ decreases with age from about 2.3 km/s to about 1.7 km/s or 1.8 km/s with increasing age, within that limit. For older tills, $\overline{V_p}$ seems to increase with increasing age. This may be due to the formation of case-hardened crusts on boulders.

ages of groups of moraines. The uncertainty windows are 2σ in the $\overline{V_p}$ and roughly the same in age. The actual values of $\overline{V_p}$ are plotted at the best guesses of the ages of the moraines, but these are arbitrary. Thus the age of Tioga II was taken to be 11,500 y, and the age of Tioga I was taken to be 25,000 y. These ages, quoted from Ch. 1, correspond respectively to the end and beginning of the Tioga glacial advance, rather than the glacial maximum (thought to be about 18,000 y BP). However, the age of the undifferentiated "Tioga" group was taken to be 18,000 y. The age of the Tenaya moraines was assumed to be 40,000 y, the mid-point of the range of possible ages, and because most of the sites in the Tahoe group were on the innermost remaining moraine of the Tahoe sequence, the age of the deposits was taken to be about 70,000 y, near the end of the Tahoe glaciation.

Although the age vs. $\overline{V_p}$ function is not well constrained by the data from Green Creek, the data are consistent with a simple logarithmic function for deposits less than about 0.1 my old. Older deposits are dominated by crusted boulders giving high values of V_p. The majority of rocks originally present at these sites has been removed from the population, probably by disintegration. Thus the values of V_p do not decrease with age, but appear to be responsive primarily to the abundance of crusted boulders and the condition of their surfaces.

Differences between the geologic interpretations of this study and those of Sharp (1972) . . .

V_p measurements in general confirmed the interpretation of Sharp (1972) of the relative ages and grouping of moraines at Green Creek. There were two significant differences between the interpretation of Sharp and that used in this study: (1) Sharp thought the moraines of sites 2, 4, 5, and 6 were of Tenaya age (instead of Tioga age); and (2) Sharp grouped the moraine

of sites 17 and 15 with the Tahoe moraines (instead of the Tenaya moraine).

$\overline{V_p}$ data support the Tioga age assignment used in this study for the moraines of sites 2, 4, 5, and 6. However, even though two sites for V_p measurement were established on the outer Tenaya moraine (this study), the V_p data failed clearly to associate the moraine within either the younger Tenaya moraine or the older Tahoe moraines. $\overline{V_p}$ for site 17 was 2.21 km/s, greater than $\overline{V_p}$ for any Tenaya site but not statistically different than $\overline{V_p}$ for Tahoe site 9. These high speeds in both cases were probably due to the high fraction of boulders with case-hardened surfaces. $\overline{V_p}$ for site 55 was 1.64 km/s, lower than $\overline{V_p}$ for any of the Tenaya sites and also lower than V_p for all Tahoe sites except site 53. However, $\overline{V_p}$ at site 55 was not significantly lower than $\overline{V_p}$ at Tenaya site 51 (86% confidence using the t-test), and more data are required to resolve this question.

Differences between the geologic interpretations of this study and those of Burke and Birkeland (1979) . .

Burke and Birkeland did not recognize the Tenaya tills of Sharp (1972) as distinct from the Tahoe till, based on their weathering characteristics. They were also unable to distinguish between the Tioga I and II groups, although their sites 25 and 45 were very close to V_p sites 15 (Tioga I) and 14 (Tioga II), respectively.

The visual weathering data for surface boulders gathered at Tioga I and Tioga II sites support the results of Burke and Birkeland. No significant differences were found. However, it should be noted that site 14 was very near the end of the moraine, where relative weathering may be anomalous or highly variable (Janda, 1966; McCulloch, 1963; Sharp, 1969, 1972). The ready distinction between these sites by the V_p method is thus encouraging, because it suggests that V_p data, at least for

young moraines, may not be subject to the same sources of variability which affect conventional methods near end moraines. This conclusion is only tentative; too few data have been taken to demonstrate conclusively that the V_p data from end moraines are not anomalous also.

Visual estimates of the weathered condition of granitic boulders in road cuts did not agree well with those reported by Burke and Birkeland (1979). The data of this study (Fig. 3-23b) showed Tenaya moraines to have a lower fraction of grusy boulders than Tahoe moraines, while Burke and Birkeland found the fractions to be the same. The results of this study are more consistent with the results from the V_p method of relative dating, which readily separated Tenaya and Tahoe tills. Thus a basic conclusion of Burke and Birkeland - - that the Tenaya moraines were indistinguishable from the Tahoe moraines - - was contradicted by the V_p data. However, inspection of Fig. 3-25 shows that this conclusion might not have been drawn had V_p data been measured at fewer sites. This suggests that the approach of Burke and Birkeland might have been successful in distinguishing between Tenaya and Tahoe moraines had data been gathered at more sites.

Repeatability . . .

V_p data were gathered at overlapping sites 1 and 54 on the biggest Tahoe moraine by different operators in different years. Twenty-five measurements were duplicates, made using the same impact points on the same boulders. Thus comparison of the results from the two sites gives a good measure of the repeatability of the V_p method under field conditions.

Values of $\overline{V_p}$ for the two sites differed by only 0.11 km/s. From the standard deviations of about 0.62 km/s and the numbers of measurements (29 and 30), the standard deviation of the mean was found to be 0.11 km/s

also. Thus the variation in V_p between sites 1 and 54 was well within expectation. Student's two-tailed t-test failed to detect any difference between the sites: $t = 0.7$ with 57 degrees of freedom, corresponding to a rejection of hypothesis H_o (no difference) with only 48% confidence. Thus the repeatability claimed by Crook and Kamb (1980) was confirmed.

Summary of results from Green Creek

V_p data from sites on moraines at Green Creek confirmed the basic relative age assignments of Sharp (1972). Values of $\overline{V_p}$ for groups of sites seemed to decrease linearly with the logarithm of the age of the till for perhaps 0.1 my. Older tills were dominated by boulders with case-hardened surfaces, and the wave speeds may thus even have increased or fluctuated with increasing age instead of decreasing monotonically.

V_p data may have enabled the discrimination of a discrete young advance within the Tioga glaciation (Tioga II), although the necessary location of the V_p sites near an end moraine raised unanswered questions about the reliability of any relative dative method in this instance. V_p data appeared to contradict the recent claim of Burke and Birkeland (1979) that the Tenaya till could not be discriminated as a separate unit but should be grouped with the older Tahoe tills. Finally, duplicated measurements of the same boulders by different operators in different years confirmed the basic repeatability of the V_p method of relative dating.

3.6 CONCLUSIONS

The measurement of acoustic wave speeds through granitic boulders appears to provide a satisfactory basis for relative dating of glacial moraines. V_p data are more effective than conventional relative weathering estimates at characterizing relative ages.

The chief benefits of the V_p method of relative dating are the repeatability of the measurements and the numerical nature of the results, which can be readily compared by standard statistical tests. The technique is intermediate in difficulty between the conventional semi-quantitative methods and most quantitative methods (e.g., measuring weathering-rind thicknesses or soil profiles). About 25 boulders at five sites may be measured in a day. This should in general correspond to one moraine per day.

Application of the V_p method of relative dating to well-studied moraine sequences at Bloody Canyon and at Green Creek showed that over at least the last 0.1 my V_p decreases with increasing age of the moraines. Because the dependency appears to be logarithmic, age resolution is reduced for older deposits. V_p dating resulted in the recognition of additional age groups in both test areas: in Bloody Canyon a pre-Mono Basin moraine was identified and the Tahoe moraine was shown to consist of different tills of at least two distinct ages; and in Green Creek the Tioga moraine sequence was divisible into at least two distinct groups. On the other hand, development of crusts on the surfaces of boulders from pre-Wisconsin moraines at Green Creek precluded the use of the V_p method on tills of Sherwin age.

It was thus demonstrated that the V_p relative dating method is a powerful addition to the array of semi-quantitative and other conventional relative dating techniques.

References Cited

Abramowitz, M. and Stegun, I.A. (ed), 1968, Handbook of Mathematical Functions: U.S. Dept. Commerce (Natl. Bureau of Standards), Applied Mathematics Series No. 55, 7th ed, 1046 p.

Birch, F., 1937, Elasticity (except compressibility): in Birch, F. (ed), Handbook of Physical Constants: Geol. Soc. America Spec. Paper 36, 325 p.

Birch, F., 1960, The velocity of compressional waves in rocks to 10 kilobars, Part I: Jour. Geophys. Research 65, 1083-1106.

Birman, J.H., 1964, Glacial geology across the crest of the Sierra Nevada: Geol. Soc. America Spec. Paper 75, 80 p.

Blackwelder, E., 1931, Pleistocene glaciation in the Sierra Nevada and Basin ranges: Geol. Soc. America Bull. 42, 865-922.

Bradley, J.V., 1968, Distribution-Free Statistical Tests: Prentice-Hall, Englewood Cliffs, New Jersey, 388 p.

Bullen, K.E., 1965, Introduction to the Theory of Seismology: Cambridge Univ. Press, London, 381 p.

Burke, R.M. and Birkeland, P.W., 1979, Reevaluation of multiparameter relative dating techniques and their application to the glacial sequence along the eastern escarpment of the Sierra Nevada, California: Quaternary Research 11, 21-51.

Chesterman, C.W., 1975, Geology of the Matterhorn Peak Quadrangle, Mono and Tuolomne Counties, California: California Div. Mines and Geology Map Sheet 22.

Chesterman, C.W., and Gray, C.H. Jr., 1975, Geology of the Bodie Quadrangle, Mono County, California: California Div. Mines and Geology, Map Sheet 21.

Clark, M.M., 1972, Range-front faulting: cause of anomalous relationships among moraines of the eastern slope of the Sierra Nevada, California: Geol. Soc. America Abstracts with Programs 4, 137.

Colman, S.M., 1981, Rock-weathering rates as functions of time: Quaternary Research 15, 250-264.

Colman, S.M. and Pierce, K.L., 1981, Weathering Rinds on Andesitic and Basaltic Stones as a Quaternary Age Indicator, Western United States: U.S. Geol. Survey Prof. Paper 1210, 56 p.

Conca, J., 1982, Case-hardening in the Aztec Sandstone, Southern Nevada: submitted to Science

Crook, R. Jr., and Kamb, B., 1980, A new method of alluvial age dating based on progressive weathering, with application to the time-history of fault activity in Southern California: Final Report, U.S. Geol. Survey Contract No. 14-08-0001-17760, 41 p.

Curry, R.R., 1968, Quaternary Climatic and Glacial History of the Sierra Nevada, California: Ph.D. thesis, Univ. of California, Berkeley; University Microfilms, Inc., No. 68-13896, Ann Arbor, MI, 204 p.

Curry, R.R., 1971, Glacial and Pleistocene History of the Mammoth lakes, Sierra Nevada, California - a Geologic Guidebook: Univ. of Montana, Dept. of Geology, Geol. Serial Publication 11, Missoula, Mont., 49 p.

Dalrymple, G.B., 1964, Potassium-argon dates of three Pleistocene interglacial basalt flows from the Sierra Nevada, California: Geol. Soc. America Bull. 75, 753-758.

Fisher, R.A., 1946, Statistical Methods for Research Workers: Oliver and Boyd, Edinburgh, 6th ed.

Griffiths, J.C., 1967, Scientific Method in the Analysis of Sediments: McGraw-Hill, New York, 508 p.

Harbaugh and Merriam, 1968, Computer Applications in Stratigraphic Analysis: Wiley, New York, 282 p.

Ide, J.M., 1937, The velocity of sound in rocks and glasses as a function of temperature: Jour. Geology 45, 689-716.

Janda, R.J., 1966, Pleistocene History and Hydrology of the San Joaquin River, California: Ph.D. thesis, Univ. California, Berkeley; University Microfilms, Inc., No. 67-5086, Ann Arbor, MI, 425 p.

Kesseli, J.E., 1941, Quaternary history of Mono Valley, California: Univ. California Pubs. Geography 6, 315-362.

Kistler, R.W., 1966, Geologic map of the Mono Craters Quadrangle, Mono and Tuolumne Counties, California: U.S. Geol. Survey Geol. Quad. Map GQ-462.

Lilliefors, H.W., 1967, On the Kolmogorov-Smirnov test for normality with mean and variance unknown: Jour. Amer. Stat. Assn. 62, 399-402.

McCulloch, D.S., 1963, Late Cenozoic Erosional History of Huerfano Park, Colorado: Ph.D. thesis, Univ. of Michigan; University Microfilms, Inc., No. 63-6922, Ann Arbor, MI., 158 p.

McGee, W.J., 1885, On the meridional deflection of ice streams: Am. Jour. Sci. 29, 3rd Ser., 386-392.

Nur, A. and Simmons, G., 1969, The effect of saturation on velocity in low porosity rocks: Earth Planet. Sci. Lett. 7, 183-193.

Nur, A., and Simmons, G., 1970, The origin of small cracks in igneous rocks: Internat. Jour. Rock Mechanics and Mining Sci. 7, 307-314.

Putnam, W.C., 1949, Quaternary geology of the June Lake district, California: Geol. Soc. America Bull. 60, 1281-1302.

Russell, I.C., 1889, Quaternary history of Mono Valley, California: U.S. Geol. Survey 8th Ann. Rept., Part I, 201-394.

Sharp, R.P. and Birman, J.H., 1963, Additions to classical sequence of Pleistocene glaciations, Sierra Nevada, California: Geol. Soc. America Bull., 74, 1079-1086.

Sharp, R.P., 1969, Semiquantitative differentiation of glacial moraines near Convict Lake, Sierra Nevada, California: Jour. Geology 77, 68-91.

Sharp, R.P., 1972, Pleistocene glaciation, Bridgeport Basin, California: Geol. Soc. America Bull. 83, 2233-2260.

Till, R., 1974, Statistical Methods for the Earth Scientist: An Introduction: John Wiley and Sons, New York, 154 pp.

Thill, R.E., Willard, R.W., and Bur, T.R., 1969, Correlation of longitudinal velocity variation with rock fabric: Jour. Geophys. Research 74, 4897-4909.

Appendix 3-A: Testing for Normality of Sample Distributions when the Population is Unknown.

Before parametric tests such as Student's t-test or analysis of variance may be used in comparing samples of a population, it is necessary to prove that the population is normally distributed (cf. Till, 1974). This is generally done using the χ^2 test, but Bradley (1968) points out several advantages of the one-sample Kolmogorov-Smirnov test. Chief among these is the freedom from the requirement to group data into cells. In the χ^2 test, especially for small numbers of measurements, the outcome of the test may vary with the choice of cells. The Kolmogorov-Smirnov test is strictly applicable only if the population is completely specified independent of the sample, but, Lilliefors (1967) has modified the test slightly so that it may be used even if the mean and variance of the population are unknown. In this test, the maximum ordinate-wise difference D_{max} between cumulative frequency distributions of (1) the ideal normal distribution having the mean and variance of the measured sample and (2) the sample itself is calculated. Values of D_{max} will tend to be large if the sample is not from a normal population. The confidence that the population is normal may be found from D_{max} using Monte Carlo methods. If D_{max} is larger than (for example) 90% of the values found in the Monte Carlo experiment, then the hypothesis that the population was normally distributed (hypothesis H_o) may be rejected with 90% confidence: there is only one chance in ten that the population is actually normally distributed. Lilliefors (1967) calculated critical values of D_{max} for samples of size N = 4,5,6,7, . . ., 30 and n = 100. However, he has tabulated the results only for selected values of 80% or

greater. In order to test H_o for groups of samples, it was desirable to know critical D_{max} for the entire range of confidences. Thus Lilliefors' Monte Carlo experiment was independently recreated and values were tabulated for the entire spectrum of confidence levels.

The experiment procedure was straightforward:

(1) A sample of N "measurements" was created using a random number generator *. The population from which the measurements were drawn was normally distributed.

(2) The mean and standard deviation for the sample were calculated and and the cumulative frequency distribution of a normal population having these characteristics was calculated.

(3) The ordinate values of the sample and population cumulative frequency distributions were compared at each value of the independent variable. The largest absolute difference, D_{max}, was retained.

(4) The above procedure was repeated for a total of 500 iterations. All values of D_{max} were ordered and displayed as a cumulative frequency distribution.

(5) This entire experiment was repeated for different values of N.

The cumulative distribution functions for all values of N listed in Table 3-A-1 are shown as contour maps at different ordinate scales in Fig. 3-A-1a and 3-A-1b. These maps show critical values of D_{max} as a function of the sample size (ordinate) and the percent of the iterations which produced smaller values. If the D_{max} value for an actual sample consisting of N measurements is known, the confidence with which H_o may be rejected can be found from the abscissa of these figures.

---

* The random number generator from the IBM Scientific Subroutine Package, for the IBM 360 series computers, was used.

Figure 3-A-1b differs from Fig. 3-A-1a only in the range of the ordinate scale. In Fig. 3-A-1a, N ranges from 4 to 100. Contour lines have been used to connect locations of equal D_{max}, although the distribution is actually discrete because N must be an integer. This was done to facilitate use of the diagrams. Finally, the contours were smoothed by hand. They thus represent an approximate "least squares fit" to the data. Critical values of D_{max} are tabulated for selected confidence levels in Table 3-A-I. These values agree with those of Lilliefors (1967).

Table 3-A-1

Sample Sizes N for which Distributions of D_{max} were Calculated

-	-	-	4	5	6	7	8	9	10
11	12	13	14	15	16	17	18	19	20
21	22	23	24	25	26	27	28	29	30
31	-	33	-	-	36	-	-	-	40
-	-	-	-	-	-	-	-	-	50
-	-	-	-	-	-	-	-	-	60
-	-	-	-	-	-	-	-	-	-
-	-	-	-	-	-	-	-	-	80
-	-	-	-	-	-	-	-	-	-
-	-	-	-	-	-	-	-	-	100

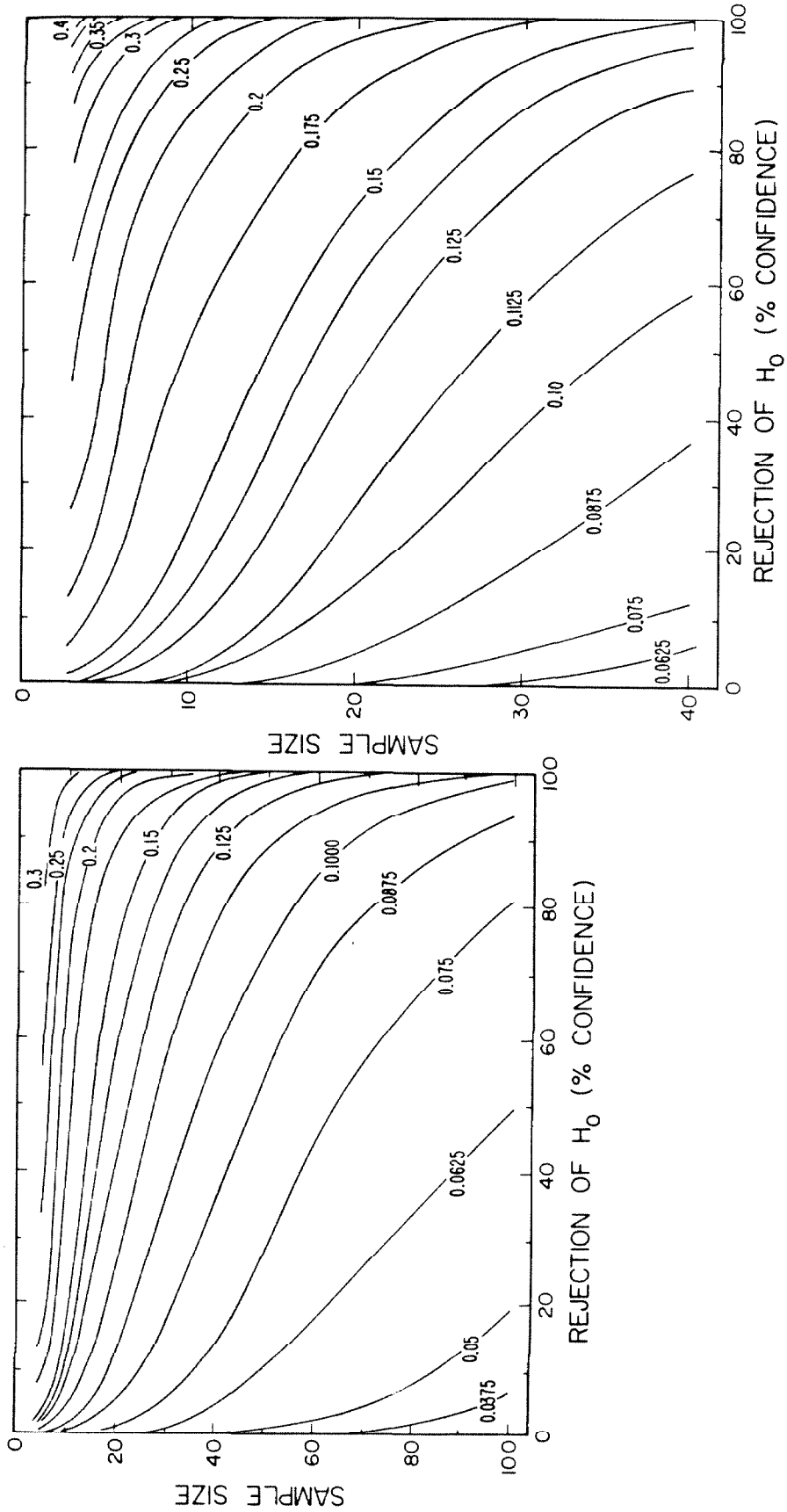

Figure 3-A-1: Contour maps showing the distribution of values of D_{max} found by the one-sample Kolmogorov-Smirnov test. Samples randomly drawn from a normal population were compared to normal populations whose means and variances were estimated from the samples. The distribution is a function of the sample size (the number of "measurements"). The abscissa shows the probability that a sample drawn from a normal population would give D_{max} less than the mapped value. Thus a value of D_{max} found for any sample of an unknown population can be used to test the hypothesis (H_0) that the population was normally distributed. The number of iterations used to generate each D_{max} distribution was 500. For simplicity, smooth contour lines were drawn but these have meaning only at integer values of sample size. Figure 3-A-1a shows distribution of D_{max} for samples containing from 4 to 100 "measurements". Figure 3-A-1b shows distributions for sample sizes of 40 or less at expanded scale.

Appendix 3-B: Comparison of the Two-Sample Kolmogorov-Smirnov Test and Student's t-Test.

It is often necessary to test two samples to determine if they were taken from the same population. Generally this is done using Student's t-test, which presumes that the samples are from normally distributed populations. If this cannot be demonstrated, a non-parametric test, which is applicable regardless of the form of the population, must be used. The Kolmogorov-Smirnov test is one of several such tests (cf. Bradley, 1968), and it is attractive because of its simplicity and because it may be used with measurements made on a ratio scale (instead of just nominal or ordinal data[1]). The purpose of this appendix is to compare the performance of the two tests on the same pairs of samples randomly drawn from a normally distributed population. From this comparison a guideline must be drawn to assist in the choice of the best test in a given situation.

Comparisons of Student's t-test and the Kolmogorov-Smirnov test were made on pairs of samples of N "measurements" randomly drawn n times from a normally distributed population. The hypothesis (H_o) that the samples were drawn from the same population was tested and the confidence with which H_o could be rejected according to Student's t-test (C_t) and the Kolmogorov-Smirnov test (C_{KS})was calculated. Values C_{KS} and $C_{KS}-C_t$ were compiled as a function of the maximum confidence (C_{NL}) with which the hypothesis of normality for population from which the samples were drawn could be rejected (App. 3-A).

In some cases it may be known a priori that the population of one sample cannot be greater in the measured parameter than that of the other. Such a situation may arise in the relative dating of moraines. A moraine

---

[1] see Griffiths (1967), p. 245-249 for a discussion of the different scales.

nested inside another cannot be the older, but may be of nearly the same age or younger. In this case the hypothesis H_1 that the population of the first sample is not greater than that of the other is tested. Both H_o and H_1 were tested in this study.

Student's t-test involves the comparison of a calculated statistic t to the frequency distribution of t for an infinite number of samples drawn from a normal population. The t distribution varies with N and tends towards the normal distribution for $N > 30$. For the two-sample test, t is a function of the difference in the sample means (x_1, x_2) scaled by the pooled sample variance and the number of measurements (N_1, N_2) and the degrees of freedom:

$$t = \left(\frac{N_1+N_2-2}{N_1+N_2} \; \frac{N_1 \; N_2}{N_1 s_1^2 + N_2 s_2^2} \right)^{-\frac{1}{2}} (x_1 - x_2) \qquad \text{(i)}$$

where s_1 and s_2 are the standard deviations of the samples:

$$s_i^2 = (N-1)^{-1} \sum_{j=1}^{n} (x_{ji} - x_i)^2 \qquad \text{(ii)}$$

and where x_{ji} are the individual measurements (cf. Griffiths, 1967). From the frequency distribution or probability density function (PDF) of t, the confidence C_t (in percent) with which H_o may be rejected for a given value of t may be found from

$$C_t = 100 \int_{-t}^{+t} \mathrm{PDF}(\eta) \, d\eta \qquad \text{(iii)}$$

where $\int_{-\infty}^{+\infty} \mathrm{PDF}(\eta) d\eta = 1$. Because of the symmetry of the integration limits about zero, this is called the <u>two-tailed</u> test. The confidence with which H_1 may be rejected is

$$C_t = 100 \int_{-\infty}^{t} \mathrm{PDF}(\eta) \, d\eta \qquad \text{(iv)}$$

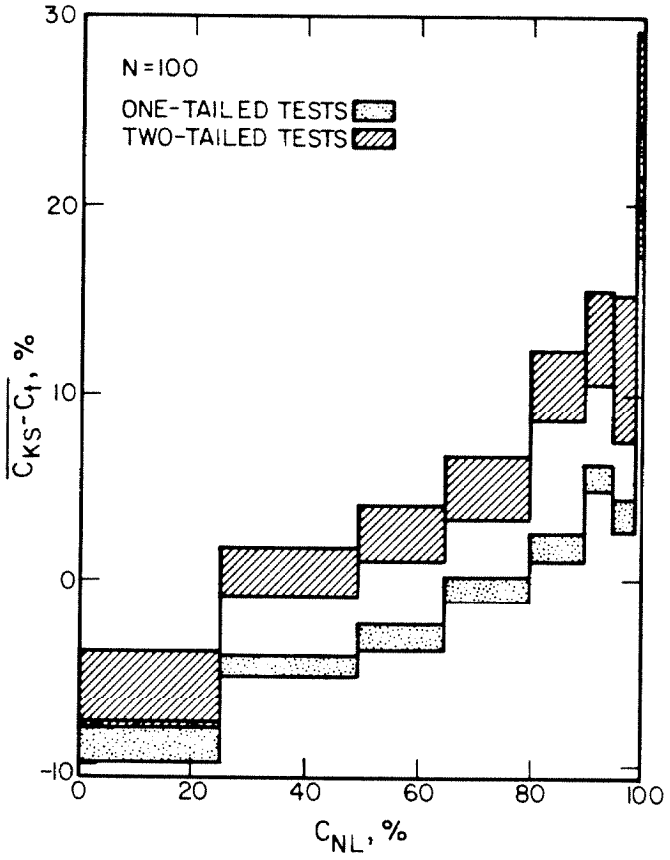

Number of Pairs (n) of Samples Tested

Range of C_{NL}, %	One-Tailed Test	Two-Tailed Test
$0 \leq C_{NL} < 25$	125	58
$25 \leq C_{NL} < 50$	462	232
$50 \leq C_{NL} < 65$	365	196
$65 \leq C_{NL} < 80$	362	176
$80 \leq C_{NL} < 90$	283	152
$90 \leq C_{NL} < 95$	220	105
$95 \leq C_{NL} < 99$	129	60
$99 \leq C_{NL} < 100$	54	21
$0 \leq C_{NL} < 100$	2000	1000

Fig. 3-B-1. The difference between the confidence with which H_o (populations are the same) is rejected by the Kolmogorov-Smirnov test (C_{KS}) and Student's t-test (C_t) increases for pairs of samples that appear to be drawn from non-normal populations for both one-tailed and two-tailed tests. However, the difference is greater for one-tailed tests. C_{NL} is the confidence with which the hypothesis that the sample is drawn from a normal population may be rejected. The mean difference between C_{KS} and C_t is plotted against the larger value of C_{NL} for the pair. Ordinate error bars are ± one standard deviation of the mean. The number of pairs (n) tested for each range of C_{NL} is tabulated at the right.

This is called the one-tailed test. Values of t for different levels of C_t are tabulated in various references (cf. Fisher, 1946). Functions describing the t distribution have also been reported (Abramowitz and Stegun, 1968, p. 948).

The two sample Kolmogorov-Smirnov test involves the calculation of the difference function

$$D(x) = CDF_2(x) - CDF_1(x) \qquad (v)$$

where CDF_1 and CDF_2 are the cumulative density functions or cumulative distributions of parameter x for samples 1 and 2 respectively. The statistic D_{max} is the largest absolute value of D(x), and is used to test H_o. To test H_1 the maximum value D_+ of D(x) is used instead. D_{max} or D_+ are compared to distributions of those statistics found by Monte Carlo experiments for samples randomly drawn from the same normal population. The confidence C_{KS_2} or C_{KS_1} with which H_o or H_1 may be rejected is found as for Student's t-test (equations (iii) and (iv)), except the PDF refers to D_{max} or D_+ instead of t.

There is no reason to presume that these different tests will generate the same confidence value in any given instance. The Kolmogorov-Smirnov test is sensitive to the shape of the distribution of the measured parameter x_{ij}, and generally neither D_{max} nor D_+ is zero even if the means x_1 and x_2 are the same. On the other hand, t is sensitive only to $(x_1 - x_2)$, and t may be zero even if the sample distributions are grossly different.

Because the t-test is insensitive to the shape of the distributions (presuming that they are normal), it will underestimate the confidence with which H_o or H_1 should be rejected if one of both populations are in fact not normally distributed. Because the Kolmogorov-Smirnov test is sensitive to shape as well as to $(x_1 - x_2)$, C_{KS} can be expected to

be larger than C_t in this case. However, if the samples are truly from normal populations, $C_t > C_{KS}$ because additional information (the distribution of the population) is used for the t-test.

In experimental situations there are bound to arise instances where normality can be neither confidently confirmed nor rejected. The purpose of this appendix is to define the relative performance of the two tests in such instances so that the proper test may be applied and so that the test results may be better interpreted. This was done by a Monte Carlo experiment in which two samples each containing N = 10, 20, or 100 "measurements" were drawn randomly from the same normal population, using a random number generator *. These pairs of samples were tested to determine with what confidence (C_{NL}) the hypothesis that the population of each sample was normally distributed could be rejected (see App. 3-A). Pairs were then grouped by the greater C_{NL}. For each pair, t, D_{max}, and D_+ were calculated. Next, the confidence with which H_o or H_1 could be rejected was was estimated from t and D_{max} or t and D_+, and the difference $C_{KS} - C_t$ was tabulated according to C_{NL}. The means of these tabulated differences, $\overline{C_{KS} - C_t}$, are plotted vs. C_{NL} in Fig. 3-B-1.

Figure 3-B-1 shows $\overline{C_{KS} - C_t}$ for one- and two-tailed tests of samples with N = 100. The number of iterations used to find the mean is shown in the included table. The error bars are $\pm$ 1 σ and are the standard deviation of the mean, not of the distribution of $\overline{C_{KS} - C_t}$. They were calculated according to $s/\sqrt{n}$ where s is the standard deviation of the n values of $C_{KS} - C_t$.

---

* The random number generator from the IBM Scientific Subroutine Package, for the IBM 360 series computers, was used.

Figure 3-B-1 shows that for both one- and two-tailed tests, $C_{KS} - C_t$ increases with C_{NL}. For $C_{NL} < 80\%$, Student's t-test rejects H_1 more often than does the Kolmogorov-Smirnov test. For $C_{NL} > 80\%$ the situation is reversed. For the two-tailed tests, the reversal occurs at $C_{NL} = 50\%$ rather than 80%. For $C_{NL} > 99\%$, $\overline{C_{KS} - C_t}$ is greater than 20%.

Figure 3-B-2 shows similar patterns for two-tailed tests when N = 10 and N = 20. As when N = 100, $\overline{C_{KS} - C_t}$ increased rapidly with C_{NL}, especially for $C_{NL} > 90\%$.

These results are important because they emphasize an undesirable aspect of statistical testing: the results may depend on the particular test as much as on the data. This problem is exacerbated when confidence level thresholds are established to define values of C_{KS} or C_t for which H_o (or H_1) may be rejected. In some instances, even small values of ($C_{KS} - C_t$) may lead to different conclusions. Furthermore, there seems to be no large range of C_{NL} for which $(\overline{C_{KS} - C_t})$ is zero or at least constant. Thus comparison of test results requires that C_{NL} be known, and even if it is, the relation between C_{KS} and C_t is only specified in a statistical sense. Partly because of the discrete values which D_{max} or D+ may assume, the distribution of $C_{KS} - C_t$ has a large standard deviation (generally ~ 15%). Thus for any individual pair of samples there is only a 25% probability that $C_{KS} - C_t$ will be within 5% of $\overline{C_{KS} - C_t}$. Individual values of C_{KS} and C_t are not easily related.

Figure 3-B-3 shows that the variation of $\overline{C_{KS} - C_t}$ with C_{NL} is paralleled by the variation of $\overline{C_{KS}}$ itself with C_{NL}, while C_t is essentially independent of C_{NL}. This was asserted at the beginning of this Appendix and attributed to the sensitivity of the Kolmogorov-Smirnov test to the

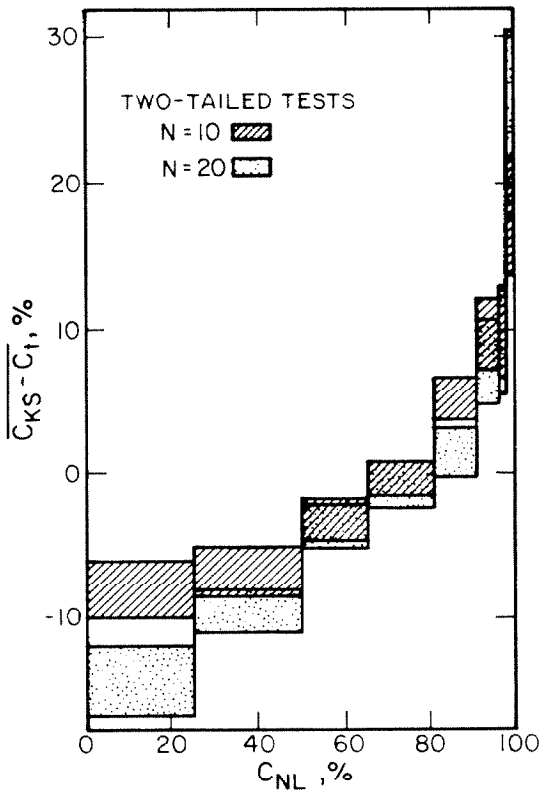

Number of Pairs (n) of Samples Tested

Range of C_{NL}, %	N = 10	N = 20
$0 \leq C_{NL} < 25$	56	60
$25 \leq C_{NL} < 50$	139	166
$50 \leq C_{NL} < 65$	160	139
$65 \leq C_{NL} < 80$	250	230
$80 \leq C_{NL} < 90$	191	208
$90 \leq C_{NL} < 95$	78	110
$95 \leq C_{NL} < 99$	84	66
$99 \leq C_{NL} < 100$	42	21
$0 \leq C_{NL} < 100$	1000	1000

Fig. 3-B-2. The difference between the confidence with which H_o (populations are the same) is rejected by the two-tailed versions of the Kolmogorov-Smirnov test (C_{KS}) and Student's t-test (C_t) increases for pairs of samples that appear to be drawn from non-normal populations. C_{NL} is the confidence with which the hypothesis that the sample was drawn from a normal population may be rejected. The mean difference bewteen C_{KS} and C_t for pairs of samples containing (a) ten and (b) twenty "measurements" (from a random number generator) is plotted against the larger value of C_{NL} for the pair. Ordinate error bars are ± one standard deviation of the mean. The number of pairs (n) tested for each range of C_{NL} is tabulated at the right.

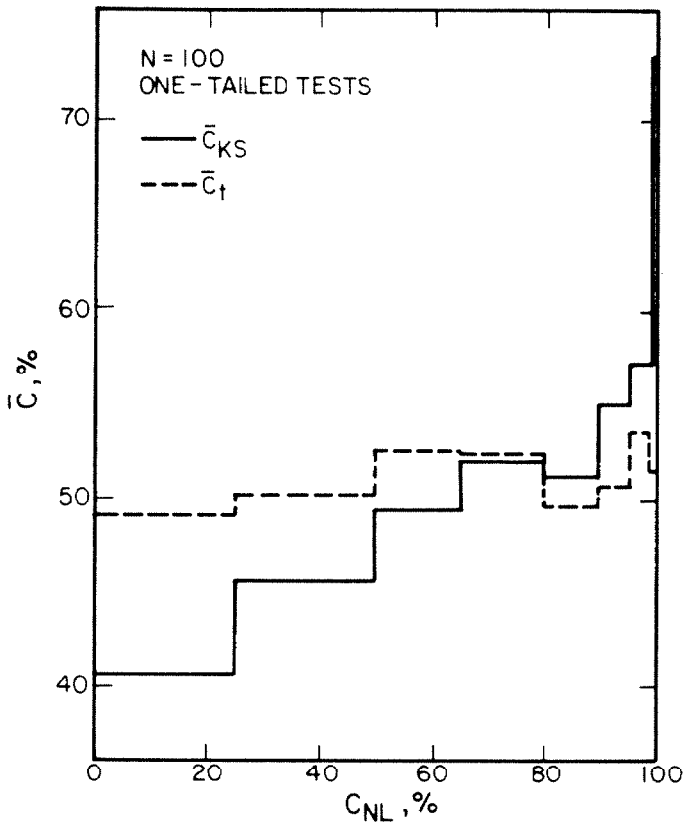

Number of Pairs (n) of Samples Tested

Range of C_{NL}, %	n
$0 \leq C_{NL} < 25$	67
$25 \leq C_{NL} < 50$	230
$50 \leq C_{NL} < 65$	169
$65 \leq C_{NL} < 80$	362
$80 \leq C_{NL} < 90$	283
$90 \leq C_{NL} < 95$	220
$95 \leq C_{NL} < 99$	129
$99 \leq C_{NL} < 100$	54
$0 \leq C_{NL} < 100$	1514

Fig. 3-B-3. The confidence C_t with which H_o (populations are the same) is rejected by Student's t-test is insensitive to C_{NL}, the confidence with which the hypothesis that the sample was drawn from a normal population may be rejected. The confidence C_{KS} with which H_o is rejected by the Kolmogorov-Smirnov test increases with C_{NL}. At high values of C_{NL}, C_t is probably too low because Student's t-test is insensitive to differences in the shape of the sample distribution. The values plotted are the means of n tests (n is tablulated at the right).

shape of the distributions, which can become a dominant factor if one or both of the samples appear to be from a non-normal population. The correlation coefficient r relating $\overline{C_{KS}}$ and $\overline{C_{KS} - C_t}$ is 0.988. For $\overline{C_t}$ and $\overline{C_{KS} - C_t}$, r= 0.286. Because both $\overline{C_{KS}}$ and $\overline{C_{KS} - C_t}$ are also correlated with C_{NL}, it is not immediately clear whether $\overline{C_{KS} - C_t}$ is actually dependent on C_{NL} or just on changes in the distribution of C_{KS}. For example, the increase in $\overline{C_{KS} - C_t}$ with C_{NL} might be due to the correlative increase in the fraction f_A of iterations for which $C_{KS} > A$, where A is some arbitrary value. In this case C_{KS} and C_t would be poorly correlated and whenever $C_{KS} > A$, $C_{KS} - C_t$ would have a high probability of being large regardless of C_{NL}. The absence of a strong correlation between f_A and $\overline{C_{KS} - C_t}$ would show that high values of $\overline{C_{KS} - C_t}$ were causally related to high values of C_{NL}. Such a relation might exist because large values of C_{NL} are found for distributions of complex shape to which the Kolmogorov-Smirnov (but not Student's t-test) is sensitive.

That a correlation does exist between F_A and C_{NL} is shown in Fig. 3-B-4a for the case where A = 90%. Figure 3-B-4b shows the correlation between f_{90} and $\overline{C_{KS} - C_t}$. Finally, Fig. 3-B-4c shows the hypothesized correlation between $\overline{C_{KS} - C_t}$ and C_{KS} is not pronounced. Consequently, it appears that the increase in $\overline{C_{KS} - C_t}$ does have a causal relationship to the complexity of one or both of the sample distributions.

The practical result of this study must be a guideline identifying the circumstances under which each text is appropriate. Such a guideline is difficult to formulate, because there is no large range of C_{NL} for which $\overline{C_{KS} - C_t}$ is zero or at least constant. In the absence of such a range of stability, the results of the two tests are not readily compared.

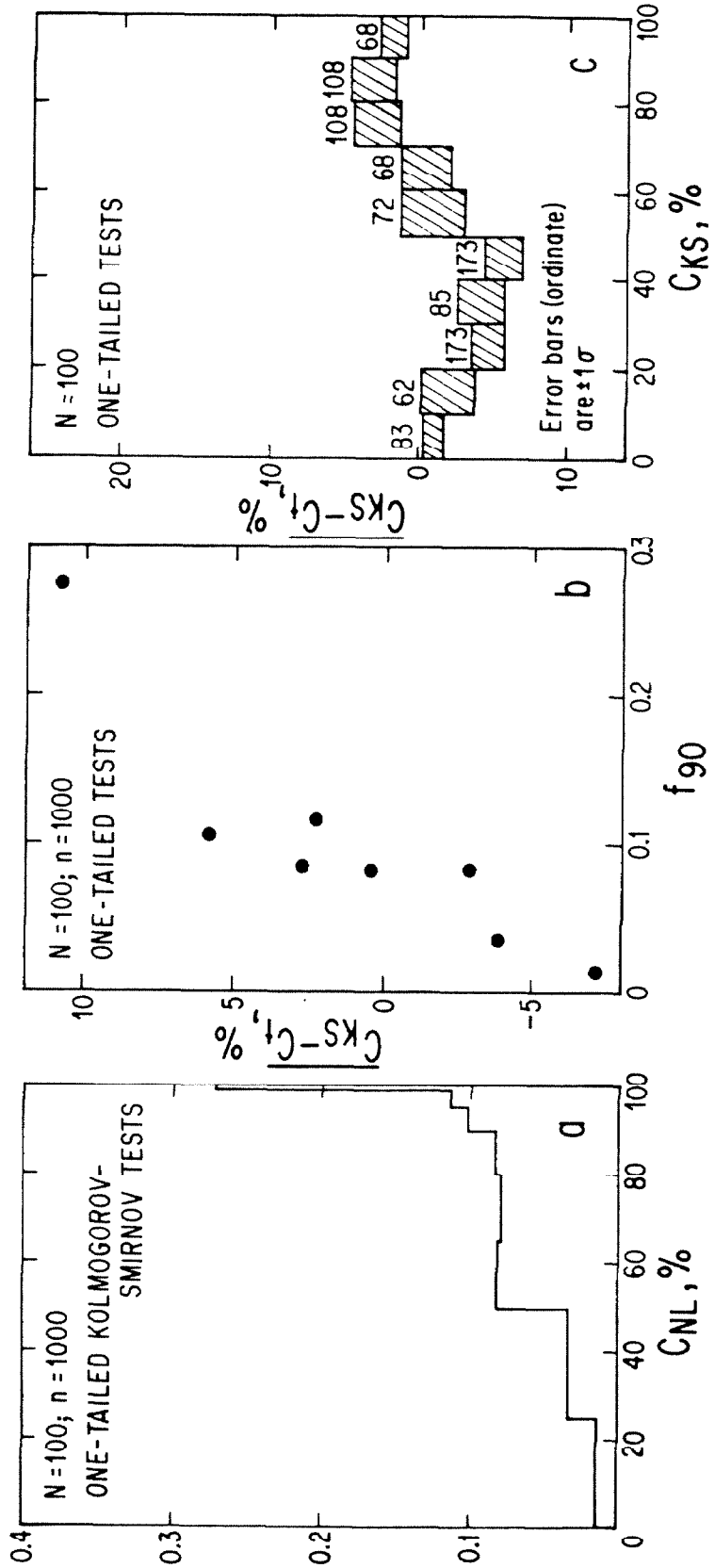

Fig. 3-B-4. The performance of the one-tailed Kolmogorov-Smirnov test. Two samples, each of 100 measurements, were drawn randomly from the same normal population. Hypothesis H_o (samples were from the same population) was tested by both the Kolmogorov-Smirnov test and by Student's t-test. The confidences with which H_o could be rejected were called C_{KS} and C_t, respectively. The samples in each pair were tested for normality using the one-sample Kolmogorov Smirnov test (see App. 3-A). The higher confidence with which the hypothesis of normality could be rejected was called C_{NL}. In all, 1000 pairs of samples were tested. The fraction f_{90} for which $C_{KS} > 90\%$ was tallied. In (a), f_{90} is seen to increase with the apparent non-normality, C_{NL}. About 28% of all tests when $C_{NL} > 99\%$ led to the rejection of H_o at the 90%-confidence level, compared to an expectation of 10%. Thus the test is too rigorous (C_{KS} is too high) for highly non-normal samples. In (b), the difference between the two tests is seen to be proportional to f_{90}. The tests agree when f_{90} is about 0.1, but for higher values of f_{90} the Kolmogorov-Smirnov test may on the average reject H_o with as much as 10% greater confidence. In (c), it is seen that this difference is probably not strongly related to C_{KS} itself. Therefore the variation in performance appears to depend on the normality of the samples rather than the results of the test per se. The Kolmogorov-Smirnov test may reject H_o too infrequently if $C_{NL} < 50\%$, but otherwise performs as expected (unless $C_{NL} > 99\%$).

There appears to be a break in slope in the $C_{KS} - C_t$ vs. C_{NL} curve between $C_{NL} = 95\%$ and $C_{NL} = 99\%$. For samples with C_{NL} greater than this, $(C_{KS} - C_t)$ may be as large as 20%. This is due to the complexity of one or both distributions, and shows that the Student t-test is inappropriate. There is no other obvious value of C_{NL} to choose as a threshold, based on the data presented in this appendix. Lower confidences (95% or 90%) are commonly used for rejecting an hypothesis. Because the t-test is predicated on the normality of the population it seems best to err on the conservative side, and for this study $C_{NL} = 90\%$ will be used as the threshold value. For $C_{NL} < 90\%$, Student's t-test (in some cases together with the Kolmogorov-Smirnov test) will be used. For $C_{NL} > 90\%$, only the Kolmogorov-Smirnov test will be used.

It should be possible to improve the Kolmogorov-Smirnov test by relating C_{KS} to D_{max} or D_+ using distributions of the test statistic calculated for random sample pairs having the same value of C_{NL} as the actual pair. In contrast, existing tables were compiled for all pairs regardless of C_{NL}. This new approach was not attempted for this study.

CHAPTER 4

DATING THE ERUPTION OF BASIC LAVAS BY ^{40}Ar - ^{39}Ar ANALYSIS OF GRANITIC XENOLITHS

The opportunity exists along parts of the escarpment on the east side of the Sierra Nevada to date glacial advances and to determine rates of tectonic displacement by analysis of lava flows interbedded with moraines or broken by faulting. Within the study area, these lava flows generally are alkalic olivine basalts, and they are extensively contaminated by fragments of the Mesozoic granitic rocks through which they were erupted. Except for very small ~ 10-μm blebs of glass or K-feldspar crystals within the groundmass, these xenocrysts and xenoliths are the most potassic components of the lava. As such they present a problem and offer an opportunity for dating the lavas by K/Ar methods.

The problem is that during immersion in the hot magma, the xenoliths are incompletely degassed of their ^{40}Ar created by radioactive decay of ^{40}K in the time since their original crystallization, about 90 my ago (Dalrymple, 1964a). Thus the sample of lava which contains a xenocryst will also contain ^{40}Ar in excess of the amount created since eruption, and this may lead to a high apparent age of eruption.

The opportunity is that by using the stepwise heating variant of the ^{40}Ar - ^{39}Ar dating method, it may prove possible at temperatures lower than those experienced by the xenolith in the magma to extract Ar free of the excess inherited ^{40}Ar. If this is the case, then the K-rich, coarse-grained xenoliths are excellent systems for dating.

In the discussion which follows, the rationale and experimental demonstration of this approach are discussed in detail. Extensive results for lava flows along the North Fork of Oak Creek and in Sawmill

Canyon, both in the study area, are presented.

4.0 INTRODUCTION

There are formidable obstacles to the precise and accurate dating of young basic lavas by conventional K/Ar methods. One of these is the presence of Ar dissolved in the magma. When trapped in young basalt, such Ar may mask the very small amounts of radiogenic ^{40}Ar ("$^{40}Ar^{*}$") created since eruption. Furthermore, the isotopic composition ($^{36}Ar/^{40}Ar$) of the trapped Ar ("Ar_t") is a priori unknown and cannot be measured by conventional K/Ar analysis. Indeed, analyses of lavas of zero age (Krummenacher, 1970; Kaneoka, 1980) have shown a significant variability in the composition of Ar_t which is attributed to mass fractionation. There is also no reason to exclude the possibility that the Ar_t may contain an admixture of pure $^{40}Ar^{*}$, perhaps derived from assimilation of wall rocks by the magma or from the original magma source.

Differences in the assumed compositions of the Ar_t affect the K/Ar age, and the effect increases rapidly as the ratio of radiogenic to trapped Ar decreases. An overestimate of 1% in an assumed composition of the Ar_t causes a 9% or a 98% increase in the K/Ar age if the amount of $^{40}Ar^{*}$ is 10% or 1% respectively of the total ^{40}Ar. An underestimate of the trapped $^{36}Ar/^{40}Ar$ could even result in a negative age.

For acidic lavas it is sometimes possible to increase the accuracy of the K/Ar age by dating two or more separates of different minerals from the same sample. As long as the different minerals have sufficiently different concentrations of K (and the same trapped $^{36}Ar/^{40}Ar$), both the $(^{36}Ar/^{40}Ar)_t$ and the K/Ar age may be accurately determined.

However, this approach is generally not applicable to young basic lavas, chiefly because these rarely have potassic phenocrysts.

A second obstacle to K/Ar dating is the presence in many lavas of microscopic fragments of ancient country rock rich in K which contain large amounts of $^{40}Ar^{*}$. Basalts of the Big Pine volcanic field are extensively contaminated by granitic xenoliths from the Mesozoic plutons through which the lavas erupted.

Hart (1964) showed that some potassic minerals heated sufficiently by the intrusion of a stock lost enough Ar that conventional K/Ar dating of the degassed crystals could in some cases give the age of the intrusion. Dalrymple (1964a) observed that if Ar loss in granitic xenoliths in lavas were complete, conventional K/Ar dating of the xenoliths could be used to measure the age of degassing of the xenoliths and hence the age of eruption of the lava. However, if such foreign material is not completely degassed during heating in the magma, the apparent eruption age of the lava will be too great.

Although the temperature of xenocrysts incorporated into basaltic magma at the time of eruption rises to ~ 1100°C within seconds and can remain this high for longer than a day while the lava flow solidifies, evidently not all the $^{40}Ar^{*}$ is diffused from the xenocryst. Dalrymple (1964a) has demonstrated Ar retention of ~ 2.5% in a 10-cm diameter granitic clast found 3 m below the top of a 25-m-thick basalt flow. Because the characteristic dimension of diffusion seems to be determined not by xenolith diameter but rather by individual grain size or width of exsolution lamellae in microcline, it must be concluded that even individual microscopic xenocrysts dispersed throughout the magma will be similarly retentive.

The increase in the K/Ar age of the whole basalt caused by such xenocrysts varies inversely with the ratio of the basalt's eruption age to the original crystallization age of the xenoliths. Inherited $^{40}Ar^*$ sufficient to increase the apparent age of a 10 my-old lava by only 0.1% will cause a 10% increase in 0.1 my-old lava. Such a bias might result if only 0.1% of a basic lava consisted of 100 my-old K-feldspar xenocrysts which were 90% degassed during eruption (i.e., if 1 g of such basalt contained a single xenocryst only 0.7 mm on a side). It is generally not possible to eliminate or even to detect contamination at this low level during preparation of samples for K/Ar analysis.

Thus conventional K/Ar dates of young basic lavas may be imprecise because of small amounts of $^{40}Ar^*$ compared to $^{40}Ar_t$ and inaccurate because of the unknown isotopic composition of Ar_t or the presence of inherited $^{40}Ar^*$ in incompletely degassed xenocrysts.

The stepwise heating ^{40}Ar-^{39}Ar method (Merrihue and Turner, 1966; Turner, 1970, 1971a) ameliorates many problems encountered in K/Ar dating. If trapped and radiogenic ^{40}Ar are contained in phases or sites with different retentivities, the resultant separation of the two types of Ar during stepwise thermal extraction may in principle permit the determination of the $^{36}Ar/^{40}Ar$ value of the trapped component, which generally dominates Ar released from the sample at low temperatures. Furthermore, Ar remaining in xenocrysts after degassing at 1100°C for many hours in the magma is unlikely to be degassed at lower temperatures in the laboratory. Therefore, it should be possible during ^{40}Ar-^{39}Ar analysis to separate the inherited $^{40}Ar^*$ from at least some of the $^{40}Ar^*$ created since cooling of the lava. At the very least this ability would serve to identify contaminated samples.

Berger (1975) has shown that ^{40}Ar-^{39}Ar age spectra of 1400 my-old biotites, hornblendes, and K-feldspars reflected thermal overprinting caused by the intrusion of the same stock studied by Hart (1964). A spectrum from biotites sampled 6 m from the stock was totally reset to ~ 63 my, the approximate age of the intrusion. Spectra from K-feldspars taken within 25 m of the stock exhibited plateaus containing four steps of similar low apparent ages and representing the ~ 25% of the total ^{39}Ar which was extracted at temperatures below ~ 900°C. During heating by the stock, ~ 95% of the ^{40}Ar in the feldspar was lost. The amount of $^{40}Ar^*$ created after cooling was ~ 6.5% of the $^{40}Ar^*$ present just before the intrusion. This situation is more favorable for the creation of plateaus than that envisioned in the present study, in which the ratio is less than 1.5% and possibly as small as 0.1%.

Radicati, Huneke, Papanastassiou, and Wasserburg (1981) have applied the ^{40}Ar-^{39}Ar method to coarse potassic crystals to determine precise ages of very young lavas. They observed well-defined plateau ages of 0.350±0.015 (2σ) my for phenocrysts of biotite and leucite from tuffs of the Roman volcanic province. The ^{40}Ar-^{39}Ar ages and the Rb-Sr ages determined on the same sample suite were found to be in good agreement. Trapped and radiogenic ^{40}Ar were well separated by their thermal release characteristics, and the large size of the phenocrysts avoided complications arising from ^{39}Ar recoil redistribution during neutron irradiation. Because most basic lavas do not have sufficiently potassic phenocrysts for ^{40}Ar-^{39}Ar dating of mineral separates, the results of Radicati et al. are not widely applicable. In this study the ^{40}Ar-^{39}Ar method has been applied to granitic xenoliths which are similar to potassic phenocrysts in that they contain large grains and are rich in

K compared to the host basalt. Thus the effects of ^{39}Ar recoil and of Ar_t are reduced compared to those expected for the ^{40}Ar-^{39}Ar dating of the lava itself.

During heating in the magma some Ar diffuses from the ancient xenocrysts. The extent of degassing depends on characteristics of the xenocrysts, the temperature of the magma, and the time it takes to cool. The extent of degassing determines the shape of the ^{40}Ar-^{39}Ar age spectrum, as shown schematically in Fig. 4-1. If there has been no degassing, the age spectrum will be undisturbed and the ages calculated from each fraction of Ar released will be constant and equal to the age of original crystallization or closure of the crystal lattice to Ar diffusion. This is the case for curve "a." If degassing has been minor, ages for the first fractions of Ar (released at low temperatures) will be younger ("b"); these may approach the age of eruption, but only for the first infinitesimal fraction will that age actually be found. As in "a," Ar released at high temperatures will yield the age of crystallization. If there has been major degassing, the amount of ^{39}Ar associated with the original crystallization age will be reduced. If even the $^{40}Ar^*$ from the most retentive sites has been partially depleted at the time of eruption, the maximum apparent age will be less than the original age of the xenocryst ("c" and "d") and no plateau at the age of crystallization will be found. However, the size of the low-temperature plateau will increase with the extent of degassing until, for complete degassing, the entire age spectrum reflects the age of eruption ("e").

As shown by Dalrymple (1964a), complete degassing of xenocrysts in basaltic magma not always achieved. We might therefore expect a xenocryst age spectrum characterized by a region of mixed ages separating

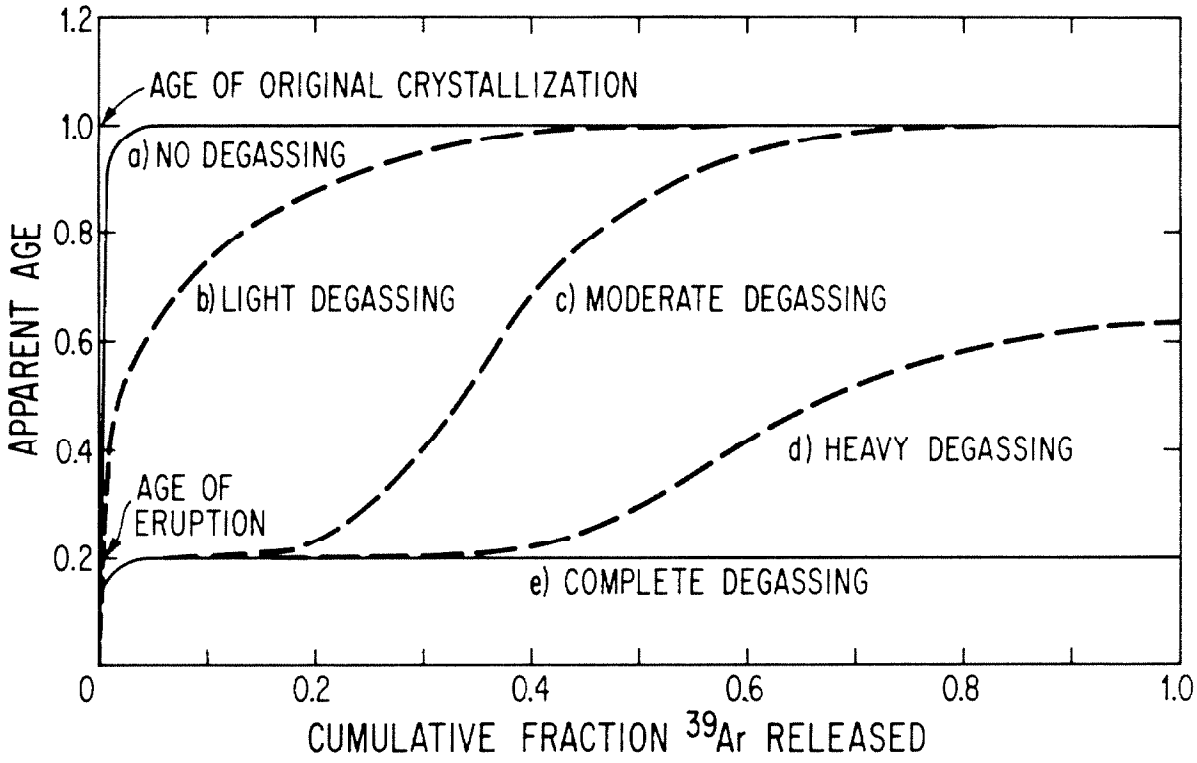

Fig. 4-1. Schematic ^{40}Ar-^{39}Ar age spectra show increasing depression of apparent age with extent of degassing of ancient xenocrysts in lava during eruption at age 0.2. Original age of crystallization is 1.0. For no degassing in the magma ("a"), entire age spectrum comprises plateau of age 1.0. Curves "b," "c," and "d" show progressive decrease in size of plateau at age 1.0 and development of plateau at age = 0.2 as level of degassing is increased. If degassing is complete ("e"), only an eruption age plateau is observed. The minor depression in age at low ^{39}Ar released reflects losses by diffusion at temperatures less than about 50°C over long periods of time.

plateaus corresponding to the times of crystallization and eruption. Depending on the degassing of the xenocryst, one or both age plateaus might not be found. If an eruption age plateau is not found, the minimum apparent age will be an upper limit to the age of eruption.

Wasserburg et al. (1956) noted discrepancies in K/Ar ages of cogenetic K-feldspar and muscovite from plutonic rocks which they have attributed to diffusive loss of Ar. Diffusive loss of Ar from silicate minerals at temperatures less than 50°C is exceedingly inefficient, and only Ar from the least retentive sites will be lost from xenocrysts after degassing in magma which has been erupted and cooled to such low temperatures. Consequently, young ages from this cause will be restricted to the first fraction of Ar released during stepwise analysis (e.g., Huneke, 1976) and will not erase the eruption age plateau. Minor diffusive loss is indicated in the age spectra of Fig. 4-1.

In the following section (§4.1) is found an assessment of those factors which determine whether or not an eruption age can indeed be determined through the study of incorporated xenoliths. It must be demonstrated that there are reasonable conditions under which a reservoir of ^{40}Ar in the xenolith may be sufficiently degassed during eruption to yield at a later date an age plateau corresponding to the time of degassing, and that during the analysis of the Ar released during the laboratory heating steps, the ^{40}Ar contributed from other incompletely degassed reservoirs is not so large as to mask this plateau.

The factors affecting the development of a plateau at the age of degassing or eruption are: (1) the extent of degassing of the xenolith in the host magma; (2) the original crystallization age of the xenolith relative to the time of degassing by the host magma; (3) the

distribution in grain size of the minerals in the xenolith; and (4) the activation energies for Ar diffusion from the minerals in the xenolith. Models using simple volume diffusion from different populations of spheres are used for an assessment of these factors.

These models demonstrate the feasibility of using "granitic" xenoliths to date Quaternary basalt eruptions and to provide both guidance in the design of dating experiments and a framework for interpreting experimental results. On the basis of these models a measure of merit is developed for the assessment of age plateaus in ^{40}Ar-^{39}Ar apparent age spectra or other problems of this type.

4.1 AN ASSESSMENT OF ^{40}Ar-^{39}Ar DATING OF INCOMPLETELY DEGASSED XENOLITHS

The Development of Eruption-Age Plateaus

To assess the feasibility of obtaining reasonable eruption ages from partially degassed xenoliths, the Ar loss in a xenolith during heating in a magma and subsequent heating in the laboratory for ^{40}Ar-^{39}Ar analysis is described by simple volume diffusion from spheres, assuming different grain-size distributions and activation-energy distributions. The diffusion characteristics of the material of each sphere are assumed to be uniform and isotropic. Diffusion out of the grains is be described by Fick's law, which for radial diffusion in isotropic spheres is

$$\frac{\partial C(r,t)}{\partial t} = D(T(t))\, r^{-2} \frac{\partial}{\partial r}\left(r^2 \frac{\partial C(r,t)}{\partial r}\right) \qquad (1)$$

where C(r,t) is the concentration of Ar, r is radial distance from the center of the sphere, t is time, and D is the diffusion coefficient. The concentration of Ar at the sphere boundaries (r=0) is taken to be zero, and the

concentration of ^{40}Ar and K is uniform for all grains at t=0, the time the xenolith is engulfed by the magma. The diffusion coefficient is related to temperature T(t) by the Arrhenius equation

$$D(T(t)) = D_o \exp(-Q/RT(t)) \tag{2}$$

where R is the gas constant, Q is the activation energy for diffusion, and D_o is a characteristic constant. The temperature of the xenolith and thus the diffusivity varies with time t after the xenolith fell into the magma at t= 0, and this variation in D is accounted for by introducing the dimensionless variable

$$\tau \equiv (D_o/a^{-2}) \int_o^t \exp(-Q/RT(\eta))d\eta \tag{3}$$

where a is the grain radius. Shortly after eruption, the lava freezes and the xenolith cools sufficiently to stop diffusion. The cumulative fraction F of Ar lost from a given grain is a function of the integrated diffusion history given by:

$$F(\tau) = 1 - (6/\pi^2) \sum_{n=1}^{\infty} n^{-2} \exp(-\pi^2 n^2 \tau) \tag{4}$$

(cf. Carslaw and Jaeger, 1959; or Crank, 1956) For reference, Eq. (4) is shown graphically in Fig. 4-2.

As seen from Eqs. (2) and (3), the three parameters that govern Ar loss from the model are the grain radius a, the activation energy Q, and D_o. A given rock sample may be considered to have different distributions of grains according to these parameters. The diffusion of Ar from grains is affected identically by changes in D_o or by changes in a^2. For the purposes of this analysis, D_o will arbitrarily be assigned a value of unity for all spheres. Thus only the two parameters a and Q are used to characterize the grains.

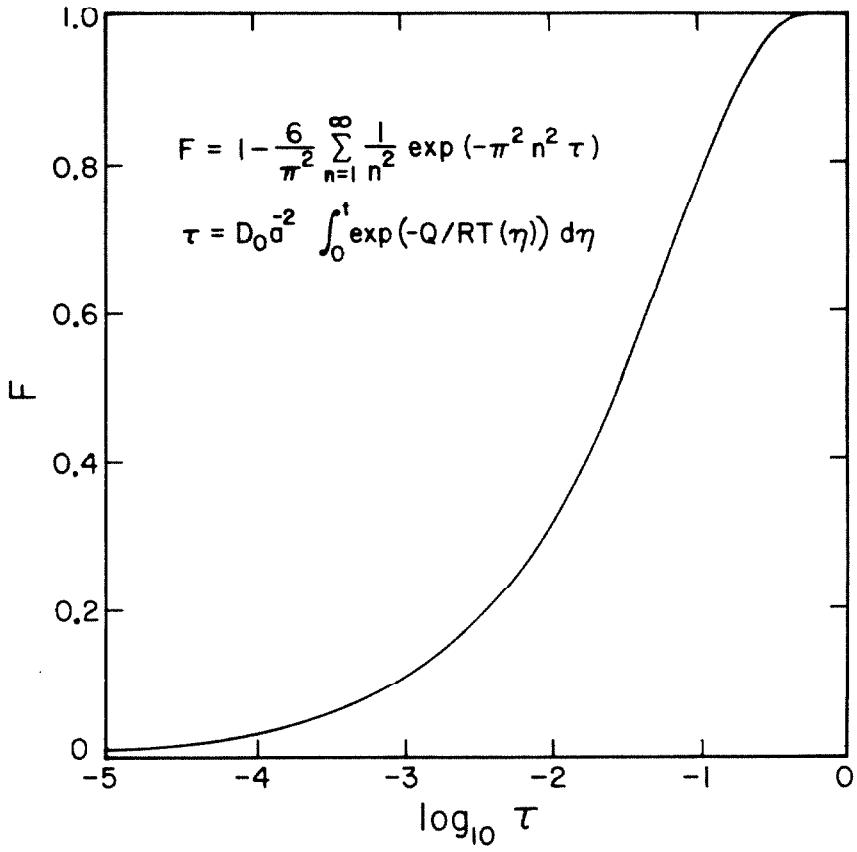

Fig. 4-2. Fractional loss F of Ar from a spherical crystal according to the exact solution of the diffusion equation.

We may express the cumulative fraction of ^{40}Ar lost by time t from a population (p) of grains by

$$F_p(t) = \frac{\int_0^\infty \int_0^\infty (4/3)\pi a^3 C_1 \, P(a,Q) \, F(\tau(a,Q,T,t)) \, da \, dQ}{\int_0^\infty \int_0^\infty (4/3)\pi a^3 C_1 \, P(a,Q) \, da \, dQ} \qquad (5)$$

where P(a,Q)dadQ is the probability that a sphere has a radius between a and (a + da) and an activation energy between Q and (Q + dQ). Each grain is taken to have the same concentration C_1 of radiogenic ^{40}Ar. It has been assumed that the Ar and K are uniformly distributed throughout each sphere, that the concentration of K in each grain is the same, and that $F_p = 0$ at $t = 0$. The ratio of C_1 to the concentration of ^{40}K is related to the age of original crystallization t_c by

$$t_c = (\lambda_e+\lambda_\beta)^{-1} \ln\left(1 + \frac{\lambda_e+\lambda_\beta}{\lambda_e} \frac{C_1}{C_{K40}}\right) \qquad (6)$$

where λ_e and λ_β are the decay constants for ^{40}K, and C_{K40} is the concentration of ^{40}K at the time of analysis.

Figure 4-3 illustrates the temperature history of the grains. Diffusive loss of Ar begins at $t = 0$ as the grains are heated. This corresponds to immersion of the xenolith in the magma. Shortly after eruption at t_c the lava freezes and the xenolith cools sufficiently to stop diffusion. In the model this occurs at $t = t_e$. For simplicity, the heating episode is assumed to be so short that ^{40}Ar created during it can be ignored. Thus a fraction $F(\tau_e)$, where $\tau_e = \tau(a,D(T),t_e)$, of the ^{40}Ar present in a grain of radius a at t=0 is lost by t_e and a fraction $F_p(t_e)$ is lost from a population of grains.*

* For notational simplicity, F_p will be referred to as $F_p(t_e)$, a function of time rather than τ_e. This is because there may be no single value of τ_e for grains in a population. $F_p(t_e)$ is implicitly a function of a, Q, P(a,Q), and T(t) (see Eq. 5).

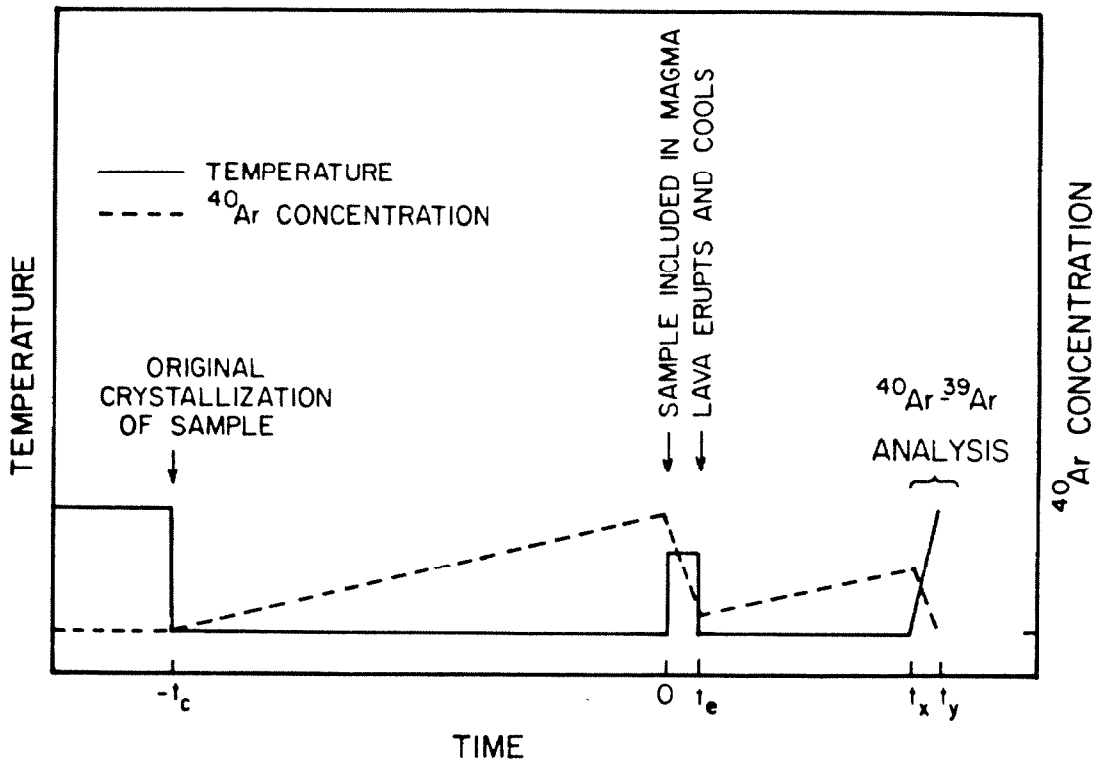

Fig. 4-3. Schematic history of temperature and ^{40}Ar accumulation in a model heated briefly from $t = 0$ to $t = t_e$ by incorporation into a magma. Prior to original crystallization, the model is hot and no ^{40}Ar accumulates. From $t = -t_c$ to $t = 0$, ^{40}Ar accumulates without loss. Most is lost from the model during heating in the magma. After cooling ^{40}Ar once again accumulates and is added to the residue which was not degassed from $t = 0$ to $t = t_e$. All ^{40}Ar is extracted during analysis. For simplicity, t_e and $t_y - t_x$ are considered to be grossly less than t_c or $t_x - t_e$, respectively, and the ^{40}Ar accumulated during these short intervals is ignored.

We assume that there is no further loss of Ar from t_e to t_x, when analysis is begun. After t_e, radiogenic ^{40}Ar again begins accumulating from the decay of ^{40}K, and this is added to the residue of radiogenic ^{40}Ar which was not degassed during heating in the magma. We denote the concentration of new ^{40}Ar by C_2. After the sample is brought to the laboratory at time t_x, it is irradiated to produce ^{39}Ar. Thus at t_x there is: (1) "new" ^{40}Ar created since t_e; (2) "residual" ^{40}Ar created before t = 0; and (3) ^{39}Ar. The number of atoms of each kind of Ar in the sphere is denoted by $N_{40(new)}$, $N_{40(res)}$, and N_{39}, respectively. The total number of atoms of ^{40}Ar is denoted by $N_{40} = N_{40(new)} + N_{40(res)}$. In the discussion which follows , the ^{40}Ar created by t = 0 is labeled "initial" ^{40}Ar.

The second step in ^{40}Ar-^{39}Ar analysis is the extraction and measurement of Ar from the sample. To do this the sample is reheated in the laboratory (L) beginning at t_x, and diffusive loss is renewed. The temperature is increased until the sample melts at t_y. ^{40}Ar created during the brief analysis is ignored. At any time t_L during the extraction $\tau_L \equiv a^{-2} \int_{t_x}^{t_L} D(T(\eta))d\eta$. For a single sphere, the fraction of the new ^{40}Ar (and also ^{39}Ar) extracted from t_x to t_L is given by $F(\tau_L)$. The rate of extraction of "new" ^{40}Ar is

$$\dot{N}_{40(new)} = (4/3)\pi\, a^3\, C_2 \frac{d\, F(\tau_L)}{d\tau_L}\, \dot{\tau}_L \qquad (7)$$

At the same time, the residual ^{40}Ar left in each sphere upon cooling at t_e is also extracted. The amount extracted in the laboratory from t_x to t_L is given by $(4/3)\pi a^3 C_1(F(\tau_e+\tau_L) - F(\tau_e))$. This residual ^{40}Ar is extracted at a different rate than the new ^{40}Ar:

$$\dot{N}_{40(res)} = (4/3)\pi\, a^3\, C_1 \frac{d\, F(\tau_e+\tau_L)}{d\tau_L}\, \dot{\tau}_L \qquad (8)$$

The total ^{40}Ar released from the sphere between t_x and t_L is simply

$$N_{40} = (4/3)\pi\ a^3 \left[C_1\ (F(\tau_e+\tau_L) - F(\tau_e)) + C_2\ F(\tau_L)\right] \qquad (9)$$

and the total rate of extraction at t_L is

$$\dot{N}_{40} = (4/3)\pi\ a^3 \left(C_1 \frac{d\ F(\tau_e+\tau_L)}{d\tau_L} + C_2 \frac{d\ F(\tau_L)}{d\tau_L} \right) \dot{\tau}_L \qquad (10)$$

The ^{39}Ar is created in proportion J to the concentration of ^{39}K (C_{K39}), and hence to the concentration of ^{40}K as well. It is degassed at the rate

$$\dot{N}_{39} = (4/3)\pi\ a^3\ J\ C_{K39} \frac{d\ F(\tau_L)}{d\tau_L}\ \dot{\tau}_L \qquad (11)$$

if ^{39}Ar and ^{40}Ar both have the same diffusivity. Thus, at any instant during analysis, the relative rate of degassing of ^{40}Ar compared to ^{39}Ar from the entire model is found from Eqs. (5), (10), and (11):

$$dN_{40}/dN_{39} = \dot{N}_{40}/\dot{N}_{39}$$

$$\frac{d\ N_{40}}{d\ N_{39}} = \frac{\int_0^\infty \int_0^\infty a^3\ P(a,Q)\ \left[C_1\ \dot{F}[\tau_e(a,D(T),t_e)+\tau_L(a,D(T(t)),t)] + C_2\ \dot{F}[\tau_L(a,D(T(t)),t)]\right] da\ dQ}{\int_0^\infty \int_0^\infty a^3\ P(a,Q)\ J\ C_{K39}\ \dot{F}[\tau_L(a,D(T(t)),t)]\ da\ dQ} \qquad (12)$$

where N_{40} and N_{39} are now understood to refer to the entire assemblage of spheres and not to just a single sphere.

From the ratio found from Eq. (12), an apparent age A for each differential amount of Ar released can be calculated by

$$A(t) = (\lambda_e+\lambda_\beta)^{-1}\ \ln\left(1 + \frac{\lambda_e+\lambda_\beta}{\lambda_e}\ J\ \frac{C_{K39}}{C_{K40}}\ \frac{\dot{N}_{40}}{\dot{N}_{39}}\right) \qquad (13)$$

Thus, the apparent age may vary throughout the analysis. A plot of A(t) versus the cumulative fraction $F_{39} \equiv F_P(t_L)$ of ^{39}Ar extracted from the population of spheres is the conventional age spectrum. The principal difference between the theoretical spectrum and the age spectrum obtained experimentally is the discrete nature of the latter. In an experiment, a finite amount of Ar must be extracted before a measurement is possible. This is done by raising the temperature of the sample in a series of large steps and extracting Ar for a long time at each step. Thus, for the experimental case the variable τ is given by

$$\tau_n = a^{-2} \sum_{i=1}^{n} D(T_i)(t_i - t_{i-1}) \quad ; \quad t_o = t_x \tag{14}$$

and Eq. (12) may be modified to

$$\left(\frac{\Delta N_{40}}{\Delta N_{39}}\right)_n = \frac{\int_0^\infty \int_0^\infty a^3 P(a,Q) \left[C_1(F(\tau_e+\tau_n) - F(\tau_e+\tau_{n-1})) + C_2(F(\tau_n) - F(\tau_{n-1}))\right] da\, dQ}{\int_0^\infty \int_0^\infty a^3 P(a,Q)\, JC_{K39} (F(\tau_n) - F(\tau_{n-1}))\, da\, dQ} \tag{15}$$

The apparent age at step n is given by

$$A_n = (\lambda_e+\lambda_\beta)^{-1} \ln\left(1 + \frac{\lambda_e+\lambda_\beta}{\lambda_e} J \frac{C_{K39}}{C_{K40}} \frac{\Delta N_{40}}{\Delta N_{39}}\right)_n \tag{16}$$

Eqs. (13) and (16) are exact descriptions of age spectra resulting from continuous measurement or stepwise heating and measurement of Ar during ^{40}Ar–^{39}Ar analysis. The solution of Eq. (13) used in the generation of several figures in this discussion is described in App. 4-A, part I.

We next turn to some simple illustrations of theoretical $\Delta N_{40}/\Delta N_{39}$ spectra and age spectra. In Fig. 4-4 three $\Delta N_{40}/\Delta N_{39}$ spectra are shown for Ar released from a single sphere from which half the initial ^{40}Ar was lost during heating in the magma ($F(\tau_e) = 0.5$). It was assumed

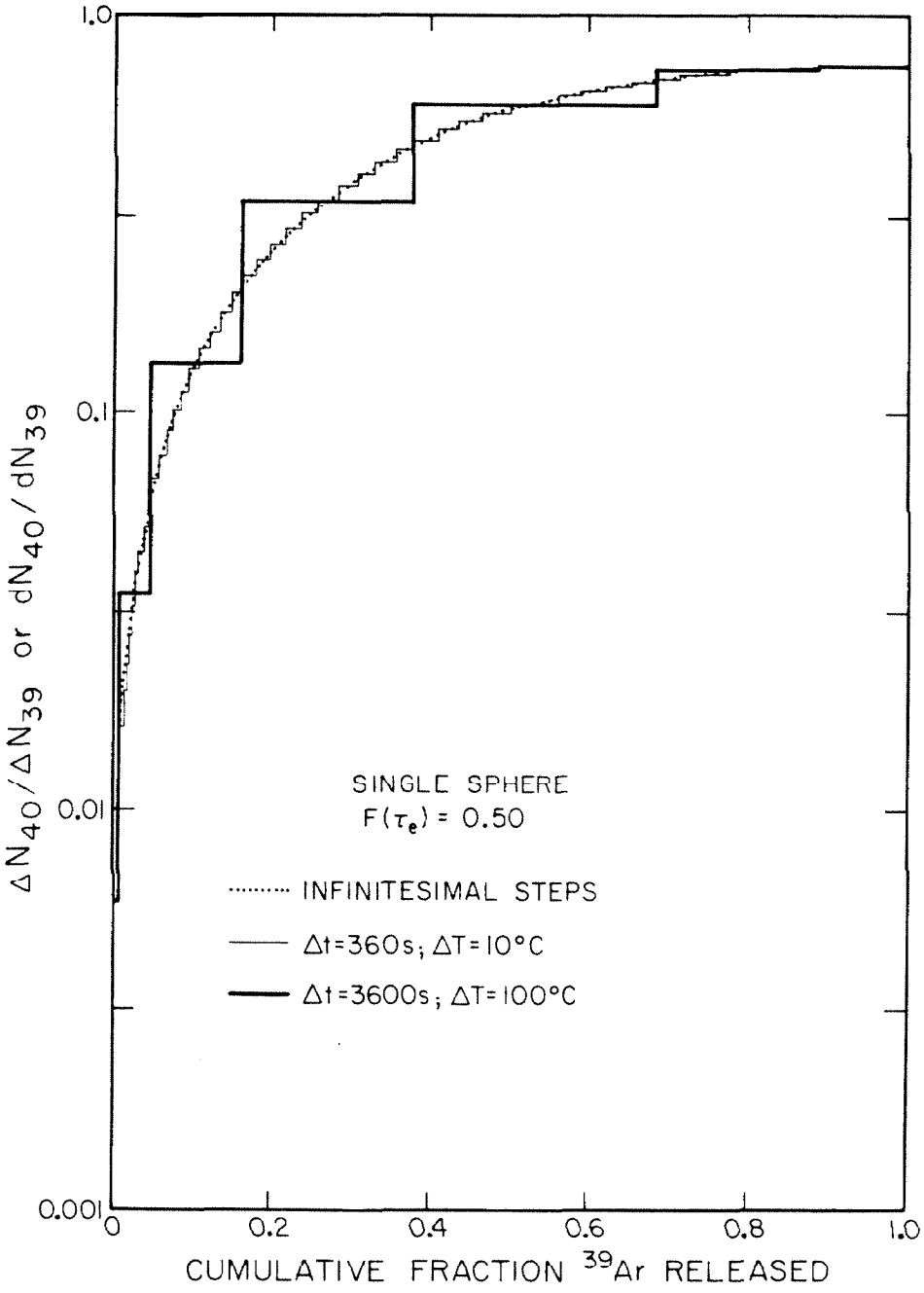

Fig. 4-4. Spectra for a single sphere degassed of half the initial ^{40}Ar before analysis show the effect of stepwise heating and measurement. For case 1, $\dot{N}_{40}$ and $\dot{N}_{39}$ were calculated for various times during "analysis" and their ratio dN_{40}/dN_{39} was plotted against $F(\tau_L)$, the fractional loss of ^{39}Ar. This spectrum would result if Ar was continuously measured as it diffused from the sphere. In experimental situations, Ar is accumulated for some Δt before measurement. At the end of each period Δt the temperature is incremented by ΔT. This results in stepped age spectra (case 2 and case 3). For these cases, ΔN_{40} and ΔN_{39} were calculated at the discrete intervals of Δt and ΔT as indicated. Case 2 is similar to the ideal differential spectrum (case 1). Case 3 most closely resembles experimental data.

that analysis immediately followed cooling of the lava so that no new ^{40}Ar was present. It was further assumed that $JC_{K39} = C_1$, so that $\Delta N_{40}/\Delta N_{39} = 1$ corresponds to the age of original crystallization (t_c).

These spectra show the influence of stepwise heating and measurement. In the first case the spectrum was found from Eq. (12) and represents continuous measurement of dN_{40}/dN_{39}. The stepped spectra were found from Eq. (15) using different values of Δt and ΔT. In the second case, Ar was extracted in a large number of small steps. The spectrum is similar to the first. In the third case Ar was extracted in only seven steps.

The continuous spectrum (first case) is independent of D and T(t). Its shape is determined solely by $F(\tau_e)$. $F(\tau_e)$ controls the overall shape of the stepped spectra, also. However, the size of the steps (fraction of ^{39}Ar released) and the exact values of $\Delta N_{40}/\Delta N_{39}$ are determined by Δt, D_o/a^2, and $Q/(RT(t))$. Thus in principal the distribution of steps in age spectra may be controlled by selection of appropriate values of Δt and T(t).

The third spectrum most closely resembles actual experimental results, but the continuous spectrum gives more insight into the behavior of the system itself, independent of arbitrary characteristics of the analysis.

It is clear from Fig. 4-4 that before 10% of the ^{39}Ar has been released from the sphere, the rate of residual ^{40}Ar loss has exceeded 10% of the rate for identical grains which were never immersed in the lava. The relative rate depends on $F(\tau_e)$. Turner (1968) has shown that even if $F(\tau_e) = 0.95$, $dN_{40(res)}/dN_{39}$ is still nearly 0.01 when 10% of the ^{39}Ar has been degassed. $F(\tau_e)$ must exceed 0.99 before a sizable fraction (e.g., 25%) of the ^{39}Ar is released unaccompanied by significant amounts of residual ^{40}Ar. This must occur if a plateau in the age spectrum identifying the age of eruption is to be developed. The actual value of $dN_{40(res)}/dN_{39}$ which may be tolerated in a

plateau is some fraction of $dN_{40(new)}/dN_{39}$, for instance 5%. Thus if $C_1/C_2 = 100$ it might be necessary for dN_{40}/dN_{39} to be less than (say) 0.0005 when 25% of the ^{39}Ar has been released for a plateau to be considered present. To achieve this, $F(\tau_e)$ must exceed 0.9991, or τ_e must exceed 0.6571. In the discussion below, this critical value of τ_e will be referred to as τ_{crit}. Turner concluded that single spheres or populations of identical spheres were unlikely to yield plateaus corresponding to the age of thermal events after original crystallization.

Equation 3 shows that τ_{crit} may be achieved by immersion of any sphere in a magma for a long enough time. This time is less if the sphere has a low activation energy, or a small radius, or if the lava temperature (T_{lava}) is high. T_{lava} and t_e are extrinsic to the sphere, and in a given lava, spheres that will achieve τ_{crit} have parameters specified by $\ln(D_o/a^2) - Q/(RT_{lava}) = \ln \tau_{crit} + \ln t_e$. This relation is shown graphically in Fig. 4-5.

Figure 4-5a shows that a single value of τ defines a plane in a cartesian space whose axes are $Q/(RT_{lava})$, $\ln (D_o/a^2)$, and $\ln t$. These planes intersect the $\left(Q/(RT_{lava}), \ln (D_o/a^2)\right)$ plane in lines having slopes of unity. In an isothermal lava, a sphere plotting at point P will evolve with time along a line parallel to the $\ln t$ axis, intersecting the τ_{crit} plane at P'. If t_e exceeds the time required to achieve τ_{crit}, the sphere will have been degassed sufficiently to develop a plateau corresponding to the age of eruption. At any given t, spheres which plot on the same line in the $\left(Q/(RT_{lava}), \ln (D_o/a^2)\right)$ plane will be equally degassed. Thus the effect on $F(\tau_e)$ of increasing $Q/(RT_{lava})$ by α is the same as decreasing D_o by a factor of e^{α} or increasing the radius by a factor of $e^{\alpha/2}$. After time t_e, only spheres plotting on or below the line of τ_{crit} will yield plateaus giving the age of eruption.

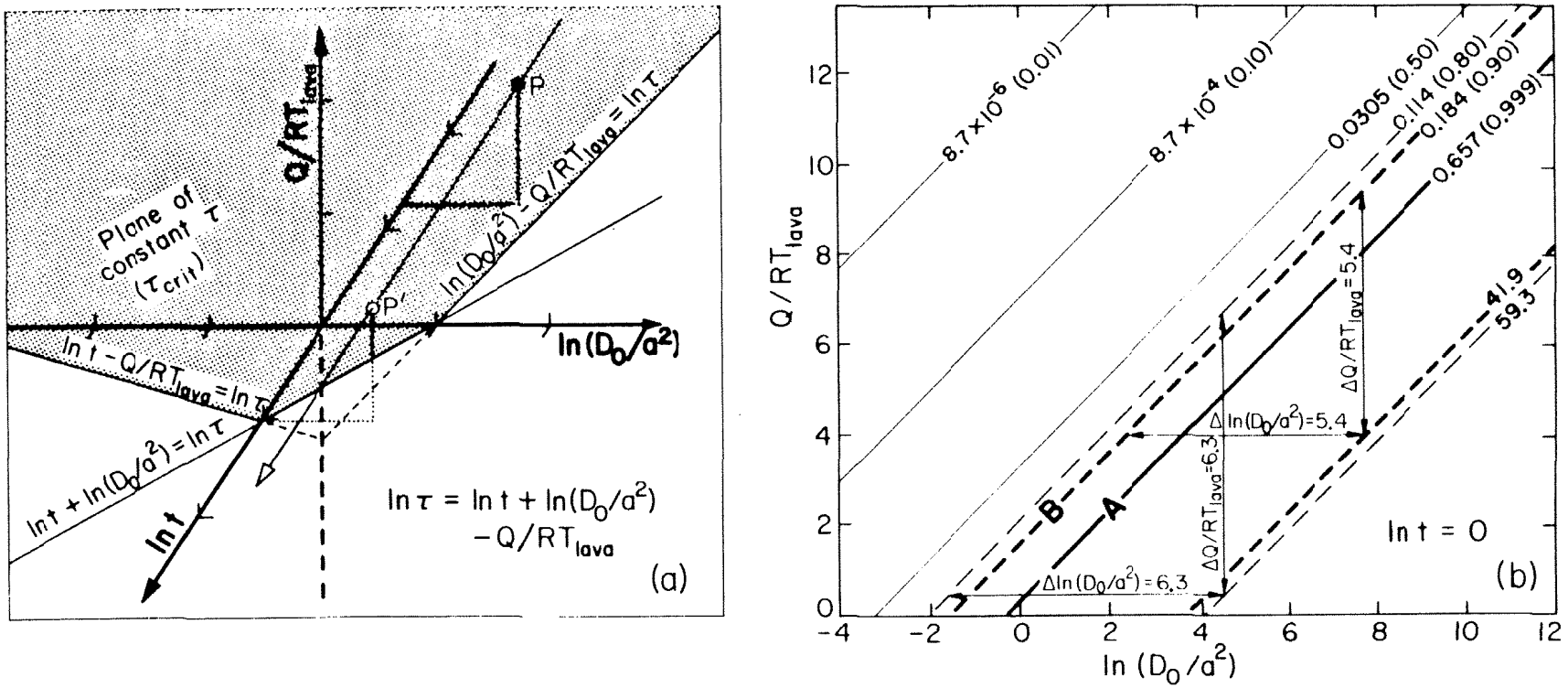

Fig. 4-5. The extent of degassing of a sphere at constant temperature is a function of the activation energy Q, the grain radius a, the value of D_o, and the time t since heating commenced. See next page for explanation.

Fig. 4-5. The extent of degassing of a sphere at constant temperature is a function of the activation energy Q, the grain radius a, the value of D_o, and the time t since heating commenced.

a) A depiction of the relation $\ln \tau = \ln t + \ln (D_o/a^2) - Q/RT_{lava}$ shows the line of intersection of a plane of constant τ and the plane $(Q/(RT_{lava}), \ln(D_o/a^2))$. The plane shown is taken to be the plane of τ_{crit} (see text). The coordinates for a grain initially plotting at point P will progress along a trajectory parallel to the ln t axis with the passage of time. At some time, the grain will plot at point P' in the plane of τ_{crit}. At this time, sufficient ^{40}Ar has been lost that a plateau in the age spectrum corresponding to the age of eruption may be established upon later analysis. If the sphere is heated longer, τ_{crit} will be exceeded. The lower hemisphere is forbidden because the activation energy Q is a non-negative number. Lines in the lower hemisphere are dashed. Stippling shows the portion of the plane of τ_{crit} which is in the first quadrant of the upper hemisphere.

b) Various lines of constant τ are shown in the $(Q/RT_{lava}, \ln (D_o/a^2))$ plane for which ln t = 0. Values of τ are shown for each line; values of $F(\tau)$ are shown in parentheses. Line A is the line of τ_{crit}. If $C_1/C_2 = 100$, a single sphere plotting on this line will have been degassed sufficiently that a plateau in the age spectrum identifying the age of eruption may be found (see text). Spheres plotting above line A will not yield such plateaus. For example, spheres plotting on line B are only degassed of 90% of their ^{40}Ar in the lava, and the apparent age over the whole spectrum will exceed the age of eruption by more than the threshold level, assumed to be 5% in this discussion.

Populations of equal volumes of two kinds of spheres differing in either (D_o/a^2) or in Q may yield plateaus giving the age of eruption, even though the total degassing F_p is such that a single sphere of $F = F_p$ would plot above line A (laboratory degassing is assumed to be at constant temperature $T_L = T_{lava}$ in this discussion). For instance, such a population consisting of spheres with τ_e = 0.114 and τ_e = 59.3 (dashed lines) would have F_p = 0.9; nevertheless, a plateau giving the age of eruption would be developed. The spheres might be characterized by grain radii different by a factor of 23 $(\Delta \ln(D_o/a^2) = 6.3)$ or by differences in Q/RT_{lava} of 6.3. These differences are reduced as F_p is increased. The heavy dashed lines (τ_e = 0.184 and τ_e = 41.9) show the requirements for a bimodal population of F_p = 0.95: $\Delta \ln(D_o/a^2)$ or $\Delta Q/RT_{lava}$ is reduced from 6.3 to 5.4.

Figure 4-5b shows the plane $(Q/(RT_{lava}), \ln (D_o/a^2))$ with several *different lines of constant* τ. *The plane was arbitrarily chosen such that* $\ln t = 0$. Line A is the line for which $\tau = \tau_{crit}$. Thus for a grain plotting on or below this line, an age spectrum with a plateau giving the age of eruption may be expected if C_1/C_2 is 100 or less.

Turner (1968) noted that while single spheres were unlikely to be degassed sufficiently to yield plateaus giving the age of reheating events, populations of spheres having different characteristics might produce such a plateau, even though the net level of degassing was the same as that of the single sphere. This can occur when a substantial fraction of the total volume of the population consists of the least-retentive spheres which are degassed in excess of their critical levels. For example, in Fig. 4-5b a population of identical spheres degassed only 90% plot on line B, well above the line of τ_{crit} (line A). No eruption-age plateau could be expected for such a population. If laboratory degassing occurred isothermally at T_{lava}, a population composed of equal volumes of two kinds of spheres for which $F_p = 0.90$ would meet the requirements for developing an eruption-age plateau if the spheres plotted on the two lines $\tau_e = 0.114$ $(F(\tau_e) = 0.80)$ and $\tau_e = 59.3$ $(F(\tau_e) \cong 1.00)$. If values of (D_o/a^2) are the same for the two kinds of spheres, the critical difference in τ_e may be achieved if ΔQ were $6.3\ RT_{lava}$. If ΔQ were zero, the same difference in τ_e would result if the radii of the spheres differ by a factor of 22.9.

The critical difference in τ_e (separation of the two lines) is inversely dependent on F_p. For example, if $F_p = 0.95$, the critical separation is achieved if $\Delta Q = 5.4\ RT_{lava}$ or if grain radii differ by a factor of 15.1. The values of τ_e for the two modes of spheres are 0.184 $(F(\tau_e) = 0.90)$ and 41.9 $(F(\tau_e) \cong 1.00)$. If either mode of spheres plots below its

critical line, the criterion for the establishment of the plateau will be exceeded.

For the above discussion, it was assumed that the temperature T_L during laboratory extraction was the same as T_{lava}, but in general T_L is much lower, except during the final steps of the analysis. This affects the age spectrum if the two kinds of spheres have different activation energies. In this case, the ratio of the values of $F(\tau_L)$ for the two kinds of spheres in the laboratory is dependent on $\exp(\Delta Q/(RT_L))$, and the value of ΔQ necessary to establish a plateau can in theory be controlled by varying T_L.

If the more retentive and the less retentive spheres are denoted R and N, respectively, then when T_L is less than T_{lava}, $(\tau_e/\tau_R)_L$ is greater than $(\tau_N/\tau_R)_{lava}$. Therefore, there is greater separation of Ar from the two kinds of spheres during analysis than when $T_L = T_{lava}$. When $T_L < T_{lava}$, residual ^{40}Ar from the retentive spheres becomes significant only after a greater fraction of ^{39}Ar has been extracted from the easily-degassed spheres. Because of this, $\tau_{N,lava}$ need not be so large in order to meet the requirements for the development of a plateau giving the age of eruption.

For a population consisting of equal volumes of two kinds of spheres of the same radius but different activation energies and if $F_p(t_e) = 0.90$, then $\Delta Q/RT_{lava} = 6.26\ T_L/T_{lava}$. The value of $\tau_{R,lava}$ is increased insignificantly, and the value of $\tau_{N,lava}$ is reduced from 59.3 to 2.59 as T_L is reduced from T_{lava} to $0.5\ T_{lava}$. Thus a plateau extending over 25% of the ^{39}Ar and having a maximum error in age of 5% if $C_1/C_2 = 100$ can be achieved if the grains have a difference in activation energies of $12.4\ T_L$ cal/mole, as long as the Ar extraction is isothermal. A practical value of T_L might be 1000°K; therefore ΔQ = 12.4 kcal/mole may be a realistic limit. (For the same plateau to be achieved if $\Delta Q = 0$ would require $(D_o/a^2)_R(D_o/a^2)_N^{-1} = 22.9$

if F_p were unchanged.)

Evaluation of dN_{40}/dN_{39} to find limiting ratios of a and differences of Q when laboratory extraction is isothermal is discussed further in App. 4-A, part II.

Generally, during analysis T_L is not constant but is increased in a stepwise fashion. In this case, after the nth step

$$[\tau_R/\tau_N]_L = \frac{\sum_{i=1}^{n} (t_i - t_{i-1}) \exp(-Q_R/(RT_i))}{\sum_{i=1}^{n} (t_i - t_{i-1}) \exp(-Q_N/(RT_i))} \quad ; \quad t_o = t_x \qquad (17)$$

so that $(\tau_R/\tau_N)_L$ may depend on actual values of Q_R, Q_N, and the heating schedule rather than simply on $\Delta Q/T_L$. This is also true for the case where T_L is changed continuously, for example when $T_L = \alpha t$. If extraction steps are of equal duration and if $(D_o/a^2)_N = (D_o/a^2)_R$, the effect of increasing T_L during analysis by 100°K increments to 1000°K compared to extracting Ar in one longer step at 1000°K is to decrease $(\tau_R/\tau_N)_L$ by about 12%. The effect of decrementing Q_N and Q_R equally is to decrease $[\tau_R/\tau_N]_L$.

For the discussion below, spectra of dN_{40}/dN_{39} have been approximated, assuming that the extraction occurred in finite steps of 360 s duration. The increment of T_L was 10°K. This heating schedule was the second case of Fig. 4-4. In the illustrations which follow, the stepped spectra have been smoothed for simplicity. Degassing in the lava was assumed to have occurred at $T_{lava} = 1400$°K. For simplicity, all spheres were assumed to have $D_o = 1$; thus discussion is in terms of grain radius a rather than $a/\sqrt{D_o}$. For populations of spheres with different activation energies, Q for one mode was set to 30 kcal/mole. Reducing this value would decrease the ΔQ required to achieve a plateau if F_p were unchanged.

Spectra of dN_{40}/dN_{39} from examples of each of three categories of models are shown in Fig. 4-6: (1) identical spheres (curves "a" and "b"); (2) spheres of two different radii a_1 and a_2 but the same activation energy ("c"); and (3) spheres of the same radius but two different activation energies Q_1 and Q_2 ("d," "e," and "f"). The examples provide simple illustrations of the effects of grain-size and activation-energy distributions on age or dN_{40}/dN_{39} spectra. These results are generalized below.

As for Fig. 4-4, we have assumed that $JC_{K39} = C_1$ and that analysis took place immediately after cooling of the lava, so that no new ^{40}Ar was created. All the ^{40}Ar released during the "analysis" was residual, and the dN_{40}/dN_{39} curves are thus measures of the apparent age in excess of the zero age of eruption of the lava.

These curves are related to differential age spectra through Eq. (13). Since $JC_{K39} = C_1$, $A = t_c$ is found from $dN_{40}/dN_{39} = 1.0$. Lesser values of dN_{40}/dN_{39} reflect Ar loss during heating in the magma. For $t_c = 100$ my, A is proportional to dN_{40}/dN_{39} within 3%.

Regardless of the model, if there was no loss of Ar during heating in the magma ($Fp(t_e) = 0$), the spectrum would have a constant value of unity and would define a plateau at t_c, the age of crystallization. This general case is shown in Fig. 4-6. Details of the six other examples and their spectra are given below.

Curve "a" is the dN_{40}/dN_{39} spectrum calculated for identical spheres after 50% of the initial ^{40}Ar was degassed in the magma and is the same spectrum shown in Fig. 4-4. Values of dN_{40}/dN_{39} rise swiftly during the release of the first ~ 20% of the ^{39}Ar, and they exceed 0.01 after only ~ 2% of the ^{39}Ar has been released. The maximum value of 0.74 is achieved for the last fraction of ^{39}Ar extracted. No finite fraction of Ar is

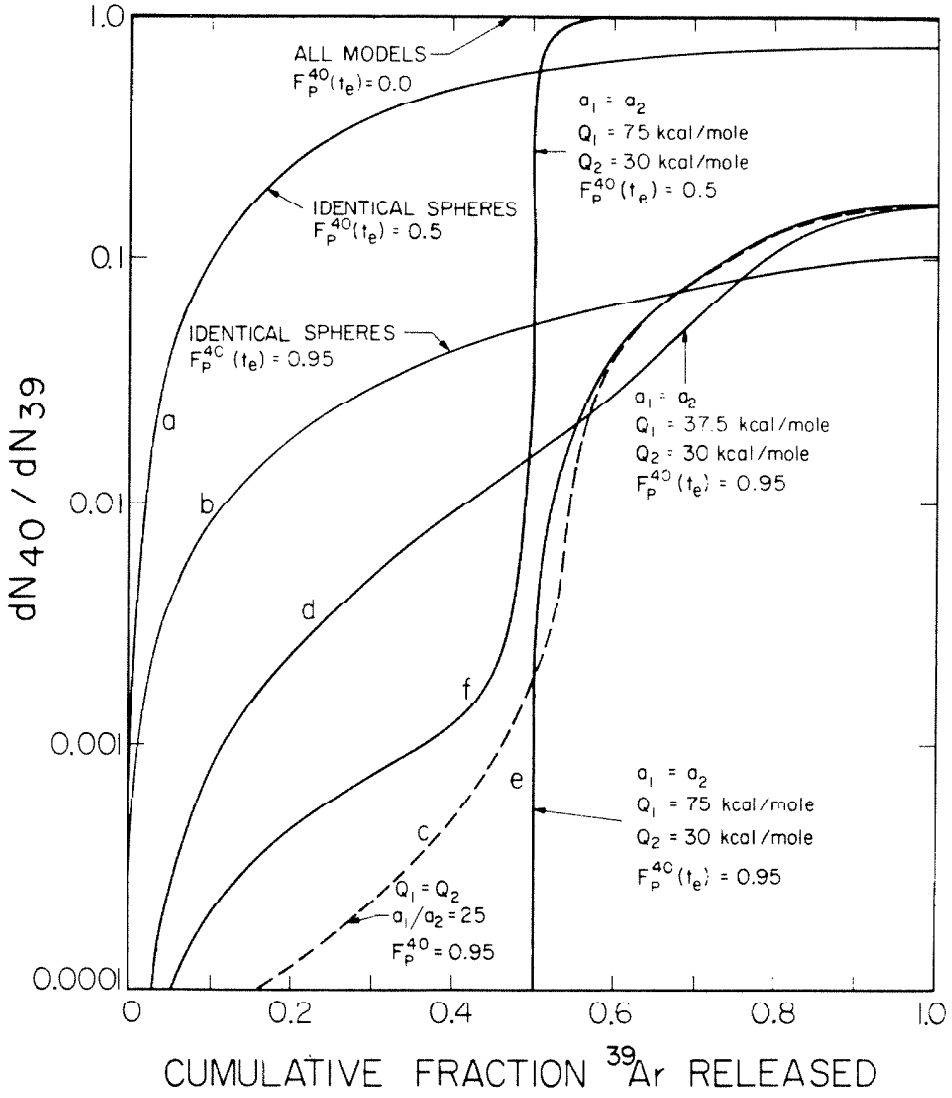

Fig. 4-6. dN_{40}/dN_{39} as a function of the cumulative fraction of ^{39}Ar released from six different models partially degassed of ^{40}Ar in magma just before ^{40}Ar-^{39}Ar analysis. Thus no new ^{40}Ar was created after cooling of the magma, and the ^{40}Ar degassed from the models was all inherited. Examples of spectra from three types of models are shown:

(1) identical spheres (curves "a" and "b");
(2) equal volumes of spheres of radii a_2 and $a_1=25a_2$ but the same activation energy ("c");
(3) equal volumes of spheres of the same size, but different activation energies Q_1 and Q_2 ("d", "e", and "f").

The different values of a_1/a_2, Q_1 and Q_2, and the fraction of ^{40}Ar degassed in the magma ($F_p(t_e)$) are indicated in the figure. Q_2 was taken to be 30 kcal/mole, a realistic value in the mid-range of values reported for K-feldspars.

Excess ^{40}Ar may be negligible over substantial fractions of the ^{39}Ar released from samples with only moderate differences in Q if $F_p(t_e)$ is as large as 0.95. Similar results are obtained if the sample contains spheres of highly different radii. Even heavily degassed samples of identical spheres release large amounts of excess ^{40}Ar except for the first small fraction of ^{39}Ar.

completely devoid of excess ^{40}Ar, and all fractions are depleted in ^{40}Ar compared to the case where $F_p(t_e) = 0$.

Even if the degassing in the magma was much greater than 50%, no finite fraction of ^{39}Ar is extracted unaccompanied by excess ^{40}Ar. Curve "b" was calculated for identical spheres for which $F_p(\tau_e) = 0.95$. The shape of "b" is similar to "a," and although the maximum value of dN_{40}/dN_{39} was reduced nearly an order of magnitude, the fraction of ^{39}Ar released before $dN_{40}/dN_{39} = 0.01$ was only ~ 0.12. Thus it appears that virtually all (>>95%) of the initial ^{40}Ar must be degassed from single spheres or groups of identical spheres before a sizable fraction of ^{39}Ar free of residual ^{40}Ar can be extracted.

We next examine instances in which populations of different spheres are analyzed. For simplicity, it was assumed that for a given model, grains varied in either a or Q but not both.

By modifying grain sizes or activation energies it is possible to reduce the amount of residual ^{40}Ar in the first fractions of Ar and to correspondingly raise the amount in the final fractions of Ar released from the xenolith, without changing $F_p(t_e)$. This is because the inherited ^{40}Ar is concentrated in the retentive reservoirs which are degassed last.

Xenoliths containing crystals of different sizes, crystals of different minerals, or crystals having exsolution lamellae would not be described by spheres of a single radius and activation energy. For example, Turner (1969) modeled Ar release from Bruderheim meteorite using spheres of log-normally distributed radii, with good agreement to the observed pattern. However, the minimum excess ^{40}Ar will be found when a xenolith contains some grains that are totally degassed at much lower temperatures or shorter times than other grains. The discussion here is accordingly restricted

to xenoliths of at most bimodal distributions of grain sizes or activation energies.

Curve "c" was calculated for a population of spheres having the same activation energy but two greatly different radii $a_1 = 25a_2$. Few real systems will have grain populations with this difference in size. The total volume of spheres of each kind was taken to be equal. The population was taken to be degassed of 95% of its ^{40}Ar upon heating in the lava ($F_p(t_e) = 0.95$). This corresponded to degassing in the magma of 90% of the initial ^{40}Ar from spheres of radius a_1 and degassing of nearly 100% from spheres of radius a_2. The spectrum is grossly different from "a" and "b." Values of dN_{40}/dN_{39} rose more slowly at low values of $F_{39} \equiv F_p(t_L)$ and over half the ^{39}Ar was extracted before $dN_{40}/dN_{39} = 0.01$. For $F_{39} > 0.5$, values of dN_{40}/dN_{39} rose steeply before finally leveling leveling off. The maximum value of dN_{40}/dN_{39} was 0.16 and occurred when $F_{39} = 1.0$. From the sigmoidal shape of the spectrum, it is clear that degassing from the large grains began only after the small ones were nearly exhausted, and in fact the amount of residual ^{40}Ar released along with the first half of the ^{39}Ar ($F_{39} < 0.5$) was as much as two orders of magnitude less than that from model "b" for equivalent values of F_{39}.

The values of dN_{40}/dN_{39} are very sensitive to the exact value of $F(\tau_e)$ for the smaller spheres. For example "c," this value was actually 0.99996 rather than 1.00 exactly. If the smaller spheres were truly completely degassed, then the amount of residual ^{40}Ar released when $F_{39} < 0.5$ would be orders of magnitude smaller. For spheres of $a_1 = 25a_2$, this cannot be achieved if $F_p(t_e) = 0.95$, but it can be achieved by further increasing the disparity in the sizes of the spheres. The spectrum for $F_{39} > 0.5$ would vary little if a_1/a_2 were increased. If a_1/a_2 were decreased,

the spectrum would rapidly approach curve "b."

Whereas large values of a_1/a_2 are necessary to minimize residual ^{40}Ar in part of the spectrum, even small differences in activation energies can achieve the same effect. If T is increased as is usual during laboratory analysis, the diffusivities for spheres of different Q will become increasingly disparate, whereas the diffusivities for spheres of different radii (but the same Q) will maintain their relative values.

Thus models consisting of spheres with different activation energies have dN_{40}/dN_{39} spectra which depend on the heating sequence during analysis. If a model consists of two spheres having the same radius but different activation energies Q_1 and Q_2, the ratio of their diffusivities is proportional to $\exp(-(Q_1-Q_2)/RT(t))$. If extraction is at constant temperature, the two spheres will degas in the same manner as two spheres with $Q_1 = Q_2$ but with different radii a_1 and a_2. The ratio of the apparent radii, a_1/a_2, will be a function of temperature. For the usual case where T is increased during analysis, the spectrum of the first system ($a_1 = a_2$, $Q_1 \neq Q_2$) lies between the spectra of different systems of the second type ($a_1 \neq a_2$, $Q_1 = Q_2$) whose values of a_1/a_2 are specified by the minimum and maximum temperatures during extraction.

Curve "d" was calculated for a model containing spheres of the same size but slightly different Q (Q_1 = 37.5 kcal/mole and Q_2 = 30 kcal/mole). Degassing of ^{40}Ar in the magma was 95% complete. As for curve "c," this was achieved by nearly complete degassing of the less retentive group of spheres.

Curve "d" was intermediate to "b" and "c" in appearance. Values of dN_{40}/dN_{39} rose less steeply than for "b," and did not exceed 0.01 until more than 40% of the ^{39}Ar had been extracted. The sigmoidal shape seen in "c" was not pronounced, but the gradient increased for $F_{39} > 0.6$, and at

$F_{39} = 1.0$, dN_{40}/dN_{39} had the same value (0.16) as for curve "c."

At T = 500°K, this model degassed as model "c" with $a_1/a_2 = 44$, and at T = 1400°K as model "c" with $a_1/a_2 = 3.9$. Within that temperature range the spectrum was intermediate between the spectra of those two endmembers. However, because degassing is inefficient at low temperatures, for much of the analysis ($F_{39} > 0.05$) the spectrum was similar to that for model "c" with $a_1/a_2 < 6$.

If Q_1 was increased to 75 kcal/mole while degassing in the magma was maintained at 95%, the change in the spectrum was profound (curve "e"). Inherited Ar released when $F_{39} < 0.5$ was more than four orders of magnitude lower than if $F_p(t_e) = 0$. Nevertheless, the maximum value of the spectrum (0.16) was unchanged.

Curves "d" and "e" show that, given a xenolith of appropriate properties, for at least a sizable fraction of the Ar released, excess ^{40}Ar might be sufficiently small to permit the measurement of the age of eruption.

Curve "f" was calculated for the previous model except that $F_p(t_e)=0.5$ (as for curve "a"). This spectrum differs from all others in that the release of initial ^{40}Ar is minimal for the first half of the spectrum and is virtually undiminished by heating in the magma for the second half. For $F_{39} < 0.4$, $dN_{40}/dN_{39} < 0.001$, and for $F_{39} > 0.6$, $dN_{40}/dN_{39} = 1.0$. Thus, for xenoliths described by this model, it might be possible to find two plateaus in the same spectrum, one at the age of eruption and one at the age of original crystallization.

For most geologic situations analysis will occur long after eruption, so that new ^{40}Ar will have a chance to accumulate in the system. Thus the spectra of Fig. 4-6 would rarely be observed. Actual spectra would have a constant bias proportional to the amount of new ^{40}Ar. In Fig. 4-7 are

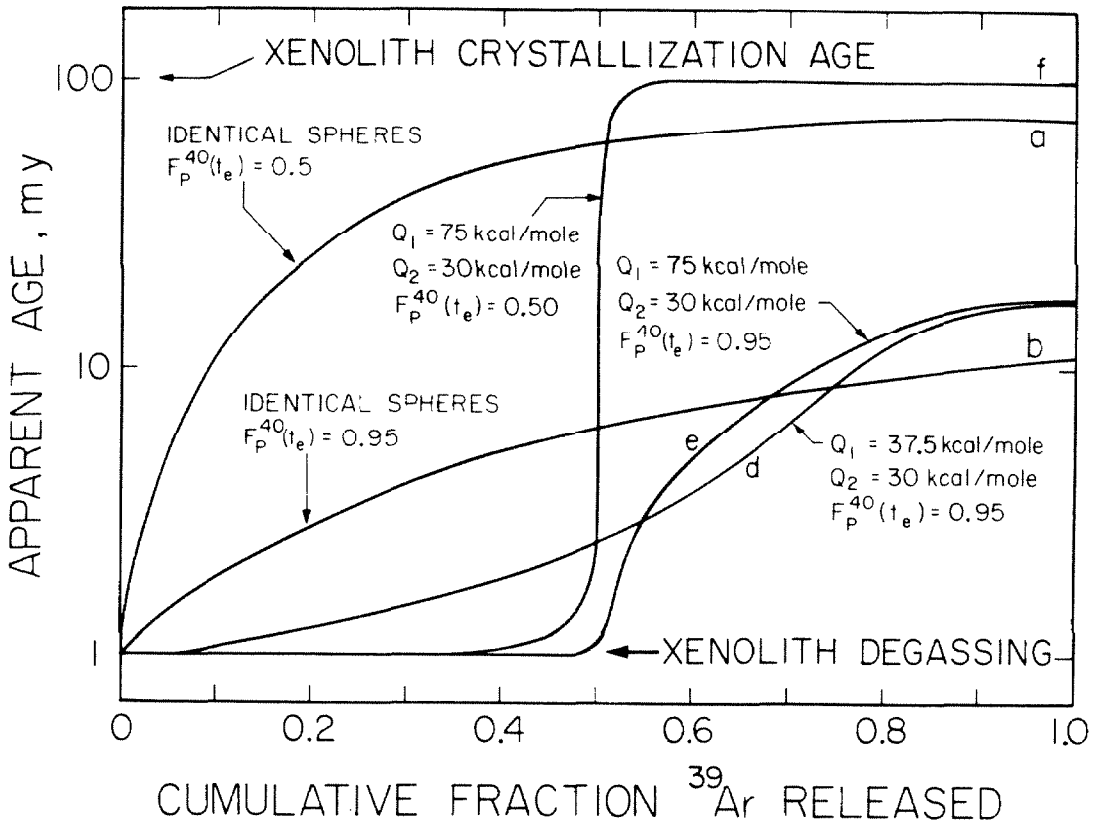

Fig. 4-7. Apparent age as a function of ^{39}Ar released from samples crystallized 100 my ago and partially degassed of ^{40}Ar 1 my ago. Letters on curves refer to the same models as in Fig. 4-6. The age spectra here differ from the dN_{40}/dN_{39} spectra of Fig. 4-6 primarily because of the uniform accumulation of new ^{40}Ar from the time of degassing in the magma to the present. Extensive low temperature plateaus at the age of eruption can be achieved by even moderate degassing of samples with a wide distribution of grain sizes on a small difference in activation energies. Essentially all ^{40}Ar must be degassed from uniform spheres in the magma to achieve low temperature plateaus of any size.

age spectra for five of the models of Fig. 4-6, for the special case where crystallization occurred 100 my ago and eruption was 1 my ago, so that $C_2/C_1 = 0.0099$. The same letters are used to identify spectra from the same models in both Fig. 4-6 and Fig. 4-7.

Curve "a" of Fig. 4-7 is the apparent age spectrum for identical spheres degassed of 50% of their initial ^{40}Ar 1 my ago. The spectrum rises rapidly from a minimum age of 1 my to a maximum of 75 my. No plateau is developed, so that neither the age of eruption nor the age of original crystallization could be determined from a xenolith described by this model.

Curve "b" was calculated for the same model degassed in the magma to $F_p(t_e) = 0.95$. Even though the maximum apparent age was only 9.4 my, no plateau was developed. For instance, after only 5% of the ^{39}Ar had been released, excess ^{40}Ar had increased the apparent age from 1 my (at $F_{39} = 0$) to 1.4 my. Even when $F_{39} = 0.01$, the apparent age of 1.1 my was already 10% greater than the age of eruption. As noted by Turner (1968), even highly degassed spheres or groups of identical spheres seem incapable of yielding low-temperature plateaus giving the age of eruption, unless $C_2/C_1 \gg 0.01$. On the other hand, the excess apparent age is always zero for the first infinitesimal fraction of ^{39}Ar released, so that an upper limit to the age of eruption should in theory be measurable regardless of $F_p(t_e)$, as long as $F_p(t_e) \neq 0$.

It was seen from Fig. 4-6 that models consisting of spheres of more than one radius or activation energy were a prerequisite for the development of well-defined low-temperature plateaus giving the age of eruption. Curve "d" in Fig. 4-7 is the age spectrum for the model with spheres of the same size but different activation energies ($Q_1 = 37.5$ kcal/mole and $Q_2 = 30$ kcal/mole), and $F_p(t_e) = 0.95$. The maximum apparent age was 17 my.

The apparent age exceeded the age of eruption by 5% after only 7% of the ^{39}Ar had been extracted. Such a spectrum is probably inadequate to determine the age of eruption but would certainly provide a closer limit than either curve "a" or "b".

Spheres in the model for curve "e" were bimodally distributed in Q with Q_1 = 75 kcal/mole (Q_2 = 30 kcal/mole), and all had radius a_1. As for curve "d", F_{39} = 0.95. The effect of increasing $|Q_1-Q_2|$ by a factor of six over model "d" was to increase seven-fold the ^{39}Ar released before the apparent age reached 1.05 my. For such a xenolith the age of eruption could certainly be determined.

Curve "f", calculated for the same model used for "e" but only degassed 50%, shows that two plateaus might be observed if C_2/C_1 = 0.01. The low-temperature plateau extends over the first 35% of ^{39}Ar relaeased before the apparent age rose to 1.05 my. It can be used to define the age of eruption. The high-temperature plateau, which defines the age of original crystallization, extends over the last 45% of the ^{39}Ar extracted. To achieve a comparable spectrum for a model with $Q_1 = Q_2$ but $a_1 \neq a_2$ would require $a_1/a_2 > 100$.

Discussion

The shape of an age spectrum and the amount of useful information conveyed by it depend strongly on the model parameters from which it was calculated. For spheres with the same activation energy, it is not reasonable to expect an age plateau of any size unless $C_2/C_1 \gg 0.01$ or unless degassing was essentially complete. On the other hand, models consisting of spheres of very different sizes or somewhat different activation energies

can produce age spectra containing two plateaus identifying both eruption and crystallization age even if C_2/C_1 is only 0.01. Thus a Cretaceous xenolith might yield an age for a Pleistocene eruption.

Multiple grain-radius models require very large differences in radii before plateaus at the age of eruption may be well developed. Such models may therefore be unrealistic for most xenoliths of igneous rocks. However, small differences in activation energies are capable of producing plateaus at the age of eruption. Activation energies of 18 and 24 kcal/mole have been reported by Evernden et al. (1960) for microcline, and activation energies of 52 kcal/mole (Baadsgaard et al., 1961) and 56 kcal/mole (Fechtig et al., 1960) have been reported for sanidine and anorthite, respectively. Consequently, activation energies different by perhaps 30 kcal/mole could be expected for real samples containing two feldspars.

From the performance of the volume diffusion models we conclude that age plateaus corresponding to the time of eruption may be found in age spectra of partially degassed xenoliths, provided that less than perhaps 10% of the ^{40}Ar has been retained. That this requirement can be fulfilled is shown by calculating τ using the thermal history T(t) of the xenolith in the magma and the Arrhenius equation. Ar retention in the xenolith may then be estimated from Eqs. (4) and (5). At the center of a spherical xenolith in an infinite low-viscosity magma, the thermal history is given by Carslaw and Jaeger (1959) as

$$T_c(t) = T_{lava} + 2T_{lava} \sum_{n=1}^{\infty} (-1)^n \exp(-\kappa n^2 \pi^2 t/a^2) \qquad (18)$$

where T_o is the magma temperature, a is the xenolith radius, and κ is the thermal diffusivity of the xenolith. If $\kappa = 0.01$ and $T_o = 1100°C$, T_c rises to 1050°C after only 40 s for a 1-cm xenolith. This might easily be

achieved during eruption itself.

Observations at the Kilauea Iki lava lake by Richter and Moore (1966) showed that although the surface of a pool of basalt magma rapidly formed a crust and cooled to ~ 100°C, only 12 m below the surface the lava was still molten more than two years after the eruption. Apparently, even for xenoliths near the rapidly cooling upper surface of a lava flow, ambient temperatures exceeding ~ 1050°C can be expected for times exceeding one day. The amount of degassing from a xenolith in such an environment can be estimated if D_o/a^2 and Q characteristic of the material comprising the xenolith are known. For orthoclase, Foland (1974) calculated $D_o a^{-2} = 245\ s^{-1}$ and Q = 43.8 kcal/mole, so that $\tau > 1.3$ if T = 1050°C for 10^5 s. For a xenolith consisting of identical spheres having the diffusion characteristics of orthoclase, Eq. (4) demonstrates that F > 99.9%, or that degassing in the magma would be nearly complete. However, F is very sensitive to Q, and if Q > 49.0 kcal/mole, F < 0.9. Only if the xenolith released Ar from grains characterized by multiple diffusion dimensions or activation energies would an age plateau be observed if F was this low.

It may be concluded that degassing in magma is probably sufficient for at least some granitic xenoliths to permit measurement of eruption-age plateaus. Indeed, Hart (1964) has demonstrated that conventional K/Ar ages of minerals from a contact zone around an intrusive stock were substantially reduced and in some cases approached the age of the stock. More recently, Berger (1975) has shown that ^{40}Ar-^{39}Ar age spectra of 1400-my-old biotites, hornblendes, and K-feldspars reflected thermal overprinting caused by the intrusion of the same stock. A spectrum from biotites sampled 6 m from the stock was totally reset to ~ 63 my, the approximate age of the intrusion. Spectra from K-feldspar taken within 25 m of the stock exhibited plateaus

containing four steps of similar low apparent ages and extending over ~ 25% of the ^{39}Ar. During heating by the stock, ~ 95% of the ^{40}Ar in the feldspar was lost. For these samples, $C_2/C_1 = 0.065$. Figure 4-6 shows that under these circumstances, even for a xenolith consisting of identical spheres, ~ 10% of the ^{39}Ar would be extracted before the apparent age became 15% greater than the age of the intrusion. Therefore, the results of Berger (1975) are not an adequate test of the models discussed herein.

Bogard and Hirsch (1980) infer from the ^{39}Ar release patterns of shocked chondrite meteorites the presence of two Ar reservoirs, one releasing Ar during ^{40}Ar-^{39}Ar analysis at temperatures >1100°C with activation energy ~ 70 kcal/mole and one releasing Ar over 500-900°C with activation energy ~ 30 kcal/mole. These 4500-my-old samples were degassed 500 my ago ($C_2/C_1 = 0.03$) of 90-99% of their ^{40}Ar. By the models presented in Fig. 4-6, it would be expected that if $Q_1 = 37.5$ kcal/mole ($Q_2 = 30$ kcal/mole), $a_1 = a_2$, and $F_p(t_e) = 0.95$, one reservoir would have been degassed of more than 99% of its initial ^{40}Ar and the ^{40}Ar-^{39}Ar age spectra should exhibit a substantial age plateau covering 30% of the ^{39}Ar with an error of less than 15%. This plateau should identify the time of episodic degassing. The age plateau for shocked chondrite samples with relatively undisturbed spectra indeed extended over ~ 25% of the ^{39}Ar released.

If multiple-site diffusion models are in fact appropriate for granitic xenoliths, then the chances are improved for finding age plateaus in xenoliths which are more than two orders of magnitude older than their host basalts. Of the three models shown in Fig. 4-6, only multiple-site models with $Q_1 = 75$ kcal/mole and $Q_2 = 30$ kcal/mole, or with $a_1/a_2 = 25$, would predict plateaus covering more than 10% of the ^{39}Ar with errors <10% if $C_2/C_1 = 0.001$ and if $F_p(t_e) = 0.95$. Were plateaus comprising ~ 25% of the

^{39}Ar realizable, then ^{40}Ar-^{39}Ar analysis of xenoliths from Mesozoic plutons might well be successfully extended to date eruptions as young as 0.1 my.

A Measure of Merit for Age Plateaus

Because of the complexity of modeling thermally disturbed systems and because of the number of parameters involved, it is desirable to have some simple measure of a sample's ability to yield an identifiable age plateau. Herein such a measure is proposed and used to explore the range of parameters for which low-temperature plateaus can be expected in age spectra of xenoliths. Ideally such a measure of merit M_ε should be applicable to both model and real systems. The critical factors are (1) the fraction of ^{39}Ar over which a plateau is defined, (2) the precision of the eruption age inferred from the plateau, and (3) the maximum difference between real and apparent age which is to be tolerated in the plateau.

M_ε is defined to be the fraction of ^{39}Ar released in analysis before the apparent age exceeds the eruption age by some threshold fraction ε. This occurs at time $t_L = t_{plat}$, and Ar extracted for $t_L < t_{plat}$ defines an age plateau. Thus

$$M_\varepsilon \equiv F_p(t_{plat}) \tag{19}$$

where F_p was defined in Eqs. (4) and (5).

For continuous analysis, values of $\tau_{plat} \equiv \tau_L(a,Q,T(t),t_{plat})$ may be determined from

$$\frac{d\,N_{40}}{d\,N_{39}} = \frac{\exp(\lambda t_e(1+\varepsilon))-\exp(\lambda t_e)}{\exp(\lambda t_c)-\exp(\lambda t_e)} \tag{20}$$

where dN_{40}/dN_{39} was defined as a function of F_p in Eq. (12) and where

t_c is the age of original crystallization, t_e is the age of degassing or eruption, and λ is the decay constant for ^{40}K. The derivation of Eq. (20) is given in App. 4-B. Equation (20) simply describes the condition when the rate of degassing of inherited Ar is such that the apparent age is increased to $(1+\epsilon)t_e$. If extraction is performed in a small number of large steps, M_ϵ will exceed the value calculated above because the apparent age for each step will be a mean age calculated for Ar extracted over a considerable fraction of the ^{39}Ar released (F_{39}).

Equation (20) allows the calculation of M_ϵ when t_c and t_e are already known. Thus it is generally appropriate only for the discussion of model systems. In real ^{40}Ar-^{39}Ar analyses, M_ϵ must be estimated by comparing the increase in apparent age from step to step.

Figure 4-8 shows M_ϵ for eruption-age plateaus as a function of four parameters: (a) the fraction of ^{40}Ar degassed from the xenolith at the time of eruption; (b) the ratio of concentration of new ^{40}Ar accumulated since the time of degassing (C_2) to the concentration which had accumulated by the time of degassing (C_1); (c) the different values of activation energy Q_1 for diffusion from distinct Ar reservoirs in the xenolith (with Q_2 = 30 kcal/mole); and (d) the ratio a_1/a_2 of grain sizes for diffusion from different reservoirs in the xenolith. In each graph a reference model consisting of identical spheres which lost 95% of their ^{40}Ar during degassing is indicated by an arrow. Baseline model spheres contain new ^{40}Ar in the ratio 0.01 to the ^{40}Ar present just prior to degassing (C_2/C_1 = 0.01). For simplicity, ϵ has been set to 0.05. Models consisted of equal volumes of spheres of different sizes or activation energies. Curves in Fig. 4-8 were calculated for c = 0.5 and c = 0.33. Otherwise, the model is the same as described for Fig. 4-6. The results in Fig. 4-8 generalize the

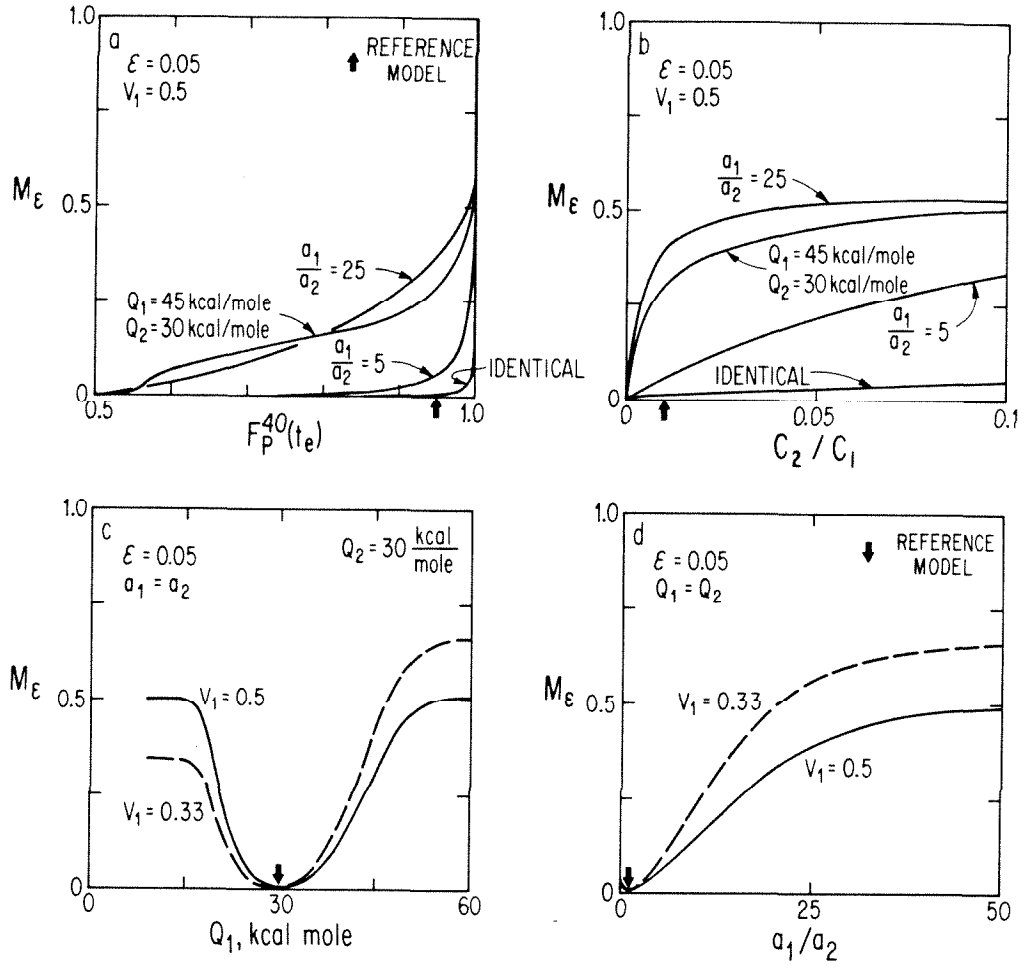

Fig. 4-8. M_ε as a function of (a) the fraction of Ar degassed by the lava, (b) the relative amounts of ^{40}Ar accumulated in the model before and after eruption of the lava, and (c,d) the characteristics of sites in the model occupied by the Ar. M_ε is the fraction of ^{39}Ar defining the eruption age plateau in the ^{40}Ar-^{39}Ar age spectrum. ε is the maximum deviation of $^{40}Ar/^{39}Ar$ from the eruption age value. The model consists of spheres bimodally distributed according to radius a or activation energy Q. The baseline model, designated by arrows in the figures, consists of uniform spheres ($a_1 = a_2$, $Q_1 = Q_2$) containing two orders of magnitude more ^{40}Ar just before degassing than new ^{40}Ar just before analysis. For all examples, Q_2 = 30 kcal/mole.

Fig. 4-8a demonstrates that M_ε increases as $F_p(t_e)$ is increased or as a_1/a_2 or $|Q_1-Q_2|$ is increased. Values of a_1/a_2 = 25 or Q_1= 15 kcal/mole were selected to show that plateaus of M > 0.25 could be achieved for Cretaceous xenoliths degassed 95% in a Pleistocene lava. M_ε decreases strongly for these models if the age difference exceeds this (Fig. 4-8b) and as grain radius or activation energies for the two spheres of the model become more similar (Fig. 4-8c and Fig. 4-8d). For Q_1 < 18 kcal/mole or Q_1 > 54 kcal/mole, or for a_1/a_2 > 25, little further increase in M_ε is achieved. The value of M_ε reaches a limit c or 1-c, which is the fraction of ^{39}Ar from the non-retentive spheres.

examples discussed above.

Figure 4-8a shows that $M_{0.05}$ ($\varepsilon = 0.05$) increases with $F_p(t_e)$, the fraction of ^{40}Ar degassed in the magma. For the baseline model, $M_{0.05} \sim 0.01$ and no plateau at the age of eruption would be identified. Not unless $M_{0.05}$ attained a level of ~ 0.25 could a plateau be reliably identified in experimental data. For the model consisting of identical spheres this would not be achieved until $F_p(t_e) > 0.99$. Other curves in Fig. 4-8a show that less degassing in the magma is necessary to achieve a given $M_{0.05}$ if the xenolith contains spheres of different radii or activation energies. If $a_1/a_2 = 5$, $F_p(t_e) \approx 0.99$ is still required for $M_{0.05} = 0.25$, but if $a_1/a_2 = 25$, only $F_p(t_e) = 0.87$ is necessary. If $a_1 = a_2$ but $Q_1 = 45$ kcal/mole a curve similar to that for $a_1/a = 25$ is obtained.

Dalrymple (1964a) has shown that degassing of granitic xenoliths in basalt in one instance exceeded 95%. Degassing at this level would be sufficient to permit the development of plateaus in the ^{40}Ar-^{39}Ar age spectra of xenoliths at the age of degassing or eruption, as long as the xenoliths were characterized by Ar in lattice sites of two or more sufficiently different diffusion radii or activation energies.

Figure 4-8b shows the sensitivity of $M_{0.05}$ to the ratio of the original age of crystallization of the xenolith and the age of eruption of the host lava. This ratio is here represented by C_2/C_1. $M_{0.05}$ increases with C_2/C_1 because the sample must be more extensively degassed in the laboratory to release residual and new ^{40}Ar in a fixed ratio when C_2 is increased with respect to C_1. Even when $C_2/C_1 = 0.1$, a model containing only identical spheres cannot produce a spectrum with $M_{0.05} > 0.05$. $M_{0.05}$ is again greater for the other three models from Fig. 4-8a. If $a_1/a_2 = 5$, $M_{0.05} > 0.25$ is achieved for $C_2/C_1 > 0.06$. If $a_1/a_2 = 25$ or if $Q_1 = 15$ kcal/mole,

$M_{0.05} > 0.25$ can be achieved even if $C_2/C_1 < 0.01$. For both of these models, $M_{0.05}$ approaches a limiting value reflecting the chosen value of c. For c = 0.5, $M_{0.05}$ cannot be significantly larger than 0.5 unless the retentive spheres also are virtually depleted of ^{40}Ar.

Figure 4-8c shows the dependence of $M_{0.05}$ on Q_1 (Q_2 is fixed) for c = 0.5 and c = 0.33. If $Q_1 > 54$ kcal/mole or if $Q_1 < 15$ kcal/mole, $M_{0.05} = 0.5$ can be achieved even if $F_p(t_e)$ is only 0.95. This value of $M_{0.05}$ is attained when the non-retentive spheres are completely depleted of residual ^{40}Ar. Degassing of new ^{40}Ar from the non-retentive spheres then occurs at temperatures low enough that residual ^{40}Ar from the other spheres is retained. Only at high extraction temperatures, when the non-retentive spheres are depleted, does degassing of the retentive spheres begin. For values of Q_1 closer to Q_2, degassing of the two populations of spheres occurs at more comparable temperatures and less new ^{40}Ar is released unaccompanied by residual ^{40}Ar. If $Q_1 > 21$ kcal/mole and $Q_1 < 43.5$ kcal/mole, then $M_{0.05} < 0.25$. Because the diffusion history for two-Q models depends on both Q_1 and Q_2 and complexities of the thermal history, $M_\varepsilon(|Q_1-Q_2|) \neq M_\varepsilon(-|Q_1-Q_2|)$, even for c = 0.5.

The graphed range of Q_1 of 9 kcal/mole to 60 kcal/mole includes most published activation energies for K-feldspars. Thus real xenoliths containing two types of feldspar could yield age spectra with $M_{0.05} > 0.25$.

Figure 4-8d shows the increase of $M_{0.05}$ with a_1/a_2. Limiting values of $M_{0.05}$ are 1-c for $a_1 > a_2$, just as for the two-Q model. For c = 0.33, $M_{0.05} > 0.25$ is attained if $a_1/a_2 > 10$. Such a disparity in the characteristic diffusion dimension might be seen in a feldspar if a were determined by the size of exsolution lamellae. Differences in values of Q required to develop plateaus in age spectra are much smaller than differences

in values of a required to develop plateaus of equivalent M_ε.

As noted, most samples will have a distribution in grain size and, if consisting of more than one phase, a distribution in activation energy. It is evident from Fig. 4-8c and Fig. 4-8d that unless either the age of crystallization and the time of eruption were comparable or degassing in the magma essentially complete, distributions of a and Q would be necessary if a meaningful eruption age were to be determined. Values of $M_{0.05}$ greater than 0.25 can be obtained if major reservoirs of ^{40}Ar in the sample differ by a factor of ten or more in grain size (Fig. 4-8d) or differ by at least ≈ 22 kcal/mole in activation energy. Extreme disparity in size or a difference in Q of 22 kcal/mole results in essentially complete degassing of one reservoir and a value for M_ε comparable to the fraction of ^{40}Ar held in that reservoir, even though degassing of the total system may be relatively low. It can be concluded that if a large M for any eruption-age plateau is observed it is likely to imply a distribution in Q or D_o/a^2, given the difficulty of achieving large M with a sample composed of similar grains. As expected, it becomes rapidly more difficult to achieve large M_ε as the fraction of ^{40}Ar degassed in the magma becomes smaller and as the eruption age and crystallization age become more disparate. It is also clear from the figures that sufficiently large M can be achieved by a combination of factors, so that variations in one parameter need not be so extreme.

The ability to extract useful dates from polymineralic whole rock systems is implied by our models, provided that individual reservoirs of Ar are sufficiently distinct in a or Q. This removes the requirement to carefully separate minerals before analysis. However, the most reliable age of eruption or degassing would still be determined from analysis of

minerals containing only reservoirs depleted of Ar during heating in the magma.

A measure of merit for actual ^{40}Ar-^{39}Ar analyses

M_ε as defined above is appropriate for analytic models. An expression incorporating experimental constraints on the definition of the age plateau is required for experimental data. For real ^{40}Ar-^{39}Ar analyses, there are generally few steps comprising the plateau at the age of eruption. Since a large number of steps increases the confidence with which a plateau can be identified, it is desirable to include this factor in the measure of merit. If the analysis is divided into too many steps, the measurement precision will be reduced along with the amount of Ar in each step. Thus the age specified by the plateau will be more uncertain. This factor also should be included in the measure of merit. We thus define a second measure of merit to be used in describing experimental results:

$$M'_\varepsilon = \frac{nF_p(t_{plat})}{(100\sigma/A)} \tag{21}$$

where n is the number of steps in the plateau and σ is the standard deviation of the age A defined by the plateau.

Usually the variance is used to weight plateau ages in the calculation of a mean age from replicate analyses. It may be desirable to additionally weight the ages by $nF_p(t_{plat})$ to reflect the degree of confidence that they are meaningful. In this case the mean age and standard deviation for N replicates would be given by:

$$\bar{A} = \frac{\sum_{i=1}^{N} M'_{\varepsilon_i}\sigma_i^{-1}}{\sum_{i=1}^{N} M'_{\varepsilon_i}(A_i\sigma_i)^{-1}} \tag{22}$$

and

$$\bar{\sigma} = \left(\frac{\sum_{i=1}^{N} M'_{\varepsilon_i} (A_i \sigma_i)^{-1}}{\sum_{i=1}^{N} M'_{\varepsilon_i} \sigma_i A_i^{-1}} \right)^{-1/2} \qquad (23)$$

This method is identical to weighting by the variance alone if $nF_p(t_{plat})$ is the same for each individual step in analysis.

Conclusions

It appears possible under some conditions to determine the age of eruption of a lava from plateaus in the ^{40}Ar-^{39}Ar age spectra of xenoliths which were only partially degassed during incorporation in the magma and eruption. In such cases two conditions are met: (1) there existed ^{40}Ar reservoirs which could be sufficiently degassed by the magma so as to yield an eruption age plateau, and (2) no reservoir released residual ^{40}Ar during ^{40}Ar-^{39}Ar analysis in quantities large enough to prevent the development of an eruption age plateau with an adequate measure of merit (M_ε). The factors which determine whether or not this is possible are interdependent, but the basic necessary conditions seem to be degassing in the lava of more than ~ 90% of the Ar and the presence of multiple sites for Ar characterized by different values of D_o/a^2 or Q. For the bimodal models considered here, values of grain size must differ by more than an order of magnitude or values of Q must differ by more than 15 kcal/mole. If these conditions are satisfied, it should prove possible to identify the age of eruption of Pleistocene lavas even if the age of original crystallization of the xenolith was two orders of magnitude greater. These conditions must be exceeded if incorporated

xenoliths are substantially older or the lavas to be dated are substantially younger.

4.2 ERUPTION AGE OF AN EARLY PLEISTOCENE BASALT FROM ^{40}Ar-^{39}Ar ANALYSIS OF PARTIALLY DEGASSED XENOLITHS

Introduction

It is the intent in this discussion to demonstrate the existence of low-temperature plateaus in age spectra of several partially degassed xenocrysts or xenoliths and to demonstrate their correspondence to the K/Ar age of eruption of the lava which incorporated and degassed the samples. Such plateaus were predicted from the considerations presented in the previous section (§4.1). To demonstrate these plateaus, xenoliths from an early Pleistocene basalt which outcrops on present-day ridges at the southern edge of the Big Pine volcanic field were analyzed. This basalt had been previously studied (Darrow, 1972) and found to have unusually high levels of K (1.3% by weight). Thus it was well suited for the K/Ar dating necessary to verify that the expected low-temperature plateaus from the xenolith age spectra did in fact give the age of eruption. The magnetic polarity of the basalt was found to be reversed; therefore, its age exceeded 0.73 my (Mankinen and Dalrymple, 1979). A sample of this age was chosen to reduce the sensitivity of the conventional K/Ar age of the basalt to contamination by inherited $^{40}Ar^*$ contributed by xenocrysts and to unusual compositions of Ar_t. In addition, it was anticipated that the age plateau would involve a higher fraction of the ^{39}Ar if an early Pleistocene lava were studied, resulting in a more confident comparison of the basalt age and the xenolith plateau age. Xenoliths from this basalt were found by preliminary K/Ar

analysis to be ~ 95% degassed.

Plateaus were in fact identified in the age spectra of xenoliths. These plateaus, obtained from Ar extracted at low temperatures (<900°C), agreed with K/Ar ages of the host basalts. They may thus be used to identify the age of eruption. Furthermore, as much as 75% of the ^{39}Ar may be involved in these plateaus. This unexpectedly large amount permits the confident identification of plateaus, and also makes the application of this technique to much younger basic lavas seem promising.

Sample Selection

Samples were chosen from three sites along the North Fork of Oak Creek (Fig. 4-9), west of Independence, California, where basalt is found on present ridge tops as much as 100 m above Oak Creek. This basalt flow is faulted and is locally capped by eroded remnants of coarse fan deposits. Darrow (1972) considered this flow to be among the oldest in the Big Pine volcanic field. At site A, the contact between weathered quartz monzonite of the late Cretaceous McGann pluton (Moore, 1963) and an overlying non-vesicular basalt is exposed in a road cut. Elsewhere such contacts are obscured by talus and scree. The unusual absence of granitic xenoliths in this basalt suggests that it may have a source separate from the contaminated basalts south of Oak Creek Creek at sites B and C, although both basalt flows cap ridges and are probably of similar age. Samples of basalt (NFOC-23a) 10 m above the base of the flow and of quartz monzonite bedrock (NFOC-109) 2 m below the contact were taken at site A. These samples were chosen to elucidate the thermal release pattern of argon from poorly degassed granitic rock and to explore the possibility of measuring eruption

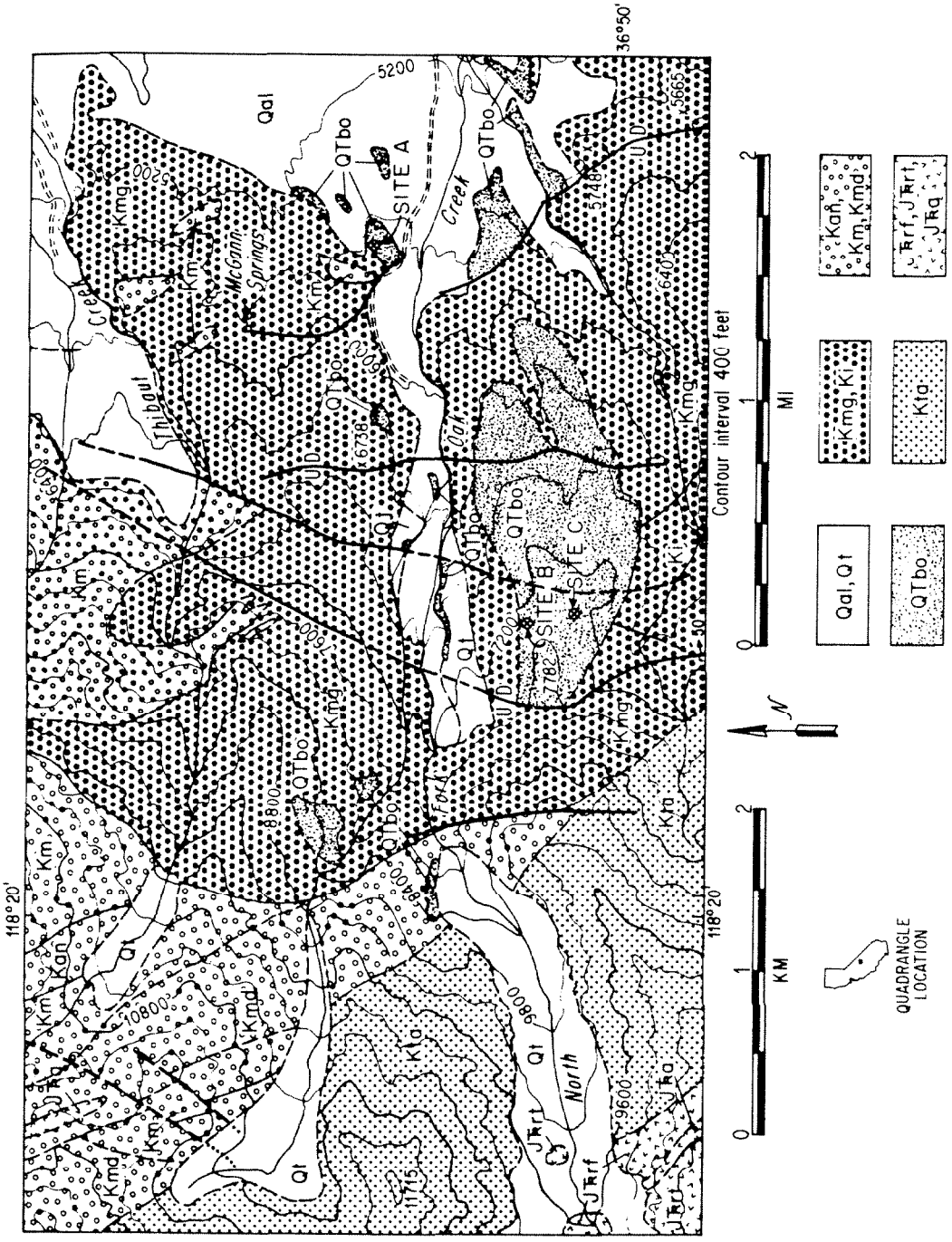

Fig. 4-9. Sample locations and generalized geology of the North Fork of Oak Creek, after Moore (1963). See next page for explanation.

Fig. 4-9. Sample locations and generalized geology of the North Fork of Oak Creek (continued).

Qal and Qt are Quaternary fan and stream gravels and Quaternary glacial deposits, respectively. Pleistocene basalts are designated Qtbo. Two Cretaceous quartz monzonites (heavy stipple) are shown; the McGann pluton (Kmg) is widespread, while the Independence pluton (Ki) crops out only in the south. The Cretaceous Tinnemaha granodiorite (KTa) is found only west of the faults along which the basalt is thought to have extruded. Kan, Km, and Kmd (open circles) are anorthosites, diorites, and gabbros of early Cretaceous age. Early Mesozoic volcanic rocks (J$\overline{\text{R}}$rf, J$\overline{\text{R}}$rt, and J$\overline{\text{R}}$a) were metamorphosed at the time of the Cretaceous intrusions. Topographic data are from the U. S. Geol. Survey, Mount Pinchot Quadrangle, Inyo County, California (1953).

ages using over-ridden material which had been only lightly degassed at much lower temperatures than xenoliths incorporated before eruption (~ 500°C vs ~ 1050°C). One piece of basalt and one sample of quartz monzonite were analyzed.

Site B was near the base of the thick (~ 50 m) sequence of basalt flows which form the ridge south of Oak Creek. The flows are expressed as distinct blocky cliffs separated by skirts of debris, but no indication of interbedded fluvial gravels has been found. Therefore, the entire sequence probably was erupted during a single episode or during closely spaced episodes of volcanism. The sample from site B, NFOC-1, consisted of a large block of basalt containing two different 1-cm granitic xenoliths (NFOC-1a, NFOC-1b). Three pieces of the basalt and duplicates of each xenolith were analyzed.

Site C was at the eroded top of the upper flow. Samples were taken 1 cm and 10 cm from the surface of a 1-m-diameter quartz monzonite xenolith (NFOC-103) and three replicates from the 10-cm depth (but no samples of basalt) were analyzed.

Petrology

The basaltic lava from site A has been called a basanite by Darrow (1972), who reported a potassium content of 1.3% and a calcium content of 7.4% (by weight). The rock contains phenocrysts of olivine and clinopyroxene in a network of smaller laths of plagioclase. Potassium probably resides to some extent in the 100-μm plagioclase grains but is found mainly in small biotite and nepheline crystals reported by Darrow and in ~ 10-μm glass blebs in the groundmass. Olivine phenocrysts show no iddingsite rims.

The ridgetop basalts south of Oak Creek are similar except that in NFOC-1 phenocrysts are larger and more numerous. A few olivine crystals show incipient iddingsite alteration; otherwise the basalt appears quite fresh. Moore (1963) reported an SiO_2 content of ~ 50%.

Most of the granitic xenoliths found in the Oak Creek lavas were probably derived from the McGann quartz monzonite, the pluton exposed at the surface in the vicinity of the vents (Fig. 4-9) and over-run by flows at site A. The K-feldspar is microcline and the dominant mafic mineral is biotite, with subordinate hornblende.

At site A the bedrock was weathered before being buried by basalt, and a thin zone of grus was present. This zone was baked by the basalts and is now cemented by iron oxides. Sample NFOC-109 was taken from below this zone, and individual feldspar grains are remarkably fresh appearing, although zones of alteration products can be seen crossing cleavage planes. Plagioclase crystals are sericitized, and mafic minerals are altered, with some replacement by iron oxides.

Xenoliths appeared to be distinctly less altered, probably because they were not weathered prior to incorporation in the magma. However, some could be disaggregated by hand, and the xenolith of NFOC-103 (site C) showed extensive replacement of biotite and hornblendes by iron oxides, which also pervaded the xenolith along series of fractures. The 1-cm xenoliths in NFOC-1 exhibited incipient phase transformation of K-feldspars from microcline to sanidine, especially at the xenolith-basalt interface. Quartz crystals, as reported by Moore (1963) and Darrow (1972), were corroded and showed reaction rims of clinopyroxene needles.

No isolated xenocrysts were seen in thin sections of NFOC-1 basalt, although the irregular xenolith interface suggests that some crystals may

have been detached from xenolith surfaces. Aggregates of microcline xenoliths were observed in similar contaminated basalts from Sawmill Canyon, a neighboring volcanic center to the north. These xenocrysts are a serious source of error in K-Ar ages of contaminated basalts; their scarcity in NFOC-1 allows us to more confidently interpret K-Ar ages of the basalt as eruption dates for comparison to xenolith plateau ages.

Analytic Techniques

Sample preparation

Basalt samples weighing ~ 0.5 gram were picked from the interior of blocks after coarse crushing. Samples from NFOC-1 were wrapped in metal foil packets to prevent their shedding particles during irradiation or loading in the Ar extraction line. It was not necessary to wrap basalt sample 8-12 (NFOC-23a) in foil. Samples were visually checked for xenocrysts, but none was found.

The granitic bedrock and xenolith samples were gently crushed in a stainless steel mortar and sieved. The 104-220 μm fraction was then magnetically cleaned of its mafic minerals. Both these steps were taken to reduce the amount of altered material analyzed. Samples were next wrapped in foil packets for irradiation. Grains of sample 8-3 (from NFOC-103) were additionally etched in 20% HF for 30 s at 25°C to further reduce fine alteration products. Isolated quartz grains were removed from 8-3 by hand-picking, so that the sample consisted of etched microcline and plagioclase crystals.

After the first analyses were made it became obvious that Ar forming the eruption-age plateaus was released at temperatures between ~ 500°C and ~ 900°C, so Sn foil packets were substituted for Al packets in subsequent

experiments. This was done to lower from 660°C to 230°C the temperature at which air incorporated in the foil was degassed. Samples of Sn or Al foil appeared to degas entirely upon melting.

Samples were irradiated with a fast neutron fluence of ~ 10^{17} n cm^{-2} in the central thimble of the TRIGA reactor facility of the United States Geological Survey at Denver, Colorado (Dalrymple et al., 1981). Sample 6-12 (NFOC-1) was irradiated at half this level. Neutron fluence inhomogeneities were monitored by measuring the ^{58}Co γ activity induced in Ni wires placed between samples.

The Bern 4M standard muscovite (Jäger et al., 1963) was used as the neutron irradiation monitor, along with samples of CaF_2 to measure interference isotopes produced by calcium. The age of the muscovite is 17.86±0.62 my, the result of ^{40}Ar-^{39}Ar analyses reported by Dalrymple and Lanphere (1971) corrected for the newly recommended ^{40}K isotopic abundance estimate and decay constant $\lambda \equiv \lambda_e + \lambda_\beta = 5.543 \times 10^{-10}$ y^{-1} (Steiger and Jäger, 1977).

Argon analysis

After neutron irradiation, Ar was extracted from samples in six to fifteen one-hour steps at successively higher temperatures from 300°C to 1700°C. Heating was by RF induction in a tungsten crucible vapor-deposited in a helium atmosphere to reduce the Ar blank. Blank levels of ^{36}Ar ranged from 10^{-10} cm^3 STP at temperatures below 800°C to 10^{-8} cm^3 STP at 1700°C, and temperature intervals between extraction steps were selected to maintain blank levels at <5% of the sample. The crucible was degassed at 1800°C for several hours between samples to reduce memory, and sequences of three to eight blank extractions were run before and after sample measurements.

Irradiation monitors were extracted totally in a single step.

After extraction, sample gases were exposed sequentially to two Ti getters at 800°C and to a final SAES Al-Zr getter prior to admission into the online mass spectrometer. Ar transfer was by absorption onto charcoal at the temperature of liquid N_2; Ar was released from the charcoal by raising the temperature to that of dry ice.

The purified Ar was analyzed using the HENEAK II gas mass spectrometer, with programmed magnetic field scanning. The mass spectrometer sensitivity for Ar was ~ 1.4×10^{-7} to ~ 2.5×10^{-6} cm^3 STP/V using a Cary 401 vibrating-reed amplifier with a 10^{11} ohm input resistor to measure the ion current collected by the Faraday cup. Sensitivity was reproducible to ±5%. For samples 1-7, 1-8, 1-11, and 1-12, a source magnet was used to increase sensitivity. The mass discrimination with a Faraday collector was (0.35±0.15)% amu^{-1} favoring heavy isotopes, and was not affected by the source magnet. Because only ~ 10^{-7} cm^3 STP/g radiogenic $^{40}Ar^*$ was present in the young rocks to be analyzed, the amounts of gas released in each step were small, and for most steps an electron multiplier was required to measure ^{36}Ar ion currents. The current from the multiplier was measured using a second Cary 401 amplifier. Use of the multiplier increased sensitivity by a factor of ~ 7500. Multiplier mass discrimination was (0.60±0.15)% amu^{-1}, favoring light isotopes. Typical analyses consisted of 10-15 individual measurements per isotope taken over about 20 min. Ion currents at each measurement were ratioed to the linearly interpolated ^{40}Ar ion current to improve precision. Data were edited to remove individual measurements that were clearly anomalous. The intensity and ratio variations with time were fit by logarithmic functions or polynomials of third order or less as appropriate (App. 4-C) to permit extrapolation to the time gas was admitted

to the spectrometer. Typical precisions in the extrapolated ratios were ~ ±0.5%. Uncertainties in the discrimination correction were overshadowed by errors introduced by measurement and by blank and interference isotope corrections. Measured ion currents of masses 36, 37, and 38 were corrected for the presence of ions of Cl and HCl in the spectrometer, as determined by measurement of mass spectrometer background prior to analyses and of mass 35 ion currents during analyses. Measured ion currents of mass 39 were corrected for spectrometer background at mass 39.

The abundances of ^{37}Ar and ^{39}Ar in the sample were corrected for radioactive decay by extrapolation to the time of irradiation, and also for relative neutron fluence differences between the sample and the muscovite monitor. Neutron fluence differences monitored by Ni wires were generally <5% and uncertainties in relative fluence were ±0.7%.

Abundances of ^{36}Ar and ^{39}Ar were corrected for $^{40}Ca(n,n\alpha)^{36}Ar$ and $^{42}Ca(n,\alpha)^{39}Ar$ according to $(^{36}Ar/^{37}Ar)_{Ca} = (3.1\pm0.3)\times10^{-4}$ and $(^{39}Ar/^{37}Ar)_{Ca} = (6.5\pm0.7)\times10^{-4}$, as determined from the CaF_2 monitor. $^{37}Ar_{Ca}$ was corrected for decay after irradiation using $\lambda = 0.01975d^{-1}$. ^{38}Ar was corrected for $^{42}Ca(n,n\alpha)^{38}Ar$ according to $(^{38}Ar/^{37}Ar)_{Ca} = (1.4\pm0.3)\times10^{-4}$ (Brereton, 1970) and ^{40}Ar was corrected for $^{43}Ca(n,\alpha)^{40}Ar$according to $(^{40}Ar/^{37}Ar)_{Ca} = 4.6\times10^{-3}$ (Dalrymple and Lanphere, 1971). Of the interference isotopes, $^{36}Ar_{Ca}$ had the greatest influence on the apparent age, but $^{36}Ar_{Ca}/^{36}Ar < 0.01$ for most Ar extractions and even for the calcic basalts no value exceeded 0.07.

Brereton (1970) found that if equal amounts of chlorine and calcium (from NaCl and CaF_2) were neutron irradiated $^{38}Ar_{Cl}$ and $^{37}Ar_{Ca}$ were produced in the ratio of 237. Consequently, correction had to be made for $^{36}Ar_{Cl}$ and $^{38}Ar_{Cl}$ created by β decay of $^{35}Cl(n,\gamma)^{36}Cl$ and $^{37}Cl(n,\gamma)^{38}Cl$.

This was done assuming that all remaining ^{36}Ar and ^{38}Ar were derived from a reservoir of atmospheric composition and from chlorine, and that $(^{36}Ar_{Cl}/^{38}Ar_{Cl})_{t=\infty} \approx 300$, the product of the isotopic abundances of $^{35}Cl/^{37}Cl$ and the ratio of their thermal neutron cross sections. This correction factor was adjusted for the time between irradiation and analysis using $\lambda = 2.258 \times 10^{-6}$ y^{-1} for ^{36}Cl and $\lambda = 1.124$ h^{-1} for ^{38}Cl. $^{36}Ar_{Cl}/^{36}Ar$ was found to be less than 6×10^{-3} for extractions from basalt and less than 1×10^{-3} for the granitic xenoliths from which hornblendes and biotites had been removed.

Finally, pro forma corrections were made for potassium-derived interference isotopes, $^{36}Ar_K$ and $^{40}Ar_K$. Correction for $^{36}Ar_K$ was made according to $^{36}Ar_K/^{39}Ar_K = 10^{-6}\ \Delta t$ (Turner, 1971b) where Δt is the time in years between irradiation and measurement. Correction for $^{40}K(n,p)^{40}Ar$ was made according to $(^{40}Ar/^{39}Ar)_K = (5.9 \pm 0.4) \times 10^{-3}$, determined by Dalrymple and Lanphere (1971) for the same TRIGA reactor which was used to irradiate samples for this study. For all measurements the correction for $^{36}Ar_K$ was negligible, while interference $^{40}Ar_K$ was less than naturally occurring radiogenic $^{40}Ar^*$ by a factor greater than 300. Tetley et al. (1980) have pointed out that production of $^{40}K(n,p)\ ^{40}Ar$ is controlled by the thermal neutron fluence, which may vary with position in the reactor and with the age of the fuel. Consequently, this pro forma correction may be a source of error.

The last correction applied to the data was the subtraction of blank ^{40}Ar and ^{36}Ar. Conservative errors of ±50% were assigned to blank levels. Measured blanks were reproducible to ±20%. Blank subtraction will not affect the step age as long as the trapped Ar released from the sample and the blank Ar have the same $^{36}Ar/^{40}Ar$.

Trapped Ar was subtracted from measured fractions using air Ar composition ($^{40}Ar/^{36}Ar = 295.5$) to produce $^{40}Ar^*/^{39}Ar$, from which an age was calculated according to

$$t = \lambda^{-1} \ln (1 + J\ ^{40}Ar^*/^{39}Ar) \qquad (24)$$

where t was in years and $J \equiv (^{40}Ar^*/^{39}Ar)_m^{-1} (\exp(\lambda t_m)-1)$ was determined from the muscovite monitor. Total ages were calculated by taking the average of step ages weighted by the associated fractional amounts of ^{39}Ar. Similarly, plateau ages were calculated by averaging the weighted ages for each step in the plateau. Ages calculated by assuming the composition of trapped argon is the same as air Ar are called model ages. To the extent that the composition of the Ar_t is unlike air, the model ages will be inaccurate. To avoid this problem it would be necessary to know the actual composition of the Ar_t, which may be found by fitting a line to the colinear array of compositions plotted in the three-isotope diagram as discussed below.

Uncertainties in ages of events must include the 3.4% systematic uncertainty in the age of the muscovite monitor. However, inclusion of this uncertainty for model total ages, or apparent ages of individual fractions of Ar from the same sample may mask trends and real differences and is therefore inappropriate.

Data presentation and systematics

Isotopic measurements of Ar released by heating during ^{40}Ar-^{39}Ar analysis are presented below in two ways: conventional age spectra, in which the apparent age at each step is plotted against the cumulative fractional amount of ^{39}Ar released; and three-isotope variation diagrams, in which the relative amounts and isotopic compositions of trapped and

K-derived Ar are made evident. Three-isotope diagrams are especially useful because they show trends in the composition of Ar released at successively higher temperatures. Fig. 4-10 schematically illustrates the use of such a diagram. Ar_t compositions ($^{36}Ar/^{40}Ar$) plot on the ordinate and K-derived Ar compositions ($^{39}Ar/^{40}Ar^*$) plot on the abscissa. Ages are related to K-derived compositions by Eq. (24). In general, Ar released from a sample contains both trapped and K-derived Ar, and plots along a mixing line connecting the two compositions. The apparent age for a sample of Ar is determined from the abscissa intercept (P') of a line passing through the measured composition (P) and the Ar_t composition (T). If several fractions of Ar released from a sample were mixtures of the same trapped and K-derived components, their compositions would plot along the mixing line connecting the endmembers. This colinear array of measured points defines an isochron whose axis intercepts specify the composition of the endmembers, which generally are not measured directly. The abscissa intercept of the isochron determines an apparent age ("isochron age") of the sample.

Measurement errors and departure of the real systems from ideal behavior (e.g., as discussed below) both contributed to uncertainties in the isochrons. If measurement was the main source of error, the least-squares method of Williamson (1968) was used to estimate the isochron. In this method, individual compositions were weighted according to their measurement precisions. Were measurement errors subordinate, Williamson's method gave unrealistically precise apparent ages because the scatter of compositions about the isochron was not considered. As recommended by York (1969) for such cases we multiplied the uncertainty of the isochron by $\sqrt{S/(n-2)}$, where S is the sum of the squares of the residua of data about the isochron and and where n is the number of compositions measured. S is distributed as

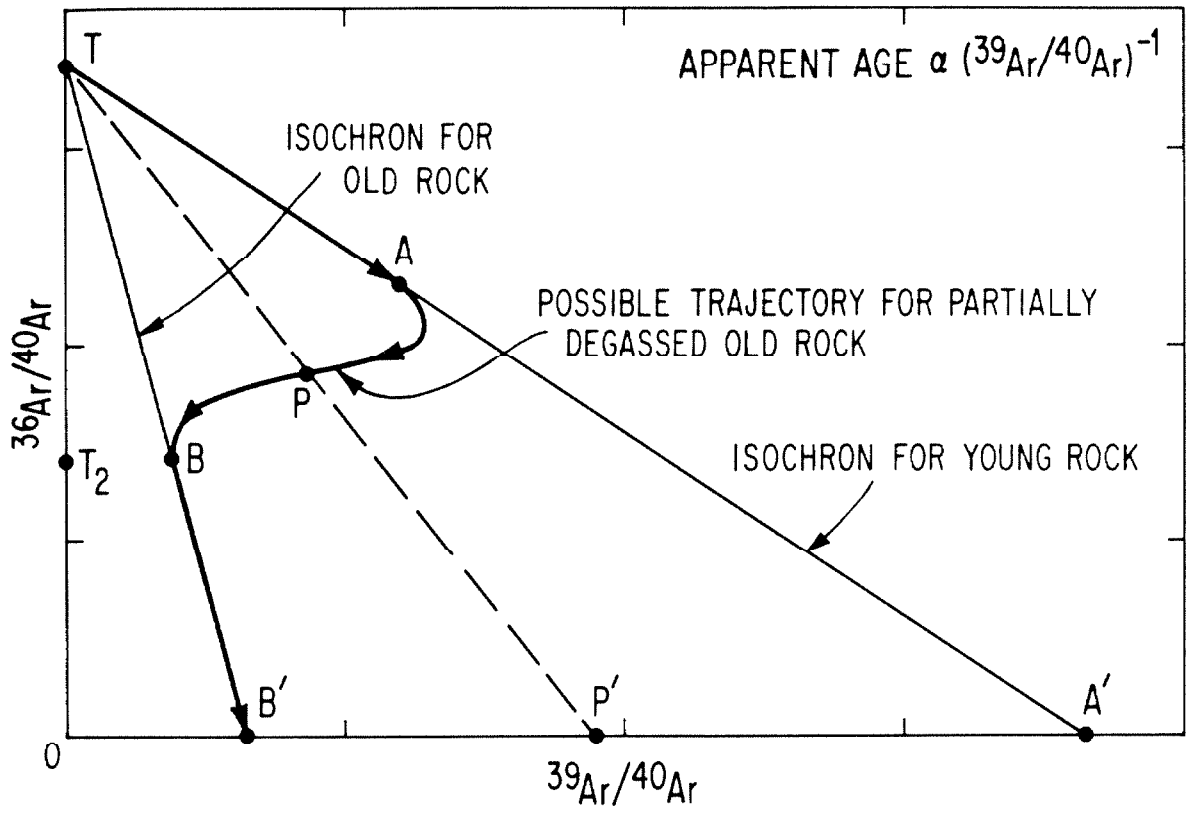

Fig. 4-10. A three-isotope correlation diagram of $^{36}Ar/^{40}Ar$ vs. $^{39}Ar/^{40}Ar$ is used to present analyses in which trapped Ar and inherited ^{40}Ar are major fractions of measured Ar. A linear array in this diagram indicates mixing of a single well-defined trapped Ar component with K-derived Ar of constant composition and hence constant age. Schematic trajectories of the isotopic compositions of Ar released during stepwise heating of degassed xenoliths are drawn to illustrate mixing among different reservoirs of Ar. In xenoliths such reservoirs may include K-derived Ar accumulated since original crystallization (B'), K-derived Ar accumulated since cooling of the host lava (A'), and trapped Ar (T and T_2). Compositions of K-derived Ar plot on the abscissa; compositions of trapped Ar plot on the ordinate. If only a single composition of trapped Ar is present, trajectories will range within the triangle TA'B'. See text for discussion.

χ^2 with n-2 degrees of freedom. If S was so large that there was less than 1% chance that the scatter of the compositions about the isochron resulted from measurement uncertainty alone, the reduced major axis (Kermack and Haldane, 1950) was taken to be the isochron. Because the scatter of compositions is due to non-experimental sources, the uncertainty of the age of the isochron must be multiplied by Student's t factor, with n-2 degrees of freedom (Brooks et al., 1972).

Isochrons shown in Fig. 4-10 connect Ar_t of composition T to K-derived Ar from undisturbed samples of two ages (A' and B'). In the context of this discussion, B' might represent the composition of Ar accumulated since original crystallization of the xenocryst, while A' might be the composition of Ar accumulated since the time of eruption. Isochron TA', then, might be anticipated for the lava and isochron TB' for the undegassed parent material of the xenocryst. The trajectory of isotopic compositions from the partially degassed xenocryst will range within the triangle TA'B'. One possibility is the curving line progressing initially along TA', but deflecting towards B near composition A and progressing finally along TB'. Arrows indicate the trend of compositions as degassing progresses during analysis. Such a trajectory would have an age spectrum similar to "c" of Fig. 4-1, which shows plateaus at the ages of eruption and of original crystallization separated by a transition zone of mixed apparent ages.

If more than a single composition of Ar_t is present (T and T_2) in a sample, trends in measured compositions will be more complicated than described above. In the presence of a single K-derived component A', compositions will range within TA'T_2, or in the presence of two K-derived components compositions will range within the quadrilateral TA'B'T_2. There is no guarantee that a true isochron will be present. Only if the

different K-derived or trapped components are derived from sites of sufficiently different Ar retentivity can compositions be expected to lie along binary mixing lines over even part of the trajectory. The differences in retentivity cannot be known in advance of the analysis, and in fact the efficacy of stepwise heating in isolating binary compositions can only be inferred from the observed trajectory. Only if separation has been achieved can trajectories be interpreted to give ages of events.

The measure of merit M'_ϵ proposed in § 4.1 can be used to facilitate comparison of plateaus from different age spectra. M'_ϵ was defined as $nF_{39}\sigma^{-1}$, where n was the number of steps comprising a plateau, F_{39} was the fraction of ^{39}Ar involved in the plateau, and σ was the standard deviation in percent of the plateau or isochron age. ϵ was the maximum systematic deviation from the "true" age to be tolerated in the plateau. Values of M'_ϵ may be used instead of the reciprocal variance to weight ages of replicate analyses for the estimation of mean ages. This is especially useful if values of σ for the different replicates are similar but F_{39} or n are different.

Results

Results are summarized in Tables 4-1 and 4-2. Ages are summarized as total ages, plateau ages, and isochron ages. As discussed earlier, total ages are the model ages calculated for all the Ar extracted from a sample assuming Ar_t is of atmospheric composition. Plateau ages are model ages calculated by averaging individual ages for steps comprising the plateau. The apparent ages for individual steps are weighted by the fraction of ^{39}Ar released during the step. Isochron ages are calculated from the $^{39}Ar/^{40}Ar$ intercept of lines regressed to Ar compositions in the three-isotope

Table 4-1

Summary of ^{40}Ar - ^{39}Ar Results

Sample	Site	Type	^{40}Ar-^{39}Ar analysis	Sample mass, mg	K†	Ca†	$^{40}Ar^*$ cm^3STPg^{-1}	^{36}Ar cm^3STPg^{-1}	$^{39}Ar/^{40}Ar$ $x10^3$	$^{36}Ar/^{40}Ar$ $x10^5$	$^{39}Ar/^{40}Ar^*$ $x10^4$
NFOC-23a	A	basalt	8-12	378	1.5	6.6	$7.5x10^{-8}$	$3.1x10^{-10}$	164	186	241
NFOC-109[1]	A	quartz monzonite	8-10	541	10.1	1.5	$>2.5x10^{-5}$	$>8.0x10^{-9}$	~ 6	~ 29	241
NFOC-1	B	basalt	6-12	592	1.3	8.5	$4.7x10^{-8}$	$2.9x10^{-9}$	9	321	122
NFOC-1	B	basalt	1-2	744	1.8	9.2	$4.4x10^{-8}$	$1.1x10^{-9}$	36	299	243
NFOC-1	B	basalt	1-3	518	1.4	9.8	$5.7x10^{-8}$	$7.5x10^{-10}$	75	269	243
NFOC-1a[2]	B	xenolith	1-7	491	4.1	-	$>1.6x10^{-7}$	$>1.9x10^{-9}$	~ 79	~ 261	243
NFOC-1a	B	xenolith	1-8	496	3.3	9.2	$6.5x10^{-7}$	$1.5x10^{-8}$	9	298	243
NFOC-1b	B	xenolith	1-11	472	>2.8	1.9	$>7.2x10^{-8}$	$>2.7x10^{-9}$	~ 28	~ 310	243
NFOC-1b	B	xenolith	1-12	436	3.6	2.9	$4.3x10^{-7}$	$9.1x10^{-9}$	10	292	243
NFOC-103	C	xenolith	8-1	88	3.1	1.9	$5.7x10^{-7}$	$1.4x10^{-8}$	13	298	241
NFOC-103	C	xenolith	8-2	119	3.4	14.6	$5.7x10^{-7}$	$2.0x10^{-8}$	10	309	241
NFOC-103	C	xenolith	8-3	113	2.0	5.1	$5.6x10^{-7}$	$2.0x10^{-8}$	6	309	241

†Weight percent calculated from ^{39}Ar and ^{37}Ar from sample normalized to isotopes from muscovite and fluorite monitors. Error is ±10%.
[1]Fusion extraction step lost.
[2]400°C extraction step lost.

Table 4-2

Summary of ^{40}Ar - ^{39}Ar Results (Continued)

^{40}Ar-^{39}Ar analysis	Model total age,my**	Retention* %	Fraction of ^{39}Ar in plateau steps	Number of steps in plateau	Model plateau age,my**	Fraction of ^{39}Ar in isochron steps	Number of steps fit by isochron	$\frac{s}{n-2}$*†	Ordinate intercept of isochron $^{36}Ar/^{40}Ar$ x10^5	Isochron age,my**	Method of regression***	M'_{10}
8-12	1.19±0.03	0	1.00	4	1.19±0.04	1.00	4	1.23	324±14	1.15±0.07	W	1.3
8-10†	61.1±0.9	>67	0	0	-	0	0	-	-	-	-	0.0
6-12	1.25±0.08	-	0.80	5	1.23±0.08	0.97	6	1.30	336±1	1.11±0.04	W	3.2
1-2	1.41±0.20	-	(0.08)	(1†††)	(1.31±0.10)	1.00	9	32.92	339±15	1.39±0.15	R	1.7
1-3	1.18±0.04	-	0.95	6	1.18±0.02	1.00	8	0.79	342±3	1.20±0.02	W	9.6
1-7†	1.26±0.16	-	<0.95	6	1.17±0.02	<0.97	7	2.33	333±4	1.15±0.02	W	>7.8
1-8	6.21±0.30	5	(0.55)	(2†††)	(1.26±0.03)	0.89	4	14.04	321±17	1.15±0.18	R	0.5
1-11††	1.32±0.22	>0	~0.76	5	1.23±0.02	1.00	9	12.63	337±11	1.20±0.12	R	1.8
1-12	6.29±0.26	6	0.58	8	1.22±0.03	0.58	8	0.87	334±4	1.19±0.02	W	5.5
8-1	3.96±0.75	3	(0.37)	(2†††)	(1.18±0.06)	0.37	3	1.26	338±1	1.17±0.06	W	0.4
8-2	3.68±0.18	3	(0.27)	(2†††)	(1.16±0.02)	0.30	4	6.29	340±13	1.16±0.10	R	0.3
8-3	5.93±0.15	3	(0.28)	(2†††)	(1.29±0.06)	0.46	4	23.44	333±12	1.17±0.16	R	0.3

*Assuming xenoliths crystallized 90 my ago, Ar retention ≈ 10 x (model total age-eruption age)/90 my.
**Uncertainty does not include 3.45% uncertainty in age of Bern 4M muscovite standard.
***W = Williamson's method. R = Reduced mean axis.
†Fusion extraction step lost.
††400°C extraction step lost.
†††Too few points to define a true plateau.
*†Determined for isochron calculated by Williamson's method.

diagram. They do not assume a composition of Ar_t and may therefore be more accurate than plateau ages. Complete tabulations of data are found in Appendix 4-D.

Basalt and subjacent country rock (site A)

We analyzed in a stepwise heating experiment the Ar from a sample of quartz monzonite found 2 m below a ~ 15-m-thick basalt flow. This was done (a) to illustrate the simplicity of trends in isotopic composition of Ar from partially degassed ancient rocks, (b) to illustrate the extreme range of apparent ages calculated from Ar released at different steps, and (c) to help establish guidelines for the selection of xenoliths which have been degassed in the magma sufficiently to permit determination of the eruption age. We also analyzed the overlying basalt, which was free of granitic fragments and presumably of inherited $^{40}Ar^*$. This analysis was used to determine the basalt's eruption age and thus the time of degassing of the underlying quartz monzonite. Results of both analyses are displayed in Fig. 4-11 and 4-12.

In Fig. 4-11 trends in the isotopic composition of Ar from the thermally undisturbed basalt are contrasted to those from the subjacent bedrock. Ar from the basalt was extracted in four steps at temperatures from 300°C to 1175°C. The compositions were colinear, indicating a binary mixture of a well-defined Ar_t with K-derived Ar of constant $^{39}Ar/^{40}Ar^*$. Little Ar_t was released from the basalt (3.3×10^{-10} cm^3 STP ^{36}Ar per gram), and even at 300°C the ^{40}Ar was about one-third radiogenic. As the temperature was increased to 900°C, the radiogenic fraction of ^{40}Ar increased. This trend was reversed for the 1175°C extraction. The small amount of Ar_t present in the basalt minimized the uncertainty in the age of the basalt due to

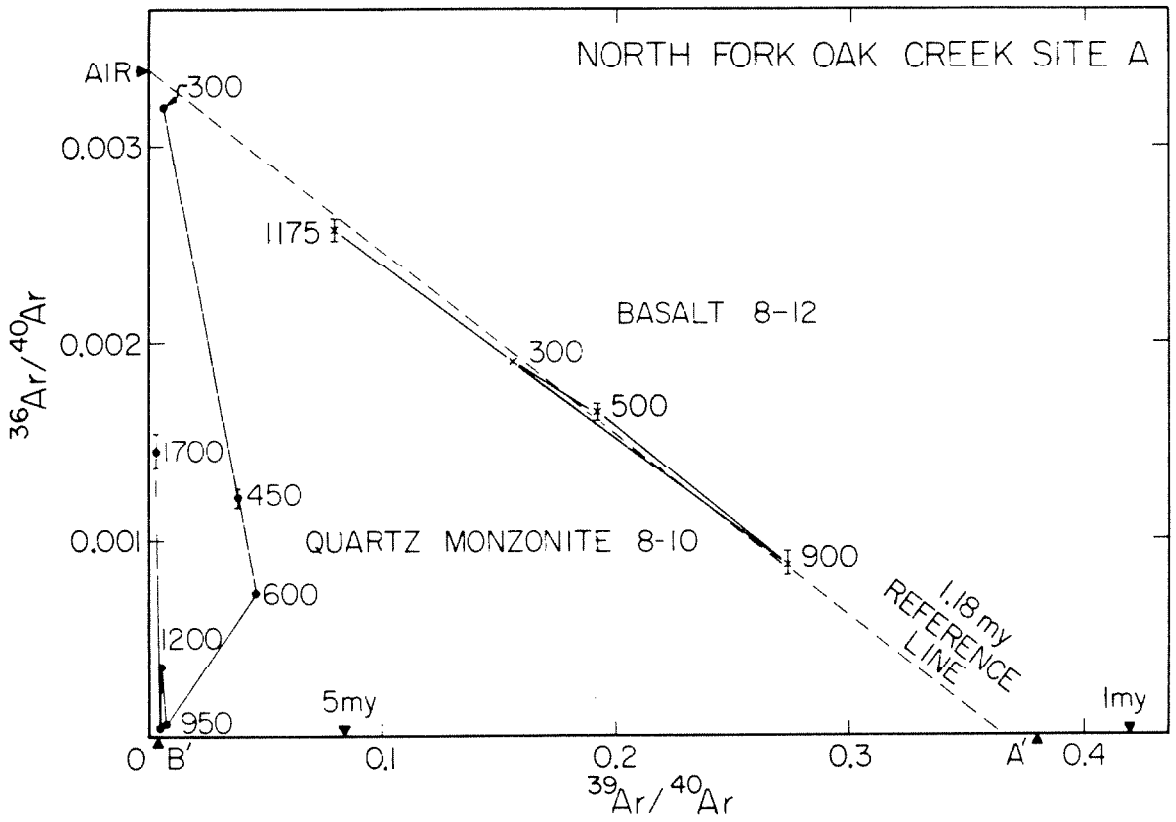

Fig. 4-11. The Ar composition trajectory in the $^{36}Ar/^{40}Ar$ vs. $^{39}Ar/^{40}Ar$ diagram for basalt 8-12 shows binary mixing between a single K-derived Ar and a single trapped Ar. The trajectory for the underlying degassed bedrock 8-10 shows ternary mixing among two K-derived Ar compositions (A' and B') and a trapped Ar. A reference line drawn from trapped Ar of atmospheric composition (AIR) to a K-derived Ar composition corresponding to 1.18 my is included for comparison in this and following figures. 1.18 my is in the middle of the range of ages found for samples from sites B and C. In this and subsequent three-isotope diagrams extraction temperatures (°C) are shown for selected steps. Plotted uncertainties are 1σ in all figures.

ill-defined Ar_t composition. The trapped component may have been slightly enriched in ^{40}Ar compared to air Ar since an isochron fit to these data intersected the ordinate at $^{36}Ar/^{40}Ar = 0.00324 \pm 0.00014$. The abscissa intercept of 0.382 ± 0.022 of corresponded to an age of 1.13 ± 0.07 my. The model age calculated from the total Ar released was 1.19 ± 0.03 my.

The composition of Ar released from the partially degassed country rock followed a more complicated trajectory. Ar was extracted in eight steps from 300°C to 1700°C, and the composition of each step plotted below the isochron of the basalt. The composition of the first step was near "AIR." Subsequent steps plotted near the origin. Lines passing through "AIR" and the compositions of the eight extractions intercepted the abscissa increasingly close to the origin as the extraction temperature was raised. This pattern corresponded to a monotonic rise in apparent age with temperature. In the context of Fig. 4-10, the entire trajectory appeared to lie between A and B, with A close to T ("AIR" in Fig. 4-11) and B close to B'. A' and B' are shown in Fig. 4-11 for reference.

The progressive dominance by inherited $^{40}Ar^*$ of Ar extracted at increasingly higher temperatures is clearly reflected in the age spectrum of the partially degassed quartz monzonite in Fig. 4-12. The apparent ages monotonically rise with the cumulative fraction of ^{39}Ar released, from an age of ~ 4 my in the lowest-temperature extraction to ages of ~ 75 my in the highest-temperature extraction. More than 90% of the ^{39}Ar is associated with apparent ages of >50 my. In the absence of a plateau the maximum apparent age of ~ 75 my is only a lower limit to the age of the late Cretaceous McGann pluton from which the sample was taken.

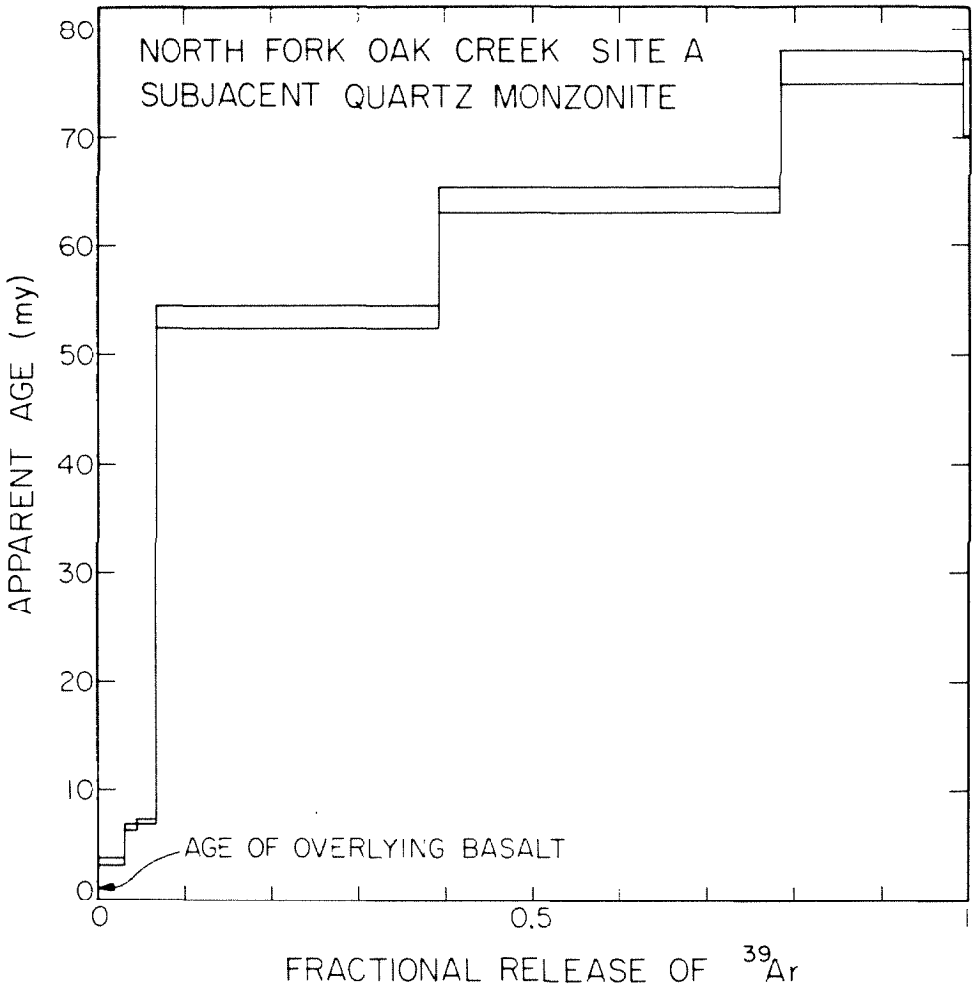

Fig. 4-12. Model age spectrum of quartz monzonite bedrock 8-10 (calculated assuming AIR trapped Ar composition) shows plateaus at neither the age of original crystallization nor the age of eruption. Nevertheless, model ages of low temperature steps provide a limit to the the time of degassing. Uncertainties are 1σ.

Degassed xenoliths and host basalt (site B)

In contrast to the preceding experiment, granitic xenoliths from within a basalt flow were analyzed to determine if eruption age plateaus were developed in age spectra of strongly degassed material. For such plateaus to be present, inherited $^{40}Ar^{*}$ must be either totally absent or present only in argon released in a restricted temperature range. Samples for this purpose were taken from the base of the basalt flow south of Oak Creek (site B, Fig. 4-9). Two samples from each of two xenoliths found only a few cm apart were analyzed. Three whole-rock basalt samples from the same block (NFOC-1) were analyzed to establish the eruption age.

$^{36}Ar/^{40}Ar$ - $^{39}Ar/^{40}Ar$ correlation diagrams for the basalt analyses and for the xenolith analyses are shown in Fig. 4-13 and Fig. 4-14, respectively. One age spectrum from each of the xenoliths is compared in Fig. 4-15 to an age spectrum from a basalt sample. The top diagram of Fig. 4-13 compares the total Ar compositions of the basalt samples from sites B and A. The compositions are distributed along a 1.18-my reference line drawn through AIR.[†] The scatter was due to different concentrations of Ar_t, which varied from 3.3×10^{-10} to 2.9×10^{-9} cm^3 STP ^{36}Ar per gram of basalt (Table 4-1). Even among the three samples from site B (6-12, 1-2, 1-3) the concentration of ^{36}Ar varied by a factor of 3.9. Sample (2-15) was powdered before analysis and atmospheric Ar presumably adhered to the new surfaces thus created, accounting for the large amount of nonradiogenic Ar (1.4×10^{-8} cm^3 STP ^{36}Ar per gram).

Model ages were calculated for each of the total compositions. Model ages for two of the basalt samples from site B (1-3 and 6-12) agreed at

---

[†] 1.18 my was chosen because it is the midrange value of isochron ages of the xenoliths in this study (Table 4-2).

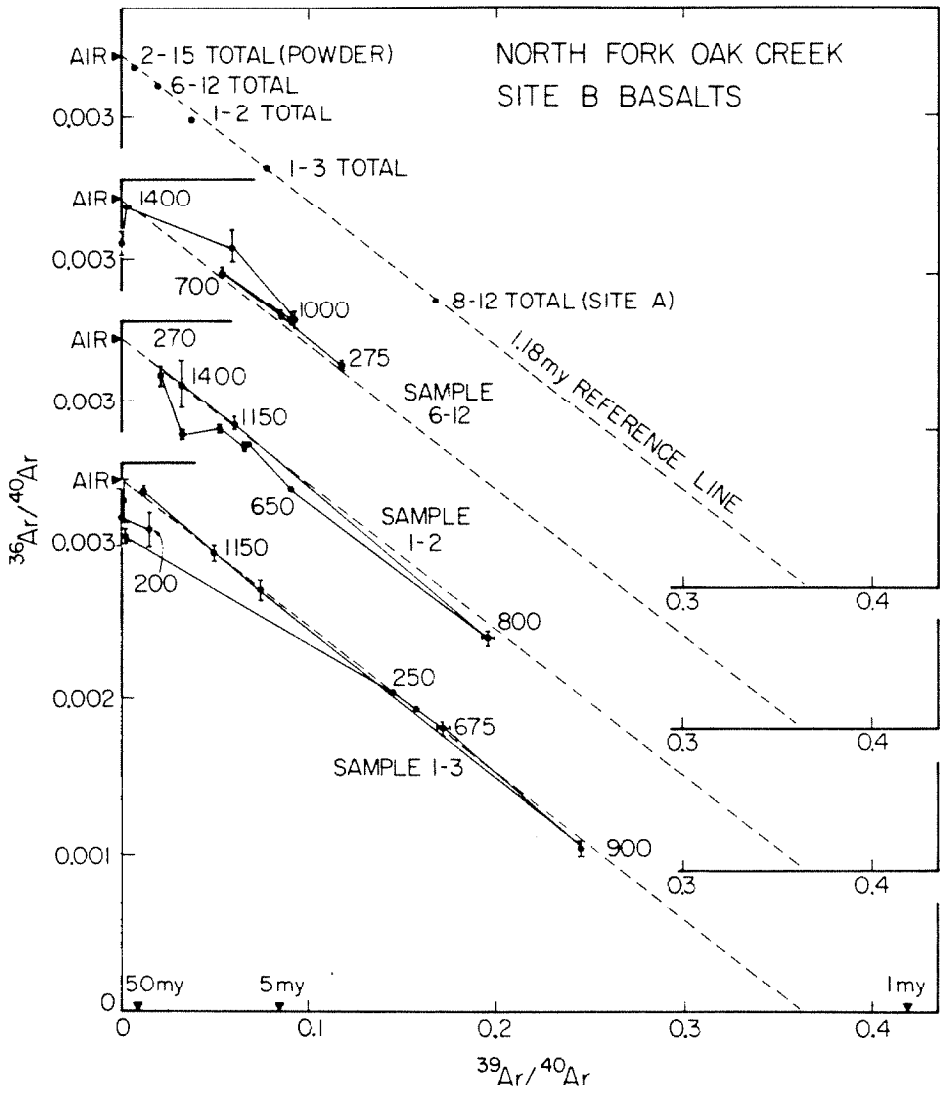

Fig. 4-13. Ar composition trajectories for basalt samples from NFOC-1 at site B show ternary mixing among two trapped compositions and a single K-derived composition. The top plot shows the composition of all the Ar released from each basalt sample. Failure of the compositions to cluster about a single point shows heterogeneity in the ratio of trapped Ar to K-derived Ar. Differences in the composition trajectories are best attributed to variable amounts of trapped Ar of different compositions.

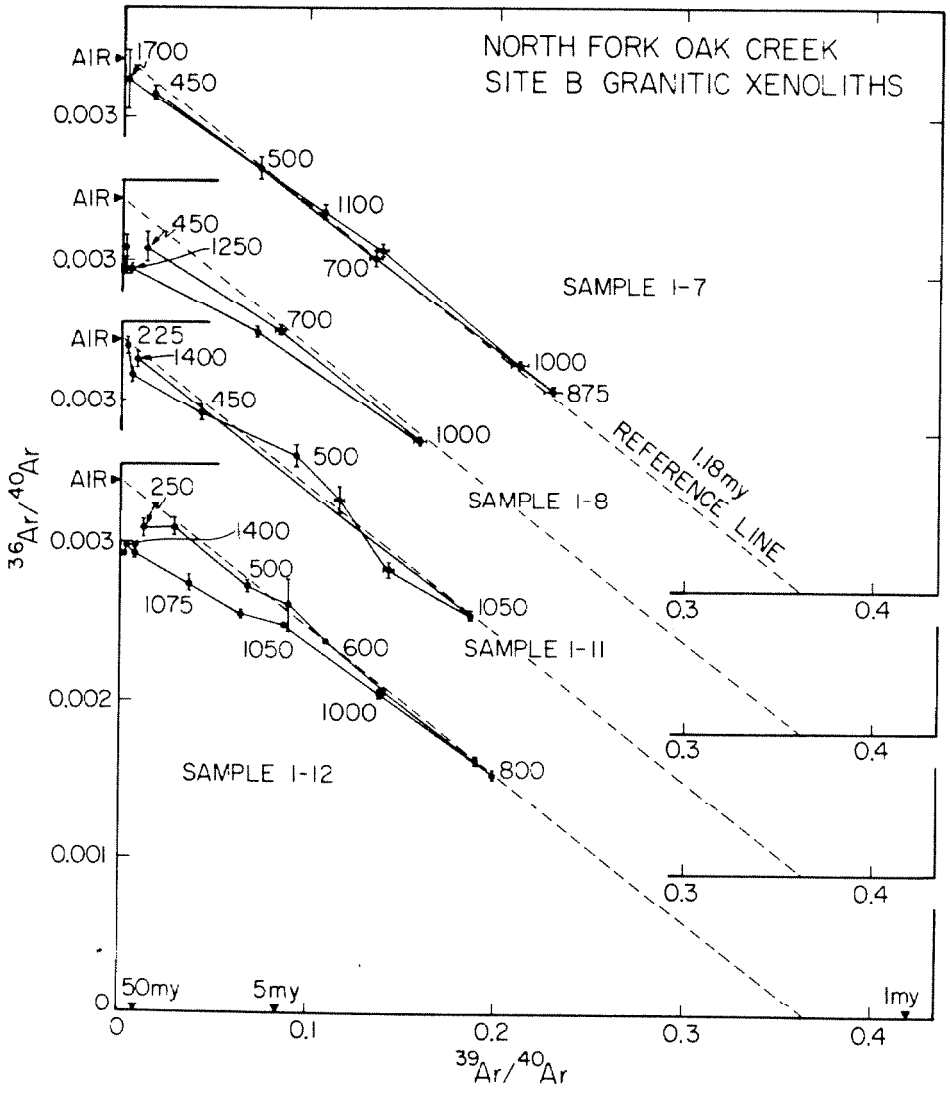

Fig. 4-14. Ar composition trajectories for granitic xenoliths from site B show ternary mixing. Two of the compositions are a trapped Ar near "AIR" and a K-derived Ar created since degassing in the magma. The third is probably ancient K-derived Ar. Compositions of Ar extracted at T < 1000°C are colinear and define an isochron giving the age of degassing of the xencliths. Compositions of Ar extracted at higher temperatures appear to show the influence of excess $^{40}Ar^{*}$ which was not degassed during heating in the host lava.

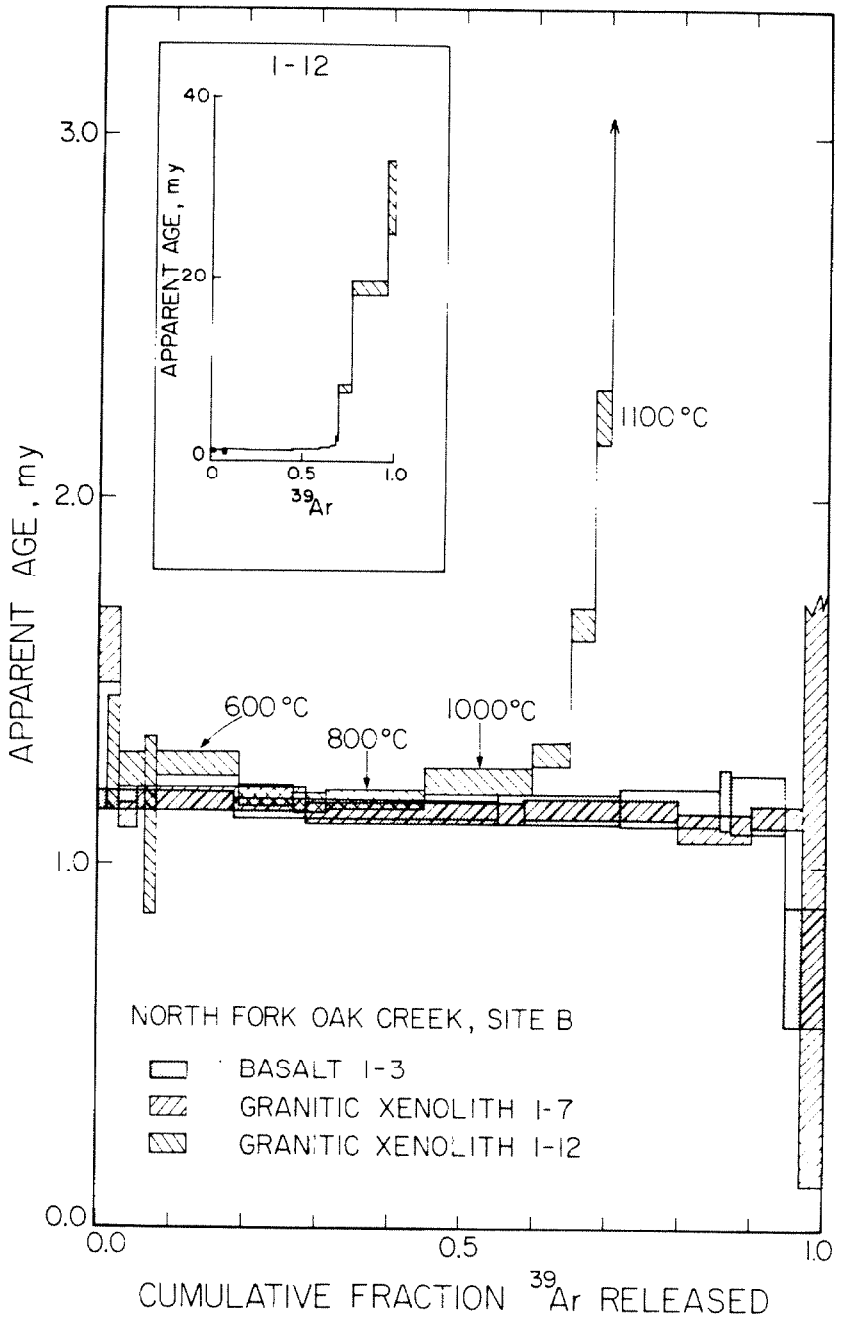

Fig. 4-15. Age spectra for basalt and two different granitic xenoliths from site B show remarkable agreement for first half of ^{39}Ar released. Plateaus for basalt 1-3 and xenolith 1-7 agree in age over more than 90% of the ^{39}Ar released. Inset shows age spectrum of xenolith 1-12 at a reduced scale which includes high-age steps. The spectrum of 1-12 shows a rapid increase in age as inherited $^{40}Ar^{*}$ is released at high temperatures. Selected extraction temperatures shown are for sample 1-12.

1.18±0.04 my and 1.25±0.08 my, but the model age of the third sample (1-2) was older at 1.41±0.20 my. Because these samples were of the same true age, this discrepancy must be explained by a variable composition of Ar_t, by local concentrations of excess ^{40}Ar, or by loss of ^{39}Ar. Because of the small fraction of radiogenic $^{40}Ar^*$ in basalts 6-12 and 1-2, minor errors in the assigned composition of the trapped component had large effects on the model age. The model age of basalt 8-12 (1.19±0.03 my) was similar to the model age of basalt 1-3, although each was from a different flow. The fact that ^{40}Ar from these two samples was rather radiogenic increased the confidence that the model ages were accurate measures of the times of eruption.

The three lower diagrams of Fig. 4-13 are the stepwise thermal release composition trajectories for the basalt samples from site B. In general, these trajectories began near "AIR" and proceeded down the 1.18-my reference line, returning towards "AIR" at fusion temperatures. This pattern was also observed for the basalt at site A (8-12). In basalts from site B, Ar released at 1400°C had compositions which all lay on the 1.18-my line close to "AIR." This constrained the Ar_t composition to a similar value. In each sample, fusion occurred during the previous step at ~ 1150°C.

Although model total ages and general patterns of isotopic variation were similar for the basalt samples from site B, each of the trajectories differed in detail. Sample 6-12 was unusual because the most radiogenic Ar was released during the first step (275°C), which accounted for 37% of the ^{39}Ar. Ar released in six of the seven steps had colinear compositions close to the reference line. The other step (1150°C) was distinctly above this array but contained only ~ 3% of the ^{39}Ar. The six colinear steps defined an isochron which intersected the abscissa at an age of 1.11±0.04 my and the ordinate at $(^{36}Ar/^{40}Ar)_t = 0.00336\pm0.00001$. Addition of the

remaining step lowered the isochron age to 1.10±0.06 my, but increased S/(n-2) from 1.34 to 3.06. This corresponded to an increase from ~ 75% to >97% confidence that the scatter in compositions was non-random. Consequently, I have accepted the six-point isochron.

The trajectory was similar to that expected for a sample containing only two well-defined constituents. There is no evidence for Ar_t of non-atmospheric composition. The single deviant step may reflect recoil redistribution of ^{39}Ar, but does not preclude interpretation of the rest of of the trajectory as an isochron.

Ar compositions for sample 1-3 (bottom) likewise followed a well-behaved trajectory. Ar was released in twelve steps, and seven of these defined a 1.20±0.02 my isochron intercepting the $^{36}Ar/^{40}Ar$ axis near AIR at 0.00342±0.00003. Ar for the first four steps (<250°C) contained very little ^{39}Ar but ranged from $^{36}Ar/^{40}Ar$ = 0.00320 to 0.00304, indicating the presence of a second Ar_t component of Ar released without accompanying ^{39}Ar. During the final two steps Ar was extracted from the molten sample. Compositions from these steps, which together contributed half the Ar_t, plotted near "AIR" in Fig. 4-13 (the 1650°C post-fusion step is not shown).

In the context of Fig. 4-10, compositions ranged within the triangle $TA'T_2$. The component T_2 was present only in small quantities in unretentive sites degassed at low temperatures. Only ~ 1% of the ^{36}Ar was released in these steps. Compositions of Ar from higher-temperature steps suggested simple mixing between T and A'. Because of the separability of T and T_2, the highly radiogenic content of several of the steps, and the colinearity of compositions at temperatures >250°C, the isochron age was accepted as the eruption age of the basalt.

In contrast to basalt samples 1-3 and 6-12, compositions of Ar

released from basalt 1-2 did not appear to define an isochron. Instead, the trajectory of compositions at steps below 800°C was somewhat erratic, with compositions falling well below the isochrons of samples 6-12 and 1-3. However, all compositions fell within the same triangle ($TA'T_2$) defined by sample 1-3. The six steps containing Ar_t apparently enriched in ^{40}Ar (T_2) together accounted for ~ 40% of the ^{39}Ar. Only at high temperatures (>1100°C) did Ar compositions plot on the isochrons of samples 6-12 and 1-3. An isochron fitted to all nine compositions gave an apparent age of 1.39±0.15 my, significantly different from isochron ages for the other two basalts. This isochron was characterized by a very large value of S/(n-2) of 32.92 which reflected the high scatter of compositions. The measure of merit $M'_{0.1}$ = 1.7 for the nine points was much lower than the values of 3.2 and 9.6 for samples 6-12 and 1-3, respectively.

Three-isotope diagrams for each of the four xenolith samples are shown in Fig. 4-14. Samples 1-7 and 1-8 (top) are from the same xenolith, and samples 1-11 and 1-12 (bottom) are from an adjacent xenolith. The general patterns of isotopic variation are similar to those for the basalt samples, and compositions again appear to range within the triangle $TA'T_2$ (Fig. 4-10). The trajectories for the xenoliths proceeded at low temperatures from an approximately atmospheric trapped component (T) to the K-derived component (A'), and returned to the ordinate along $A'T_2$ at high temperatures. Thus at high extraction temperatures, Ar released from the xenoliths was enriched by excess ^{40}Ar. In contrast, Ar released from the basalts contained Ar_t enriched in ^{40}Ar only at low temperatures. Thus the trajectories were fundamentally different. Although observed compositions for xenoliths departed from trajectories expected for simple binary systems (TA'), it was not possible from the three-isotope diagrams

alone to infer whether the departure at high extraction temperatures was due to the presence of a second Ar_t component (T_2) or to the admixture of inherited $^{40}Ar^*$ from retentive sites. In this latter case, mixing would have occurred within TA'B' rather than TA'T_2, but compositions would be restricted to the lines TA and AB, with B plotting close to T.

The four trajectories for site B xenoliths were not identical. Measured compositions for 1-7 were colinear, and at 1700°C Ar_t was released which was not statistically distinct from air Ar. Ar released from 1-8 at 450°C may have been enriched in ^{40}Ar or depleted in ^{39}Ar, and Ar released at temperatures of >1250°C was clearly enriched in ^{40}Ar. The trajectory for 1-11 was somewhat erratic but began and ended virtually at "AIR" and showed no sign of inherited $^{40}Ar^*$. The initial composition of Ar from 1-12 was excessively radiogenic, while the next seven fractions defined an isochron passing through "AIR." As was the case for 1-8, the final several steps were distinctly enriched in ^{40}Ar, defining a mixing line intersecting the ordinate at ~ 0.0030.

Because the poorly degassed sample of country rock from the same pluton as the xenoliths unmistakably showed the presence of inherited $^{40}Ar^*$, we attribute the departure from binary mixing of the site B xenolith trajectories primarily to the release of inherited $^{40}Ar^*$.

Model total ages for the xenoliths were <6.5 my, corresponding to degassing of >94% by the basaltic lava. Although model total ages for xenoliths exceeded ages for basalts by as much as a factor of five, by excluding those high temperature steps which seemed to contain inherited $^{40}Ar^*$ it was possible to fit isochrons whose abscissa intercepts gave ages clustered around 1.18 my (Table 4-2). These ages are in excellent agreement both among themselves and with the isochron age of 1.20±0.02 my

for basalt 1-3. $M'_{0.1}$ for the four isochrons ranged from 0.5 to 7.8, reflecting the different number of steps and different amounts of ^{39}Ar released without interfering inherited $^{40}Ar^*$, but especially echoing the strikingly different uncertainties of the isochrons. These are proportional to values of S/(n-2) and reflect disturbances in the colinearity of the isochrons. The mean of the xenolith isochron ordinate intercepts (weighted by the reciprocal of the variances) indicated $(^{36}Ar/^{40}Ar)_t = 0.00333 \pm 0.00003$, perhaps enriched slightly in ^{40}Ar compared to air Ar.

Fig. 4-15 demonstrates the remarkable agreement among model age plateaus from the two different xenoliths and from the basalt that enclosed them. Model ages from xenolith sample 1-7 and from basalt 1-12 agreed within 1σ over more than 90% of the spectrum.† Model ages from xenolith 1-12 were within 2σ of model ages of the basalt over the first 60% of the spectrum.

Model ages are calculated assuming trapped argon of atmospheric composition. Were they calculated using the isochrons' ordinate intercepts for the compositions of Ar_t, agreement among the samples in Fig. 4-14 would be even better. Ages calculated from Ar released from xenolith 1-12 at temperatures >1000°C rose rapidly to ~ 30 my, regardless of which trapped compositions were assumed. The complete spectrum is shown in the inset, at reduced scale. This spectrum resembles "d" in Fig. 4-1, while age spectra from xenolith 1-7 and basalt 1-3 resemble "a."

The age spectrum for xenolith 1-7 shows that if degassing in the magma was nearly complete the eruption age may be measured from analysis of xenoliths as well as from analysis of the basalt itself. The age

---

† Ar released during fusion of 1-7 was not measured, and abscissa values were calculated assuming that step contained no ^{39}Ar. By comparison with other xenolith samples, it would appear that only ~ 5% of the ^{39}Ar was released during the fusion step.

spectrum for xenolith 1-12 shows that even if degassing in the magma was only ~ 94% complete, new $^{40}Ar^*$ created after eruption may be completely separated from inherited $^{40}Ar^*$ by stepwise heating, and that the eruption age may still be confidently determined.

Degassed xenoliths (site C)

A final set of ^{40}Ar-^{39}Ar analyses was performed on three samples from a xenolith found at site C near the top of the series of basalt flows sampled at site B. The purpose of this experiment was to demonstrate that the appearance of plateaus in the age spectra of extensively degassed xenoliths was not exceptional.

For this experiment, three fragments were taken from xenolith NFOC-103. From one of these samples (8-3), ~ 1-mm feldspar grains were hand-picked and etched in HF to reduce the amount of altered material analyzed.

Ar isotopic variation trajectories for the three analyses are plotted in Fig. 4-16. Overall, the patterns were distinct from those for all other samples, but closely resembled the predicted trajectory for degassed xenoliths shown in Fig. 4-10. Compositions of Ar released at temperatures below ~ 1100°C described patterns like those in Fig. 4-14, proceeding from an atmospheric Ar_t towards a K-derived component and returning towards an ordinate intercept somewhat lower than 0.0034. However, Ar released at the highest temperatures was increasingly radiogenic. In the context of Fig. 4-10, the trajectories seemed to have followed a path from T to A, then returned towards B (located close to T) before ranging from B towards B' and back. Despite the similarity to the model trajectory, compositions of Ar released at high temperatures did not define isochrons. Instead, as for partially degassed country

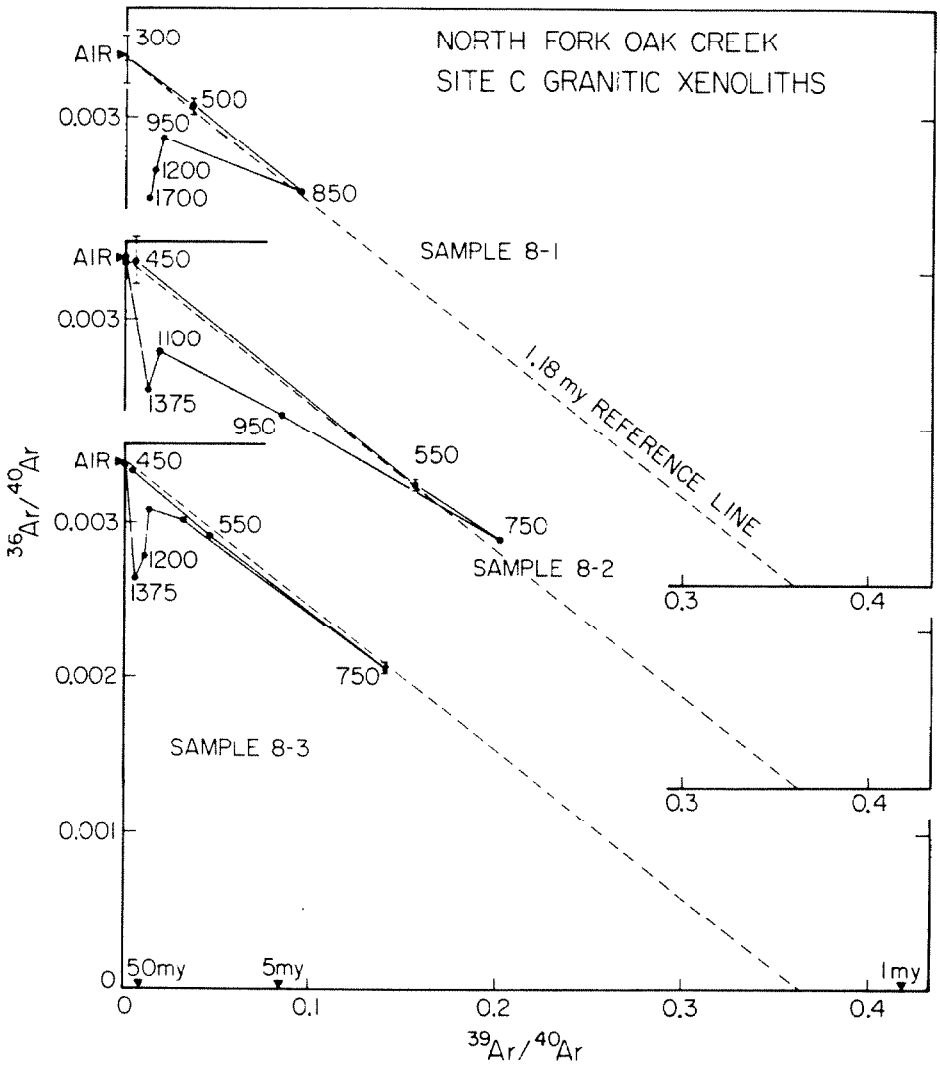

Fig. 4-16. Ar composition trajectories for xenoliths from site C show the presence of only new $^{40}Ar^*$ at low temperatures but show the clear admixture of inherited $^{40}Ar^*$ at temperatures above about 850°C. This admixture is responsible for the trend of the trajectories towards the origin for extractions at T > 1000°C. Sample 8-3 was etched in HF and quartz was removed.

rock (8-10), lines projected from "AIR" through measured compositions intersected the abscissa increasingly closer to the origin as extraction progressed. The model age spectrum of such a pattern resembled curve "d" of Fig. 4-1, wherein a plateau at the age of degassing was established by the first fractions of Ar. Subsequent fractions included some inherited $^{40}Ar^*$ and corresponded to a region of mixed age.

No trajectory for xenoliths from site C had more than four colinear points. In part, this was because less ^{39}Ar (<46%) was released before inherited ^{40}Ar became significant, compared to >58% ^{39}Ar released from xenoliths from site B. However, isochrons fit to these points gave apparent ages of ~ 1.17 my. These ages were the same as those from site B.

Model plateau ages for the two untreated fragments (Table 4-2), calculated for Ar released at temperatures $\leq$ 850°C, averaged 1.17±0.04 my. This agreed well with ages from the xenoliths and basalt of site B. Although the model plateau age of the treated sample (8-3) was older at 1.29±0.06 my, an isochron fit to the first four compositions gave a lower age of 1.17±0.16 my, which agreed better with other estimates of the age of the eruption. Otherwise, the isotopic variation pattern showed no striking differences from the patterns of the untreated samples.

Model ages and isochron ages for analyzed samples

Ages calculated for all samples analyzed are given in Table 4-2. Model total ages showed considerable scatter due to inherited $^{40}Ar^*$ and possibly to non-atmospheric Ar_t. Maximum ages for all xenolith samples (both sites) were less than about 25 my, lower than the ~ 75 my maximum from the poorly degassed rock (8-10) underlying basalt at site A. Model total ages for all xenolith samples were less than about 6.5 my, despite

the difference in appearance between trajectories from sites B and C. Differences in the trajectories appeared to reflect only the relative distributions of ^{36}Ar and $^{40}Ar^*$ in sites of different retentivities, rather than differences in the total amounts of ^{36}Ar (Table 4-1). Variations in ^{36}Ar among xenoliths from the same site were as great as differences between the sites.

Model ages were calculated for plateaus containing steps unaffected by inherited $^{40}Ar^*$. The mean model plateau age for all seven xenoliths was 1.22±0.10 my. The uncertainty in the mean was almost twice the uncertainty of any individual age. For replicate measurements of the same physical system, the scatter in the mean ages should be less than the scatter of the individual measurements. Since the xenoliths were degassed in the magma at the same time, this suggests that they may have had different Ar_t compositions. The mean isochron age was 1.17±0.04 my, which was more than twice as certain as the mean model plateau age. Only two individual isochron ages had uncertainties smaller than the uncertainty of the mean. Different compositions of Ar_t would explain the reduced scatter in isochron ages, for which a fixed composition is not assumed.

Ordinate intercepts of the seven xenolith isochrons indicate that Ar_t had a mean composition of $^{36}Ar/^{40}Ar$ = 0.00335±0.00018. This value is not statistically different from atmospheric Ar (0.00338), but at the 95% confidence level four xenolith isochrons did have non-atmospheric ordinate intercepts. If Ar_t had a non-atmospheric composition, then model ages are inaccurate and isochron ages must be used to determine the actual age of events.

The best estimate of the age of degassing of the xenoliths is probably the mean of the individual isochron ages weighted by their

variances. The mean ages are 1.17±0.01 my and 1.17±0.05 my for the xenoliths from sites B and C respectively and are indistinguishable both from each other and from the weighted mean age of 1.18±0.02 my found for basalt samples 1-3 and 6-12. Thus these ages may be pooled. Including Student's t factor (cf. Brooks et al., 1972) and the systematic uncertainty for the Bern 4M monitor, the weighted mean age of degassing for all nine samples from sites B and C is 1.18±0.05 my.

Summary of results, with commentary

Basalts . . .

The isotopic variation trajectories of each of the three basalt samples from site B (Fig. 4-13) were consistent with mixing between atmospheric Ar_t and a single K-derived component with admixture of different amounts of a ^{40}Ar-rich Ar_t component from unretentive sites (Fig. 4-10). This enriched Ar_t component was released at low temperatures only. Where two individual isochron ages had uncertainties smaller than the uncertainty the excess ^{40}Ar derived from ancient xenocrysts, its presence would be expected at high temperatures only. The large amount of this component in sample 1-2 together with the high model total age argues that this component is indeed Ar_t (T_2 in Fig. 4-10) rather than K-derived Ar depleted of ^{39}Ar by recoil redistribution. At low temperatures, compositions ranged between T and T_2, while at moderate temperatures they ranged within TA'T_2. At high temperatures the T_2 reservoir appears to have been depleted and compositions ranged along TA'. Sample 6-12 appeared to be devoid of T_2, while sample 1-3 had minor amounts of T_2 and sample 1-2 contained major amounts of T_2.

The source of the excess ^{40}Ar in the enriched Ar_t might well have been

ancient xenocrysts, even if no xenocrysts were found in the samples themselves. Once the host lava had cooled sufficiently, $^{40}Ar^*$ released from a xenocryst may have diffused only a short distance through the viscous melt or hot glassy matrix. A halo of excess ^{40}Ar might thus enclose each xenocryst, and a sample of basalt could include part of this halo without including the xenocryst itself. Indeed, were the diffusivity of ^{40}Ar in the cooling basaltic lava the same as that of moldavite ($D/a^2 \sim 10^{-6}s^{-1}$ at T = 900°C, Fechtig et al., 1961) then such a halo sufficient to increase the apparent age by a few hundred thousand years might extend 1 cm from a microscopic 100 my old xenocryst after degassing for one day at 900°C. Some of this excess ^{40}Ar might remain in small late-crystallizing grains after cooling of the basalt, to be degassed at relatively low temperatures during analysis. Thus, inherited $^{40}Ar^*$ need not be the only source for non-radiogenic trapped components. Krummenacher (1970) and Kaneoka (1980) have identified non-atmospheric Ar_t in several volcanic rocks which do not appear to have been contaminated by ancient xenocrysts. Nevertheless, localized halos of excess ^{40}Ar are an attractive explanation for variable or multiple trapped components in the same rock. It is apparent that K/Ar dating, even in the absence of xenocrysts, may be unreliable for basic lavas erupted through ancient rocks. ^{39}Ar–^{40}Ar dating may be likewise inconsistent, but affected measurements can be more readily identified. Because of the demonstrated presence of non-atmospheric Ar_t, it is necessary to infer the age of eruption from isochron ages rather than model ages.

Fusion of basalt sample 1-3, with minor amounts of T_2, occurred during the 1150°C step, and was accompanied by bursts of both $^{37}Ar_{Ca}$ and trapped ^{36}Ar, the latter an order of magnitude above blank. Release of $^{37}Ar_{Ca}$

at high temperatures has been attributed to its occurrence in refractory minerals such as pyroxene (Jessberger et al., 1974). Similarly retentive sites for ^{36}Ar are thus indicated in sample 1-3, with the Ar_t probably trapped at the time of crystallization of the refractory grains. There is a common tendency of the Ar isotopic variation trajectories for many different minerals and rocks to return to atmospheric composition at high temperatures (cf. Jessberger et al., 1974; Brereton, 1972). The existence of Ar_t within crystal lattices and its implications for K/Ar or ^{39}Ar-^{40}Ar dating are discussed below.

Recoil of ^{39}Ar during neutron irradiation does not appear to have upset the correlation of $^{40}Ar^*$ and ^{39}Ar. Huneke and Smith (1976) observed significant recoil of ^{39}Ar from μm-sized grains, and because most K in basalts probably resides in crystals and shreds of glass <50 μm in diameter, at least some effects were anticipated. Recoil depletes ^{39}Ar from sites near rims of potassic grains, and some recoiled ^{39}Ar will be implanted in neighboring grains in sites of various retentivities. Although the possible distortions of the composition trajectories are numerous, one commonly observed effect of recoil is a deficiency of ^{39}Ar in Ar extracted at low temperatures and an excess at high temperatures. Ar released from basalt 8-12 at both low and high temperatures was less radiogenic than Ar released at intermediate temperatures. Thus the effect of recoil redistribution of ^{39}Ar might be only a reduction in the colinearity of compositions rather than a systematic change in the slope of the trajectory. Too few steps were taken in the analysis of basalt 8-12 to rule out recoil distribution, but the observed colinearity of compositions suggests that any effects were minor. The apparently high model age of the 1175°C step implies a deficiency of ^{39}Ar in Ar

extracted at high temperatures and is therefore not readily explained by recoil. A more satisfactory explanation is the radiogenic composition of Ar_t indicated by the isochron or the presence of inherited $^{40}Ar^*$ from undetected xenocrysts (Fig. 4-11, Table 4-2). Ar released from basalt 8-12 did not indicate more than one trapped component. For the purposes of this paper the eruption age of the basalt of site A is taken to be the isochron age, 1.13±0.08 my (including systematic uncertainties).

Granitic xenoliths and bedrock . . .

Argon isotopic variation trajectories for the two 1-cm granitic xenoliths (Fig. 4-16) showed a strong resemblance to the trajectories for Ar from the basalt samples, except that the steps having the highest apparent ages were taken at the highest temperatures. The excess ^{40}Ar released in these steps may be explained either by the presence in retentive lattice sites of Ar_t enriched in ^{40}Ar or by the presence of inherited $^{40}Ar^*$. In view of the ancient original crystallization of the xenoliths and the clear evidence for inherited $^{40}Ar^*$ in the trajectories of the site C xenolith and the poorly degassed bedrock, all from the same pluton, the latter explanation is favored. Nevertheless, the obvious tendency of the trajectories to return to a composition near that of air Ar together with the large amounts of ^{36}Ar ($\sim 3\times10^{-9}$ $cm^3STP\ g^{-1}$, two orders of magnitude above blank) released during fusion demonstrates the presence of Ar_t in retentive sites in the xenoliths as well as in the basalts.

If the xenoliths indeed contained multiple At_t components of different compositions, then their isochrons would have to be interpreted cautiously. More work is needed to resolve this problem, but it does not obviate the dramatic agreement between xenolith degassing ages and basalt eruption ages.

In each of the four xenolith samples from site B more than half of the ^{39}Ar was released in steps whose colinear compositions defined isochrons of the same age (Table 4-2), even though degassing in the magma was as little as ~ 94% complete and even though two of the samples (1-8 and 1-12) showed large contributions of inherited $^{40}Ar^*$ in steps about 1000°C, sufficient to raise apparent ages to >20 my. The isochrons of sample 1-7 and 1-12 (Fig. 4-14) provided the best estimates from xenoliths of the actual age of eruption. Sample 1-7 showed no evidence of excess ^{40}Ar at temperatures below fusion, but with a value of $S/(n-2) = 2.33$ may have had scatter in excess of measurement errors. Sample 1-12 had less scatter but a smaller plateau. At 1.15±0.02 my and 1.19±0.02, these ages were distinct but neither was greatly different from the isochron age of 1.20±0.02 my for basalt sample 1-3.

Isotopic variation trajectories for the xenolith of site C showed the effects of inherited ^{40}Ar more clearly than those for xenoliths of site B, despite a similar retention of Ar after heating in the lava. Inherited $^{40}Ar^*$ is responsible for the trend of high-temperature steps towards the origin of the three-isotope diagrams. This bias towards old model ages began at ~ 750°C, lower than for xenoliths from site B.

The isotope variation pattern from the etched sample 8-3 (Fig. 4-16) did not differ strikingly from those of the untreated xenolith fragments 8-1 and 8-2, suggesting that the intergranular alteration products removed during etching did not play an important role in xenolith dating. However, the model age of the plateau in the age spectrum of the treated sample was much greater than the model ages of plateaus for the untreated xenoliths (Table 4-2). This could have been caused by removal during etching of some atmospheric Ar adsorbed onto main surfaces or incorporated into fine-grained

alteration products, leaving a slightly ^{40}Ar-enriched trapped component in lattice sites.

Compositions of Ar from the poorly degassed bedrock (8-10) ranged within the triangle approximately bounded by isochrons of the age of eruption and the age of original crystallization. The trajectory was straightforward, and can be interpreted to show mixing first between Ar_t and K-derived Ar corresponding to the age of eruption (A' in Fig. 4-10), followed by admixture of inherited $^{40}Ar^*$ (B' in Fig. 4-10) in higher-temperature releases. Because degassing by the lava was incomplete, inherited $^{40}Ar^*$ was present in all fractions of Ar analyzed. Despite this, apparent ages for the first fractions of Ar released (<10% of the ^{39}Ar) were a factor of ~ 24 less than the age of original crystallization of ~ 90 my (Fig. 4-12). It is remarkable that the age of the overlying basalt (indicated by the arrow on the ordinate of Fig. 4-12) was even approached when total degassing did not exceed ~ 33%. Poorly degassed xenoliths, overridden cobbles, or contact rock may provide useful upper limits to the time of eruption, but degassing at the relatively low temperatures (~ 500°C) expected in bedrock within a meter or so of an overlying lava flow appears to be insufficient to permit measurement of an eruption age plateau. Failure to find an eruption age plateau in 8-10 does not preclude the possibility of finding one in samples from other contact zones, but does suggest that attention should be directed towards separates of high K minerals with low activation energies such as biotite, which has been found to be more completely degassed than feldspars near intrusions (Hart, 1964; Berger, 1975).

From the excellent agreement of apparent ages over the major part of the age spectra shown in Fig. 4-15 it indeed appears to be possible to determine eruption age plateaus from granitic xenoliths, even if degassing

was incomplete and even if individual high-temperature steps yield ages more than an order of magnitude greater than the age of eruption. Agreement of isochron ages among different xenoliths and basalt samples from sites B and C showed that credible eruption ages could consistently be determined by analysis of xenoliths. The fraction of ^{39}Ar involved in plateaus at the age of eruption was sufficiently large that it seems reasonable to apply ^{40}Ar-^{39}Ar dating to xenoliths from younger flows in the expectation of finding smaller but nevertheless distinct age plateaus.

Discussion

Two topics are addressed in this section to clarify the application of the ^{40}Ar-^{39}Ar method to partially degassed xenoliths. These topics are (1) the existence and effect of multiple reservoirs of Ar_t, and (2) the extent of diffusive loss of Ar after cooling of the host lava.

Trapped argon

Success in interpreting Ar release patterns in terms of isochrons or step ages depends on the assumption that measured Ar is a simple mixture of two components: trapped and K-derived end-members. It appears that appreciable quantities of non-radiogenic Ar were released at all temperatures during analyses of both basalts and granitic xenoliths. This may be interpreted to mean that Ar was trapped within mineral lattices during crystallization (Frechen and Lippolt, 1965; Musset and Dalrymple, 1968; Lanphere and Dalrymple, 1971) as well as adsorbed onto grain surfaces. While adhered Ar was presumably atmospheric in composition, lattice Ar need not have been. Our analyses of basalts strongly indicated the presence of a trapped component of non-atmospheric composition.

Were different compositions of Ar_t indeed present, the compositions of Ar released from incompletely degassed xenoliths would be confined only to a quadrilateral in the three-isotope diagram as discussed above. A linear trajectory might still be developed but its interpretation in terms of an age would generally be inappropriate. In basalts, little inherited $^{40}Ar^*$ is present and Ar isotopic variations during stepwise release might begin at one Ar_t endmember, proceed towards a single K-derived endmember, and return to a different Ar_t endmember. This was probably the case for sample 1-2. Interpretation of the variation pattern to give an eruption age would require the Ar_t endmembers to be thermally separable, so that the variation trajectory would consist of two linear segments. This did not occur for 1-2, and it was not possible to infer an eruption age.

For xenoliths with significant amounts of inherited $^{40}Ar^*$ and with multiple Ar_t reservoirs, it is highly unlikely that such an isotopic variation pattern could be clearly interpreted over its whole course. Identification of an eruption age plateau would depend upon thermal release characteristics of inherited $^{40}Ar^*$ as well as separation of the trapped components.

Multiple reservoirs of Ar_t (of whatever composition) were indicated by the ^{36}Ar release patterns. These are clearly displayed in Fig. 4-17, which contrasts the release patterns of ^{36}Ar to those of ^{37}Ar, ^{39}Ar, and $^{40}Ar^*$ for xenolith sample 1-12. Amounts of each Ar isotope released during each extraction step have been normalized by the total amount of that isotope in the sample and by the temperature difference between steps. This was done to reduce the effect of irregularities in the heating schedule on the release patterns. In this representation, a curve describing gas

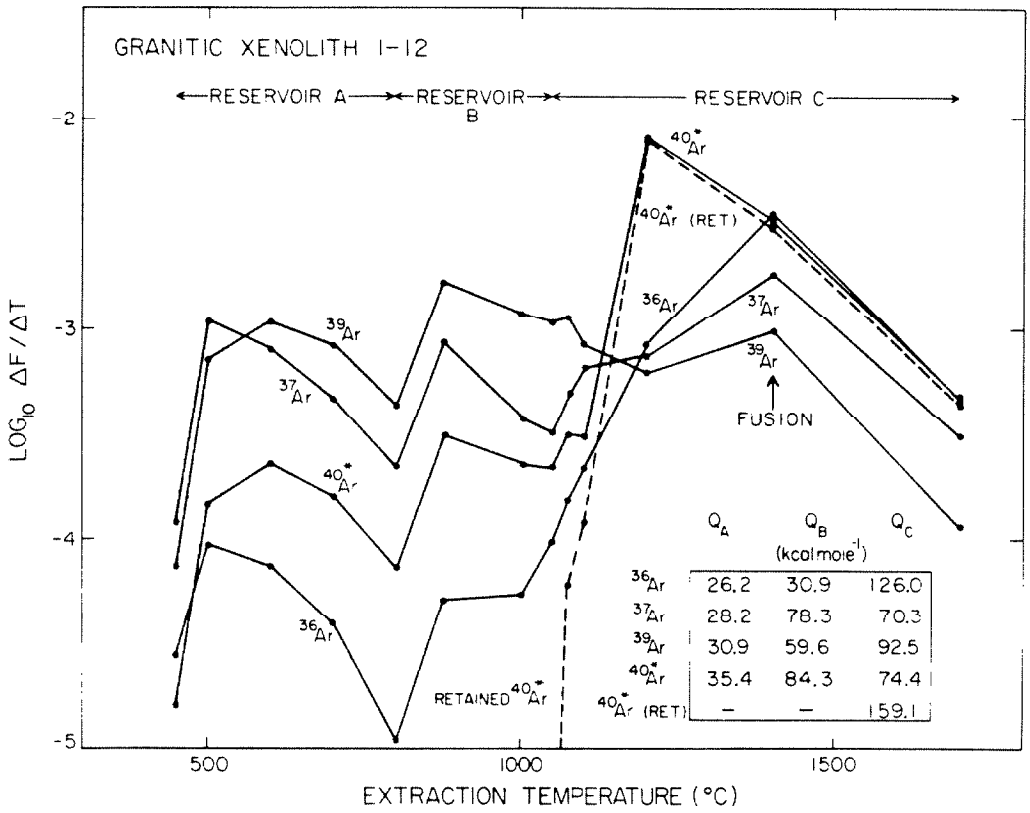

Fig. 4-17. Ar release patterns for xenolith sample 1-12. The fraction of Ar (ΔF) released at each extraction temperature (abscissa) was normalized by the change in temperature (ΔT) between extraction steps and is shown on the ordinate. The plots show clearly that Ar was released from at least three distinct reservoirs. The prominent rise in $\Delta F/\Delta T$ for $^{40}Ar^*$ and ^{36}Ar compared to ^{39}Ar and ^{37}Ar in reservoir "C" is attributable to inherited radiogenic and trapped Ar from retentive sites. Dotted curve shows $\Delta F/\Delta T$ for inherited $^{40}Ar^*$ retained during degassing in the lava (RET). The apparent activation energies Q shown in the box below the curves were calculated from Ar released from each reservoir alone. Q for $^{40}Ar^*$ was calculated for the new $^{40}Ar^*$ accumulated since degassing and the inherited $^{40}Ar^*$ retained during degassing (RET). The apparent Q for $^{40}Ar^*_{RET}$ is about twice that calculated for $^{40}Ar^*$.

released from uniform grains rises with extraction temperature until the reservoir is nearly exhausted, whereupon it reverses slope. Each reservoir in a system is characterized by its own peak, although separation need not be sufficient to permit unambiguous identification of each peak.

The temperature range in which Ar is released from a reservoir is controlled by an activation energy Q. Temperature T and Q are related through the diffusivity D by the Arrhenius relation (Eq. 2), If Q is large or D_o is small, the reservoir is retentive and Ar is released at high temperatures.

In sample 1-12 (Fig. 4-17) there appear to be three separate reservoirs, characterized by different activation energies, which release Ar over different temperature ranges. The amounts of ^{37}Ar and ^{39}Ar in each reservoir are about the same, while $^{40}Ar^*$ and ^{36}Ar are dominated by gas released from the most retentive reservoir. Because ^{36}Ar exceeded blank levels by an order of magnitude or more in most extraction steps, the ^{36}Ar release pattern clearly reflects a characteristic of the xenolith. In this study the increase in $^{40}Ar^*$ has been attributed to radiogenic Ar remaining in the xenolith upon cooling of the host lava, and it is reasonable that non-radiogenic ^{36}Ar trapped during original crystallization was similarly partially retained.

^{37}Ar and ^{36} Ar are created during neutron irradiation and are not subject to degassing by the magma. Apparent activation energies calculated for these two isotopes are largest for the high-temperature reservoir, but in no case do the activation energies exceed those cited for feldspars (e.g., Gerling and Morozova, 1962). In contrast, the activation energy calculated for the high-temperature reservoir "C" of inherited $^{40}Ar^*$ is ~ 160 kcal/mole if new $^{40}Ar^*$ created in the 1.2 my since eruption is subtracted from the measured amounts so that only Ar retained during heating in the magma is considered. This activation energy is a factor

of ~ 1.8 greater than the activation energy of ^{39}Ar from the same reservoir. ^{36}Ar likewise shows a large activation energy of 126 kcal/mole for the high-temperature reservoir "C." To explain these high activation energies, I have generated Arrhenius plots for diffusion from identical spheres subjected to different amounts of degassing but treated (as above) as if none had occurred (Fig. 4-18). It is evident that the effect of only 5% degassing is to practically double the apparent activation energy calculated from a line least-squares fit to the Arrhenius plot. This apparent activation energy is insensitive to changes in the amount of degassing if the reservoir is more than 20% depleted. Thus the high apparent activation energies for ^{36}Ar and ^{40}Ar calculated for sample 1-12 indicate that both ^{36}Ar and ^{40}Ar released at high temperatures (reservoir "C") were retained during degassing in the magma. Consistent with this, more ^{36}Ar was released at high extraction temperatures from xenolith 1-12, which was 6% retentive, than from xenolith 1-11, which showed no inherited $^{40}Ar^*$ at all. The existence of isochrons with air Ar_t intercepts defined by Ar released from NFOC-1 at temperatures below ~ 1000°C (Fig. 4-14) and from NFOC-103 below ~ 850°C (Fig. 4-16) demonstrate that if strongly non-atmospheric trapped components were present in the xenoliths, they occupied only retentive sites, together with inherited $^{40}Ar^*$, and their influence on inferred age of eruption was negligible. $^{40}At_t$ released from xenoliths at low temperatures could arise from either or both of two sources: Ar diffused into the xenolith from the basaltic magma (cf. Harrison and McDougall, 1980), or air Ar adhered to surfaces or incorporated during weathering or alteration. Ar trapped in the xenolith at the time of original crystallization was presumably dissolved in the magma of the pluton. However, the presence of inherited $^{40}Ar^*$ in Ar released at high temperatures masked the composition of Ar_t from retentive sites. Thus we must in general

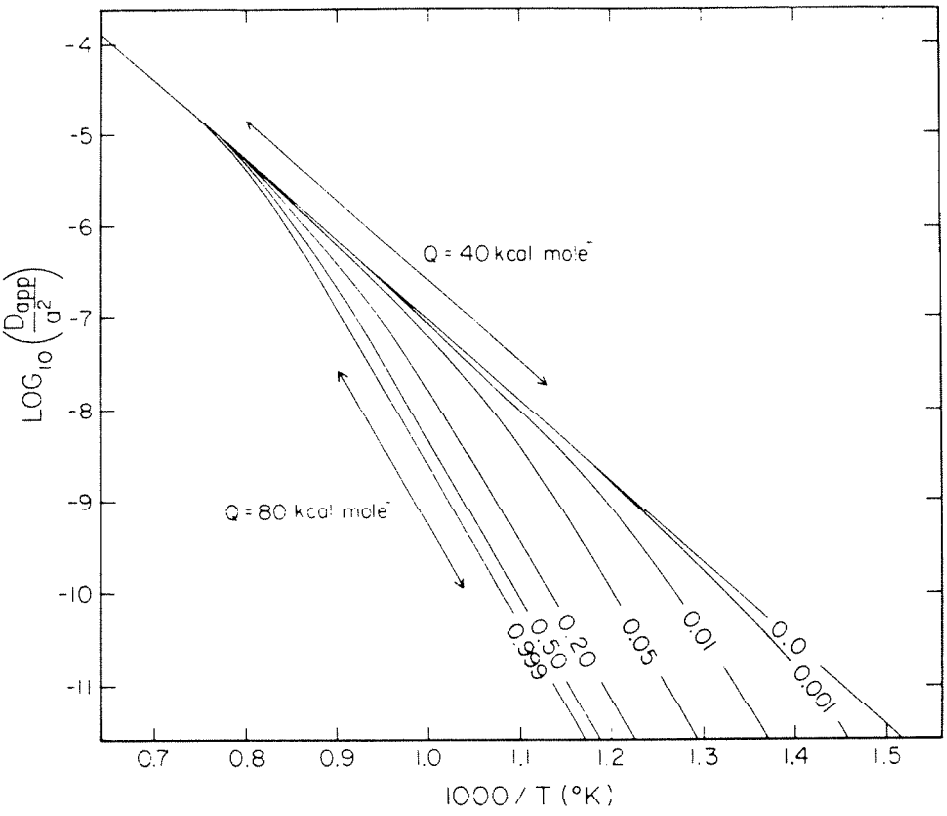

Fig. 4-18. Arrhenius diagrams for an ideal sphere degassed of different fractions F of its ^{40}Ar immediately before analysis. Ordinarily, F = 0 and Q may be found from the slope of the straight line relating $\log(D/a^2)$ to T^{-1}. For the examples shown, ^{40}Ar extracted during analysis was calculated assuming $D = 50 \exp(-4x10^{-4}/(RT))$, extraction steps lasting 1 hr, and a temperature increment of 0.1 T °K between steps. In all cases, the diffusivities were calculated at different temperatures as though F were zero. Thus the ordinate is in terms of apparent diffusivity, D_{app}.

Degassing before analysis resulted in a reduction of D_{app} at low temperatures and convex curves instead of straight lines. The apparent value of Q was increased from its actual value of 40 kcal/mole to a maximum of ~80 kcal/mole, calculated for the linear portion of the curve for F = 0.999 as indicated.

The high values of Q calculated for ^{40}Ar and ^{36}Ar extracted from xenoliths at high temperatures (Fig. 4-17) may thus be explained by only partial loss of Ar from the retentive sites during degassing in the lava. For partially degassed spheres, the apparent Q decreases with increasing T. In contrast, for undegassed samples containing multiple reservoirs of Ar, the apparent Q generally increases with T.

consider the possibility that Ar_t released at different temperatures has different compositions. In ^{40}Ar-^{39}Ar analysis of xenoliths, generally only the composition of the Ar_t released at low temperatures will have an effect on the apparent eruption age. In all cases most original Ar_t should have diffused out of the grains from those sites which also lost inherited $^{40}Ar^*$. That portion of the Ar composition trajectory corresponding to the eruption-age plateau in the age spectrum should generally lie on a mixing line connecting new $^{40}Ar^*$ to new Ar_t created or introduced in the xenolith since cooling of the lava. The chief opportunities for complexity in the Ar release patterns occur when the release of inherited $^{40}Ar^*$ already precludes interpretation of step ages as dates.

Diffusive loss after cooling of the lava

There may be diffusive loss of $^{40}Ar^*$ from K-feldspars over extended periods of time (Wasserburg et al., 1956). The effect on age spectra of such loss was shown schematically in Fig. 4.1. Because we have calculated the diffusivity of ^{39}Ar in the xenolith sample 1-12, it is possible to estimate the extent of loss of Ar after the xenolith cooled. $D_{40°C}$ for ^{39}Ar from the least retentive reservoir (Q = 30.9 kcal/mole) was about 3.6×10^{-17} cm^2/s. After 1 my at 40°C, the expected loss could be ~ 1%. This loss is consistent with the experimental results of Khutsaidze (1962), who found negligible loss from microcline at <100°C. This minor amount would not distort the composition trajectory, except for the first low-temperature extraction. In addition, agreement of total Ar ages of host basalt and isochron ages from low-temperature extractions from xenoliths suggests that there has been little diffusive loss of Ar.

Conclusions

We have measured the age of eruption of a Pleistocene basalt by ^{40}Ar-^{39}Ar stepwise analysis of the host basalt and of granitic xenoliths originally crystallized >75 my ago. The existence of low-temperature plateaus in age spectra of the xenoliths and the good agreement of these plateau ages with model and isochron ages of the host basalt establishes ^{40}Ar-^{39}Ar analysis of xenoliths as a viable method of dating the eruption of the host lava. The identification of granitic xenoliths as appropriate material for ^{40}Ar-^{39}Ar dating is significant because it permits measurement of eruption ages for young lavas which would otherwise be difficult to date.

From the excellent agreement between isochron ages derived for these different systems, I conclude that the weighted mean apparent age of 1.18 ± 0.05 (2σ) my is the eruption date of the basalt capping the ridge south of the North Fork of Oak Creek. Ages for xenoliths from the base and at the eroded top of the basalt flows south of the North Fork of Oak Creek were indistinguishable. Apparently the ~ 50-m-thick sequence of flows was erupted within a short period of less than ~ 0.1 my. It was necessary to use isochron ages because of the presence of Ar_t enriched in ^{40}Ar compared to air Ar.

Multiple reservoirs of Ar_t were shown to exist in both the basalt and xenoliths. In the basalt, at least two trapped components of different composition appeared to be present. The resulting disagreement of model total ages of adjacent samples emphasized the unreliability of conventional K/Ar analysis for dating complicated systems. The presence of multiple trapped components of different compositions necessitates dating young samples by ^{40}Ar-^{39}Ar instead of K/Ar analysis.

Only a small fraction of the Ar in the xenoliths was retained after

heating in the lava. If the xenoliths degassed as uniform spheres, even this amount would have been sufficient to preclude the development of plateaus in the xenolith age spectra. As discussed in §4.1, the large plateaus actually observed are characteristic of diffusion models with two or more sites of different dimensions or activation energies. The behavior of such models suggests that the xenolith dating technique can be successfully applied to yet younger lavas.

4.3 ^{40}Ar-^{39}Ar ANALYSES OF XENOLITHS FROM LATE PLEISTOCENE BASALT FLOWS

Introduction

In §4.2 it was shown that the age of eruption of an early Pleistocene basalt determined by ^{40}Ar-^{39}Ar dating of the lava itself could also be found from plateaus in the ^{40}Ar-^{39}Ar age spectra of partially degassed xenoliths. In this section it will be shown that similar plateaus are observed in the age spectra of xenoliths from basalt flows an order of magnitude younger, even though the xenoliths in both lavas were from plutons which crystallized during the late Cretaceous Epoch. ^{40}Ar-^{39}Ar analysis of the younger samples are much more difficult because they contain about an order of magnitude less new $^{40}Ar^*$ than xenoliths from the older lava. Therefore, a similar fractional increase in the younger apparent age will be found for an order of magnitude less inherited $^{40}Ar^*$. Such a small amount of inherited $^{40}Ar^*$ might be released even at very low extraction temperatures, and it is not at all obvious a priori that enough ^{39}Ar and new $^{40}Ar^*$ can be extracted free of inherited $^{40}Ar^*$ to define a plateau at an age of eruption.

If plateaus can be found in age spectra of xenoliths from very young lavas, then the possibility exists of accurately dating many late

Pleistocene lavas which could not be dated directly. Obviously, in such cases the convincing agreement between K/Ar or ^{40}Ar-^{39}Ar ages of the host lava and ^{40}Ar -^{39}Ar ages of the xenoliths cannot be expected, and for the lavas and xenoliths discussed in this section, identification of meaningful plateaus in age spectra must depend upon characteristics of the spectra or of the $^{36}Ar/^{40}Ar$ vs. $^{39}Ar/^{40}Ar$ trajectories of the xenoliths themselves.

One motivation in developing the methodology for dating thermal events by ^{40}Ar-^{39}Ar analysis of ancient material which contained inherited $^{40}Ar^*$ was the dating of interglacial basalt flows in the Sierra Nevada. This is necessary if the chronology of glacial advances is to be understood. Because many of these flows are so young (< 0.1 my old) very little $^{40}Ar^*$ has accumulated, and the accuracy of ages found by K/Ar or ^{40}Ar-^{39}Ar is strongly dependent on the accuracy of the estimated value of $(^{36}Ar/^{40}Ar)_t$. Thus conventional K/Ar methods applied to the K-poor lava itself are potentially inaccurate, and analyses of coarse-grained K-rich granitic inclusions in the magma may be a better method of dating the eruptions, even though the xenoliths were only partially degassed of Ar during heating by the magma.

In the southeastern Sierra Nevada there are several interglacial basalt flows where method of xenolith analysis might prove useful. In the Toowa Range, at the headwaters of the South Fork of the Kern River, a volcanic center has been active repeatedly during the late Pleistocene. Webb (1950) recognized five ages of basalt flows. Near Little Whitney Meadows, two of these are separated by a bed of gravels and rounded boulders larger than 1 m in diameter which may be glacial outwash. Three canyons through the Sierra escarpment in the Mt. Pinchot quadrangle have intercalated basalt flows and moraines. These are the North Fork of Oak Creek, Sawmill Canyon, and Goodale Canyon.

One basalt flow in Sawmill Canyon has been analyzed using conventional K/Ar methods and appears to be < 0.1 my old (Dalrymple, 1964a, 1964b). In the Mammoth embayment, the Casa Diablo till of Curry (1968) lies between andesite flows which have been independently dated by Curry and by Bailey et al., (1976). These analyses of the same flows gave K/Ar dates which disagreed by more than a factor of two, resulting in the identification of the Casa Diablo glaciation as pre-Wisconsin (Curry, 1971) or early Wisconsin (Bailey et al., 1976; Burke and Birkeland, 1979). The younger andesite overrode and presumably degassed potassic grains in the till. Perhaps these could be dated by the $^{40}Ar/^{39}Ar$ method to resolve the controversy.

Finally, Putnam (1950) has mapped a basalt flow east of June Lake that was erupted between the Tioga (late Wisconsin) and Tahoe (early Wisconsin) glaciations. It should thus be 0.025-0.065 my old. Dating such a young basalt would be difficult by any K/Ar method, and the analyses of potassic xenoliths would seem to afford the greatest chance for success.

Of the three interbedded lava and moraine sequences within the study area, the ^{40}Ar-^{39}Ar dating effort focussed on the one in Sawmill Canyon (Fig. 4-19), which appeared to be the most important. This is because two moraines and at least two lava flows are intercalated. This relationship affords the best opportunity to obtain absolute limits on the age of two Sierran glacial stages and to strengthen correlations with the better understood chronology of continental glaciation. Additionally, the moraines of Sawmill Canyon have previously been studied by different researchers (Knopf, 1918; Moore, 1963; Dalrymple, 1964b; Burke and Birkeland, 1979), and are probably better understood than those of the adjacent canyons of Oak Creek and Goodale Creek.

Figure 4-19 shows a simplified map of the Quaternary geology in

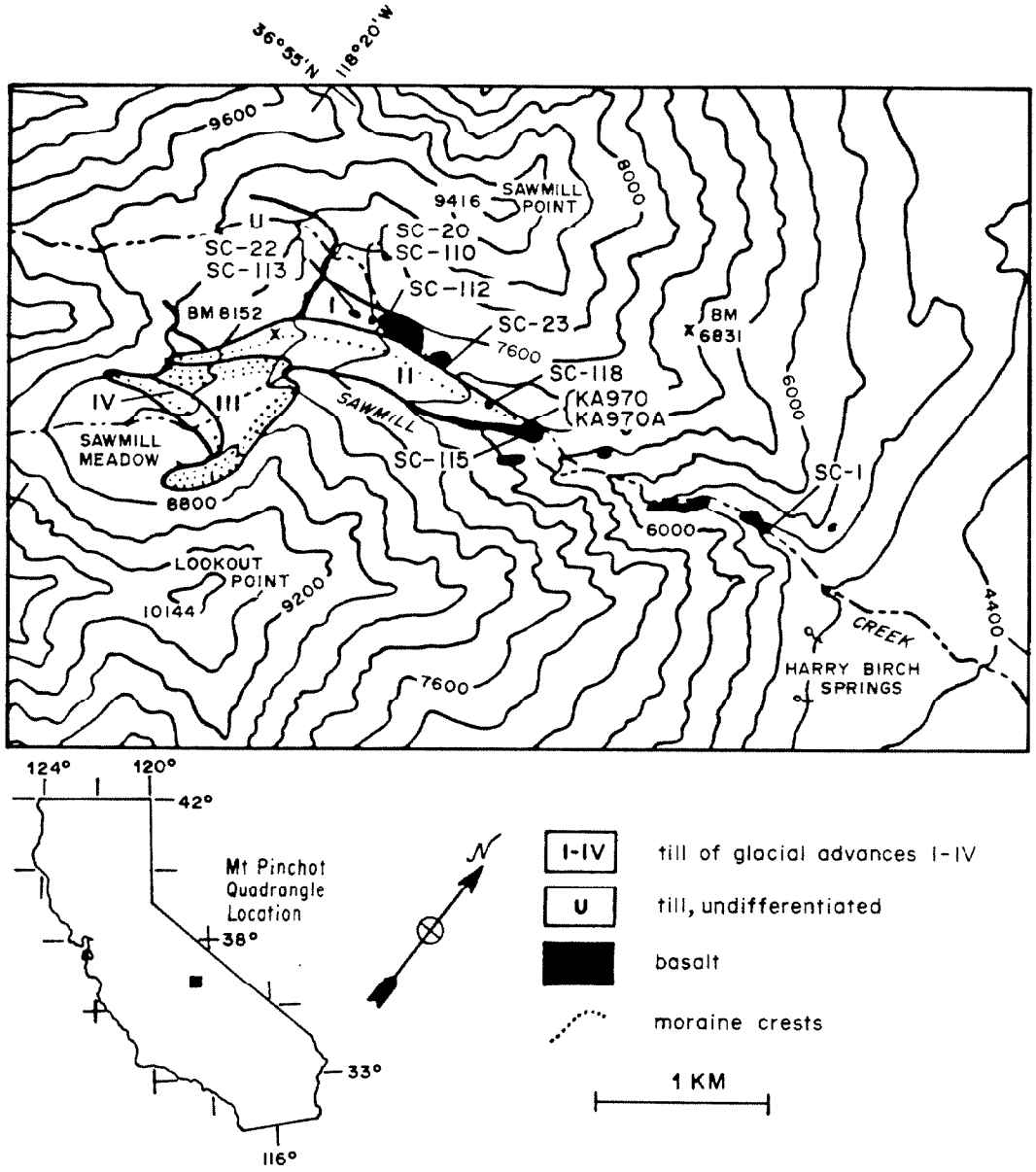

Fig. 4-19. Map shows sample locations in Sawmill Canyon. Glacial geology and most basalt outcrops are from Dalrymple (1964). The small outcrop of basalt at sites SC-20 and SC-110 was not mapped in earlier studies. Samples from KA970 and KA970A were analyzed by Dalrymple (1964). Generalized topography with 400-ft contours is from the U. S. Geological Survey, Mt. Pinchot Quadrangle (1953).

Sawmill Canyon. The oldest moraine (I) appears to have been deposited over basalt which today outcrops only in a small area next to the Sawmill Pass trail. Younger basalt issued from the north slopes of Sawmill Canyon and overrode the end of this old moraine. Pyroclastic deposits are found on both the lava flow and on the moraine itself. Some time later an advancing glacier deposited till (moraine II) atop erosional remnants of this flow. No volcanic bombs or cinders are found on moraine II.

The basalts are contaminated by granodiorite xenoliths probably derived from the late Cretaceous Spook pluton (Moore, 1963) through which the basalts erupted. The age of crystallization of the xenoliths is about three orders of magnitude greater than the age of eruption of at least the basalt dated by Dalrymple (1964b). If it is possible to detect a plateau in the age spectra of such xenoliths, the ages of eruption will bracket glacial advance I and provide an upper (older) limit for glacial advance II.

In addition to the lavas of Sawmill Canyon, lavas from the North Fork of Oak Creek, Taboose Creek, and two sites outside the study area were analyzed. Lavas from these last two sites were included because there were published independent estimates of the ages of eruption.

Sample Sites In Sawmill Canyon

We sampled the basalt at several locations in Sawmill Canyon (Fig. 4-19). SC-1 is near the range-front fault. SC-23 is ~ 10 m north of the contact between moraine II and the eastern of the two basalt remnants on the north side of Sawmill Canyon. Sites SC-116, SC-115, and SC-118 underlie moraine II. From the geologic relationships it is not necessary that SC-1 or even SC-23 be older than moraine II. The basalt K/Ar dated by Dalrymple

(1964b) at < 0.1 my was found under moraine II. His samples, KA970 and KA970A in Fig. 4-19, were taken from the same outcrop on which is located site SC-115.

Sites SC-22 and SC-113 were established in the pyroclastic deposits above moraine I. Site SC-112 was in the basalt flow covering the end of the moraine. Sites SC-20 and SC-110 were from the 20-m-long ledge of basalt found under moraine I. Despite its small size, this basalt outcrop is easy to find because the Sawmill Pass trail passes through it.

At each location samples were chosen which contained xenoliths. By working with a number of xenoliths from different positions in the outcrops, the chances were improved of finding one degassed sufficiently to yield an eruption age.

Other sites . . .

Other sample sites were established elsewhere in adjacent canyons, in the Coso Range to the south, and near Mono Lake to the north. Details of these site locations are presented with the results of the analyses.

Petrology of the Samples from Sawmill Creek

The lava at site SC-1 (Sawmill Creek) is a non-vessicular olivine basalt which contains abundant clinopyroxene and plagioclase phenocrysts in a matrix of smaller (~ 100 μm) plagioclase laths and pyroxene crystals. K probably resides primarily in small crystals and glass blebs in the groundmass. Electron microprobe analysis showed one glass bleb to have the composition of leucite. Rare xenocrysts of microcline or granodiorite xenoliths are encountered. These were apparently derived from the late Cretaceous Spook pluton (Moore, 1963) through which the lava erupted. Most xenoliths

are small, but some as large as 10 cm have been found. The edges of the xenoliths are corroded by reaction with the basaltic lava. Xenoliths appear fresh in thin section, but some may be easily crumbled with a hammer.

Samples of basalt of ~ 0.5 g (samples 2-2 and 2-3) were taken more than 20 cm from the nearest observed xenoliths at SC-1. Two of the freshest xenoliths were sampled (sample 6-8; and samples 6-17, 9-1, and 9-2). These xenoliths were less than 5 mm in diameter and were not easily disaggregated.

At SC-23 the olivine basalt was similar to that at SC-1 but more vessicular. It may be a higher part of the same flow, or a different flow. Numerous granodiorite xenoliths up to 15 cm in diameter were found at this site. Five samples (6-16, 6-25, 9-4, 9-5, and 9-6) from the largest xenolith were analyzed. One of these, 6-16, was part of a 2-cm orthoclase phenocryst. The others were whole pieces of the xenolith with several mineral phases. The surface of the xenolith was pitted where feldspars in contact with the basaltic lava had been melted.

Granodiorite xenoliths from the basalt under moraine II were collected at SC-115 and SC-118. These xenoliths were similar to the one from SC-23. Dalrymple (1964b) determined that K from the host basalt near SC-115 constituted ~ 1.4% of the rock by weight.

Granitic xenoliths were common in the volcanic bombs and fragments atop moraine I. Care was taken to sample only from obvious volcanic bombs to reduce the chance of accidentally dating reworked lava from the throat of the vent. Many xenoliths were rounded and easily broken from the lava. These might have been grus from the vent area included in the lava just before eruption. Such material would likely be only lightly degassed by the rapidly cooling lava in the bombs, and was therefore not likely to yield an age of eruption. Care was taken to avoid sampling these

inclusions. Sampled xenoliths were angular and were well bonded to the lava. These xenoliths were probably included during passage of the magma up through feeders to the vent, although obviously such determinations could not always be made reliably in the field. Basalt samples were selected from relatively non-vessicular portions of the interior of bombs.

Granitic xenoliths from the basalt below moraine I were extremely rare. They were very fresh, and could not be crumbled by hand. The basalt was non-vessicular.

Samples from other sites . . .

Both basalt and xenolith samples from Oak Creek were similar to those described for sites A and C in §4.2. The lava from the Taboose Creek fan was an olivine basalt similar to those found widely in the Big Pine volcanic field, including Sawmill Canyon and Oak Creek. The granitic xenoliths from Black Point were from basalt which was never submerged by the Pleistocene Lake Russell. Lajoie (1968) pointed out that these sub-aerial lavas were typically altered, and some effort was made to obtain fresh-looking samples. The xenoliths were somewhat crumbly, but none better was found. In contrast, the xenoliths from the basalt at Fossil Falls in the Coso Range south of the study area were extremely fresh. These xenoliths consisted of aggregates of microcline crystals.

Analytic Techniques

Analytic techniques were the same as described in §4.2, with only minor exceptions. These are listed below.

Different xenolith samples were treated in different ways. Samples 6-16 (orthoclase), 6-25, 9-4, and 9-5 from SC-23 were irradiated in foil

and then unwrapped before analysis to reduce the amount of non-radiogenic Ar. They were simply pieces of the xenoliths. Sample 9-6 (also from SC-23) was gently crushed and etched in 20% HF at 25°C for 100 s. This was done to remove fine-grained intergranular alteration products. Feldspars larger than ~ 0.5 mm were then hand-picked and wrapped in Sn foil. Xenolith samples from sites SC-115, SC-118, SC-1, sites SC-116 and all xenolith samples from sites on morine I were crushed and sieved. Felsic grains from the size fraction from 104 μm to 160 μm were then separated magnetically and wrapped in foil. The intent was to simplify the mineralogy by excluding biotite, hornblende, and (from SC-1) fragments of basalt.

Xenolith samples from other locations were treated in the same ways. Xenoliths from Oak Creek and Black Point (Mono Lake) were crushed, sieved, and purified. The microcline aggregates from the Coso Range were not treated in any way except for wrapping in foil.

Basalt samples weighing ~ 0.5 g were picked from the interior of hand samples after coarse crushing. Samples were visually checked for xenocrysts, and none were found on exposed surfaces. The samples were wrapped in Al foil packets for neutron irradiation.

Analyses of Ar were especially sensitive to blank composition because of the small amounts of $^{40}Ar^*$ found in the young samples. To minimize the Ar blank, extraction was accomplished in a W crucible vapor-deposited in a He atmosphere. Blank levels of ^{36} Ar ranged from ~ 10^{-10} cm $^{-3}$ STP at temperatures below ~ 800° C for several hours between to reduce memory. Nevertheless, after several samples had been run in a crucible the composition of blank Ar had become somewhat enriched in ^{40}Ar, typically to values of $^{36}Ar/^{40}Ar \approx 0.0032$. Sequences of three to eight blank extractions were run before and after sample measurements.

As in §4.2 Ar data are presented primarily as compositional variation trajectories in plots of $^{36}Ar/^{40}Ar$ vs. $^{39}Ar/^{40}Ar$. The Ar compositions of the first few extractions tend to plot in a colinear array which may define an isochron. The intercept of the isochron with the $^{39}Ar/^{40}Ar$ axis corresponds to the ratio of K-derived ^{39}Ar to new $^{40}Ar^*$ created since degassing of the xenolith in the lava. The K-derived $^{39}Ar/^{40}Ar^*$ is proportional to $(\exp(\lambda t) -1)^{-1}$, where t is the age, but for Quaternary events $^{39}Ar/^{40}Ar^*$ is proportional to t^{-1} with < 0.05% error. Samples in this study were neutron irradiated in several different batches, so there are different factors necessary to relate $(^{39}Ar/^{40}Ar)^{-1}$ to age. Consequently, the abscissa of the three-isotope diagrams has been standardized to the equivalent units of reciprocal age, in my^{-1}. However, only if $^{36}Ar/^{40}Ar = 0$ does the measured $^{39}Ar/^{40}Ar$ actually specify an age.

In §4.2 it was shown that in some samples Ar_t was often slightly enriched in ^{40}Ar compared to atmospheric Ar. This limits the usefulness of conventional presentations of Ar data such as age spectra, which are usually constructed assuming an atmospheric composition of Ar_t. In that case, colinear arrays of compositions in the three-isotope diagram will not yield flat plateaus in age spectra unless Ar_t has atmospheric compositions (cf. Lanphere and Dalrymple, 1976). I have used age spectra in this study to exhibit the fraction of ^{39}Ar released before inherited $^{40}Ar^*$ was detected, which is vital information not evident in three-isotope diagrams. However, in the construction of these spectra, Ar_t has been subtracted according to the $^{36}Ar/^{40}Ar$ intercept of isochrons in the three-isotope diagram in order to calculate meaningful step ages.

The isochrons were determined by linear regression of the low-temperature Ar compositions which appear to be colinear in the three-isotope

diagram. The method of Williamson (1968), which accommodates compositions of different precisions, was used as discussed in §4.2.

If S is much larger than unity, weighting of compositions by their measurement variances is inappropriate, and regression to the reduced major axis (Kermack and Haldane, 1950) may be necessary instead. The reduced major axis was used if S was sufficiently large that there was only a 1°/°° chance that measurement errors were the only source of scatter about the regression line. If the isotopic ratios are precise and if they are co-linear in the three-isotope diagram, then S is small and the regression line may be an isochron. Lanphere and Dalrymple (1978) pointed out that in some situations colinear arrays may be spurious. If S is large enough, the regression line probably has little significance in terms of an actual age. In this study the principal opportunity for such a quandary arose when compositions affected by inherited $^{40}Ar^*$ were inadvertently used to define the line. In this case, the regression line would provide only a lower limit to the age of eruption.

A "measure of merit" M'_ε used to describe the credibility of an age plateau or isochron was introduced in §4.2. M'_ε is a useful measure for the comparison of different isochrons. The plateau was defined as consisting of steps having apparent ages within a fraction ε of the true age. In experimental situations the true age is unknown, and in this discussion we take the plateau to end at the first step for which the apparent age is (a) more than 10% greater than the mean of earlier steps and (b) less than the apparent ages of subsequent steps. In the following discussion M'_ε is is denoted simply as M'. Values of M' may be used to weight individual ages to calculate a mean age (§4.2).

Results

Measured Ar abundances and isotopic ratios for each step in the $^{40}Ar/^{39}Ar$ analyses are summarized in Appendix 4-E. In Table 4-3 are found total amounts of ^{40}Ar and ^{36}Ar released from each sample, and the corresponding compositions $^{36}Ar/^{40}Ar$ and $^{39}Ar/^{40}Ar$. From these compositions, model ages for the sample are calculated by subtracting trapped ^{40}Ar using $(^{40}Ar/^{36}Ar)_t = 295.5$. Abundances of K and Ca inferred from ^{39}Ar and $^{37}Ar_{Ca}$ are also reported. Information pertaining to isochrons and inferred ages of degassing or eruption is given in Table 4-4.

Samples from site SC-1

Isotopic composition diagrams for basalt samples 2-2 and 2-3 from site SC-1 are shown in Fig. 4-20. Ar from 2-3 was extracted in nine steps at temperatures from ~ 275° C to ~ 1375° C. Fusion of the basalt occurred during the ninth step. Low-temperature steps were dominated by Ar_t. ^{40}Ar extracted at higher temperatures up to ~ 850°C was as much as 85% radiogenic, but the amount of Ar released was so small that blank Ar made sample Ar compositions uncertain. As the extraction temperature was raised to the fusion point the basalt released large amounts of Ar_t. This pattern was described in §4.2 for basalts from the nearby North Fork of Oak Creek, and the burst of Ar at the highest extraction temperatures was attributed to loss of Ar_t trapped in sites of high activation energies within lattices of low-K minerals such as pyroxenes which comprised most of the basalt.

Perhaps the most significant feature of the trajectory of Ar isotopic compositions from 2-3 is the apparent trend for the first four steps of compositions along a line connecting Ar_t plotting near AIR and K-derived Ar indicating an age of ~ 0.5 my. This trend may reflect recoil loss or

Table 4-3

Summary of ^{40}Ar - ^{39}Ar Results

Sample	Site		^{40}Ar $cm^3STP\ g^{-1}$ $x10^8$	^{36}Ar $cm^3STP\ g^{-1}$ $x10^{10}$	$^{36}Ar/^{40}Ar$ $x10^6$	$^{39}Ar/^{40}Ar$† $x10^4$	Bern 4M Muscovite $^{39}Ar/^{40}Ar$* $x10^4$	K wt.%	Ca wt.%	Total age,my
2-2	SC-1	basalt	20.6	6.61	3202±54	831±7	243	1.4	12.2	0.28±0.07
2-3	SC-1	basalt	15.7	5.06	3221±60	829±19	243	1.2	11.4	0.25±0.08
6-8	SC-1a	xenolith	208.	57.4	2755±51	121±2	122	4.0	2.9	3.3±0.1
6-17	SC-1b	xenolith	90.2	26.2	2905±68	331±5	122	4.7	2.1	0.9±0.1
9-4	SC-1b	xenolith	229.	69.0	3044±82	156±7	119	5.5	7.2	1.4±0.4
9-5	SC-1b	xenolith	211.	63.8	3008±29	167±1	119	5.4	2.4	1.4±0.2
6-16	SC-23	orthoclase	200.	26.0	1302±25	264±4	122	7.1	0.7	5.1±0.3
6-25	SC-23	xenolith	129.	29.3	2325±41	184±1	122	3.3	2.8	3.7±0.2
9-1	SC-23	xenolith	58.9	14.4	2452±25	225±1	119	4.6	2.0	2.6±0.3
9-2	SC-23	xenolith	148.	31.9	2150±74	181±4	119	4.4	8.4	4.3±0.3
9-6	SC-23	microcline	1050.	23.0	204±5	31±0	119	5.2	3.4	64.8±0.7
7-82	SC-115	xenolith	50.3	6.27	1005±67	193±2	104	3.4	1.5	6.8±0.2
7-83	SC-116	xenolith	226.	68.0	3001±48	71±1	104	3.0	3.0	3.0±0.4
7-63[1]	SC-118	xenolith	>86.0	>16.5	2318±24	104±1	104	>2.4	>1.5	5.7±0.4
6-23	SC-22	basalt	44.3	14.4	3213±68	222±3	122	1.4	10.2	0.5±0.2
7-80	SC-112	xenolith	89.7	26.0	2873±55	157±1	104	2.6	1.1	1.8±0.3
7-61	SC-113	xenolith	554.	33.6	591±9	52±0	104	5.4	1.5	29.5±0.5
7-60	SC-113	xenolith	288.	17.4	714±58	66±5	104	3.3	1.1	22.9±3.7
6-15	SC-20	basalt	13.8	4.90	3355±79	712±11	122	1.6	10.2	0.03±0.7
7-54	SC-110	xenolith	154.	42.3	2734±51	91±1	104	2.5	2.2	4.0±0.2
7-55	SC-110	xenolith	84.0	21.5	2478±23	150±0	104	2.6	2.6	3.3±0.1
9-20	Tab-201	basalt	8.30	2.74	3297±106	838±2	119	0.4	4.2	0.07±0.08
9-9	BPt-11	xenolith	165.	34.6	2227±25	118±2	119	3.6	1.6	6.2±0.3
9-32	FF-101	microcline	190.	58.6	3127±19	259±1	119	9.3	0.6	0.63±0.06
7-86[1]	NFOC-29	xenolith	>170.	>29.2	1716±42	166±3	104	>5.4	>1.8	5.6±0.2
7-27	NFOC-51	basalt	8.00	2.49	3110±14	104±0	228	2.0	6.8	3.2±0.2
7-107	NFOC-25	basalt	236.	75.3	3192±8	42±0	103	1.9	5.3	2.4±0.1

*Normalized to neutron fluence for muscovite irradiation monitor. Uncertainties are <0.5%.
†Normalized to neutron fluence for muscovite irradiation monitor.
[1]Step lost in analysis.

The first two columns show amount of Ar extracted from each sample normalized by the sample mass (App. 4-E, Table 4-E-I). Next columns show isotopic composition. Error bars are 2σ. Apparent age (sixth column) is found from compositions normalized by $^{39}Ar/^{40}Ar^*$ of the muscovite irradiation monitor. Concentrations of K and Ca were calculated from ^{39}Ar and ^{37}Ar compared to abundance of some isotopes in the Bern 4M and fluorite irradiation monitors of known K and Ca.

Table 4-4

Summary of ^{40}Ar - ^{39}Ar Results (Continued)

Sample	Site		Fraction of ^{39}Ar in plateau	Number of steps	Isochron age, my	Ar_t $^{36}Ar/^{40}Ar$ x10^6	$\frac{S}{n-2}$	Regression method	M'
2-2	SC-1	basalt	1.00	5	0.076±0.051	3255±54	1.85	W	0.15
2-3	SC-1	basalt	1.00	9	0.126±0.066	3245±61	2.40	W	0.34
6-8	SC-1a	xenolith	0.47	8	0.119±0.008	3324±41	12.99	R	1.10
6-17	SC-1b	xenolith	0.54	4	0.122±0.022	3335±36	4.72	W	0.23
9-4	SC-1b	xenolith	0.52	3	0.084±0.028	3353±52	35.61	R	0.13
9-5	SC-1b	xenolith	0.56	4	0.115±0.024	3356±17	26.70	W	0.21
6-16	SC-23	orthoclase	0.19	5	0.161±0.024	3254±71	6.84	R	0.12
6-25	SC-23	xenolith	0.55	8	0.117±0.011	3332±26	6.75	R	0.92
9-1	SC-23	xenolith	0.53	5	0.125±0.023	3370±74	12.32	R	0.28
9-2	SC-23	xenolith	0.53	4	0.104±0.037	3340±90	12.50	R	0.12
9-6	SC-23	microcline	0.00	0	-	-	-	-	-
7-82	SC-115	xenolith	0.32	4	0.124±0.085	2839±96	3.64	W	0.06
7-83	SC-116	xenolith	0.66	9	1.135±0.015	3322±11	2.01	W	8.81
7-63	SC-118	xenolith	>0.26	5	0.34±0.13	3391±97	5.92	R	0.07
6-23	SC-22	basalt	1.00	5	0.20±0.21	3280±43	0.10	W	0.09
7-80	SC-112	xenolith	0.52	5	0.131±0.010	3359±9	0.54	W	0.67
7-61	SC-113	xenolith	0.13	3	0.179±0.051	3372±11	0.63	W	0.03
7-60	SC-113	xenolith	0.00	0	-	-	-	-	-
6-15	SC-20	basalt	-	-	-	-	-	-	-
7-54	SC-110	xenolith	0.26	3	0.405±0.109	3359±22	4.20	W	0.06
7-55	SC-110	xenolith	0.33	6	0.468±0.052	3361±13	1.72	W	0.36
9-20	Tab-201	basalt	-	-	-	-	-	-	-
9-9	BPt-11	xenolith	0.00	0	-	-	-	-	-
9-32	FF-101	microcline	0.18	8	0.123±0.020	3344±40	16.38	R	0.14
7-86[1]	NFOC-29	xenolith	>0.08	2	(0.195±0.074)	(3182±93)	-	*	(0.01)
7-27	NFOC-51	basalt	-	-	-	-	-	-	-
7-107	NFOC-25	basalt	-	-	-	-	-	-	-

*The "isochron age" and Ar_t were determined from the line passing through the two compositions.

[1]Step lost in analysis.

Explanation

Lines were fit to Ar compositions thought to be free of inherited $^{40}Ar^*$. These regression lines were interpreted as isochrons. The isochron age was calculated from the intersection of the isochron and the $^{39}Ar/^{40}Ar$ axis. The composition of Ar_t is specified by the intersection of the isochron and the $^{36}Ar/^{40}Ar$ axis. $S/(n-2)$ is a measure of the scatter of compositions about the isochron determined by the method of Williamson (1968). In general, values of $S/(n-2) > 1$ indicate more scatter than expected from the measurement uncertainties alone. If $S/(n-2)$ is so large that there is less than a 1°/°° chance that the scatter is allowed by the known measurement uncertainties, the isochron was taken to be the reduced major axis (Kermack and Haldane, 1950). The method of regression is indicated by a W (Williamson) or an R (reduced major axis) in the penultimate column. The final column shows values of $M' = nF/\sigma_{\%}(\S 4.2)$ where n is the number of steps to be fit, F is the fraction of ^{39}Ar released in those steps, and $\sigma_{\%}$ is the standard deviation in percent of the isochron age.

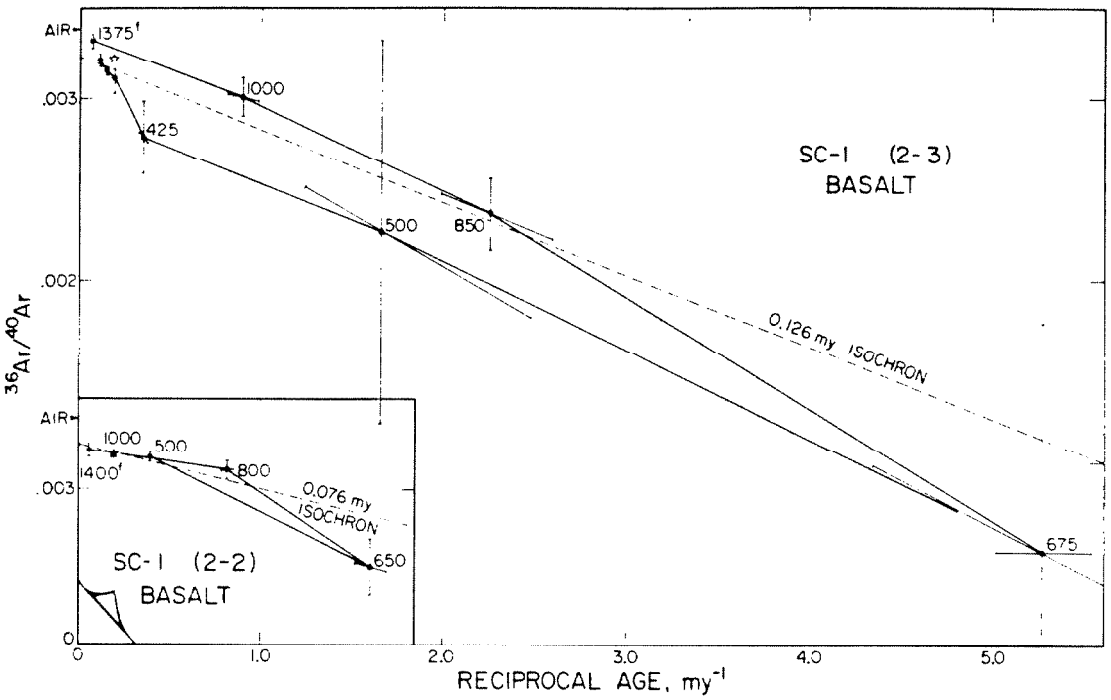

Fig. 4-20. Poorly defined isochrons from ^{40}Ar-^{39}Ar analysis of basalt samples 2-3 and 2-2 from site SC-1 yield ages consistent with earlier K/Ar ages for basalt samples KA970 and KA970A (Dalrymple, 1964), taken from a different outcrop probably of the same flow. Total compositions (stars) yield total ages of ~ 0.27 my, considerably older than isochron ages. One explanation is that Ar_t is enriched in ^{40}Ar compared to air AIR. Error bars in this and subsequent three-isotope diagrams are 1σ. Diagonal error bars reflect uncertainties in blank subtraction. Extraction temperatures (°C) are shown by selected steps. Superscript f identifies step in which fusion occurred.

redistribution of ^{39}Ar from small K-rich grains during neutron irradiation. The variation pattern may also reflect the presence of multiple reservoirs of Ar_t, at least one of which is enriched in ^{40}Ar compared to atmospheric Ar (cf. §4.2). Such an explanation cannot be ruled out for this sample.

A line fit to Ar compositions from sample 2-3 intercepts the $^{36}Ar/^{40}Ar$ axis at 0.00325±0.00006, suggesting an Ar_t enriched in ^{40}Ar compared to air Ar. If this is true, then the model total or K/Ar age of 0.25±0.08 my, calculated assuming Ar_t = 0.00338, is too large and the age corresponding to the abscissa intercept of the fitted line (0.13±0.07 my) is the only measure of the age of eruption. Because of the complexity of the isotopic variation trajectory, the regression line is of uncertain significance.

The model total age of basalt sample 2-2, also from site SC-1, is 0.28±0.07, similar to the total age of 2-3. The trajectory of compositions is somewhat simpler than for 2-3, although this may be due in part to the relatively high temperature of ~ 500°C for the first extraction. The regression line again implies a radiogenic Ar_t. The age indicated by this line is only 0.08±0.05 my, which is not significantly younger than the 0.13±0.07 my age for 2-3. Isochron ages from both samples are consistent with Dalrymple's (1964b) K/Ar ages of 0.06±0.10 my and 0.09±0.18 my (2σ) (for samples taken near SC-115). Total model ages are older than Dalrymple's K/Ar ages at >95% confidence. Abundances of K and Ca inferred for these samples were ~ 1.3% and ~ 11.8% by weight, respectively.

Xenolith sample 6-8, from site SC-1a, was analyzed in fourteen steps at temperatures from ~ 275°C to ~ 1700°C (Fig. 4-21). Ar compositions for the first eight steps were colinear in the three-isotope diagram, indicating mixing between a single Ar_t and a well-defined $^{39}Ar/^{40}Ar^*$ corresponding to an age of 0.119±0.008 my. The radiogenic fraction of the ^{40}Ar increased

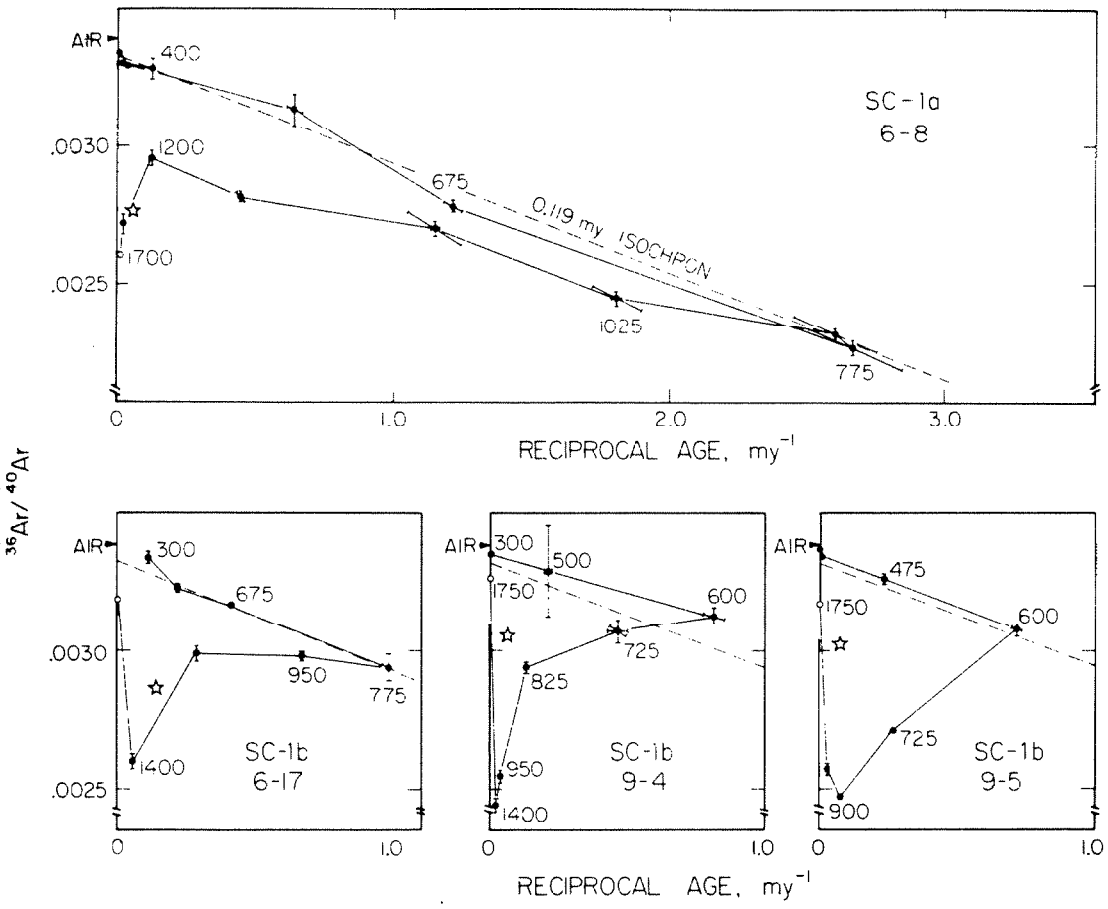

Fig. 4-21. Ar compositions for granodiorite xenolith samples from site SC-1. Top diagram shows Ar compositions for xenolith SC-1a (sample 6-8). The 0.119-my line is probably an isochron and was fit to the first eight compositions. At higher temperatures Ar appeared to include inherited $^{40}Ar^*$. Bottom row shows compositions from three replicates of a second xenolith, SC-1b. The dashed line is the isochron from sample 6-8, included for reference. In general the first three or four steps produce Ar of compositions consistent with mixing between Ar_t and a young K-derived Ar. This is most pronounced for sample 6-17.

with temperature to a maximum of ~ 33% at a 775°C. At higher extraction temperatures the Ar_t became increasingly dominant, although this trend was offset by the presence of increasing amounts of what was probably inherited $^{40}Ar^*$, especially above 1200°C. This resulted in a spurious colinear array of six compositions, extracted at temperatures from ~ 775°C to 1200°C. A line fit to these points would intersect the $^{36}Ar/^{40}Ar$ axis at ~ 0.003. Were it not for the large burst of inherited $^{40}Ar^*$ released during the last two steps, this pattern could not be confidently distinguished from ternary mixing among two compositions of Ar_t and one composition of K-derived Ar. So much inherited $^{40}Ar^*$ was released at 1700°C that the total composition of Ar from 6-8 was well below the mixing lines established at lower temperatures and corresponded to a model age of 3.3±0.2 my. If the xenolith first crystallized in late Cretaceous time, the degassing in the lava was more than 95% complete.

The line fit to compositions of Ar extracted at or below ~ 875°C gave a very precise age. This precision resulted from the large number of steps defining the line, from the high colinearity of compositions in the three-isotope plot, and from the high $^{40}Ar^*$ content of Ar released at 775°C and 875°C. The regression line was probably an isochron.

Only ~ 20% of the Ar measured in the two steps at 775°C and 875°C was attributable to the blank, so the Ar compositions were well known. Furthermore, the effect of blank subtraction was to shift the plotted compositions along a line very nearly parallel to the isochron. This minimized the influence of blank Ar on the apparent age of eruption for sample 6-8.

To demonstrate the insensitivity of the isochron for sample 6-8 to uncertainties in the blank Ar, we randomly chose different blank Ar amounts for each step according to the uncertainties listed in App. 4-A. Lines

were fit and ages tabulated for 100 iterations. The distribution of ages calculated in this way was 0.119±0.002 my. As the uncertainties in age from measurement precision were ±0.008 my, the uncertainties due to blank subtraction were negligible.

The high value of S/(n-2) indicates scatter of compositions about the isochron in excess of that predicted from measurement errors alone. The correlation coefficient relating the variation of $^{36}Ar/^{40}Ar$ and $^{39}Ar/^{40}Ar$ for the points fit by the isochron is -0.997, suggesting that the high value of S may result from underestimation of measurement errors or random effects but that the data were sufficiently linear that fitting a reduced mean axis is justified. The colinearity of the compositions increases the confidence that the isochron age is physically significant.

Because of the high radiogenic content of Ar from the 775°C and 875°C steps, the influence of uncertainties in the composition of Ar_t on the apparent ages was reduced. Apparent ages for these steps (assuming Ar_t of atmospheric composition) averaged 0.122±0.005 my, within 2σ of the isochron age. Remarkably, almost half of the total ^{39}Ar was released before inherited $^{40}Ar^*$ was detected. This characteristic of the xenolith allowed the measurement of the large number of steps (eight) which defined the isochron. From the amounts of $^{39}Ar_K$ and $^{37}Ar_{Ca}$ in sample 6-8, it was inferred that xenolith SC-1b contained 4.0% K and 2.9% Ca by weight. This is reasonable for a granodiorite. The composition of Ar_t, $^{36}Ar/^{40}Ar$ = 0.003324±0.000041, was enriched in ^{40}Ar compared to air.

^{40}Ar-^{39}Ar analyses of three replicates of the second xenolith, SC-1b, produced three-isotope diagrams similar to that of sample 6-8 (Fig. 4-21). However, for no step free of inherited Ar in any of the three analyses did $^{40}Ar^*$ exceed 13% of the ^{40}Ar released in that step. Since total ages

were less than 1.5 my, degassing in the lava was more complete than for sample 6-8. Despite this, inherited $^{40}Ar^*$ was detected at temperatures as low as 725°C in two of the samples (9-4 and 9-5). This was 300°C lower than for sample 6-8. In each of the samples >50% of the total ^{39}Ar was still released before inherited $^{40}Ar^*$ was detected.

Regression lines for each of the xenolith samples from SC-1b indicated slightly radiogenic Ar_t compositions. Although precisions were lower than for sample 6-8, isochron ages for samples 6-17 and 9-5 (Table 4-4) were within 1σ of 0.119 my, the mean age of eruption found from sample 6-8. Only three extraction steps for sample 9-4 appeared to be free of inherited $^{40}Ar^*$, and these were of low analytic precision. As a consequence, $S/(n-2) = 35.61$ was the highest for any sample. The plateau or isochron had a very low M' of 0.13, a factor of 8.5 lower than M' for sample 6-8. The mean age calculated by weighting all four individual isochron ages by their respective values of nF_{39} (§4.1) was 0.118±0.006 my. (The uncertainty of this mean age does not include the systematic 3.4% uncertainty of the monitor age, which raises the uncertainty to ±0.007 my.)

Thus the age of degassing of the xenoliths from the basalt at site SC-1 appeared to be 0.12 my. This age is based chiefly on one sample (6-8) but is supported by three other analyses of xenoliths and is consistent with analyses of the basalt itself. This age is also consistent with the geological context.

Samples from site SC-23

Five samples of a single granodiorite xenolith from SC-23 were analyzed. Three of these (9-1, 9-2, and 6-25) were simply ~ 0.25 g pieces of the xenolith. Sample 6-16 was a piece of an orthoclase phenocryst, and sample 9-6

contained etched feldspar grains picked from the crushed xenolith. Only 9-6 was wrapped in foil.

Ar from sample 9-1 was released in eight steps (Fig. 4-22). Compositions followed the usual pattern, with the trajectory in the three-isotope diagram proceeding from near AIR towards a young K-derived component, then reversing direction and returning towards a point on the ordinate lower than AIR. Fusion occurred during the 1400°C step, and Ar from this step was strongly enriched in inherited $^{40}Ar^*$. Over half the ^{39}Ar was released unaccompanied by inherited $^{40}Ar^*$, in five steps up to 900°C. The compositions plotted in a concave array in the three-isotope diagram. The reduced major axis fit to these points yielded an apparent age of 0.125±0.023 my and Ar_t within 1σ of AIR composition. However, the composition at 600°C plotted well below this line. Such a pattern could result if the sample contained multiple reservoirs of Ar_t. In this case a regression line has uncertain meaning.

Compositions of Ar released from sample 9-2 did not follow the same concave trajectory seen for 9-1. A line fit to the first four compositions gave an age of 0.104±0.037 my. This was closer to the younger of the apparent ages found for 9-1, but the uncertainties in the ages were so large that the age for 9-2 differed from the older age for 9-1 at less than the 95% confidence level.

Ar released from sample 6-25 in eight steps at temperatures below 1050°C defined a linear array of compositions. A line fit to these points passed through AIR and gave an age of 0.117±0.011 my. Over half of the ^{39}Ar was released in these steps, but only 15% was released during the three most radiogenic steps. Sample Ar released during those three steps was only two to five times above blank levels. The regression line for sample 6-25 was the best of all from site SC-23. This is reflected by

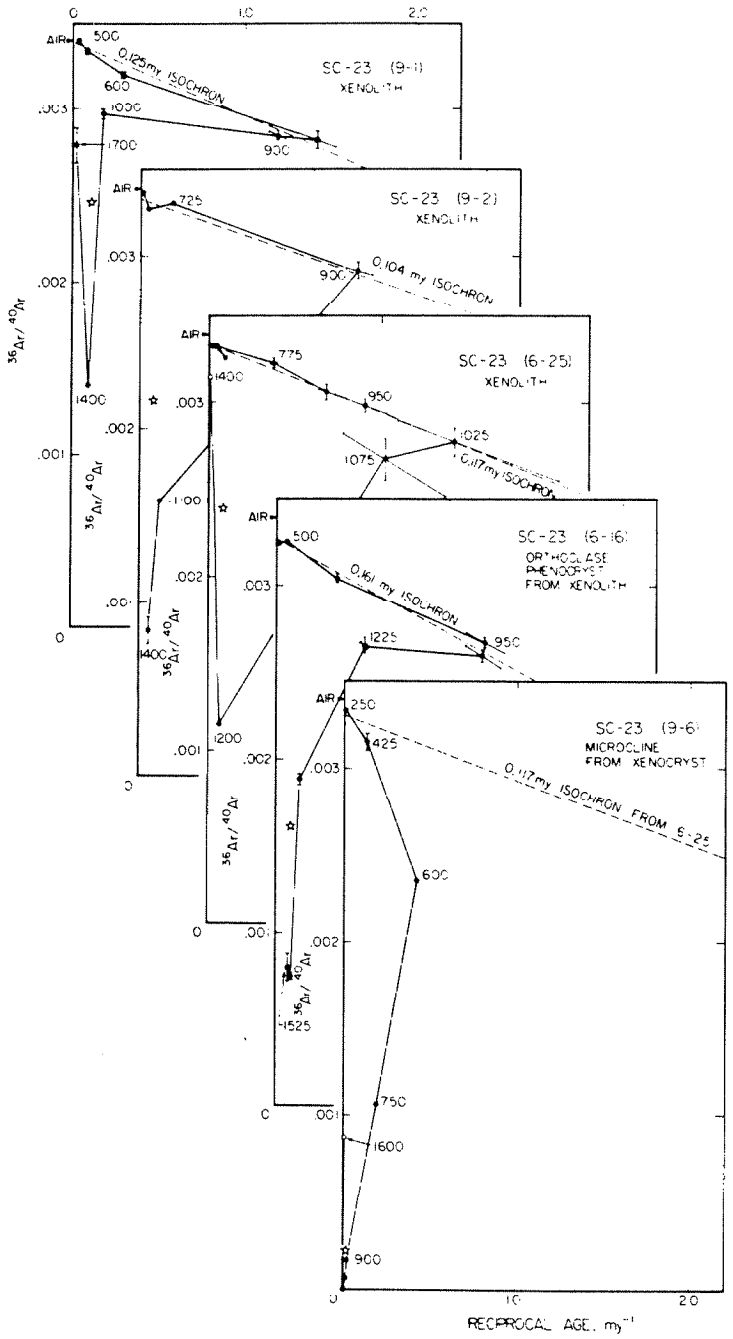

Fig. 4-22. Ar compositions for xenolith samples from site SC-23 clearly show the tendency to lie along a line between a well-defined Ar_t on the ordinate and a young K-derived $^{39}Ar/^{40}Ar$ (proportional to reciprocal age) on the abscissa. All samples released inherited $^{40}Ar^*$ at temperatures above 1050°C. Sample 9-6 alone was etched in HF. This may be responsible for its failure to define an isochron.

$M' = 0.92$, second only to $M' = 1.10$ for sample 6-8 from site SC-1 and a factor of three higher than M' for sample 9-1. Although $S/(n-2) = 6.25$, implying excess scatter in compositions, inspection of Fig. 4-22 shows the high degree of colinearity (correlation coefficient $r = -0.994$) which supports the interpretation of the reduced major axis as an isochron giving the age of eruption.

Compositions of Ar released from sample 6-16, part of a single orthoclase phenocryst from xenolith SC-23, followed a trajectory similar to those of other xenolith samples. Ar_t clearly contained excess ^{40}Ar, with $^{36}Ar/^{40}Ar = 0.003254 \pm 0.000071$. Only 3.1×10^{-10} cm^3 STP ^{36}Ar (per gram sample) was degassed in the first two steps (300°C and 500°C), compared to 1.4×10^{-9} cm^3 STP ^{36}Ar for adjacent sample 6-25. This might reflect lower amount of atmospheric Ar adhered to the reduced surface area of the single crystal compared to the aggregate of small grains in sample 6-25.

Four or five increments of Ar from sample 6-16 were measured before inherited $^{40}Ar^*$ was detected. However, only 19% of the ^{39}Ar was released in these steps below 1100°C, compared to 58% for sample 6-25. The reduced major axis fit to the five points apparently free of inherited $^{40}Ar^*$ gave an age of 0.161 ± 0.024 my. This was the oldest apparent age for any of the xenoliths from SC-1 or SC-23.

The apparent high age for sample 6-16 could result from the presence of $^{40}Ar^*$ in the 950°C and 1075°C steps. Fitting the reduced major axis to only the first four compositions (eliminating the 1075°C step) reduced the age to only 0.151 ± 0.031 my, not significantly lower and still anomalously high. In fact, no line younger than 0.135 my could be fit to any two points. The weighted mean age of isochrons from site SC-23 was 0.119 ± 0.008 my (± 0.009 my, if the monitor uncertainty is included). This age is not

different from the mean age for site SC-1.

Total ages for all of the unetched xenoliths from SC-1 and SC-23 ranged from 0.9 my to 5.1 my. Degassing in the lava was more than 92% complete, based on an assumed lower limit of 65 my for the age (late Cretaceous) of the parent pluton. In contrast to the other samples, sample 9-6 consisted of feldspars etched in HF, and although it was from the same xenolith SC-23, its total age was 65 my. It is unlikely that such a disparity in the levels of degassing of similar grains would be found in the same xenolith. Consequently, it appears that etching removed or damaged parts of the crystal lattices which were degassed in the lava.

The three-isotope diagram (Fig. 4-22) shows that the age of eruption could not be identified from the pattern of Ar compositions for sample 9-6. However, Ar released at 1300°C gave a model age of 116 my, which may be considered a lower limit to the age of the late Cretaceous Spook pluton through which the basalt erupted.

Samples from sites SC-116, 115, and 118

Site SC-116 was near the base of the basalt flow sampled by Dalrymple (1964b) for K/Ar dating of the basalt underlying the glacial moraine (Fig. 4-19). Site SC-115 was near the top of the same flow. Site SC-118 was a second smaller outcrop of basalt beneath the same moraine. These outcrops are close to the present level of Sawmill Creek, and from this geomorphic relationship the basalt appears to be relatively young.

Xenolith sample 7-83 from site SC-116 showed a familiar isotopic composition trajectory (Fig. 4-23), with low-temperature compositions plotting near AIR and progressing towards a single K-derived composition for eight steps at temperatures up to 775°C. At higher temperatures,

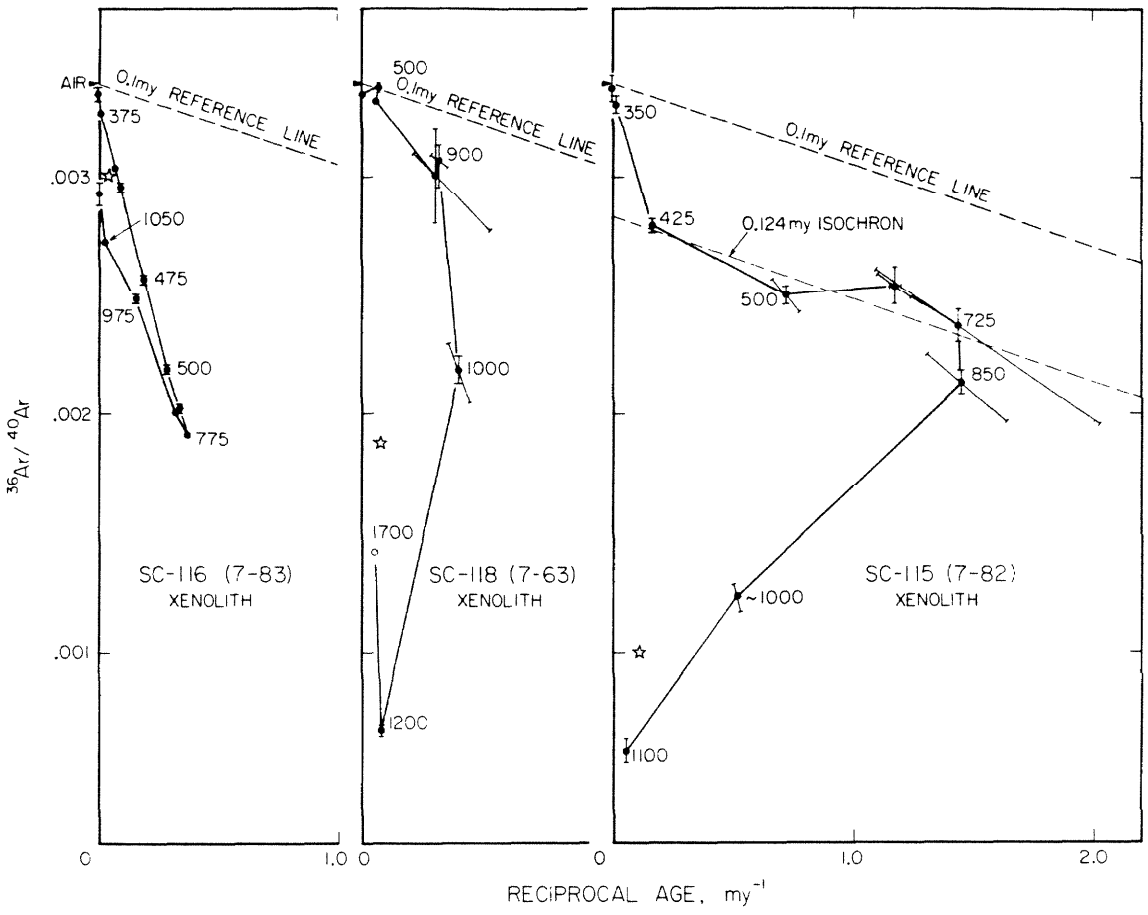

Fig. 4-23. Ar compositions for three granodiorite xenoliths from basalt cropping out beneath moraine II showed different trajectories or patterns of variation with extraction temperature. For sample 7-83 compositions of Ar released in nine steps at temperatures below 975°C defined an isochron giving an age of ~ 1.1 my. Ar compositions for neither of the other xenoliths defined such simple linear patterns. Steps at temperatures of 900°C or less could be interpreted as an isochron giving an age of ~ 0.35 my for sample 7-63. The complicated trajectory for sample 7-82 could be interpreted as showing the effects of recoil redistribution of ^{39}Ar or mixing of multiple compositions of Ar_t, one of them enriched in ^{40}Ar compared to air Ar. In the first case, regression lines would be of uncertain significance. The 0.124-my line shown was fit to the compositions for the four steps made at temperatures from 425°C to 725°C, assuming a mixture of compositions for Ar_t.

the trajectory reversed direction and returned to the ordinate at $^{36}Ar/^{40}Ar < 0.003$ for T > 1000°C. The eight low-temperature steps appear to define an isochron giving an age of 1.14±0.02 my. This age is an order of magnitude greater than the K/Ar ages of Dalrymple (1964b). It would be geologically improbable to find a 1-my-old lava flow within a few tens of meters of the rapidly down-cutting Sawmill Creek. (Only 20 km to the north, Coyote Creek has cut down ~ 300 m in the past 1 my; Bateman, 1965). Yet the isochron for sample 7-83 appears to be well defined.

Moore (1963) noted basaltic dikes on the north side of Sawmill Point and mapped a similar outcrop on the south side, in the drainage of Sawmill Creek. He guessed the dikes north of Sawmill Point could be older than the basalt flows of Oak Creek (1.2 my). Thus ancient lava may well be found in Sawmill Canyon. If volcanism in Sawmill Canyon was not restricted to a single episode, then perhaps the xenolith of sample 7-83 was from a large block of ancient basalt incorporated in a younger flow. No conclusions should be drawn without new K/Ar or ^{40}Ar-^{39}Ar analyses confirming the presence of ancient basalt in Sawmill Canyon.

Site SC-115 was the same outcrop sampled by Dalrymple (1964b) for K/Ar dating of the basalt underlying the glacial moraine (Fig. 4-19). Site SC-118 was a second smaller outcrop of basalt under the same moraine. One xenolith from each site was analyzed. Xenolith sample 7-63 from SC-118 had a total age of only 5.7 my but no reliable isochron could be fit to compositions in the three-isotope diagram (Fig. 4-23). It appears that inherited $^{40}Ar^*$ was released at extraction temperatures as low as 700°C.

While more than one quarter of the ^{39}Ar was released in the first six steps which appeared to be unaffected by inherited $^{40}Ar^*$, compositions clustered around two values. Thus the trends in composition used

to identify isochrons were not present.

Sample 7-82 from site SC-115 had an isotopic variation trajectory (Fig. 4-23) which was too complex to permit confident identification of an isochron. Ar released at 350°C or less plotted close to AIR, but after progressing towards an old K-derived $^{39}Ar/^{40}Ar$ (~ 1 my) the trajectory flattened out. Model ages of subsequent steps decreased to ~ 0.2 my. At steps above 850°C the trajectory changed direction again and progressed towards an ancient K-derived argon plotting near the origin.

If Ar extracted below ~ 500°C was a mixture of new $^{40}Ar^*$ created since degassing in the lava, an Ar_t of atmospheric composition, and a second Ar_t enriched in ^{40}Ar, then compositions of extractions from 500°C to 725°C might define an isochron. A line fit to these compositions indicated an age of 0.12±0.09 my. This imprecise age is at least consistent with ages from the adjacent site SC-23. However, the 500°C point may well include atmospheric Ar_t also, in which case the regression line provides only an upper limit to the age.

Sample 7-63 from site SC-118 had a composition trajectory which did not appear to define an isochron. One of the critical steps (600°C) was lost during analysis. However, the next three steps all had similar apparent ages (~ 0.35 my), which may be interpreted as indicating an absence of inherited $^{40}Ar^*$ until the 1000°C step. A line fit to the five steps at 900°C or lower gave an age of 0.34±0.13 my. Because of the ambiguity in the trajectory and the missing step, this age should probably be viewed only as an upper limit to the age of eruption.

Samples from sites atop moraine I

Four samples were analyzed from two basalt outcrops atop moraine I, an old deposit of till north of the main moraine (II) of Sawmill Canyon

(Fig. 4-19). Site SC-112 was at the west end of the basalt flow covering the lower portion of the moraine. Sample 7-80 from this site was part of a 5-cm granodiorite xenolith from a 1-m volcanic bomb resting on the flow atop the moraine. Site SC-113 was at the center of a small patch of pyroclastic basalt bombs, cinders, and fragments on the crest of the same moraine to the west, and samples 7-60 and 7-61 were granodiorite xenoliths from a 25-cm bomb from this site. Sample 6-23 was basalt from a different 25-cm bomb from site SC-22, a few meters away.

Sample 6-23 was analyzed in six steps, at temperatures from 300°C to 1700°C. Ar released at 500°C was the most radiogenic, but the total amount of Ar released in this step was so small that only a low-precision apparent step age of 0.05±0.05 my resulted. No plateaus were found in the erratic age spectrum. The total age was 0.50±0.16 my. However, an Ar_t composition enriched in ^{40}Ar only 5% compared to air AR would reduce that age to zero. Because non-atmospheric compositions of Ar_t have been observed in lavas (Krummenacher, 1970; Kaneoka, 1980; see also §4.2) this age should probably be viewed with scepticism.

Xenolith samples 7-60 and 7-61 were apparently only poorly degassed: they yielded total ages of 22.9 and 29.5 my. Because of the large amount of inherited $^{40}Ar^*$, no low-temperature isochron was developed for either sample (Fig. 4-24). Compositions of steps extracted at temperatures of 500°C or less yielded apparent ages as low as 0.18±0.04 my which could be regarded as upper limits to the age of eruption, but these are extremely sensitive to the composition of Ar_t. The highest apparent age (66 my) was found for the fusion step, and confirmed that the source of the xenoliths was at least Cretaceous in age. No plateau was developed for Ar released at high temperatures, and the age is therefore only a lower limit to

the age of original crystallization.

Xenolith sample 7-80 from SC-112 was much more completely degassed than the xenoliths from SC-113, despite the fact that it was from a similar bomb. Its total age was only 1.8 my. Figure 4-24 shows that compositions of Ar extracted in five steps at temperatures up to 775°C formed a linear array in the $^{36}Ar/^{40}Ar$ vs. $^{39}Ar/^{40}Ar$ diagram, defining a distinct isochron of 0.131±0.010 my age. Ar released from sample 7-80 at temperatures above 900°C was clearly enriched in $^{40}Ar^*$, yielding an apparent age at fusion of 14 my.

The five-step plateau represented 52% of the ^{39}Ar released. The precise isochron indicated an Ar_t composition of 0.003359±0.000009, only slightly enriched in ^{40}Ar compared to air Ar. M' = 0.67 was comparable to values of M' for samples 6-8 and 6-25, which produced the best isochrons from sites SC-1 and SC-23. The isochron age appears to be a valid measure of the age of eruption of the host bomb.

Thus the pyroclastic deposits atop moraine I may have been erupted ~0.13 my ago, possibly contemporaneously with the lava flows underlying moraine II and also with those at the canyon bottom farther east (site SC-1). These analyses show that moraine I was certainly pre-Wisconsin, an important conclusion that has not been satisfactorily demonstrated before.

Sites SC-20 and SC-110

Underlying moraine I is an outcrop of basalt distinct from the basalt of site SC-112. One sample of basalt (6-15) and two samples from a granodiorite xenolith (7-54 and 7-55) were analyzed. The basalt and xenolith were from different locations a few meters apart (SC-20 and SC-110, respectively).

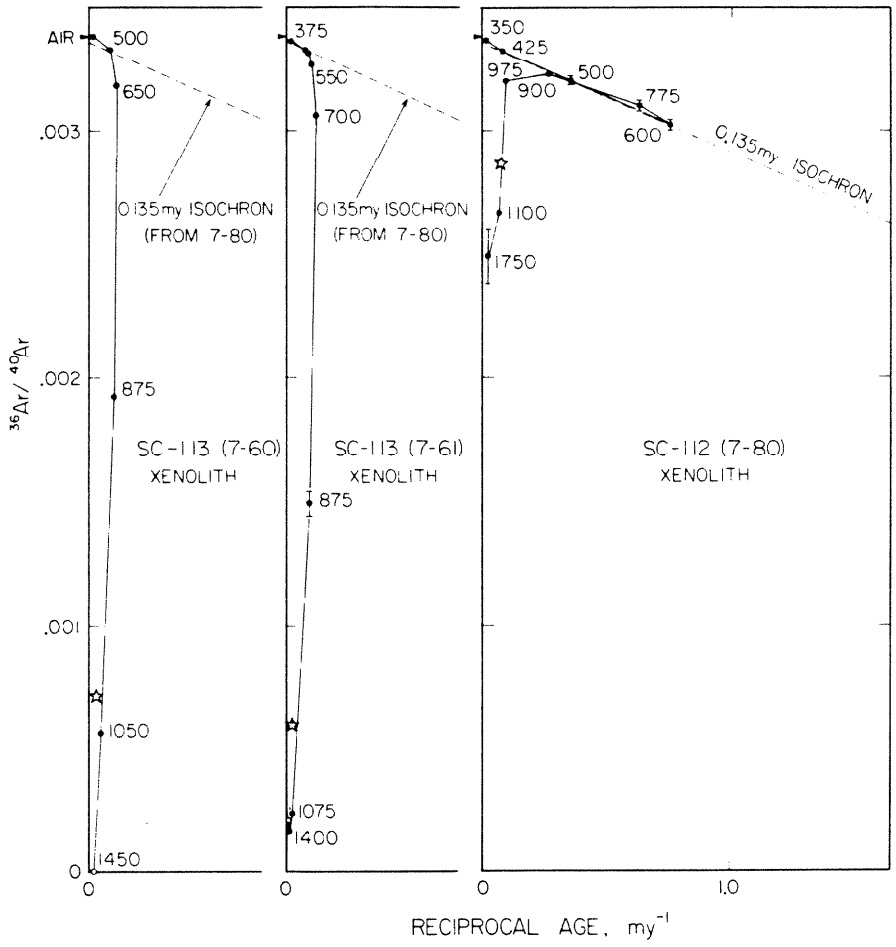

Fig. 4-24. Ar compositions for xenoliths from volcanic bombs atop moraine I show effects of different levels of degassing. Only about 62% of the Ar from the xenolith from site SC-113 was lost during heating in the the basalt, assuming an age of 65 my for the pluton which donated the xenolith. Although compositions of Ar extracted at very low temperatures <550°C could well lie along a young isochron, these data do not define one and can only be interpreted to give an upper limit to the age of degassing. In contrast, the xenolith from site SC-112 was more thoroughly degassed in the magma (97.4%) and compositions of Ar extracted in six steps at temperatures $\lesssim$ 900°C clearly defined an isochron which gave an age of 0.135 my. Ar released at higher temperatures included large amounts of inherited ^{40}Ar.

Basalt sample 6-15 was analyzed in two steps at 1075°C and 1400°C. Most of the Ar and 88% of the ^{39}Ar was released in the first step, but this Ar contained no $^{40}Ar^*$. During the post-fusion step enough $^{40}Ar^*$ was released to give a step age of 0.19±0.23 my, raising the total age to 0.03±0.07 my. ^{40}Ar from the second step was only 5% radiogenic, and thus the apparent age was highly sensitive to the composition of Ar_t.

Xenolith samples 7-54 and 7-55 gave a much more precise and older estimate of the age of eruption than basalt 6-15 did. Fig. 4-25 shows that Ar compositions for each sample appeared to define isochrons at extraction temperatures below 900°C. For sample 7-54 only three steps were made below 900°C, and for the line fit to these points $M' = 0.06$. However, for sample 7-55 six steps representing 33% of the ^{39}Ar were included in the isochron and $M' = 0.36$. This isochron indicated $(^{36}Ar/\ ^{40}Ar)_t = 0.003361\pm0.000013$ and an age of 0.468±0.052 my. The mean age of both isochrons, weighted by their values of M', was 0.463±0.041 my.

Thus the lava found under moraine I establishes an upper age limit of ~0.46 my for the pre-Wisconsin glaciation that left the moraine. This demonstrates the existence of an ancient but post-Sherwin (<0.7 my BP) glaciation in the southern Sierra Nevada.

Samples from Sites Adjacent to Sawmill Canyon

Basalt 9-20 from Taboose Creek (Tab-201)

A single sample of basalt from the fan of Taboose Creek was analyzed. Taboose Creek is the northernmost in the study area. The basalt flow, sampled at 37°0.2'N, 118°18.3'W, is part of the Big Pine volcanic field. The lava flow is probably interglacial in age (see §5.9), and was therefore probably erupted >0.025 my ago. The lava was deposited on a late

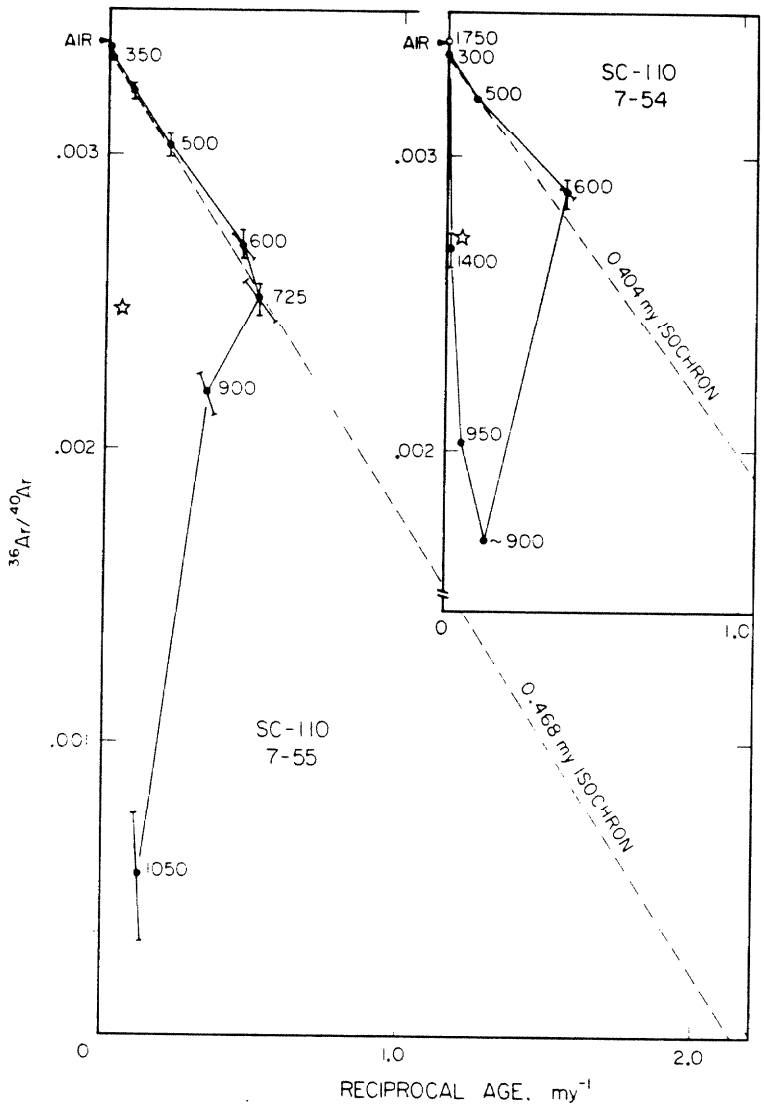

Fig. 4-25. Compositions of Ar released at temperatures ≤725°C from two samples of granodiorite xenoliths from site SC-110 defined isochrons which gave ages of ~ 0.46 my. These isochrons identified an eruption distinctly older than those 0.115-0.135 my ago which were responsible for the pyroclastics atop moraine I and the basalt flows near the bottom of the present-day Sawmill Canyon. As usual, compositions of Ar released at high temperatures reflected the presence of inherited $^{40}Ar^*$.

The Ar composition variation trajectory for sample 7-54 does not by itself define an isochron. Only three steps were made before inherited $^{40}Ar^*$ was released. However, the compositions of Ar from those three steps lay along a line similar to the isochron fit to five compositions from 7-55.

Pleistocene fan, and has been locally covered by boulders which appear to have weathered at most for only a few tens of thousands of years. Analysis was undertaken to test the possibility of obtaining a date for this event.

Ar from sample 9-20 was analyzed in one step at 1300°C. ^{40}Ar was slightly radiogenic and indicated an age of 0.005±0.079 my. Because $^{36}Ar/^{40}Ar = 0.00332$, this age was very sensitive to the actual Ar_t composition. The apparent age was therefore probably not accurate.

Basalt samples from the North Fork of Oak Creek

Two samples of basalt from the north side of the canyon of the North Fork of Oak Creek (Fig. 4-26) were analyzed in single-step experiments. Sample 7-27 (site NFOC-51) was found on the ridge top near site A (§4.2). The total age for 7-27 was 3.2±0.2 my, considerably older than the age of ~ 1.1 my for the basalt at site A. Geologically, this flow appears to be younger than the 1.1 my basalt at site A (§5.4). Hence this apparent age must be regarded with suspicion until corroborating information is obtained.

The second sample (7-107) was taken from site NFOC-25, a basalt flow on a terrace cut 72 m above the present-day stream. This sample yielded an age of 2.4±0.1 my, although geologically this sample must also be younger than the 1.1-1.2 my-old basalt flows on the present-day ridges on both sides of the stream canyon. Until better analyses are obtained, this apparent age must therefore be considered untrustworthy.

Granodiorite xenolith 7-86 from the North Fork of Oak Creek

Sample 7-86 was taken from a basalt flow only 15 m above the present-day North Fork of Oak Creek at NFOC-29 (Fig. 4-26). The basalt underlies a glacial moraine thought by Moore (1963) to be of Tahoe (early Wisconsin) age, probably <0.1 my old. Fig. 4-27 shows that Ar compositions appeared

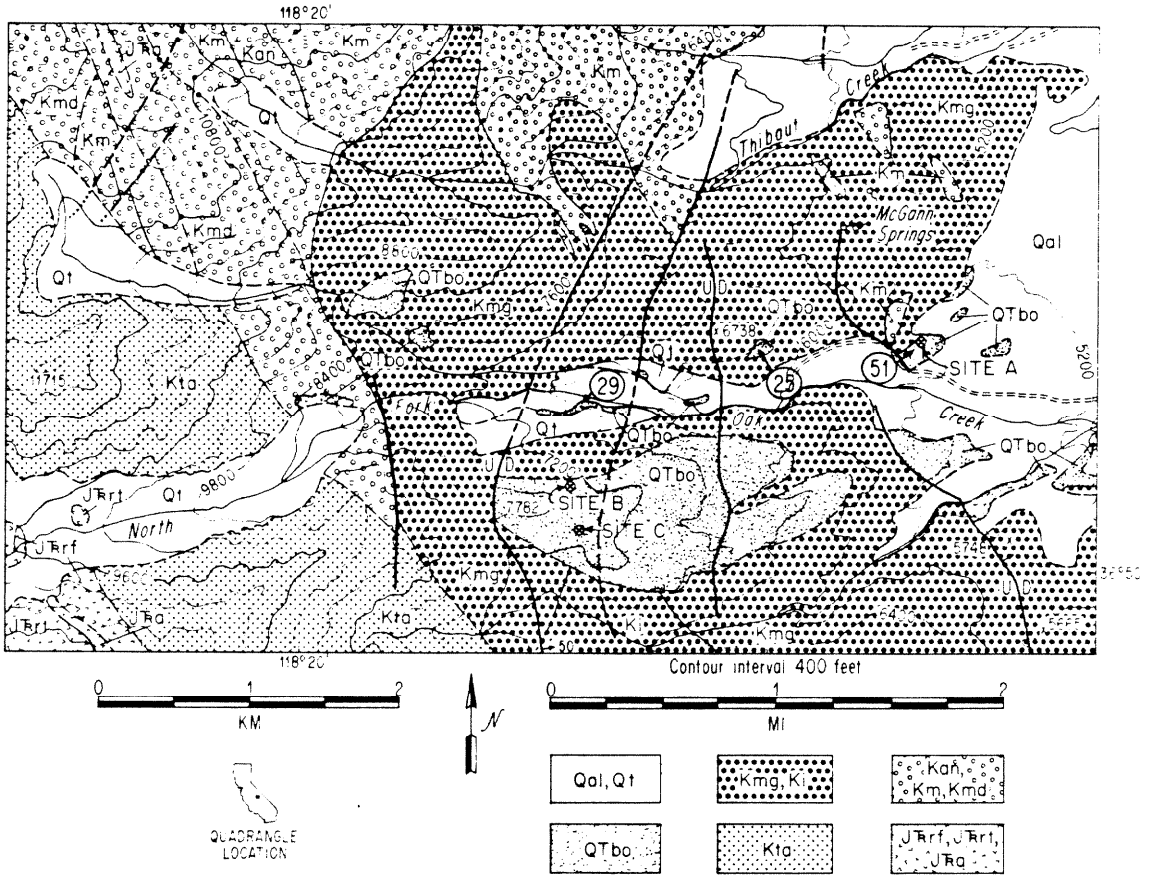

Fig. 4-26. Location of basalt and xenolith samples NFOC-29, 25, and 51 from the North Fork of Oak Creek. Sample sites A, B, and C were discussed in §4.2. Bedrock geology, basalt outcrops, and glacial geology are after Moore (1963). See Fig. 4-9 for an explanation of mapped units. Topography is from the United States Geological Survey, Mt. Pinchot Quadrangle (1953).

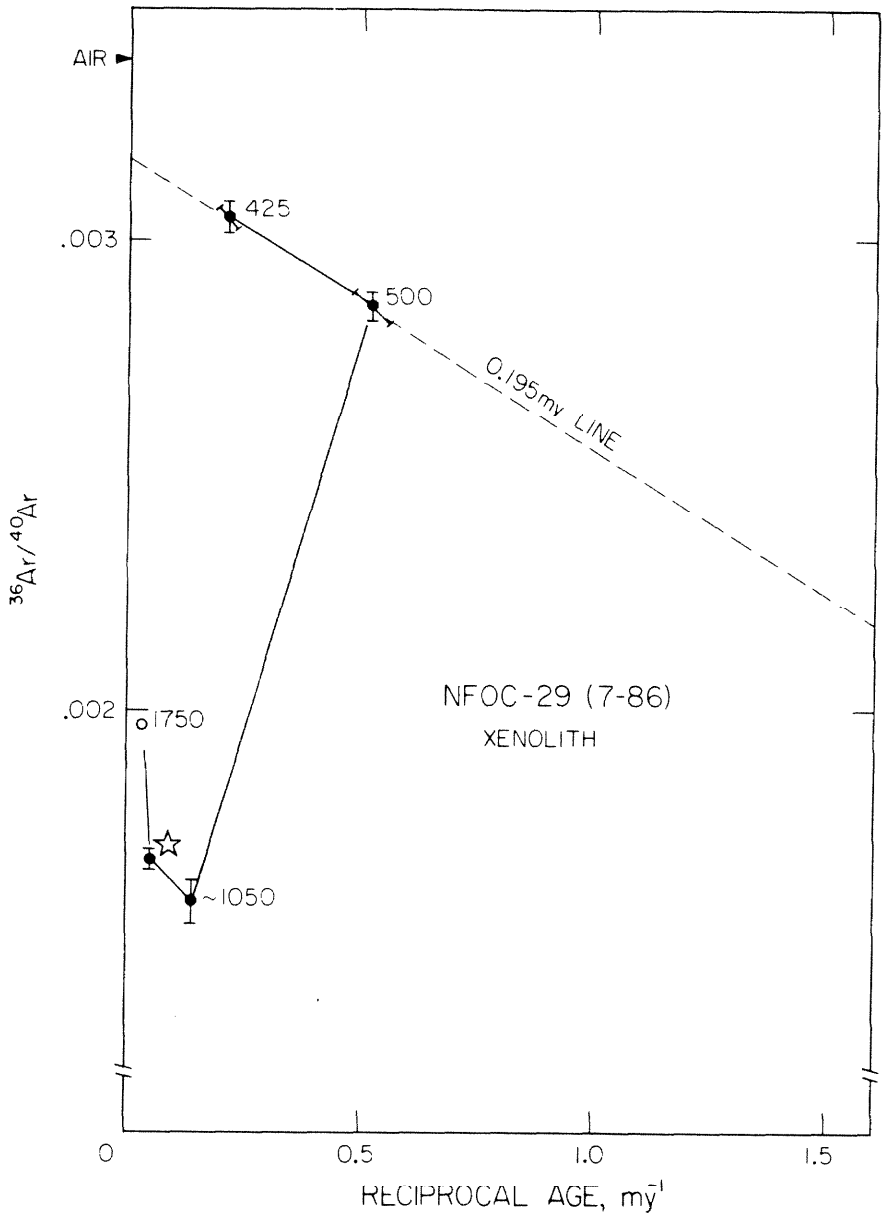

Fig. 4-27. Variation of Ar composition during stepwise extraction from a granodiorite xenolith from a basalt underlying a Tahoe (early Wisconsin) moraine at the North Fork of Oak Creek. The first step was lost. Ar from the steps at 425°C and 500°C may be free of inherited ^{40}Ar. If so, they may indicate an age for the basalt of ~ 0.2 my.

to follow the familiar trajectory, starting near AIR and progressing towards a young K-derived component on the $^{39}Ar/^{40}Ar$ axis at low temperatures. Compositions at high temperatures plotted closer to the origin because of admixture of inherited $^{40}Ar^*$. The initial (300°C) step was lost, so that Ar_t could not be well defined. During the fourth step, the RF generator used to heat the sample in an induction furnace became unstable and overheated the sample to ~ 1050°C. Consequently, Ar compositions for only two steps unaffected by inherited $^{40}Ar^*$ are known. A line passed through these steps indicates an age of 0.195±0.074 my. Only 8% of the ^{39}Ar actually measured was extracted in these steps. This apparent age does not contradict the geological information, but unless it is only a grossly upper limit to the actual age of eruption of the basalt flow, it does suggest that further effort would not improve our understanding of the glacial chronology.

Granitic Xenoliths from Other Dated Basalts in the Sierra Nevada

To further explore the application of ^{40}Ar-^{39}Ar analysis to partially degassed granitic xenoliths and the development of isotopic composition trajectories in $^{36}Ar/^{40}Ar$ vs. $^{39}Ar/^{40}Ar$ diagrams, xenoliths from Black Point and Fossil Falls were studied. At both locations basalts were extruded through Mesozoic granitic plutons (Lajoie, 1968; Duffield and Smith, 1978). Black Point (Fig. 4-28) was a sub-lacustrine volcano in glacial Mono Lake at the end of the Pleistocene Epoch (Christensen and Gilbert, 1964; Lajoie, 1968). Tufa on the flanks of the volcano has yielded a corrected ^{14}C age of ~ 13,000 y (Lajoie, 1968), which places the volcano prior to the end of the last glacial advance of the Pleistocene Epoch. Sample 9-9 was a xenolith from a block of basalt found at the top of the volcano, above the highest

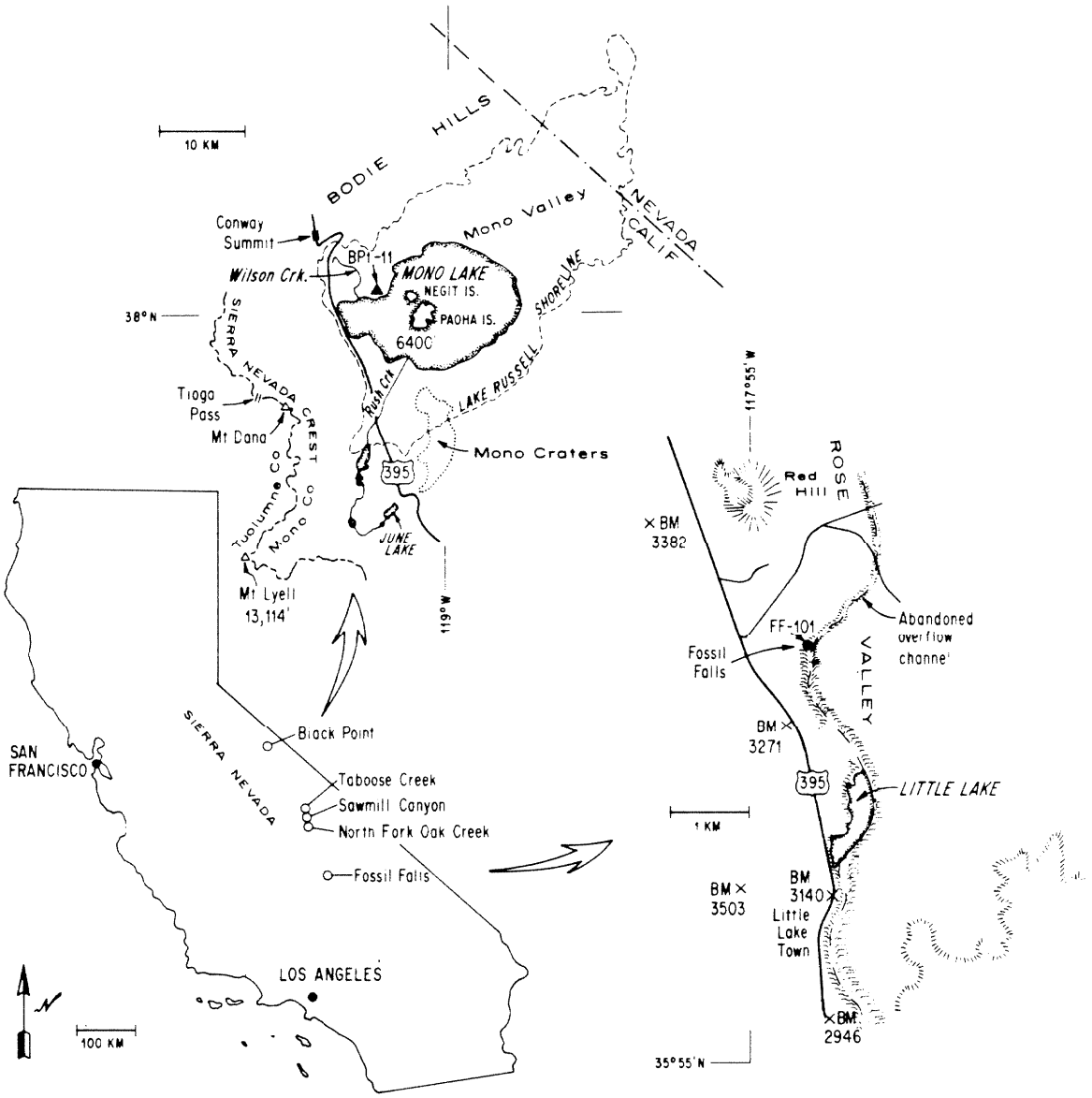

Fig. 4-28. Location of samples 9-9 and 9-32. Sample 9-9 was from site BPt-11, on the top of Black Point at Mono Lake, California (the map is after Lajoie, 1968). Sample 9-32 was from site FF-101 at the lip of Fossil Falls, a dry falls in the overflow channel draining Owens Lake during pluvial or glacial periods. Site is near town of Little Lake, California (the map is after Duffield and Smith, 1978). Sawmill Creek, Taboose Creek, and the North Fork of Oak Creek are shown for reference.

level of the lake. The total ^{40}Ar-^{39}Ar age of the xenolith was 6.2±0.3 my, only slightly greater than total ages for xenoliths from Sawmill Canyon which produced meaningful isochrons. However, most of the ^{39}Ar was released at above 1100°C, and compositions of Ar released at lower temperatures clustered near AIR (Fig. 4-29). It was not possible to define an isochron. A 0.013-my line passing through AIR is shown in Fig. 4-29 for reference.

Fossil Falls is located 2 km northwest of the town of Little Lake, California, between the Coso Range and the Sierra Nevada (Fig. 4-28). The Quaternary history of the Coso Range has been reported by Duffield and Smith (1978) and Duffield and Bacon (1980). Fossil Falls is in a dry overflow channel from Owens Lake. The channel and the falls cut into the basalt of Red Hill, which issued from a vent near the cinder cone of that name, and the underlying basalt of Upper Little Lake Ranch. The overflow channel was thought to have carried water during glacial or pluvial periods in the Pleistocene Epoch. The basalt of Red Hill must therefore be Pleistocene in age. It was thought by Duffield and Smith (1978) to be less than 0.3 my old, based on erosion rates of the basalt in the channel. Sample 9-32 was from a 1-cm aggregate of fresh-appearing microcline xenocrysts found at the lip of the dry falls in the basalt of Red Hill (Fig. 4-28). The basalt of Red Hill overlies the basalt of Upper Little Lake Ranch. Duffield and Bacon (1980) reported a K/Ar age of 0.14±0.18 (2σ) my for this basalt, and Lanphere et al. (1975) obtained a K/Ar age of 0.77±0.16 my on sanidine from a rhyolite dome younger than the basalt.

Sample 9-32 was an ideal xenolith for ^{40}Ar-^{39}Ar analysis because it was mono-mineralic and unaltered. It appeared to be highly degassed and yielded a total ^{40}Ar-^{39}Ar age of only ~ 0.6 my (Table 4-3). Figure 4-29 shows its Ar composition variation trajectory in the three-isotope diagram. The

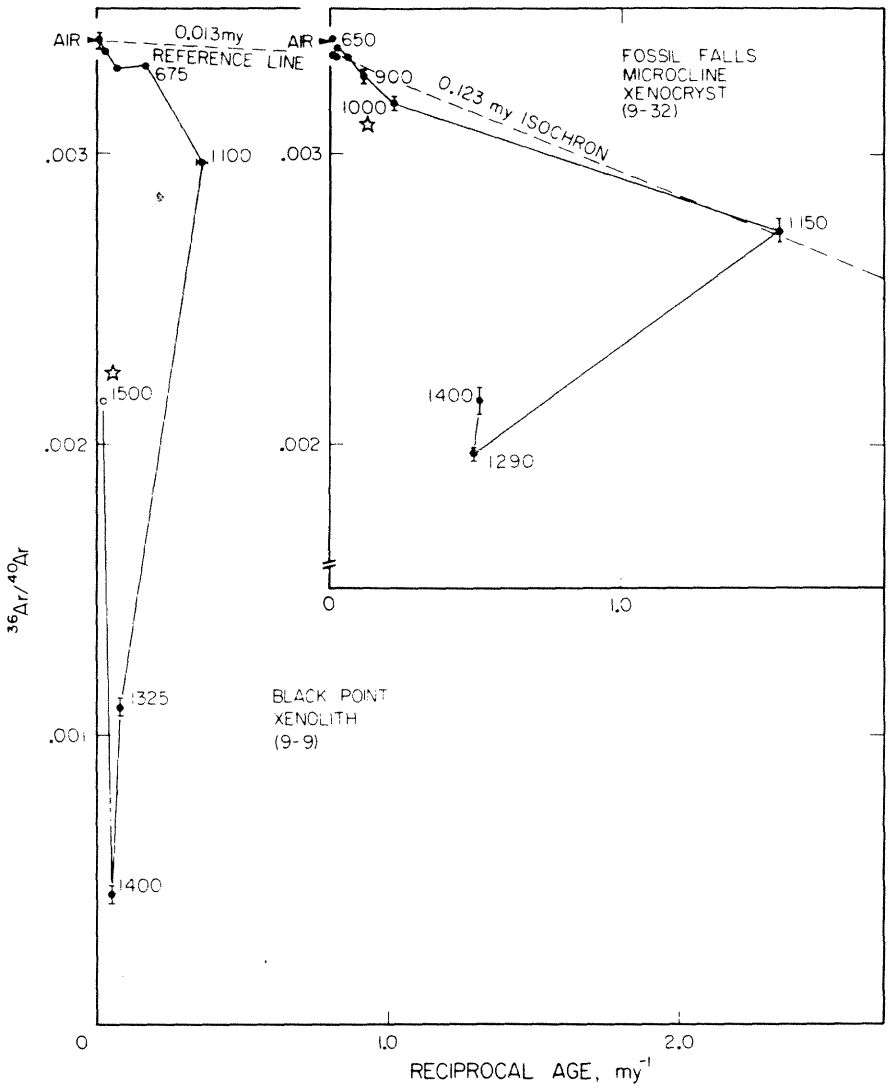

Fig. 4-29. Variation with extraction temperature of isotopic composition of Ar released from xenoliths in basalts of known young age. Ar from 9-9 (BPt-11) failed to define an isochron. Black Point was an active volcano during the last high stand of Mono Lake at the end of the Pleistocene Epoch. A ^{14}C date of 0.013 my has been determined for ostracods from silts underlying ash from Black Point (Lajoie, 1968), and for reference a 0.013-my line passing through AIR is shown in the figure.

Ar from sample 9-32 (FF-101) formed a concave, saddle-shaped trajectory below 1150°C. This may represent disturbance of the trajectory (e.g., by recoil) or mixture of different compositions of Ar_t. A line fit to compositions of Ar extracted in the eight steps at or below 1150°C gave an age of ~ 0.123 my, greatly in excess of the ~ 0.03 my estimated by Duffield and Smith (1978). Additional steps at temperatures from 1000°C to 1150°C would be required to understand the trajectory.

trajectory below 1150°C was concave, perhaps reflecting multiple Ar_t compositions. A line fit to the first eight points (taken at temperatures up to 1150°C) gave an age of 0.123±0.025 my, greatly in excess of the estimate of Duffield and Smith (1978). Perhaps the regression line is not an isochron and does not give a meaningful age. This could be because no step at T > 900°C was free of $^{40}Ar^*$, or because multiple compositions of Ar_t were present. The first explanation cannot be ruled out because no steps were taken between 1000°C and 1150°C,and details of the composition variation are therefore unknown in this part of the trajectory.

The concave trajectory for steps up to 1150°C is compatible with the mixing of two or more compositions of Ar_t. Assuming the 1150°C step to be free of inherited $^{40}Ar^*$, to achieve an isochron age less than 0.03 my, a $(^{36}Ar/^{40}Ar)_t$ less than 0.0029 would be required. For such an Ar_t there is no evidence. It is also possible that the age of the basalt of Red Hill is somewhat greater than estimated by Duffield and Smith (1978). Conclusive interpretation of the data for sample 9-32 must await further analyses of additional xenoliths from the same basalt. For the present, it is best to regard the 0.123±0.025-my isochron age as an upper limit to the age of the basalt of Red Hill.

Discussion

Stepwise ^{40}Ar-^{39}Ar analyses of seven partially-degassed xenoliths from three different sites in the basalt flows of Sawmill Canyon reveal consistent patterns of isotopic composition variation. Lines fit in $^{36}Ar/^{40}Ar$ vs. $^{39}Ar/^{40}Ar$ diagrams to compositions of Ar extracted in low-temperature steps (below ~ 950°C) consistently indicate Ar_t compositions

enriched in ^{40}Ar compared to air Ar and ages which cluster around ~0.015 my (Table 4-4). I interpret at least two of these regression lines as isochrons (6-8 and 6-25). Most of the other lines are similar in slope and intercept to the two isochrons and are probably isochrons also.

Figure 4-30 shows the distribution of the isochron ages. Data are grouped by site. The bottom ages are for basalt samples 2-2 and 2-3; the rest are for xenoliths. The top three ages are mean ages weighted according to values of M' shown with each isochron age. The shaded region shows the mean age (0.118±0.006 my) for all samples. Error bars are 95% confidence limits.

The unweighted mean age for all analyses was 0.115±0.046 my. Two samples (6-16 and 9-4) had ages more than 3σ from the mean. However, of the remaining nine, only basalt 2-2 was more than 1σ from 1.15 my. That samples 6-16 and 9-4 were so deviant probably indicates that their ages were not accurate. If anything, the other ages appeared to be more tightly grouped than expected by chance alone. The ages with the lowest M' were also the most different from the mean age. The two ages with $M' > 0.5$ were very close to 0.115 my. It appears that the best analyses also give the most repeatable ages. If the isochrons were fit to meaningless composition variation trajectories, this would not be the case.

The scatter of data points about the isochrons is indicated by the parameter S/(n-2) (Table 4-4). S is distributed according to χ^2 with n-2 degrees of freedom (Williamson, 1968). Six of the nine isochrons or regression lines for xenoliths had scatter in excess of measurement uncertainties at >99.9% confidence. This could have been caused by underestimation of measurement uncertainties but was more likely caused by the presence of inherited $^{40}Ar^*$ or multiple compositions of Ar_t (§4.2), recoil of ^{39}Ar,

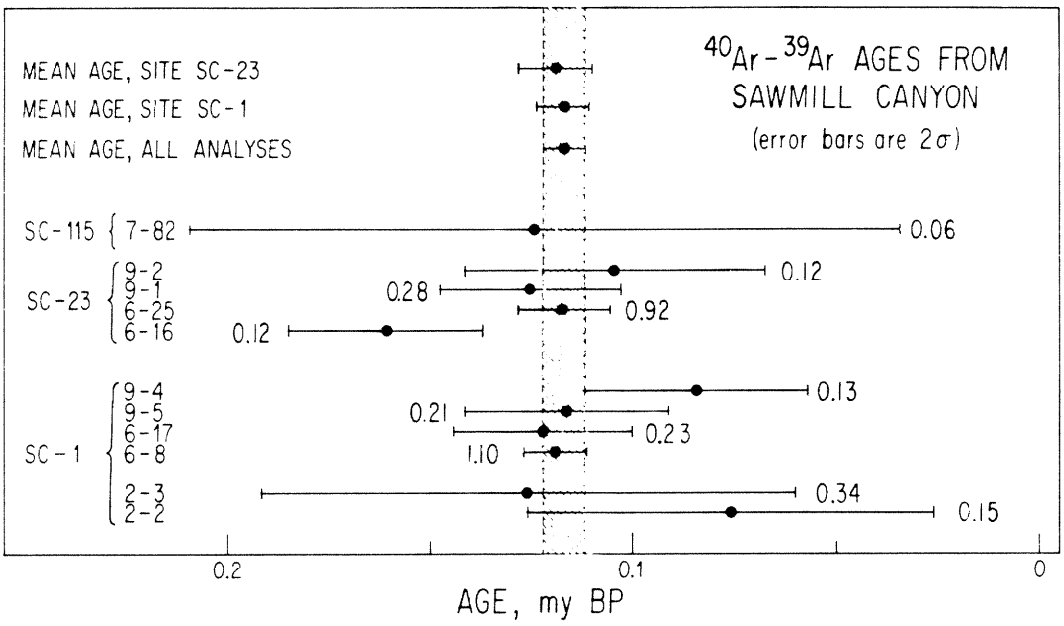

Fig. 4-30. Isochron ages for samples from sites SC-1, SC-23, and SC-115. Sites are in basalt outcrops near the level of the present-day Sawmill Creek. Samples 2-2 and 2-3 are basalt; the others are granodiorite xenoliths. Site and sample are shown to left. Ages are stacked above the time line. Top three ages are means for site SC-1, site SC-23, and all analyses. Mean ages were calculated by weighting isochron ages by $nF\sigma^{-2}$, where n is the number of steps comprising the isochron, F is the fraction of ^{39}Ar released in those steps, and σ is the standard deviation of the isochron age (see §4.2). Numbers by each isochron age are values of M'. Stipple pattern shows the 95% confidence window for the mean age of all analyses.

or other effects. Causes of inaccuracy in isochron ages found from lines fitted to ^{40}Ar–^{39}Ar data for xenoliths are discussed below.

The most obvious source of error in the isochron ages was the undetected presence of $^{40}Ar^*$ in steps thought to define a plateau. This may be seen in Fig. 4-31, which contrasts age spectra for xenolith samples 6-8 and 6-16. The eight steps in the plateau for sample 6-8 comprised at least 47% of the ^{39}Ar. The correlation coefficient for mean values of $^{36}Ar/^{40}Ar$ vs. $^{39}Ar/^{40}Ar$ for these steps was -0.99, indicating a high degree of linearity. The presence of inherited $^{40}Ar^*$ should be marked by a monotonic rise in the apparent age as increasing amounts of ^{39}Ar are extracted. The rise in apparent age was not detected until over half the ^{39}Ar was released. Therefore the isochron age is unaffected by inherited $^{40}Ar^*$. Sample 6-16 showed the same increase in apparent age at similar extraction temperatures. However, far less ^{39}Ar was released without inherited $^{40}Ar^*$ and it is not clear which step was the first affected. Thus it is possible that the regression line for sample 6-16 was fit to affected compositions. This would be consistent with the high age for the sample.

Diffusive loss from microcline of new $^{40}Ar^*$ created after eruption is probably an unimportant source of error. Khutsaidze (1962) measured <2% loss at temperatures <400°C. Reported loss of Ar from microcline (Wasserburg et al., 1956) could have taken place at elevated temperatures before exposure at the earth's surface. Microcline crystals from xenoliths have not been heated above 50°C since cooling of the host lava.

Diffusion of Ar from crystal lattices damaged during neutron irradiation would be most severe in fine-grained samples. Its presence might not be marked by a disruption of the isotopic composition trajectory if escape of proportional amounts of ^{39}Ar occurred also.

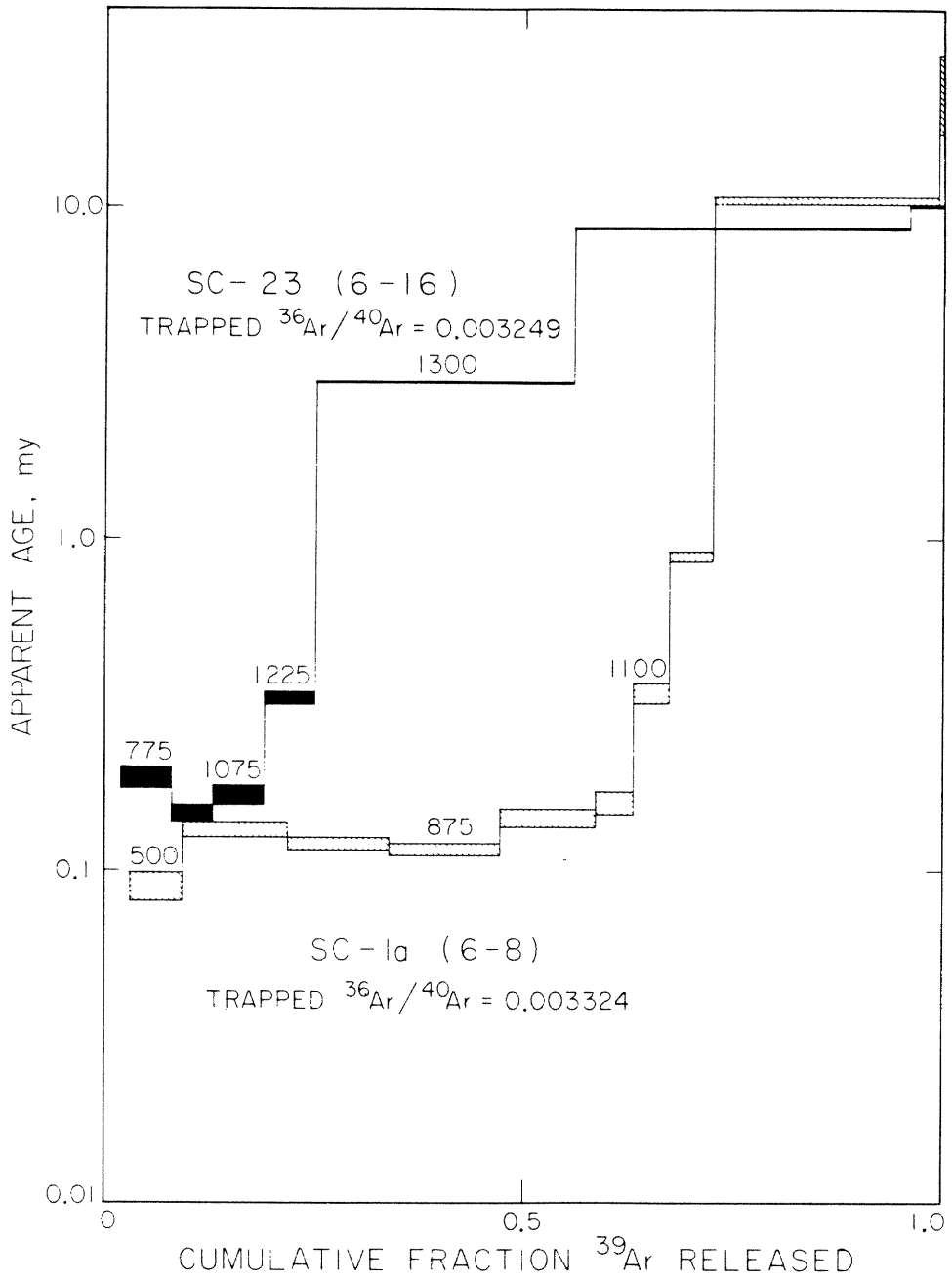

Fig. 4-31. Age spectra for granodiorite xenolith SC-1a (6-8) and orthoclase phenocryst 6-16 from a xenolith from SC-23 show that the age of degassing may have been the same for each. Half or more of the ^{39}Ar from 6-8 was released in low-temperature steps defining a plateau at the age of degassing or eruption of the host basalt. A much smaller fraction was released from 6-16 in comparable low age steps. Error bars are 1σ. Ages are calculated assuming a composition for Ar_t given by the ordinate intercept of a line fit to Ar compositions thought to be free of inherited $^{40}Ar^*$ (Table 4-4).

Recoil redistribution of ^{39}Ar is a more serious problem (Huneke and Smith, 1976; Turner and Cadogan, 1974). Recoil of ^{39}Ar from small, easily degassed grains could masquerade as excess ^{40}Ar in the trapped component. One result might be an excessively low isochron age. Huneke and Villa (1981) have reported loss of up to 60% from five samples of very fine-grained inclusions in Allende. There is no evidence of recoil effects in the composition trajectories for xenolith samples. Isochron ages are within 2σ of K/Ar determinations for the host basalts (Dalrymple, 1964b). However, total ages of basalt samples 2-2 and 2-3 are decidedly older than the K/Ar ages (0.265±0.08 my vs 0.07±0.09 my). There is no evidence in the trajectories that this is caused by inherited $^{40}Ar^{*}$, and I have attributed the higher age of samples 2-2 and 2-3 to variable compositions of Ar_t enriched in ^{40}Ar. However, it could also be explained by ~ 75% loss of ^{39}Ar. While this large loss appears possible in light of the findings of Huneke and Villa (1981), it seems unlikely that the isochron ages would coincide with the isochron ages of the xenoliths and with the K/Ar ages of the basalts were this the case. Loss of ^{39}Ar should also be reflected in low values of K, but such were not found (Table 4-3).

Tetley et al. (1980) have shown most $^{40}K(n,p)^{40}Ar$ is due to thermal rather than fast neutrons. They point out that the ratio of thermal neutrons to fast neutrons varies spatially and temporally for a given reactor. The thermal neutron flux of the Herald reactor (Turner, 1971b) varies by a factor <2.5 with time; the flux of the HIFAR reactor varies by a factor of <0.5 with position of the monitor in the reactor. Thus the pro forma correction we applied for $^{40}Ar_K$ may be in error by much more than the indicated uncertainty.

The effect of uncorrected $^{40}Ar_K$ is to increase the apparent age by

an amount proportional to ^{39}Ar. The trajectory of compositions in the three-isotope diagram is steepened, corresponding to an apparent increase in the isochron age, but the linearity of compositions is undisturbed. We found that the maximum $^{40}Ar_K/^{40}Ar^*$ was about 2% for basalt samples 2-2 and 2-3. The maximum value was 1% for xenolith 6-8. For the young ages of interest in this study, the error in age resulting from $^{40}Ar_K$ is linear with this factor. Because the $(^{40}Ar/^{39}Ar)_K$ correction factor was probably correct within a factor of 3, maximum bias to the apparent age of an individual step was <6% (basalt) or <3% (6-8). This source of inaccuracy was subordinate to measurement uncertainties.

Non-atmospheric compositions of Ar_t appear to be indicated by many regression-line intercepts. Most convincing is sample 6-16, part of a single orthoclase phenocryst. In thin section this sample was seen to consist of interlocking grains of orthoclase and albite, with rounded and embayed boundaries. Characteristic grain diameters were 100μm. Because of the large grain size, recoil effects should have been minimal, and because of the small grain surface-to-volume ratio, adhered Ar_t of atmospheric origin should also have been minimal. Thus the radiogenic Ar_t may well be real. If it is, then mixture of a radiogenic and an atmospheric Ar_t, rather than recoil or other effects, may explain the concave low-temperature composition trajectories observed for sample 9-1 (Fig. 4-22) and perhaps for sample 7-82 (Fig. 4-23). Such a mixture of trapped components would have the effect of increasing the apparent isochron age. Protection against effects of mixed components seems to lie in analyzing large samples using many extraction steps so that real trends in composition can be identified.

Comparison of K/Ar and ^{40}Ar-^{39}Ar analyses of basalts

Compositions of the total Ar from each basalt sample in this study are plotted in Fig. 4-32, along with compositions of basalts from Sawmill Canyon measured by Dalrymple et al. (1982) using conventional K/Ar analysis. These latter samples were taken from the site labeled "KA970" and "KA970A" in Fig. 4-19. In Fig. 4-32 the $^{39}Ar/^{40}Ar$ compositions for each sample have been scaled to compensate for different neutron fluences. The abscissa is in units of reciprocal age. Conventional K/Ar data were represented in this diagram by scaling the measured $K/^{40}Ar$ ratio in a similar fashion.

All samples had $^{36}Ar/^{40}Ar > 0.0031$, and hence all total ages were very sensitive to the actual value of Ar_t. Because age spectra for sample 2-3 and other basalts from the same volcanic field (§4.2) indicate an Ar_t enriched in ^{40}Ar compared to air Ar, caution must be exercised in interpreting total ages.

Of particular interest is the observation that the samples analyzed by Dalrymple using the K/Ar method all seem to have less radiogenic Ar than basalt samples 2-2 and 2-3, which were sampled from what is probably the same flow in Sawmill Canyon. The total ages of 2-2 and 2-3 averaged $\sim$ 0.27 my, considerably older than their isochron ages of $\sim$ 0.1 my.

The disparity between the total ^{40}Ar-^{39}Ar ages and isochron ages would be eliminated if $(^{36}Ar/^{40}Ar)_t = 0.00332$, but if that were true for the entire flow the samples of Dalrymple would all have negative apparent ages. This dilemma could be resolved if $(^{36}Ar/^{40}Ar)_t$ were variable within a flow, or the samples were from different (but roughly coeval flows), or if the neutron irradiation resulted in loss of ^{39}Ar through recoil.

Recoil loss cannot be ruled out, but it seems unlikely that sufficient ^{39}Ar could have been lost to increase the apparent age more than

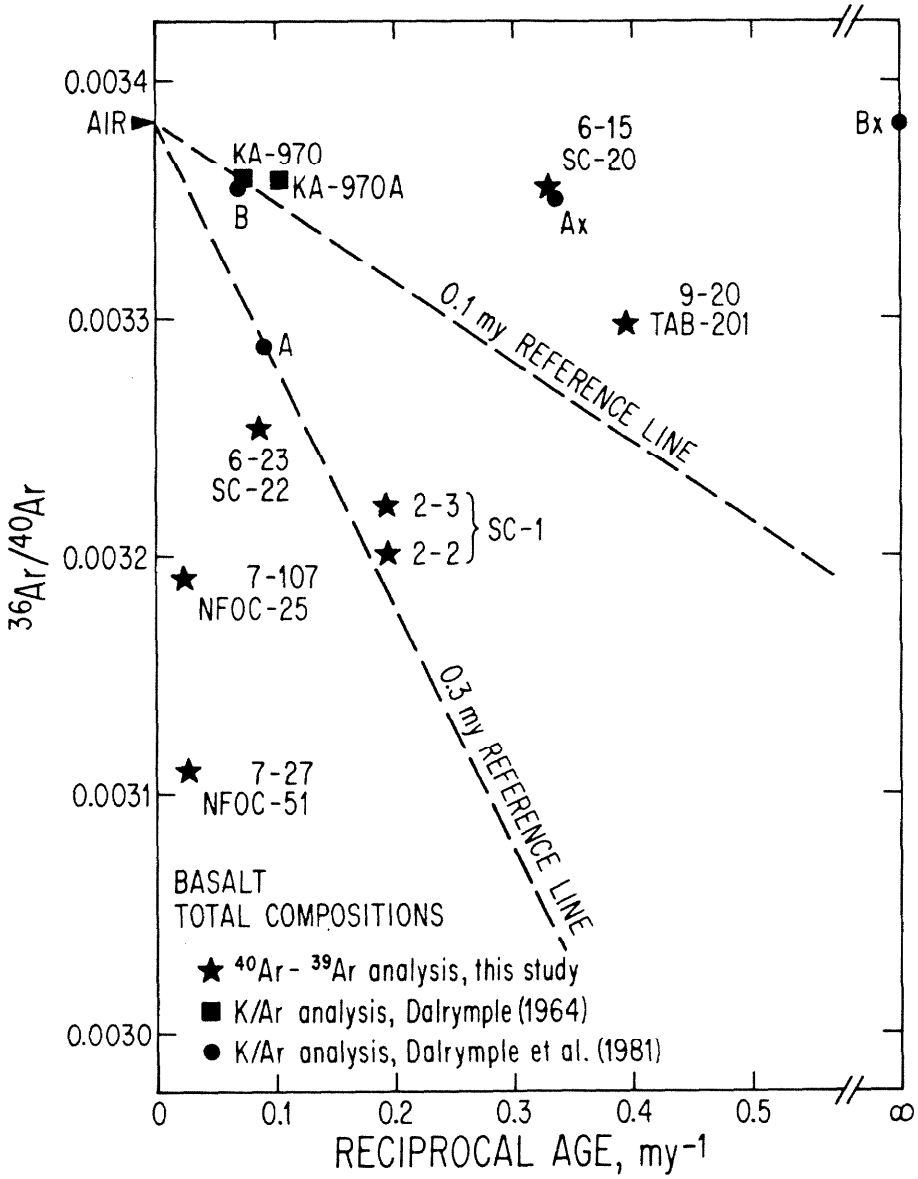

Fig. 4-32. Total composition of Ar from basalt samples. For comparison, K/Ar data from Dalrymple et al. (1982) has been included. For these samples, the plotted location was found from the intersection of a horizontal line passing through the measured $^{36}Ar/^{40}Ar$ and a diagonal line passing through AIR and the reciprocal K/Ar age on the abscissa. All samples were dominated by Ar_t.

two-fold. This is because the total ^{39}Ar remaining with the samples indicated an abundance of K (~ 1.3% by weight) very close to the value of 1.37% obtained by Dalrymple et al. (1982) by flame photometry of unirradiated samples. K of 3% or more would be greater than expected for a basalt. Consequently it appears that $(^{36}Ar/^{40}Ar)_t$ is variable, at least among flows and perhaps within flows.

If $(^{36}Ar/^{40}Ar)_t$ is variable, then it is not possible to obtain accurate ages by K/Ar analysis of whole rock basalt samples, and ^{40}Ar-^{39}Ar isochrons must be established to deduce the ages of eruption. For basalts as young as 0.1 my, the results presented in this discussion show that ^{40}Ar-^{39}Ar analysis of xenoliths leads to more precise ages than analysis of the lava itself.

Conclusions

Ten partially degassed xenoliths and two host basalt samples from Sawmill Canyon have been analyzed using stepwise ^{40}Ar-^{39}Ar dating techniques. Lines fit in $^{36}Ar/^{40}Ar$ vs. $^{39}Ar/^{40}Ar$ diagrams to compositions thought to be free of inherited $^{40}Ar^*$ gave ages in agreement among themselves and with previous K/Ar dates of basalt from Sawmill Canyon (Dalrymple, 1964b). In some instances more than half the ^{39}Ar was released in steps used to define the regression line. At least some of these lines were isochrons identifying the age of eruption of the host basalt. The best estimate of the age of eruption was 0.118±0.07 my. Uncertainties of isochron ages were variable but were as little as 11% of the combined uncertainties of the K/Ar dates of the basalts. The high precision of isochron ages from partially degassed granitic xenoliths is comparable to precisions of K/Ar ages from sanidines of equivalent age. This is alone

justification for dating basic lava flows by this method when possible.

Isochrons indicated Ar_t may be enriched in ^{40}Ar compared to air Ar. ^{40}Ar-^{39}Ar analysis is more accurate than conventional K/Ar analysis because such effects can be recognized and corrected. However, neutron irradiation causes other effects which complicate analysis and interpretation. Chief among these may be loss of ^{39}Ar due to recoil during irradiation. Because of the simple linear character of some of the isotope composition trajectories for Ar extracted below ~ 950°C, there appears to be no evidence for recoil or other complications in at least some of the analyses. If this is true, the best isochron ages may well represent the actual age of eruption of the host basalt. That the eruption is three orders of magnitude younger than the age of original crystallization of the xenoliths emphasizes the exceptional ability of stepwise heating to separately release Ar from different reservoirs or sites.

Ages of Eruptions for Sawmill Canyon

Analyses of granitic xenoliths from lavas at different sites within Sawmill Canyon clearly show that there were at least two different episodes of volcanic activity in Sawmill Canyon. Fig. 4-33 shows age spectra for the three most critical analyses. The lava flow at the bottom of the present-day canyon (SC-1) was erupted 0.118±0.007 my ago. It underlies moraine II (Fig. 4-19). Volcanic bombs atop moraine I (SC-112) appear to be clearly coeval, although the isochron defined by the first five steps in the analysis of sample 7-80 gave an age of 0.131±0.010 my, which was a little older. Xenoliths from site SC-110, the basalt flow underlying moraine I, gave an eruption age of 0.46±0.04 my, distinctly

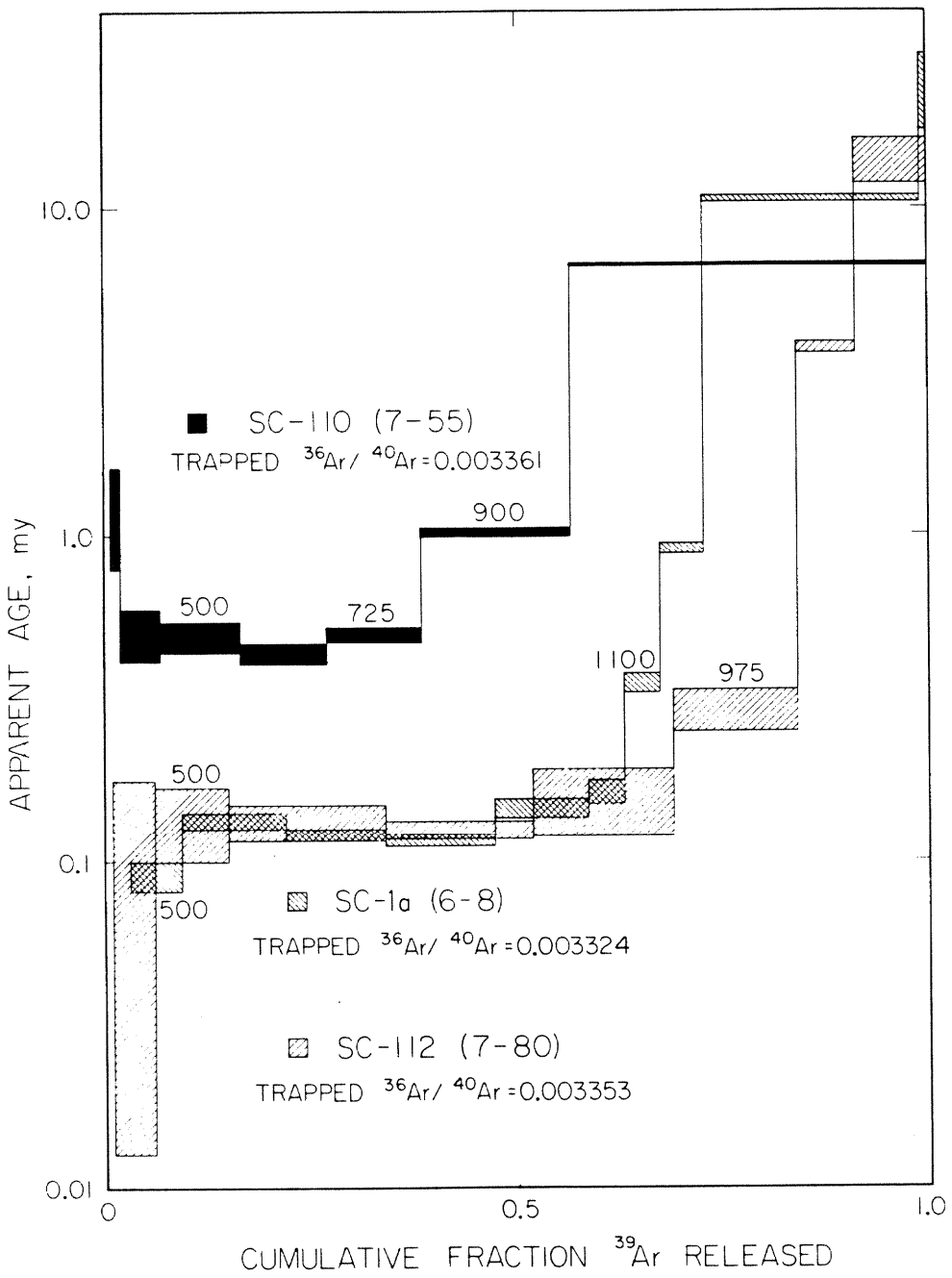

Fig. 4-33. Age spectra for granodiorite xenoliths from the bottom of Sawmill Canyon (SC-1a), a basalt bomb atop moraine I, and a basalt flow from beneath moraine I show two distinct episodes of volcanism at 0.115 to 0.135 my ago and ~ 0.45 my ago. Moraine I was deposited between those events. Moraine II was deposited after the final episode > 0.115 my ago . The volcanic bombs and basalt flows were clearly coeval. Error bars are 1σ. Apparent ages were calculated assuming for Ar_t the composition specified by the ordinate intercept of the line fit to compositions thought to be free of inherited $^{40}Ar^*$.

older than the other flows. Fig. 4-33 shows this difference clearly.

The precise age of 0.118±0.007 my provides an upper limit to the age of glacial advance II of Dalrymple (1964b) in Sawmill Canyon. Dalrymple considered this advance to be of early Wisconsin age. The age of eruption is consistent with that interpretation. The other analyses provide age limits that bracket the glacial stage during which moraine I was deposited. These results show this stage to be 0.13 - 0.46 my old, pre-Wisconsin but post-Sherwin.

One xenolith (sample 7-83) from the recent flow (site SC-116) gave an anomalously high eruption age of ~ 1.1 my. This is geologically improbable and must represent either reworking of older lava from the vent area or a blunder in sample book-keeping.

4.4 SUMMARY

Technique

From theoretical considerations it appears that xenoliths containing Ar in sites of sufficiently different diffusion dimensions or activation energies should yield plateaus at the age of eruption in ^{40}Ar-^{39}Ar age spectra. Diffusion dimensions must differ by a factor of ten or more, but activation energies need not differ by more than ~12 kcal/mole (in the range of activation energies published for K-feldspar) to achieve this as long as degassing at the time of eruption exceeded 90%. Apparently one or both of these conditions are met in real xenoliths, because plateaus in age spectra extending over 60% of the ^{39}Ar are found in at least some xenoliths. These plateaus are formed by Ar released at low temperatures. They identify an age which is the same as the age of

eruption found by analysis of the host lava, and at least for early Pleistocene lavas it seems clear that these plateaus can be used to define the age of eruption. Similar plateaus are found in age spectra of xenoliths from late Pleistocene lavas, but analysis of the lavas themselves does not yield precise ages, so concordance cannot be determined. These plateaus probably define the age of eruption of the young lavas. The ages are much more precise than K/Ar ages of basic lavas, and are about as precise as K/Ar ages of sanidines. Furthermore, the ages are at least potentially more accurate than K/Ar ages because, in principle, the composition of Ar_t can be identified in ^{40}Ar-^{39}Ar analysis. Most important, this study shows that coarse-grained potassic inclusions can be used in the dating of K-deficient lavas and fine-grained lavas which may have lost Ar since cooling. These lavas are difficult to date by conventional methods. Thus this approach to K/Ar dating extends its applicability in a significant way.

Geology

Lavas capping ridges 125 m above the modern North Fork of Oak Creek were shown to be about 1.1 - 1.2 my old. Lavas on the floor of the modern canyon, cut through the ridge-top basalts, were much younger, possibly ~0.2 my old.

Two volcanic episodes were dated at Sawmill Canyon. The older lava, ~ 0.46 my old, underlay a glacial moraine (moraine I). Pyroclastic deposits from the younger eruptions, 0.12 - 0.13 my BP, were found atop the same moraine. Lava flows from the younger eruptions were found at the canyon bottom, underneath a second moraine (moraine II). Thus two glaciations were separated by the younger of the eruptions.

Moraine II must be younger than 0.12 my, and moraine I must be from 0.13 - 0.46 my old. Although these age limits are not close together, they establish two significant conclusions: (1) moraine I is pre-Wisconsin, and (2) moraine I is post-Sherwin.

References Cited

Baadsgaard, H., Lipson, J., and Folinsbee, R.E., 1961, The leakage of radiogenic argon from sanidine: Geochim. et Cosmochim. Acta 25, 147-157.

Bailey, R.A., Dalrymple, G.B., and Lanphere, M.A., 1976, Volcanism, structure, and geochronology of Long Valley Caldera, Mono County, California: Jour. Geophys. Research 81, 725-744.

Bateman, P.C., 1965, Geology and Tungsten Mineralization of the Bishop District, California, with a Section on Gravity Study of Owens Valley by L.C. Pakiser and M.F. Kane and a Section on Seismic Profile by L.C. Pakiser: U.S. Geol. Survey Prof. Paper 470, 208 p.

Berger, G.W., 1975, ^{40}Ar-^{39}Ar step heating of thermally overprinted biotites, hornblendes, and potassium feldspars from Eldora, Colorado: Earth Planet Sci. Lett. 26, 387-408.

Bogard, D.D. and Hirsch, W.C., 1980, ^{40}Ar-^{39}Ar dating, Ar diffusion properties and cooling rate determinations of severely shocked chondrites: Geochim. et Cosmochim. Acta 44, 1667-1682.

Brereton, N.R., 1970, Corrections for interfering isotopes in the $^{40}Ar/^{39}Ar$ dating method: Earth Planet Sci. Lett. 8, 427-433.

Brereton, N.R., 1972, A reappraisal of the $^{40}Ar/^{39}Ar$ stepwise degassing technique: Geophys. Jour. Royal Astr. Soc. 27, 449-478.

Brooks, C., Hart, S.R., and Wendt, I., 1972, Realistic use of two-error regression applied to rubidium-strontium data: Rev. Geophys. Space Phys. 10, 551-577.

Burke, R.M., and Birkeland, P.W., 1979, Reevaluation of multiparameter relative dating techniques and their application to the glacial sequence along the eastern escarpment of the Sierra Nevada, California: Quaternary Research 11, 21-51.

Carslaw, H.S., and Jaeger, J.C., 1959, Conduction of Heat in Solids: Clarendon Press, 510 p.

Christensen, M.N., and Gilbert, C.M., 1964, Basaltic cone suggests constructional origin of some guyots: Science 143, 240-247.

Crank, J., 1956, The Mathematics of Diffusion: Clarendon Press, 347 p.

Curry, R.R., 1968, Quaternary Climatic and Glacial History of the Sierra Nevada, California: Ph.D. dissertation, Univ. of Calif. Berkeley; University Microfilms, Inc., No. 68-13896, Ann Arbor, MI., 204 p.

Dalrymple, G.B., 1964a, Argon retention in a granitic xenolith from a Pleistocene basalt, Sierra Nevada, California: Nature 201, 282.

Dalrymple, G.B., 1964b, Potassium-argon dates of three Pleistocene interglacial basalt flows from the Sierra Nevada, California: Geol. Soc. America Bull. 75, 753-758.

Dalrymple, G.B. and Lanphere, M.A., 1971, $^{40}Ar/^{39}Ar$ technique of K-Ar dating: a comparison with the conventional technique: Earth Planet. Sci. Lett. 12, 300-308.

Dalrymple, G.B., Alexander, E.C. Jr., Lanphere, M.A., and Kraker, G.P., 1981, Irradiation of Samples for $^{40}Ar/^{39}Ar$ Dating Using the Geological Survey TRIGA Reactor: U.S. Geol. Survey Prof. Paper 1176, 55 p.

Dalrymple, G.B., Burke, R.M., and Birkeland, P.W., 1982, Note concerning K-Ar dating of a basalt flow from the Tahoe-Tioga interglaciation, Sawmill Canyon, southeastern Sierra Nevada, California: Quaternary Research, in press.

Darrow, A.C., 1972, Origin of the Basalts of the Big Pine Volcanic Field, California: unpublished Univ. of Calif., Santa Barbara, MS thesis, 61 p.

Duffield, W.A., and Bacon, C.R., 1980, Late Cenozoic volcanism, geochronology, and structure of the Coso Range, Inyo County, California: Jour. Geophys. Research 85, 2381-2404.

Duffield, W.A., and Smith, G.I., 1978, Pleistocene river erosion and intracanyon lava flows near Little Lake, Inyo County, California: Calif. Geology 31, 81-89.

Evernden, J.F., Curtis, G.H., Kistler, R.W., and Obradovich, J., 1960, Argon diffusion in glauconite, microcline, sanidine, leucite, and phlogopite: Am. Jour. Sci. 258B, 583-604.

Fechtig, F., Gentner, W., and Zahringer, J., 1960, Argonbestimmungen an Kaliummineralien - VII. Diffusionsverluste von Argon in Mineralien und ihre Auswirkung auf die Kalium-Argon-Alterbestimmung: Geochim. et Cosmochim. Acta 19, 70-79.

Fechtig, H., Gentner, W., and Kalbitzer, S., 1961, Argonbestimmungen an Kaliummineralien - IX: Messungen zu den verschiedenen Arten der Argondiffusion: Geochim. et Cosmochim. Acta 25, 297-311.

Foland, K.A., 1974, Ar^{40} diffusion in homogeneous orthoclase and an interpretation of Ar diffusion in K-feldspars: Geochim. et Cosmochim. Acta 38, 151-166.

Frechen, J. and Lippolt, H.J., 1965, Kalium-Argon Daten zum Alter des Laacher Vulkanismus der Rheinterrassen und der Eiszeiten: Eiszeitalter u. Gegenwart 16, 5-30.

Gerling, E.K. and Morozova, I.M., 1962, Determination of the activation energy for the release of argon and helium from minerals: Geochemistry 12, 1255-1268.

Harrison, T.M. and McDougall, I., 1980, Investigations of an intrusive contact, northwest Nelson, New Zealand - II. Diffusion of radiogenic and excess ^{40}Ar in hornblende revealed by $^{40}Ar/^{39}Ar$ age spectrum analysis: Geochim. et Cosmochim. Acta 44, 2005-2020.

Hart, S.R., 1964, The petrology and isotopic-mineral age relations of a contact zone in the Front Range, Colorado: Jour. Geol. 72, 493-525.

Huneke, J.C., 1976, Diffusion artifacts in dating by stepwise thermal release of rare gases: Earth Planet. Sci. Lett. 28, 407-417.

Huneke, J.C. and Smith, S.P., 1976, The realities of recoil: ^{39}Ar recoil out of small grains and anomalous age patterns in ^{39}Ar-^{40}Ar dating: Proc. 7th Lunar Sci. Conf., Geochim. et Cosmochim. Acta Supp. 7, 2, 1987-2008.

Huneke, J.C. and Villa, I.M., 1981, ^{39}Ar loss during neutron irradiation and the aging of Allende inclusions (abstract): submitted to 44th Meteoritical Soc. Mtg., Bern, Switzerland, August, 1981.

Jäger, E., Niggli, E.E., and Baethge, H., 1963, Two standard minerals, biotite and muscovite, for Rb-Sr and K-Ar age determinations, sample Bern 4B and Bern 4M from a gneiss from Brione, Valle Verzasca (Switzerland): Schweiz. Mineral. Petrog. Mitt. 43, 465-470.

Jessberger, E.K., Huneke, J.C., Podosek, F.A., and Wasserburg, G.J., 1974, High resolution argon analysis of neutron-irradiated Apollo 16 rocks and separated minerals: Proc. 5th Lunar Sci. Conf., Geochim. et Cosmochim. Acta Supp. 5, 2, 1419-1449.

Kaneoka, I., 1980, Rare gas isotopes and mass fractionation: an indication of gas transport into or from a magma: Earth Planet. Sci. Lett. 48, 284-292.

Kermack, K.A., and Haldane, J.B.S., 1950, Organic correlation and allometry: Biometrika 37, 30-41.

Khutsaidze, A.L., 1962, Experimental investigation of diffusion of radiogenic argon in feldspars and micas: Geochemistry II, 1063-1068.

Knopf, A., 1918, A Geologic Reconnaissance of the Inyo Range and the Eastern Slope of the Southeastern Sierra Nevada, California, with a Section on the Stratigraphy of the Inyo Range by Edwin Kirk: U.S. Geol. Survey Prof. Paper 110, 130 p.

Krummenacher, D., 1970, Isotopic composition of argon in modern surface volcanic rocks: Earth Planet. Sci. Lett. 8, 109-117.

Lajoie, K.R., 1968, Late Quaternary Stratigraphy and Geologic History of Mono Basin, Eastern California: Ph.D. Thesis, Univ. of Calif., Berkeley; University Microfilms, Inc. No. 69-14936, Ann Arbor, MI., 271 p.

Lanphere, M.A. and Dalrymple, G.B., 1971, A test of the $^{40}Ar/^{39}Ar$ age spectrum technique on some terrestrial materials: Earth Planet. Sci. Lett. 12, 359-372.

Lanphere, M.A., Dalrymple, G.B., and Smith, R.L., 1975, K-Ar ages of Pleistocene rhyolitic volcanism in the Coso Mountains, California: Geology 3, 339-341.

Lanphere, M.A., and Dalrymple, G.B., 1976, Identification of excess ^{40}Ar by the $^{40}Ar/^{39}Ar$ age spectrum technique: Earth Planet. Sci. Lett. 32, 141-148.

Lanphere, M.A., and Dalrymple, G.B., 1978, The use of ^{40}Ar-^{39}Ar data in evaluation of disturbed K-Ar systems: in Zartman, R.E., ed., Short Papers of the Fourth International Conference, Geochronology, Cosmochronology, and Isotope Geology: U.S. Geol. Survey Open-File Report 78-701.

Mankinen, E.A., and Dalrymple, G.B., 1979, Revised geomagnetic polarity time scale for the interval 0-5 my B.P.: Jour. Geophys. Research 84, 615-626.

Merrihue, C.M. and Turner, G., 1966, Potassium-argon dating by activation with fast neutrons: Jour. Geophys. Research 71, 2852-2857.

Moore, J.G., 1963, Geology of the Mount Pinchot quadrangle, southern Sierra Nevada, California: U.S. Geol. Survey Bull. 1130, 152 p.

Musset, A.E. and Dalrymple, G.B., 1968, An investigation of the source of air Ar contamination in K-Ar dating: Earth Planet. Sci. Lett. 4, 422-426.

Putnam, W.C., 1950, Moraine and shoreline relationships at Mono Lake, California: Geol. Soc. America Bull. 61, 115-122.

Radicati di Brozolo, F., Huneke, J.C., Papanastassiou, D.A., and Wasserburg, G.J., 1981, ^{40}Ar-^{39}Ar and Rb-Sr age determinations on Quaternary volcanic rocks: Earth Planet. Sci. Lett. 73, 445-456.

Reichenberg, D., 1953, Properties of ion-exchange resins in relation to their structure - III. Kinetics of exchange: Jour. Am. Chem. Soc. 75, 589-597.

Richter, D.H. and Moore, J.G., 1966, The Petrology of the Kilauea Iki Lava Lake, Hawaii: U.S. Geol. Survey Prof. Paper 537-B, 26 p.

Steiger, R.H. and Jäger, E., 1977, Subcommission on Geochronology: convention on the use of decay constants in geo- and cosmochronology: Earth Planet. Sci. Lett. 36, 359-362.

Tetley, N., McDougall, I., and Heydigger, H.R., 1980, Thermal neutron interference in the $^{40}Ar/^{39}Ar$ dating technique: Jour. Geophys. Research 85, 7201-7205.

Turner, G., 1968, The distribution of potassium and argon in chondrites: in Ahrens, L.H. (ed.), Origin and Distribution of the Elements: Pergamon Press, New York, pp. 387 - 398.

Turner, G., 1969, Thermal histories of meteorites by the ^{39}Ar-^{40}Ar method: in Millman, P. (ed), Meteorite Research: Reidel Publishing Co., Holland, pp. 407-417.

Turner, G., 1970, Argon 40/argon 39 dating of lunar rock samples: Proc. of the Apollo 11 Lunar Sci. Conf., Geochim. et Cosmochim. Acta. Supp. 1, 2, 1665-1684.

Turner, G., 1971a, ^{40}Ar-^{39}Ar ages from the lunar maria: Earth Planet. Sci. Lett. 11, 169-191.

Turner, G., 1971b, Argon 40-argon 39 dating: the optimization of irradiation parameters: Earth Planet. Sci. Lett. 10, 227-234.

Turner, G. and Cadogan, P.H., 1974, Possible effects of ^{39}Ar recoil in ^{40}Ar-^{39}Ar dating of lunar samples: Proc. 5th Lunar Sci. Conf., Geochim. et Cosmochim. Acta Supp. 5, 2, 1601-1615.

Wasserburg, G.J., Hayden, R.J., and Jensen, K.J., 1956, A^{40}-K^{40} dating of igneous rocks and sediments: Geochim. et Cosmochim. Acta 10, 153-165.

Webb, R.W., 1950, Volcanic geology of Toowa Valley, southern Sierra Nevada, California: Geol. Soc. America Bull. 61, 349-357.

Williamson, J.H., 1968, Least-squares fitting of a straight line: Canada Jour. Phys. 46, 1845-1847.

York, D., 1969, Least squares fitting of a straight line with correlated errors: Earth Planet. Sci. Lett. 5, 320-324.

APPENDIX 4-A. Part I: Evaluation of dN_{40}/dN_{39}

Values of dN_{40}/dN_{39} were approximated by values of $\Delta N_{40}/\Delta N_{39}$, which were calculated using finite element methods for each sphere in the population by evaluation the series of Eq. (4) for $F(\tau_e+\tau(a,Q,T_i,t_i))$ and $F(\tau(a,Q,T_i,t_i))$, where t_i was the time during analysis (t_L; see Eq. 14) at which the equation was evaluated. Values of F_p were found at at each (T_i,t_i) according to Eq. (5), and values of $\Delta N_{40}/\Delta N_{39}$ were found using Eq. (15).

In solving Eq. (4), the series was allowed to converge until the subsequent iteration contributed < 0.05% to the sum. In no instance did calculated values differ by more than 0.5% from values calculated by Reichenberg (1953). For $F < 0.01$, the number of required iterations exceeded 250 and the approximation $F = \sqrt{36\tau_i/\pi}$ was used instead (τ_i was defined in Eq. 14). Solutions are shown graphically in Fig. 4-2. Equation (4) was evaluated for $T_i = 300 + 10i$ ^oK and $t_i = 360i$ s. Index i was incremented until $F(\tau(a,Q,T_i,t_i)) \approx 1.0$ for the most retentive grain in the model. The increments of t and T were chosen to give small enough values of $F_i - F_{i-1}$ so that curves of $(\Delta N_{40}/\Delta N_{39})$ vs. $F_p(t_i)$ were not grossly stepped (cf. Fig. 4-4). The curves of Fig. 4-6, Fig. 4-7, and Fig. 4-8 were drawn through these points and smoothed by hand. A superior method would be to evaluate the derivative of the series in Eq. (4) directly, although the resulting changes from the curves as drawn would be indistinguishable.

Part II: Calculation of limits of $\Delta \ln(D_o/a^2)$ and $\Delta Q/RT_{lava}$ which will yield plateaus in dN_{40}/dN_{39} spectra giving the age of degassing of bimodal populations of spheres.

If Ar extraction in the laboratory is isothermal, three simultaneous equations may be solved to specify differences in activation energies or ratios of grain radii which will permit the development of an age spectrum or a dN_{40}/dN_{39} spectrum featuring a plateau corresponding to the age of degassing of a poulation of spheres incorporated in a lava some time after their original crystallization. (For simplicity, the dN_{40}/dN_{39} spectrum is considered herein. Extension to the age spectrum is straightforward.) The spheres are taken to be bimodally distributed in (D_o/a^2) or Q, but as shown in §4.1 they may be distributed along two parallel lines in the $(Q/RT_{lava}, \ln(D_o/a^2))$ plane (e.g., Fig. 4-5b) with equal validity. These lines are defined by the equation

$$\ln(D_o/a^2) - Q/RT_{lava} = \ln t_e + \ln \tau_e \qquad \text{(i)}$$

and finding the critical values of τ_e is the goal of solving the simultaneous equations.

These equations are:

$$\varepsilon = \frac{C_1\left(n_R(4/3)\pi a_R^3 \dot{F}(\tau_{e,R}+\tau_{L,R}) + n_N(4/3)\pi a_N^3 \dot{F}(\tau_{e,N}+\tau_{L,N})\right)}{C_2\left(n_R(4/3)\pi a_R^3 \dot{F}(\tau_{L,R}) + n_N(4/3)\pi a_N^3 \dot{F}(\tau_{L,N})\right)} \qquad \text{(ii)}$$

$$M_\varepsilon = \frac{n_R(4/3)\pi a_R^3 F(\tau_{L,R}) + n_N(4/3)\pi a_N^3 F(\tau_{L,N})}{n_R(4/3)\pi a_R^3 + n_N(4/3)\pi a_N^3} \qquad \text{(iii)}$$

$$F_p = \frac{n_R(4/3)\pi a_R^3 F(\tau_{e,R}) + n_N(4/3)\pi a_N^3 F(\tau_{e,N})}{n_R(4/3)\pi a_R^3 + n_N(4/3)\pi a_N^3} \qquad \text{(iv)}$$

where ε is the maximum error allowed for the values of N_{40}/N_{39} found in the plateau; the subscripts N and R refer to the non-retentive and retentive spheres, respectively; n is the number of spheres in the population; M_ε is the fraction of ^{39}Ar released from the population before ε is exceeded; and the remainder of the symbols are used as in §4.1.

Several simplifications are possible. It is obvious from degassing patterns of single spheres that $F(\tau_{e,N})$ must be very nearly unity if a plateau is to be achieved. Thus, Eq. (iv) may be rewritten as

$$F(\tau_{e,R}) \approx F_p - (n_N/n_R)(a_n/a_R)^3 (1 - F_p) \qquad (v)$$

where F_p refers to the fractional degassing for the population.

Solution of all three equations is simplified if the approximations of Reichenberg (1953) for $F(\tau)$ are used instead of the series of Eq. (4). These approximations are listed here for convenience:

$$F(\tau) = 6\sqrt{\tau/\pi} \quad ; \quad F(\tau) \leq 0.1 \qquad (vi)$$

$$F(\tau) = 6\sqrt{\tau/\pi} - 3\tau \quad ; \quad 0.1 < F(\tau) \leq 0.9 \qquad (vii)$$

$$F(\tau) = 1 - (6/\pi^2)\exp(-\pi^2\tau) \quad ; \quad 0.9 < F(\tau) \qquad (viii)$$

The choice of the correct approximations must be made from inspection of Eq. (iii) and Eq. (v).

For a wide range of values of M_ε, $0.1 < F(\tau_{e,N}) \leq 0.9$ and $F(\tau_{e,R}) \leq 0.1$. Furthermore, if $\dot{T}(t) = 0$ then $\tau_{e,R} = xy\ \tau_{e,N}$, where $x \equiv (D_o/a^2)_R(D_o/a^2)_N^{-1}$ and $y \equiv \exp(-(Q_R-Q_N)/RT_L)$. Eq. (iii) may be rewritten as

$$\left(1 + \frac{n_R}{n_N}\left(\frac{a_R}{a_N}\right)^3\right)\frac{\sqrt{\pi}}{6} M_\varepsilon = \left(1 + \frac{n_R}{n_N}\left(\frac{a_R}{a_N}\right)^3\sqrt{xy}\right)\sqrt{\tau_{L,N}} - \frac{\sqrt{\pi}}{2}\tau_{L,N} \qquad (viii)$$

Equation (viii) is a quadratic equation for $\sqrt{\tau_{L,N}}$. The root in the region of interest is

$$\sqrt{\tau_{L,N}} = \frac{b}{\sqrt{\pi}} - \left(\frac{b^2}{\pi} - \left(1 + \frac{n_R}{n_N}\left(\frac{a_R}{a_N}\right)^3 \right)\frac{M_\varepsilon}{3} \right)^{-1/2} \qquad \text{(ix)}$$

$$b = 1 + \frac{n_R}{n_n}\left(\frac{a_r}{a_N}\right)^3\sqrt{xy}$$

Therefore, unless $F_p(t_e)$ is itself quite large (e.g., > 0.99), $\dot{F}(\tau_{e,R}) >> \dot{F}(\tau_{e,N})$. If $F(\tau_{e,R}) \leq 0.9$, Eq. (ii) may be rewritten and solved iteratively for xy by substitution of pairs of $(xy, \tau_{L,N})$ found from Eq. (ix):

$$\varepsilon \frac{C_2}{C_1} \approx \frac{n_R a_R^3 xy \left[(\tau_{e,R} + xy\ \tau_{L,N})^{-1/2} - \sqrt{\pi} \right]}{(n_R a_R^3\sqrt{xy} + n_N a_N^3)\frac{1}{\sqrt{\tau_{L,N}}} - \sqrt{\pi}\ n_N a_N^3} \qquad \text{(x)}$$

The single value of xy specifies the relative values of (D_o/a^2) and Q for the spherical crystals in the population. Because of the dependence of y on T_L, the value of xy that satisfies Eq. (x) is different for different laboratory extraction temperatures (T_L).

Commonly, extraction of Ar is not isothermal, but T_L is increased in a systematic fashion. The above analysis applies only to isothermal extraction.

APPENDIX 4-B. Derivation of Equation (20)

Let t_c be the age of original crystallization of a sphere and let t_e be the age of degassing in the host lava during eruption. It must be noted that this usage of t_c is new: previously, t_c has been used as the age of the model at the time it was immersed in the magma. For simplicity, the derivation is in terms of time rather than age. Time t is herein defined such that t = 0 is the time of crystallization and t increases towards the future. Thus the time of an event is related to its age A by $t = t_c - A$. The sphere was immersed in magma at some time t_m, and the eruption and cooling occurred at time $t_c - t_e$. The amounts of ^{40}K and ^{40}Ar in the sphere vary with time. The amount of ^{40}K present upon crystallization at time t = 0 is

$$^{40}K(0) = {}^{40}K(t_c)\exp(\lambda t_c) \qquad \text{(i)}$$

where $\lambda \equiv \lambda_e + \lambda_\beta$ is the decay constant for ^{40}K. The amount of ^{40}Ar some time t after crystallization is

$$^{40}Ar(t) = {}^{40}K(t)R(\exp(\lambda t)-1) \qquad \text{(ii)}$$

where $R = \lambda_e(\lambda_e+\lambda_\beta)^{-1}$. The amount of initial ^{40}Ar accumulated at the time of eruption is thus

$$^{40}Ar(t_c-t_e) = {}^{40}K(0)R(1-\exp(-\lambda(t_c-t_e))) \qquad \text{(iii)}$$

and the new ^{40}Ar created since eruption is

$$^{40}Ar_{(NEW)} = {}^{40}K(0)R(\exp(-\lambda(t_c-t_e))-\exp(-\lambda t_c)) \qquad \text{(iv)}$$

During degassing in the magma, a fraction $F(\tau_e)$ of the initial ^{40}Ar is lost. F and τ were defined by Eqs. (3) and (4), and here τ_e is found using integration limits of t_m and t_c-t_e. The remaining or residual $^{40}Ar_{RES} = {}^{40}K(0)R\ (1-\exp(-\lambda(t_c-t_e))(1-F(\tau_e))$ is said to be inherited.

In ^{40}Ar-^{39}Ar analysis, a fraction J of the ^{39}K is converted to $^{39}K(n,p)^{39}Ar$, and ^{39}K is found in constant proportion X to the ^{40}K present in the crust today ($t = t_c$). Thus

$$^{39}Ar = {}^{40}K(0)JX\exp(-\lambda t_c) \qquad (v)$$

so that equations (iii) and (iv) may be rewritten as

$$^{40}Ar(t_c-t_e) = {}^{39}Ar\ C(\exp(\lambda t_c)-\exp(\lambda t_e) \qquad (vi)$$

and

$$^{40}Ar_{NEW} = {}^{39}Ar\ C(\exp(\lambda t_e)-1) \qquad (vii)$$

where $C \equiv R/JX$.

In ^{40}Ar-^{39}Ar analysis, the apparent age A may vary during extraction and is a function of $\frac{d^{40}Ar}{d^{39}Ar}$. In analysis of thermally undisturbed models,this ratio is unity. However, in the analysis of partially degassed models, ^{40}Ar is drawn from two sources: $^{40}Ar_{NEW}$ and $^{40}Ar_{RES}$. Thus the age equation may be written:

$$A = \frac{1}{\lambda} \ln\left(1 + \frac{1}{C}\ \frac{^{40}Ar(t_c-t_e)}{^{39}Ar}\ \frac{dF(\tau_e+\tau_L)}{dF(\tau_L)} + \frac{^{40}Ar_{NEW}}{^{39}Ar}\ \frac{dF(\tau_L)}{dF(\tau_L)}\right) \qquad (viii)$$

substituting for ^{40}Ar according to Eqs. (vi) and (vii), the expression of Eq. (viii) may be simplified:

$$A = \frac{1}{\lambda} \ln\left(\exp(\lambda t_e)+(\exp(\lambda t_c)-\exp(\lambda t_e)) \frac{dF(\tau_e+\tau_L)}{dF(\tau_L)} \right) \qquad \text{(ix)}$$

By choosing a maximum bias ε for apparent ages considered to belong to a plateau, it is now possible to write an indirect equation for τ_{plat}, which defines through Eq. (4) the extent of degassing during analysis before the bias exceeds ε. The maximum allowed age is $A = (1+\varepsilon)t_e$. Substituting for A in Eq. (ix), it may be seen that

$$\frac{d^{40}Ar}{d^{39}Ar} = \frac{dF(\tau_e+\tau_{plat})}{dF(\tau_{plat})} = \frac{\exp(-\lambda(1+\varepsilon)t_e)-\exp(\lambda t_e)}{\exp(\lambda t_c)-\exp(\lambda t_e)} \qquad \text{(x)}$$

which is Eq. (20). The generalization of this derivation for a single sphere to a population of spheres is straightforward.

APPENDIX 4-C. Extrapolation of measured ion currents to the time of admission of Ar into the mass spectrometer

After the mass spectrometer is opened to admit Ar at time $\tau = 0$, there is an unavoidable delay before measurement can begin at $\tau = \tau_1$. However, as soon as the Ar is admitted, exchange begins with gas resident in the accelerating and focussing plates of the source and in the walls of the flight tube. The amount of Ar, $P(\tau)$, available for measurement and the amount of resident Ar, $Q(\tau)$, thus both vary with time. Consequently, the amount of Ar in the measured sample must be estimated by extrapolation of ion currents measured n times from $\tau = \tau_1$ to $\tau = \tau_n$. Usual practice is to perform a linear regression of $P(\tau)$ on τ or of log $P(\tau)$ on τ to permit the estimation. However, there are instances when neither method results in a good fit of the function to the measured data. In such cases we have fitted polynomials of order $N < 4$ to the data.

If $P(\tau)$ and $Q(\tau)$ both describe a single isotope, then

$$\dot{P}(\tau) = -\alpha P(\tau) + \beta\alpha P(\tau)Q(\tau) + \gamma \qquad \text{(i)}$$

where the mass spectrometer is a closed system ($P(\tau) + Q(\tau) = T$) and where α and β are constants respectively describing the efficiency of ion implantation and of escape of resident atoms as a result of ion implantation. The final term γ arises because observations show that even if $P(0) = 0$, $\dot{P}(0) > 0$. This may be caused by diffusion from the resident reservoir or by exchange of resident atoms with other implanting ions (e.g., N_2^+) from the mass spectrometer chamber. For this discussion it is assumed that these processes are of constant rate γ.

The solution to Eq. (i) is not straightforward, but some simplifying assumptions can be made. If $\int_{\tau_o}^{\tau_n} \dot{Q}(\eta)d\eta \ll Q(0)$ then $Q(\tau)$ is approximately constant during the period of measurement, so that

$$\dot{P}(\tau) \approx -\lambda P(\tau) + \gamma \qquad \text{(ii)}$$

where $\lambda = -\alpha(1-\beta Q(0))$. Thus

$$P(\tau) \approx a + be^{-\lambda t} \qquad \text{(iii)}$$

where $a = \gamma/\lambda$ and $b = P(0) - a$. If for $\tau_1 < \tau < \tau_n$, $\lambda P(t) \gg \gamma$, then $P(\tau) \approx P(0)e^{-\lambda t}$ and regression of log $P(\tau)$ on τ is appropriate. If $\lambda P(\tau) \ll \gamma$, $P(\tau) \approx \gamma\tau$ and linear regression is adequate. If $\lambda P(0)$ is of the same order of magnitude as γ then neither approach may be acceptable. Equation (iii) may be expanded to give

$$P(\tau) \approx a + b\left(1 - \lambda\tau + \frac{(\lambda\tau)^2}{2!} - \frac{(\lambda\tau)^3}{3!} + \ldots + \frac{(-\lambda\tau)^n}{n!}\right) \qquad \text{(iv)}$$

if b or λ is sufficiently small and if $0 < \tau < \tau_n$, most of $P(\tau)$ is contributed by the first few terms, and provided that the number of terms of the truncated expansion is less than n-1, polynomial regression may be used to estimate P(0).

The actual order N of the polynomial must be chosen carefully. If N is too small, the curvature of the polynomial may be inadequate to model $P(\tau)$ well over $0 < \tau < \tau_n$. The fit may be improved by increasing N or decreasing n. However, if n is decreased there will be an increased uncertainty in the extrapolated amount of Ar because the estimated standard deviation s is proportional to an integral α of

Student's t distribution such that

$$s = t_{(n-2,\alpha)} \sum_{i=1}^{n} (R(\tau_i)-\hat{P}(\tau_i))^2 \left(1/n + \frac{(\sum_{i=1}^{n} \tau_i)^2}{n \sum_{i=1}^{n} (\tau_i-\bar{\tau})^2} \right)^{1/2} \quad (v)$$

where τ_i are the times of measurement, $\bar{\tau}$ is the mean of all τ_i, α is the confidence with which we want to estimate P(0), and $\hat{P}(\tau)$ is an estimate of $P(\tau)$ from the fitted polynomial. For 95% confidence and n = 3, $t_{(1,0.95)} > 12$ while for n = 10 $t_{(8,0.95)} = 2.1$. For $n > 30$, $t_{(n-2,0.95)} \approx 1.96$.

If N is increased too much in an effort to improve the fit, $\hat{P}(0)$ would fluctuate strongly with n because of the influence of random measurement errors. In the presence of such instability s is too small an estimate of the uncertainty of $\hat{P}(0)$. If N is adequate to fit the data, values of $\hat{P}(0)$ will neither drift nor fluctuate strongly as n is changed. In practice it appears that a polynomial of $N < 4$ can be successfully fit to n = 10 data points, but this varies with the quality of measurement. For instance, if $\lambda > 0.0025\ s^{-1}$ and ion currents were sampled every 120 s over 1200 s (n = 10), then a stable fit by a polynomial of adequate curvature, as discussed above, does not appear to be achievable.

To minimize uncertainties, instead of ion currents themselves generally ratios of one ion current to a linearly interpolated reference ion current are estimated. In this case

$$r(\tau) = \frac{a + b \exp(-\lambda\tau)}{a_{REF} + b_{REF} \exp(-\lambda_{REF}\,\tau)} \qquad \text{(vi)}$$

is the function describing the variation with time of the ratios $r(\tau_i)$. Because of the complicated form of $r(\tau)$, when linear or logarithmic regression are inappropriate, it is difficult to find $\hat{r}(0)$ without the use of polynomial regression.

APPENDIX 4-D. Tabulated data from ^{40}Ar-^{39}Ar analyses for §4.2

Data from ^{40}Ar - ^{39}Ar analyses for samples discussed in §4.2 are presented in two tables. In Table 4-D-I information necessary for the reduction of the stepwise ^{40}Ar-^{39}Ar analyses is given. Data from the analyses are given in Table 4-D-II.

The metal foils used to wrap some samples contributed Ar to the measured gas. This contribution was assumed to affect only the step during which the foil melted. Measured ^{40}Ar from Al foil was 2×10^{-7} $cm^3STP\ g^{-1}$; measured ^{40}Ar from Sn foil was 2.7×10^{-7} $cm^3STP\ g^{-1}$.

Table 4-D-I

Delay Between Neutron Irradiation and ^{40}Ar-^{39}Ar Analysis, and Neutron Fluence of Sample Relative to Bern 4M Muscovite Monitor

^{40}Ar-^{39}Ar Analysis	Delay, Days	Relative Fluence
8-12	66	0.954
8-10	61	1.006
6-12	243	0.915
1-2	125	1.016
1-3	127	1.016
1-7	295	0.987
1-8	297	1.000
1-11	225	1.020
1-12	227	1.002
8-1	159	0.998
8-2	160	1.006
8-3	161	0.979

Table 4-D-II

Stepwise Summary of ^{40}Ar-^{39}Ar Analyses of Basalts, Subjacent Bedrock, and Granitic Xenoliths from the North Fork of Oak Creek, Inyo County, California

Data are presented for twelve ^{40}Ar-^{39}Ar analyses. Each matrix gives data for one sample. Rows give data for individual 60 min. steps at the temperature indicated in the first column. Temperatures above 700°C were estimated by pyrometry before analysis of the samples. Temperatures below 700° C were estimated from the melting of Al and Sn foils and by interpolation. The second column shows the total ^{40}Ar released in each step, including blank ^{40}Ar (third column). Background mass 40 from the spectrometer has been subtracted. Uncertainties in the amount of mass 40 are ± 10% and the blank is known to ± 25%. The next four columns show measured ion current ratios for the indicated masses. Ratios have been corrected for spectrometer background and mass discrimination and for the blank of the extraction line (except for air Ar), but not for interference isotopes, radioactive decay of ^{39}Ar and ^{37}Ar, nor neutron fluence (Table 4-D-I). Ratios of ^{39}Ar and ^{36}Ar to ^{40}Ar (after all corrections, including removal of the blank air Ar) are shown in columns nine and ten. Column 11 gives the cumulative fraction of ^{39}Ar released up to an including the indicated step, and the final column shows the age indicated by the Ar compositions in columns nine and ten, assuming $(^{36}Ar/^{40}Ar)_t = 0.003384$. All uncertainties are 2σ and do not include systematic uncertainties.

TABLE 4-D-IIa.

NFOC-23a basalt 8-12 (site A)

T°C	^{40}Ar $cm^3STPx10^8$	^{40}Ar(blank) $cm^3STPx10^8$	39/40 x10^3	38/40 x10^5	37/40 x10^5	36/40 x10^5	$^{39}Ar/^{40}Ar$ x10^3	$^{36}Ar/^{40}Ar$ x10^5	$\frac{^{39}Ar}{\Sigma^{39}Ar}$	model age,my
300	2.43	0.02	146±1	228±3	418±3	192±3	155±1	191±3	0.36	1.21±0.03
500	1.98	0.02	176±0	754±4	2742±8	174±4	187±0	169±7	0.35	1.15±0.05
900	7.61	0.03	252±0	764±8	13523±60	113±9	274±0	89±11	0.20	1.16±0.05
1175[f]	1.56	0.35	59±0	411±2	31347±62	312±5	79±0	259±12	0.09	1.28±0.20

TABLE 4-D-IIb.

NFOC-109 quartz monzonite bedrock 8-10 (site A)

T°C	^{40}Ar $cm^3STPx10^8$	^{40}Ar(blank) $cm^3STPx10^8$	39/40 x10^3	38/40 x10^5	37/40 x10^5	36/40 x10^5	$^{39}Ar/^{40}Ar$ x10^3	$^{36}Ar/^{40}Ar$ x10^5	$\frac{^{39}Ar}{\Sigma^{39}Ar}$	model age,my
300	42.8	0.08	6±0	70±3	32±1	320±3	6±0	320±3	0.03	3.70±0.63
450	4.04	0.08	39±0	78±4	94±2	126±7	39±1	122±7	0.02	7.01±0.24
600	4.39	0.08	46±0	76±1	76±1	77±1	46±0	73±1	0.02	7.33±0.05
950	400.0	0.13	8±0	11±0	12±0	6±0	8±0	6±0	0.33	54.9±0.2
1200	640.0	0.83	6±0	21±4	2±0	36±1	6±0	36±1	0.39	66.0±0.4
1400	377.0	2.24	5±0	8±0	42±1	7±0	5±0	5±0	0.21	78.2±0.1
1500[f]	-	-	-	-	-	-	-	-	-	-
1700	35.0	25.8	1±0	56±1	3±0	288±4	3±0	146±33	0.00	75.8±7.0

"f" denotes step in which fusion occurred.

TABLE 4-D-IIc.

NFOC-1 basalt 6-12 (site B)

T°C	^{40}Ar $cm^3STPx10^{-8}$	^{40}Ar(blank) $cm^3STPx10^{-8}$	39/40 x10^3	38/40 x10^5	37/40 x10^5	36/40 x10^5	$^{39}Ar/^{40}Ar$ x10^3	$^{36}Ar/^{40}Ar$ x10^5	$\frac{^{39}Ar}{\Sigma^{39}Ar}$	model age,my
275	3.08	0.05	53±0	112±17	0±0	233±4	59±0	232±4	0.37	1.16±0.05
500	2.28	0.05	39±0	130±24	3±32	265±4	43±0	264±5	0.20	1.12±0.07
700	1.48	0.05	26±0	107±37	17±49	291±6	29±0	288±6	0.09	1.11±0.14
900	0.91	0.05	39±0	91±62	48±82	2682±7	45±1	263±8	0.08	1.08±0.12
1000	0.73	0.05	40±1	96±74	77±97	270±7	46±1	262±8	0.07	1.06±0.12
1100	0.61	0.10	23±1	86±94	32±127	315±12	30±1	309±15	0.03	0.65±0.32
1400[f]	46.6	1.96	2±0	69±1	14±2	334±1	2±0	333±1	0.17	1.96±0.45

TABLE 4-D-IId.

NFOC-1 basalt 1-2 (site B)

T°C	^{40}Ar $cm^3STPx10^{-8}$	^{40}Ar(blank) $cm^3STPx10^{-8}$	39/40 x10^3	38/40 x10^5	37/40 x10^5	36/40 x10^5	$^{39}Ar/^{40}Ar$ x10^3	$^{36}Ar/^{40}Ar$ x10^5	$\frac{^{39}Ar}{\Sigma^{39}Ar}$	model age,my
270	17.6	0.02	20±0	90±3	28±1	315±9	20±0	315±9	0.28	1.52±0.59
270	1.28	0.02	32±0	111±3	79±2	280±3	33±0	279±3	0.03	2.36±0.11
450	1.78	0.02	52±0	174±2	41±2	283±2	52±0	281±3	0.08	1.42±0.06
500	1.55	0.02	66±0	186±2	562±5	272±4	66±0	269±4	0.08	1.35±0.08
600	1.26	0.02	65±0	169±3	567±6	275±3	67±0	271±3	0.07	1.31±0.06
650	0.89	0.02	86±0	204±5	1052±9	246±3	89±0	240±3	0.06	1.45±0.04
800	0.82	0.02	139±1	341±7	2578±14	215±2	141±1	202±4	0.09	1.25±0.04
1150	5.09	0.04	60±0	307±3	1949±8	294±2	60±0	286±4	0.12	1.14±0.09
1400[f]	12.0	0.52	18±0	167±9	1634±34	328±16	31±1	311±29	0.18	1.16±1.21

"f" denotes step in which fusion occurred.

TABLE 4-D-IIe.

NFOC-1 basalt 1-3 (site B)

T°C	^{40}Ar $cm^3STPx10^8$	^{40}Ar(blank) $cm^3STPx10^8$	39/40 x10^3	38/40 x10^5	37/40 x10^5	36/40 x10^5	$^{39}Ar/^{40}Ar$ x10^3	$^{36}Ar/^{40}Ar$ x10^5	$\frac{^{39}Ar}{\Sigma^{39}Ar}$	model age,my
~170	0.05	0.02	9±0	82±16	60±30	320±12	13±1	308±19	0.00	2.9±1.8
~180	0.04	0.02	1±0	57±18	8±43	328±11	2±1	316±28	0.00	12.2±15.5
~190	0.05	0.02	0±0	68±16	10±35	331±11	0±1	326±21	0.00	45.9±80.3
~200	0.32	0.02	0±0	60±3	4±5	304±6	0±0	302±6	0.00	139.9±23.3
250	1.37	0.02	147±0	235±3	120±2	205±2	147±0	202±2	0.18	1.20±0.02
270	2.57	0.02	159±0	269±2	103±2	195±1	159±0	194±2	0.37	1.18±0.01
675	1.24	0.03	146±1	492±5	1625±9	213±3	148±7	203±6	0.17	1.18±0.06
900	0.99	0.04	157±1	328±4	3283±25	207±4	248±1	108±10	0.14	1.20±0.05
900	0.20	0.05	55±0	183±7	884±12	292±7	74±1	269±10	0.01	1.21±0.18
1150	1.83	0.15	46±0	256±4	2575±34	308±4	49±0	294±6	0.08	1.17±0.15
1400[f]	5.68	0.52	10±0	122±1	1282±3	338±2	11±0	332±3	0.05	0.70±0.32
~1650	3.61	2.61	1±0	68±1	98±5	337±2	3±0	331±27	0.00	3.6±14.0

"f" denotes step in which fusion occurred.

TABLE 4-D-IIf.

NFOC-1a quartz monzonite xenolith 1-7 (site B)

T°C	^{40}Ar $cm^3STPx10^8$	^{40}Ar(blank) $cm^3STPx10^8$	39/40 x10^3	38/40 x10^5	37/40 x10^5	36/40 x10^5	$^{39}Ar/^{40}Ar$ x10^3	$^{36}Ar/^{40}Ar$ x10^5	$\frac{^{39}Ar}{\Sigma^{39}Ar}$	model age,my
450	4.47	0.03	17±0	85±7	0±4	317±3	17±0	316±3	0.03	1.62±0.20
500	1.01	0.03	72±1	149±42	5±20	270±10	75±1	268±10	0.03	1.20±0.17
700	4.47	0.03	138±1	220±8	1±3	208±3	141±1	207±14	0.23	1.20±0.03
875	3.64	0.03	228±1	332±12	2±6	128±1	234±1	126±3	0.31	1.17±0.02
1000	2.70	0.03	209±1	305±13	1±8	145±1	214±1	143±3	0.21	1.18±0.02
1050	2.26	0.03	135±1	241±18	2±9	218±5	139±1	217±5	0.11	1.13±0.05
1100	1.76	0.04	105±0	194±33	0±5	242±3	109±0	241±3	0.07	1.16±0.04
1400f	-	-	-	-	-	-	-	-	-	-
1700	22.9	7.96	3±1	60±4	0±2	317±7	5±1	323±22	0.03	4.1±5.7

TABLE 4-D-IIg.

NFOC 1-a quartz monzonite xenolith 1-8 (site B)

T°C	^{40}Ar $cm^3STPx10^8$	^{40}Ar(blank) $cm^3STPx10^8$	39/40 x10^3	38/40 x10^5	37/40 x10^5	36/40 x10^5	$^{39}Ar/^{40}Ar$ x10^3	$^{36}Ar/^{40}Ar$ x10^5	$\frac{^{39}Ar}{\Sigma^{39}Ar}$	model age,my
450	5.62	0.03	12±0	75±5	1±3	309±17	12±0	309±17	0.03	3.26±1.87
700	4.96	0.03	86±1	149±8	2±4	255±3	87±1	254±3	0.19	1.25±0.05
1000	5.16	0.03	157±1	251±6	4±2	185±2	158±1	184±3	0.36	1.26±0.02
1150	3.57	0.04	73±0	159±5	0±1	256±2	74±0	255±3	0.12	1.45±0.05
1250	9.05	0.30	5±0	57±1	6±2	297±2	5±0	297±2	0.20	11.5±0.7
1400f	99.5	0.60	2±0	55±2	2±3	297±2	2±0	296±2	0.09	27.0±1.6
1775	4.33	8.59	1±1	56±4	0±1	308±4	1±1	308±10	0.02	1.4±10.5

"f" denotes step in which fusion occurred.

TABLE 4-D-IIh.

NFOC-1b quartz monzonite xenolith 1-11 (site B)

T°C	^{40}Ar $cm^3STPx10^8$	^{40}Ar(blank) $cm^3STPx10^8$	39/40 $x10^3$	38/40 $x10^5$	37/40 $x10^5$	36/40 $x10^5$	$^{39}Ar/^{40}Ar$ $x10^3$	$^{36}Ar/^{40}Ar$ $x10^5$	$\frac{^{39}Ar}{\Sigma^{39}Ar}$	model age,my
225	0.12	0.02	2±0	65±16	0±6	336±8	2±0	336±9	0.00	1.39±4.81
300	1.11	0.02	7±1	77±3	2±1	317±5	7±0	317±5	0.01	4.17±0.92
400	-	-	-	-	-	-	-	-	-	-
450	0.72	0.02	42±0	119±4	14±2	294±5	42±0	292±6	0.02	1.40±0.17
500	0.60	0.03	91±1	181±6	181±6	273±6	93±1	266±7	0.04	1.00±0.09
500	0.13	0.03	93±1	176±17	22±6	260±12	117±2	238±15	0.01	1.11±0.17
675	1.94	0.04	153±2	234±5	21±1	186±3	153±2	182±3	0.22	1.32±0.03
1050	3.26	0.06	187±2	285±4	15±1	167±2	187±2	164±2	0.46	1.20±0.02
1400[f]	34.5	0.92	8±0	73±2	5±0	328±6	8±0	328±6	0.21	1.67±1.02
1600	8.89	3.32	3±0	66±4	1±0	339±11	5±0	341±18	0.02	-

"f" denotes step in which fusion occurred.

TABLE 4-D-IIi.

NFOC-1b quartz monzonite xenolith 1-12 (site B)

T°C	^{40}Ar $cm^3STPx10^8$	^{40}Ar(blank) $cm^3STPx10^8$	39/40 x10^3	38/40 x10^5	37/40 x10^5	36/40 x10^5	$^{39}Ar/^{40}Ar$ x10^3	$^{36}Ar/^{40}Ar$ x10^5	$\frac{^{39}Ar}{\Sigma^{39}Ar}$	model age,my
250	1.60	0.02	11±0	79±3	3±0	309±6	11±0	309±6	0.01	3.56±0.77
300	0.73	0.02	27±1	97±6	16±1	311±7	28±1	310±7	0.02	1.33±0.32
500	0.74	0.03	65±1	139±1	36±2	275±3	67±1	271±4	0.04	1.28±0.07
500	0.19	0.02	79±1	144±11	34±3	269±30	89±1	261±34	0.01	1.12±0.49
600	1.36	0.03	108±0	186±2	30±1	239±4	110±0	236±4	0.11	1.20±0.05
675	0.74	0.03	151±0	235±4	31±1	196±2	158±0	189±3	0.08	1.22±0.02
800	0.33	0.03	180±1	272±10	33±2	171±5	200±1	153±6	0.05	1.19±0.04
900	0.96	0.04	179±1	271±3	33±1	171±2	188±1	163±2	0.13	1.21±0.02
1000	1.42	0.04	136±1	229±4	15±0	206±6	139±1	202±6	0.15	1.26±0.06
1025	0.86	0.04	85±1	180±4	9±1	250±2	88±1	247±2	0.06	1.33±0.04
1050	0.72	0.08	56±0	146±5	8±1	263±3	63±0	255±4	0.03	1.70±0.07
1075	0.93	0.13	31±0	106±3	9±1	282±4	36±0	274±5	0.02	2.31±0.17
1100	12.1	0.24	7±0	66±1	3±0	294±4	7±0	293±4	0.06	8.4±0.7
1400[f]	96.5	0.75	3±0	59±0	2±0	297±2	3±0	297±2	0.20	19.4±0.7
1700	26.1	7.06	2±0	60±1	2±0	301±3	2±0	291±6	0.03	30.0±5.3

"f" denotes step in which fusion occurred.

TABLE 4-D-IIj.

NFOC-103 quartz monzonite xenolith 8-1 (site C)

T°C	^{40}Ar $cm^3STPx10^8$	^{40}Ar(blank) $cm^3STPx10^8$	39/40 $x10^3$	38/40 $x10^5$	37/40 $x10^5$	36/40 $x10^5$	$^{39}Ar/^{40}Ar$ $x10^3$	$^{36}Ar/^{40}Ar$ $x10^5$	$\frac{^{39}Ar}{\Sigma^{39}Ar}$	model age,my
450	18.5	0.18	0±0	68±0	0±0	338±1	1±0	338±1	0.00	-
550	1.09	0.18	31±0	114±3	71±2	312±3	36±0	307±4	0.07	1.11±0.12
850	1.93	0.18	85±0	164±2	176±2	260±4	94±1	251±4	0.30	1.19±0.06
950	6.96	0.18	21±0	83±1	28±1	289±1	21±0	287±1	0.27	3.08±0.06
1200	5.85	0.18	16±0	73±1	28±1	268±1	16±0	266±1	0.17	5.65±0.08
1375[f]	14.9	6.80	7±0	65±0	33±0	289±1	13±0	248±9	0.19	9.05±0.85

TABLE 4-D-IIk.

NFOC-103 quartz monzonite xenolith 8-2 (site C)

T°C	^{40}Ar $cm^3STPx10^8$	^{40}Ar(blank) $cm^3STPx10^8$	39/40 $x10^3$	38/40 $x10^5$	37/40 $x10^5$	36/40 $x10^5$	$^{39}Ar/^{40}Ar$ $x10^3$	$^{36}Ar/^{40}Ar$ $x10^5$	$\frac{^{39}Ar}{\Sigma^{39}Ar}$	model age,my
350	13.1	0.04	0±0	64±1	0±0	338±1	3±0	338±1	0.00	-
450	3.43	0.04	42±0	109±15	13±1	338±5	6±0	338±5	0.03	0.11±1.02
550	0.65	0.04	128±1	233±6	331±6	207±5	154±1	194±5	0.12	1.20±0.05
750	0.63	0.04	29±0	287±6	424±9	175±2	201±1	160±3	0.15	1.13±0.02
950	1.04	0.04	10±0	160±2	117±1	243±3	85±0	238±3	0.11	1.51±0.04
1100	22.0	0.04	9±0	76±0	32±0	279±1	18±0	279±1	0.49	4.31±0.05
1375	0.81	0.18	4±0	64±1	50±1	256±1	10±0	254±1	0.10	10.7±0.10
1700[f]	28.4	1.31	0±0	64±1	1±0	339±1	0±0	339±1	0.01	-

"f" denotes step in which fusion occurred.

TABLE 4-D-IIℓ.

NFOC-103 quartz monzonite xenolith 8-3 (site C)

T°C	^{40}Ar $cm^3STPx10^8$	^{40}Ar(blank) $cm^3STPx10^8$	39/40 $x10^3$	38/40 $x10^5$	37/40 $x10^5$	36/40 $x10^5$	$^{39}Ar/^{40}Ar$ $x10^3$	$^{36}Ar/^{40}Ar$ $x10^5$	$\frac{^{39}Ar}{\Sigma^{39}Ar}$	model age,my
450	19.21	0.03	11±0	65±1	7±0	336±1	12±0	336±1	0.05	-
550	1.32	0.03	42±0	112±2	147±2	291±3	44±0	289±3	0.12	1.43±0.09
750	0.57	0.03	128±1	215±7	454±7	219±5	139±1	208±5	0.16	1.19±0.05
950	1.93	0.03	29±0	100±1	69±2	303±2	30±1	302±2	0.12	1.55±0.08
1050	6.02	0.04	10±0	77±1	39±0	309±1	11±0	309±1	0.14	3.60±0.11
1200	13.1	0.04	9±0	69±1	43±0	280±1	10±0	280±1	0.27	7.8±0.15
1375	13.7	0.89	4±0	58±0	74±0	270±1	5±0	264±1	0.13	19.9±0.3
1700[f]	20.5	1.58	0±0	64±1	3±0	338±1	0±0	338±1	0.00	-

"f" denotes step in which fusion occurred.

APPENDIX 4-E. Tabulated data from ^{40}Ar-^{39}Ar analyses for §4.3

Data from ^{40}Ar - ^{39}Ar analyses for samples discussed in §4.3 are presented in two tables. In Table 4-E-I information necessary for the reduction of stepwise ^{40}Ar-^{39}Ar analyses are given. The results of the stepwise analyses are given in Table 4-E-II.

The metal foils used to wrap some samples contributed Ar to the measured gas. This contribution was assumed to affect only the step during which the foil melted. Measured ^{40}Ar from Al foil was $2x10^{-7}$ $cm^3STP\ g^{-1}$; measured ^{40}Ar from Sn foil was $2.7x10^{-7}$ $cm^3STP\ g^{-1}$. Extraction bottle blanks were consistently rich in ^{40}Ar compared to air Ar.

Table 4-E-I

Summary Data for Samples

Sample	Site		mass,mg	Foil mass,mg	Delay, days	Relative neutron fluence*	Blank $^{36}Ar/^{40}Ar$ x10^6	Sensitivity v cm^{-3}STP x10^{-4}
2-2	SC-1	basalt	533	120 Al	120	1.003	3044±136	431
2-3	SC-1	basalt	411	58 Al	222	0.994	3214±136	417†
6-8	SC-1a	xenolith	422	35 Al	40	1.059	3384±100	847†
6-17	SC-1b	xenolith	228	43 Al	34	0.934	3384±100	813†
9-4	SC-1b	xenolith	105	70 Sn	291	0.997	3347±93	249
9-5	SC-1b	xenolith	111	57 Sn	296	1.022	3284±60	249
6-16	SC-23	orthoclase	361	0	18	1.028	3304±120	877†
6-25	SC-23	xenolith	343	0	30	0.999	3304±120	800†
9-1	SC-23	xenolith	222	0	305	1.025	3354±60	249
9-2	SC-23	xenolith	275	0	294	0.999	3204±72	249
9-6	SC-23	microcline	340	87 Sn	161	0.949	3384±100	306
7-82	SC-115	xenolith	442	86 Sn	224	1.110	3384±100	249
7-83	SC-116	xenolith	544	83 Sn	226	1.139	3351±45	249
7-63[1]	SC-118	xenolith	330	85 Sn	101	1.154	3314±56	191
6-23	SC-22	basalt	682	0	240	0.967	2784±120	041
7-80	SC-112	xenolith	411	104 Sn	231	1.037	3354±67	249
7-61	SC-113	xenolith	524	82 Sn	232	1.141	3325±60	249
7-60	SC-113	xenolith	655	105 Sn	98	1.141	3384±100	306
6-15	SC-20	basalt	1417	0	244	0.981	3184±40	041
7-54	SC-110	xenolith	187	43 Sn	216	1.079	3204±72	249
7-55	SC-110	xenolith	160	65 Sn	221	1.097	3252±132	249
9-20	Tab-201	basalt	1410	0	161	0.973	3384±100	191
9-9	BPt-11	xenolith	433	88 Sn	81	0.995	3384±100	379
9-32	FF-101	microcline	332	96 Sn	79	0.983	3384±100	375
7-86[1]	NFOC-29	xenolith	530	94 Sn	236	1.159	3354±80	249
7-27	NFOC-51	basalt	469	0	97	1.009	3384±100	306
7-107	NFOC-25	basalt	1017	0	99	1.120	3384±100	306

*Normalized to neutron fluence for muscovite irradiation monitor.
Uncertainties are <0.5%.
†With source magnet.
[1]Step lost in analysis.

The first column gives the sample number assigned to each irradiated sample. Several samples may come from the same site (second column). The next columns identify the type of sample ("xenoliths" are granodiorite), the mass of the sample, and the mass and type of foil used to wrap it for neutron irradiation. The sixth and seventh columns give the time from irradiation to analysis and the neutron fluence during irradiation (relative to the Bern 4M monitor). The final two columns give the composition of blank Ar at low extraction temperatures (< 900° C) and the sensitivity of the mass spectrometer to ^{40}Ar.

Table 4-E-II
Stepwise Summary of ^{40}Ar-^{39}Ar Analysis of Late Pleistocene Basalts and Xenoliths.

Each matrix gives data for one sample. Rows give data for individual 60 min. steps at the temperature indicated in the first column. Temperatures above 700° C were estimated from pyrometry before analysis. Temperatures below 700° C were estimated from the melting of Al or Sn foils and by interpolation. The second column shows the total ^{40}Ar released in each step, including blank ^{40}Ar (third column). Next four columns show measured ion current ratios for the indicated masses. Ratios have been corrected for spectrometer background and mass discrimination and for the blank of the extraction line, (except for air Ar) but not for interference isotopes, radioactive decay, or neutron fluence (Table 4-E-I). Ratios of ^{39}Ar and ^{36}Ar to ^{40}Ar (after all corrections, including removal of the blank air Ar) are shown in columns nine and two. Column 11 gives the cumulative fraction of ^{39}Ar released up to and including the indicated step, and the final column shows the age indicated by the Ar compositions in columns nine and ten, assuming $(^{36}Ar/^{40}Ar)_t = 0.003384$. ^{40}Ar from foil wrappings has been subtracted. Uncertainties are ± 5%. Blank levels of ^{40}Ar are generally repeatable to ± 50% (2σ). In a few cases uncertainties were ± 25%.

TABLE 4-E-IIa: Sample 2-2 - Basalt from Sawmill Creek (SC-1)

T,°C	^{40}Ar $cm^3STP\ g^{-1}$ $x10^8$	^{40}Ar(blank) $cm^3STP\ g^{-1}$ $x10^8$	39/40 $x10^4$	38/40 $x10^5$	37/40 $x10^5$	36/40 $x10^5$	$^{39}Ar/^{40}Ar$ $x10^4$	$^{36}Ar/^{40}Ar$ $x10^5$	^{39}Ar $\sum^{39}Ar$	model age, my
500	5.5	0.05	1722±9	427±5	781±9	320±4	1736±9	318±5	0.56	0.15±0.04
650	0.29	0.05	5681±18	1651±66	8901±29	295±17	6979±22	258±30	0.66	0.15±0.05
800	0.37	0.05	3065±25	731±14	6639±101	331±8	3574±30	311±12	0.72	0.10±0.05
1000	1.0	0.06	809±1	271±6	2049±13	326±1	857±1	323±3	0.77	0.27±0.05
1400[f]	14.	0.87	271±1	181±2	3769±18	333±6	285±1	322±7	1.00	0.72±0.31

TABLE 4-E-IIb: Sample 2-3 - Basalt from Sawmill Creek (SC-1)

T,°C	^{40}Ar $cm^3STP\ g^{-1}$ $x10^8$	^{40}Ar(blank) $cm^3STP\ g^{-1}$ $x10^8$	39/40 $x10^4$	38/40 $x10^5$	37/40 $x10^5$	36/40 $x10^5$	$^{39}Ar/^{40}Ar$ $x10^4$	$^{36}Ar/^{40}Ar$ $x10^5$	^{39}Ar $\sum^{39}Ar$	model age, my
275	2.6	0.06	453±2	133±2	7±1	321±8	467±3	321±8	0.09	0.47±0.22
300	1.5	0.08	613±7	184±6	15±1	315±3	651±7	315±4	0.17	0.47±0.08
375	0.47	0.08	704±14	391±21	64±6	315±10	853±17	311±16	0.19	0.41±0.24
425	0.40	0.08	1197±11	1077±36	187±11	292±11	1525±14	278±40	0.23	0.51±0.34
500	0.16	0.09	3042±18	3047±90	574±12	296±8	7201±42	228±209	0.27	0.20±0.37
675	0.22	0.10	12076±1208	5230±524	1813±183	221±43	22925±2294	51±127	0.48	0.16±0.14
850	0.33	0.12	6245±27	1480±22	1037±14	291±7	9801±43	237±40	0.64	0.13±0.05
1000	0.55	0.15	2787±18	723±24	612±8	321±7	3893±25	301±20	0.76	0.12±0.06
1375[f]	13.	3.1	234±1	158±2	433±1	340±3	305±1	332±7	1.00	0.28±0.29

[f]denotes step in which fusion occurred.

TABLE 4-E-IIc: Sample 6-8 - Granodiorite xenolith, Sawmill Creek (SC-1a)

T,°C	^{40}Ar $cm^3STP\ g^{-1}$ $x10^8$	^{40}Ar(blank) $cm^3STP\ g^{-1}$ $x10^8$	39/40 $x10^4$	38/40 $x10^5$	37/40 $x10^5$	36/40 $x10^5$	$^{39}Ar/^{40}Ar$ $x10^4$	$^{36}Ar/^{40}Ar$ $x10^5$	^{39}Ar $\sum^{39}Ar$	model age, my
275	7.6	0.11	15±0	66±1	16±1	333±1	15±0	333±1	0.004	2.4±0.4
300	2.5	0.14	81±0	84±3	102±2	330±1	81±0	329±1	0.01	0.7±0.1
400	1.1	0.14	261±1	112±6	607±9	330±7	283±1	328±8	0.02	0.23±0.2
400R	4.2	0.14	39±0	69±2	85±3	331±1	39±0	330±1	0.03	1.4±0.2
500	1.3	0.14	1318±14	309±8	1628±37	317±1	1400±15	313±2	0.09	0.115±0.009
675	1.3	0.14	2185±4	362±5	1203±9	292±1	2624±4	278±3	0.22	0.146±0.008
775	0.68	0.14	4859±29	722±11	2114±9	250±3	5797±34	227±5	0.34	0.124±0.005
875	0.73	0.14	4831±22	720±8	2042±11	254±3	5657±26	233±4	0.47	0.120±0.005
950	0.87	0.14	3484±25	553±11	1350±8	261±5	3928±28	245±6	0.59	0.151±0.010
1025	0.58	0.14	2007±7	371±12	708±19	287±3	2499±9	270±5	0.63	0.175±0.014
1100	1.3	0.14	914±1	209±5	447±7	288±2	971±1	281±3	0.67	0.377±0.019
1200	4.9	0.14	285±1	105±3	221±3	296±1	277±1	295±1	0.73	1.02±0.02
1700[f]	180.	4.5	40±0	53±1	117±2	273±1	39±0	271±1	0.99	11.3±0.2
1700	11.	4.5	13±1	63±3	43±3	292±10	20±2	260±19	1.00	24.9±6.2

TABLE 4-E-IId: Sample 6-15 - Basalt beneath the outer moraine, Sawmill Creek (SC-20)

T,°C	^{40}Ar $cm^3STP\ g^{-1}$ $x10^8$	^{40}Ar(blank) $cm^3STP\ g^{-1}$ $x10^8$	39/40 $x10^4$	38/40 $x10^5$	37/40 $x10^5$	36/40 $x10^5$	$^{39}Ar/^{40}Ar$ $x10^4$	$^{36}Ar/^{40}Ar$ $x10^5$	^{39}Ar $\sum^{39}Ar$	
~ 1075[f?]	12.	0.07	708±3	226±4	40±6	339±5	727±3	338±6	0.88	0.00±0.04
~ 1400	3.3	1.4	354±3	186±9	439±15	336±11	616±4	320±21	1.00	0.19±0.21

[f]denotes step in which fusion occurred.
R denotes re-extraction.

TABLE 4-E-IIe: Sample 6-16 - Orthoclase from granodiorite xenolith, Sawmill Creek (SC-23)

T,°C	^{40}Ar $cm^3STP\ g^{-1}$ $x10^8$	^{40}Ar(blank) $cm^3STP\ g^{-1}$ $x10^8$	39/40 $x10^4$	38/40 $x10^5$	37/40 $x10^5$	36/40 $x10^5$	$^{39}Ar/^{40}Ar$ $x10^4$	$^{36}Ar/^{40}Ar$ $x10^5$	^{39}Ar $\sum^{39}Ar$	model age, my
300	5.8	0.32	22±0	64±4	63±4	325±1	23±0	324±1	0.003	4.0±0.4
500	4.4	0.32	125±0	81±5	244±6	325±1	131±1	325±1	0.02	0.67±0.07
775	4.3	0.32	722±1	156±6	680±6	306±2	760±1	304±3	0.08	0.29±0.02
950	1.2	0.32	1967±14	325±20	563±19	284±3	2630±19	267±6	0.13	0.17±0.02
1075	1.2	0.32	1987±10	326±19	374±17	277±5	2602±13	259±8	0.19	0.20±0.02
1225	2.8	0.32	1014±11	185±7	240±3	272±6	1111±13	265±7	0.25	0.4±0.0
1300	46.	0.41	309±0	76±1	61±1	191±1	303±0	189±1	0.56	3.2±0.0
1500[f]	97.	2.5	190±1	40±1	34±1	81±1	190±1	75±1	0.96	8.9±0.1
1525	24.	13.	80±1	50±1	16±0	211±3	164±3	80±15	1.00	10.1±1.0
1750	41.	35.	3±0	71±5	17±1	335±4	21±2	358±68	1.00	-

TABLE 4-E-IIf: Sample 6-17 - Granodiorite xenolith, Sawmill Creek (SC-1b)

T,°C	^{40}Ar $cm^3STP\ g^{-1}$ $x10^8$	^{40}Ar(blank) $cm^3STP\ g^{-1}$ $x10^8$	39/40 $x10^4$	38/40 $x10^5$	37/40 $x10^5$	36/40 $x10^5$	$^{39}Ar/^{40}Ar$ $x10^4$	$^{36}Ar/^{40}Ar$ $x10^5$	^{39}Ar $\sum^{39}Ar$	model age, my
300	1.8	0.22	199±3	116±38	195±17	334±3	243±3	334±3	0.01	0.13±0.09
500	7.1	0.27	432±2	129±9	570±6	324±1	481±2	324±1	0.12	0.20±0.02
675	5.8	0.27	784±4	164±11	377±6	318±2	832±5	317±2	0.29	0.16±0.02
775	3.8	0.33	1826±6	303±18	757±17	298±2	2137±7	294±2	0.54	0.13±0.01
950	4.6	0.33	1257±1	228±15	466±7	301±2	1450±2	298±2	0.75	0.18±0.01
1100	4.7	0.33	545±2	149±15	290±10	302±3	627±2	299±3	0.84	0.40±0.03
1400[f]	42.	2.3	99±1	62±2	247±6	265±5	113±1	260±5	0.99	4.5±0.3
1750	51.	27.	4±0	61±2	13±1	329±6	9±1	319±17	1.00	14.6±12.6

[f]denotes step in which fusion occurred.

TABLE 4-E-IIg: Sample 6-23 - Basalt above outer moraine, Sawmill Creek (SC-22)

T,°C	^{40}Ar $cm^3STP\ g^{-1}$ $x10^8$	^{40}Ar(blank) $cm^3STP\ g^{-1}$ $x10^8$	39/40 $x10^4$	38/40 $x10^5$	37/40 $x10^5$	36/40 $x10^5$	$^{39}Ar/^{40}Ar$ $x10^4$	$^{36}Ar/^{40}Ar$ $x10^5$	^{39}Ar $\sum^{39}Ar$	model age, my
300	1.7	0.72	119±2	57±135	0±44	299±40	217±4	314±72	0.02	0.7±2.1
500	0.82	0.72	796±19	281±281	32±100	280±84	5916±163	280±709	0.10	0.05±0.65
950	4.6	0.72	735±6	331±86	37±31	296±27	901±7	297±33	0.52	0.29±0.24
1050	2.4	0.72	636±5	254±129	100±42	298±38	935±8	301±55	0.71	0.26±0.38
1400[f]	33.	1.1	74±0	87±9	50±3	326±3	79±0	326±3	1.00	1.0±0.3
1700	20.	13.0	1±0	51±14	1±5	303±5	2±0	348±25	1.00	-

TABLE 4-E-IIh: Sample 6-25 - Granodiorite xenolith, Sawmill Creek (SC-23)

T,°C	^{40}Ar $cm^3STP\ g^{-1}$ $x10^8$	^{40}Ar(blank) $cm^3STP\ g^{-1}$ $x10^8$	39/40 $x10^4$	38/40 $x10^5$	37/40 $x10^5$	36/40 $x10^5$	$^{39}Ar/^{40}Ar$ $x10^4$	$^{36}Ar/^{40}Ar$ $x10^5$	^{39}Ar $\sum^{39}Ar$	model age, my
300	12.	0.36	61±1	67±9	19±4	332±1	63±1	332±1	0.03	0.67±0.15
500	30.	0.36	102±1	74±6	85±3	332±1	104±1	332±1	0.16	0.37±0.09
675	14.	0.36	207±1	89±8	274±4	325±1	213±1	325±1	0.28	0.41±0.04
675R	5.4	0.36	94±1	71±14	115±7	332±4	101±1	332±4	0.30	0.39±0.25
775	2.7	0.36	711±3	155±9	1013±12	324±4	821±3	322±5	0.38	0.13±0.04
875	1.6	0.36	1132±12	207±31	1381±58	312±5	1482±16	306±8	0.46	0.14±0.03
950	1.1	0.36	1252±6	235±47	1111±29	310±3	1976±10	298±8	0.51	0.13±0.03
1025	0.67	0.36	1410±9	243±19	999±43	307±4	3112±20	278±17	0.55	0.13±0.04
1075	0.64	0.36	975±29	251±69	739±50	303±8	2241±67	267±24	0.58	0.20±0.07
1200	62.	4.1	160±0	45±0	356±2	128±1	172±1	114±1	0.99	8.4±0.0
1400	47.	40.	3±0	56±2	7±0	328±4	22±1	316±72	1.00	-

[f]denotes step in which fusion occurred.
R denotes re-extraction.

TABLE 4-E-IIi: Sample 7-27 - Basalt of North Fork Oak Creek (NFOC-51)

T,°C	^{40}Ar $cm^3STP\ g^{-1}$ $x10^8$	^{40}Ar(blank) $cm^3STP\ g^{-1}$ $x10^8$	39/40 $x10^4$	" 38/40 $x10^5$	37/40 $x10^5$	36/40 $x10^5$	$^{39}Ar/^{40}Ar$ $x10^4$	$^{36}Ar/^{40}Ar$ $x10^5$	^{39}Ar $\sum^{39}Ar$	model age, my
1300[f]	240.	16.	98±0	96±2	254±5	313±1	104±0	311±1	1.00	3.2±0.2

TABLE 4-E-IIj: Sample 7-54 - Granodiorite xenoliths from the basalt beneath the outer moraine, Sawmill Canyon (SC-110)

T,°C	^{40}Ar $cm^3STP\ g^{-1}$ $x10^8$	^{40}Ar(blank) $cm^3STP\ g^{-1}$ $x10^8$	39/40 $x10^4$	38/40 $x10^5$	37/40 $x10^5$	36/40 $x10^5$	$^{39}Ar/^{40}Ar$ $x10^4$	$^{36}Ar/^{40}Ar$ $x10^5$	^{39}Ar $\sum^{39}Ar$	model age, my
300	28.	1.3	5±0	68±1	1±0	335±1	5±0	336±1	0.01	3.1±1.3
500	10.	1.4	178±1	95±3	-4±1	320±2	192±1	320±2	0.14	0.52±0.07
600	3.6	1.4	494±5	139±7	44±5	303±5	758±8	288±10	0.26	0.37±0.08
~ 900	25.	1.4	259±0	70±1	20±0	177±1	255±0	168±1	0.72	3.7±0.0
950	36.	2.0	103±1	64±4	14±1	210±2	101±1	203±2	0.98	7.3±0.2
1400	18.	9.9	19±1	73±5	5±1	298±2	39±2	269±11	1.00	9.7±1.6
1750[f]	110.	64.	0±1	60±2	0±0	328±5	0±2	340±17	1.00	-

[f]denotes step in which fusion occurred.

TABLE 4-E-IIk: Sample 7-55 - Granodiorite xenoliths from the basalt beneath the outer moraine, Sawmill Canyon (SC-110)

T,°C	^{40}Ar $cm^3STP\ g^{-1}$ $x10^8$	^{40}Ar(blank) $cm^3STP\ g^{-1}$ $x10^8$	39/40 $x10^4$	38/40 $x10^5$	37/40 $x10^5$	36/40 $x10^5$	$^{39}Ar/^{40}Ar$ $x10^4$	$^{36}Ar/^{40}Ar$ $x10^5$	^{39}Ar $\sum^{39}Ar$	model age, my
275	30.	0.86	2±0	65±1	0±0	336±1	2±0	337±1	0.004	5.7±4.1
350	14.	0.86	14±0	68±1	2±1	333±2	14±0	333±2	0.02	2.2±0.8
425	4.8	0.86	140±1	87±3	13±2	324±3	156±1	322±5	0.06	0.56±0.18
500	3.6	0.86	317±2	107±2	34±4	310±4	380±3	303±7	0.14	0.51±0.10
600	2.3	0.86	592±2	138±3	48±5	292±3	851±3	270±9	0.23	0.45±0.06
725	2.2	0.86	637±4	145±4	62±5	283±3	958±6	251±10	0.33	0.50±0.06
900	4.0	0.78	567±2	135±2	43±3	242±2	643±2	219±4	0.48	1.02±0.04
1050	33.	12.	166±1	52±1	12±1	151±2	233±1	55±8	0.85	6.7±0.2
1750[f]	60.	68.	37±0	59±1	6±0	277±1	-	-	1.00	-

TABLE 4-E-IIℓ: Sample 7-60 - Granodiorite xenoliths, Sawmill Canyon (SC-113)

T,°C	^{40}Ar $cm^3STP\ g^{-1}$ $x10^8$	^{40}Ar(blank) $cm^3STP\ g^{-1}$ $x10^8$	39/40 $x10^4$	38/40 $x10^5$	37/40 $x10^5$	36/40 $x10^5$	$^{39}Ar/^{40}Ar$ $x10^4$	$^{36}Ar/^{40}Ar$ $x10^5$	^{39}Ar $\sum^{39}Ar$	model age, my
375	13.	0.38	19±1	66±1	2±0	337±1	17±1	337±1	0.01	0.3±0.4
500	14.	0.38	169±0	84±1	70±0	334±1	152±0	333±1	0.14	0.18±0.04
650	17.	0.38	233±0	90±1	59±1	318±1	209±0	318±1	0.34	0.54±0.02
875	17.	0.38	214±0	64±0	51±1	196±1	192±0	192±1	0.52	4.2±0.0
1050	25.	0.38	100±0	25±0	29±0	61±1	89±0	56±1	0.65	17.3±0.1
1450[f]	210.	35.	33±0	18±3	14±0	44±3	34±0	-12±6	1.00	55.4±0.7

[f]denotes step in which fusion occurred.

TABLE 4-E-IIm: Sample 7-61 - Granodiorite xenolith, Sawmill Canyon (SC-113)

T,°C	^{40}Ar $cm^3STP\ g^{-1}$ $x10^8$	^{40}Ar(blank) $cm^3STP\ g^{-1}$ $x10^8$	39/40 $x10^4$	38/40 $x10^5$	37/40 $x10^5$	36/40 $x10^5$	$^{39}Ar/^{40}Ar$ $x10^4$	$^{36}Ar/^{40}Ar$ $x10^5$	^{39}Ar $\sum^{39}Ar$	model age, my
375	20.	0.48	35±0	69±0	1±0	336±1	31±0	336±1	0.02	0.38±0.16
425	10.	0.48	149±0	83±1	5±0	333±1	137±0	333±1	0.07	0.22±0.04
500	12.	0.48	173±0	85±1	5±0	332±1	158±0	332±1	0.13	0.23±0.04
550	9.6	0.48	193±1	87±1	4±0	326±1	178±1	326±1	0.19	0.40±0.04
700	8.8	0.48	234±1	89±1	4±1	308±2	217±1	306±2	0.25	0.82±0.05
875	31.	0.48	201±1	56±2	4±0	152±9	179±1	149±9	0.44	5.9±0.3
1075	220.	0.48	47±0	10±0	1±0	24±1	41±0	23±1	0.76	41.9±0.2
1100	220.	0.54	32±0	7±0	1±0	16±1	28±0	16±1	0.98	62.1±0.4
1750[f]	38.	15.	18±0	32±1	1±0	148±6	26±1	20±11	1.00	66.1±2.7

TABLE 4-E-IIn: Sample 7-63 - Granodiorite xenolith, Sawmill Canyon (SC-118)

T,°C	^{40}Ar $cm^3STP\ g^{-1}$ $x10^8$	^{40}Ar(blank) $cm^3STP\ g^{-1}$ $x10^8$	39/40 $x10^4$	38/40 $x10^5$	37/40 $x10^5$	36/40 $x10^5$	$^{39}Ar/^{40}Ar$ $x10^4$	$^{36}Ar/^{40}Ar$ $x10^5$	^{39}Ar $\sum^{39}Ar$	model age, my
350	48.	0.95	8±0	99±10	5±1	334±1	7±0	334±1	0.03	3.5±1.2
500	6.8	0.95	141±1	96±10	89±5	337±3	142±1	337±3	0.09	0.07±0.13
600*	-	0.95	-	-	-	-	-	-	-	-
700	18.	0.95	116±0	74±2	81±1	332±1	106±0	331±1	0.24	0.37±0.08
700R	1.5	0.95	239±2	75±14	138±6	325±15	570±5	300±40	0.26	0.37±0.38
900	2.8	0.95	459±4	92±9	223±6	318±9	599±5	306±13	0.35	0.30±0.12
1000	3.1	0.95	605±2	101±15	192±4	256±8	753±3	218±11	0.48	0.88±0.08
1200	41.	1.4	163±1	37±1	97±1	77±1	146±1	67±1	0.94	10.2±0.1
1700	15.	7.9	56±0	56±2	35±1	245±4	102±1	142±7	1.00	10.6±0.4

*step lost
[f]denotes step in which fusion occurred.
R denotes re-extraction.

TABLE 4-E-IIo: Sample 7-80 - Granodiorite xenolith, Sawmill Canyon (SC-112)

T,°C	^{40}Ar $cm^3STP\ g^{-1}$ $x10^8$	^{40}Ar(blank) $cm^3STP\ g^{-1}$ $x10^8$	39/40 $x10^4$	38/40 $x10^5$	37/40 $x10^5$	36/40 $x10^5$	$^{39}Ar/^{40}Ar$ $x10^4$	$^{36}Ar/^{40}Ar$ $x10^5$	^{39}Ar $\sum^{39}Ar$	model age, my
350	13.	0.29	6±0	65±1	0±0	336±1	6±0	336±4	0.01	2.5±1.0
425	5.1	0.29	141±1	81±1	11±1	333±2	144±1	333±2	0.06	0.22±0.07
500	2.2	0.29	585±3	142±3	22±2	323±3	654±4	320±3	0.15	0.16±0.03
600	2.1	0.29	1256±3	228±3	45±3	309±2	1409±4	302±4	0.34	0.143±0.014
775	2.3	0.29	1063±3	202±3	28±2	315±2	1174±3	310±3	0.52	0.132±0.014
900	5.1	0.29	466±1	124±2	7±1	323±2	478±1	322±2	0.69	0.19±0.02
975	12.	0.29	120±1	82±1	3±0	321±1	168±1	321±1	0.84	0.59±0.03
1100	8.3	0.39	104±0	64±1	3±1	270±1	105±0	266±1	0.91	3.8±0.08
1750[f]	52.	15.	25±2	55±1	2±0	274±9	34±2	249±13	1.00	14.3±2.2

TABLE 4-E-IIp: Sample 7-82 - Granodiorite xenoliths, Sawmill Canyon (SC-115)

T,°C	^{40}Ar $cm^3STP\ g^{-1}$ $x10^8$	^{40}Ar(blank) $cm^3STP\ g^{-1}$ $x10^8$	39/40 $x10^4$	38/40 $x10^5$	37/40 $x10^5$	36/40 $x10^5$	$^{39}Ar/^{40}Ar$ $x10^4$	$^{36}Ar/^{40}Ar$ $x10^5$	^{39}Ar $\sum^{39}Ar$	model age, my
275	9.	0.36	4±0	65±1	2±0	338±1	3±0	338±1	0.00	-
350	4.8	0.36	22±0	77±3	2±1	330±3	21±0	330±4	0.01	2.3±1.0
425	2.3	0.36	295±1	99±2	15±2	289±3	316±1	279±4	0.04	1.0±0.1
500	1.1	0.36	991±2	182±4	45±5	282±4	1348±3	250±8	0.10	0.36±0.03
600	1.3	0.36	1729±104	262±8	64±3	281±10	2183±131	254±15	0.21	0.21±0.04
725	1.6	0.77	1506±6	261±4	67±3	290±4	2684±11	237±13	0.33	0.21±0.03
850	0.86	0.36	1728±7	283±4	-29±4	265±4	2720±11	213±11	0.41	0.25±0.02
~ 1000	2.6	0.36	924±2	157±2	26±1	153±2	968±2	122±3	0.53	1.24±0.02
1100	66.	0.46	121±1	251±4	5±0	41±4	110±1	39±9	0.94	14.9±0.5
1750	32.	36.	40±1	46±1	3±0	213±19			1.00	

[f]denotes step in which fusion occurred.

TABLE 4-E-IIq: Sample 7-83 - Granodiorite xenolith, Sawmill Canyon (SC-116)

T,°C	^{40}Ar $cm^3STP\ g^{-1}$ $x10^8$	^{40}Ar(blank) $cm^3STP\ g^{-1}$ $x10^8$	39/40 $x10^4$	38/40 $x10^5$	37/40 $x10^5$	36/40 $x10^5$	$^{39}Ar/^{40}Ar$ $x10^4$	$^{36}Ar/^{40}Ar$ $x10^5$	^{39}Ar $\sum^{39}Ar$	model age, my
350	69.	0.21	5±1	65±1	1±0	334±5	4±1	334±5	0.02	5.8±6.3
375	12.	0.21	31±0	66±1	4±0	327±1	28±0	327±1	0.04	2.2±0.2
425	6.6	0.21	144±1	77±1	14±1	306±2	130±1	304±2	0.09	1.46±0.07
375R	2.2	0.31	172±1	81±2	14±2	302±2	176±1	296±2	0.11	1.34±0.08
475	2.8	0.21	385±1	102±2	28±2	265±2	366±1	257±2	0.17	1.22±0.04
500	3.1	0.21	573±2	121±2	37±2	229±3	540±2	219±3	0.27	1.22±0.03
575	3.0	0.21	672±3	131±2	37±2	214±2	635±2	203±2	0.39	1.18±0.02
775	4.2	0.21	753±3	143±1	26±1	201±2	696±3	192±2	0.56	1.16±0.02
875	2.7	0.21	628±2	135±1	11±2	222±1	599±2	212±2	0.66	1.17±0.02
975	3.3	0.21	414±2	112±2	19±2	255±2	389±2	249±2	0.73	1.27±0.03
1050	44.	0.20	71±1	622±1	11±0	274±8	63±1	273±20	0.91	5.7±1.8
1125	59.	0.30	27±1	63±1	4±1	293±6	23±1	293±6	0.99	10.7±1.4
1400	17.	3.4	8±6	63±1	-7±1	330±11	9±7	330±14	1.00	5.2±9.1

TABLE 4-E-IIr: Sample 7-86 - Granodiorite xenolith, North Fork Oak Creek (NFOC-29)

T,°C	^{40}Ar $cm^3STP\ g^{-1}$ $x10^8$	^{40}Ar(blank) $cm^3STP\ g^{-1}$ $x10^8$	39/40 $x10^4$	38/40 $x10^5$	37/40 $x10^5$	36/40 $x10^5$	$^{39}Ar/^{40}Ar$ $x10^4$	$^{36}Ar/^{40}Ar$ $x10^5$	^{39}Ar $\sum^{39}Ar$	model age, my
350*	-	-	-	-	-	-	-	-	-	-
425	2.2	0.48	356±2	149±3	5±2	312±4	394±2	305±6	<0.02	0.47±0.08
500	2.2	0.48	869±3	227±4	13±2	298±3	962±3	286±5	<0.08	0.30±0.03
~ 1050	67.	0.48	300±1	101±50	9±5	161±6	261±1	159±7	<0.70	3.8±0.1
1100	73.	0.55	106±1	48±1	2±0	169±3	93±1	168±3	<0.94	10.1±0.2
1750[f]	40.	12.	52±1	54±1	1±0	239±6	64±1	197±9	<1.00	12.2±0.8

*step lost
[f]denotes step in which fusion occurred.
R denotes re-extraction.

TABLE 4-E-IIs: Sample 7-107 - Basalt, North Fork Oak Creek (NFOC-25)

T,°C	^{40}Ar $cm^3STP\ g^{-1}$ x10^8	^{40}Ar(blank) $cm^3STP\ g^{-1}$ x10^8	39/40 x10^4	38/40 x10^5	37/40 x10^5	36/40 x10^5	$^{39}Ar/^{40}Ar$ x10^4	$^{36}Ar/^{40}Ar$ x10^5	^{39}Ar $\sum^{39}Ar$	model age, my
1300[f]	240.	4.5	46±0	71±0	137±0	320±1	42±0	319±1	1.00	2.44±0.10

TABLE 4-E-IIt: Sample 9-1 - Granodiorite xenolith, Sawmill Canyon (SC-23)

T,°C	^{40}Ar $cm^3STP\ g^{-1}$ x10^8	^{40}Ar(blank) $cm^3STP\ g^{-1}$ x10^8	39/40 x10^4	38/40 x10^5	37/40 x10^5	36/40 x10^5	$^{39}Ar/^{40}Ar$ x10^4	$^{36}Ar/^{40}Ar$ x10^5	^{39}Ar $\sum^{39}Ar$	model age, my
400	13.	0.24	63±0	72±1	0±0	340±1	63±0	340±1	0.06	-0.1±0.1
500	7.8	0.24	161±1	85±1	1±1	334±1	162±1	334±1	0.15	0.18±0.05
600	2.7	0.24	573±2	139±2	3±2	322±2	615±2	320±3	0.27	0.19±0.03
725	0.72	0.24	2060±12	332±8	10±6	300±5	3020±18	281±9	0.38	0.12±0.02
900	1.0	0.24	1993±8	328±3	11±4	297±3	2536±10	284±6	0.53	0.13±0.01
1000	3.0	0.24	355±2	104±3	0±2	300±3	378±3	297±3	0.61	0.69±0.05
1400[f]	28.0	3.9	180±1	57±0	1±0	167±1	205±1	140±1	0.98	6.13±0.04
1750	21.0	13.0	15±2	89±5	0±0	314±5	37±5	279±16	1.00	9.9±3.0

[f]denotes step in which fusion occurred.

TABLE 4-E-IIu: Sample 9-2 - Granodiorite xenolith, Sawmill Canyon (SC-23)

T,°C	^{40}Ar $cm^3STP\ g^{-1}$ $x10^8$	^{40}Ar(blank) $cm^3STP\ g^{-1}$ $x10^8$	39/40 $x10^4$	38/40 $x10^5$	37/40 $x10^5$	36/40 $x10^5$	$^{39}Ar/^{40}Ar$ $x10^4$	$^{36}Ar/^{40}Ar$ $x10^5$	^{39}Ar $\sum^{39}Ar$	model age, my
300	3.1	0.97	15±1	97±4	6±2	332±3	22±1	336±6	0.002	0.7±1.6
600	35.	0.97	91±1	108±4	11±2	328±1	94±1	327±2	0.12	0.7±0.1
725	17.	0.97	377±2	136±2	12±1	333±1	401±2	330±2	0.36	0.13±0.04
900	2.7	0.97	1733±19	308±6	18±4	309±5	2700±29	291±10	0.53	0.11±0.02
~ 1100	22.	0.97	234±1	68±1	2±0	166±1	246±1	158±1	0.73	4.6±0.0
1400[f]	61.	6.7	119±1	30±2	1±0	110±14	134±1	83±16	1.00	12.0±0.7
1750	48.	29.	1±2	24±47	0±1	326±5	1±5	336±18	1.00	-

TABLE 4-E-IIv: Sample 9-4 - Granodiorite xenolith, Sawmill Canyon (SC-1b)

T,°C	^{40}Ar $cm^3STP\ g^{-1}$ $x10^8$	^{40}Ar(blank) $cm^3STP\ g^{-1}$ $x10^8$	39/40 $x10^4$	38/40 $x10^5$	37/40 $x10^5$	36/40 $x10^5$	$^{39}Ar/^{40}Ar$ $x10^4$	$^{36}Ar/^{40}Ar$ $x10^5$	^{39}Ar $\sum^{39}Ar$	model age, my
300	37.	2.3	6±0	70±3	0±1	336±2	6±0	336±2	0.01	2.8±1.8
500	22.	2.3	407±23	205±8	11±2	330±29	458±26	329±33	0.28	0.13±0.45
600	6.9	2.3	1158±9	221±8	31±1	323±3	1740±14	313±6	0.52	0.09±0.02
725	7.3	2.3	676±135	157±4	6±3	316±5	990±198	307±8	0.67	0.20±0.06
825	19.	2.3	257±1	105±2	2±1	299±2	295±1	294±2	0.82	0.95±0.05
950	48.	2.3	95±1	73±3	2±1	259±1	101±1	255±2	0.96	5.2±0.1
1400	34.	18.	32±1	61±8	2±1	292±2	68±2	244±5	0.99	8.8±0.5
1750	150.	76.	4±5	458±8	91±5	331±9	9±11	327±19	1.00	-

[f]denotes step in which fusion occurred.

TABLE 4-E-IIw: Sample 9-5 - Granodiorite xenolith, Sawmill Canyon (SC-1b)

T,°C	^{40}Ar $cm^3STP\ g^{-1}$ $x10^8$	^{40}Ar(blank) $cm^3STP\ g^{-1}$ $x10^8$	39/40 $x10^4$	38/40 $x10^5$	37/40 $x10^5$	36/40 $x10^5$	$^{39}Ar/^{40}Ar$ $x10^4$	$^{36}Ar/^{40}Ar$ $x10^5$	^{39}Ar $\sum^{39}Ar$	model age, my
275	57.	2.4	2±0	64±1	0±0	336±1	2±0	337±1	0.004	5.5±4.3
350	24.	2.4	16±0	67±1	1±1	333±1	18±0	334±2	0.02	1.7±0.6
475	11.	2.4	409±2	122±1	3±2	327±2	508±2	326±3	0.15	0.15±0.04
600	11.	2.4	1226±2	229±2	3±1	313±2	1533±3	308±4	0.56	0.12±0.02
725	16.	2.4	497±2	133±1	3±1	279±1	573±2	271±2	0.79	0.75±0.02
900	28.	2.4	155±1	73±1	1±2	254±1	166±1	247±2	0.92	3.5±0.1
1400	47.	10.	55±1	62±1	1±0	273±3	69±1	257±4	1.00	7.4±0.4
1750	100.	72.	0±1	62±1	0±0	325±1	0±4	317±16	1.00	-

TABLE 4-E-IIx: Sample 9-6 - Microcline from xenolith, Sawmill Canyon (SC-23)

T,°C	^{40}Ar $cm^3STP\ g^{-1}$ $x10^8$	^{40}Ar(blank) $cm^3STP\ g^{-1}$ $x10^8$	39/40 $x10^4$	38/40 $x10^5$	37/40 $x10^5$	36/40 $x10^5$	$^{39}Ar/^{40}Ar$ $x10^4$	$^{36}Ar/^{40}Ar$ $x10^5$	^{39}Ar $\sum^{39}Ar$	model age, my
350	29.	0.09	5±0	70±21	0±0	338±1	5±0	338±1	0.01	0.8±0.9
425	7.4	0.09	257±1	116±3	14±1	316±2	275±1	315±2	0.07	0.5±0.0
600	4.1	0.09	831±3	163±2	64±1	237±1	896±3	235±2	0.18	0.7±0.0
750	6.2	0.09	377±1	75±0	28±1	110±1	403±1	107±1	0.26	3.6±0.0
900	110.	0.09	48±0	10±0	2±0	17±3	51±0	16±3	0.43	39.7±0.5
1100	810.	0.09	20±0	5±0	1±0	6±0	21±0	6±0	0.95	98.7±0.2
1300	81.	9.4	15±0	11±1	3±0	31±1	18±0	-8±2	1.00	116.1±1.9
1600	28.	19.	5±0	58±1	48±7	259±1	16±1	87±22	1.00	94.4±5.3

TABLE 4-E-11y: Sample 9-9 - Granitic xenolith, Black Point (BPt-11)

T,°C	^{40}Ar $cm^3STP\ g^{-1}$ $x10^8$	^{40}Ar(blank) $cm^3STP\ g^{-1}$ $x10^8$	39/40 $x10^4$	38/40 $x10^5$	37/40 $x10^5$	36/40 $x10^5$	$^{39}Ar/^{40}Ar$ $x10^4$	$^{36}Ar/^{40}Ar$ $x10^5$	^{39}Ar $\sum^{39}Ar$	model age, my
325	59.	0.31	8±0	66±3	6±0	339±5	8±0	339±5	0.02	-
425	19.	0.31	50±1	81±1	22±1	335±0	51±1	335±0	0.06	0.47±0.07
525	9.8	0.31	140±1	94±1	76±1	329±1	145±1	329±1	0.13	0.41±0.06
675	4.6	0.31	331±1	108±2	169±3	330±2	357±1	330±2	0.20	0.15±0.03
1100	7.1	0.31	734±45	166±4	243±17	297±2	771±47	297±2	0.44	0.34±0.03
1325[f]	53.	1.1	169±2	46±2	68±4	109±5	174±2	109±5	0.84	8.3±0.2
1400	33.	4.5	92±1	29±1	48±2	45±6	107±1	45±6	0.98	17.2±0.4
1500	16.	2.3	24±0	55±2	13±1	215±9	44±0	215±9	1.00	17.8±1.3

TABLE 4-E-11z: Sample 9-20 - Basalt, Taboose Canyon (Tab-201)

T,°C	^{40}Ar $cm^3STP\ g^{-1}$ $x10^8$	^{40}Ar(blank) $cm^3STP\ g^{-1}$ $x10^8$	39/40 $x10^4$	38/40 $x10^5$	37/40 $x10^5$	36/40 $x10^5$	$^{39}Ar/^{40}Ar$ $x10^4$	$^{36}Ar/^{40}Ar$ $x10^5$	^{39}Ar $\sum^{39}Ar$	model age, my
1300[f]	11.	2.7	614±1	304±2	1407±4	342±1	838±2	330±11	1.00	0.065±0.079

[f]denotes step in which fusion occurred.

TABLE 4-E-[Iaa: Sample 9-32 - Microcline xenolith, Fossil Falls (FF-101)

T,°C	^{40}Ar $cm^3STP\ g^{-1}$ $x10^8$	^{40}Ar(blank) $cm^3STP\ g^{-1}$ $x10^8$	39/40 $x10^4$	38/40 $x10^5$	37/40 $x10^5$	36/40 $x10^5$	$^{39}Ar/^{40}Ar$ $x10^4$	$^{36}Ar/^{40}Ar$ $x10^5$	^{39}Ar $\sum^{39}Ar$	model age, my
325	134.	0.42	0±0	63±1	0±0	340±1	0±0	340±1	0.000	-
400	20.	0.42	2±0	64±1	62±4	334±1	2±0	334±1	0.001	18.3±4.0
500	4.2	0.43	19±0	65±4	6±2	334±2	21±0	334±3	0.002	1.3±0.8
650	7.5	0.45	36±0	8±2	62±2	337±1	39±0	337±2	0.007	0.2±0.3
800	4.3	0.46	108±0	75±4	7±2	333±2	123±0	333±3	0.016	0.3±0.1
900	5.5	0.48	219±0	90±3	10±2	328±2	245±0	327±3	0.037	0.3±0.1
1000	5.0	0.66	401±1	114±4	15±2	320±2	470±1	317±3	0.074	0.29±0.04
1150	2.8	1.0	2020±3	322±4	68±4	298±2	3278±5	274±7	0.18	0.12±0.01
1290	9.0	1.5	861±3	155±2	29±1	220±2	1051±4	197±3	0.32	0.85±0.02
1400	41.	6.4	913±2	162±5	30±1	234±7	1101±2	215±9	1.00	0.71±0.05

PART II

QUATERNARY GEOLOGY

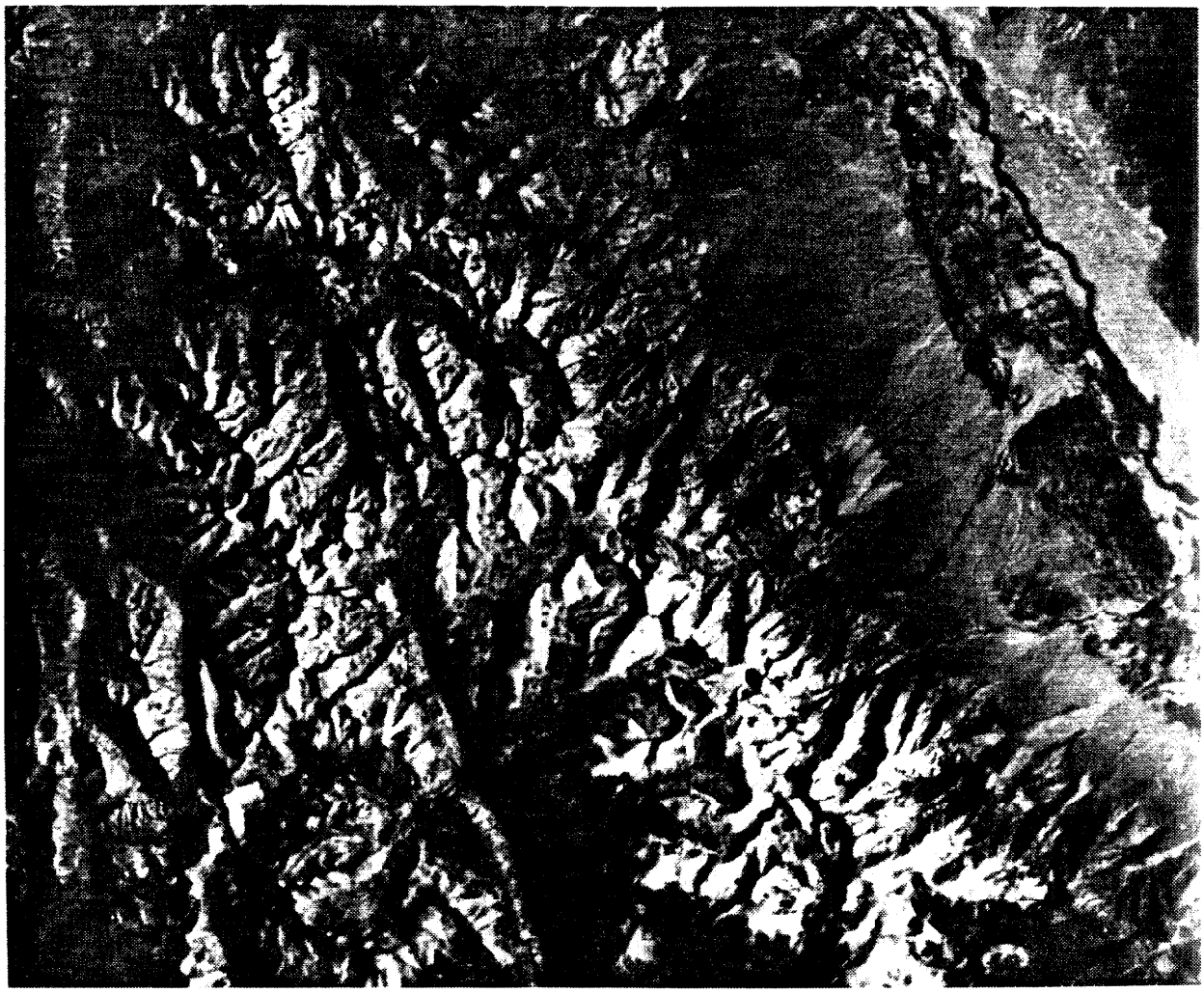

The southeastern Sierra Nevada from orbit. The Owens Valley from Independence (top) south to Lone Pine and the Alabama Hills contrasts markedly with the rugged glaciated Sierra. The irregular eastern margin of the mountains is a 2-km-high escarpment developed along a series of normal faults. A second escarpment of comparable relief lies buried under the alluvium in the central Owens Valley. The major drainage near the top is the South Fork of the Kings River. The large canyon parallel to the escarpment at the bottom of the image is the canyon of the Kern River. The adjacent round feature is the Kaweah range, a Tertiary volcanic complex. The study area is east of the Sierra crest, near the top of the image. Both forks of Oak Creek and Onion Valley may be seen. North is towards the top of the NASA Landsat MSS image. The scale is ~ 1:275,000.

CHAPTER 5

QUATERNARY GEOLOGY: FIELD RELATIONS

Geologic mapping covered the region from the Sierra Nevada crest east to the distal ends of the alluvial fans, and from Independence Creek north to Taboose Creek. The area studied included about 400 km^2, but investigation focused mainly on the canyons, fan heads, and the zone of the range-front fault. Only Quaternary and late Tertiary geology was mapped, to minimize duplication of J.G. Moore's earlier mapping of the Mount Pinchot Quadrangle (Moore, 1963). Field work was concentrated in two four-month periods during the summers of 1978 and 1979. The discussion below is organized geographically, by canyon, and from south to north. Discussion is focused on Onion Valley, because of the well preserved and accessible sequence of Pleistocene moraines, and on Sawmill Canyon, because of the interbedded lavas and tills and of their importance in understanding the chronology of Quaternary processes and events in the southeastern Sierra Nevada. A generalized geologic map at a scale of 1:62,500 is found in Plate I. Maps of the bedrock geology at the same scale are found in Moore (1963), Bateman (1965), and Moore (1981). Ross (1965) has mapped the geology of the Independence Quadrangle, which includes the distal ends of the fans of the western side of the Owens Valley. More detailed maps of Quaternary deposits at scales of about 1:25,000 are presented with the discussions of individual valleys. A map and profiles of the Sierra crest and details of the eastern escarpment of the Sierra Nevada are found in Plate II.

5.1 ONION VALLEY

Introduction

The glaciers of Onion Valley were the southernmost late Pleistocene glaciers of the eastern Sierra Nevada to cross the range-front fault system. The lowest of these terminated at the top of the broad coalescing alluvial fans that flank the 2-km-high escarpment. The moraines left by these glaciers serve as time markers with which to measure offset and erosion rates. Onion Valley is particularly attractive for this purpose, because the sequence of moraines and glacial outwash is unusually complete and because the valley has good access. Quaternary deposits are well exposed in numerous road cuts.

In this study Onion Valley is regarded as that reach of the canyon of Independence Creek occupied by trunk glaciers during the late Pleistocene Epoch. The trunk glaciers were formed of three tributary glaciers confluent at the present-day meadow at the end of the Onion Valley Road, at an elevation of 2800 m (9180 ft). In upper Onion Valley, Independence Creek flows through a broad trough only slightly incised by running water since the retreat of the last glacier. Largely intact bouldery moraines flank the freshly cut cliffs. This trough is typical of recently glaciated canyons in crystalline rocks. Figure 5-1 illustrates the characteristic U-shaped cross section, the oversteepened cliffs along the canyon sides, and the lack of incision by the post-glacial river.

About 1700 m east of the confluence, Independence Creek turns northeast and its gradient steepens. The incision of the stream through the ground till and outwash increases to ~ 10 m, and the lateral moraines

Fig. 5-1. Onion Valley from the southeast. This photograph shows the upper valley, last occupied by the glaciers of the Tioga stage at the end of the Pleistocene Epoch perhaps 11,000 y ago. The steep cliffs and U-shaped trough are especially well developed. Independence Creek has incised the floor of the valley to a depth of only ~ 4 m since the retreat of the glaciers. Boulders in the right foreground are on the flank of a Tioga moraine. The unnamed peak in the center background is on the crest of the Sierra Nevada.

are less bouldery than their counterparts in the upper valley. They are also deeply cut by ravines. The stream drops 850 m through the escarpment in 2.9 km. At 1950 m (6400 ft) elevation Independence Creek emerges from between the lowest of the lateral moraines onto the alluvial fan. For another 3 km the river flows against low foothills which bound the upper portion of the fan on the north. Below 1585 m (5200 ft) elevation, these foothills are themselves submerged beneath the coalescing fans of Independence Creek and of the South Fork of Oak Creek.

Independence Creek heads at a broad and low U-shaped notch in the crest of the Sierra (Kearsarge Pass). This notch has the cross-section of a glaciated valley, and in the early Pleistocene Epoch or late Pliocene Epoch a large crest-crossing glacier may have flowed into the headwaters of Independence Creek from the west. By the late Pleistocene Epoch, the floor of this hypothetical valley had been plucked from the east and from the west until only the narrow arete of Kearsarge Pass remained. Certainly the most recent glaciers did not overtop this ridge.

A brief summary of the bedrock geology is presented below. In the discussion which then follows, the Quaternary geology of the drainage basin of Independence Creek is divided into five topics: (1) geology of the alluvial fan of Independence Creek; (2) geology of the foothills; (3) late Pleistocene moraines of Onion Valley and the geology of the three tributary canyons above Onion Valley; (4) age of the fan; and (5) evidence for episodic faulting along the range-front faults.

Summary of Bedrock Geology Along Independence Creek

For convenient reference, some aspects of the bedrock geology along

Independence Creek originally reported by Moore (1963) are summarized below.

Most of the main fork of Independence Creek and all of its principal southern tributary are cut into a single pluton of alaskitic quartz monzonite--the Bullfrog pluton. This rock contains only 1.8% biotite (by volume), on the average. Grain size is about 5 mm. The rock is coarsely jointed and, as Moore points out, not too susceptible to glacial plucking. It therefore forms large domes and peaks. In the southern tributary, Bullfrog quartz monzonite is relatively enriched in biotite (to as much as 6.2%) and impoverished in quartz. The increase in the amount of biotite probably renders the rock more easily weathered.

Separating the Bullfrog quartz monzonite from other granitic rocks to the east is an older mafic pluton, about 1 km wide. The northern tributary is largely cut into this pluton. Rock types within the pluton near Onion Valley are chiefly quartz diorite and hornblende diorite.

Upper Onion Valley is cut into the mafic pluton and into the Dragon granodiorite. This latter rock is quartz-poor and rich in mafic minerals. It is susceptible to glacial erosion and forms basins and low passes. It is probably unsuitable for relative age dating.

Lower Onion Valley is cut into Tinemaha granodiorite, which is slightly porphyritic. This pluton is cut by the numerous dikes of the Independence swarm. Separating the Dragon and Tinemaha plutons on the north wall of Onion Valley is about 500 m of metarhyolite and quartz monzonite of the Sardine pluton.

The foothills east of the Independence fault consist of metaandesite and quartz monzonite of the Independence pluton. The quartz

monzonite is enriched in K-feldspar compared to the Bullfrog quartz monzonite.

The Alluvial Fan of Independence Creek

Description

The alluvial fan of Independence Creek covers an area of 20 km^2 from its head at the mouth of the canyon at the Sierra Nevada range front to the distal end in the alluvium of the Owens River. Its surface (Fig. 5-2) forms a smooth concave arc, with slopes from 2.5° at its eastern end to 6.3° at its western head. The fan does not appear to be segmented, and no scarps are found east of the foothills. The major part of the fan is covered by granitic sand, fragments, and boulders up to several meters in diameter. The modal boulder size appears to decrease with distance down the fan, but to the eye the boulders appear remarkably similar in their degree of weathering. Few heavily weathered or disintegrating boulders are encountered, but glacially abraded surfaces have already been removed by weathering.

Along traverses perpendicular to Independence Creek east of the foothills, visual inspection revealed no obvious differences in the extent of weathering of boulders on the fan surface, and in general the fan appeared to be homogeneous. However, within the foothill block levees containing fresher boulders as large as 5 meters in diameter were found near Independence Creek. These appear to have been deposited by debris flows that may have followed the melting of the last glaciers of the Pleistocene, when there was an abundance of water to move such rocks.

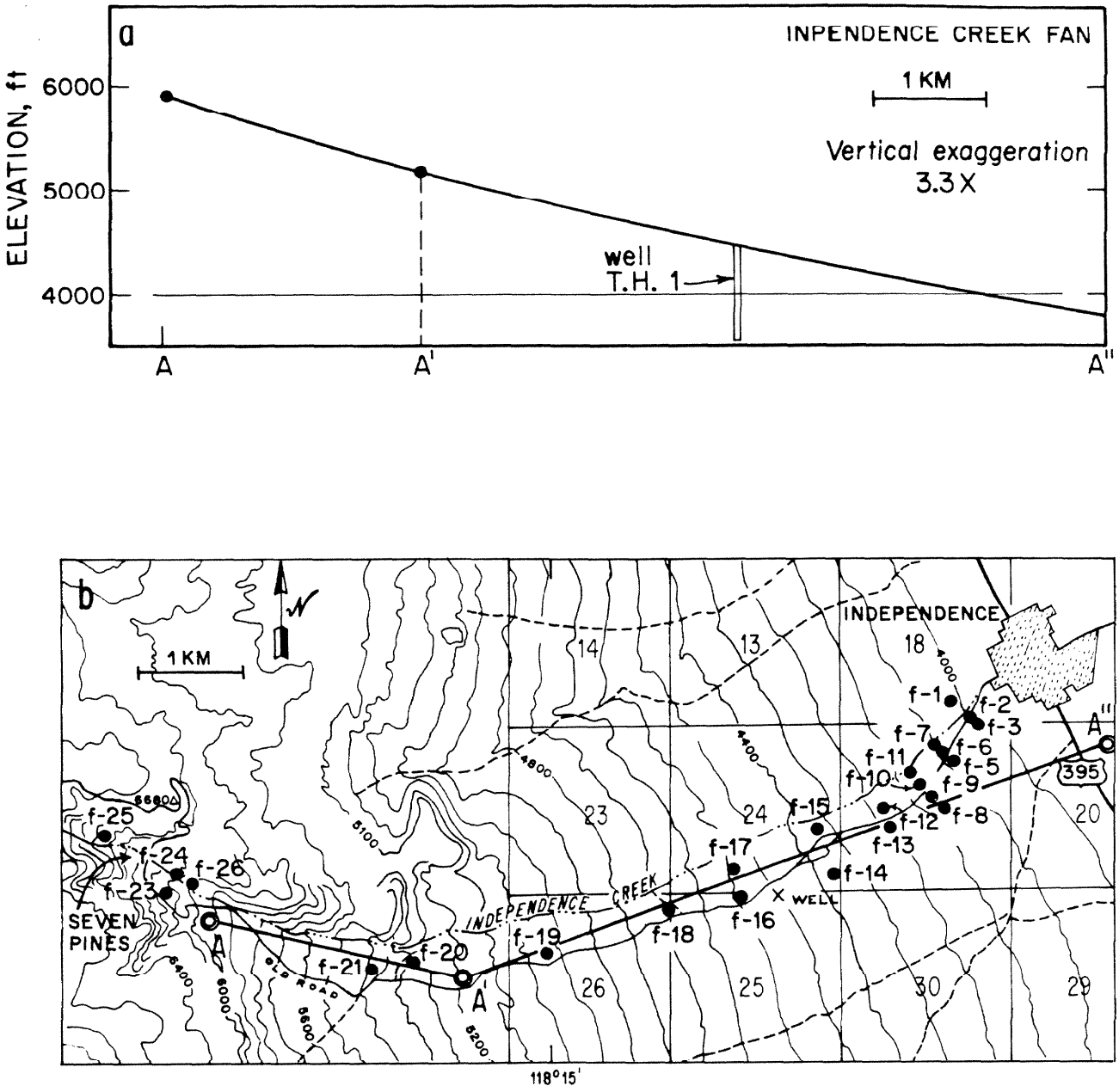

Fig. 5-2. The alluvial fan of Independence Creek. Topographic data are from the U. S. Geol. Survey, Mt. Pinchot Quadrangle (1953) and Independence Quadrangle (1951). The scale is 1:62,500, and contour intervals are 80 ft or 24.4 m.

a) Longitudinal profile of the alluvial fan of Independence Creek (vertical exaggeration is 3.3x). The surface of the fan forms a smooth concave arc, with slopes ranging from 2.5° to 6.3°.

b) Location of the longitudinal profile and locations of sites where relative weathering data were collected on the fan and outwash. The location of a water well, T.H. 1, drilled 280 m into the fan is marked by "X" (Los Angeles Dept. of Water and Power, 1978).

To detect boundaries in the age of fanglomerate along the profile of Fig. 5-2, the frequencies of fresh and weathered boulders (Ch. 2) were estimated at several sites (Fig. 5-2b). These semi-quantitative measurements are summarized in Table 5-1. Granodiorite weathering ratios (GWR) and boulder burial or boulder relief ratios (BR) are plotted in Fig. 5-3. The GWR values define two distinct clusters. From this it may be inferred that the fan contains at least two regions, each with a distinctive abundance of weathered boulders.

The lowest of the two regions is found east of the foothills. Here, as seen on Fig. 5-3a, 60% of the boulders were "heavily weathered", although no cavernous boulders were found. Less than 5% appeared to have remnants of abraded surfaces. The remainder had lost their abraded surfaces but showed no evidence of deep weathering; e.g., surfaces were not grusy, and joints, aplite dikes, and diorite inclusions did not stand in relief to the surface of the boulder.

The second zone contains the fan head. Heavily weathered boulders were more abundant than lower on the fan and comprised 85% of the total. Only 1% could be considered fresh. Student's t-test could be used to test the significance of the differences between the two clusters of GWR values, because the data were from normally distributed populations (Fig. 5-4). These two clusters consisted of a total of 15 GWR values (13 degrees of freedom). The value of t was found to be 3.77, so the populations from which the samples were drawn were different with more than 99% confidence (with 13 degrees of freedom, t must exceed 3.05 for this to be true). Thus it appears that the upper part of the fan is significantly more weathered and hence probably older than the lower part.

Table 5-1

Relative Weathering Data for Boulders in the Independence Creek Alluvial Fan

Site	Boulder Abundance* m^{-2}	No. of Boulders Counted**	Granodiorite Weathering Ratio (GWR)*†	Granodiorite Boulder Relief (BR)†*	Boulder Type MGR†	Maximum Diameter cm	Average Diameter†† cm
f-1	0.66	66	52/44/5	83/16/2	7/84/9	117	28
f-2	0.54	54	61/32/7	80/17/4	8/78/14	61	33
f-3	0.02	-	-	-	-	84	15
f-5	<0.14	-	-	-	-	69	20
f-6	0.46	34	68/29/3	63/20/17	11/80/9	107	36
f-7	0.50	45	78/20/2	30/40/30	8/88/4	130	28
f-8	<0.21	-	-	-	-	76	15
f-9	0.04	4	-	-	-	147	8
f-10	0.30	30	50/47/3	67/23/10	3/94/3	165	-
f-11	2.24	47	34/66/0	26/43/32	11/84/5	188	-
f-12	<0.07	-	-	-	-	427	-
f-13	0.16	57	61/32/7	-	-	122	-
f-14	0.06	54	69/26/6	-	-	234	-
f-15	0.54	63	60/33/6	42/45/13	12/78/10	366	-
f-16	0.14	57	63/32/5	-	-	381	-
f-17	0.49	50	80/16/4	58/34/8	12/84/4	305	-
f-18	0.45	59	85/15/0	85/ 8/7	2/92/6	231	-
f-19	0.47	52	96/ 4/0	82/14/4	2/94/4	191	-
f-20	~0.60	46	78/10/2	33/58/8	2/96/2	183	-
f-21	0.55	55	85/15/0	85/13/2	17/78/6	74	-
f-22	0;2.0	54	-	-	-	206	-
f-23	0	-	-	-	-	-	-
f-24	0	-	-	-	-	-	-
f-25	~0.70	55	64/27/9	9/18/73	14/82/4	244	-
f-26	0.53	62	66/31/3	79/17/4	17/79/4	-	-

* Boulders are considered to have intermediate axes longer than 30 cm.

** Number counted for the granodiorite weathering ratio

*† Granodiorite Weathering Ratio: granodiorite or quartz monzonite boulders are classified as heavily weathered, weathered, or fresh (see Ch. 2). The tabulated numbers are the relative abundance (in %) in each category (in sequence).

†* Granodiorite Boulder Relief: boulders counted for the GWR are classified as largely buried, partly buried, or exposed. "Largely buried" boulders are no more than one-quarter exposed. "Exposed" boulders are no more than one-quarter buried (see Ch. 2). The tabulated numbers are the relative abundance (in %) in each category (in sequence).

† Boulder type: Matic, Granitic, or "Resistate" (see Ch. 2). Mafic boulders are ultramafic rocks or rocks having more than 10% mafic minerals. Granitic rocks are granodiorites or quartz monzonites. "Resistates" include fine-grained granitic rocks (e.g., aplites) and metavolcanic rocks. Only metavolcanic and plutonic rocks are counted.

†† Estimated value

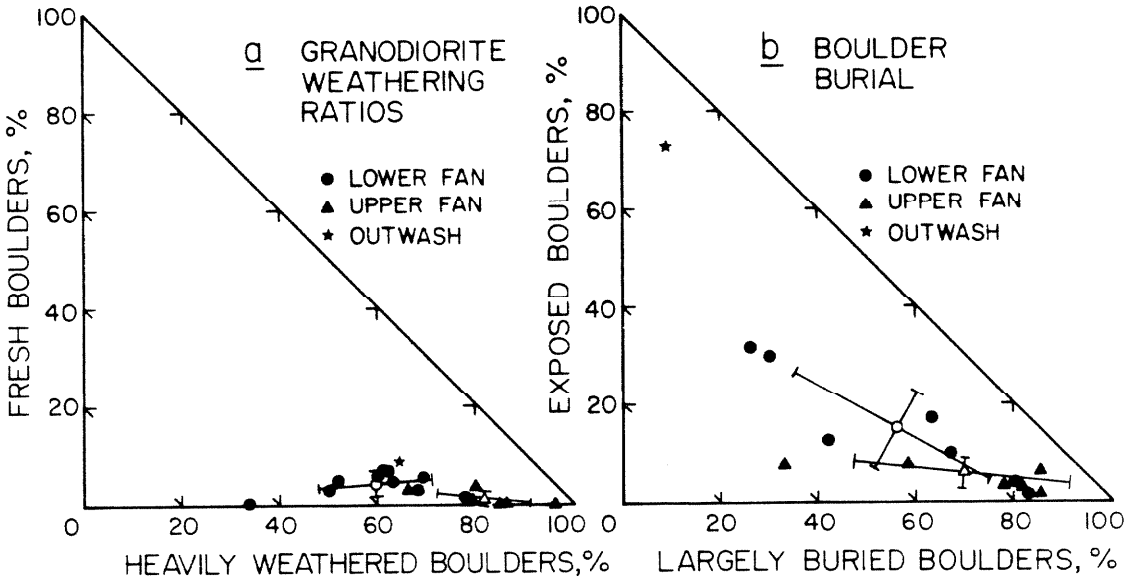

Fig. 5-3. Distribution of relative weathering data for boulders on the alluvial fan of Independence Creek.

a) Granodiorite weathering ratios (GWR) for boulders from 17 sites (ten sites on the lower fan, six sites on the upper fan, and one site on the outwash head) define two distinct clusters. Normal populations defined by the samples are shown with an open circle or triangle for the mean and 1σ error bars. The two populations are separable with >99% confidence. The outwash sample is 1.5 σ from the mean of the sites of the lower fan, but 2.7 σ from the mean of the sites of the upper fan.

b) The degree of burial of boulders ("boulder relief") in the fan surface is depicted. Clusters of sites grouped by GWR values are not distinct in this presentation and cannot be separated with 90% confidence or more.

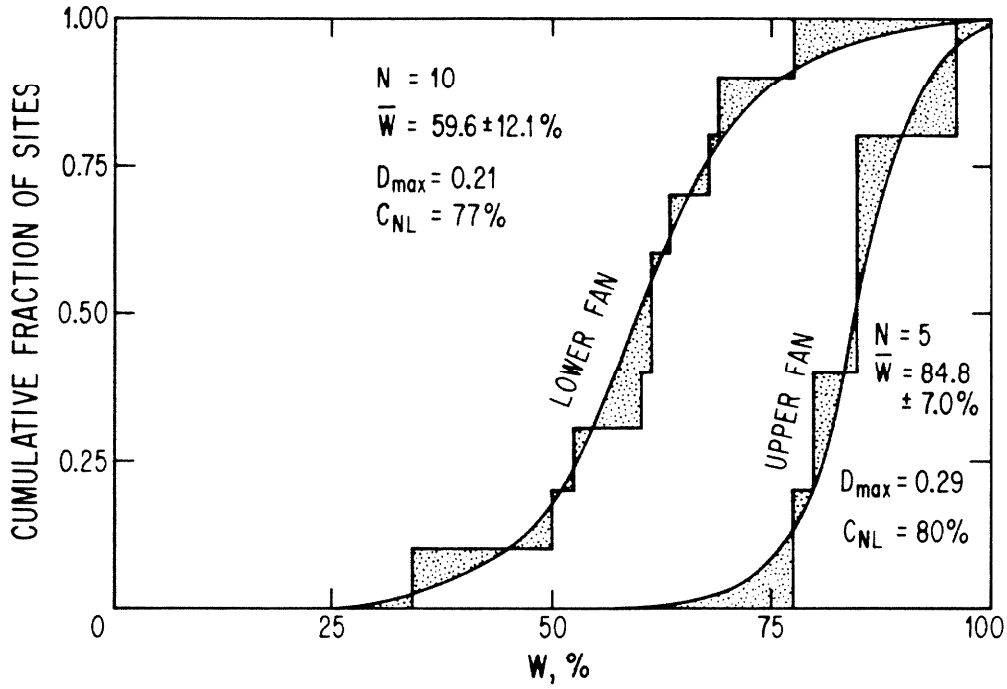

Fig. 5-4. One-sample Kolmogorov-Smirnov test for normality of the distribution of the proportion of boulders which are heavily weathered ("W"), for two groups of sites on the alluvial fan of Independence Creek. C_{NL} is the confidence with which the hypothesis that observed distributions result from sampling normal populations may be rejected. C_{NL} is found from D_{max} (Fig. 3-A-1b), the maximum difference between ordinate values of the cumulative distributions of the normal populations estimated from the samples (smooth curves) and the samples themselves (stepped curves). The test shows that the proportions of weathered boulders at sites on the upper fan and the lower fan are both normally distributed.

No other measured parameter shows two distinct clusters. The degree of burial of boulders in the fan surface, shown in Fig. 5-3b, cannot be used to separate the same groups of sites with more than 90% confidence ($t = 1.73$; 11 degrees of freedom). The correlation between the relative frequencies of heavily weathered and deeply buried boulders is poor ($r = 0.3$). Figure 5-5a shows that the relative abundance of deeply buried boulders is also uncorrelated with the distance down the fan, and it seems that this parameter reflects local abundance of fluvial sands and gravels more than age or some systematic spatial trend.

Like the depth of boulder burial, the maximum diameter of boulders shows no obvious correlations with distance down the fan (Fig. 5-5b), except perhaps for a tendency towards smaller boulders at the distal end of the fan, where the gradient is only 2.5°. The largest boulders seem to be found in the middle elevations of the fan, but this could be a sampling artifact. Large boulders are encountered closer to the bridge on levees along Independence Creek and elsewhere, but their distribution is irregular. Perhaps this may be attributed to the infrequent occurrence of stream floods large enough to transport meters 2 m or more in diameter.

The distribution of rock types over the fan was very uniform. Only 8% of the boulders were mafic, while 86% were quartz monzonite or granodiorite. The remaining 6% were "resistates", chiefly granitic dike rocks or metavolcanic boulders. Sharp (1969, 1972) has argued that the ratio of granitic boulders to "resistates" decreases with age as the granitic rocks disintegrate. Apparently most of the fan is sufficiently young that this process has not yet begun. The boulder abundance showed no

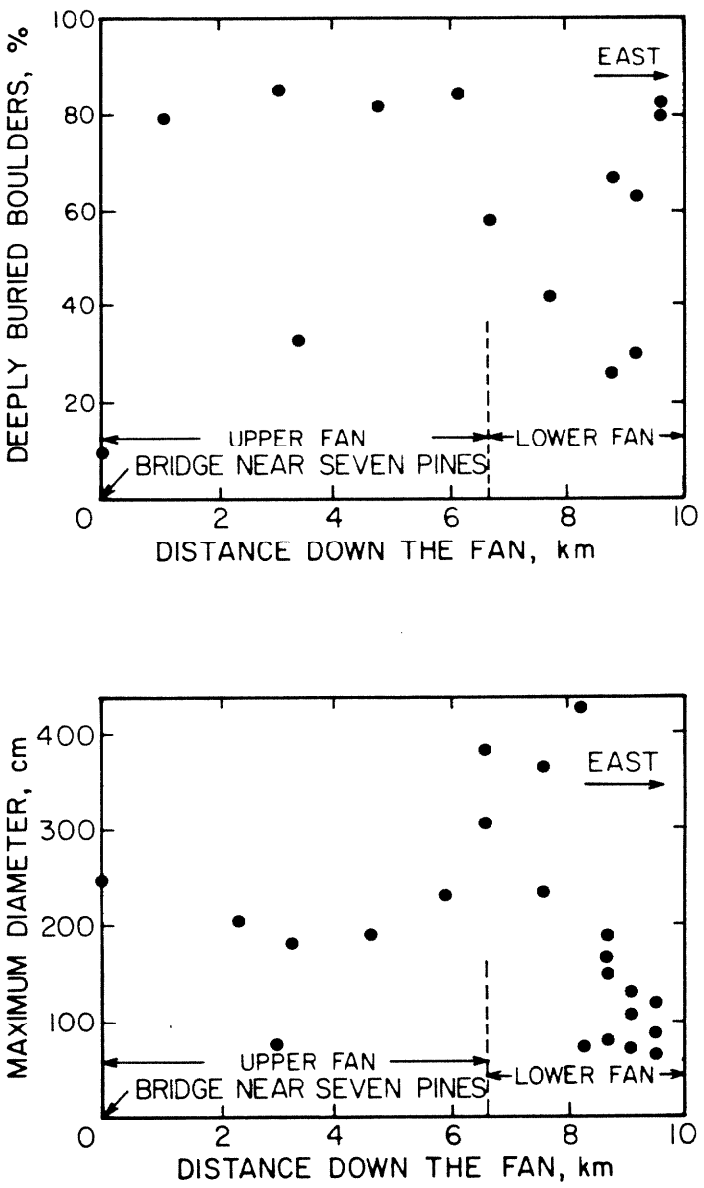

Fig. 5-5. The fraction of boulders which are deeply buried in the fan surface (top) and the estimated maximum diameter (bottom) are plotted against the distance down the fan (measured eastward from the bridge on the new Onion Valley road west of Seven Pines). No trend in the degree of burial is seen.

Although the variation in maximum diameter shows more order than the variation in the degree of boulder burial, there are no obvious trends except at the distal (eastern) end of the fan, where the boulder size decreases. The largest boulders are found at the contact (as defined by the GWR values) between the lower and upper fan.

obvious trends, either. It seems likely that heterogeneous deposition of sand and gravel in channels now abandoned has obscured any trends, if such existed.

Site f-25 was on the boulder terrace between the glacial moraines at the head of the fan. As seen on Fig 5-3a, the GWR is not significantly different from GWR values for the lower fan. Thus the lower fan and the outwash appear to be roughly coeval.

A third surface is found in the lee of the bedrock hill just east of the confluence of Piñon and Lime Creeks. This small region is characterized by few boulders and a somewhat redder soil. This is the oldest deposit on the active fan. The contrast with the younger fanglomerate encroaching from the north and south is unmistakable.

The old surface occupies a topographic low region, about 9 m below the adjacent fan. If this surface dates from the Sangamon interglacial period (~ 0.1 my BP), then an average aggradation rate of only 0.09 mm/y is indicated. This is certainly a low value, because the surrounding fan has not been active for some time; it is the older of the surfaces discussed above. If the adjacent fan were of early Wisconsin age, then the rate might be as much as a factor of four greater. The Milner Creek fan on the west side of the White Mountains north of Bishop, California, appears to have grown at about 0.075-0.150 mm/yr since 0.7 my BP (Beaty, 1970).

The depth of the oldest surface below the fan's current surface in the lee of the bedrock hill may not be representative of the average depth elsewhere. Independence Creek has incised about 10 m into the fan, but no evidence of a paleosol was found even in good exposures on road

cuts in the embankment.

Large granitic boulders several meters in diameter are perched atop the bedrock hill that shields the ancient fan surface east of the confluence of Piñon and Lime Creeks. These are several meters above the current fan surface, and in the absence of any evidence of degradation of the fan, are taken to be relics of ancient debris flows such as those which left the levees with similar boulders near the current Independence Creek.

Incision of Independence Creek is greatest where its fan lies within the foothill block. At the western end of the fan this is not obvious, because the new surface is rather wide (Grays Meadow) and its margins are somewhat irregular. However, a remnant of the older fan surface has been left as an "island" between channels of Independence Creek just east of Seven Pines. The top of this remnant, 6.5 m above the meadow, shows the amount of incision of the fan head since deposition of the older fan.

Below Grays Meadow the stream channel narrows. Incision is about 10 m until the stream crosses the eastern boundary of the foothill block. Farther down the fan, incision lessens until the the stream flows within 2 m of the fan's surface near the contact between the two fanglomerates of different age. Thus, Independence Creek appears to be most deeply incised into the older fan.

No fault scarps were found anywhere on the Independence Creek fan. Thus in the late Quaternary Period, faulting does not seem to have occurred within the foothill block, but has instead been restricted to the range front (Independence Fault) or to the mid-valley fault (the Owens Valley fault zone which ruptured in the 1872 earthquake).

Discussion

In addition to the meadows and fluvial deposits of the current Independence Creek, there are at least three different ages of fanglomerates on the Independence Creek fan. As seen on Plate I, the youngest of these is found in the lower, eastern part of the fan. Thus the boulders and gravels must have been shuttled through the older fan along an incised Independence Creek rather than moved over its surface by sheet floods (cf. Davis, 1938). This pattern was observed in other canyons, also. Such a situation could generally arise in one of several ways: (1) because of faulting, the headward portion of a fan may be uplifted and incised, with a new fan being constructed below the scarp; (2) because of a change in climate, the efficiency of the stream may be increased such that the upper and steeper part of the fan is degraded, with aggradation beginning at a lower elevation (cf. Mabbutt, 1977); (3) because of headward erosion of the stream, its channel is deepened everywhere, leading to fan-head incision even in the absence of continued faulting or climatic change; or (4) because of regional tilting, the gradient of the stream may be increased, resulting in fan-head incision and redeposition of the eroded fanglomerate farther from the mountain front (cf. Hooke, 1972).

With so many possibilities, it is not now possible to identify a single cause for the observed incision of the head of the Independence Creek fan and the deposition of young fanglomerate near the base of the fan. However, the absence of even old eroded fault scarps or linear zones of enhanced incision across the fan itself shows the first alternative to have been inoperative.

In the Sierra Nevada, the second alternative is clearly important: evidence of the advance and retreat of glaciers resulting from climatic change is well displayed in many canyons of the Sierra escarpment, among them Onion Valley. During and at the end of a glacial advance, enormous amounts of debris are made available by the glacier. This debris generally forms a steep outwash plain which grades into the fan below. Boulders from the outwash are reworked by periodic flooding, so that the entire head of the fan may be steepened. With the retreat of the glaciers, debris is no longer added to the fan in such large quantities, and the fan head may be incised.

While climatic change is certainly an important process in the incision of the alluvial fans and in the distribution of fanglomerate in the study area, neither headward erosion nor regional tilting can be ruled out. In particular, headward erosion must certainly accompany the relative uplift of the Sierra along the Independence Fault, which has been active during the Holocene. Eastward tilting of the Owens Valley between the range-front and mid-valley faults has been measured geodetically (Savage et al., 1975). The tilting results in a drop of the base level of ~ 2.2 mm/y for the streams of the eastern Sierra Nevada.

In recent times, deposition by Independence Creek appears to have been largely limited to alluvium at Grays Meadow. The fresh-appearing outwash above grades into the meadow and is deposited on a surface cut into the old fan. Thus morphologic and relative weathering data lead to the same conclusion.

From the GWR measurements it would be difficult to assign any of the bouldery surfaces of the fan to the Tioga glaciation. Thus the fan

appears to be mid-Wisconsin in age at the latest. In this study the older fan head is thought to be early- to mid-Wisconsin. The younger deposits on the distal end of the fan are probably mid-Wisconsin, and the outwash is early Tioga at the latest. However, the observations on which these age assignments are based have been made on moraines and may not be directly applicable to fans.

Lubetkin (1980) has made one of the few studies of fans in the Owens Valley which includes relative weathering and age information. He argued that the abandoned fan of Lone Pine Creek, west of Lone Pine, California, postdates the time of the high-water stand of Owens Lake, because beach deposits and wave-cut cliffs found nearby are not found on the fan, and because channels on the fan appear to be graded to a base level as much as 21 m below the high-water line. Lubetkin found that tufa from the beach gravels yielded a ^{14}C date of 21,000 ± 130 y. This must be an upper limit for the age of the fan, which thus appears to have been deposited during the Tioga stage or later.

On the basis of relative weathering data and geomorphic evidence, Lubetkin (1980) argued that the abandoned fan of Lone Pine Creek is distinctly older than the modern fan, and also distinctly younger than the larger fans west of the Alabama Hills. He therefore felt that the abandoned fan was deposited during the Tioga glaciation.

Lubetkin (1980) measured the maximum weathering relief (from granular disintegration) of granitic boulders on the surface of the abandoned Tioga fan to be as great as 6 cm. Boulders were observed to have larger diameters below the soil line, and as many as 5% of the buried boulders exposed in trenches and natural embankments were grusy. All of these

observations would point to a mid-Wisconsin age if the boulders were from tills rather than fans. For example, Burke and Birkeland (1979) found a maximum pit depth of only 2.8 cm in boulders from Tioga moraines in Sawmill Canyon (Inyo County) and Bloody Canyon (Mono County). More extensive weathering of youthful boulders has been observed in the High Sierra (M. M. Clark, oral comm., 1979), but generally only in highly exposed locations on domes, passes, or in high cirques. Thus if the ^{14}C date is accurate, boulders in fans may weather faster than those in tills.

It is possible that the abandoned fan at Lone Pine Creek is little younger than the limit of 21,000 y; in this case, it would predate many Tioga moraines that were constructed some time after the glacial maximum, ~ 18,000 y ago. If this were true, the fan could be nearly twice as old as some Tioga moraines, and the apparently excessive weathering would be less difficult to reconcile with observations elsewhere.

Relative weathering parameters for coeval fans and moraines may have different values for at least three reasons. (1) Fanglomerate is likely to be reworked several times during its transit down the fan and mixed with debris eroded during interglacial periods, whereas till is generally deposited only once, during episodic glacial advances. (2) Boulders in till are usually abraded by the glacier so that upon deposition their surfaces are unweathered, although exceptions can occur (cf. Birman, 1964). In fans, boulders from glaciers are mixed with talus transported by stream floods, so that there is no single characteristic degree of weathering upon deposition, but on the average boulders may be somewhat weathered compared to moraines of the same age.

(3) The climate on the fans is drier and warmer than in mountain valleys, but water retention in fans is probably different than in moraines, so that weathering may proceed at a different rate than on moraines.

A rough calculation of the amount of corrasion during the Wisconsin glaciation . . .

If the Independence Creek fan consisted of lamina of constant thickness, it would be possible to estimate erosion rates in Onion Valley since the time the oldest fanglomerate was deposited (~ 0.1 my BP ?). In this model, the latest layer would be 9 m thick and would contain ~ 0.18 km^3 of debris. The glaciers of Onion Valley covered 11.2 km^2. Allowing for the parabolic cross-section of the glaciers, about 14 km^2 of bedrock were in contact with ice. Thus the uppermost layer on the model fan could be generated by corrasion of only 13 m on all glacier-bedrock surfaces during the Wisconsin glaciation. Actual corrasion would be greater because some till still resides in Onion Valley above the fan and was not included in the volume calculation.

The Foothills Near Independence Creek

The foothills east of the Sierra escarpment are a block of quartz monzonite and meta-andesite bounded on the west by the Independence Fault, a normal fault on which the Sierra escarpment appears to have been developed, and on the east by the aggrading alluvial fans. Moore (1963) shows only one fault within the foothills near Independence Creek, but undoubtedly there are more. I recognized two previously unmapped faults south of Independence Creek, and these will be discussed below.

Springs within the foothills may arise along faults. However,

bedrock faults are difficult to map in the absence of lithologic contrasts, because good exposures are limited by the mantle of weathering products. Morphologic expression is inconclusive, probably because the faults have not been active since early Wisconsin time.

The eastern boundary of the foothills may also be a fault, so that the foothills could be a fault-bounded block intermediate between the Sierra Nevada and similar blocks at the floor of Owens Valley. However, there is no direct evidence of this, and gravity surveys by Kane and Pakiser (1961) and Pakiser et al. (1964) show that there is no large buried bedrock escarpment comparable to the one of the mid-valley fault.

A well 2.8 km east of the foothills (Fig. 5-2b) has been drilled 280 m into the valley fill (Los Angeles Dept. Water and Power, 1978) without encountering bedrock. This depth of fill does not necessarily imply faulting; the bedrock surface of the foothill block need only dip east 9° to exceed a depth of 280 m under the well.

The foothill block north of Independence Creek (Fig. 5-6) is capped by a flat upland surface at about 2165 m (7100 ft) elevation, and an incised ramp sloping gently to the east. There is a smaller bench north of the creek at about 1830 m (6000 ft) elevation, 100 m above the fan. Valleys cut through this bench and into the eastern edge of the upland plateau are ~ 50 m deep and generally have smooth, rounded contours. The ancient surfaces are cut into bedrock and mantled by locally derived rock fragments and soil. No exotic boulders were found, and there were no deposits of any kind.

South of Independence Creek the ancient highest surface is easily recognized. The high points consist of intensely weathered quartz

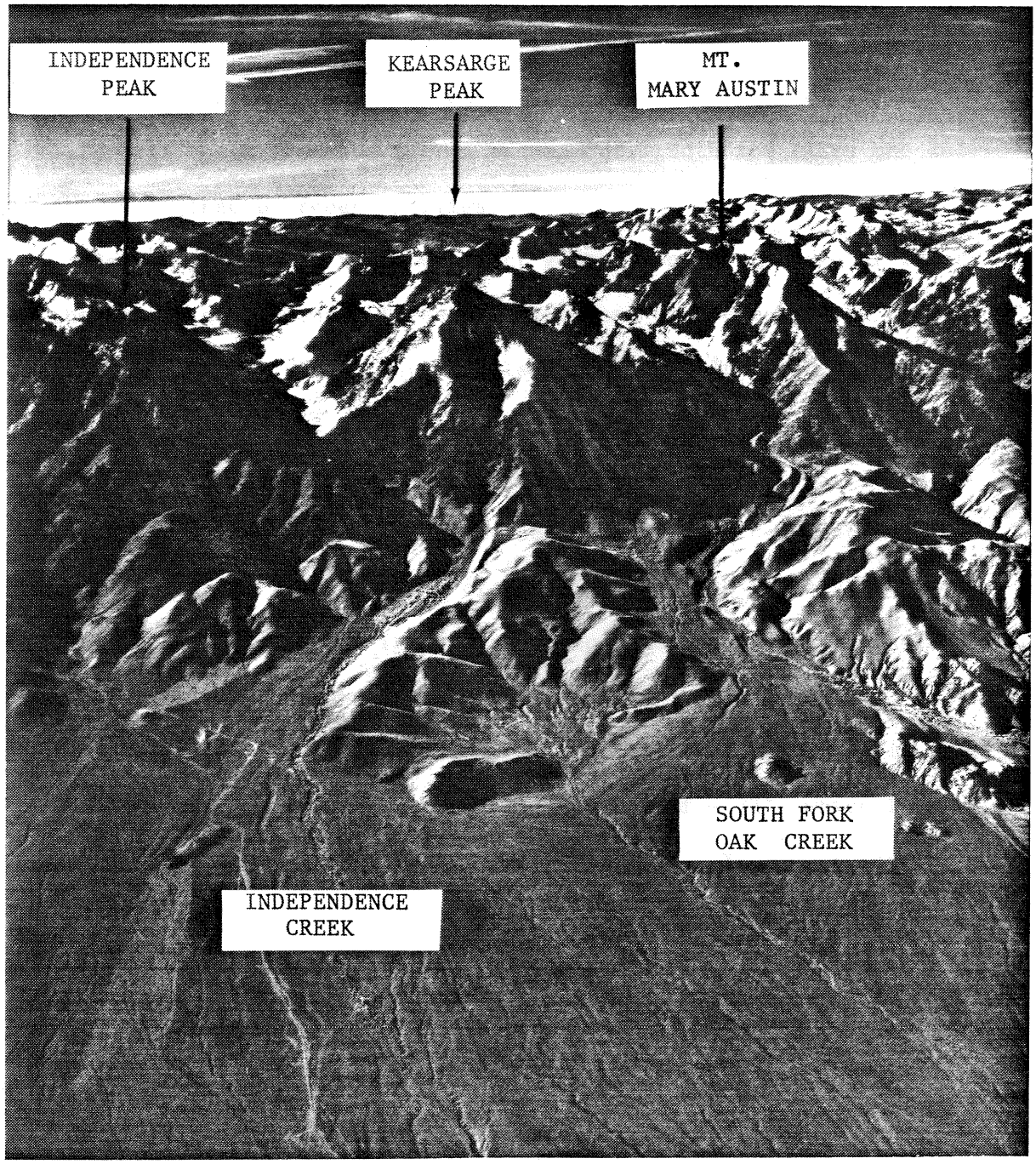

Fig. 5-6. Oblique aerial photograph of the Sierra escarpment near Independence Creek. View is towards the west. At least three generations of triangular facets can be seen on the east face of Kearsarge Peak. These testify to the grossly episodic character of the subsidence of Owens Valley. U. S. Geol. Survey Photograph GS-OAI 5-24 (11-25-55).

monzonite bedrock. The surface also features a flat deposit of locally derived rock fragments and soil which is now being slowly buried by steep debris cones from the Sierra escarpment. Both the flats and debris cones are incised by recent gullies.

There appear to be three distinct generations of triangular facets on the Sierra escarpment. These are best seen on the east face of Kearsarge Peak (Fig. 5-6), but are also visible on Independence Peak. Locations of apices are shown in Plate II. The elevations are about: 2315 m (7600 ft), 3170 m (10,400 ft), and 3780 m (12,400 ft). The lowest appears to record vertical offset of 170 m on the Independence Fault. The second records 850 m of displacement, and the highest records about 600 m. Only the upper two zones of facets were consistently recognized throughout the study area.

The highest apex is Kearsarge Peak itself. Its upper face is heavily eroded and the remnant of the facet has a slope of ~ 22°, which is less than the 30° gradients of the younger facets. The lower facets are only slightly modified by erosion. Faulting along the Independence Fault appears to have been grossly episodic.

The foothills south of Independence Creek do not extend as far east as do the foothills to the north. They terminate just east of the lower of two large scarps of normal faults (Fig. 5-7). The freshest and eastern scarp is about 25 m high, and although its morphology was not studied in detail, it is clear that it is just the most recent part of a scarp with an older and more eroded part about 70 m high. The western scarp is about 80 m high.

The two faults appear to have offset the ancient alluvial fan,

Fig. 5-7. Photograph looking south from the vicinity of Independence Creek, east of the Independence Fault Piñon Canyon is in the background. Two scarps of normal faults parallel to the Independence Fault can be seen in the foothills (arrows). The lower scarp is 95 m high; the upper is 80 m high. Both faults offset the ancient alluvial fan of Independence Creek, and heavily weathered remnants of fanglomerate can be found west of the scarps in the foothills as much as 170 m above the modern fan.

although scarps are not seen across the current fan surface. Diamictons with heavily weathered cavernous boulders are found south of Seven Pines on steps above each fault, 75 m and 170 m above the fan (Plate I). The presence of boulders of hornblende diorite showed unmistakably that the source of these deposits included the mafic pluton in Onion Valley or Lime Canyon.

Additionally, 25 m above the fan but below the lower scarp, was a third patch of diamicton, on a low ridge. The occurrence of the deposit on a ridge surrounded by the recent fan is incompatible with simple faulting. Possibly the ridge is an erosional remnant, left by lateral cutting of Independence Creek or Lime Creek, but since no other erosional remnants are found elsewhere in the fan or its margins, it is more likely a heavily eroded scarp. Similar scarps eroded to a lesser degree are found only 7 km to the south.

Rates of tectonic offset within the foothill block

At Coyote Creek, west of Bishop, California, and 50 km northwest of this study area, Bateman (1965) found that Sherwin till (> 0.7 my BP) and underlying bedrock had been incised ~ 245 m. Assuming that this incision reflects tectonic displacement, the average rate of that displacement was less than 0.35 mm/y since deposition of the Sherwin till. If this rate applies at Independence Creek, then the age of the three diamictons remnants would be more than 0.07, 0.21, and 0.49 my, respectively. Thus the lowest remnant could be as young as the Tahoe stage of the Wisconsin glaciation, and hence coeval with the fan below.

The occurrence of the lowest deposits on a ridge surrounded by the late Pleistocene fan implies a period of deposition following faulting

or incision, so that most of the ancient scarp was buried under an aggrading fan. It is unlikely that the remnant and the aggrading fan are close in age. It follows that: (1) the displacement rate at Coyote Creek may be faster than that at Independence Creek; (2) displacement also occurred elsewhere than along these faults; or (3) the Sherwin till at Coyote Creek is significantly older than its lower age limit. Insufficient information is available to choose among the alternatives, but the second at least does appear to have happened: the scarp of the Independence Fault itself offsets late Pleistocene moraines and glacial outwash of Independence Creek (see below).

The intermediate fan remnant near Lime Creek occupies a small bench which from its height above Independence Creek appears to be correlative with the lower surface on the foothills north of the creek. The highest surfaces north and south of the creek (2165 m or 7100 ft elevation) likewise appear to be correlative. The highest fan remnant is below this level and has no obvious match in the foothills to the north. Into the highest surface (which has no remnants of ancient fanglomerate) Independence Creek and Lime Creek have cut 190 m. Piñon Creek has cut 300 m through the same feature. Arguing as before, the incision probably took more than 0.54 my or 0.86 my, respectively. This discrepancy may be explained by faster aggradation of the Independence Creek fan than the Piñon Creek fan. The former extends 150 m higher in elevation, and has an unknown depth. Between the remnants of the highest surface, Piñon Creek flows in a narrow gorge close to bedrock. If the actual incisions of the two rivers through bedrock are the same depth, then the gravels of the upper Independence fan might be about 100 m thick. This is

considerably less than the thickness of > 250 m estimated by Gutenberg et al. (1932) from seismic refraction profiles at Shepard Creek. Shepard Creek is only 6 km south of Piñon Creek, and is one valley south of the exposed hills of the foothill block. Thus it appears that even the deepest alluvium within the foothills is much shallower than alluvium south of the foothills.

Offset of Independence Creek

During the past century there has been continuing debate over the existence and sense of lateral offset across the Owens Valley. Most of the controversy has centered on the mid-valley Owens Valley fault zone, the site of the earthquake of 1872. Recently, Moore and Hopson (1961) and Ross (1962) have placed limits on the total Cenozoic lateral offset of a few km, based on correlated dikes and granitic plutons (respectively) on either side of the Owens Valley. Lubetkin (1980) has attributed ~ 6.4 m of right-lateral offset along the Lone Pine Fault (within the Owens Valley fault zone) to the 1872 earthquake. On the other hand, Pakiser (1960) and Pakiser et al. (1964) argue for left-lateral offset to explain the distribution of Pleistocene volcanic eruptive centers.

Because of clear evidence of late Quaternary faulting along the Independence Fault, only 10 km west of the Owens Valley fault zone at Independence, geomorphic evidence of possible lateral offset across the range front merits attention. Mayo (1941) observed the flexure in the

course of Independence Creek as it crosses the range front and foothill region, and considered the possibility that this might have recorded right-lateral displacement along the frontal fault zone.

The amount of offset supposedly indicated by Independence Creek is more than 1.56 km. However, no more than 0.32 km of offset could have occurred along the Independence Fault itself since incision of the stream into the foothill block (Fig. 5-8). This limit is the distance from the modern Independence Creek south to the northernmost of the foothills near Lime Creek. Thus more than 1.24 km horizontal displacement must have occurred along the two sub-parallel faults east of Independence Fault. If this were true, they would be dominantly strike-slip rather than normal faults, but there is no evidence for this: the ravines which cross these faults south of Lime Canyon show no sign of horizontal displacement. Furthermore, neither Lime Creek nor Piñon Creek is offset across the range front. Thus it seems probable that the bend in Independence Creek is unrelated to horizontal displacement along the range-front faults. It follows that at least in the area of this study, any major lateral offset on the east side of the Sierra Nevada is restricted to the Owens Valley Fault or occurred before incision of the foothill block.

History of the foothill block

The old surfaces of the foothill block are cut into bedrock. Apparently at least some were once buried by the alluvial fan. From the rate of incision estimated elsewhere for the Sierra as a whole, the highest of these old surfaces appears to be older than ~ 0.5 my. The actual age is probably significantly greater than this limit. This is because much of the tectonic displacement has occurred on the Independence Fault, west

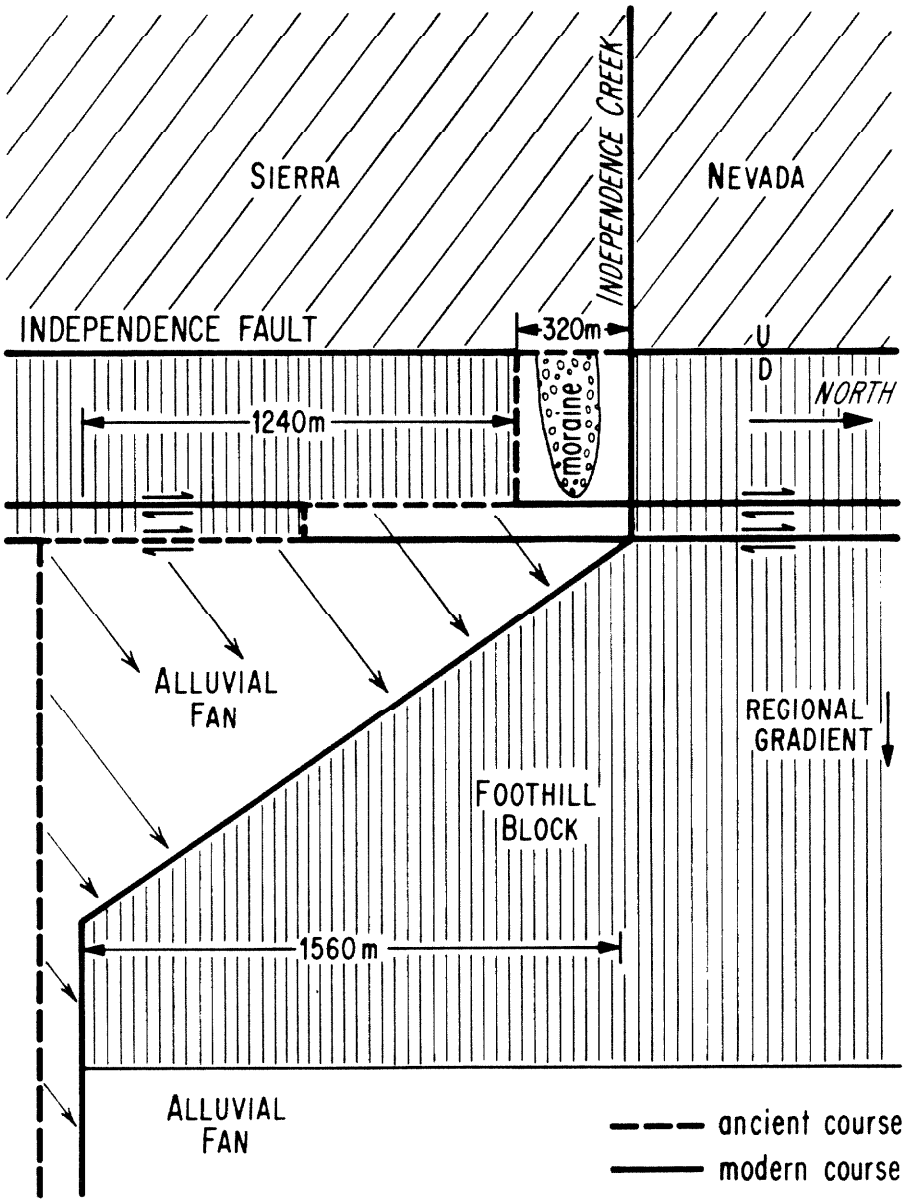

Fig. 5-8. Schematic representation of hypothetical right-lateral offset of Independence Creek along the frontal fault system (not to scale). Independence Fault can not have had more than 320 m of such offset since it incised the foothill block, so most offset would have to have been on faults further east. There is no direct evidence for strike-slip faults in the foothill block.

The figure shows the hypothetical ancient offset Independence Creek (dashed line) gradually assuming its present course by erosion down the regional gradient of the foothills.

of the foothill block. The surface is thus probably early Pleistocene or even older. It must have originated as a pediment at a time when the deep graben to the east had yet to form, so that it was not yet deeply incised. Fans covered at least its lower reaches. Normal faulting during the Pleistocene disrupted the ancient pediment and dropped the entire block relative to the Sierra Nevada. The presence of relict debris cones and fans suggests that stable periods occurred within this period, and that displacement was episodic on a finer time scale than recorded by the giant facets of the escarpment. The quiesence of faults within the foothills in the late Pleistocene contrasts with their earlier activity and supports this contention. Richardson (1975) attributed a similar history to the Alabama Hills, south of Independence.

Pakiser et al. (1964) have suggested that the Poverty Hills, a foothill block in the middle of Owens Valley between Big Pine and Independence, originated as a giant landslide. A similar genesis for the foothill block from Symmes Creek to Thibaut Creek is unlikely, because the Independence quartz monzonite which comprises most of the foothills is found west of the Independence Fault only in small outcrops on Lookout Point, well to the north of the foothills.

Late Pleistocene Glacial Deposits in Onion Valley

Onion Valley was repeatedly glaciated during the Pleistocene Epoch. The catchment area was the largest in the area of this study. Above 2680 m (8800 ft) elevation, glaciers covered 9.6 km^2. The typical elevation of cirque walls was 3600 m. In addition, at least during some early glaciations, ice originating west of the bedrock crest may have flowed east

across Kearsarge Pass, adding to the glaciers cutting Onion Valley. Late Pleistocene glaciers left moraines as low as 1950 m (6400 ft) elevation, east of the Independence Fault.

Moore (1963) identified the glacial deposits of upper Onion Valley as belonging to the Tioga advance. He considered the moraines of the lower valley and foothills to be of the Tahoe advance. This view is basically correct. However, Quaternary deposits in lower Onion Valley reveal a complicated history of multiple glaciations, each distinguished by different degrees of weathering of boulders in moraines. A generalized map of these moraines is given in Fig. 5-9.

In the discussion which follows, moraines of different advances of the glaciers will be identified by Roman numerals, with I identifying the oldest moraines. These will be correlated to conventional Sierra Nevada glacial stages in a later section. When possible, moraines throughout the study area will be correlated with the advances of Onion Valley, and thus indirectly tied to the conventional Sierra chronology.

Distinction among moraines of different advances was made morphologically and by semi-quantitative relative weathering measurements. Relative weathering data are summarized in Tables 5-2 and 5-3. Site locations in Onion Valley and in the tributary canyons are shown in Fig. 5-10.

Lower Onion Valley

There are tills of seven or eight distinct ages in Onion Valley and its tributary canyons. Three or four of these are found in the lower reaches of Onion Valley. Recognition of these units is facilitated by excellent exposure along the two roads up Independence Creek, but the deposits may be distinguished by surface exposures alone.

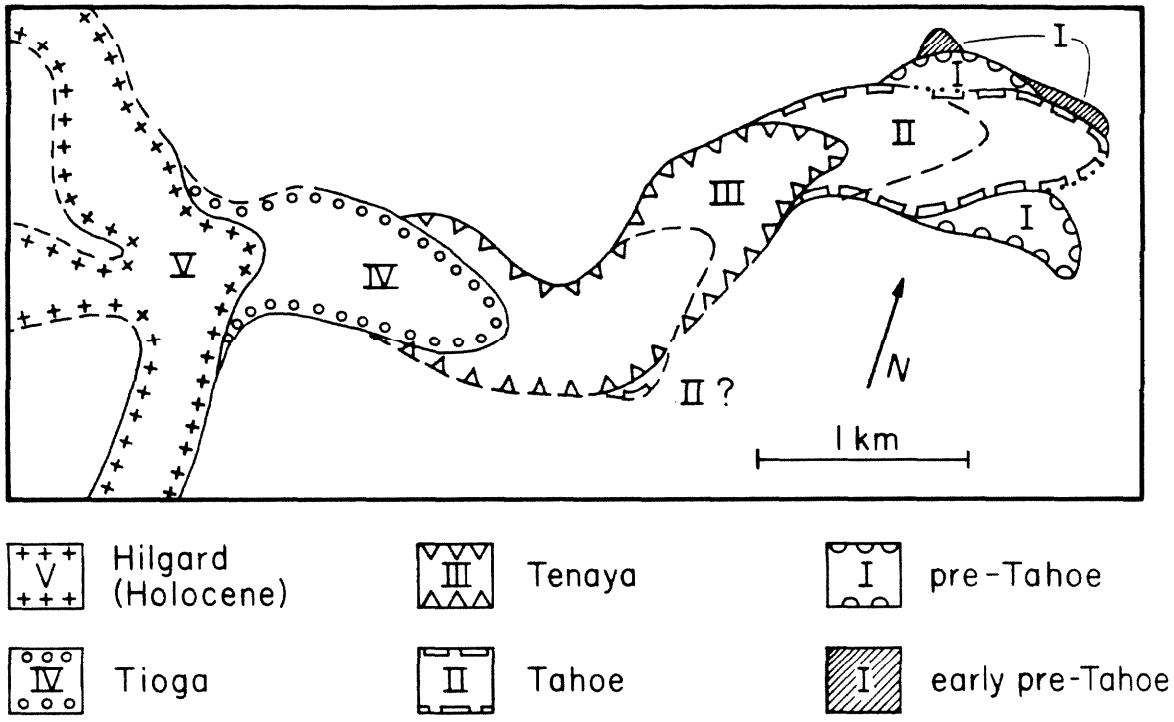

Fig. 5-9. Glacial moraines of Independence Creek. Roman numerals identify the relative ages of the glacial deposits: I is the oldest till and V is the youngest shown on this map. Probable equivalent glacial stages from the conventional Sierra Nevada sequence are shown below. Contacts have been generalized somewhat and are dotted where buried by talus or outwash or removed by erosion.

Table 5-2

Semi-Quantitative Weathering Data for Moraines of Onion Valley

Right-Lateral Moraines

Site[1]	Age[2]	No. of Boulders[3]	GWR[4]	BR[5]	U/G/M[6]	BFC[7] m^{-2}
8-3	VII	100	0/100/0	----	----	----
8-2	VI	100	7/93/0	8/20/72	----	----
3-6	V_{RC}	104	50/50/0	----	----	----
3-5	V_{RC}	94	78/22/0	----	----	----
3-1	IV_{RC}	71	56/41/3	----	----	----
2-7	III	41	44/49/7	69/19/12	33/67/0	0.29
2-6a	III	35	69/31/0	51/31/17	12/78/0	0.72
2-6b	III	48	65/35/0	46/35/19	20/80/0	0.93
6-14	III	100	99/ 1/0	----	----	----
2-5	II?	74	73/27/0	64/29/7	11/85/4	0.58
2-22	II	43	51/47/2	32/57/11	6/85/9	0.44
2-23	II	37	78/22/0	50/32/18	19/73/8	0.22
2-4	II	49	33/65/2	56/37/7	8/91/1	0.61
1-1	I	59	59/39/2	----	17/68/14	0.51
2-3	I	34	88/12/0	50/36/14	15/63/22	0.28

Left-Lateral Moraines

Site[1]	Age[2]	No. of Boulders[3]	GWR[4]	BR[5]	U/G/M[6]	BFC[7] m^{-2}
9-1	V_{GT}	36	11/83/6	----	----	----
9-2	V_{GT}	100	----	----	60/40/0	----
9-3	V_{GT}	110	0/95/5	----	45/55/0	1.53
9-4	V_{GT}?	76	84/16/0	26/36/38	1/99/0	----
2-16	IV	134	10/79/11	24/45/32	8/85/7	0.96
1-4	IV	178	0/94/6	----	8/85/7	1.78
8-1	III	90	57/39/4	----	----	----
2-17	III	80	19/73/9	----	12/85/3	0.64
2-18	III	66	45/44/11	28/32/35	21/77/2	0.75
1-3	III	85	34/55/11	----	17/65/18	0.84
2-2	III	109	29/64/7	49/36/15	11/72/17	0.82
1-6	II	87	43/55/2	----	20/69/11	0.87
2-1	II	121	45/54/2	11/76/13	41/47/12	0.72
1-2	I	84	11/78/11	----	0/74/26	1.40
2-19	I	20	80/20/0	50/29/21	0/59/41	0.28

1 Measurement site locations are shown in Fig. 5-10. "RC" denotes Robinson Creek; "GT" denotes Golden Trout Creek.

2. Glacial advances in Onion Valley were numbered from I to VII in order of decreasing age. Correlation with the conventional Sierra Nevada sequence is given in Table 5-10.

3. Number of boulders counted for GWR.

4. Granodiorite weathering ratios. The relative frequencies of boulders (in %) are listed in order of decreasing weathering class (Ch. 2).

5. Boulder burial or "boulder relief" (Fleisher,1967). Relative frequencies (in %) are for classes of decreasing burial (Ch. 2).

6. Ultramafic / Granitic / "resistate" ratio (in %). See Ch. 2.

7. Boulder frequency on the moraine surface (Ch. 2).

Table 5-3

Semi-Quantitative Weathering Data from Road Cuts in Moraines of Onion Valley

Site[1]	Glacial Advance[2]	No. of Boulders in Sample	GWR [3]	B-Horizon Munsell Color
9-5	IV_L	67	16/36/48	10 YR 5/4
9-6	III_L	50	28/32/40	10 YR 5/4
9-7	III_L	74	41/28/31	5 Y 7/2
9-8	III_L	79	42/29/29	10 YR 7/2
2-24	III_L	67	42/58/0	-----
2-20	III_L	97	56/39/5 *	10 YR 6/2
2-21	II_L	93	68/29/3 *	10 YR 7/2
9-9	II_L	86	47/42/12	10 YR 6/4
2-19	I_L	20	----	7.5 YR 7/4
9-10	I_R	84	74/19/7	5 Y 6/1

1. Measurement site locations are shown in Fig. 5-10. "L" and "R" refer to left-lateral and right-lateral moraines, respectively.

2. Glacial advances in Onion Valley were numbered from I to VII in order of decreasing age. Correlation with the conventional Sierra Nevada sequence is given in Table 5-10.

3. Granodiorite weathering ratios. The relative frequencies of boulders (in %) are listed in order of decreasing weathering class: e.g., heavily weathered (class 3) / lightly weathered (class 2) / unweathered (class 1). See Ch. 2 for further discussion. Boulders counted were from the C-horizon, except for those ratios marked by asterisks (B-horizon).

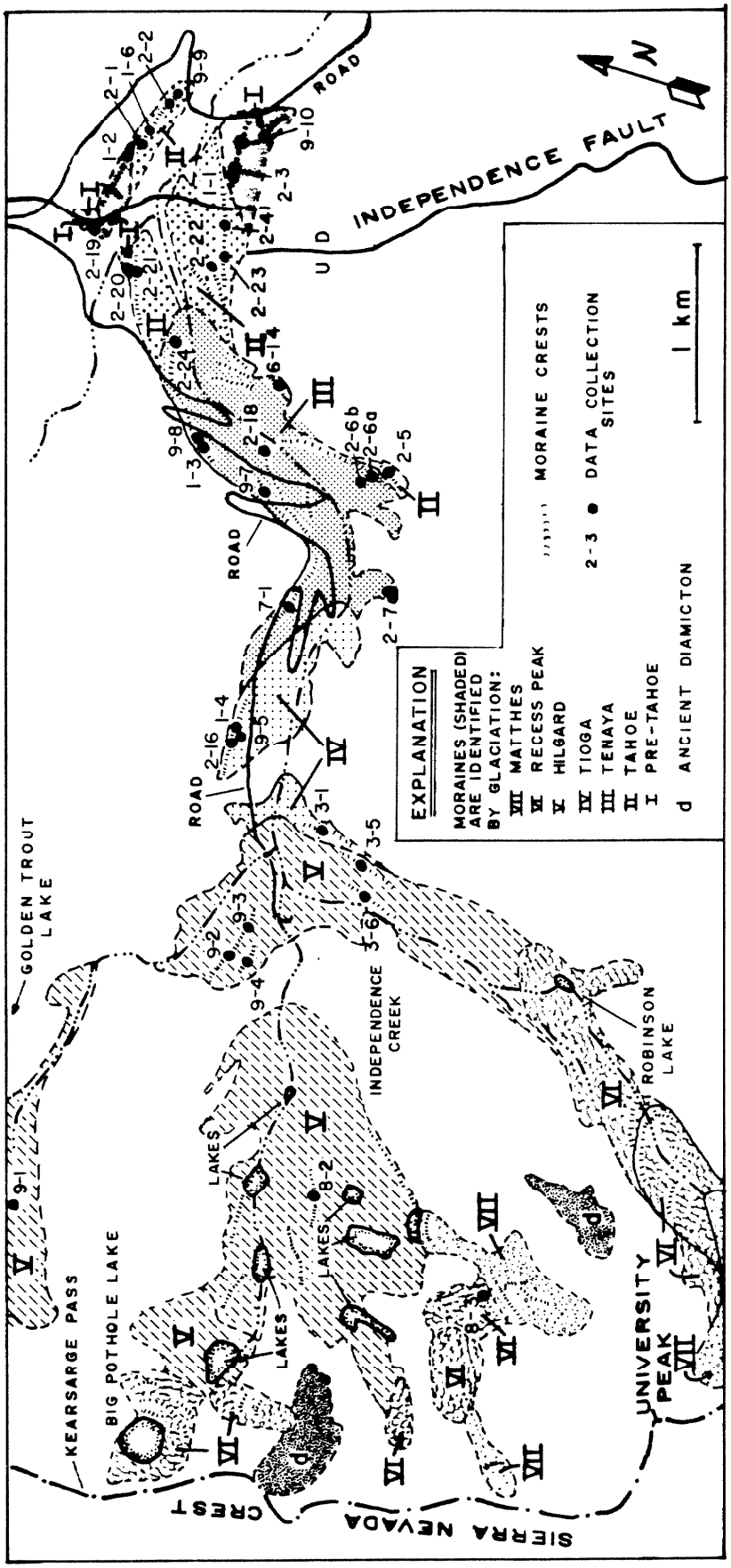

Fig. 5-10. Locations of sites where semi-quantitative weathering data were gathered in Onion Valley. Moraines of different ages I - VI are also shown (see Fig. 5-16 or Plate I for a more complete geologic map). Data for sites are summarized in Tables 5-2 and 5-3. The road shown is the modern Onion Valley road, not the abandoned road shown on the Mt. Pinchot Quadrangle (1953).

Right-lateral moraines . . .

Glacial deposits south of Independence Creek in the vicinity of the range front consist of a massive right-lateral moraine, a number of smaller lateral and recessional moraines, and an outwash plain near the river. These are of progressively younger ages. The core and the eastern end of the massive moraine were the oldest till found south of Independence Creek; the thin layers of till which cover the massive moraine near the range front and the recessional moraines east of the range front are distinctly younger. A third series of moraines found west of the range front, within lower Onion Valley itself, are younger still. The glacial outwash appears to truncate geomorphic features of this third series of moraines and probably dates from the retreat of the glaciers which constructed them. The three glacial advances probably represent distinct stages, denoted I, II, and III in order of decreasing age in this study. These stages probably bracketed the early Wisconsin glaciation.

Till of the major right-lateral moraine is exposed in a large road cut 50 m south of the bridge over Independence Creek above Seven Pines. Large numbers of disintegrating quartz monzonite boulders from the Bullfrog pluton were found alongside surprisingly fresh ones. The A horizon is only a few cm thick, but the B horizon is as much as 3 m deep and is somewhat oxidized. The maximum Munsell color in the road cut is 5Y6/1; colors of 10YR5/4 were found in 30-cm-deep pits on the crest. The C horizon forms most of the road cut. Its color is neutral (Munsell N7 to 10YR8/2).

The moraine crest contains heavily weathered boulders largely buried

in a grusy matrix. Only 28 boulders over 30 cm in diameter were found in 100 m^2. Most were from the Bullfrog pluton, but about 14% were "resistates" (chiefly fine-grained granitic rocks) and about 17% were mafic rocks, especially diorites and gabbros. The roundness of the boulders is noteworthy and appears to be caused by removal of loosened crystals from the surface of the boulders. The degree of roundness contrasts with the more angular boulders from younger moraines upstream. If granitic boulders are classified as "round", "sub-round", "subangular", or "angular", then the frequency distribution found for 111 boulders in the lowest right-lateral moraine is 47/31/22/1.

Just above the road cut this lowest moraine appears to have two crests. The outer and lower crest seems to be buried by a younger moraine. The two crests are separated by a shallow gully. However, no weathering differences can be seen in the boulders exposed in the road cut; thus it may be that the till was all deposited at about the same time.

Just north of the higher (inner) moraine crest a veneer of less-weathered boulders covers the moraine. The contact may be seen easily from the Onion Valley road north of Seven Pines. The veneer of boulders is the remnant of a thin layer of till left by a glacier distinctly younger than that which deposited the massive older moraine. The contact rises upstream, and 200 m west of the road cut the old moraine crest itself is buried by the younger till. The younger till contains more boulders on its surface (61 per 100 m^2) than the older moraine, and they are more angular (26/34/34/5, for 87 boulders). Granodiorite weathering ratios (Table 5-2) showed that fewer boulders in the younger

till are heavily weathered, and the grusy quartz monzonite boulders which typified the surface of the lowest moraine are not evident. Thus the morphologic moraine appears to be composite, consisting of till deposited at distinctly different times. The older till is denoted by "I" and the younger by "II" in this study.

The younger moraine is continuous at least as far west as the range front. At about the point where the canyon bends, yet younger moraines of subdued expression bury it. Exposed in shallow cuts of the old road through these moraines are seen buried disintegrating boulders. Few grusy boulders are seen on the surface, and the distinction between the two tills based on weathering characteristics is not great.

In part this may be because the subdued moraines are end moraines. Most workers have felt that age estimates based on weathering of till in end moraines were unreliable compared to those for lateral moraines (Janda, 1966; McCulloch, 1963; Sharp, 1969,1972). Birman (1964) argues that weathering data for end moraines are likely to be excessively large. Thus the end moraines in lower Onion Valley may have been left by a glacier younger than advance II. They may be the terminal moraines of the glaciers of advance III.

A final set of three well preserved moraine crests in lower Onion Valley is found from 2650 m to 2680 m elevation. The highest moraine is less bouldery than the lower two. Weathering of boulders indicates a difference in age between the highest and the lower two moraines. The degree of burial of boulders along the moraine crest is greatest for the highest moraine. This is consistent with the relative age deduced from the nesting of the moraines, but care must be exercised in interpreting

these results because the lower moraine crests are little more than inflections in the slope of the massive uppermost one. As such they are subject to burial by slopewash and also to loss of fine particles down slope. However, the youthful appearance of boulders on the lower moraines cannot have been caused by the addition of weathered boulders from the highest moraine; thus the lower moraines are probably significantly younger than the highest one. They may also be significantly younger than the end moraines found at 2315 m elevation, based on their GWR values (Table 5-2).

While it is logical to assign the highest moraine to advance II and the lower ones to an advance III, this is not defensible on the basis of semi-quantitative weathering data alone, for the reasons of limited exposure and possibilities of contamination.

The outwash plain above Seven Pines can be traced to a point at or just west of the terminal moraines of advance III. The shallow swales separating the three end moraines appear to be truncated by the outwash. Thus the outwash seems on geomorphic grounds to have been last deposited during and after the maximum advance of the glaciers of advance III.

In summary, from inspection of weathering and morphologic characteristics of the right-lateral moraines of lower Onion Valley, there appear to be at least three recognizable glacial advances. Advance I left broad, rounded moraines as low as 1900 m elevation. Boulders are heavily weathered. The crest of this oldest moraine was buried by till of advance II above 2070 m (6800 ft) elevation. This till is found in the inner flank of the oldest moraine as a thin veneer of sub-angular boulders down to an elevation of 1950 m (6400 ft). Above 2315 m (7600

ft) elevation the main crest of the moraine of advance II was buried by a series of end moraines which arguably might be assigned either to advance II or to advance III, based on semi-quantitative weathering observations alone. The snout of the glacier that left the lowest of these end moraines might have extended to 2150 m (7040 ft) elevation. Glaciers of advance III certainly descended at least to an elevation of 2240 m (7360 ft). Moraines of advance III left unburied short lengths of older moraine crests, probably of advance II.

Left-lateral moraines . . .

The same three stades represented south of Independence Creek may also be recognized in the left-lateral moraines. However, interpretation is complicated by the presence of an ancient till which may predate any found south of the creek, and by the unusual distribution of moraines from advances I and II. This ancient till, here designated as an early deposit of advance I, is found immediately west of the Independence Fault.

Upon careful inspection, the lowest (easternmost) moraine, which at first glance appears to correlate with the massive right-lateral moraine of advance I, is seen to correlate better with the moraines of advance II. The right-lateral moraine of advance I is inconspicuous, stream erosion having obliterated the original morphology of the southern flank of the moraines so that moraines I and II share a common embankment. Furthermore, the crest of moraine I is largely buried by a wedge of debris, probably a kame terrace, which also drowns its northern flank. Nevertheless, distinction of the tills appears to be possible by careful observation of weathering characteristics of boulders exposed

on moraine crests and in road cuts. This evidence is summarized in the discussion below.

The lowest left-lateral moraine of Independence Creek extends down valley to an elevation of 1950 m (6400 ft). Like right-lateral moraine I, it is cut by the Onion Valley road. This exposure reveals a single till resting on weathered bedrock and debris shed therefrom.

Obvious differences in weathering suggest that the road cuts expose till of different ages on either side of Independence Creek. The color of the B and C horizons were Munsell 10YR6/4 and N7.5 respectively. Although the B horizon had a redder color than seen in the right-lateral moraine, weathering characteristics in the C horizon appeared to be less well developed. Fewer boulders were grusy, and the weathering ratio was 42/42/17, compared to 63/27/10. Reflecting the lesser weathering, more boulders in the road cut protruded from the matrix of the left-lateral till than from the right-lateral till.

To some extent these differences might be caused by differences in the weathering rates of rocks found in the source regions for the tills. Most right-lateral till probably originated along Robinson Creek or the northern cliffs of University Peak, a region consisting almost entirely of Bullfrog quartz monzonite. Left-lateral tills probably originated on the southern slopes of Mt. Gould and in the drainage of Golden Trout Creek, where the dominant rocks in addition to Bullfrog quartz monzonite are granodiorites from the Dragon pluton, hornblende gabbros, and other mafic plutonic rocks. Thus the right- and left-lateral moraines have different compositions, and even boulders from the same pluton may have come from sites far apart. However, it seems unlikely that GWR values

for boulders of the same pluton would be as different as observed unless the moraines were of different ages.

Additional information suggests that the lowest left-lateral moraine was left by a glacier of advance II rather than advance I. From the crest of the right-lateral moraine (Fig. 5-11) the inner face of the lower left-lateral moraine is seen to be bouldery. About 435 m upstream from the roadcut the bouldery till abruptly ends. On the stream-cut inner face of the moraine there is no morphologic expression of this boundary; west of the boundary the till is simply less bouldery. The crest of the bouldery moraine seems to end at the contact. It is replaced by a second moraine crest which is slightly higher and somewhat further from the stream. The two crests are separated by a shallow gully which leads northeast, away from Independence Creek. Apparently the bouldery moraine was once nested inside an older moraine which did not extend as far downstream. Most of both moraines have been removed by erosion by Independence Creek and by the intermittent stream which has cut the deep ravine in the east face of Kearsarge Peak.

The older moraine has impounded a deep wedge of alluvium or outwash behind it. Two channels leading from the truncated southern edge of the deposit show that drainage was from the southwest. These channels must have been cut by streams flowing off the glacier or alongside its moraines. Their presence shows that very little of the terrace was derived by mass wasting of the local hillsides. The deposit was probably a kame terrace alongside the glacier or its moraine. The moraine character of the southern edge of this terrace can be seen in the presence of the large rounded boulders.

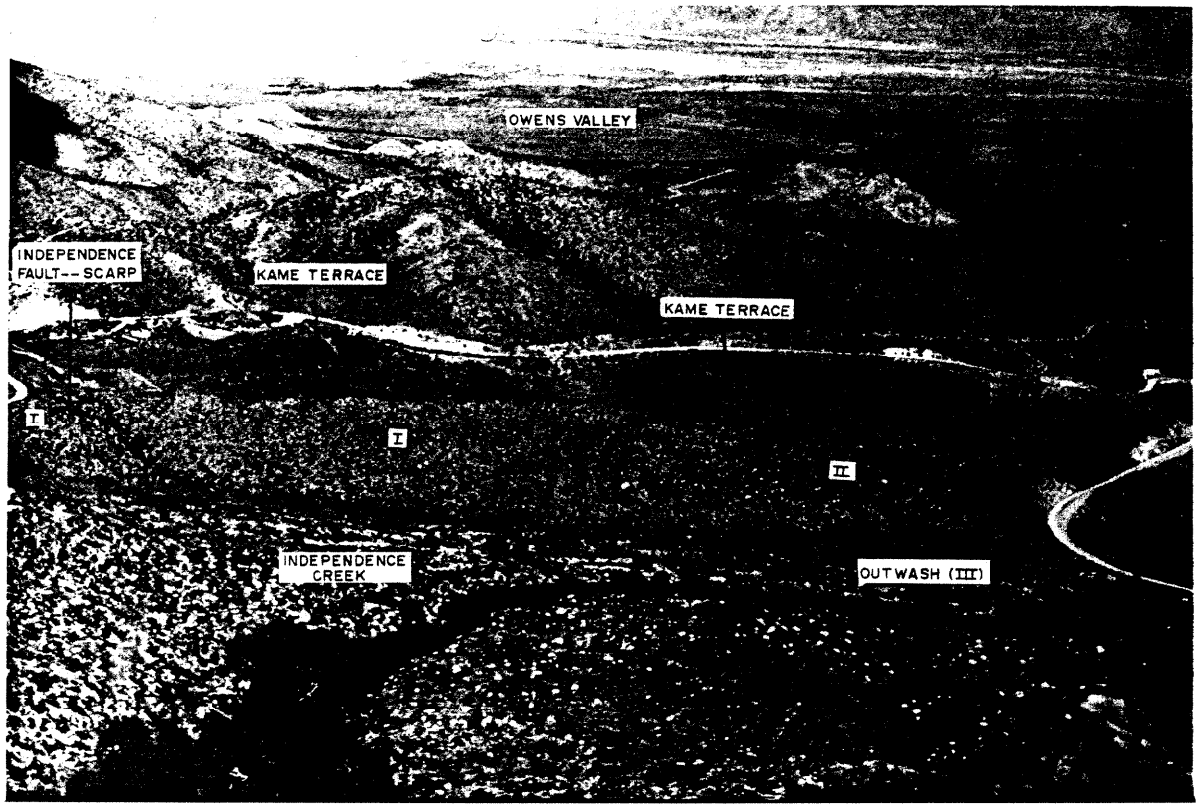

Fig. 5-11. View of the left-lateral moraines of Independence Creek, from the south. The older moraine of advance I is seen on the left; the moraine of advance II forms the eastern end of the ridge. The original morphology of the southern flank of the moraines has been largely obliterated by stream erosion. The till of advance II can be distinguished from the older till of advance I by its greater abundance of boulders exposed on its flank and crest. On the left, the moraine ends against the late Quaternary scarp of the Independence Fault. West of the scarp is a till which may predate advance I.

A remnant of a depositional terrace may be seen just under the Onion Valley road at 2040 m (6700 ft) elevation. A deeply entrenched intermittent stream now separates this from the main terrace, and in the northern wall of the stream cut may be found rounded boulders of Dragon granodiorite that must have been derived from upstream. These exotic boulders are not found at the surface of the deposit, which is covered by locally derived colluvium. The genesis of this deposit is arguable, but it probably involved glacial rather than colluvial processes. The deposit may be a remnant of the kame terrace or of an earlier moraine. This remnant could not have formed behind the crest of the bouldery moraine (advance II), which is too low to have impounded it. It must have been deposited against the side of an earlier glacier or a more extensive moraine removed by erosion sometime before the bouldery moraine was created. It was thus deposited during or before advance I.

Moore (1963) has mapped the glacial deposits as truncated against the Independence Fault. Inspection of a road cut where the old road crosses the scarp of the fault shows that this is not correct, and that till is also found west of the fault. The road cut exposes a diamicton that can be divided into three strata. The disordered fabric and disoriented rounded clasts of the lowest stratum (largely buried by debris fallen from the road cut) point to a glacial origin.

Large subangular boulders in the middle stratum are oriented with their long axes parallel to the regional slope and their short axes dipping into the road cut. This suggests some different process, possibly colluvial reworking of the upper part of the moraine. The top zone consists of smaller chips of rock which probably are colluvium

from the slopes above the moraine.

The buried till exposed in the road cut is more oxidized than any other of Onion Valley. Only the B horizon is exposed. Its color in the Munsell system is 7.5YR7/4, compared to 10YR6/4 for the B horizon of the left-lateral moraine in the road cut at 1950 m elevation. The B horizon of the moraine of advance I exposed in the road cut south of the creek had a color of 5Y7/2.

Boulders exposed in the road cut on the Independence Fault are typically heavily weathered, and boulders on the surface of the moraine which are exposed here and there through the colluvium have a GWR of 80/20/0, with a BR of 50/29/21. Both measures may underestimate the actual degree of weathering characteristic of the moraine, because colluvium may have hidden some grusy boulders which would otherwise have risen a few cm above the surface. The older of the two moraines east of the fault gave GWR values of 11/79/11 and 44/54/2. The first was from a site probably contaminated by material from the kame terrace, but second site was near the eastern limit of the moraine where its crest is a few meters above the terrace. Even this more trusted count indicated less weathering than in the till just west of the fault. The ancient till exposed in the road cut is therefore at least as old as advance I.

There is distinctly more clay in the B horizon of the old moraine than was found in the B horizon of the moraine of advance II. This is taken to indicate a significant difference in age between the two moraines.

Thus there appear to be left-lateral moraines of three ages found along the Independence Fault and eastward. The youngest is the bouldery moraine, which is certainly of advance II. The age assignment of the

other two is not so obvious. Most probably the moraine impounding the kame terrace is of advance I, and the moraine exposed in the old road cut is even older. However, it is also possible that the moraine of the old road cut correlates with the right-lateral moraine I, and that the other moraine is of intermediate age. The limited exposure of the older moraine and the erosion of the crest of the younger moraine preclude a more definitive application of relative age dating techniques.

The contact between moraines of advances I and II is especially well exposed in an embankment of the abandoned road, 250 m southwest of its crossing of the Independence Fault. The older of the moraines has been buried by alluvium from the intermittent stream flowing off the east face of Kearsarge Peak. The maximum thickness of this alluvium is about 50 m. It was able to accumulate to this depth because the stream was impounded by the moraines emplaced across its channel. The crest of the inner moraines protrudes a few meters from the wedge of alluvium above the abandoned road, but the outer moraine has been completely buried and is exposed only in the road cut.

Striated quartz monzonite boulders and clasts of hornblende diorite from the headwaters of Independence Creek confirm the glacial character of the buried diamicton. The GWR measurements for boulders from the road cut (Table 5-3) indicate that the outer moraine is older than the inner one, but younger than the ancient moraine exposed at the Independence Fault. The inner moraine is here assigned to advance II, correlative with the bouldery till near Seven Pines, on the basis of the similar values of the GWR.

About 150 m southwest of the intermittent stream, the old road passes

from the side of the moraine onto the old outwash head. The change in character of the diamicton can be seen in the roadcuts just northeast of Independence Creek. Near this point was the plunging snout of the glacier of advance III. The left-lateral moraines are well exposed in cuts of the new Onion Valley road. Boulders found there were decidedly less weathered than those in tills exposed in road cuts down canyon: GWR values were 28/32/40, 34/31/45, and 29/29/42. Nevertheless, heavily decomposed Bullfrog quartz monzonite boulders were found in all road cuts in this till.

Glacial trim lines are seen only on the south walls of lower Onion Valley. The location of left-lateral moraines shows that glaciers apparently stood away from the cliffs at the base of the east face of Kearsarge Peak.

Glacial outwash . . .

From Seven Pines west for 1250 m the entire width of the valley of Independence Creek is choked by glacial outwash. Within this outwash plain the creek flows in an incised channel. At first glance the boulders of this outwash plain appear quite fresh and unweathered. Closer inspection reveals very few with any trace of original glacially abraded surface, and most surfaces are somewhat pitted. The state of weathering is roughly akin to that found on the fan east of the foothills. The large number of large boulders gives an unwarranted appearance of youth to the outwash.

At the bridge for the Onion Valley road just west of Seven Pines the creek is incised only 2-3 m into the outwash plain. Farther west the incision deepens and two additional terrace levels can be discerned. The outwash head mentioned in the previous section grades into the main

outwash plain. At 2170 m (7120 ft) elevation, Independence Creek is incised ~ 30 m into this outwash, and this incision increases to as much as 50 m upstream. The GWR for boulders in the outwash was 42/58/0, not unlike the values for the lower fan or the outwash above Seven Pines (Table 5-1). The next younger terrace is roughly 7 m above the creek, at 2160 m (7080 ft) elevation. The present flood plain of the stream is everywhere only ~ 1.5 m above the creek.

West of the lower limit of till III the oldest outwash head was no longer recognized. Instead the creek is incised as much as 20 m into the diamicton comprising the floor of the valley, which grades smoothly into the lateral moraines. Furthermore, near the snout of the advance III glaciers the fosses separating the moraine crests appear to terminate against the outwash and thus may predate it. Therefore the uppermost outwash plain seems to have been created by drift discharged from the glaciers of advance III during an extended period after the maximum down-valley advance but before rapid retreat.

Runoff from the east face of Kearsarge Peak has cut through the impounded alluvium and now deposits material directly onto the old outwash surface. It is possible that incorporation of weathered alluvium from the ancient terrace has increased the apparent age of the outwash.

Upper Onion Valley

Above 2545 m (8350 ft) elevation Independence Creek runs due east. It is incised only 4 m into the broad floor of upper Onion Valley, much less than in the steeper reach below. Massive talus cones mantle the thin moraines on the south side of the upper valley. Some cones even reach mid-valley, deflecting the creek to the north. Moraine crests are

poorly developed and preserved below 2850 m (9360 ft) elevation, where moraines of the Robinson Creek glacier entered Onion Valley from the south. On the north side moraines are less buried by rockfall, and road cuts assist in the discrimination of relative ages. Remarkably, although subtle moraine crests can be traced to within a few tens of meters from Independence Creek, no massive terminals characteristic of youthful moraines elsewhere in the Sierra Nevada (e.g., Blackwelder, 1931, Sharp, 1972; Sharp and Birman, 1963) are observed anywhere in Onion Valley.

Upper Onion Valley contains glacial deposits of three ages (III - V), ranging from mid-Wisconsin to Holocene. Moraine crests are generally covered by talus, except locally on the north side of the valley. The contact betwen tills of advances III and IV is well exposed in road cuts, however. Moraines of advance V are heavily vegetated in Onion Valley itself, although they are well exposed in all three main tributary canyons.

Just south of the prominent rib of Kearsarge Peak at the lower end of upper Onion Valley, till exposed in road cuts contains grusy boulders typical of moraines of advance III. At 2560 m (8400 ft) elevation close to the creek the till is distinctly less weathered. Grusy boulders of quartz monzonite are conspicuously absent, and heavily weathered clasts are half as numerous as in roadcuts through lower moraines (Table 5-3). Granodiorite weathering ratios from the limited exposed crests are less conclusive (Table 5-2). Perhaps this is because of contamination by weathered talus of till on moraine surfaces. The contrast in the tills exposed in the roadcuts is sufficient to define a younger advance (IV)

above 2560 m (8400 ft) elevation. The contrast is best seen in the road cut in the left-lateral moraine at 2640 m (8660 ft) elevation, well above the creek.

Just west of the highest hairpin turn of the new Onion Valley road the crest of the left-lateral moraine of advance III is seen to the south. Between this moraine and the road lies a low manzanita-covered ridge which contains rounded cobbles of hornblende diorite not found locally. This low feature is probably an older moraine.

Above 2740 m (9000 ft) elevation a largely unbreached end moraine is encountered. This is probably the terminal moraine of the early Holocene glaciation (advance V). West of this moraine Independence Creek flows within 1-2 m of the surface of a marshy area, perhaps a filled lake. Unconsolidated sand and gravel deposits alternate with peats in strata exposed in road cuts. The gravels may mark surges of outwash into the meadow during or just following Holocene advances, or they may simply be gravel bars of the post-glacial Independence Creek. Detailed study of this easily accessible location could lead to useful ^{14}C dates for Holocene events.

Because of the meager incision through the end moraine enclosing the meadows, it is regarded in this study as the terminal moraine of a recent glacial advance V. The assignment is unsupported by relative weathering data, and the moraine might simply be a recessional moraine of advance IV.

As in lower Onion Valley, the most recent Pleistocene glaciers appear to have left moraines a short distance from the canyon walls on the northern side of Independence Creek. Thus trim lines are better developed on the south side of the valley. However, at the meadow two

distinct lines of cliffs leading into the canyon of the northern tributary were recognized. The upper (~ 165 m above the valley floor) is considerably less pronounced and more eroded than the lower (only ~ 75 m above the valley floor). Even the lower line of cliffs is higher than the crests of the moraines of advance IV; thus, it may have been cut or at least refreshed during an earlier stage (perhaps advance III).

The presence of two trim lines is mentioned because it is unusual for glaciers to have such different depths this far from their snouts (Clark, 1967). Perhaps the simplest explanation in this instance is that when the older and higher line of cliffs was cut the bedrock step on Golden Trout Creek, now a few hundred meters to the north, stood closer to the confluence, as the comparable step on Robinson Creek does today. In this way the upper surface of the glacier would have been higher, without an increase in its depth.

Above the trim line on the south wall of upper Onion Valley are several truncated spurs, now ~ 270 m above the modern stream. Although these are developed mainly in the mafic pluton, their apices are only approximately near its contact with the Bullfrog quartz monzonite. Thus the truncation is probably not simply a consequence of differential erosion rates. It probably records the sudden incision of an ancient and shallower Onion Valley through the agency of tectonic displacement or climatic change.

Moraines of the southern tributary

Till in the canyons and cirques above Onion Valley are Holocene or perhaps latest Pleistocene in age. Three different periods of deposition can be detected (advances V, VI, and VII). These probably

correlate with the Hilgard, Recess Peak, and Matthes glaciations recognized elsewhere in the Sierra Nevada. The Matthes moraines are found only in the highest cirques.

The southern tributary to Independence Creek reaches the meadows at the head of upper Onion Valley in a cascade over a 150-m-high bedrock step. During the last glaciation this was an icefall. Moraines, probably of equivalent age to the terminal moraine below the confluence (advance IV or V) are found up to an elevation of 3200 m (10,500 ft), below Robinson Lake. Most of the moraines are found near the lip of the old ice fall. Apparently the snout of the glacier was there for a considerable time, or else the moraines would not have formed. Proximity to the snout may also be indicated by the low crests of the moraines near the creek from Robinson Lake. These are ~ 30 m below the crests of the moraines of the advance IV glaciers. The GWR for these moraines, composed entirely of the easily weathered Bullfrog quartz monzonite, were 78/22/0 and 50/50/0. These values are little different from those for till of advance IV (Table 5-2).

Robinson Lake itself is located behind an end moraine, probably of advance V. Pocket glaciers have occupied the cirque just south of the lake more recently. Unlike the forested moraines below the lake, they are unvegetated and have less soil. These are assigned to advance VI. The most important moraine of advance VI are found up-canyon above 3410 m (11,200 ft) elevation. The terminal moraine is unbreached, has extensive lichens on sheltered boulders, and minor sedges. Boulders are firmly seated in the moraine and provide stable footing. Dwarf white pines are found on the slopes just beyond the moraine itself.

At the head of the canyon, two rock glaciers descend from the south face of University Peak. The upper of these may be still active. The surfaces are essentially unstable boulder fields. Especially on the upper moraine, even lichens are missing. These are assigned to advance VII, the most recent of Onion Valley.

Two additional features along the southern tributary are of interest. First, on the southeast face of University Peak there has accumulated a thick deposit of sand, silt, and clay. This material is found as high or higher than the glacial trim line; it may be loess deposited alongside the glaciers or silt reworked by nivation. Second, deep erosion by Robinson Creek and its glaciers has beheaded the canyons of two streams draining east into Piñon Canyon from the ridge south of Robinson Lake. These stream-cut canyons have left characteristic V-shaped notches in the ridge. No alluvium is seen in the bottom of the exposed canyons. These are of interest because the contrast with the U-shaped profile of Sardine Canyon Canyon and other truncated valleys to the north which will be discussed later.

Moraines of the main fork

The main fork of Independence Creek enters Onion Valley from the west. Two main ice streams composed the glacier that cascaded into Onion Valley by this route. The larger arose in the cirques of the north face of the 4155-m-high University Peak (13,632 ft), entirely within the Bullfrog pluton. The other originated against the arete south of Mt. Gould near Kearsarge Pass.

Moraines of perhaps three ages are found in the headwaters of Independence Creek. By far the greatest area is covered by till of advance V.

Moraines of this advance, like those below Robinson Lake, are bouldery but stable. Few of the boulders of Bullfrog quartz monzonite have preserved patches of glacially abraded surfaces, and based on weathering alone, may look as old or older than boulders from moraines of advance III in upper Onion Valley. Advance V could thus be of similar age to advance IV, and could even be merely a recessional event. However, there seems to be consistently less burial of boulders in moraines of advance V, which argues against a similar age. Birman (1964) considers such apparent "weathering reversals" to be characteristic of Hilgard neoglacial moraines. Later discussion will focus on this topic. Soil development has been extensive enough to support forests.

Lakes in areas once covered by moraines of advance V are largely free of alluvial margins, except close to the inlets. An exception is Little Pothole Lake, which is the lowest lake and is largely meadow and marsh today. The highest lakes which were once covered by advance VI glaciers are completely devoid of alluvium and have shores composed of blocky fresh talus or till. Thus there seems to be a progression to the degree of sedimentation which must correlate with the age of the lake. The lowest lakes have received sediment from retreating glaciers the longest. The most heavily sedimented lakes appear to have received discharge from two glaciers.

Above ~ 3350 m (11,000 ft) elevation moraines are largely devoid of trees. Stability of boulders on the moraines is high in general, but loose ones are encountered. Sedges grow in sheltered locations. Many different lichens are well established, with minor axes of colonies of the yellow-green variety as large as 15 cm. These moraines are classified

as advance VI.

Glaciers of the youngest advance (VII) are found in the headwaters of the main fork only under the steep northeast face of University Peak and possibly at one location along the crest itself. Boulders comprising the moraines are sharp and angular and show no signs of glacial abrasion. Small boulders are commonly unstable and footing may be treacherous. Lichens are small and there are few coalescing colonies. The largest minor axes of the yellow-green lichens are 1.5 - 2 cm. No soil is developed, but small particles from silt up to small rock fragments are abundant.

The Mt. Pinchot quadrangle shows a small pocket glacier in the northeast cirque of University Peak above the moraines of advance VII. Inspection in the late summer failed to reveal a bergschrund, and there is no fresh moraine at its base. If it is a glacier, it is now inactive.

On the northeast ridge of University Peak a fresh line of cliffs can be seen as much as 150 m below the ridge top but far above the small moraines in the basin below. This line probably was last actively eroded during advance IV. There is no evidence that glaciers of the present drainage system ever attained a greater depth. At the same time, the crest of the ridge preserves a U-shaped chute high above the level of these glaciers. This trough contrasts strikingly with the complex of recent avalanche chutes on the ridge and appears to be a relic land form. Interestingly, the feature is about the same height above recent basins as is Kearsarge Pass.

During ancient glaciations a large ice cap between Mt. Gould and Kearsarge Pinnacles, west of the Sierra crest, may have fed ice eastward

through the U-shaped pass and down Onion Valley. Other passes through which such crest-crossing glaciers flowed (e.g., Tioga Pass and Taboose Pass) are today broad troughs generally sculpted on the east by cirques of later and smaller glaciers. All that remains of such a hypothetical trough at Kearsarge Pass is a narrow arete standing 125 m above the young glacial basins to the east and west. In this interpretation, the arete is the relic of the ancient floor of a glaciated canyon which has been incised and glacially eroded until only a thin septum remains. That this process occurs is amply evident at Taboose Pass (§ 5.9), where the septum is still hundreds of meters thick. Alternatively, the U-shaped profile of the arete could have been created simply by plucking from both sides, even in the absence of a pre-existing valley crossing the crest. This latter hypothesis is rejected for the following reasons: (1) other aretes on the same ridge are just as thin and delicate but show no evidence of a U-shaped profile; and (2) judging from the size of the neoglacial moraines, the glaciers near Kearsarge Pass eroded less than other cirque glaciers of the main fork of Independence Creek, yet the pass is the lowest point of the crest.

If Kearsarge Pass was once part of the floor of a glaciated valley, then the glaciers which carved it must have predated those which have left moraines in the modern Onion Valley. It must have required many successive glaciers great amounts of time to so nearly obliterate the ancient valley.

Thus the southern Sierra Nevada may have supported large ancient glaciers which have left little trace of their presence except for infrequent morphologic relicts unobliterated by the extensive glaciers of the late Pleistocene Epoch.

The old surface of University Peak . . .

The top of the ridge above the U notch at an elevation of 3660-3780 m (12,200 - 12,400 ft) is covered by as much as 5 m of diamicton. This mantle extends about 700 m along the ridge (Fig. 5-12). The surface dips gently towards Robinson Lake and is no more than 140 m wide. Along the northwest side of the ridge the diamicton is exposed in contact with the underlying Bullfrog quartz monzonite. The contact also dips to the northeast. In contrast to the gradational contact zone expected for nivated surfaces or felsenmere (cf. Matthes, 1900, 1933), this contact is extremely sharp, with silt, sand, and boulders directly overlying a smooth rock surface or a rock surface littered with a thin zone of blocks (Fig. 5-13). Because of the nature of its contact with the bedrock ridge, the diamicton appears to be depositional rather than the product of in situ weathering.

The bedrock surface exposed on three promontories shows signs of polish and fluting, with an orientation of N64°E (Fig. 5-14). The origin of the surface is unclear. The flutes are characteristically wider (1-3 mm) than glacial striations but their intersections with the boulder surface are not parabolic, as seen on wind-blasted quartz monzonite boulders elsewhere in the Sierra Nevada (e.g., at Green Creek, near Bridgeport, Mono Co., Calif.). It is certainly possible that this is a water-worn or glaciated surface modified by wind erosion. Boulders on the surface of the diamicton also seem to be polished by the wind.

The arete rising towards University Peak is quite smooth (Fig. 5-15). On either side the cliff is blocky and angular, showing the effects of plucking and rockfall. If the smooth arete itself resulted recently from

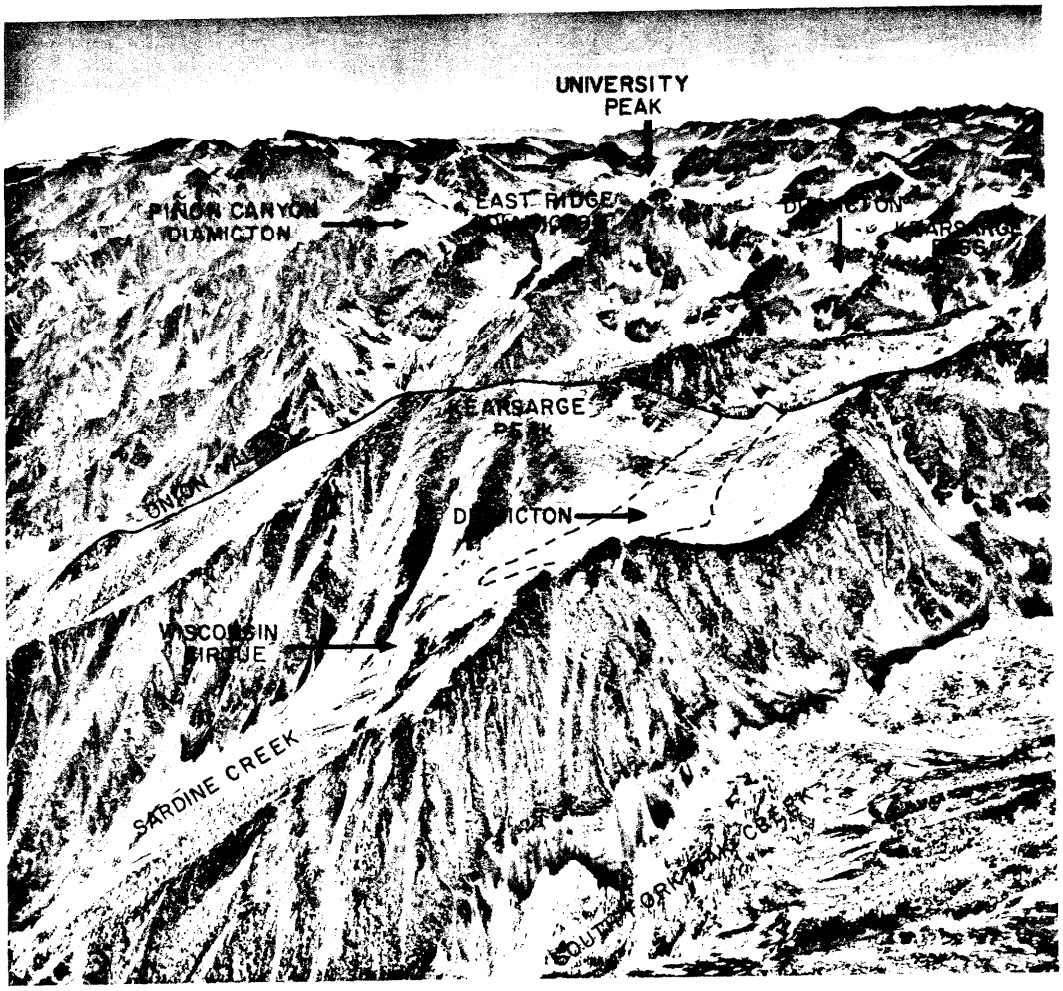

Fig. 5-12. Aerial photograph of the headwaters of Independence Creek from the north, showing the location of ancient diamictons high above the modern canyon. The diamicton of the eastern ridge of University Peak is truncated by 240-m-high cliffs of the cirque under the northwest face of the peak. The diamicton, ~ 5 m thick, appears to be depositional and must predate the cutting of the cirque. Other similar deposits are found above Piñon Canyon, near Kearsarge Pass, and above the Wisconsin cirque in Sardine Canyon. Each is at roughly the same elevation and may be a remnant of a regional surface of moderate relief. The diamicton in Sardine Canyon and the beheaded end of the canyon have been outlined for for clarity.

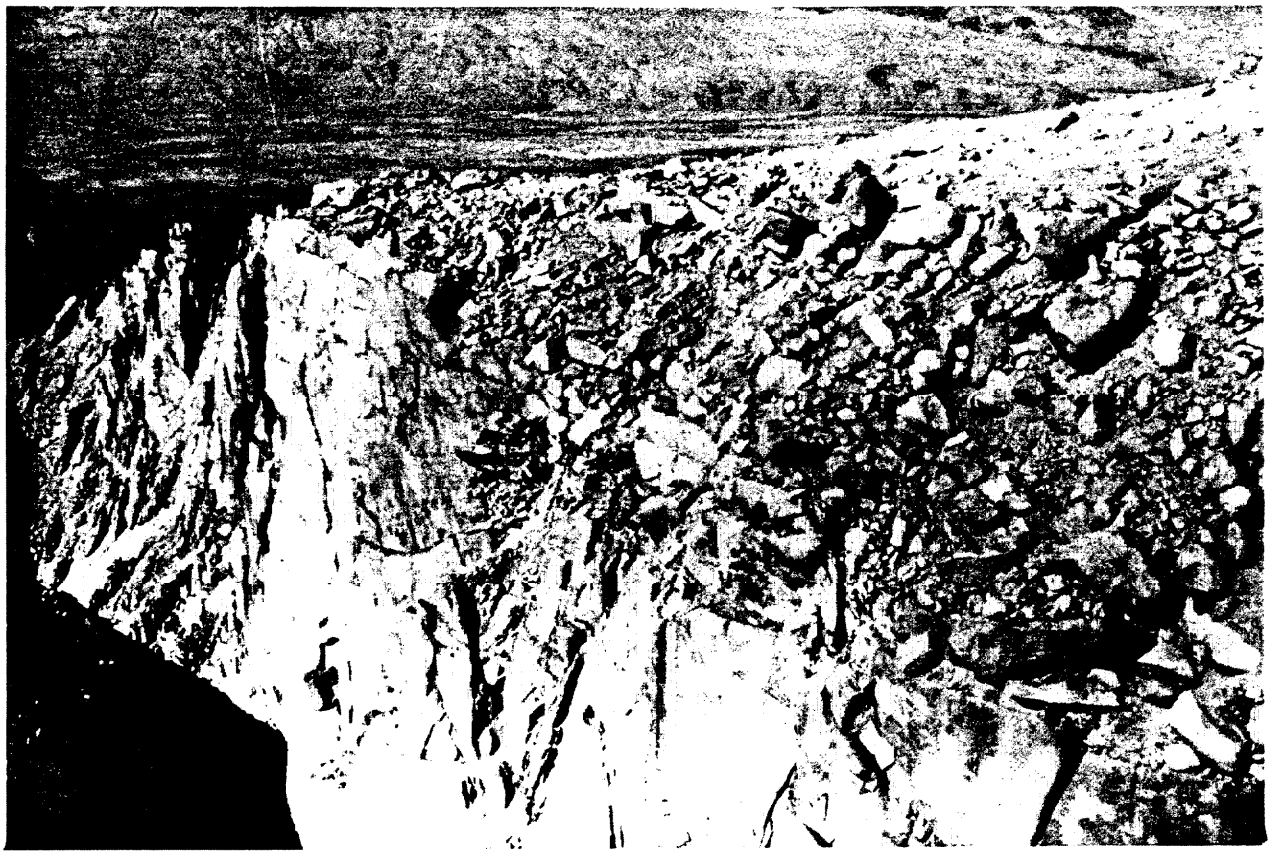

Fig. 5-13. The diamicton atop the eastern ridge of University Peak, looking east. The boulders in the foreground are ~ 1 m long. The sharp contact with the lightly weathered bedrock and the high concentration of silt-sized particles indicates that the diamicton was deposited, not created in situ.

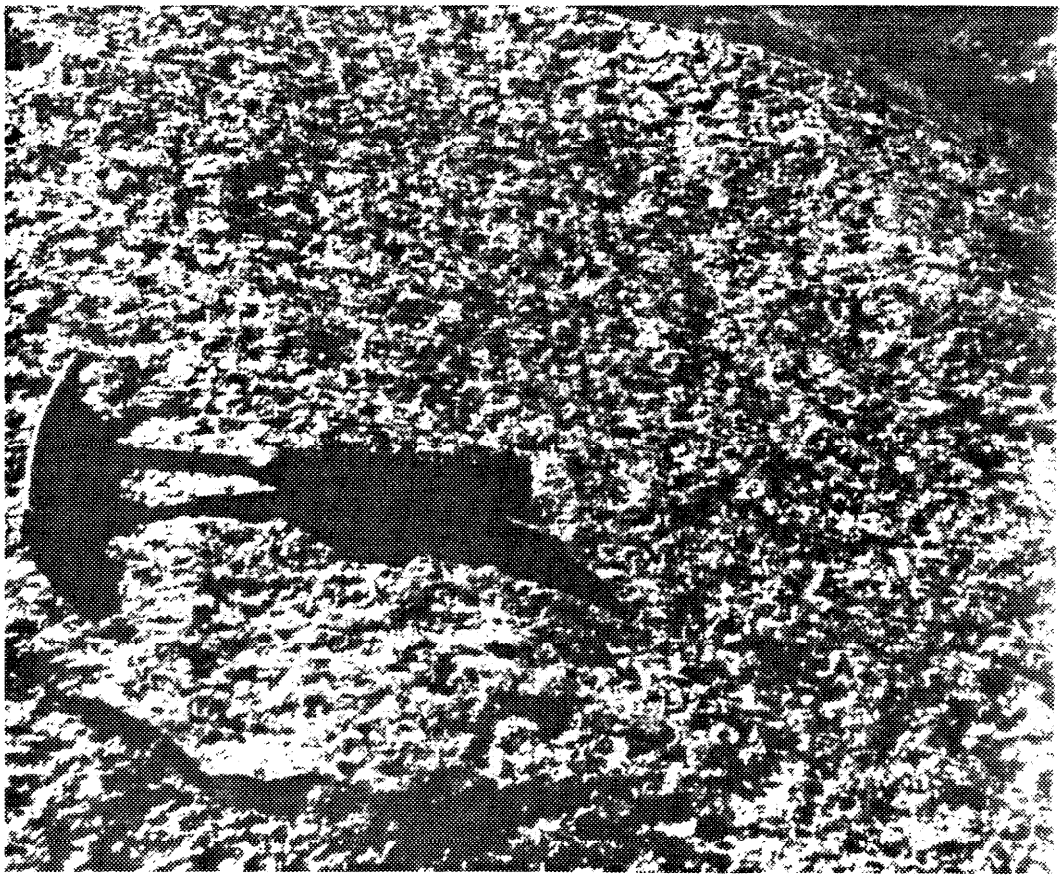

Fig. 5-14. Detail on the bedrock surface of the eastern ridge of University Peak. The rock is the quartz monzonite of the Bullfrog pluton. Striations and gouges parallel to the hammer head (N64°W) may be seen in the case-hardened surface. The ridge is capped by a diamicton.

Fig. 5-15. The arete above the diamicton on the eastern ridge of University Peak. The view is to the west. The flat face of the arete with the deeply eroded joints contrasts strikingly with the more freshly plucked cliffs on either side. Generally, aretes on Sierra Nevada peaks are narrow, with prominent spires or gendarmes. This arete, about 10 m wide, may be the last vestige of an ancient glacially sculpted valley wall.

frost riving and exfoliation, enormous blocks would be seen to either side, especially to the southeast where a long debris slope leads to the glacial trim line. The absence of such blocks indicates the surface has been inactive for a long time. Furthermore, joints in the face of the arete are deeply weathered, flaring widely in a fashion not observed in recently glaciated competent granodiorite or quartz monzonite in Yosemite Valley or Tuolumne Meadows. Pehaps this arete is a relict part of an ancient valley wall whose alluviated floor is likewise partially preserved on the ridge below. Downcutting of about 300 m must have occurred since deposition of the diamicton, implying at least an early Pleistocene age.

Characteristics of the diamicton itself do not necessarily lend strong support to the hypothesis of ancient origin. Below an armored surface a few cm thick on the middle promontory the soil color was reddish. Some buried clasts were grusy. However the matrix of the diamicton was virtually devoid of clay, and rock fragments did not have clay coatings. From this standpoint, the soil seemed no better developed than Tioga tills in Onion Valley. Since it is highly unlikely that the 300-m-deep cirque on the northeast face of University Peak has been cut since the late Pleistocene Epoch, it follows that chemical weathering at high altitudes in well-drained soils may be extremely slow.

The relative scarcity of the boulders at least near the surface of the diamicton may be explained by either weathering or the original character of the deposit. Because of the extremely fresh-appearing bedrock surface only a few meters below, it seems unlikely that boulders in the deposit would completely disintegrate. The original deposit may have been enriched in fine material, just as the late Pleistocene or

Holocene deposits on the slopes on the southeast flank of the same ridge are dominated by "loess".

Other ancient surfaces . . .

A second ancient depositional surface is preserved at 3720 m (12,200 ft) elevation on the peak between Bench and Heart Lakes. Diamicton on this surface may be as much as 50 m deep. It is being rapidly eroded on the north, and a large cone of debris has been built up southwest of Heart Lake. Presumably this has happened during previous interglacial periods also, with the weathered material being reworked by later glaciers. Such reworking of ancient debris could seriously effect apparent relative ages of moraines, in this case by the addition of grusy boulders to fresh till.

Approximately in line with the Sierra crest the diamicton thins. West of this point the weathered bedrock surface rises 100 m to the peak. Clearly the great depth of diamicton has not been created in situ. At the same time, no exotic boulders which indicated a distant origin were found. Like the presumably ancient diamicton of University Peak, the diamicton was poor in clay but oxidized sufficiently to have a Munsell color of 10YR7/4.

A third surface was found at 3960 m (13,000 ft) elevation on Mt. Gould, north of Kearsarge Pass. Here too the bedrock was buried by debris, but the thickness was much less and did not exceed a few meters. Furthermore, there seemed to be a one-to-one correspondence between the variable bedrock lithology and the composition of the deposit, so that the surficial material was undoubtedly derived in situ, albeit from a surface not strongly modified in recent times. This surface is probably

a felsenmere, or nivated surface.

Moraines of the northern tributary

Moraines of two ages are preserved in the canyons between Mt. Gould and Kearsarge Peak. These were left by glaciers of advances V and VI. Below the bedrock step at 2990 m (9800 ft) elevation are preserved several forested low end moraines. Weathering ratios are not necessarily related to ratios for moraines of other canyons, because boulders were mainly granodiorite of the Dragon pluton or mafic plutonic rocks. Boulders of the Bullfrog quartz monzonite were present locally; these appear to have been derived by rock fall onto the moraine and thus might be expected to give anomalously high apparent ages.

At 3290 m (10,800 ft) elevation, the two forks of the northern tributary meet in a silted-up lake, now a meadow. The western fork leads to Golden Trout Lake, which has itself had little sedimentation. Up to this elevation glacial deposits appear to belong to advance V. The head of the canyon, above a step at 3660 m (12,000 ft) elevation, arguably contains an old rock glacier of advance VI or VII. Here talus from Mt. Gould has coalesced in the bottom of a cirque to form a bouldery mass of convex profile. Missing, however, is clear evidence of mobility.

Of particular interest are the trim lines of the earlier glaciers (at least of advance IV). The most obvious line of cliffs is at an elevation of about 3580 m (11,750 ft), at the low point of the eastern ridge of Mt. Gould just above Golden Trout Lake. This is only a few tens of meters short of overtopping the ridge. To the east, the ridge rises to 3660 m (12,000 ft) elevation. Here the cliff line is lower, at about 3580 m (11,500 ft), and the northern face is deeply eroded by closely

spaced avalanched chutes. Generally, such chutes terminate at the trim line because the rock below is shielded from erosion by the glacial ice (Matthes, 1936). However, the deep chutes stop at ~ 3580 m (11,750 ft) elevation below the end of the ridge, and this is considerably higher than the trim line. The face of the ridge between the cliffs and the chutes is gullied also, but not deeply. This could result from differential erosion of facies within the mafic pluton, or it could be an earlier trim line.

The second fork of the northern tributary drains the east face of Dragon Peak. Above 3205 m (11,500 ft) elevation obvious rock glaciers about 300 m long are found. From the similarity of these to the rock glaciers of the southern and middle tributaries they have been assigned to advance VI.

Relative ages of moraines from acoustic wave speeds

Relative age determination of moraines by conventional semi-quantitative methods (Ch. 2) was somewhat unsatisfactory in Onion Valley. To some extent, this may have been because of problems with repeatability and consistency (different "operators" or even the same operator at different times might classify the same boulder differently). However, all semi-quantitative approaches rely on large numbers of observations well distributed over the moraines to be compared. In Onion Valley exposures were locally excellent but frequently limited. Many critical sites were subject to rockfall. These factors certainly reduced the effectiveness of relative dating. Because of the complexity of the glacial sequence at Onion Valley and because of its importance as an easily accessed reference sequence for correlation to other studies, relative dating was attempted using as a measure of age the speed of acoustic waves propagating through weathered

boulders found on moraine crests (Ch. 3). The chief virtue of this method is that quantitative data are gathered objectively. Repeatability is good, and the resulting data form a satisfactory basis for statistical testing and comparison. I felt these advantages would outweigh the difficulties presented by limited exposures and talus.

Twenty-eight sites for the measurement of P-wave speeds were distributed along glacial moraine crests, chiefly in Onion Valley. Site locations are shown in Fig. 5-16. Sites were established on most of the usable portions of each moraine crest. Two additional sites were established on talus of the Bullfrog quartz monzonite and the Tinemaha granodiorite. Data are summarized in Table 5-4. From 16 to 50 boulders were measured at each site, except for one site on talus (6-19). Mean P-wave speeds ranged from a high of 2.5 km/s for moraines in the cirques to a low of 0.8 km/s for the oldest moraines near the range-front. P-wave speeds for individual boulders ranged from 4.5 km/s (fresh) to 0.5 km/s (grusy). Except for one site (8-4) on a cirque moraine, the standard deviations ranged from $\sim$ 0.2 to $\sim$ 0.6 km/s.

The final two columns in Table 5-4 show values of the statistic D_{max} and the corresponding confidence (C_{NL}) that the distribution of measured speeds was from a non-normal population, according to the one-sample Kolmogorov-Smirnov test (Ch. 3). Values of C_{NL} ranged from 1% to > 99%, but seven were 90% or more. This is twice as many as nominally anticipated, but because only a small number of sites (28) were studied some deviation from ideal behavior is expected.

Figure 5-17 shows the cumulative frequency distribution of all 28 values of C_{NL} compared to expectation (solid diagonal line). The parallel dashed lines are the 90% and 95% confidence intervals within which

Table 5-4

Summary of Acoustic Wave-Speed Data for Onion Valley

Site	Advance[1]	Mean Speed, km/s	Std. Deviation of Speeds km/s	No. of Boulders	D_{max}[2]	C_{NL}[3] %
1-1	I-R	0.807	0.277	36	0.172	99
1-2	I-L	1.477	0.528	16	0.127	32
1-3	III-L	1.658	0.584	36	0.083	18
1-4	IV-L	1.712	0.540	28	0.139	90
2-1	II-L	1.619	0.449	21	0.119	39
2-2	II-L	1.514	0.411	20	0.090	9
2-3	I-R	0.895	0.176	20	0.130	52
2-4	II-R	1.430	0.243	20	0.127	46
2-5	II?-R	1.332	0.290	20	0.110	25
2-6	III-R	1.248	0.301	20	0.077	1
2-7	III-R	1.625	0.229	20	0.124	42
2-16	IV-L	1.896	0.368	16	0.155	66
2-17	III-L	1.514	0.427	16	0.157	68
3-1	IV-R	1.556	0.357	30	0.112	57
3-2	I-R	0.883	0.386	29	0.187	99
3-3	II-R	1.480	0.497	30	0.077	8
3-4	t-R	1.769	0.480	30	0.178	>99
3-5	V-R	1.512	0.453	30	0.128	90
3-6	V-R	1.574	0.461	30	0.236	>99
6-14	III-R	1.591	0.364	50	0.059	87
6-15	t-R	2.000	0.294	12	0.159	48
6-16	III-R	1.641	0.394	28	0.138	81
6-17	IV-R	1.728	0.421	30	0.109	54
7-1	III-L	1.757	0.398	30	0.072	6
8-1	IV-L	1.950	0.361	31	0.139	88
8-2	V-R	1.956	0.290	30	0.092	25
8-3	VI-R	2.118	0.350	30	0.108	52
8-4	VII-R	2.502	0.960	30	0.198	>99

1 Roman numerals I - VII identify the glaciation. "t" - talus; "R" - right-lateral moraine; "L" - left-lateral moraine.

2 D_{max} is the statistic generated by the Kolmogorov-Smirnov test for normality of the distribution of speeds (Ch. 3).

3 C_{NL} is the confidence with which the hypothesis that the sampled population was normal may be rejected (App. 3-A).

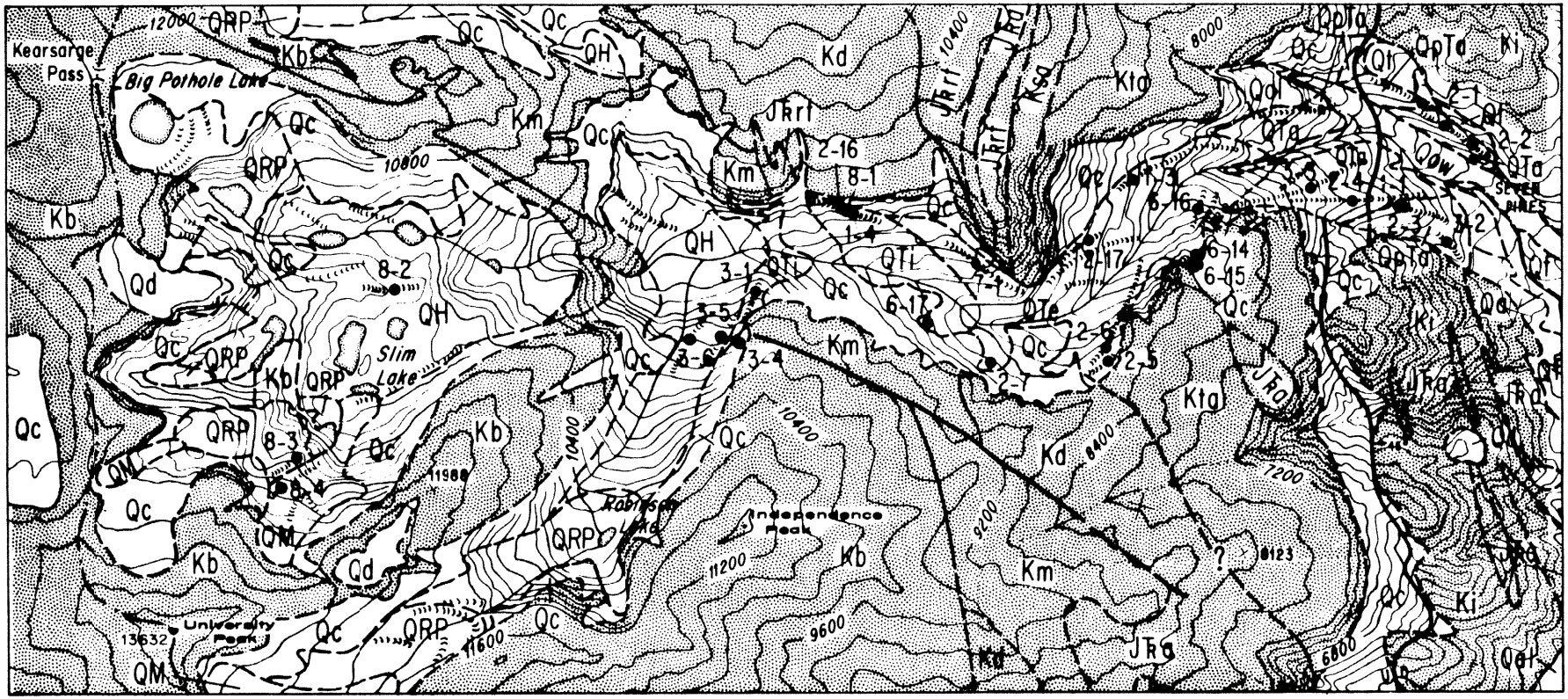

Fig. 5-16. Sites in Onion Valley where V_p data were acquired, and a geologic map of the drainage of Independence Creek. See next page for explanation.

Fig. 5-16. Onion Valley: V_p measurement sites and geology (continued)

Topographic data are from the U. S. Geol. Survey, Mt. Pinchot Quadrangle (1953) and the Mt. Whitney Quadrangle (1956). The scale has been increased from 1:62,500 to ~ 1:32,300; contour intervals were 80 ft (24.4 m). Outside of the vicinity of Independence Creek, only 400-ft contours were reproduced. Neither the new Onion Valley road nor the old road shown on the 1953 map is shown on this reproduction. The new road may be seen in Fig. 5-10

The bedrock geology is after Moore (1963). Cretaceous plutonic rocks are:

- Ki..... alaskitic quartz monzonite (Independence pluton)
- Kb..... alaskitic quartz monzonite (Bullfrog pluton)
- Ksa.... quartz monozonite (Sardine pluton)
- Kmg.... quartz monzonite (McGann pluton)
- Kta.... granodiorite (Tinemaha pluton)
- Kd..... granodiorite (Dragon pluton)
- Kdk.... Independence dike swarm: diorite and granodiorite porphyry
- Kgd.... granitic dikes
- Km..... mafic pluton: gabbro, hornblende diorite

Jurassic - Triassic metamorphosed volcanic rocks are:

- JTra... meta-andesite tuffs, breccias, and flows
- JTrf.. metarhyolite flows
- JTrt.. metarhyolite tuffs

The Quaternary deposits shown were mapped in this study. These units are:

- Qc..... talus
- Qal.... alluvium
- Qow.... glacial outwash
- Qf..... alluvial fan
- Qt..... kame terrace (probably pre Wisconsin)
- QM..... moraines of advance VII (Matthes glaciation, late Holocene)
- QRP.... moraines of advance VI (Recess Peak glaciation, Holocene)
- QH..... moraines of advance V (Hilgard glaciation, early Holocene)
- QTi.... moraines of advance IV (Tioga or late Wisconsin glaciation, late Pleistocene)
- QTe.... moraines of advance III (Tenaya or mid Wisconsin glaciation, late Pleistocene)
- QTa.... moraines of advance II (Tahoe or early Wisconsin glaciation, late Pleistocene)
- QpTa... moraines, kame terraces of advance I (pre-Wisconsin, Pleistocene)
- Qd..... diamicton, mid or early Pleistocene. The diamicton on University Peak may be glacial, but those near Seven Pines are remnants of alluvial fans.

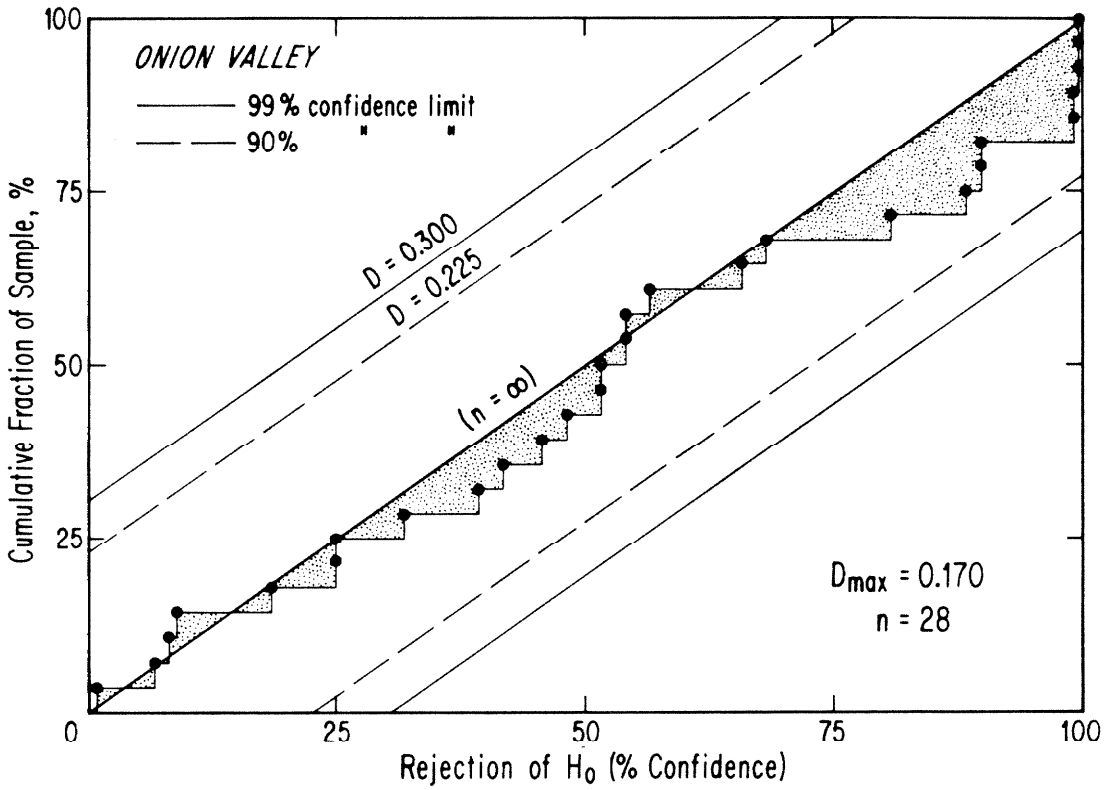

Fig. 5-17. Tests for normality of distributions of acoustic wave speeds measured at 28 sites in Onion Valley. The one-sample Kolmogorov-Smirnov test was applied to data from each site (Ch. 3). Each test produced a confidence with which H_0, the hypothesis that the data were from normally distributed populations, could be rejected. The figure shows the cumulative distribution of these 28 values, compared to the ideal distribution (heavy diagonal line) of an infinite number of samples from normal populations. For finite numbers of sites, the distributions will deviate about this ideal; the limits within which 90% and 99% of all distributions for 28 sites will fall are indicated by light dashed and solid lines, respectively. The actual distribution lies well within these limits. It may be concluded that the population of acoustic wave speeds in boulders of Onion Valley is normally distributed.

the actual data are expected to plot in 90% or 95% (respectively) of all cases. The samples for Onion Valley appeared to be from a normally distributed population; therefore conventional statistical tests for differences (Student's t-test) and analysis of variance could be used.

In Table 5-5 acoustic wave speeds were grouped by morphologic and semi-quantitative weathering criteria. Acoustic wave speeds were measured only for boulders from the Bullfrog (quartz monzonite) and Tinemaha (granodiorite) plutons. These rocks were of different grain size and composition. The only other granitic rock, the dark Dragon granodiorite, was excessively mafic according to Crook and Kamb (1980).

The Bullfrog quartz monzonite was leucocratic and medium-grained to coarse-grained. Coarse-grained rocks contained biotites as large as 5 mm, and weathering of these micas appeared to be one factor in the rapid decomposition of these rocks (e.g., Clark, 1967) Disintegrated quartz monzonite boulders typified the right-lateral moraine of advance I that gave the slowest wave speeds.

Tinemaha granodiorite was fine-grained compared to the Bullfrog quartz monzonite and did not seem so susceptible to disintegration. Wave speeds in quartz monzonite talus at 2865 m (9400 ft) elevation were 1.77 ± 0.48 km/s (site 3-4). In contrast, speeds in Tinemaha granodiorite talus at 2670 m (8600 ft) elevation were 2.00 ± 0.29 km/s (site 6-15). The higher talus covered a moraine of advance IV; the lower covered a moraine of advance III. Thus the granodiorite boulders transmitted acoustic waves marginally faster even though they may have been older.

The difference in wave speeds probably reflects an intrinsic property of the rocks. Thus the ratio of quartz monzonite to granodiorite boulders

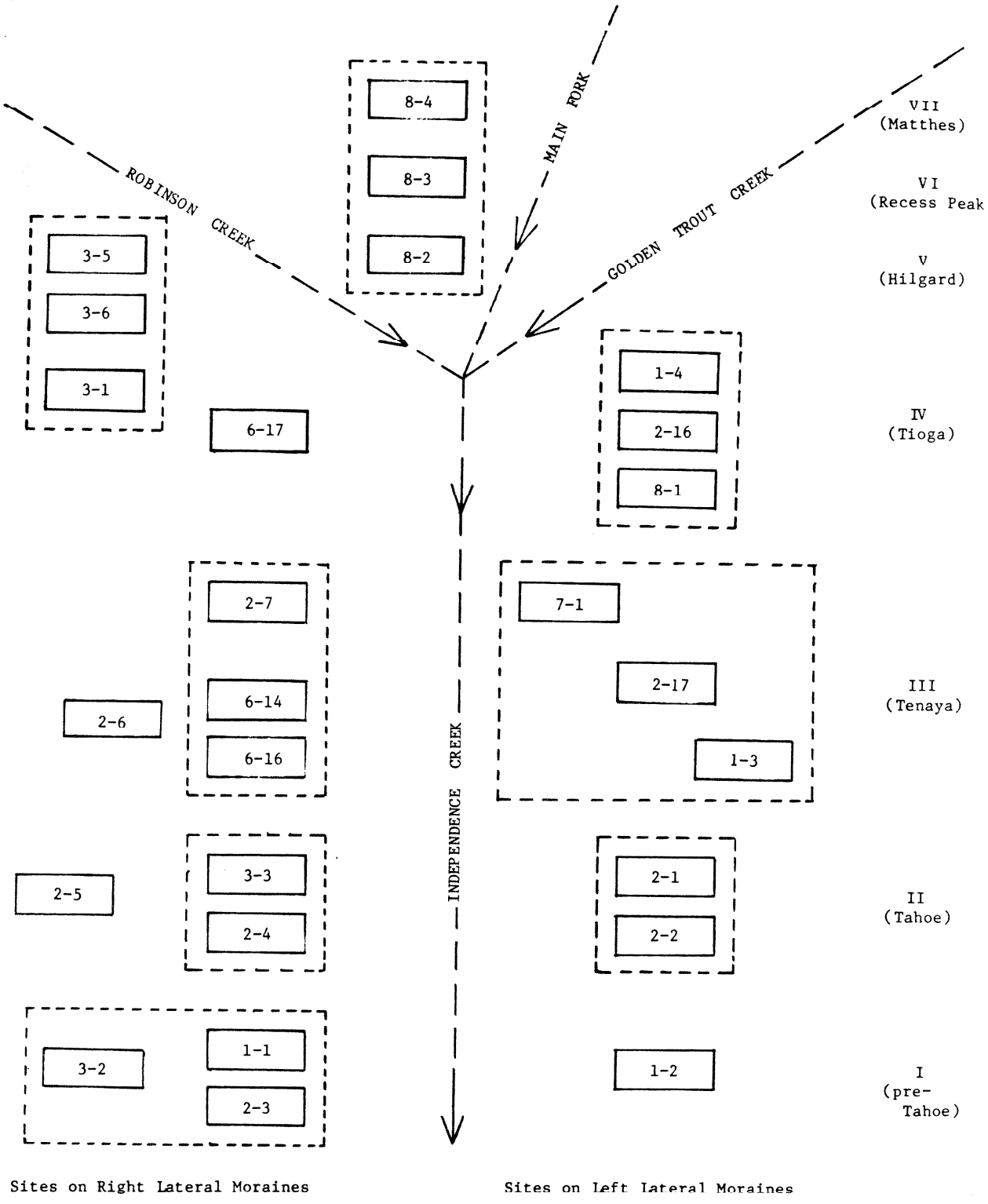

Table 5-5. Schematic representation of the geographic distribution of sites about Independence Creek and its two tributaries. Arrows indicate stream direction. North is to the right. Actual locations are found in Fig. 5-16. In this table, sites on youngest moraines are at top; age of moraines increases down the table. Relative ages and their probable conventional equivalents are found to the right. Grouping of sites for statistical testing is indicated by boxes.

in the sample may affect the distribution of measured speeds. However, were this a severe problem the wave-speed distributions would be bimodal and hence non-normal; this they were not. Consequently, use of acoustic wave speeds for samples of mixed populations seems justified unless the mixing ratios are strongly different among moraine crests.

There was no indication that this was so for moraines on the same side of the valley. However, speeds on left-lateral sites were consistently higher than speeds in right-lateral moraines of equivalent age (Table 5-4). Left-lateral moraines had fewer of the easily weathered quartz monzonite boulders than did right-lateral moraines, because of differences in provenance. This gross difference in mixing ratios was probably responsible for the disparity in speeds between moraines of the same advance but different sides of the stream.

Because of the complexities of the left-lateral moraine sequence east of the Independence Fault and because of the widespread burial of right-lateral moraine crests by talus in upper Onion Valley, an entire suite of good sites on only one side of the creek could not be found. The fall of weathered talus onto a moraine will make young moraines appear too old, and ancient moraines appear too young.

Wave-speed data were grouped according to the age of the moraine on which they were measured. The distribution of sites and their organization into groups is shown schematically in Table 5-5. Two kinds of statistical tests were performed on wave speed (V_p) data organized as shown: 1) tests of homogeneously for sites within a group (analysis of variance); and (2) test for differences between groups. Because the population of all V_p appeared to be normally distributed, the latter

tests required only that the means ($\overline{V_p}$), standard deviations (s), and the numbers of measurements for each group be known. These are displayed in Table 5-6.

Analysis of variance was done three ways: Fisher's method of randomization; Student's t-test (if a group contained only two sites); and Fisher's F-test (Ch. 3). Results are displayed in Table 5-7. The F-test is attractive because it is conventional and computationally simple. However, it was probably inapplicable in several instances (marked in the table by an asterisk) because variances were too dissimilar among sites within groups. All groups tested appeared to be homogeneous (less than 95% chance of error). The t-test gave similar results where it could be applied.

Fisher's method of randomization was the most useful test, because it produces directly a confidence with which the group may be regarded as homogeneous. It may also be used in circumstances where the F-test is applicable. These tests also showed that all groups of Table 5-5 were homogeneous (less than 90% confidence of rejection). Thus the organization of data into groups was not arbitrary and tests for differences between groups may yield valid geological conclusions. Confidence values from Fisher's method of randomization (C_{F*}) and from Student's t-test (C_t) are shown in Table 5-6, along with $\overline{V_p}$ and s, for groups of data.

Table 5-8 summarizes the results from Student's t-test comparing sites and groups shown in Table 5-6. Two different confidences, C_1 and C_2, are shown for each test. These correspond to the one-tailed and two-tailed tests, respectively. The one-tailed test is used when the relative age is known from morphologic or other considerations, but the

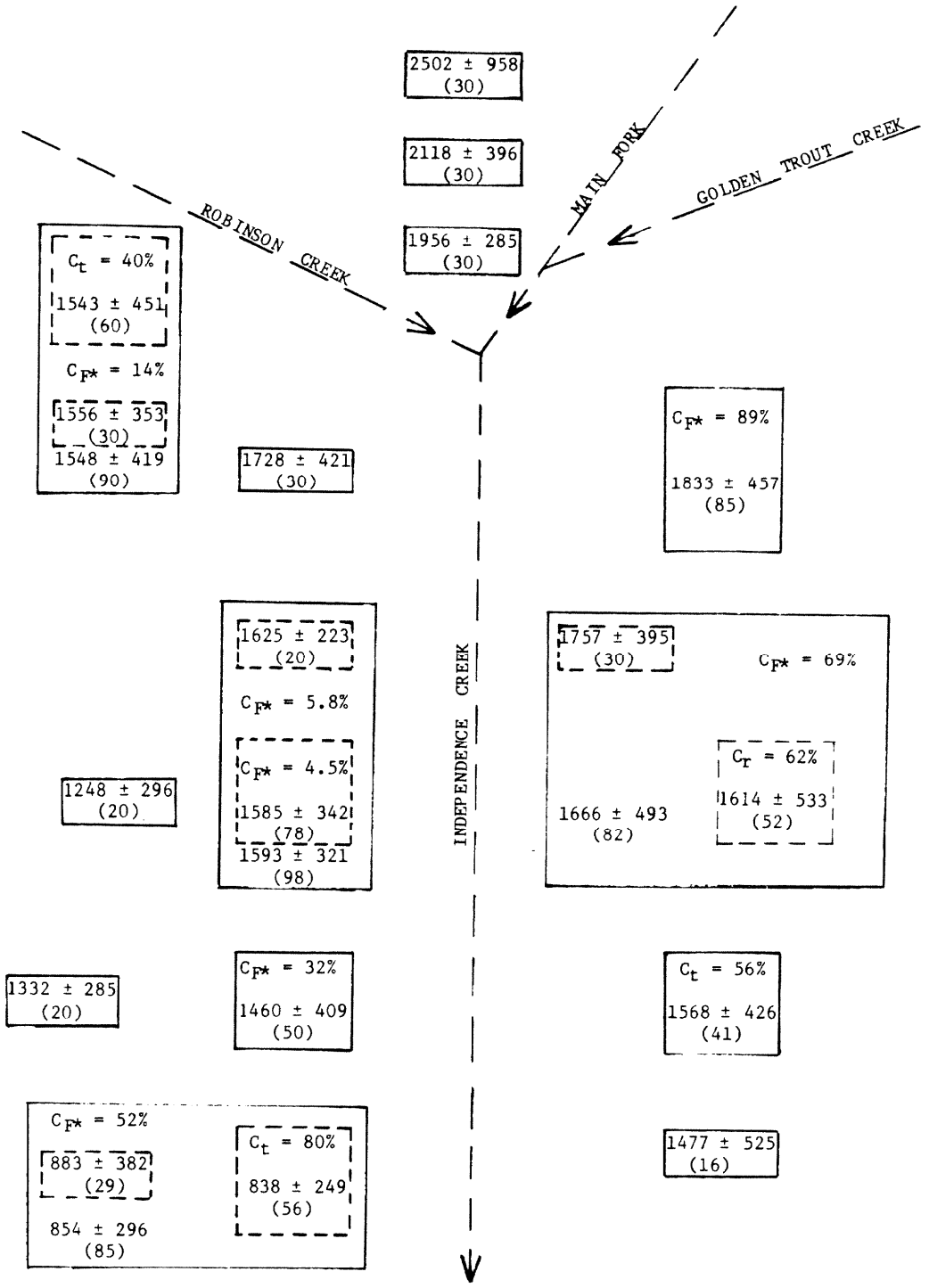

Table 5-6. Mean ($\overline{V_p}$) and standard deviations (s) for distributions of acoustic wave speeds (V_p) for sites and groups of sites used in tests for differences between moraines (Table 5-8).

(Table 5-6, continued)

The schematic distribution of sites and groups reflects their geographic locations (Fig. 5-16). Site numbers are found in Table 5-5. $\overline{V_p}$ and s are in m/s. The number of measurements for each site or group is in parentheses below $\overline{V_p}$ and s.

Results of the analyses of variance for groups of sites (Table 5-7) are shown also. The values listed give the confidence with which H_o (samples are drawn from the same population) may be rejected: C_F is the confidence found by Fisher's method of randomization; and C_t is the confidence found by Student's t-test (two-tailed), for groups of two sites.

Table 5-7

Analysis of Variance for Groups of V_p Data from Onion Valley

a) Right-Lateral Moraines

Sites[1]	Age[2]	Fisher's Method of Randomization[3] F*	Fisher's Method of Randomization[3] C,%	t-Test[4] Degrees of Freedom	t-Test[4] t	t-Test[4] C_2,%	F - Test[5] Hartley's Test	F - Test[5] Degrees of Freedom	F - Test[5] Cochran's Test	F
3-5,3-6 (RC)	V	-	-	58	-0.53	40	1.04(2.23)	30	0.51(0.69)	$F_{1,58}$ = 0.28(4.01)
3-5,3-6,3-1(RC)	IV-V	0.17	13.5	-	-	-	1.68(2.69)	30	0.39(0.50)	$F_{2,87}$ = 0.17(3.10)
6-14,6-16	III	0.01	4.6	76	-0.57	43	1.17(2.00)	39	0.54(0.68)	$F_{1,76}$ = 1.13(3.97)
2-7,6-14,6-16	III	-	-	-	-	-	3.06(2.62)*	32.7	0.46(0.49)	$F_{2,95}$ = 0.76(3.09)
3-3,2-4	II	0.18	32.0	48	0.42	32	4.35(2.41)*	25	0.81(0.70)*	$F_{1,48}$ = 0.18(4.04)
1-1,2-3	I	-	-	54	-1.31	80	2.47(2.29)*	28	0.71(0.69)*	$F_{1,54}$ = 1.65(4.02)
1-1,2-3,3-2	I	0.76	53.0	-	-	-	5.19(2.77)*	28.3	0.59(0.50)*	$F_{2,82}$ = 0.76(3.11)

b) Left-Lateral Moraines

Sites	Age[2]	Fisher's Method of Randomization[3] F*	Fisher's Method of Randomization[3] C,%	t-Test[4] Degrees of Freedom	t-Test[4] t	t-Test[4] C_2,%	F - Test[5] Hartley's Test	F - Test[5] Degrees of Freedom	F - Test[5] Cochran's Test	F
1-4,2-16,8-1	IV	2.56	89.0	-	-	-	2.27(2.77)	28.3	0.53(0.50)*	$F_{2,82}$ = 2.56(3.11)
2-17,1-3	III	-	-	50	-0.89	62	-	-	-	-
7-1,2-17,1-3	III	1.27	69.0	-	-	-	2.17(2.80)	27.3	0.50(0.50)	$F_{2,79}$ = 1.27(3.13)
2-1,2-2	II	-	-	39	0.78	56	1.20(2.62)	20.5	0.54(0.72)	$F_{1,39}$ = 0.61(4.09)

1 Site locations are shown in Fig. 5-16. Organization of sites into age groups is shown in Table 5-5. Correlation to the conventional Sierra Nevada glacial sequence is presented in Table 5-10. RC denotes sites on Robinson Creek.

2 Roman numerals identify the glacial stage, for Onion Valley.

3 Analysis of variance by Fisher's Method of randomization (Ch. 3) is necessary if conditions of the F-test are not fulfilled. F* is the calculated statistic, similar to F. C is the confidence with which H_o (all samples were drawn from the same population) may be rejected.

4 Student's t-test was used when a group contained only two sites. The degrees of freedom are n + m - 2, where n and m are the number of measurements at the two sites; t is the t-statistic, calculated from $\overline{V_p}$ for the site listed second subtracted from $\overline{V_p}$ for the site listed first; C_2 is the confidence that the samples were not drawn from the same population (two-tailed test).

5 F-test: application of the F-test requires that several conditions be met (Ch. 3). Similarity of the variance among sites (homoscedasticity) is tested by Hartley's and Cochran's tests: the degrees of freedom listed in the second column of the group refer to these tests. In only 5% of all cases where the samples are drawn from populations of the same variance will the test statistics exceed the limits shown in parentheses. Asterisks mark the tests in which the critical value was exceeded; in these cases the F-test may not be valid. The final column lists the value of F (the degrees of freedom are subscripted). The critical limit in parentheses is the value at which H_o may be rejected with 95% confidence.

Table 5-8

Results of t-Tests on Groups of V_p Data from Sites on Moraines in Onion Valley

a) Right-Lateral Moraines

Sites*	Age**	t*†	Degrees of Freedom†*	C_1,%†	C_2,%††
8-4 vs. 8-3	VII vs. VI	2.06	58	98	96
8-3 vs. 8-2	VI vs. V	1.98	58	98	95
8-2 vs. (3-5,3-6,3-1)	V vs. IV(RC)	4.96	118	>99	>99
8-2 vs. 6-17	V vs. IV	2.46	58	99	98
(3-5,3-6,3-1) vs. 6-17	IV(RC) vs. IV	-2.06	118	0	96
6-17 vs. 2-7	IV vs. III	1.00	48	84	68
2-7 vs. (6-14,6-16)	III vs. III	0.49	96	69	38
(6-14,6-16) vs. (3-3,2-4)	III vs. II	1.88	126	97	94
(3-3,2-4) vs. (1-1,2-3,3-2)	II vs. I	9.95	133	>99	>99
(1-1,2-3) vs. 3-2	I vs. I	-0.65	83	0	48
2-6 vs. 2-5	II vs. III	-0.92	38	0	64
2-6 vs. (2-7,6-14,6-15)	III vs. III	-4.43	116	>99	>99
2-5 vs. (3-3,2-4)	III vs. II	-1.28	68	0	80
2-5 vs. (1-1,2-3,3-2)	III vs. I	6.55	103	>99	>99

b) Left-Lateral Moraines

Sites*	Age**	t*†	Degrees of Freedom†*	C_1,%†	C_2,%††
(1-4,2-16,8-1) vs. 7-1	IV vs. III	0.82	113	79	58
(1-4,2-16,8-1) vs. (2-17,1-3)	IV vs. III	2.55	135	99	99
(1-4,2-16,8-1) vs. (7-1,1-3,2-17)	IV vs. III	2.28	165	99	98
7-1 vs. (2-17,1-3)	III vs. III	1.28	80	90	80
(2-17,1-3) vs. (2-1,2-2)	III vs. II	0.45	91	67	34
(7-1,1-3,2-17) vs. (2-1,2-2)	III vs. II	1.08	121	86	72
(2-1,2-2) vs. 1-2	II vs. I	0.68	55	75	50

c) Cross-Canyon Comparisons

Sites*	Age**	t*†	Degrees of Freedom†*	C_1,%†	C_2,%††
8-2 vs. (1-4,2-16,8-1)	V(RL) vs. IV(LL)	1.38	113	92	83
6-17 vs. (1-4,2-16,8-1)	V(RL) vs. IV(LL)	-1.11	113	0	73
(2-7,6-14,6-16) vs. (7-1,1-3,2-17)	III(RL) vs. IV(LL)	-1.19	178	0	77
(3-3,2-4) vs. (2-1,2-2)	II(RL) vs. II(LL)	-1.23	89	0	78

Table 5-8 (footnotes)

* Site locations are shown in Fig. 5-16. Organization of sites into age groups is shown in Table 5-5.

** Roman numerals identify the relative age by glacial stage. Correlation to the conventional Sierra Nevada sequence is presented in Table 5-10. RL and LL denote right- and left-lateral moraines, respectively. Advance IV includes sites in Robinson Creek ("RC").

*† In calculating the t-statistic, $\overline{V_p}$ for the group of sites listed second was subtracted from $\overline{V_p}$ for the group listed first.

†* The degrees of freedom are n + m - 2, where n and m are the number of measurements in each group.

† C_1 is the confidence with which the hypothesis H_1 (that $\overline{V_p}$ for the first group is not greater than $\overline{V_p}$ for the second group) may be rejected (one-tailed test).

†† C_2 is the confidence with which the hypothesis H_o (that the mean speeds are the same) may be rejected (two-tailed test).

significance of the age difference is uncertain. The two-tailed test is used when the relative ages are thought to be the same.

Appropriate values of C_1 or C_2 are displayed in Table 5-9, on tie lines connected to the groups or sites tested. These results confirm that, in general, wave speeds are distinctly different for moraines of different advances. In contrast, $\overline{V_p}$ for right- and left-lateral moraines are not different at even the 90% confidence level, although values for left-lateral moraines are consistently higher. Thus in general V_p data seem to confirm that advances I-VII represent glacial advances distinctly separated in time. Special considerations for individual tests are discussed below.

Speeds for sites on right-lateral moraines east of the Sierra escarpment clearly show the difference in weathering between tills of advances I and II. Moraines of advance II are younger with more than 99% confidence. On the other hand, the two speed distributions for the sites on different moraine crests of advance II are not statistically different. The locations of sites 1-1 and 2-3 (advance I) were overlapping. These were chosen to demonstrate repeatability--different operators made the measurements during different field seasons. They could not be distinguished at even the 75% confidence level. Analysis of variance of all three sites on right-lateral moraines of advance I showed that samples were all from the same population. This reinforced the conclusion from conventional study that the outermost ridge (site 3-2) was the same age as the larger moraine.

The right-lateral moraines east of the range front are favorable for relative dating because they are far from source areas of boulders

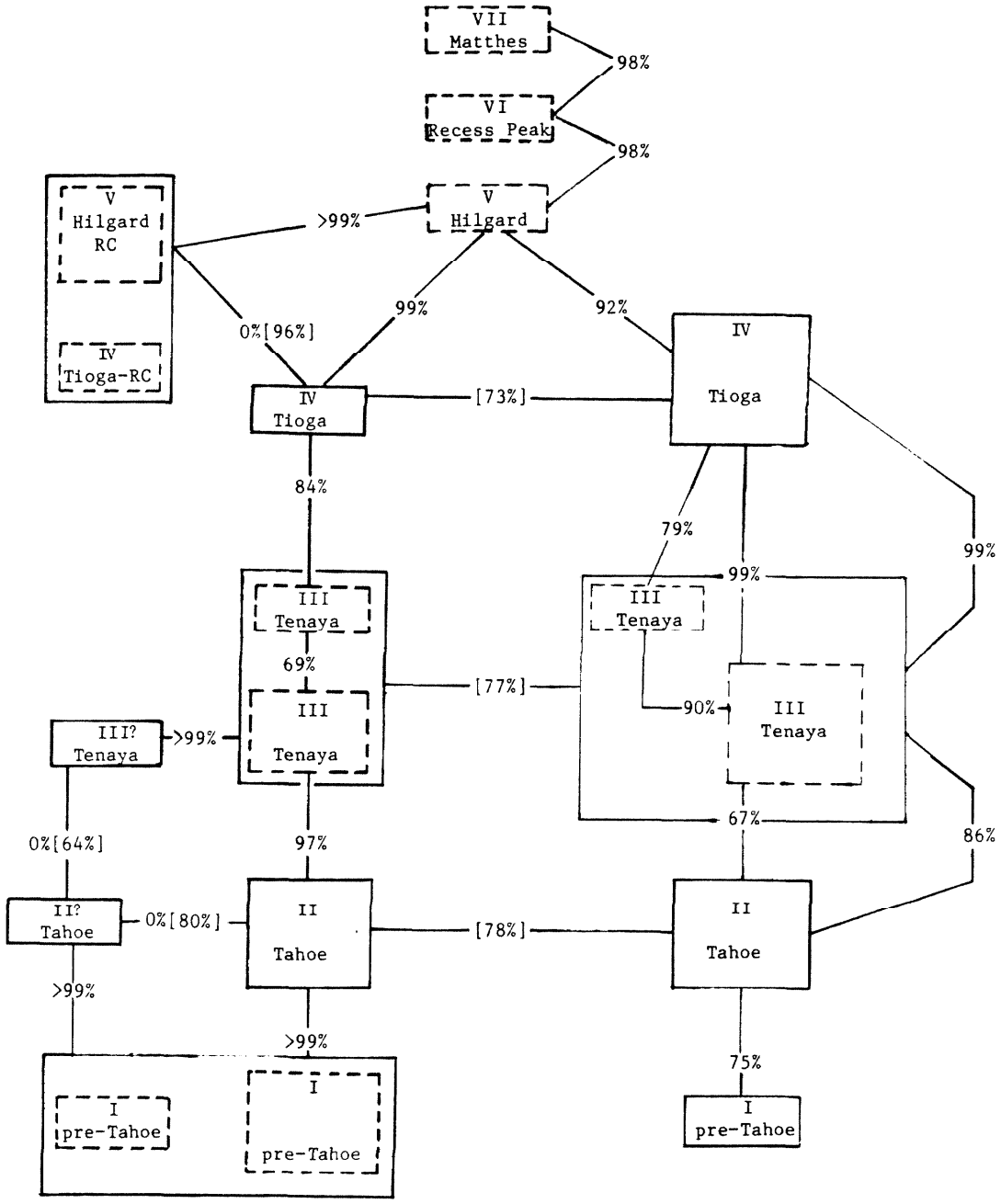

Table 5-9 Comparisons of $\overline{V_p}$ between sites and groups of sites in Onion Valley. Values shown on tie bars are C_1, the confidence found from the one-tailed Student's t-test that $\overline{V_p}$ for the site closer to the top of the table is smaller than $\overline{V_p}$ for the lower group. Where appropriate, values of C_2 (from the two-tailed version of the test) are shown in square brackets. A more extensive summary of the testing is found in Table 5-8. Ages of sites and groups are shown in boxes. Site locations are schematic only. Site identifications are found in Table 5-5.

and rockfall. Thus homogeneity in till of the same age is maximized.

Beginning with sites 6-14 and 6-16 (advance III), the moraines are found under cliffs, so the opportunity for recent rockfall is present. At these sites, the cliffs and any talus are composed of Tinemaha granodiorite. Measurements were restricted at these two sites to quartz monzonite boulders, to eliminate the possibility of contamination. This should also have minimized the difference between mean speeds at these sites and at sites on the older moraines downstream (for which granodiorite boulders were not excluded). However, mean speeds were still greater than for advance II moraines at the >95% confidence level. This appears to justify the assignment of these moraines to the younger advance III. Furthermore, within advance III the higher moraine (6-14) was not different from the morphologically younger recessional (6-16), although the mean speed was 0.05 km/s lower. It was concluded from conventional relative dating methods that the higher moraine might be of advance II. From this new evidence, this conclusion seems to have been in error. Acoustic wave-speed data strongly support the recognition of three distinct glacial advances in lower Onion Valley.

Sites 2-5 and 2-6 were located in a region of minimal rockfall on right-lateral moraines. Site 2-6 was on an advance III moraine; site 2-5 may have been on an older one. Talus was Tinemaha granodiorite only. No effort was made to measure quartz monzonite boulders only, but the effect of recent rockfall probably would be to increase the mean speed. It is possible that glacial boulders from site 2-5 rolled down onto the moraine of site 2-6. Sites 2-5 and 2-6 were not different statistically. The mean speed for site 2-6 was lower than $\overline{V_p}$ for sites 6-14 and 6-16.

This difference is significant at the >99% confidence level. The low mean speed at site 2-5 on the upper moraine was anticipated because the moraine was thought to have been an ancient remnant.

Site 2-5 appeared to have lower speeds than the two advance II sites (2-4 and 3-3), but the mean speeds were different at only the 80% confidence level. The absence of grusy boulders contrasts markedly with the moraines of advance I. Thus it might be argued that the upper moraine (site 2-5) was of similar age as the moraines of advance II, or that it was intermediate in age between advances I and II, but it could not have been as old as advance I. The lower moraine (site 2-6) is constrained by its location to be younger than the advance III moraines of sites 6-14 and 6-16. Its anomalous age could be explained if it was buried by mass wasting of till from the upper moraine. This argument is difficult to believe since there was little geomorphic evidence to support it. Thus the discrepancy must be attributed to (1) an intrinsic defect in the acoustic wave-speed method; (2) gross heterogeneity of boulders in the till, or (3) some unrecognized blunder in the actual measurement of the wave speeds. It is interesting that the nearby site 2-7 (also on a moraine of advance III) gave a mean speed of 1.63 km/s, indistinguishable from the speeds at sites 6-14 and 6-16 also on advance III moraines. Because this site was measured the same day as the others, the third possibility seems unlikely. The demonstrated consistency of acoustic wave-speed data at Bloody Canyon and Green Creek appears to rule out the first possibility. Thus the second possibility must be considered.

In the discussion below it will be shown that Bullfrog quartz monzonite boulders from the southern tributary transmit acoustic waves slower

than similar boulders from the main fork. Thus the unusually low speeds at sites 2-5 and 2-6 could be due to mixing of boulders from different source regions. If this is true, acoustic wave speeds and perhaps other weathering data on right-lateral moraines in Onion Valley would be unreliable indicators of age. Sites below the range front would be less affected because of the greater opportunity for mixing.

The contact between till of advances III and IV was not recognized in V_p data from right-lateral moraines. Site 6-17 was 300 m west of site 2-7, on a lateral moraine of advance IV. The mean speed was greater than at site 2-7, but only at the 84% confidence level. It is not possible to tell from these data whether this is because the last glaciers of "advance III" and the first glaciers of "advance IV" were not separated much in time, or because of mixing and other problems encountered in right-lateral moraines.

To characterize the effect of till from the southern tributary on apparent ages in Onion Valley, three sites were established on moraines within its drainage (3-1, 3-5, and 3-6). Although 3-1 was on a moraine of advance IV and the others were on moraines of age V, analysis of variance showed that the samples were from the same population. Site 3-1 was on a promontory free of rockfall, and sites 3-5 and 3-6 were shielded from rock fall by the higher moraine of site 3-1 and deep fosses. Thus it must be concluded that these moraines were of the same apparent age. The mean speed at these three sites was less than at 6-17, and the groups were different at the 96% confidence level.

From the above information it appears that Bullfrog quartz monzonite from the southern tributary weathered faster than that from the main fork.

Partly to verify the above conclusion, sites were established on moraines of ages V, VI, and VII in the drainage of the main fork. These samples represented different populations at the 95% confidence level or or greater, and there was a clear decrease in mean speed with increasing age of the moraine. Site 8-2 (advance V) was at the lowest possible elevation (3235 m or 10,620 ft) to facilitate comparison with the sites from the southern tributary. Nevertheless, it was higher by ~ 300 m. The main fork site was clearly "faster", at >99% confidence. It was also "faster" than sites on both right- and left-lateral moraines of advance IV in Onion Valley. This appears to preclude the possibility that the anomalous values of $\overline{V_p}$ for the Robinson Creek sites resulted from a "weathering reversal" such as Birman (1964) claimed for Hilgard and Tioga tills in Rock Creek and Mono Creek, north of this study area. The simplest explanation is that quartz monzonite from the southern tributary weathers exceptionally quickly.

Unlike right-lateral moraines, the left-lateral moraines of upper Onion Valley contain boulders of Bullfrog quartz monzonite only from the main fork. About 80 m of crest of one left-lateral moraine of advance IV was suitable for acoustic wave-speed measurements. Three sites (1-4, 2-16, and 8-1) were established here. Talus was from the Dragon granodiorite and was recognized and excluded from the samples. Analysis of variance shows that the three samples were taken from a single population.

The three sites treated as a group were "slower" than the single site of advance V (8-2), but the difference was decidedly less pronounced than the difference between 8-2 and the sites of the southern tributary. Because left-lateral sites were in general "faster" than right-lateral

sites, this distinct difference probably should be attributed to a significant difference in age. The increased contrast seen between sites 8-2 and 6-17 appears to reinforce the hypothesis of variable weathering rates within the Bullfrog pluton.

Moraines of advance IV and advance III were readily distinguished in roadcuts by the fraction of quartz monzonite boulders which are disintegrated. At site 7-1 a segment of crest of a left-lateral moraine of advance III was preserved both from rockfall and road builders. The mean speed at site 7-1 was lower than two of the three advance IV sites. It was lower than that of the combined three sites, but only at the 79% confidence level. This does not appear to justify the separation of advances III and IV.

Two other sites were established on left-lateral moraines of advance III (2-17 and 1-3). Site 2-17 was directly comparable in composition to site 7-1, because it was only 300 m east of the westernmost outcrops of Tinemaha granodiorite. Site 1-3 was another 500 m farther east, so the fraction of Tinemaha boulders may have been greater. However, sites 2-17 and 1-3 were not significantly different, and the hypothesis that these three sites on left-lateral moraines of advance III sampled the same population could be rejected at only the 69% confidence level. Despite this, site 7-1 was "faster" than the two older sites at the 99% confidence level. Advance III was separable from advance IV, also at the 99% confidence level.

Addition of Tinemaha granodiorite boulders to the quartz monzonite boulders at the lower sites of advance III would probably increase their mean speeds. Perhaps this explains the observed increase in V_p from site 2-17 to site 1-3.

The mean speed of P waves at the three sites on left-lateral moraines of advance III from lower Onion Valley was not significantly greater than

the speed for the two sites on the moraine of advance II (sites 2-1 and 2-2). This contrasts with the marked difference found for right-lateral moraines. Sites on left-lateral moraines east of the Independence Fault were not on original moraine crests, which were removed by erosion. This does not explain the discrepancy in any obvious way, however. Again, this may be related to the abundance of Tinemaha boulders.

It is likewise unclear why the contrast between the sites on the left-lateral moraine of advance II was not greatly different from the contrast with site 1-2 on the moraine of advance I. Site 1-2 may have been partly buried by alluvium, but as alluvium tends to be already weathered at the time of deposition this should have enhanced the contrast, not reduced it.

Summary of relative dating using acoustic wave speeds . . .

Three distinct ages of moraines (I, II, and III) were recognized on the south side of Independence Creek in lower Onion Valley and the foothills below (Fig. 5-16). In upper Onion Valley burial of moraine crests by talus and a mixture of rapidly weathering boulders from the southern tributary of Independence Creek appeared to preclude confident interpretation of the data. Still farther upstream, three distinct ages of moraines (V, VI, and VII) were found along the main fork of Independence Creek west of Onion Valley. Advance V appeared younger than advance IV moraines on the north side of Onion Valley. Left-lateral moraines in lower Onion Valley and the foothills should decrease in mean speed with distance down valley, but distinct jumps between IV, III, II, and I were not observed. Instead there seemed to be a gradual progression more in keeping with continuous slow retreat than with the episodic advances indicated by semi-quantitative weathering data, especially from road

cuts. It must be concluded that glacial advances III and IV were closer in weathering age than advances I and II, and possibly II and III. Moraines of advances III and IV show nearly as much scatter within the groups as between the groups. Some of the scatter in data from the left-lateral moraines may have been due to admixture of granitic boulders from a more resistant pluton near the range front.

Correlation of glacial advances in Onion Valley to the conventional sequence for the Sierra Nevada

Table 5-10 lists the glacial advances in Onion Valley and their probable counterparts in the rest of the Sierra Nevada. Moraines of advance VII are found just below permanent snowfields or glaciers high in cirques. Moraines are unstable, there is no soil or vegetation, and boulders show no sign of weathering since deposition. The infrequent small lichens indicate a very young age, probably only a few hundred years (Curry, 1968, 1969). These characteristics are typical of the Matthes neoglacial advance (Birman, 1964).

Moraines of advance VI are also found in or just below cirques. Stability of boulders is greater than on Matthes moraines. There is more soil, and occasional grasses and even dwarf white pines are found. Boulders may show flakes on surfaces. Lichens are abundant and indicate an age of a few thousand years (Curry, 1968, 1969). This is appropriate for the Recess Peak neoglacial advance of Birman (1964).

Moraines of advance V are stable and forested. Many boulders are somewhat weathered but burial in the moraine crest is slight. Sedimentation in lakes is generally minor. Terminal and recessional moraines are

Table 5-10

Correlation of Glacial Advances in Onion Valley to the Conventional Named Glaciations for the Sierra Nevada and their Continental Equivalents.

Glacial Advances in Onion Valley	Sierra Nevada Equivalents	Age†	Continental Glaciations
VII	Matthes	~ 400 y	
VI	Recess Peak	~ 2500 y	Neoglacial
V	Hilgard (?)	~ 9500 y	
IV	Tioga	0.010-0.025 my	
III	Tenaya	0.035-0.045 my	Wisconsin
II	Tahoe	0.065-0.090 my	
I	pre-Tahoe (Mono Basin?)	~ 0.13 my ?	Illinoian ?
older I (?)	pre-Tahoe (post-Sherwin)	< 0.7 my	Illinoian ?

† The ages quoted are from the literature. For references, see Ch. 1.

breached only slightly. Streams are incised very little. Advance V may correspond to the Hilgard neoglacial advance of Birman (1964), but no strong evidence was found to indicate that this was not simply a recessional stage of the Tioga glaciation. Birman argued that the Hilgard advance was distinct from the Tioga because he found large moraines which were more weathered than the Tioga moraines, although they were clearly younger. This he attributed to accelerated weathering on canyon walls and bottoms (but not on Tioga moraines) during the warm interglacial period, which provided abundant weathered debris for moraines. The Hilgard of Onion Valley met neither of these criteria: the terminal moraine was small, and weathering was not necessarily severe more than on older moraines. Curry (1971) argues from ^{14}C dating that the Hilgard glaciation may actually have preceded rather than followed the "altithermal" period.

Moraines of advance IV are widely breached. Boulders are generally substantially buried. Many show evidence of weathering, although no cavernous, deeply pitted, or disintegrated boulders are found. Independence Creek is incised 4 m into the valley floor. Advance IV correlates with the Tioga stage at the end of the Wisconsin glaciation.

Moraines of advance III differ from younger moraines mainly in the presence of disintegrated quartz monzonite and mafic plutonic boulders. Although these are rare on the surface, they are a significant minor component of the boulders exposed in road cuts. Advance III is either a distinct early Tioga or a Tenaya advance. Because moraines of advance III are recognizably different from Tioga moraines and are mappable as a different unit, they are considered to be Tenaya in this study.

Till of advance II contains a high proportion of disintegrated or

highly weathered boulders. Road cuts show no strong oxidation in the thin B horizon. Subsurface boulders are heavily coated with clay. Advance II probably correlates with the Tahoe glaciation, although the deeply cavernous boulders found on Tahoe moraines farther north are absent.

Advance I was distinctly older than advance II. Most boulders at the surface are disintegrating and have low relief. Deep pitting is common. The B horizon is several meters deep and lightly oxidized. Its age should be regarded as pre-Tahoe rather than early Tahoe because of the strong contrast in weathering characteristics compared to advance II (Tables 5-2, 5-3).

If Crook and Kamb (1980) were correct in claiming a logarithmic relationship of acoustic wave speed to age, then mean speeds through groups of boulders at different sites plotted against the logarithm of the age of the site can be extrapolated to give a rough indication of the age of advance I. As Fig. 5-18 shows, for the right-lateral moraine this age clearly exceeds 100,000 y. Thus the assignment to a pre-Tahoe glacial advance appears to have been justified. The nominal age, > 1 my, is inconsistent with the obvious morainal form of the deposit and appears to be excessive. Sherwin till (e.g., at Green Creek; Sharp, 1972) is generally sufficiently eroded that the original morphology is largely obscured.

The old till on the Independence Fault scarp north of Independence Creek was included with advance I in this study. However, it appeared to be even older, based on the intense oxidation in the B horizon and on the GWR data. Elsewhere in the Sierra such red soils on tills indicate great age. At lower Rock Creek, Sharp (1968) found a red till underlying Sherwin till. At Big Pine Creek, a red till underlies a thin veneer of till assigned by Fleisher (1967) and Bateman (1965) to the Tahoe advance.

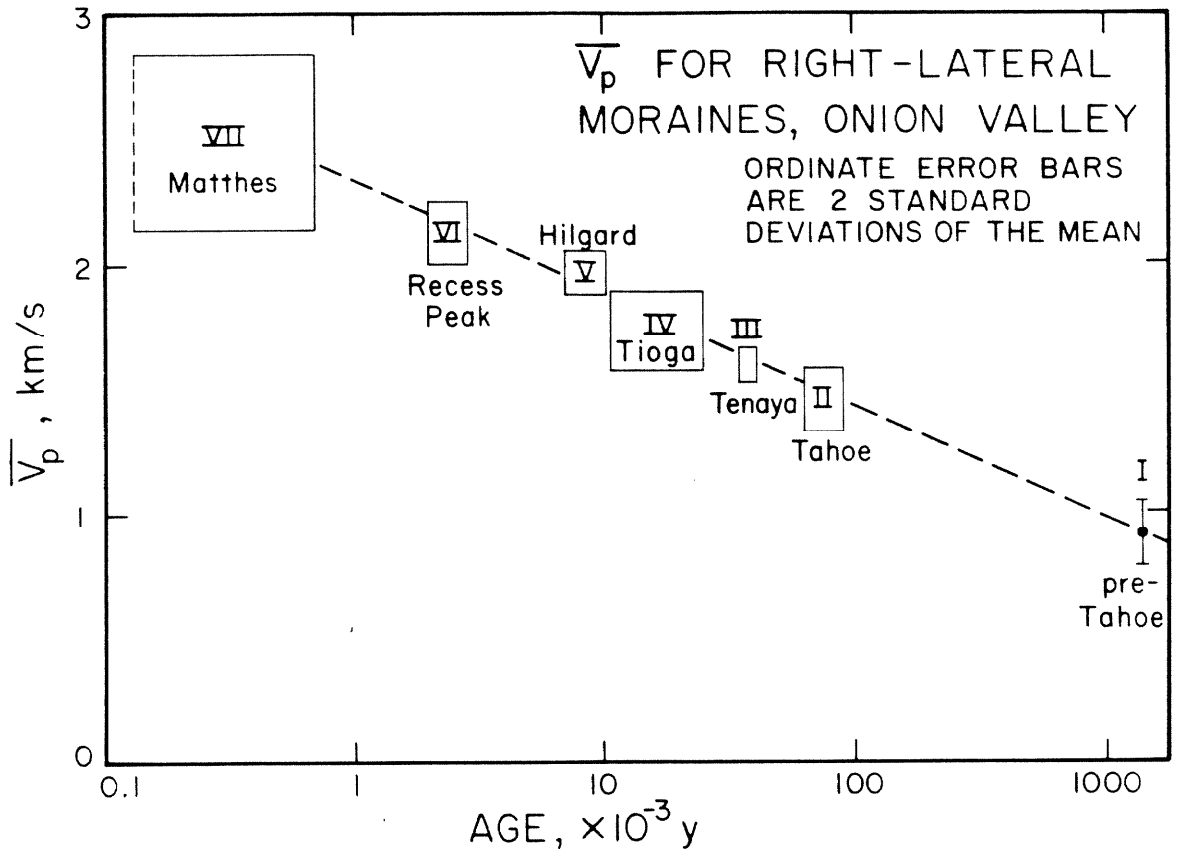

Fig. 5-18. Mean wave speeds ($\overline{V_p}$) for sites on right-lateral moraines grouped according to apparent age decrease with the logarithm of the age. Ages for groups II - VII were assigned as discussed in Ch. 1. A line passing through these boxes indicates that the age of advance I exceeded 1 my, which is probably excessive. From the data, it appears unlikely that the age could be less than 100,000 y, which is consistent with the assignment of advance I to a pre-Tahoe glacial stage.

Thus the old right-lateral moraine in Onion Valley does appear to be pre-Tahoe and is probably quite old. However, the specific glaciation to which it belongs is unknown.

Age of deposition on the alluvial fan of Independence Creek

From weathering characteristics, three different ages for parts of the active alluvial fan of Independence Creek were recognized. These were discussed earlier. The oldest surface, in the lee of a bedrock ridge, was depleted of granitic boulders, probably by disintegration. It must correlate with advance I or a still older advance of glaciers down Onion Valley. Valley. It is probably pre-Wisconsin in age.

The lower fan east of the foothills was equivalent in weathering to the outwash plain west of Seven Pines. The outwash was deposited during glacial advance III, or possibly during the early part of advance IV. The fan surface was thus probably of mid-Wisconsin (Tenaya to early Tioga) age. The remainder (and largest fraction) of the fan was older and was probably early Wisconsin (Tahoe) in age. Although this interpretation is satisfying in that the longest Wisconsin stage (Tahoe) is associated with the greatest area of fanglomerate, it is surprising that very little of the fan was of Tioga age. This is, however, consistent with the distribution of fan deposits reported by Lubetkin (1980) at Lone Pine Creek, south of the study area. Probably any Tioga debris has been mixed with older fanglomerate along the stream channels of the mid-Wisconsin fan surface.

Deposition on the fan surface in the last 0.1 my has exceeded 10 m, the maximum observed incision into the early Wisconsin fanglomerate. However, deposition may not have been much greater than this limit because the pre-Wisconsin fanglomerate in the lee of the bedrock ridge is exposed

only ~ 9 m below the early Wisconsin surface.

Evidence for Episodic Faulting: Multiple Sets of Truncated Ridges

Knopf (1918) remarked that the eastern escarpment of the Sierra Nevada consisted of two levels, each defined by sets of truncated spurs. He took this observation to show that the escarpment was formed in two periods, separated by a long hiatus during which the initial escarpment (now the upper level) weathered to a lower gradient. Matthes (1950) felt that he could discern traces of an ancient 900-m-deep valley parallel to the escarpment but east of the modern crest of the Sierra Nevada near Mt. Whitney. The evidence for this was the presence of ancient east-dipping erosion surfaces preserved on east-west ridges. These fragments may have once been the eastern side of the valley. Matthes thought this valley predated the beginning of faulting on the modern range front.

It is also possible that cross-sectional profiles of ancient valleys which drained eastward into the young Owens Valley might have been partially preserved during the rejuvenation and rapid erosion accompanying episodic glaciation, increases in the rate of normal faulting along the range-front or mid-valley faults, or other causes. Shortly after rejuvenation, the base of the canyon wall may be over-steepened if erosion in side canyons is unable to match erosion in the main canyon. This is common during regional tilting or during glaciation. Eventually, the hanging canyons will be cut down through the cliffs of the main canyon, leaving only segments intact. Ultimately only triangular facets or even rock ribs which once were part of the ancient valley walls or floor may be preserved. However, if these are not excessively eroded they may

still provide clues to the erosional environment of the ancient valleys.

Truncated spurs along Independence Creek

On the south side of upper Onion Valley is at least one set of three truncated spurs, with apices ~ 135 m above the late Pleistocene trim line (Fig. 5-19a). The tops of these facets coincide approximately with the contact between the mafic pluton and the Bullfrog quartz monzonite, but this relationship appears to be only coincidental. The apices are found at 2975 m (9760 ft) elevation (below the contact) at the mouth of the southern tributary, and at 3000 m (9840 ft) and 2900 m (9520 ft) elevation farther east. If the elevations of these apices reflect an ancient stream gradient, it was roughly 65 m/km or 4° compared to 120 m/km or 9° for the modern Independence Creek in upper Onion Valley.

The cross-section presented in Fig. 5-19b clearly shows the over-steepening at the base of the southern wall of Onion Valley. This zone extends well above the level of the top of the Wisconsin glaciers. If indeed ancient glaciers were responsible for the over-steepening, then they were much deeper than the late Pleistocene glaciers, or the valley has been excavated considerably since their time.

Clark (1967) argues that for a given valley it is unusual for glaciers of different advances to have grossly different depths, at least far from their snouts. However, this presumes that the gradient of the valley is unchanged between advances. For valleys of the eastern escarpment, this presumption may not be valid.

According to the model Clark (1967) used to describe glacial flow, the depth of ice is proportional, among other factors, to sin α , where α is the slope of the valley floor. If the gradient of the ancestral

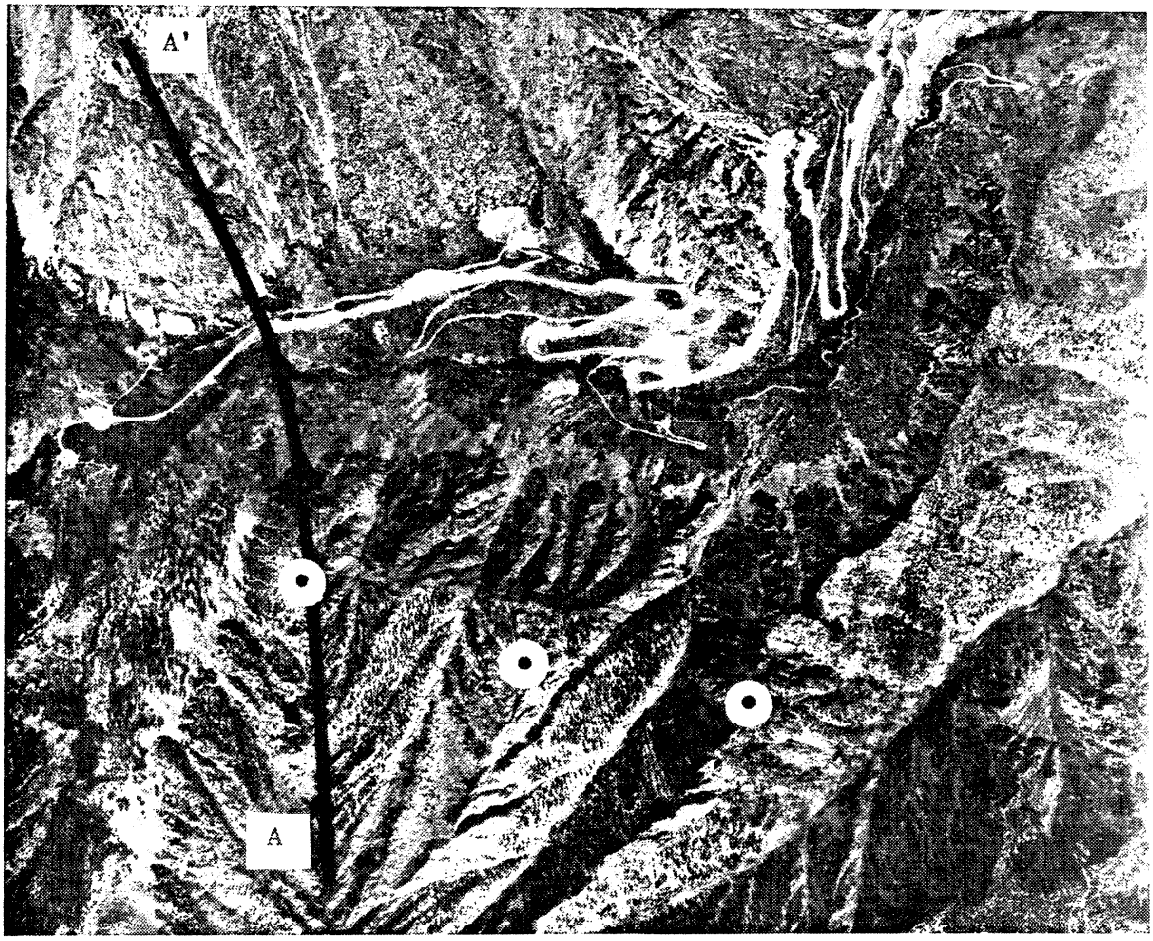

a

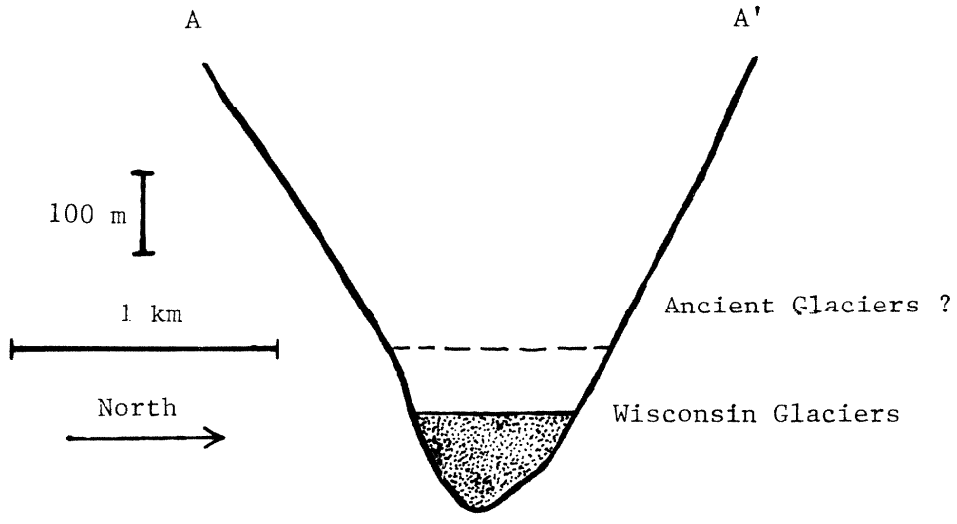

b

FIGURE 5-19

Fig. 5-19. Apices of three truncated ridges on the south wall of Onion Valley may record an episode of increased erosion caused by down-faulting of Owens Valley or by ancient glaciers. Figure a is from an aerial photograph of Onion Valley. North is towards the right; the scale is ~ 1:24,000. The three apices of the faceted end of the spurs are marked by dots. The line is the location of the topographic cross-section of figure b. It appears curved because of foreshortening in the photograph (U. S. Dept. Agriculture, IN04 06027 2372, 9-10-74).

Figure b shows the cross-section of Onion Valley just east of Robinson Creek. Vertical exaggeration is a factor of 2.3 The cross-section shows over-steepening at the base of the south wall of the valley. The depth of the late Pleistocene glaciers is shown by the stippling. If the truncated ridges above the level of the late Pleistocene glaciers was caused by ancient glaciers, their surfaces were ~ 135 m higher (dashed line). Those glaciers may have been deeper than more recent ones, but the difference could also reflect erosion of the canyon bottom.

Independence Creek was in fact only 4°, then the ancient glaciers would have been roughly a factor of two deeper than the late Pleistocene glaciers. Thus if the over-steepening in Onion Valley resulted from glaciation, then either the valley has been deepened by ~ 100 m or the valley gradient has been increased by a factor of two since its end.

Either option requires the considerable passage of time. For example, Blackwelder (1931) reported that there has characteristically been about 15 m of stream incision since the retreat of the Tahoe glaciers; Bateman (1965) reported 300 m of incision at Coyote Creek since the Sherwin glaciation. Thus the ancient glaciers in Onion Valley would probably have retreated a few hundred thousand years ago.

Truncated spurs are also found on Kearsarge Peak, north of Independence Creek. Here they are best represented by the facet on the ridge north of the Onion Valley pack station, at the end of the road. The apex of this facet is at 3170 m (10,400 ft) elevation, higher than the apices on the south wall. If these facets are truly related to the tectonic or climatic history of the Sierra Nevada and not merely to lithologic influence on erosion, they point to a more complex and interesting ancient history than can be understood at this time.

Morphology of the Sierra escarpment near Independence Creek

Near Independence Creek the Sierra escarpment rises about 1800 m from the alluvial fans to the first row of peaks. The crest itself is another 3000 m higher. The escarpment does not consist of a single unbroken slope, but as Knopf (1918) observed, it is composed of at least two segments. At Kearsarge Peak the upper ~ 650 m of the escarpment appears to be a deeply dissected slope of low gradient which has been preserved as ridges

separating ravines. The gradient on Kearsarge Peak is ~ 20°; on the east face of Independence Peak it is ~ 25°. Apices of the steeper triangular facets of the lower escarpment are found at ~ 3170 m (10,400 ft) elevation on Kearsarge Peak and ~ 2740 m (9000 ft) elevation on Independence Peak. The segmented character of the escarpment is clearly revealed in Fig. 5-20. Especially on Kearsarge Peak, a second lower facet can be seen below ~ 2865 m (9400 ft) elevation. The gradients of these facets are ~ 36° (upper) and ~ 32° (lower), as measured from the topographic map. A third set of truncated ridges is found below ~ 2300 m (7550 ft) elevation on both Kearsarge Peak and Independence Peak. These morphologic features probably record changes in the faulting rate along the range front. In later discussion they will be compared to correlative features elsewhere on the escarpment.

Offset of the Independence Fault across moraines of Independence Creek

A prominent low scarp extends about 5 km along the Independence Fault, from a point between Independence Creek and Lime Canyon (Fig. 5-21) north to Sardine Creek. The maximum height of the scarp, corrected for the local slope of the terrain, was found to be ~ 15 m. There has been no discernible horizontal offset. Offset is progressively less in younger deposits, and the low scarp has either been obliterated or was never formed above the banks of the modern Independence Creek.

Measured offsets are listed in Table 5-11 and measurement locations are shown in Fig. 5-22. Because the scarp crosses deposits whose ages are roughly known, an average rate of dip-slip offset for the late Pleistocene Epoch may be calculated. This rate probably lies between 0.06 mm/y and 0.13 mm/y, with a best estimate of 0.09 mm/y. If the rate is correct,

Fig. 5-20. Oblique aerial photograph looking south at the eastern escarpment of the Sierra Nevada. The eastern ridge of Kearsarge Peak is in the immediate foreground; Onion Valley is the next canyon to the south (note the old Onion Valley road). The segmented character of the escarpment is best seen near Symme's Creek in this view. Symme's Creek (arrow) crosses the range front just south of the low foothills (lower left). U. S. Geol. Survey photograph GS-OAL 1-49 (11-5-56).

Fig. 5-21. Late Pleistocene scarp of the Independence Fault, looking south from the Onion Valley road above Seven Pines. The scarp cuts Pleistocene moraines of three ages, glacial outwash, and post-glacial river terraces. The arrow shows the scarp on the crest of the right-lateral moraine of advance II. From the progressively greater vertical offset of increasingly older deposits of known age, it is possible to estimate an average offset rate for the Independence Fault during the late Pleistocene Epoch. The best value for this rate is ~ 0.09 mm/y.

Table 5-11

Measured Dip-Slip Offsets on the Independence Fault.

Site*	Offset Deposit	Age of Deposit** Geological Age	Absolute Age x 10^3 years	Offset† m	Offset Rate mm/y
1	Terrace	Modern	0	0	- - -
2	Terrace	Late Tioga	10.5 - 18	1.4	0.08 - 0.13
3	Moraine	Pre-Tahoe	?	1.6	- - -
4	Landslide	Holocene	< 10.5	~2.0	> 0.19
5	Outwash	Early Tioga - Tenaya	20 - 35	2.3	0.07 - 0.12
6	Outwash	Early Tioga - Tenaya	20 - 35	2.3	0.07 - 0.12
7	Moraine	Late to mid-Tahoe	65 - 75	3.8	0.05 - 0.06
8	Moraine	Tahoe	65 - 90	5.7	0.06 - 0.09
9	Moraine	Pre-Tahoe	?	≥15.2	- - -
10	Bedrock	- - -	- - -	~10	- - -

* Locations of sites are found in Fig. 5-22

** Age assignments are those of this study. Estimates of absolute age follow the chronology developed elsewhere and summarized in Ch. 1.

† Vertical offsets were measured with hand-level and measuring tape, corrected for regional slope measured above and below the scarp. The offset at site 3 is for a fresh scarp at the base of the degraded scarp of site 8. The offset at site 4 was measured at a distance, from the angle subtended by the scarp; it is probably accurate to ± 0.5 m. The moraine crest below the scarp at site 9 was not identified and may have been buried by later glacial deposits. Hence the offset is a lower limit. The offset at site 10 was estimated on aerial photographs from the displacement of the road built across the scarp.

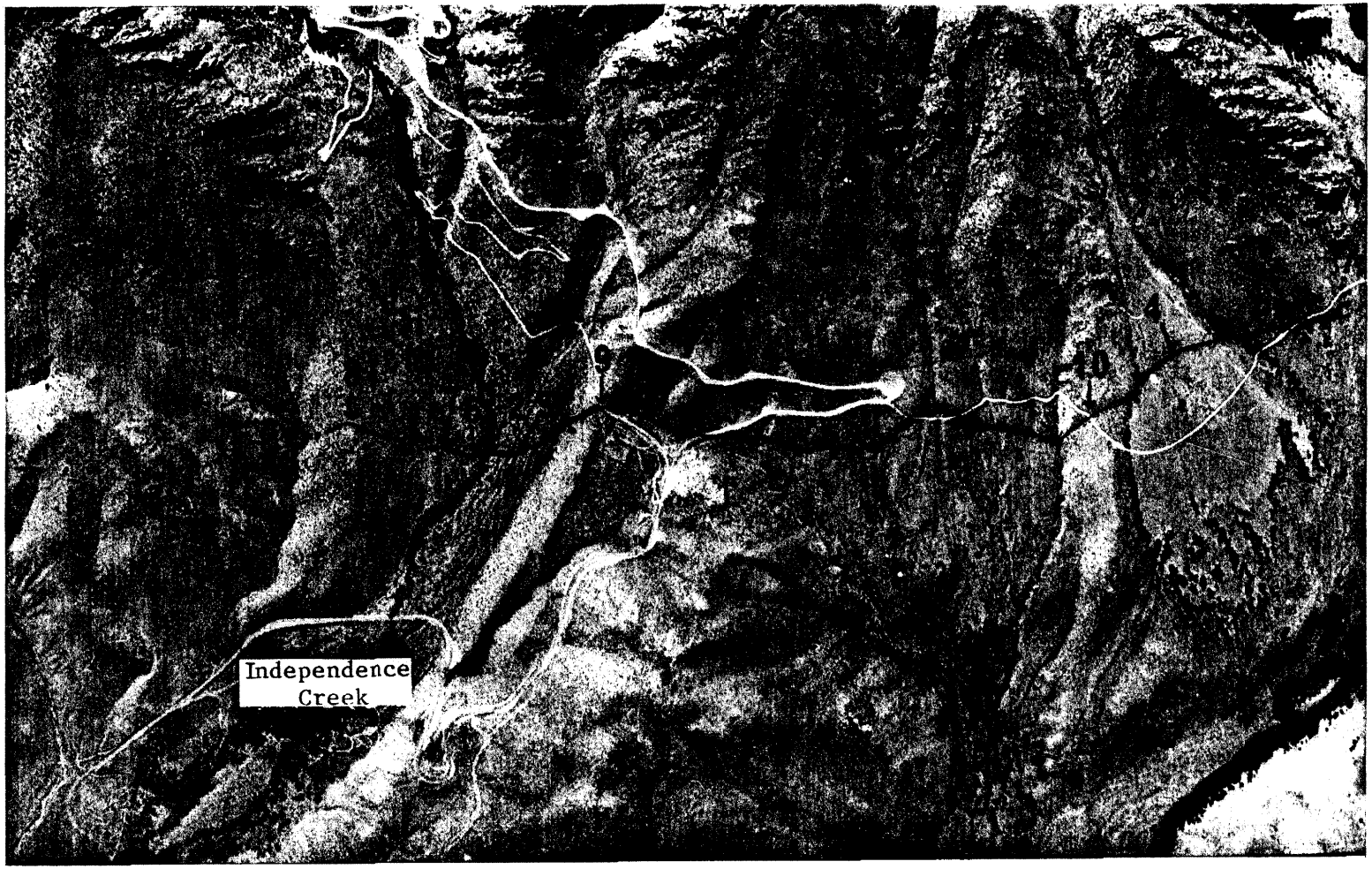

Fig. 5-22. Locations of sites on the Independence Fault where vertical offsets were measured, near Independence Creek. The fault scarp has been inked. The down-thrown side is marked by balls. Sites, indicated by arrows, are numbered. The offset at each site is given in Table 5-11. Scarp is about 5 km long. North is to the right; the scale of the figure is ~ 1:20,000. U. S. Geol. Survey aerial photograph GS-VDYM 2-190 (8-31-75).

the old left-lateral moraine offset 15 m or more is probably older than 0.1 my and could be older than 0.25 my. This is consistent with its pre-Tahoe age assignment based on boulder weathering characteristics.

The offset of the old left-lateral moraine (15.2 m) is only a lower limit because it was never identified east of the fault. The limit itself is uncertain because of the correction for the slope of the faulted moraine crest (~ 17°), which was partly buried by colluvium from the range front.

The 15-m-high scarp may be composite. At its base appears to be a low 1.6-m-high youthful scarp, with a slope of 34°. This scarp is best seen north of the old moraine, but it may have been modified locally when the road was built. This low scarp must be Holocene or latest Pleistocene in age, from its steep slope (cf. Wallace, 1977).

The outwash of early Tioga or Tenaya age on either side of Independence Creek has been offset 2.3 m. This observation is important because it shows that even this close to the southern end of the scarp there does not seem to have been a strong gradient in the amount of offset, although only a few hundred meters farther south the scarp can no longer be seen.

Within the outwash plain is cut a terrace, probably of late Tioga or early Holocene age. Here the scarp is 1.4 m high. This is virtually the same height as the youthful scarp to the north.

The final surface above the creek is the late Holocene flood plain, which is probably still active. This narrow zone is choked with boulders and brush, and no scarp was detected. Even if a low scarp once existed, it probably would have been obliterated during periods of high stream flow such as were probably common at the end of the Matthes glaciation.

South of the glacial outwash plain, the low recessional moraine of late Tahoe age was offset 3.8 m. This value may be confidently compared

to those measured in the outwash, because the moraine is only a few tens of meters south of those sites.

The crest of the major right-lateral moraine is more distant from the other measurement sites, and closer to the southern end of the scarp. Its 5.7-m offset may thus give a low rate for the fault as a whole. If it does not, then it implies the considerable passage of time between deposition of the main moraine and deposition of the younger recessional moraine. Both were thought to be of Tahoe age, and both had boulders which were weathered similarly. Thus the offset rate may have been greater before ~ 50,000 y BP than it was at the end of the Pleistocene.

Offset rates (Table 5-11) were calculated using the best estimates for the ages of the offset deposits. The most useful measurements for this purpose are probably the 3.8-m offset of the recessional moraine and the 2.3-m offset of the outwash plain. Even if the ages I have assigned these deposits are too old by one sub-stage of the Wisconsin glaciation, the offset rate does not exceed 0.2 mm/y. The most probable value is about 0.09 mm/y.

In contrast, the vertical strain reported by Savage et al. (1975) for the Owens Valley was 2.2 mm/y, more than an order of magnitude greater. This high rate applies to the mid-valley fault zone, and if it is representative of the long-term average rate, then it appears that most of the displacement across the Owens Valley is currently on the mid-valley fault zone, not the range-front fault.

It is unlikely that these relative rates have been constant over the Pleistocene Epoch, because near Independence the bedrock east of the Owens Valley fault zone is only ~ 1100 m below the surface of the valley fill (Pakiser et al. 1964). Thus total vertical offset across the mid-valley faults is comparable to but no greater than offset across the Independence Fault.

5.2 SARDINE CANYON

Introduction

In contrast to the deeply incised and rugged canyons to the north and south, Sardine Canyon is shallow and has subdued topography. Neither the modern Sardine Creek nor even the late Pleistocene glaciers have strongly eroded the upper reaches of Sardine Canyon. Sardine Canyon heads at 3660 m (12,000 ft) elevation north of Kearsarge Peak, 1.75 km east of the crest of the Sierra Nevada. At this distance from the crest, other canyons have been cut to about 3350 m (11,000 ft) elevation, 310 m lower. Perhaps this difference in erosion may be attributed to the rapid drop in precipitation from west to east across the Sierra (cf. Curry, 1968), compounded by the small area of the drainage. Sardine Canyon is underfit by the intermittent modern Sardine Creek, which is often dry by late July. Streams in adjacent canyons flow all year.

The principal interest in Sardine Canyon is in its ancient history. That this may be complex is suggested by the segmented longitudinal profile of the canyon: below ~ 3300 m elevation the stream gradient is ~ 23°, while in the upper canyon it is only ~ 8°. In other canyons in the study area, stream profiles were simple and concave, except as modified by glacial corrasion. However, the upper part of Sardine Canyon probably has not been glaciated during the Pleistocene Epoch, and it may be a topographic relic from the ancient Sierra Nevada.

A small, fresh-looking cirque is found at about 3290 m (10,800 ft) elevation in Sardine Canyon. Below the cirque the U-shaped profile, fresh cliffs on the canyon walls, and till exposed in road cuts testify

to recent glaciation.

There are thus two important questions concerning Sardine Canyon: (1) of what age are the moraines of glaciers arising in the low cirque?; and (2) is there any evidence that the canyon above the cirque was ever glaciated?

Summary of Bedrock Geology (Moore, 1963)

Sardine Canyon is developed in roughly equal amounts of granitic and metavolcanic rocks, chiefly meta-andesites and metarhyolites. Above 3655 m (11,500 ft) elevation, bedrock is the quartz-poor granodiorite of the Dragon pluton. Below the late Pleistocene cirque, which is not found at the valley head but rather at ~ 3290 m (10,800 ft) elevation, alaskitic quartz monzonite of the Sardine pluton crops out for ~ 500 m. Near the mouth of the canyon there is a comparable outcrop of Tinemaha granodiorite. Thus similar rock types are found as compared to Onion Valley, but in different proportions. These differences are reflected in the boulders of the moraines.

Glaciation of Lower Sardine Canyon

Sardine Canyon does not have the large and fresh moraines so prominent in Onion Valley. In part, this may be attributed to the small size of the glaciers and to the steep gradient of the canyon. Below the small cirque at 3290 m (10,800 ft) elevation, the canyon was glaciated, at least during the late Pleistocene Epoch. Till and outwash can be identified in road cuts. The distribution of Quaternary deposits and the geography of Sardine Canyon are shown in Fig. 5-23.

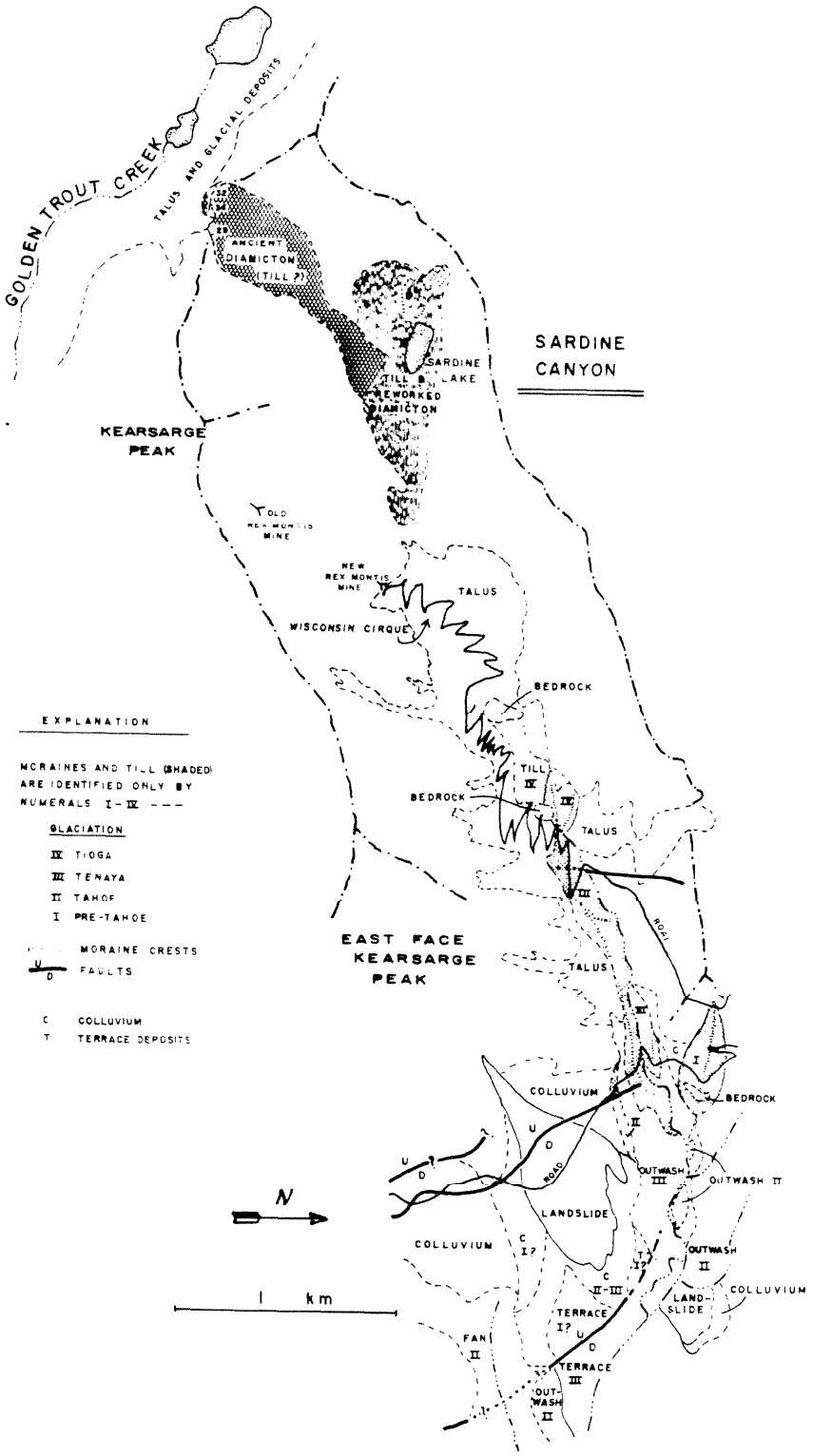

Fig. 5-23. The Quaternary geology and the geography of Sardine Canyon. Sites where relative weathering data were acquired are indicated. The map base was a ~ 1:80,000-scale aerial photograph enlarged to a scale of ~ 1:16,000. Vertical relief exceeding 1500 m introduced large amounts of foreshortening; hence, the scale is approximate. U.S. Geol. Survey photograph GS-VDYM 2-190 (8-31-75).

Road cuts on both sides of Sardine Creek at the range front at 2195 m (7200 ft) elevation expose three outcrops of till. Two of these, south of the creek, are of different ages. The third, north of the creek, is coeval with the younger of the others. The age difference may be inferred from the difference of the GWR of boulders in the roadcut (Table 5-12): the outer till (farther from the creek) contains a factor of six more heavily weathered boulders than the inner till (closer to the creek). Yet disintegrated boulders are found in the inner till, and competent ones in the outer. From its degree of weathering, the younger inner till appears to be equivalent to advance III of Onion Valley (Tenaya stage), and the outer till is equivalent to advance II (Tahoe stage).

The three road cuts appear to be sections through moraines. However, the features do not have the characteristic morphology of typical valley moraines. The most obvious difference is that they rise only a few meters above their outwash plains to the east. Sardine Creek has cut deeply through both the moraines and the outwash. Channels on the outwash plain south of the creek are parallel to Sardine Creek and do not radiate from the breach in the inner moraine. These channels probably transported runoff from the southern flank of the advance III glacier.

Outwash caps the right-lateral inner moraine. This can be seen from the sharp change in the fabric of the diamicton exposed in the road cut. Below the contact the boulders are disoriented and fine material is abundant. Above, boulders and cobbles have a distinct orientation with their major axes aligned and parallel to Sardine Creek. The proportion of sand and clay is reduced and the color of the matrix is darker (as was observed at a similar roadcut in Onion Valley). Outwash must have overtopped the low moraine during the retreat of the glacier and before

Table 5-12

Relative Weathering Data for Moraines in Sardine Canyon

Site*	Advance**	No. of Boulders†	GWR†*	G/R*†	BFC†† m^{-2}	GWR (road cut)
1	IV_R	37	----	----	----	5/30/65
2	III_R	43	----	----	----	12/40/49
3	III_R	53	----	----	----	11/43/45
4	III_R	35	23/77/0	47/53	1.08	----
5	II_R	71	----	----	----	68/24/8
6	II_R	23	57/43/0	29/71	2.13	----
7	III_L	66	24/64/12	56/44	1.10	----

---

* Site locations are on moraine crests and road cuts shown in Fig. 5-23 "R" and "L" denote right- and left-lateral moraines, respectively.

** The notation for the glacial advance is that of Onion Valley: advances I - VII are ordered by decreasing age (see Fig. 5-10 for the correlation to the conventional Sierra Nevada sequence).

† The number of boulders used for the GWR (see Ch. 2).

†* Granodiorite weathering ratio (Ch. 2). Frequencies in % are ordered by decreasing degree of weathering.

*† Granodiorite/"Resistate" boulder ratio (in %).

the terminus was breached. Perhaps because of the high gradient (23° compared to 11° for Onion Valley) the moraines were low and distributed, as occurs below hanging glaciers elsewhere, such that floods and debris flows from the retreating glacier were able to override them.

The left-lateral moraine does not seem to have been buried by outwash, and is the more prominent of the two. Outwash is nevertheless found to its north, where it could not have been deposited by Sardine Creek after the retreat of the advance III glacier. Thus the deposition of the outwash plain appears to have been contemporaneous with the construction of the moraines.

The outwash grades to an inner terrace in the fan of the South Fork of Oak Creek. This permits the correlation of moraines from Sardine Canyon to the South Fork, and will be discussed in §5.3.

The older right-lateral moraine (advance II) forms part of a ridge which bounds the outwash plain (advance III). The higher surface to the south is covered by colluvium, and the ridge also is thinly covered. This high surface is itself cut into a yet higher surface, best preserved south of the prominent landslide on the east face of Kearsarge Peak. Thus at least four surfaces are present. Further discussion of these surfaces will be found in the §5.3.

Moraines of two ages were found within lower Sardine Canyon. These were best exposed in road cuts south of the creek. Left-lateral moraines of the lower of the two series were not found and appear to have been eroded from the steep canyon walls. Till from the lower series was best exposed in road cuts above ~ 2470 m (8100 ft) elevation (Table 5-12). The degree of weathering of boulders in these road cuts was the same as found for the right-lateral moraine of advance III at the range front;

thus, the lower till was assigned to advance III also.

Moraines of the upper series were found on both sides of the canyon below the cirque, at elevations from 2590 m (8500 ft) to 3050 m (9800 ft). Till from these moraines also was exposed in a series of roadcuts. No disintegrating clasts were seen in these exposures. Relative weathering data gathered there indicate a 30% increase in the proportion of fresh boulders over the moraines of advance III. Thus these moraines are probably the equivalent of advance IV of Onion Valley (Tioga stage).

No neoglacial moraines were recognized in the cirque.

Upper Sardine Canyon

Above the Wisconsin-age cirque, the canyon widens into a broad basin composed of two parts: a minor northern pocket containing Sardine Lake, a small clear tarn, and a southern branch whose head has been truncated by the northern tributary of Independence Creek (Fig. 5-23). The truncated profile reveals a maximum of ~ 20 m of diamicton covering steeply dipping bedrock (Fig. 5-24). The bedrock-diamicton contact is strikingly similar to that on University Peak (§5.1). Attitudes of the bedrock surface, (Fig. 5-23) suggest that the eroded head of the canyon lay not far to the west. The contact between the diamicton and the deeply weathered sides of the canyon can be seen on aerial photographs from the albedo contrast and on the ground from the increase in the numbers of blocks on the slopes.

West of the Wisconsin-age cirque, primary evidence for glaciation is not obvious. Above Sardine Lake, there is the subdued trace of an old cirque or nivation hollow. Fresh-appearing lobate ridges of debris indicate that the old cirque may have supported pocket glaciers in the late Pleistocene

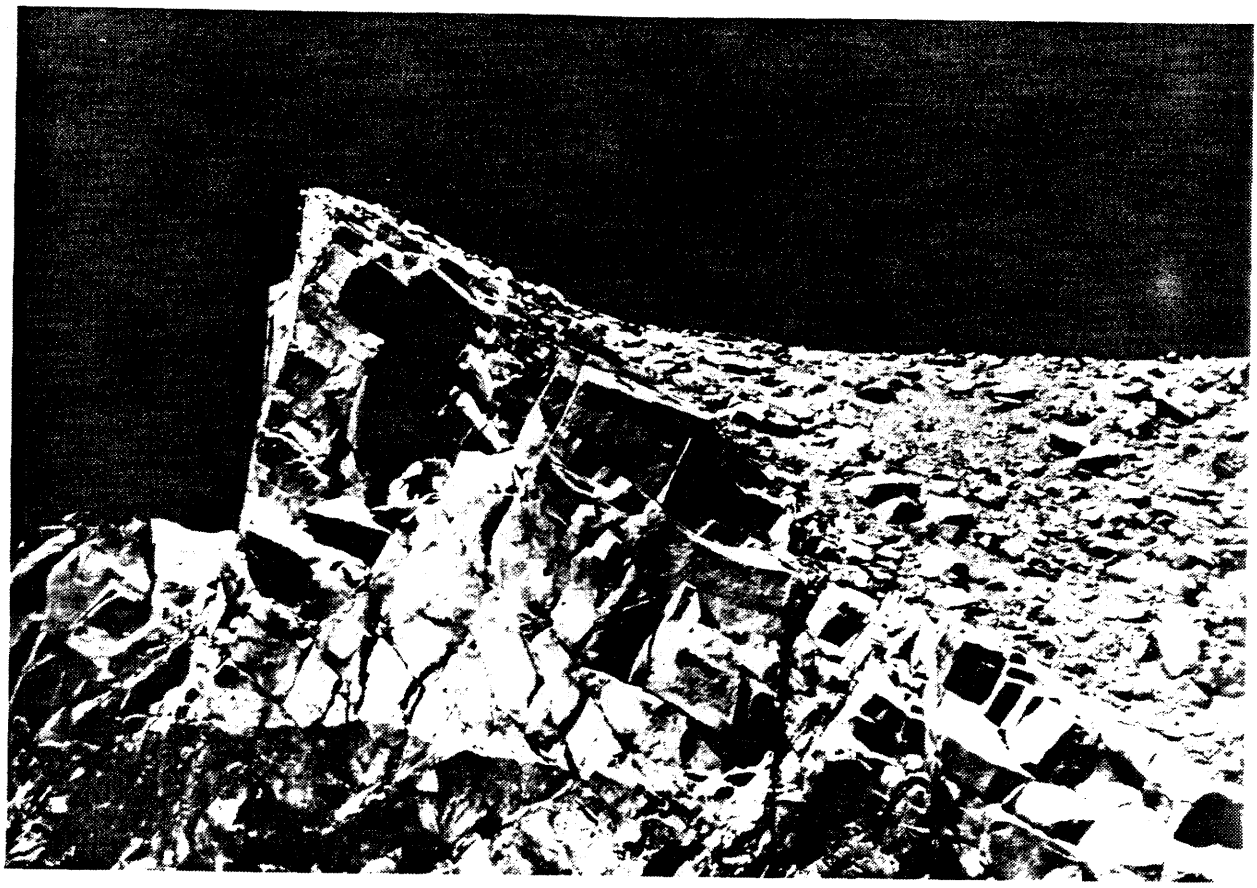

Fig. 5-24. The diamicton at the col between Sardine Canyon and the northern tributary to Independence Creek. As much as 20 m of diamicton overlies granodiorite bedrock. The sharp contact dips 34° to the east. The heavily weathered diamicton may be till from an ancient glacier. Photograph was taken looking north.

Epoch or even more recently. Minor solifluction lobes near the lake may be active now. However, above the large cirque at 3290 m (10,800 ft) elevation there is no trace of trim lines, nor any evidence of moraines in the main canyon. The youthful features near Sardine Lake were not created by glaciers large enough to affect the overall character of the canyon.

It seems possible that the canyon above 3290 m (10,800 ft) elevation was never glaciated, and that its deep diamicton resulted only from slope wash into a fluvial valley. Yet three observations suggest the influence of ancient glaciers.

The first observation is the broad trough itself (Fig. 5-25). In Fig. 5-26 several topographic profiles across this trough are contrasted to profiles across Onion Valley and lower Sardine Canyon, both of which were glaciated, and to a profile across Lime Canyon, which was not. The walls of upper Sardine Canyon clearly lack the steep cliffs which characterize the classical glaciated valley (e.g., Onion Valley). Instead, the walls have a constant slope which only lessens near the contact with the diamicton. Two possible interpretations are shown in the inset of Fig. 5-26. In the first (1), a fluvial canyon is simply filled by slope wash. In the second (2), a glaciated valley is filled with ground till or outwash that may be buried by slope wash. Extrapolation of the valley walls under the diamicton suggests that the fill should be about 60 m deep if "1" is correct. Instead, it was found to be only about 20 m deep where it was exposed at the col between Sardine Canyon and the drainage of Independence Creek. This is consistent with a flat-bottomed or U-shaped canyon, but not with a V-shaped canyon. Thus a glacial history is indirectly implied.

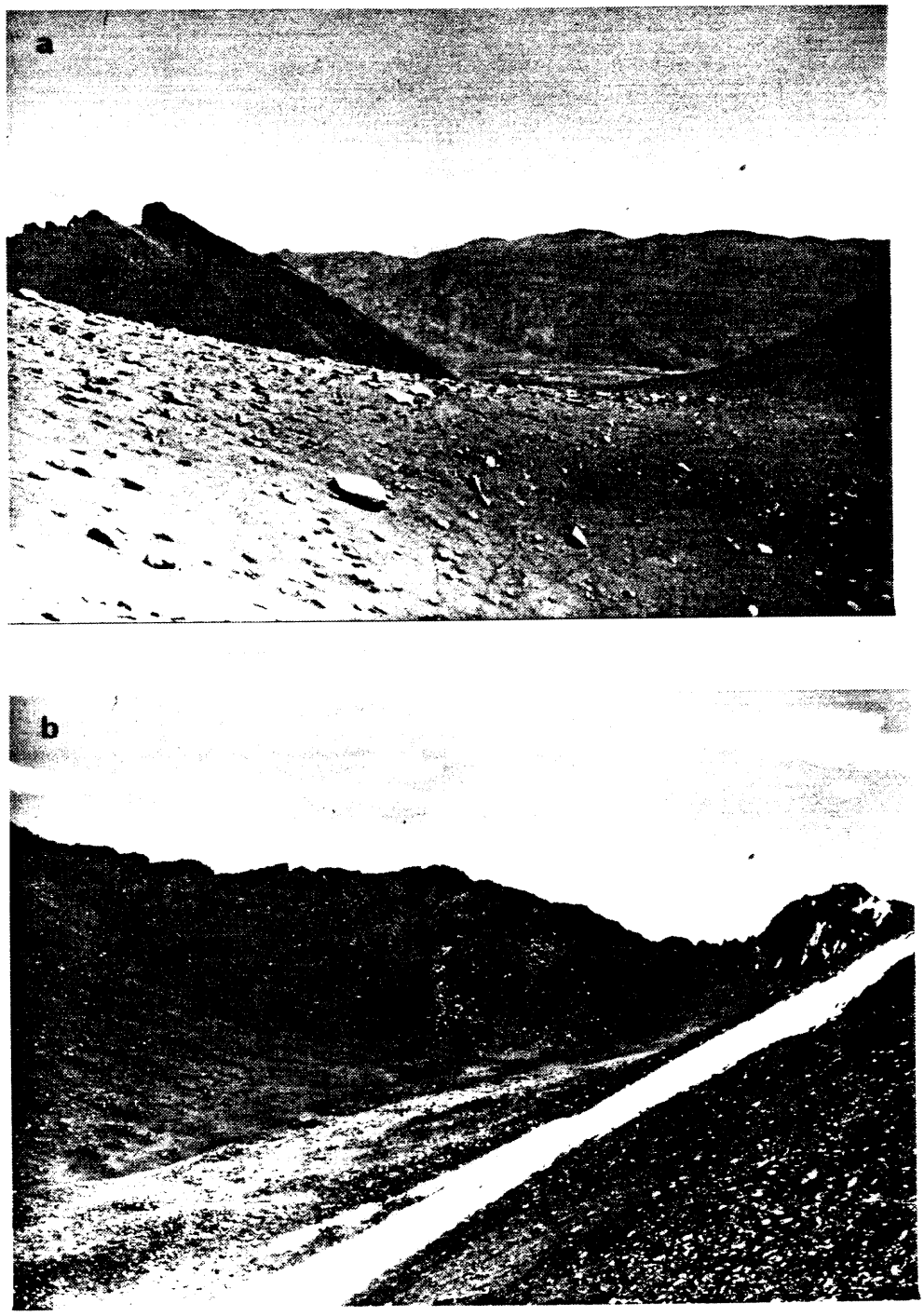

Fig. 5-25. The broad trough of Sardine Canyon. a) Photograph, taken from the pass between the drainages of Sardine and Independence Creeks looking northeast. The ancient diamicton is in the foreground; the Inyo Mts. across Owens Valley are the skyline. b) Photograph of upper Sardine Canyon, looking south from the ridge above Sardine Lake. The truncated head of the canyon is seen below University Peak (right), 5 km distant.

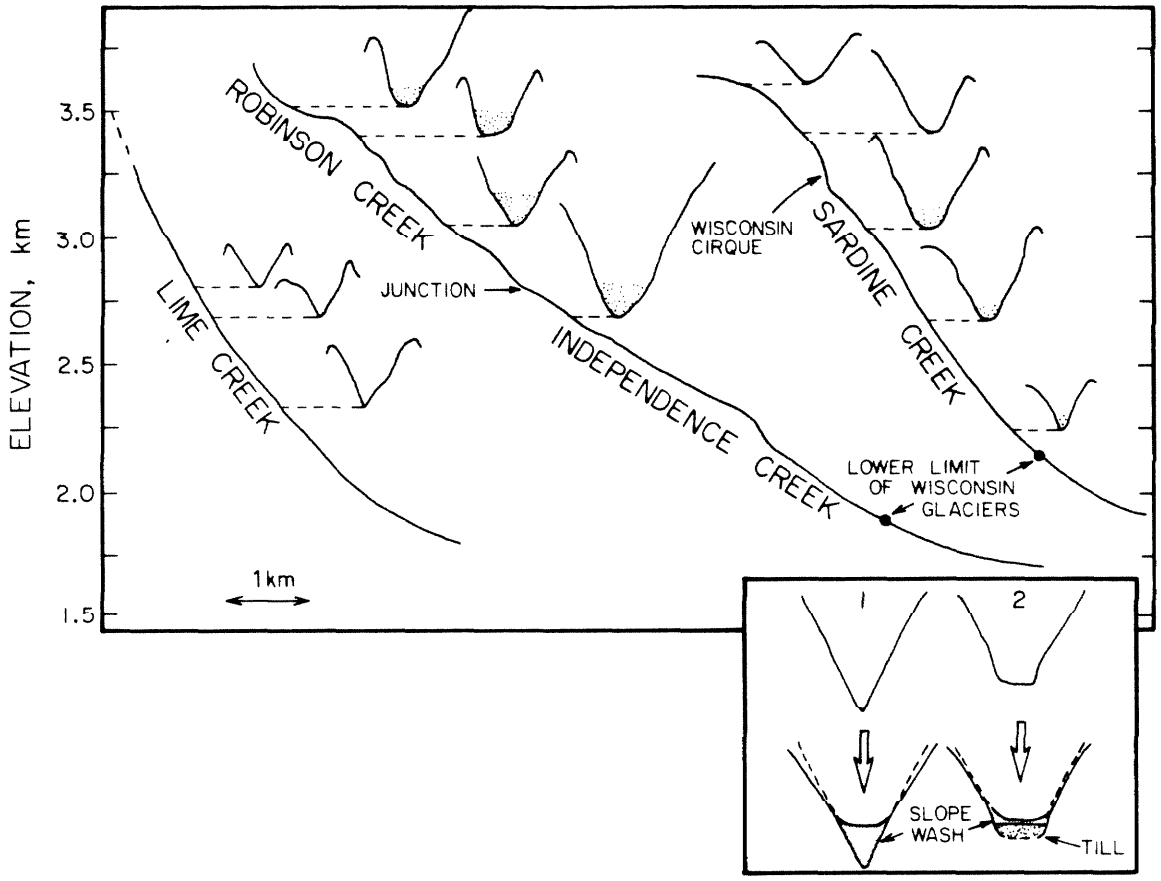

Fig. 5-26. Topographic cross sections of Sardine Canyon compared to cross sections from the southern tributary to Independence Creek (glaciated) and to Lime Canyon (never glaciated). Depth of the late Pleistocene glaciers is indicated by shading. Inset shows two explanations for the breadth of upper Sardine Canyon: in (1), the shallow V-shaped trough of an ancient stream was never glaciated, but assumed a U-shaped profile after beheading, through the agency of slope wash. In (2), the over-steepened cliffs of an ancient glaciated valley are reduced by erosion and masked by slope wash, which buries the ground till. The depth of the canyon fill may be too shallow to permit the first explanation; hence, the second is preferred.

The broad character of the valley is especially significant because the bedrock surface at the truncated head of the low-gradient (8°) valley dips steeply (29° - 34°) downstream, indicating that the ancient valley had a staircase longitudinal profile, or that the headwall of the valley was quite close to the modern col. A fluvial valley this broad and shallow would require a divide much farther to the west. A steep headwall is characteristic of glaciated valleys. Furthermore, sudden changes of gradient themselves are uncommon in equilibrated fluvial systems but are typical of glacial valleys.

The second observation is the presence of faceted boulders above the Wisconsin cirque. Facets on boulders are created when the boulder is dragged over bedrock by a glacier, abrading one side (cf. Flint, 1971, p. 165-168). These boulders were exposed in Sardine Canyon where the gradient was steep enough that fine components of the diamicton were washed away.

Boulders with crescentic gouges or fractures may also indicate a glacial history. Generally, these features are thought to develop in bedrock abraded by glaciers (Matthes, 1930). However, during this study boulders with crescentic gouges or fractures were found on moraines or in glacial outwash also. Such fractures are seen in several boulders in upper Sardine Canyon. Because arcuate fractures are also seen in rocks which were never transplanted glacially, such evidence is suggestive of glacial history but not diagnostic.

Glacial striations were found neither on bedrock nor on boulders in upper Sardine Canyon. Their absence close to the cirque is not surprising, however. As seen in neoglacial moraines, few boulders are striated

unless they have been transported a kilometer or more. Scratches and striae are easily obliterated from granitic rocks by weathering.

The third observation is the relatively fresh character of the bedrock exposed under the diamicton at the truncated head of the canyon. The gradient of the valley here is less than 7°, and in a fluvial environment little erosion would have occurred. Deposition should have been gradual. Consequently, the sharp contact of low relief between diamicton and bedrock (Fig. 5-24) similar to the contact between bedrock and diamicton on University Peak, should not be found. Instead the contact should be gradational, with large blocks of weathered bedrock which could not be moved by the low-gradient stream.

Characteristics of the diamicton

The diamicton at the truncated top of Sardine Canyon is similar to that of University Peak, but is much more deeply weathered. On either side of the canyon it is in contact with bedrock and its margins are covered by slope wash. Its lower contact is with steeply dipping granodiorite bedrock and thin exfoliation slabs. The exposed bedrock underlying the diamicton has been weathered sufficiently that no original abraded surface remains, if there ever was one. Near the col at the head of Sardine Canyon, the bedrock is covered by no more than ~ 20 m of diamicton.

The diamicton appears to consist of at least two parts, the original valley fill and a surfical coating of lag gravels and grus. This upper layer is especially pronounced near the sides of the canyon. The origin of this may be slope wash from the canyon walls, enhanced by the removal of sand and clay farther down slope. The upper layer of the

diamicton has been reworked such that the major axes of the pebbles now point down slope.

Near the axis of the canyon, fewer pebbles and grus are found. A few cm down, the diamicton is dominantly yellow-brown (10YR6/4 or 10YR7/4) sand and clay. The clay content is sufficient to form aggregates in the soil and to roll into cohesive plastic cylinders when wet. All pebbles and lithic fragments are heavily coated by clay.

The diamicton also has rare boulders on its surface. Some of these are heavily weathered and cavernous (Fig. 5-27). The exceptions are concentrated near the sides and may be rockfall. Some of the cavernous boulders are aplitic or are fine-grained granodiorites. Most are flush with the surface.

Thus regardless of the genesis of the diamicton, it appears to be of great age. A comparable level of soil development is not seen at lower elevations in till younger than Sherwin age (>0.7 my). Soil was much more developed than on the similar diamicton of University Peak, which must be at least several hundred thousand years old.

The origin of upper Sardine Canyon as a nivated valley

Matthes (1900, 1933) has noted numerous instances in the Big Horn Mountains, Wyoming, and in the Sierra Nevada where periglacial terrain was modified solely by nivation, the action of permanent snowfields. Nivated surfaces are gentle and rounded, in strong contrast to the steep-sided glaciated valleys and amphitheaters. Upper Sardine Canyon appears to fit Matthes conception of a nivated valley rather well: there is no trace of a stream channel, and the floor of the valley is filled with clay and mud. These Matthes (1900) felt were deposited via water

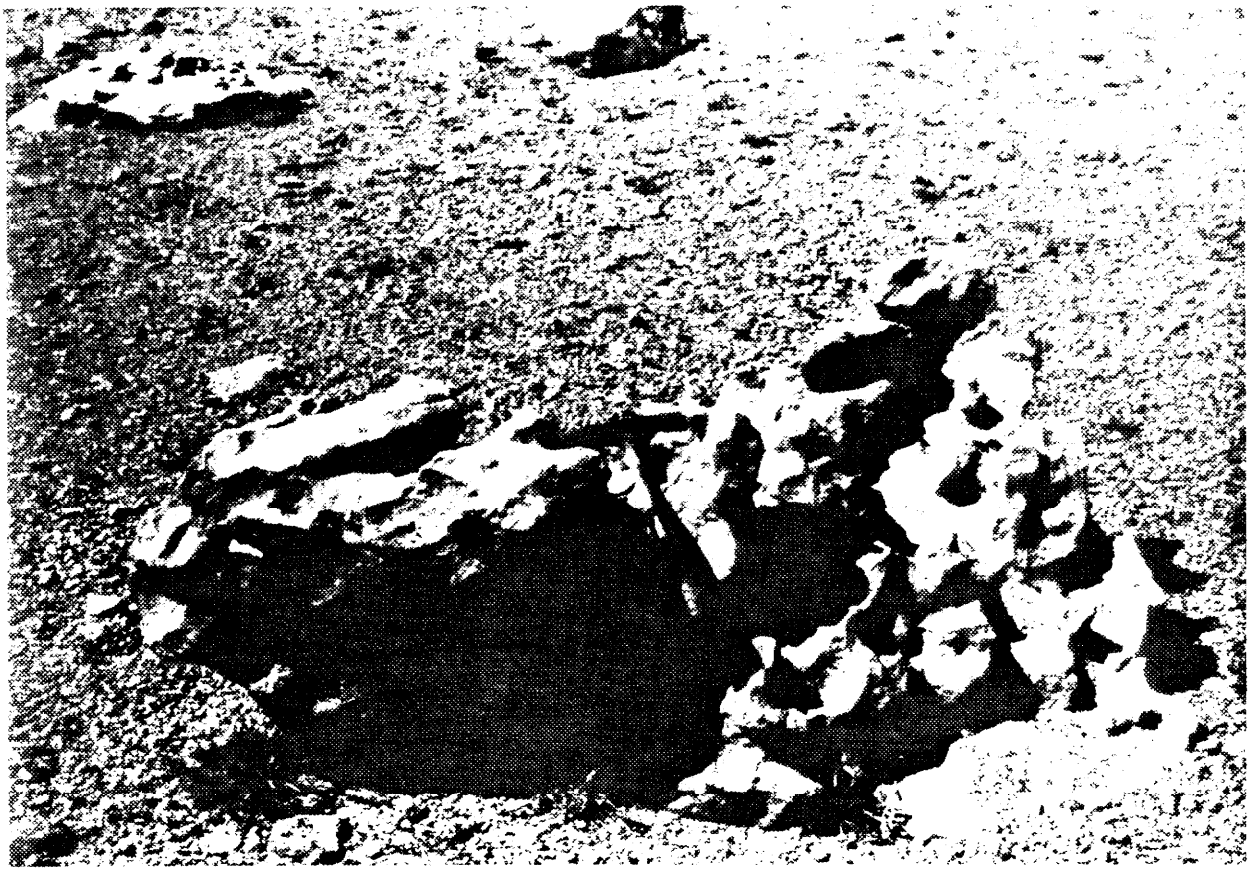

Fig. 5-27. A cavernous boulder of fine-grained granodiorite, found in a diamicton near the col at the head of Sardine Canyon. Boulders this heavily weathered argue that the diamicton is of great age, certainly predating the Wisconsin glaciation.

percolating through the snowfields. The fine sediments could be derived from in situ processes on the flanks of the mountains on either side of the canyon, and transported by wind, water or avalanche to the snowfields below. Thus an anomalously high degree of soil development is to be expected. Transport of such boulders as are seen in the diamicton could also result from avalanching.

Certainly, upper Sardine Canyon must have been nivated during the late Pleistocene glaciations. However, Matthes (1900) argues that nivation has but little effect on gross topography; hence the canyon itself, its concave-convex longitudinal profile, and perhaps its U-shaped cross section derive from other causes. As discussed above, ancient glaciation is consistent with these observations.

Summary

Sardine Canyon probably owes its broad geomorphic form to glacial erosion, even though the late Pleistocene glaciers formed in a small cirque cut into a step midway up the canyon instead of the canyon head. The broad and gently sloping canyon above the cirque may show the existence of an ancient glacier in the southern Sierra Nevada.

An ancient heavily weathered diamicton fills the upper reaches of Sardine Canyon. It is in sharp contact with the underlying bedrock. Some boulders at the surface of the diamicton are cavernously weathered, and others are faceted or show crescentic gouges or fractures which are suggestive of a glacial history. From its color and clay content, this diamicton appears to be grossly older than the one on University Peak, at a comparable elevation. It is weathered comparably to tills of the Sherwin

glaciation found at much lower elevations, and it must have an age of at least several hundred thousand years.

During the Pleistocene and Holocene glaciations, the hollow now filled by Sardine Lake appears to have supported small glacierettes. These left fresh-appearing arcuate lobes of debris and low moraines. The rest of upper Sardine Canyon may have been heavily nivated during these glaciations.

5.3 SOUTH FORK OF OAK CREEK

The South Fork of Oak Creek arises in cirques east of the Sierra crest near Black Mountain and flows east through "Little Onion Valley", between Mt. Mary Austin and Kearsarge Peak. After crossing the Independence Fault at the range front, it passes between foothills for 6 km before flowing down its alluvial fan to the confluence with the North Fork. The Quaternary geology along the South Fork is of interest primarily because of its complex of four nested moraines, which lie across the Independence Fault at the mouth of Little Onion Valley, and because of the correlative sequence of outwash plains and river terraces terraces in the fan below.

Discussion is organized as for Onion Valley, with sections on the bedrock geology, the fan, the foothills, the Pleistocene moraines, and the Quaternary geology of the upper canyon.

Summary of Bedrock Geology (Moore, 1963)

The glaciers of Little Onion Valley cut into granodiorite, alaskite quartz monzonite, and metavolcanic bedrock. The cirque of the main glacier is in the dark granodiorite of the Dragon pluton. A tributary cirque on the western flank of Mt. Mary Austin appears to have been cut along a thin exposure of the Diamond pluton (alaskitic quartz monzonite). Here the Dragon granodiorite, which is generally easily eroded, forms a bold ridge. Mt. Mary Austin itself is part of a large metavolcanic roof pendant. From the Parker Lakes to about 2560 m (8400 ft) elevation, the South Fork of Oak Creek passes through a succession of meta-andesites

and metarhyolites. One of these, a metarhyolite tuff, is colored purple by the presence of piedmontite. This distinctive and resistant rock crops out primarily in the North Fork of Oak Creek, but a smaller outcrop is found on the south face of Mt. Mary Austin. The purple boulders are found in moraines and alluvial fans of both forks.

Below 2560 m (8400 ft) elevation, the walls and floor of Little Onion Valley consist of the slightly prophyritic granodiorite of the Tinemaha pluton, intruded by granodiorite porphry dikes of the Independence swarm. The foothill block east of the Independence Fault is composed of the Independence pluton (alaskitic quartz monzonite) and the quartz-poor quartz monzonite of the McGann pluton. Minor stringers of brown meta-rhyolite tuffs are found on top of the foothills north of the South Fork.

The Alluvial Fan of the South Fork of Oak Creek

East of the Independence Fault the South Fork debouches through its lowest lateral moraines, through a deeply incised outwash plain, and onto an alluvial fan. This fan consists of three sections (Plate I; Fig. 5-28): (1) an ancient abandoned fan east of the foothills; (2) terraces incised in the ancient fan within the foothills; and (3) a recent fan to which the creek is constrained by a bedrock gap just northeast of the Bright ranch at 1585 m (5200 ft) elevation.

The abandoned fan

Two ages of fan deposits were recognized on the abandoned fan of the South Fork. These are unmistakably different in age, based upon their weathering characteristics, and correspond to the ancient and early or

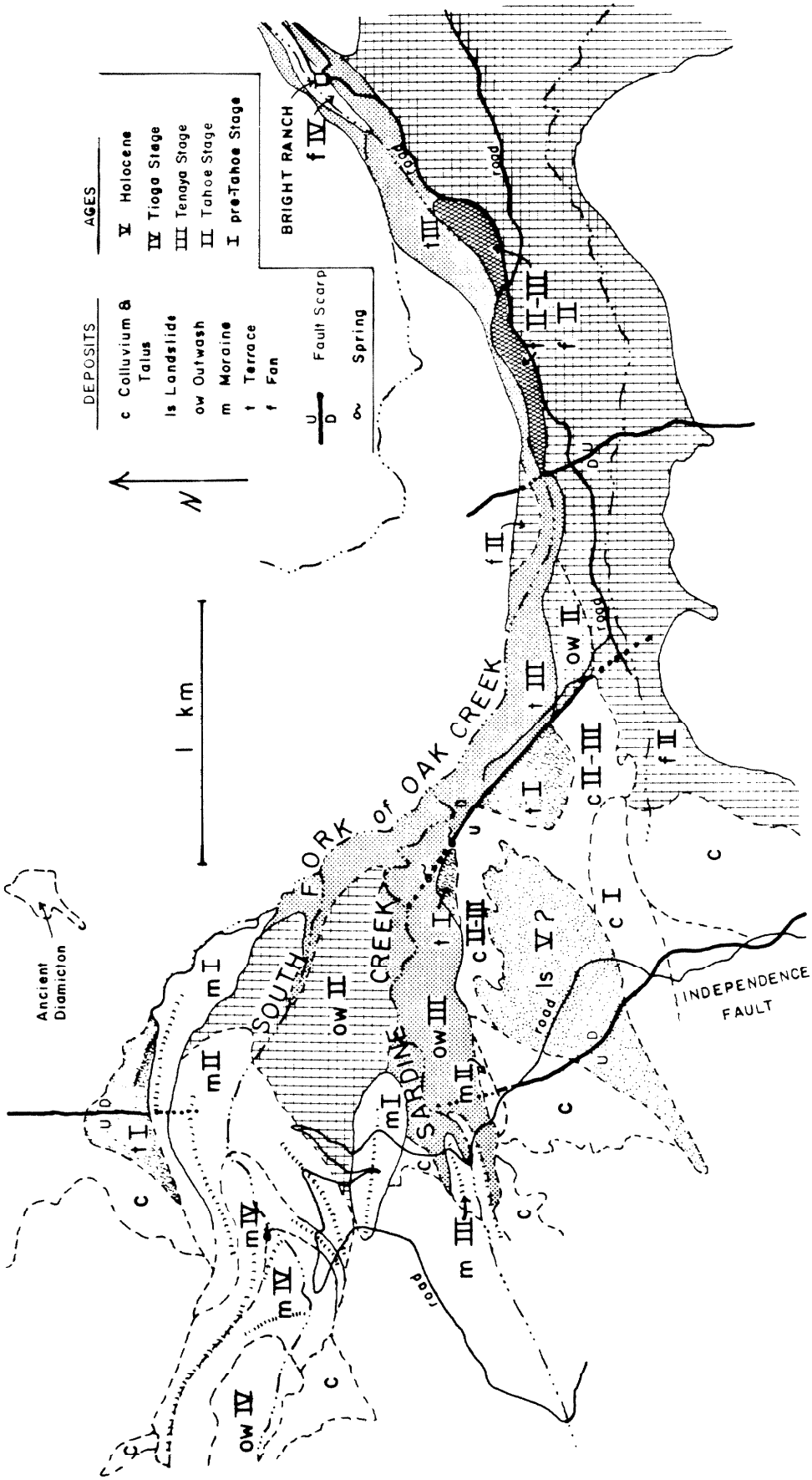

Fig. 5-28. Map of the upper alluvial fan of the South Fork of Oak Creek, showing multiple terraces left during the late stages of the Wisconsin glaciation. Ages of deposits are indicated by Roman numerals corresponding to the glacial advances of Onion Valley. The map was traced from U.S. Geol. Survey aerial photograph GS-VDYM 2-192 (8-31-75) enlarged from a scale of ~ 1:80,000 to ~ 1:15,000.

mid-Wisconsin (advance II) fan surfaces of Independence Creek.

The older fan deposits were found in two locations: along the southern margin of the South Fork fan, and in the lee of an isolated bedrock knob at ~ 1525 m (5000 ft) elevation. The scarcity of boulders on the surface (less than 1 m^{-2}) and the low Granodiorite/Resistate boulder ratio (~ 0.05) are indicative of great age. The fan is certainly pre-Wisconsin. The resistant boulders are largely metavolcanic, and purple piedmontite-bearing metadacite clasts clearly identify the provenance of this ancient fanglomerate as the flanks of Mt. Mary Austin. Those few granitic boulders exposed are grusy or cavernous and are nearly flush with the surface. They have clearly been selectively removed by weathering, increasing the proportion of "resistates" among the survivors. The color of the matrix of the fanglomerate is distinctly reddish brown, with a Munsell color of 5YR5/6.

The adjacent sediments from the reentrant at Boron Springs are roughly equivalent in age to the ancient fanglomerate. Granitic boulders exposed on the surface at the narrow mouth of the reentrant are grusy and flush with the ground, but subsurface boulders exposed along the banks of the small ephemeral stream leading from the reentrant are typically competent. The degree of weathering is similar to that of the right-lateral advance I (pre-Tahoe) moraine at Onion Valley.

Within ~ 250 m of the south edge of the South Fork fan, lightly weathered granitic boulders only partially buried in the fan surface are encountered. Beyond a short transition zone the entire fan surface consists of these younger boulders and light colored grus. About 30% of boulders are granitic, and many of these are covered with a dark desert

varnish. As seen in the banks of the arroyo leading to Tub Springs, the frequency of disintegrated boulders increases with depth in the fan, at least to 10 m. The B horizon has a color of 5YR6/6. No paleosols were seen in the embarkment. From comparison to the fan of Independence Creek, this surface appears to be of early Wisconsin age (advance II).

The increase of boulders with depth in the fan appears to reverse the usual trend. Because the early Wisconsin fan clearly buries the older one, one possible explanation is that there is a strong increase in the age of deposition with depth.

The pre-Wisconsin fanglomerate exposed in the lee of the isolated knob is found in a hollow about 10 m below the level of the early Wisconsin fan. Thus 10 m may be the approximate depth of the fanglomerate deposited during the Tahoe glacial advances. This is comparable to the depth of the equivalent fan of Independence Creek.

Incision along the arroyo from Tub Springs increases from ~ 2 m at the ford east of Boron Springs to ~ 10 m at the prominent dogleg, at about the 1610 m (5280 ft) contour (Plate I). Farther west, the incision lessens to ~ 2 m again. The dogleg is on line with springs and a zone of disturbed ravines in the Boron Springs reentrant and with a zone of reddish gouge in the foothills north of the South Fork. These features may lie along a fault, although there are no consistent offsets in the reentrant and no scarp on the fan. However, the zone of deep incision straddles this possible fault, and smaller ravines to the north show no deepening where they cross the "fault". Thus faulting does not seem to have been responsible for the incision of the ravine, which may have resulted from some non-tectonic cause.

West of the Bright ranch, at 1770 m (5800 ft) elevation, an antithetic normal fault (west side down) breaks the early Wisconsin fan surface. The maximum height of the back facing scarp is ~ 4 m, of which ~ 2 m is perhaps attributable to erosion. The fault scarp can be traced only a short distance into the foothills to the north and south. The scarp appears to be sufficiently old that it has been obliterated by slope wash in the foothills and is preserved only on the early Wisconsin fan, where it is enhanced by erosion. The scarp appears to cut none of the young or (mid-Wisconsin) terraces along the South Fork (Fig. 5-28). This is also an indication that the scarp is quite old.

Terraces in the old fan

Four stream levels are preserved west of the antithetic fault. These are: the modern stream and its banks; a terrace supporting willow and oak, 2 m above the stream; a sage-covered terrace, 5 m above the steam; and the old fan surface, 15 m above the stream. A fifth level, intermediate between the upper two, is found east of the scarp. A sketch profile across the South Fork west of the fault is shown in Fig. 5-29.

The 2-m terrace probably dates from the latest Pleistocene or early Holocene Epochs. The 5 m terrace is continuous with the outwash (advance III) from Sardine Canyon. It is littered with fresh-appearing boulders, some of which may be overflow from younger floods. There seems to be a considerable difference in the age of the terrace and the fan surface nonetheless. The 5-m terrace probably was formed during the Tenaya (III) or early Tioga (IV) glacial stages. Thus the scarp on the antithetic

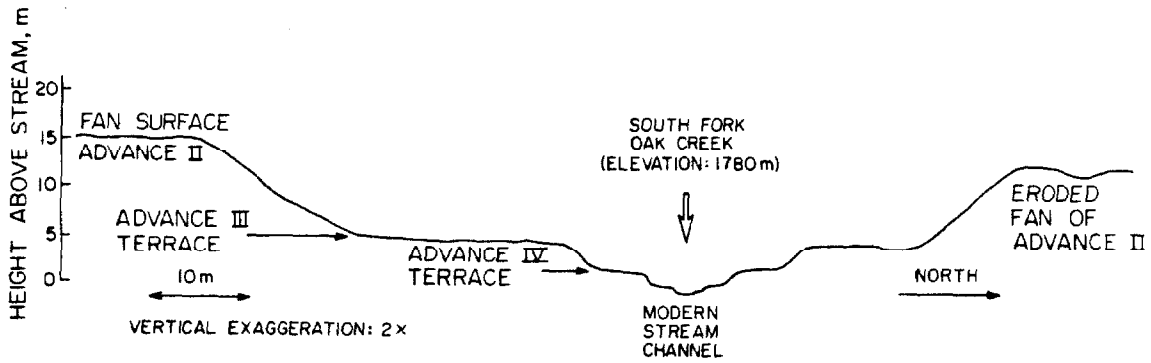

Fig. 5-29. Sketch profile showing terraces of the South Fork ~ 100 m west of the antithetic fault.

fault, which does not break the terrace, must have formed more than ~ 18,000 years ago.

The fifth terrace, east of the antithetic fault, is intermediate in character between the Tenaya terrace and the fan surface. It has fresh granitic boulders and a somewhat lighter matrix (10YR8/2) than the fan surface (10YR7/4). This terrace is steeper than either the fan or the Tenaya terrace, and grades to the advance III (Tenaya) surface at the meadows near the Bright ranch. This might record an ancient channel of the South Fork dating from the time when it overtopped the bedrock sill and became trapped in its northern course. Just after this event the stream cut through the bedrock, its efficiency enhanced by the steep gradient of the new course. A channel or terrace abandoned at this time, before the knick point worked all the way headward, would have an especially steep gradient. The old fan and younger terraces created after equilibrium was reestablished would have similar and lower gradients. The change in the course of the South Fork must have occurred before the Tenaya (III) stage and during or after the Tahoe (II) stage during which the highest surface was created. Its age is thus from ~ 45,000 years to ~ 90,000 years.

Bedrock is found shallowly buried by the old fan on both sides of the antithetic scarp south of the creek. West of the scarp, bedrock lies under ~ 4 m of fanglomerate; to the east it is buried only ~ 2 m. This is consistent with the sense of offset indicated by the scarp, but because there is no compelling reason to assume that the original stream-cut bedrock surface was flat, no value for the total displacement can be deduced. Nevertheless, bedrock spurs north of the creek are cut to a level similar

to the aforementioned outcrops. Thus relief may have been only a few meters and it is possible that total displacement on the fault since creation of the bedrock surface has been no more than about 10 meters. The presence of the pre-Wisconsin fanglomerate lower on the same fan suggests that the bedrock surface was cut more than ~ 0.1 my ago. Thus total displacement on this fault has not been large during the late Pleistocene Epoch, and activity seems to be sporadic with recurrence intervals of tens of thousands of years or more.

The bedrock has apparently been incised about 11 m since the advance II fan was abandoned when the South Fork assumed its modern course.

The modern fan

Sediment being deposited on the active fan is shuttled through the advance II fan and later terraces, just as at Onion Valley, and largely deposited east of the foothill block. When the old fan overlapped a bedrock sill near the site of the Bright ranch, the South Fork gained access to an unsedimented region in the lee of the foothills. This hole may have been as deep as 100 m below the fans to the north and south, and it has not yet been completely filled. The course of the South Fork will remain fixed until the surface of the new fan exceeds the height of the old. The pronounced development of distinct terraces along the South Fork is probably a consequence its chance capture rather than trends in climate or tectonic rates.

The surface of the modern fan appears to be quite young. There are few heavily weathered boulders, and some retain glacial polish. Into this surface the stream is cut ~ 3 m. A low terrace is found ~ 1.5 m below the fan surface also. The fan surface may correspond to the 2-m

terrace upstream and because of the number of fresh boulders it seems to have been formed during the Tioga stage.

The head of the fan at the range front

West of the antithetic fault the 5-m terrace widens to 150 m or more. It may be traced up the South Fork as far as 400 m through the incised outwash plain. As discussed above, (§5.2) the advance III outwash plain of Sardine Canyon grades to this terrace. The surface of the outwash from the South Fork stands ~ 30 m above that from Sardine Canyon and must have been emplaced during an earlier advance of the glaciers. The surface of the older (advance II) right-lateral moraine of Sardine Canyon is comparably (but not so deeply) incised. Both were probably part of a single coalescing outwash plain which thinned southeast from the glaciers of little Onion Valley. This surface graded to the upper surface of the old fan west of the antithetic fault.

An ancient surface is preserved between Tub Springs and the prominent landslide south of Sardine Creek. It has been incised as much as ~ 45 m by rills from the east face of Kearsarge Peak. Below Tub Spring these rills grade to the advance II fan. The ancient surface is truncated on the east by an escarpment about 60 m high. It may correlate with the outermost of the South Fork moraines, or with the earlier ancient deposits on the southern margin of the fan near Boron Springs, or with neither.

On aerial photographs this escarpment is part of a faint diffuse linear shaded zone ~ 200 m northeast of Tub Springs. However, the advance II surface does not appear to have been offset, and the shaded zone across it may reflect a change in the density of vegetation (sage).

The photo-lineament projects through the springs near the confluence of Sardine Creek and the South Fork. The coincidence of springs along the escarpment raises the possibility that this feature is an ancient fault scarp, more or less on strike with the faults in the foothills south of Independence Creek. It cannot be followed into the foothills themselves, nor does it break the outwash head below Little Onion Valley. Any offset along this zone therefore predated the Wisconsin glaciation. On the other hand, faulting is not necessary to explain the escarpment, which may simply be an ancient terrace riser. The springs could arise where bedrock is nearly exposed by downcutting.

Summary of the South Fork fan

There appear to be at least four and possibly five surfaces on the fan of the South Fork of Oak Creek. The youngest (latest Pleistocene) is found along the South Fork northeast of the Bright ranch and in a narrow terrace upstream. A mid-Wisconsin age fan (advance III) probably underlies the youngest fan. Fanglomerate of this age is exposed on the surface only in a wide terrace 5 m above stream level west of the ranch. The major part of the fan was deposited when the South Fork flowed due east through the foothills. This surface grades upward to the large outwash head below Little Onion Valley. It is probably of early Wisconsin age (advance II). Largely buried beneath ~ 10 m of this fanglomerate is a distinctly older surface. It is probably pre-Wisconsin in age. Near Tub Springs is found another old surface. Its relation to other surfaces and its age are unknown.

The Foothills

The South Fork of Oak Creek has cut a canyon as deep as 425 m through the foothills east of the Independence Fault. The foothill block north of the South Fork is capped by two plateaus, at ~ 2285 m (7500 ft) elevation and at ~ 2070 m (6800 ft) elevation. These probably correspond to the surfaces north of Independence Creek at ~ 2145 m (7040 ft) and 1830 m (6000 ft) elevation. If this is true these surfaces dip less than 5° south. The eastern side of the foothills is an eroded and gullied surface which dips ~ 9.5° E. It is truncated on the east by a deeply eroded line of cliffs ~ 150 m high. To the north the foothill block is cut by Charlie Canyon, which drains only the east face of Mt. Mary Austin. This canyon is as deep as the canyon of the South Fork.

Moore (1963) has mapped the foothill block as consisting of quartz monzonite and small stringers of metamorphosed rhyolitic tuff. Both upper surfaces of the foothill block are bedrock covered by locally derived weathering products. However, on the highest surface there is one small hilltop composed of a diamicton (Plate I) containing exotic rounded and grooved metamorphic and granitic boulders.

The diamicton is about 20 m thick. Some of the metamorphic boulders must have been derived from the upper reaches of either fork of Oak Creek or from above the 3050 m (10,000 ft) level on the east face of Mt. Mary Austin. The degree of rounding shows that they were fluvially (or glacially) transported. Fig. 5-30 shows one such boulder. Parallel grooves in its surface points towards a glacial history but in the absence of distinctive scratches another mechanism cannot be ruled out. The presence of the grooves on both the exposed and buried surfaces of this and other

Fig. 5-30. Rounded metadacite boulder from the ancient fanglomerate found atop the foothills east of the Independence Fault, and 125 m above the late Pleistocene moraine crests. Distinct grooves parallel to the hammer handle suggest a glacial history. Darkened part of the boulder (left) was buried. Grooves appear both on the buried and exposed surfaces.

boulders shows that they were created before deposition. Grooved boulders were common among boulders of the ~ 2.5-my-old McGee till (central Sierra Nevada), although distinctive scratches were rare (Blackwelder, 1931).

The diamicton probably originated as an ancient fan. At the same distance from the range front its base is about 125 m above the top of the outer left-lateral moraine. This indicates that it is considerably older. If the downcutting rate at Coyote Creek (< 0.33 mm/y) is applicable here, the age difference must exceed 0.37 my. Later it will be shown that the old moraine is probably of pre-Wisconsin age. Thus the diamicton probably is older than 0.5 my.

The Independence Fault and the Sierra escarpment

Evidence of recent offset along the Independence fault was not observed north of Sardine Creek. The Independence Fault has not offset the largest moraine of the South Fork glaciers. The outer left-lateral moraine (advance I) does not seem to be broken either, but it emerges from a skirt of colluvium just about on the probable trace of the fault. A wedge of diamicton impounded between this or an earlier moraine and the foothills to the north was clearly faulted an estimated 10 m. If the faulting rate on this part of the Independence Fault is similar to the rate at Independence Creek, then this diamicton must be comparable in age to the oldest moraines of Independence Creek and would therefore be pre-Wisconsin in age.

The long-term offset along the Independence Fault is recorded in the immense eastern escarpment of the Sierra Nevada. The faceted nature of this escarpment is as well illustrated on Mt. Mary Austin as anywhere in the Mt. Pinchot quadrangle. This may be seen in the oblique aerial

photograph of Fig. 5-6. The apices of the lower facets are at 2925 m (9600 ft) elevation and 2805 m (9200 ft). The facets rise 660 m with an average slope of 31.4°. Above, the ridges of Charlie Canyon define a facet with an apex at 3815 m (12,520 ft) elevation and an average slope of 25°. From here a narrow ridge leads up 300 m to the Sierra crest, 2.9 km to the west. The facets do not appear to be controlled by the contact between the Tinemaha granodiorite and the metavolcanic rocks.

The Moraines of Little Onion Valley

Four nested pairs of moraines are found along the South Fork at the range front (Fig. 5-31). These may correlate to the moraines of advances I-IV along Independence Creek, and this numbering scheme will be used provisionally in the discussion below. The outermost (I) extends down to 2070 m (6800 ft) elevation. The till rests on bedrock, which is exposed by extensive erosion near the lower limits of both lateral moraines. The moraines of advance II are the most massive of the four pairs. The crests are as much as 73 m above the South Fork, and together both lateral moraines contain ~ 0.007 km^3 of till. The moraine overtops a thick outwash head. The moraine provisionally assigned to advance III are widely breached by the South Fork, but the youngest moraines (IV) are not.

The crest of the left-lateral moraine I north of the South Fork is as much as 25 m below the crest of moraine II. This amount exceeds the height of an ancient scarp on the Independence Fault through the filled hollow. The left-lateral moraine II is in turn buried to a depth of ~ 10 m by a moraine of advance III. The difference in the elevation of the crests could well be caused by down-faulting of the

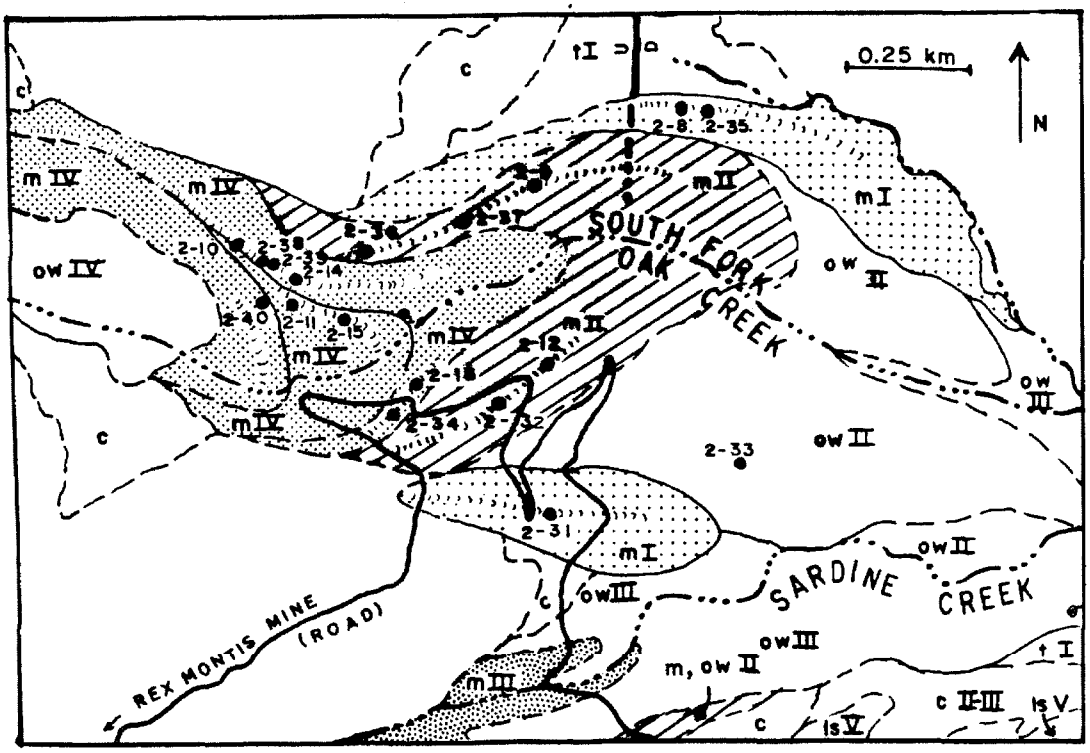

Fig. 5-31. Relative weathering data collection sites on the Pleistocene moraines of Little Onion Valley. Sites where conventional semi-quantitative measurements were made are shown by open circles. Sites where V_p data were gathered also are shown by filled circles. Map base is U.S. Geol. Survey aerial photograph GS-VDYM 2-192 (8-31-75) enlarged from a scale of ~ 1:80,000 to ~ 1:15,000.

outer moraine before the younger ones were deposited (Clark, 1972), but if this is the case, displacement must have occurred in a zone west of the Independence Fault. It is noteworthy that the crest of moraines of advances III and IV are at the same elevation. If faulting occurred at the same rate over the last ~ 0.25 my, then advances I, II, and III may be significantly different in age, but advances III and IV appear to be close in age.

The outermost right-lateral moraine (I) was not mapped as such by Moore (1963). It appears to be a moraine for the following reasons: (1) It is composed of a diamicton containing massive rounded boulders more than 2 m in diameter; (2) Many boulders are metavolcanic and appear to have originated more than 1 km to the west. The local bedrock from which the diamicton might be derived is only granodiorite and porphyritic granodiorite dike rock; (3) The "moraine" heads on a ridge and there is no obvious source for the diamicton; (4) Some boulders exhibit arcuate fractures found in similar boulders in tills; (5) It resembles a moraine morphologically; (6) A moraine of the same age as the outermost left-lateral moraine should have been present south of the creek after the retreat of the glacier. While this could have been eroded or over-ridden by subsequent moraines, the presence of an old right-lateral moraine today is not unexpected.

Arguments against this intepretation are: (1) Metamorphic rocks could have been derived locally from pods within the granodiorite similar to those mapped by Moore (1963) 0.6 km to the west; (2) The debris could have originated on a larger spur now reduced in size by cutting of later glaciers; (3) No piedmontite-bearing metarhyolitic boulders were found,

nor any boulders with undisputable glacial striae. Piedmontite-bearing boulders are found in the younger right-lateral moraines, even though the only source appears to be on the north side of the canyon. Nevertheless, the feature was mapped as a moraine in this study.

An early left-lateral moraine apparently isolated a hollow against the foothills to the north, just as did the early moraines on Independence Creek. This may have been the outermost moraine preserved today, or an earlier one. The hollow filled with diamicton, containing massive black metabasalt boulders about 50 cm in diameter which came from Little Onion Valley. The deposition of the sediment could not have been after the retreat of the glacier which created the present outermost left-lateral moraine.

Semi-quantitative relative weathering data were of some use in assigning ages to moraines in Little Onion Valley. These data are given in Table 5-13. Metamorphic "resistates" on the crest of the oldest left-lateral moraine (I) outnumbered granitic boulders by a factor of nine. About 74% of the granitic boulders exposed at the surface at two sites were heavily weathered, and some were cavernous. Half the boulders were largely buried. The surficial soil had a Munsell color of 10YR4/2 to 10YR4/3, increasing in chroma to 10YR6/5 ~ 30 cm below the surface. Although granitic boulders were rare, the numerous metavolcanic clasts observed maintained the BFC at levels exceeding 0.5 m^{-2}. The high proportion of weathered granitic clasts and the large number of boulders nearly flush with the moraine surface are indicators of great age. The abundance of resistates is consistent with this, but could also result from the abundance of metavolcanic rocks in drainage of the South Fork.

Table 5-13

Semi-Quantitative Relative Weathering Data for Pleistocene Moraines of Little Onion Valley

Right-Lateral Moraines

Site[1]	Advance[2]	No. of Boulders[3]	GWR[4]	G/R[5]	BR[6]	BFC[7] m^{-2}	Color[8]
2-31	I	24	54/38/8	18/82	-	1.41	5Y7/2*
2-32	II	72	32/64/4	68/32	-	2.13	10YR8/2*
2-12	II	43	81/19/0	83/17	62/17/21	0.34	10YR7/3†
2-33(OW)	II	34	29/53/18	34/66	-	0.94	-
2-34	III	82	15/44/41	67/33	-	1.58	N7-5Y8/1*
2-13	III	62	44/45/11	82/18	24/55/2	0.78	10YR6/4†

Left-Lateral Moraines

Site[1]	Advance[2]	No. of Boulders[3]	GWR[4]	G/R[5]	BR[6]	BFC[7] m^{-2}	Color[8]
2-35	I	7	29/71/0	10/90	-	1.48	-
2-8	I	28	86/14/0	10/90	50/21/29	0.56	10YR6/5†
2-36	II	65	9/48/43	48/52	-	1.79	-
2-37	II	28	32/57/11	15/85	-	1.17	-
2-9	II	26	77/23/0	25/75	22/25/53	1.10	10YR6/4†
2-38	III	39	8/59/33	52/48	-	1.53	-
2-39	III	80	5/49/46	62/38	-	1.58	-
2-10	III	36	28/56/17	45/55	18/30/53	0.54	10YR5/2†
2-14	III	38	50/45/5	79/21	29/21/50	0.63	10YR6/3†
2-40	IV	101	3/30/67	72/28	-	2.85	-
2-11	IV	87	22/51/28	70/30	27/56/17	1.48	10YR4/2†
2-15	IV	43	35/42/23	7/93	-	0.80	-

Table 5-13 (continued)

[1] Sites are shown in Fig. 5-31. "OW" denotes outwash; other sites were on moraine crests. Sites 2-36 (II) and 2-11 (IV) were both subject to rockfall from the adjacent moraine (III). Site 2-10 (III) may have been partially buried by boulders from the advance IV glacier.

[2] Advances I-IV are Pleistocene glaciations of Independence Creek in order of decreasing age. For correlation to the conventional Sierra Nevada sequence, see Table 5-10.

[3] Number of boulders used for the GWR. In some instances only a few boulders were counted due to limited exposure or simply because virtually all granitic rocks had disintegrated.

[4] Granodiorite Weathering Ratio: the percent of granodiorite or quartz monzonite boulders in each of three classes based on degree of weathering (heavily weathered; lightly weathered, or fresh, respectively). See Ch. 2.

[5] Granodiorite/Resistate boulder ratio (in %). See Ch. 2.

[6] Boulder burial or relief: the percent of granodiorite or quartz monzonite boulders exposed at the surface, in each of three classes based on the depth of burial (less than 25% exposed; 25% to 75% exposed; more than 75% exposed, respectively). See Ch. 2.

[7] Boulder Frequency Count: the number of boulders with diameters exceeding 30 cm, regardless of composition, per m^2. See Ch. 2.

[8] Munsell color notation. "*" indicates color measured in roadcuts, ~ 2 m below the surface. "†" indicates color measured in pits at a depth of ~ 0.3 m.

On the right-lateral moraine I the enhancement of resistate abundance was less pronounced. Fewer of the granitic boulders exposed at the surface were heavily weathered (54%), but most boulders in road cuts were grusy and oxidized red. The color of the till matrix in road cuts was 5Y7/2. The difference between lateral moraines in the resistate abundance may have been due to differences in the bedrock geology between sides of the canyon of the South Fork.

These measurements contrasted strongly with those for the moraine of advance II: The boulder frequency on the younger left-lateral crest was twice as great, the surficial soil color (10YR7/2) was lighter, and metamorphic boulders outnumbered granitic boulders by only a factor of 3. In part, some of this apparent relative youthfulness could have been caused by undercutting of the inner flank of the moraine by the South Fork, removing the original crest and leaving fresh subsurface till exposed on the new top of the moraine. The inner slope was 34°, in contrast to only 26° for the left-lateral moraine I.

Comparable contrasts were observed between the two oldest (I and II) right-lateral moraines also, except the GWR values were not necessarily different (Table 5-13). However, the difference in the abundance of resistates was pronounced, with more granitic boulders preserved on the younger (II) moraine. In road cuts, granitic boulders were typically grusy, but not oxidized, and matrix color was 10YR7/3-10YR8/2. Thus the moraine appeared to be younger than the moraine of advance I.

The second glacier of advance II terminated at about 2130 m (7000 ft) elevation against the outwash head which grades into the highest fan surface (also of advance II). Apparently outwash was deposited before

the moraine was completed: the right-lateral moraine buries an old channel cut into the outwash head. This channel was cut by water pouring off the earlier glacier.

Because of its size, weathering characteristics, and position in the stratigraphic sequence, the correlation of the moraine with the moraines of advance II (Tahoe stage) along Independence Creek is probably valid. The outermost moraine, which appears to be distinctly older than advance II, is regarded as advance I (pre-Tahoe stage), although its age equivalence with advance I of Independence Creek was not established.

The moraine tentatively assigned to advance III terminates at about 2240 m (7360 ft) elevation. At first glance it seems to be obviously younger than the massive moraine of advance II. However, the semi-quantitative weathering data (Table 5-13) show considerable overlap with the earlier moraine, and also considerable heterogeneity within each moraine. The most convincing evidence of the difference in ages is the incidence of fresh granodiorite boulders in both lateral moraines of advance III, and the markedly higher incidence of "resistates" in the left-lateral moraine II. Although few grusy granodiorite boulders were found on the surface of moraine III, they were found in roadcuts south of the creek. Thus the moraine does appear to be correlative with moraines of advance III in Onion Valley.

The South Fork has had time to cut only a narrow slot through the southern part of the terminus of the moraine tentatively correlated with advance IV of Onion Valley. In contrast, the older moraines have been extensively breached. West of the terminus, the South Fork is incised less than 2 m into the floor of Little Onion Valley. The valley

strongly resembles the upper Onion Valley of Independence Creek in general appearance, and is certainly no older than advance IV (Tioga stage). From the lack of stream incision alone, it could even be correlated with advance V.

The left-lateral moraines of advance IV rise westward to about the level the crest of the moraine of advance III. They are not massive, and have left only a thin veneer on this older moraine. Because the general appearance of the constituent boulders is similar, it is difficult to tell whether the advance III moraine was actually overtopped. There exists the strong possibility that the apparent moraine crest contains tills of both ages. Sites for the collection of relative weathering data were selected to minimize the possibility of mixing of till of different ages.

Despite possible contamination, sites on the younger moraines (III and IV) tended to show greater fractions of fresh and unburied granodiorite bolders than found on the older moraines (I and II). Perhaps the most dramatic difference was the reduction in the abundance of resistates (granodiorite/resistate ratio, Table 5-13), from 52-90% to 21-55% of the boulders exposed on left-lateral moraines (with one exception on the youngest moraine). Even casual inspection in the field showed a high variability in the G/R among sites on the youngest moraines. Perhaps this variability was caused by incomplete mixing of till from different cirques. It reduced the reliability of the G/R ratio as a relative age criterion, at least for this valley. Nevertheless, the younger (III and IV) and older (I and II) moraines were readily distinguished by weathering criteria in the field. However, distinction between the younger moraines

provisionally assigned to advances III and IV was not possible. The fact that the terminus of the youngest moraine has barely been breached shows that this is at the oldest of late Tioga advance (IV). Because in Onion Valley (and elsewhere in the Sierra; cf. Birman, 1964) Hilgard moraines (advance V) are not found close to Tioga (advance IV) terminal moraines, these youngest moraines were assigned to advance IV in this study. From the weathering data, the provisional advance III appears to be an earlier Tioga advance, and thus should be assigned to advance IV rather than advance III.

Thus on the basis of field inspection only, three ages of moraines were recognized in Little Onion Valley. The two most recent advances are probably correlative with advances II and IV of Onion Valley. The correlation of the oldest moraine is uncertain, but it predates advance II and is assigned to advance I in this study. Because of the high variability in the semi-quantitative parameters among sites on the same moraine, acoustive wave speeds were measured to provide an additional basis for age discrimination.

Acoustic wave speeds in boulders of South Fork moraines

Acoustic wave speeds were measured at eight sites shown in Fig. 5-31. Summary data are given in Table 5-14. One of the sites (2-11) was in a location where mixing of till of different advances was a possibility. A duplicate site was established to test this possibility. Wave speeds for about 15 boulders were measured at each site. Mean wave speeds for these sites ranged from a low value of 1.3 km/s to a maximum value of 2.0 km/s; the standard deviations ranged from 0.26 to 0.41 km/s. Wave speeds at each site appeared to be normally distributed. Thus Student's

Table 5-14

Acoustic Wave-Speed Data for Moraines

Along the South Fork of Oak Creek

Site*	Advance**	No. of Boulders	$\overline{V_p}$, km/s	s,km/s	D_{max} †	C,%††
2-12	II (R)	15	1.61	0.26	0.160	70
2-13	III (R)	15	1.98	0.27	0.139	52
2-8	I (L)	15	1.29	0.37	0.121	37
2-9	II (L)	15	1.78	0.32	0.127	42
2-10	III (L)	15	1.80	0.26	0.108	28
2-14	III (L)	18	1.88	0.41	0.105	31
2-11[1]	IV (L)	15	1.86	0.28	0.142	55
2-15	IV (L)	15	2.00	0.37	0.142	24

* Measurement localities are indicated in Fig. 5-31

** Advances are those of Onion Valley and are numbered I-VII in order of decreasing age. Correlation with the conventional Sierra Nevada sequence is found in Fig. 5-10. "R" and "L" denote right- and left-lateral moraines, respectively.

† D_{max} is the statistic for the one-sample Kolmogorov-Smirnov test, comparing the actual distribution of wave speeds (V_p) to a normal population with the same mean ($\overline{V_p}$) and standard deviation (s). See Ch. 3 for details.

†† C is the confidence with which D_{max} allows us to reject the hypothesis that the population was normally distributed.

1 Site 2-11 may have been contaminated by boulders rolling off the adjacent and higher moraine of advance III (sites 2-10, 2-14).

t-test rather than the non-parametric Kolmogorov-Smirnov test was used to compare sites. Results are shown in Table 5-15.

Advances I and II were clearly separable, with > 99% confidence. Comparison of sites 2-12 and 2-13 shows that right-lateral moraines of advances II and III were likewise different. However, the technique failed to discriminate between adjacent left-lateral moraines of advances II, III, and IV, although moraines of advances II and IV were separable with 96% confidence. By comparing both sites from the left-lateral moraine of of advance III (2-10 and 2-14) to the contamination-free site on the moraine of advance IV (2-15), enhanced separability, still with only 91% confidence, was achieved. The relatively low $\overline{V_p}$ for site 2-11 is consistent with the presence of older boulders "(III)" among those measured. Even excluding this site, the differences between the V_p data for the two moraines were not so great as to make a separate stage mandatory for the moraine "III". Instead, this moraine could be simply an early Tioga stade. Thus in this study moraine "III" will be classified with advance IV.

It is remarkable that in this instance V_p data were unable to distinguish between advance "III" (early advance IV) and advance II moraines, since conventional methods were sufficient to do so.

It is possible that exposure of fresh buried boulders by the undercutting of the advance II moraine by the South Fork resulted in the continued exposure of new fresh boulders on the "crest" and an anomalously high V_p, and hence reduced the contrast with the advance "III" data. However, the weathered appearance of the measured boulders belies this, and it seems more likely that some boulders were case-hardened, as

Table 5-15

Comparisons of $\overline{V_p}$ Using Student's t-Test

Right-Lateral Moraines

Sites*	Advances**	Degrees of Freedom†	t††	C_1,%*†	C_2,%†*
2-12 vs 2-13	III vs IV (R)	28	-3.93	>99	>99

Left-Lateral Moraines

Sites*	Advances**	Degrees of Freedom†	t††	C_1,%*†	C_2,%†*
2-8 vs 2-9	I vs II (L)	28	-3.88	>99	>99
2-9 vs (2-10,2-14)	II vs III (L)	46	-0.69	75	51
2-9 vs (2-15)	II vs IV (L)	28	-1.78	96	93
(2-10,2-14) vs (2-15)	III vs IV (L)	46	-1.32	91	81
2-9 vs (2-10,2-14, 2-11,2-15)	II vs (III, IV) (L)	76	-1.07	86	72

* Measurement localities are indicated in Fig. 5-31.

** Advances are those of Onion Valley and are numbered I-VII in order of decreasing age. Correlation with the conventional Sierra Nevada sequence is found in Fig. 5-10. "R" and "L" denote right- and left-lateral moraines, respectively.

† Degrees of freedom = n + m - 2, where n and m are the numbers of V_p measurements in the two groups being compared.

†† t is the test statistic calculated from the difference between the means ($\overline{V_p}$ for the group listed second is subtracted from $\overline{V_p}$ for the group listed first). See Ch. 3 for details.

*† C_1 is the one-tailed confidence that $\overline{V_p}$ for the second group is higher than $\overline{V_p}$ for the first group.

†* C_2 is the two-tailed confidence that the groups are not the same.

observed at Green Creek. Because moraines II and III were so obviously separable based on conventional relative dating methods, and on V_p data south of the creek no additional data were taken to test this possibility.

Thus acoustic wave-speed distributions support the classification of the moraines into at least three groups. These are correlated with advances I (?), II, and IV in Onion Valley.

Glaciation in Upper Little Onion Valley

Quaternary deposits along the South Fork of Oak Creek were mapped all the way to the Sierra crest (Fig. 5-32). These were chiefly talus and neoglacial till. Three ages of till were recognized, correlative with tills of advances V, VI, and VII in Onion Valley. Of these, the oldest (V) was present largely as thin ground till and erratic boulders on bedrock. The terminus of the glacier of this advance was not identified; it was probably on the step between East Parker Lake and Little Onion Valley. Granitic boulders from this till were often deeply weathered, with diorite inclusions standing as much as 6 cm above the degraded surfaces. Boulders in moraines were stable, and locally dense forests were supported.

Above East Parker Lake, most of the terrain was last glaciated during advance V (Recess Peak). Boulders in these moraines were somewhat unstable; occasional shrubs and grasses were supported; and boulders in favorable locations were heavily covered by lichens. Minor axes of colonies of yellow-green lichens were up to ~ 20 cm in length.

Under the cirque walls, fresh moraines and rock glaciers of the most recent glaciation (advance VII) were found. These moraines are steep-sided,

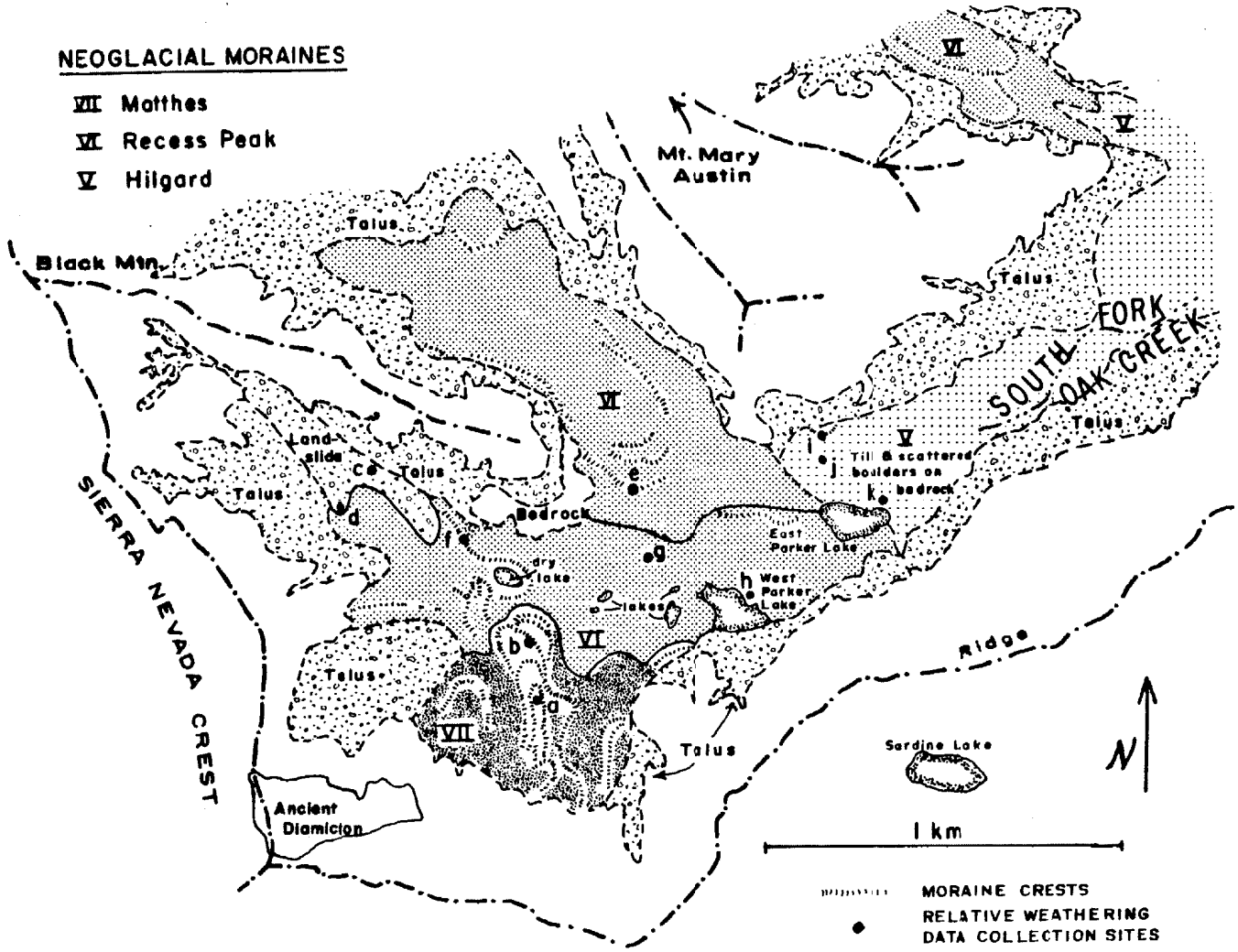

Fig. 5-32. Relative weathering data collection sites on neoglacial moraines and talus in the headwaters of the South Fork of Oak Creek. Map base is U.S. Geol. Survey aerial photograph GS-VDYM 2-192 (8-31-75) enlarged from a scale of ~ 1:80,000 to ~ 1:19,000.

unstable, and support neither grasses nor lichens. In addition, a lake at the base of the south wall of the cirque had the distinctive milky color of rock flour, indicating the presence of active glaciers.

The principal basis for comparison of neoglacial tills and moraines with those at the range front did not exist, because the headwater regions of the South Fork were developed primarily in metavolcanic rocks. The Tinemaha granodiorite terminated against the metamorphic pendant 1.5 km west of the Independence Fault. Quartz monzonites of the Sardine and Diamond plutons were exposed at two restricted locations in the headwaters of the South Fork, but the only abundant granitic rocks were quartz-poor granodiorites of the Dragon pluton. Because of widespread assimilation of mafic minerals and xenoliths from dioritic and volcanic wallrock (Moore, 1963) these rocks were probably unsuitable for relative dating.

Semi-quantitative measurements (Table 5-16) are therefore probably of use only for relative dating of deposits within the headwater region and cannot be reliably compared to those for lower moraines. These measurements were used to support the assignment of the deposits to the different advances.

Boulders from the youngest moraines (advance VII) under the present-day glaciers and from talus overtopping older neoglacial till were dominately unweathered, with the hackly surfaces characteristic of fresh glacially plucked rock. This close to the source, no boulders were polished. The yellow-green lichens used in lichenometric dating were not found, although as many as 10% of the boulders had incipient colonies of the fast-growing brown lichens.

Boulders from the older moraines (advance VI) of the cirque

Table 5-16

Granodiorite Weathering Ratios for Neoglacial Moraines and Talus of the South Fork of Oak Creek

Site[1]	Advance[2]	No. of Boulders[3]	GWR[4]	Weathering Relief[5] cm	Lichen Thalli Diameter[6] cm	Fraction of Boulders with Lichen[7]
a	VII	-	0/ 0/100*	0	0	0.05
b	VII	-	20/80/0*†	0	0	0.1
c	VII(talus)	100	0/ 0/100	0	0	0.0
d	VII(talus)	49	0/10/90	0	0	0.1
e	VI	65	31/31/38	-	5	0.75
f	VI	79	33/44/23	-	-	-
g	VI	177	33/44/23†	4	-	-
h	VI	140	37/46/17†	2	20	0.6
i	VI	83	10/25/65	6	-	0.9
j	V	118	47/44/8†	-	-	-
k	V	51	51/49/0	1.5	20	0.8
k	V	119	46/45/9			

* Rough estimate only.

† Heavily weathered boulders were grusy or strongly pitted.

1 Sites are shown in Fig. 5-32.

2 Glacial advances V, VI, and VII probably correspond to the Hilgard, Recess Peak, and Matthes neoglacial advances, respectively.

3 Number of boulders counted for the GWR.

4 Granodiorite Weathering Ratio: the percent of granodiorite or quartz monzonite boulders in each of three classes based on degree of weathering (heavily weathered; lightly weathered, or fresh, respectively). See Ch. 2.

5 Weathering relief: maximum depth of pits or maximum height of diorite inclusions above the boulder surface.

6 The diameter of the lichen thalli or colonies refers only to the yellow-green lichen. See Ch. 2. Because colonies may grow together from different nucleii, if this is suspected the largest minimum diameter is reported. Diameters are approximate.

7 Lichens of all species were counted.

region were roughly equally distributed among weathering classes. The most heavily weathered boulders had grusy surfaces, with diorite inclusions standing as much as 4 cm in relief. In general, lichens were well established and were found on more than half the boulders. Yellow-green lichens were present; at the two locations were their sizes were measured they were ~ 5 cm and ~ 20 cm. These correspond roughly to ages of 1000 y and 4000 y, if the growth-rate charts of Curry (1968) are applicable here.

Few boulders from the neoglacial till below the cirque region (advance V) were unweathered. The contrast with the younger till (VI) was pronounced. Lichen cover and weathering relief were similar, however.

An old bench supporting perhaps 50 m of diamicton is seen above 3660 m (12,000 ft) elevation just east of the Sierra Crest and southwest of the upper Parker Lake. This surface was not visited. However, it is cut by the late Wisconsin cirque, which it thus predates. Other evidence for relict geomorphic features in Little Onion Valley is scarce. The south wall contains only numerous avalanche chutes terminating on the steep cliffs of the trim line. On the north wall, the ridges leading S30°E and S70°E from the summit of Mt. Mary Austin are truncated at 3660 m (12,000 ft) and 3535 m (11,600 ft) elevation, respectively. The truncated spurs form triangular facets whose apices are 370 m above the present-day South Fork. If they are remnants of an ancient line of cliffs, their equivalents on the south side of Little Onion Valley would be at least as high as the present-day ridge.

Summary

The moraines of the South Fork of Oak Creek are among the best preserved in the Southern Sierra. Four pairs of moraines of late Pleistocene age were found at the range front. These could only be assigned to three different stages, correlating to I(?), II, and IV of Independence Creek. Advance III, so prominent in Onion Valley, appeared to be missing. It may be that the two moraines assigned to advance IV would be separable if more V_p data were taken, and that the older actually belongs to advance III, or it may simply be that moraines of advance II were thin veneers of till which were readily eroded from the inner flanks of the massive Tahoe (II) moraine by undercutting by the South Fork.

As at Independence Creek, three different ages of fan deposits were recognized. The oldest deposits (I?) were found at the margins of the advance II fan. The latest Pleistocene and Holocene fan was deposited north of the advance II fan following overtopping by the fan of a ridge of the foothills and subsequent capture of the South Fork, probably near the end of advance II. Rapid down-cutting of the creek following this event was probably for the well-preserved terraces found in the upper fan. The cirque and upper reaches of the canyon of the South Fork contained neoglacial deposits of three ages, corresponding to advances V-VII of Onion Valley, or the Hilgard, Recess Peak, and Matthes glacial stages. Minor glaciers are still found under the steep and shady cliffs in the southern part of the cirque today.

Ancient diamictons were found on a bench above the Wisconsin-age cirque and on a ridge in the foothills, east of the range-front fault. Grooved boulders in the diamictite of the foothills may indicate a glacial

history, but these boulders may have been redeposited and there is no evidence that the diamicton was actually a till. If the grooves were of glacial origin, then this is evidence of early Pleistocene glaciation in the southern Sierra Nevada, even if the diamicton were a fanglomerate. If incision rates of the foothills are comparable to that of Coyote Creek (Bateman, 1965), then the diamicton may be roughly equivalent in age to the Sherwin glaciation.

5.4 NORTH FORK OF OAK CREEK

Introduction

The North fork of Oak Creek arises at 3595 m (11,800 ft) elevation under Diamond Peak on the Sierra Crest. After joining with a tributary which drains the northern slopes of Black Mt., it flows east 5 km to the Independence Fault on the range front and 5 km through the foothills to the confluence with the South Fork at 1325 m (4350 ft) elevation.

The southernmost lavas of the Big Pine volcanic field are found on the foothill ridges between the North Fork and Charlie Canyon and in the alluvial fan and canyon of the North Fork itself. These consist of flows of olivine basalts, which generally overlie pyroclastic beds of basalt bombs and blocks in a matrix of lapilli, ash and granitic cobbles and grus. Petrographic descriptions are found in Moore (1963), Darrow (1972), and Moore and Dodge (1980). Moore (1963) identified a vent at 2560 m (8400 ft) elevation in the unnamed northern tributary to the North Fork.

Darrow (1972) felt that more than one eruptive center was active because the lava flows rested on extensive beds of pyroclastic debris. Both Darrow and Moore agreed with Knopf (1918) that the lava flows of Oak Creek are among the earliest of the volcanic field, citing the extensive erosion and alluviation of the outcrops. Moore argued that the flows conformed to the present topography but were buried by Tahoe moraines, and he concluded that they were early Pleistocene in age. Darrow attempted to establish eruptive sequences but could not, because of the lack of contiguity of outcrops and lack of petrographic similarities. Moore and Dodge (1980) have since recognized at least two different

basalts from Oak Creek based on K_2O and SiO_2 content and on mineralogy. Potassic olivine basalts were found on ridges and on the fan, while alkalic olivine basalts were found in the canyon itself. In one sample of the latter group (at 36°50.3'N, 118°16.5'W) plagioclase was the dominant phenocryst, but in all other flows olivine was dominant. Both Moore and Dodge (1980) and Darrow (1972) commented that throughout the Sierra Nevada and the Big Pine volcanic field in particular, compositional trends with time were difficult to identify and were subordinate to apparently random differences.

At least three different ages of lava are indicated by the morphologic setting: (1) old lavas on present ridges; (2) lavas on high terraces; (3) young lavas near the present stream channel. Morainal deposits and perhaps outwash lie atop the youngest lavas. The Quaternary geology of the North Fork is of interest primarily because of the insights into erosion and tectonic rates and glacial chronology afforded by these relationships. ^{40}Ar-^{39}Ar dating of several basalt samples was used to provide chronologic control for these studies (Ch. 4).

Discussion of the geology is divided into a summary of the bedrock geology, discussions of the Quaternary geology of the alluvial fan and the foothills, and discussions of the late-Pleistocene moraines near the range front and of the geology of the headwaters of the North Fork.

Summary of Bedrock Geology (Moore, 1963)

The upper reaches of the North Fork of Oak Creek erode the same rock units as the South Fork, with the addition of sheared and gneissic granodiorite of the White Fork pluton. Near the lower end of the

Pleistocene glaciers, the drainage contains the dark granodiorite of the McDoogle pluton and a wide variety of mafic plutonic rocks. The northern tributary to the North Fork is cut primarily into Tinemaha granodiorite. Below about 2620 m (8600 ft) elevation basalts have erupted through the McGann (quartz monzonite) or the McDoogle pluton. Inclusions of the McGann quartz monzonite and also dunite xenoliths are common in these basalts.

The foothill block consists mainly of McGann quartz monzonite, intruded locally by granitic dikes. Several normal faults besides the Independence Fault break the foothills. Most of these also break the basalt flows.

The Alluvial Fan of the North Fork of Oak Creek

The alluvial fan of the North Fork of Oak Creek covers an area of about 16 km^2. It may be divided into two parts, the larger of which contains roughly 70% of the fan and is currently inactive. Most of this older fan lies north of the modern stream. Its latest deposits appear to be of early Wisconsin age. The younger fan is found along the modern channel of the North Fork, chiefly southeast of Oak Creek Camp (see Plate I).

The older fan contrasts with the younger in the redder color of its soil and in the greater proportion of weathered boulders exposed on its surface. However, the fan was apparently constructed over an extended period, and its weathering characteristics are variable. Fanglomerate from the period is exposed well in cuts along the new road just northwest of Oak Creek Camp. The soil is deeply weathered and rich in clay.

Disintegrated granitic boulders are common. On the same fan surface is found debris containing relatively unweathered granodiorite boulders, chiefly near the fan head at 1585 m (5200 ft) elevation and also north of the isolated low bedrock hills near Oak Creek Camp. These relatively fresh deposits probably mark the final course of the North Fork down the main axis of the fan before the stream shifted south and ultimately overtopped the bedrock ridge below Oak Creek Camp. When this occurred, the stream flowed into a depression previously shielded from alluviation; in consequence of the new steep gradient, the bedrock ridge and the fan behind it were quickly incised about 15 m so that the North Fork became trapped in its modern course.

Basalt from at least two early volcanic eruptions flowed over the older fan and is exposed at the fan surface or on the walls of the arroyo leading east from McGann Springs. The older basalt yielded a ^{40}Ar-^{39}Ar age of 1.13 ± 0.07 my (Ch. 4). At least on the fan the older basalt commonly has distinctive light-colored polygonal segregations that seem to contain fewer opaque minerals than the rest of lava. Granitic xenoliths are rare. In contrast, the younger basalt is devoid of the segregations and has abundant granitic inclusions. However, the most significant difference appears to be in the alluvial cover. Some outcrops of the older basalt are buried by an ancient fanglomerate from which most of the granitic boulders have been removed by granular disintegration. Boulders exposed in the arroyo below the level of the older basalt were thoroughly grusy. On the other hand, granitic cobbles exposed beneath the younger flows were still competent.

The eruption of the 1.13-my-old basalt predated the cutting of the

modern canyon of the North Fork through the foothills. The lava is now found on the highest ridge tops. An erosion remnant of this lava caps the end of the northern ridge of the canyon, at 1700 m (5600 ft) elevation. In the roadcut at the top of the ridge the underlying surface of disintegrated quartz monzonite bedrock is well exposed, dipping steeply eastward. The contact can be traced down the northeastern side of this ridge for about 100 m to the aquifer recharge canal at the head of the fan. It does not appear to have been faulted.

As much as 10 m of the ancient fanglomerate covers an equivalent thickness of the 1.13-my-old lava near the northern edge of the alluvial fan. The depth of burial decreases to zero along the banks of the arroyo from McGann Springs. Hypothetical coeval flows along the axis of the fan might be buried more deeply; where the fan is incised ~ 25 m by the modern North Fork, no ancient lava is exposed.

The ancient fanglomerate that buries the old basalt forms a smooth reddish surface of rock chips and sand, with few boulders. Those resistant boulders that stand above the surface are chiefly metavolcanic rock from the headwaters of the North Fork. Granitic boulders were weathered flush with the surface of the fan.

Exposed beneath the level of the basalt in the arroyo are thoroughly decomposed and rounded boulders of McGann quartz monzonite. The ancient surface on which the flow ended was apparently depositional and probably much like the fan today. That no exotic boulders were found shows that the basalt did not exit from the foothills through the main channel of the ancient North Fork. If it had, underlying deposits would have included the metavolcanic boulders from the headwaters of the river. The lava either

flowed down a broad pediment away from the North Fork, or flowed down the North Fork's shallow channel, overtopping its banks at the eastern end of the foothills and flowing onto locally derived alluvium below.

To the south and east of the older basalt, the ancient fan surface is buried by younger debris. This appears to have originated from a point near the 1700 m (5600 ft) contour on the modern channel of the North Fork. The younger basalt flows are associated with this younger fanglomerate, and they appear to have radiated from the same point. Thus these flows seem to have postdated the cutting of at least most of the canyon of the North Fork through the foothills. Finally, these younger flows are at most thinly covered by debris, and much of the flows crop out well above the fan surface. Thus the eruption of the younger lava was close in time to the abandonment of the older fan.

The modern North Fork has cut a channel at least 20 m deep through the older fan west of Oak Creek Camp. This is now partly filled by mid- to late-Wisconsin glacial outwash. Near the confluence of the North Fork and Charlie Creek, a young basalt flow is capped by this outwash. The base of the flow is only a few meters above the modern stream level, and it seems clear that this flow predates the later stages of the Wisconsin glaciation and postdates the abandonment of the fan.

Thus at least three episodes of volcanism are recorded on the fan of the North Fork, ranging in age from 1.13 my BP to perhaps less than 0.1 my BP. Dating of the two younger flows would be of interest in establishing growth rates for fans of the eastern Sierra Nevada; it is unfortunate that to do so was not feasible during this study.

The younger fan, probably consisting of reworked glacial outwash of

the Wisconsin glaciation, has not yet filled the depression southeast of Oak Creek Camp. This fan probably has a volume of about 0.026 km^3. If deposition occurred in the last 0.1 my, an average aggradation rate of only ~ 0.2 mm/y is implied for the larger old fan. Thus the 1.13-my-old lava might be buried by an average of 22 m of fanglomerate, assuming constant deposition rates. Incomplete burial of the younger flows argues for an age of less than perhaps 0.25 my.

Summary

The North Fork fan consists of a smaller modern fan and a larger ancient fan abandoned no later than the early Wisconsin glaciation. Three different lava flows, two on the abandoned fan and one beneath mid- to late-Wisconsin glacial outwash in terraces of the modern fan, provide an unusual opportunity for dating the growth of the fan. The oldest flow was dated at 1.13 my; the others have not yet been dated.

From the estimated volume of the younger fan, created since the early stage of the Wisconsin glaciation, the growth rate of the older fan appears to be about 0.2 mm/y. This rate is comparable to those estimated for the Independence Creek fan (~ 0.1 mm/y) and in the White Mountains, California (0.22 mm/y; Beaty, 1970).

The Foothills

For 2.5 km west of Oak Creek Camp the North Fork flows against the foothills to the south. The ridges of the foothills here are part of the ancient gently east-dipping eroded surface found below 1700 m (5600 ft) elevation on the ridge between Charlie Canyon and the South Fork. Two

higher surfaces found there were not recognized near the North Fork. Instead, both ridges now dip eastward about 10°. Fig. 5-33 compares the longitudinal profiles of the three ridges between the South Fork and Thibaut Creek. A generalized topographic map showing these ridges and the North Fork is also shown. The ridges on either side of the North Fork have remarkably similar profiles east of the range-front fault. The northern of the two is the one that is capped by the small outcrop of 1.13-my-old basalt. More extensive basalt outcrops dated at 1.18 ± 0.05 my (Ch. 4) cap the southern ridge, and both ridges appear to be relics of the same ancient erosion surface. The lavas capping the southern ridge (Fig. 5-34) are as thick as 50 m; however, dates of samples from high in the flow are not significantly lower than those from the base. The entire series of flows therefore seems to have been erupted over a short period of at the most a few tens of thousands of years. The ridges on both sides of the North Fork now stand more than 175 m above the creek, and both are at least a comparable amount lower than the foothills to the south. Thus the ancient lavas appear to have flowed across the ancient foothills at a time when the North Fork had already cut deeply into them. The geometry of the foothill surface ~ 1 my ago may be seen in the generalized topographic map of Fig. 5-33b. The modern canyons of the South Fork and of Charlie Creek have been smoothed over in this map to emphasize the general topography of the foothills. The location of the modern Charlie Creek appears to be on the southern margin of an embayment whose bedrock floor was at least 200 m below the foothills to the south.

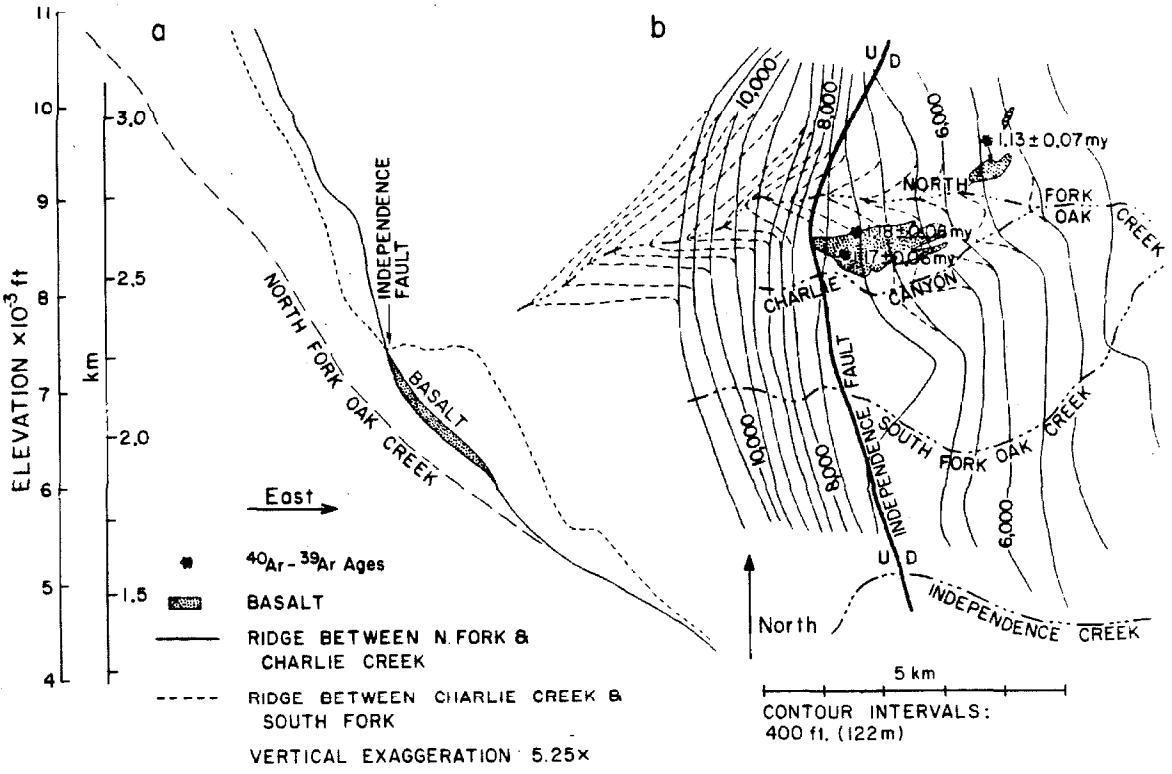

Fig. 5-33. Topography of the foothills near the North Fork of Oak Creek. Basaltic lavas were erupted 1.2 my ago from vents on the Independence Fault or farther west. The basalt outcrops preserved today are found capping ridges. The east-west profile of the major ridge (a) is similar to but ~ 150 m higher than the profile of the modern North Fork. However, the basalt-capped ridge is as much as 390 m lower than the foothills to the south. A generalized topographic map (b) with the modern canyons smoothed over shows that the lava seems to have flowed through a broad channel or embayement through the ancient foothills. Thus the ancient erosion surface of the foothills signficantly predates the eruption of the basalts. If erosion rates have been constant over the Pleistocene Epoch, the surface probably dates from the late Pliocene Epoch. Topographic data are from the U.S. Geol Survey, Mt. Pinchot Quadrangle (1953).

Fig. 5-34. The foothill ridges between Charlie Creek (foreground) and the North Fork of Oak Creek are capped by 20 m to 60 m of basalt flows overlain by as much as 25 m of fanglomerate. The basalt has been dated at 1.18 ± 0.05 my. The outcrop of fanglomerate is about 600 m in length. Charlie Canyon is about 200 m deep. View is to the north.

Incision rate of the North Fork

The incision rate of the North Fork during the last 1.2 my can be calculated since the ridge-top basalts have been dated. This rate is ~ 0.14 mm/y, about a factor of two less than the incision rate inferred for Coyote Creek (Bateman, 1965). Furthermore, this rate for the North Fork must be a lower limit, because subsequent to the eruption of the lavas enough time passed for the North Fork to deposit at least ~ 25 m of fanglomerate atop the basalt. At late Pleistocene deposition rates for the North Fork fan this may represent a ~ 0.13-my period. Thus the average down-cutting rate may have been ~ 0.16 mm/y. This figure is still a lower limit, because there may have been a lengthy period after eruption and before deposition of the fanglomerate. If this incision rate applies to the entire Pleistocene Epoch, then the highest surface of the foothills may have been formed during the late Pliocene Epoch, about 2.5 my ago. This suggests great antiquity for the fan deposits with the grooved boulders (§5.3) found on this surface near the South Fork.

The fanglomerate atop the 1.2-my-old basalt

The fanglomerate overlying the ridge-top basalt (Fig. 5-34) is at about the same elevation as the diamicton north of the South Fork. Metavolcanic boulders from the ancient fan deposits were examined for glacial scratches or other direct evidence of weathering. While no striated boulders were found, other features characteristic of glacial erosion were plentiful. These included rounded and facetted metavolcanic boulders, boulders with crescentic gouges (Fig. 5-35), and boulders with parallel grooves oblique to foliation. These grooves were somewhat coarser (1 mm across) than the distinctive fresh scratches, but they have no obvious

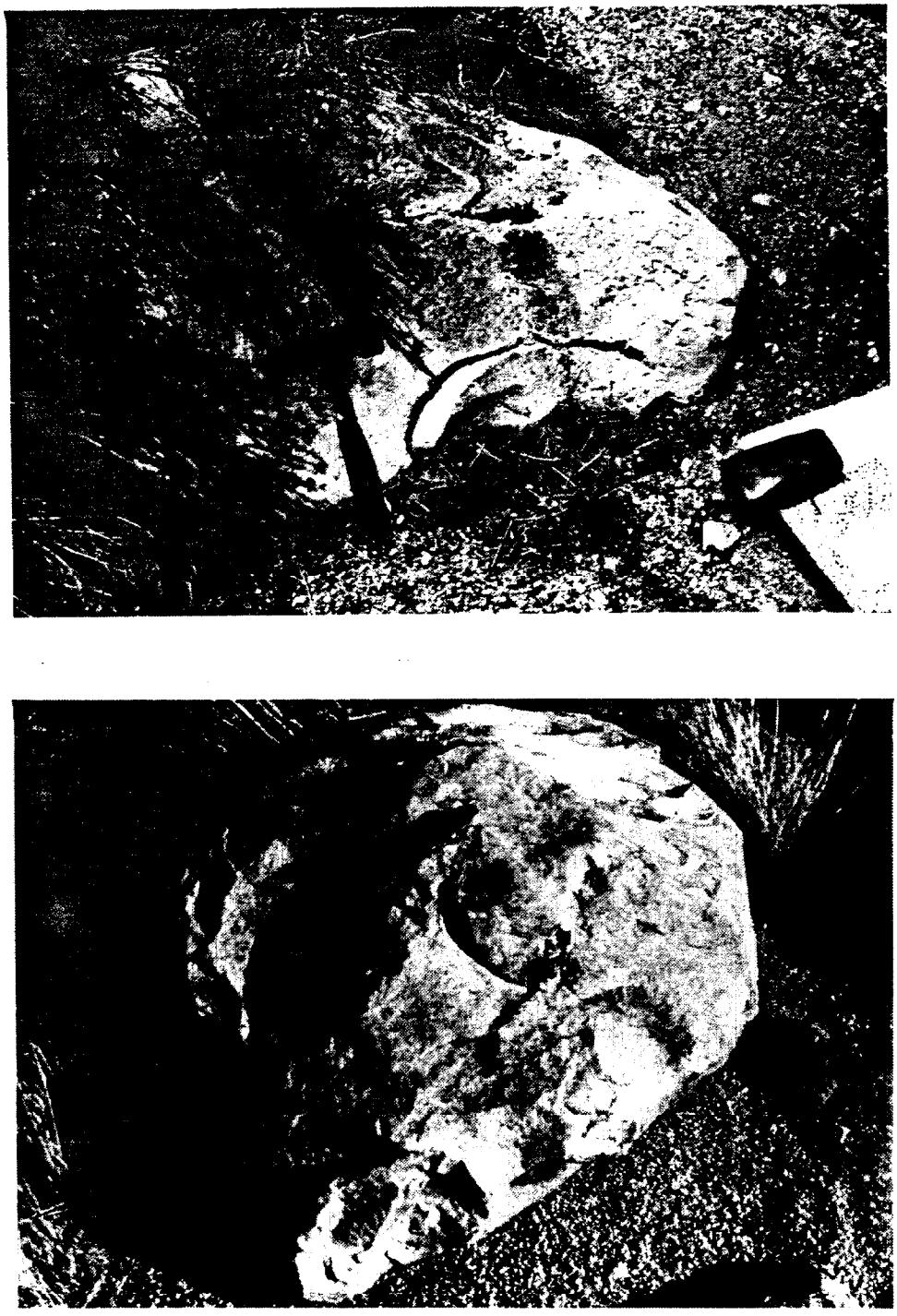

Fig. 5-35. Metavolcanic boulders showing crescentic fractures and gouges. Hammer (top) and knife (bottom) give scale. Boulders were found in fanglomerate overlying a 1.2-my-old basalt, on a ridge top about 125 m above the North Fork of Oak Creek.

origin other than glacial abrasion. Thus while unproven, an ancient glaciation after 1.2 my BP but long before the Tahoe glaciation is a definite possibility, from this evidence. This would seem to correlate with the Sherwin glaciation (>0.7 my BP) elsewhere in the Sierra Nevada. Presently, no good lower age limit for the ancient fan gravels can be determined. They predate early Wisconsin moraines found near the bottom of the modern North Fork, however.

Terraces in the canyon of the North Fork

The modern canyon of the North Fork apparently did not cut through the ridge-top basalt and the underlying bedrock in a single episode. At least one and perhaps two terraces are cut into the bedrock northwest of the Baxter Pass trail head at 1830 m (6000 ft) elevation. These terraces are 35 m and 20 m above the prominent mid- or late-Wisconsin glacial outwash plain into which the North Fork has cut an additional 17 m. The highest preserved terrace, 52 m above the North Fork, is marked on the north side of the canyon only by a thin outcrop of flow basalt. The lower of the ancient terraces is revealed by deeply weathered and eroded bedrock ribs that once formed a continuous bench. These are best seen on the north canyon wall 150 m downstream from the lowest deposits of early Wisconsin glacial outwash. Fifteen meters below the lava flow of the top terrace, a dense concentration of basalt blocks and boulders is found. This may represent an individual flow, or it may be talus from the higher flow.

The south wall of the canyon likewise has at least one cut terrace. This is best displayed about 200 m southeast of the confluence of the North Fork and its northern tributary (Plate I). Large blocks of flow

basalt on these ledges are partially buried by quartz monzonite and basalt talus from the ridge above. These blocks may simply have fallen to the terrace from the outcrops on the ridge top. Thus there seems to have been at least one hiatus in the incision of the foothills, after 1.2 my BP but before the Wisconsin glaciation. This time could be found by dating the basalts of the 52-m-high terrace. This date would also provide a lower limit to the age of the fan deposits atop the ridge south of the creek. The ages of the terraces may be estimated from the average incision rate of the North Fork (~ 0.16 mm/y): the highest terrace, 52 m above the creek, may be about 0.33 my old; the lower terrace, which at 37 m above the creek is at about the level of the abandoned fan and the top of the early Wisconsin glacial outwash, appears to be about 0.23 my old.

Basalt flows underlying the early Wisconsin glacial deposits are found only a few meters above the modern stream level. These may be ~ 0.1 my old or more. Thus incision of the North Fork through bedrock in the last ~ 0.1 my has been negligible, and the average rate of incision before that was more like 0.18 mm/y. The reason for this apparently variable rate is uncertain. It could simply be that repeated volcanic flows and the subsequent continuing influx of large amounts of outwash during the Wisconsin glaciation reduced the ability of the North Fork to erode efficiently.

Faulting and tilting within the foothills

The 3-km-long ridge between Charlie Creek and the North Fork, capped by the 1.2-my-old basalt flows affords an opportunity to estimate the amount of normal faulting within the foothill block during the last half of the Pleistocene Epoch.

The ridge now slopes about 10° to the east, compared to the gradient of 8.6° for the modern North Fork through the foothills. The ridge has been offset vertically along at least four normal faults (Plate I), and three of these appear to have broken the basalt flows. However, the offset on each fault appears to have been less than 15 m, and two are even antithetic (west side down). Thus cumulative offset across a 2.5-km-wide zone of the foothills during the last 1.2 my was neglible, and the 10° slope for the ridge is probably close to the ancient slope, unless there has been regional tilting. Eastward tilting of even 5° appears to be ruled out, though, because the east-west ridge between Charlie Creek and the South Fork is virtually level for 1.6 km, and such a regional tilt would have dropped the eastern end 140 m. Thus the foothill block does not appear to have been tilted during the Quaternary Era, and faulting appears to have been concentrated on the range front itself and not distributed throughout the foothill block.

Normal faulting within the foothills but east of the basalt-capped ridge is not ruled out by the discussion above. The stepped appearance of the foothills, especially south of the confluence of Charlie Creek and the North Fork, certainly seems to indicate as much as ~ 280 m of vertical displacement (east side down). Still other normal faults are possible at the eastern edge of the foothill block. However, as observed farther south, there were scarps on the early Wisconsin fans, so the offset history is problematical and activity, if there was any, seems to have been confined to the early Pleistocene Epoch. The Independence Fault appears to have been active as recently as the late Pleistocene Epoch. Two parallel scarps ~ 50 m apart and perhaps ~ 10 m high (Fig. 5-36)

can be seen in the foothills north of the North Fork. The eroded scarps clearly do not break the mid- to late-Wisconsin outwash in the channel of the North Fork, and they were not recognized in the foothills south of the river. The scarps do not intercept the early Wisconsin left-lateral moraines and outwash, and it is not clear whether the equivalent left-lateral moraine was offset. Thus the scarps are at least several tens of thousands of years in age, and may exceed ~ 65,000 y, the probable lower age limit of the early Wisconsin glacial stage.

Glacial Moraines and Outwash

Advance II

Glacial deposits of at least three ages can be seen below 2745 m (9000 ft) elevation (Fig. 5-37). The oldest is the right-lateral moraine and outwash found east of the Independence Fault. The moraine appears to have extended down to at least 1950 m (6400 ft) elevation. It has been heavily eroded, perhaps because it lies atop basalt which is easily undercut by the river. Granitic boulders tend to be well weathered, but the cavernous forms seen on many old moraines are not present. No morphologic moraine north of the creek remains; the high terrace consists mostly of glacial outwash. The top is level with the lower cut terrace in the canyon wall 20 m above the mid-Wisconsin outwash. Exotic rounded boulders found on the northern wall of the canyon upstream at the level of the projected top of the outwash confirm that the deposit was once more extensive. From its degree of preservation and weathering, this moraine is assigned to the Tahoe stage. It is probably correlative with advance II of Onion Valley. The age of the underlying basalt is an

Fig. 5-36. Late Pleistocene scarp of the Independence Fault, north of the North Fork of Oak Creek. The scarp, accentuated by late afternoon shadows, is about 10 m high and cuts a skirt of debris fallen from the eastern escarpment of the Sierra Nevada. View is to the north.

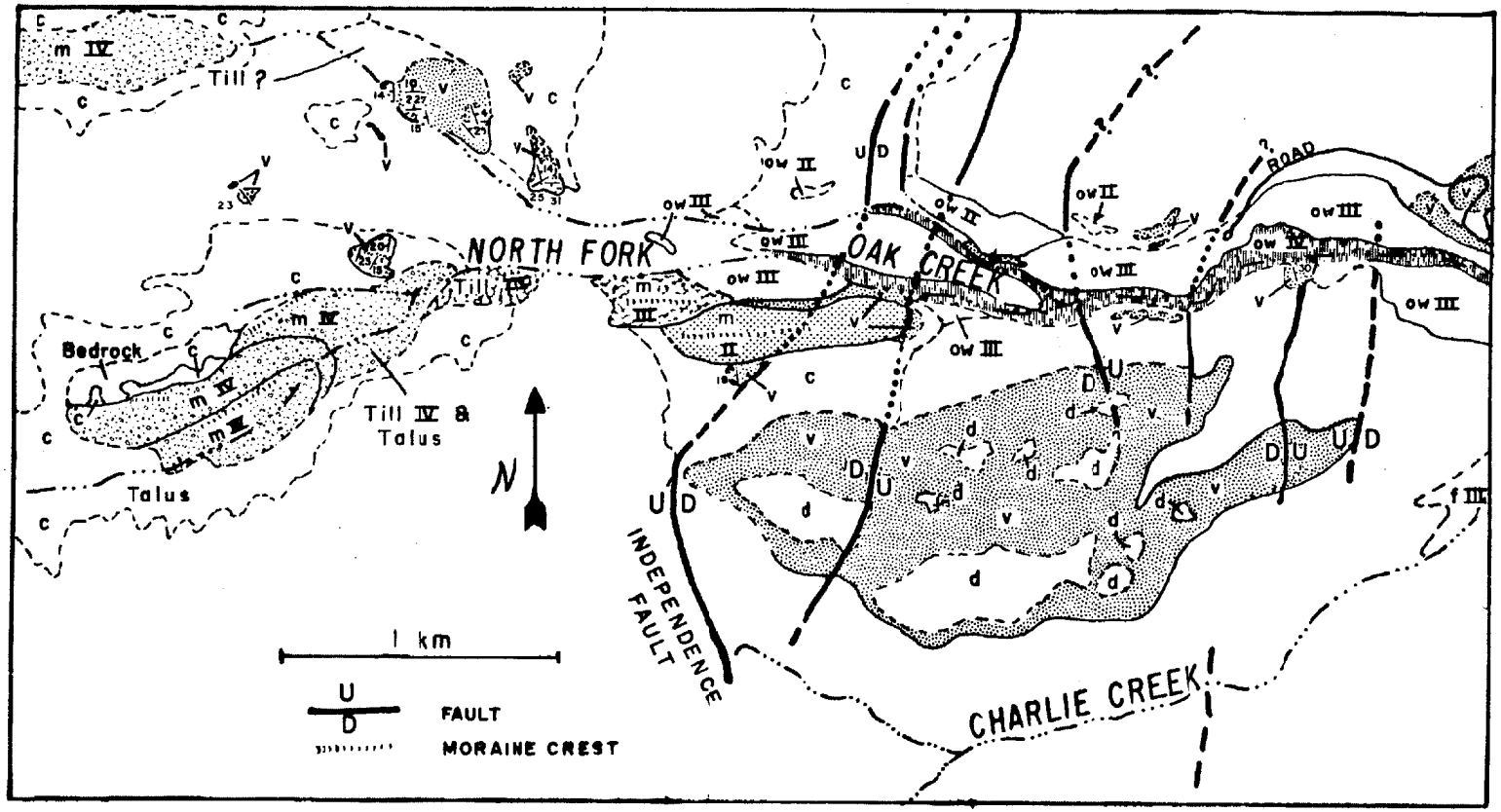

EXPLANATION

DEPOSITS	AGE
c Colluvium & Talus	
m Moraine	IV Tioga
ow Outwash	
f Fan	III Tenaya
d Diamicton (ancient fanglomerate)	II Tahoe
v Basalt	

Fig. 5-37. Map of the Quaternary deposits along the North Fork of Oak Creek. Map base is U.S. Geol. Survey aerial photograph GS-VDYM 2-192 (8-31-75), enlarged from a scale of ~ 1:80,000.

upper limit to the age of the Tahoe-stage glaciers of the North Fork. The basalt, whose base is only a few meters above the modern stream, appears to be quite young, so that even as a limit its age could be important. Unfortunately, this age was not successfully measured. A tentative value from a single sample was ~ 0.2 my, but the 2σ uncertainty is probably close to 75%.

Advance III

The fill terrace between the moraine and the Tahoe outwash may be traced on the narrow septum separating the North Fork from its northern tributary to about 2240 m (7350 ft) elevation. Ancient shallow river channels are preserved on the top of the ridge. South of the North Fork, the outwash appears to grade into a small erosional remnant of the right-lateral moraine at 2135 m (7000 ft) elevation. The Baxter Pass trail proceeds up this moraine whose morphologic crest is no more than ~ 25 m higher than the septum. Boulders from this eroded feature are less weathered than those from the lowest moraine, but no fresh boulders with original glacially abraded surfaces were found. Together with the deep incision of the outwash by the North Fork--17 m to 25 m at the rock septum--this argues that the age is at least mid-Wisconsin, probably the equivalent of advance III of Onion Valley (Tenaya stage). No left-lateral moraine of this advance was observed.

It must be noted that not all the erosion of the bedrock septum need have occurred after the Tenaya glaciation. M. M. Clark (oral comm., 1979) has observed deep steam-cut notches with glacial striae on the walls near Sonora Pass in the northern Sierra Nevada. Apparently the glacier may fill and polish the subsurface topography without necessarily

obliterating it. Subglacial stream erosion has also been observed (e.g., Embleton and King, 1975) and could help explain the deep incision in bedrock.

Advance IV

Scattered glacially transported boulders are found above the Baxter Pass trail from 2345 m (7700 ft) to 2560 m (8400 ft) elevation. No moraine is seen on either wall of the canyon. However, above 2390 m (7840 ft) elevation on the North Fork a massive left-lateral moraine is found. This probably correlates to advance IV of Onion Valley (Tioga stage). No corresponding right-lateral moraine is preserved, but above 2560 m (8400 ft) elevation for 275 m the Baxter Pass trail crosses forested slopes which appear to be till partly buried by talus. This till is probably from the eroded moraine.

The left-lateral moraine has been largely unmodified by erosion. Much of the moraine crest south of a narrow, delicate bedrock ridge (which may have been a nunatak in earlier glaciations) has been covered by talus. The moraine blocked off the drainage behind this ridge, and the alluvium thus impounded apparently overtopped the moraine. Where this happened, the moraine was breached by the tributary and has been severely eroded, leaving a plunging, sharp ridge which may be mistaken for the moraine crest. The moraine east of the incision buried an old basalt flow. At some point a stream flowing alongside the glacier cut a channel perhaps 6 m deep in the top of the lava. A second 2-m-deep channel cut in the first shows there were two episodes of erosion. This abandoned channel probably marks the downstream limit of the glacier of advance IV. The elevation at this point on the North Fork is 2340 m (7680 ft).

Because of the massive character of the moraine upstream and the absence of streams, had the moraine extended farther downstream to blanket the septum it would probably still be evident today.

The North Fork at the downstream limit of the advance IV glaciers has cut only an estimated 4 or 5 m through bedrock, probably since the last glacier retreated. Boulders on rare unmodified and unvegetated parts of the crest are moderately weathered but do not appear greatly younger than those from the advance III moraine below. The trim line on the southern wall is distinct and fresh west of the terminus. To the east it is not so obvious. The above features certainly stand in sufficient contrast to the advance III (Tenaya) moraine to warrant a separate age assignment. Only a short distance upstream from the advance IV terminus is nested a fourth moraine. Both lateral moraines may be seen near its terminus at 2500 m (8200 ft) elevation. Indeed, the moraine is barely breached by the river. About 200 m upstream the right-lateral moraine is largely buried by fresh talus. The left-lateral moraine is very brushy, and no good exposures of crest were found.

Above the terminal of the fourth moraine, the valley of the North Fork has the same broad character distinguishing the recently glaciated upper Onion Valley. The stream is incised only 5 m through ground till. A terrace is found about 2.5 m above the modern stream. The moraine certainly is of latest Pleistocene age (late Tioga stage), and the terrace may have been cut during the retreat of a Holocene glacier higher in the valley.

Basalt outcrops west of the Independence Fault . . .

The basalt beneath the oldest preserved moraine of advance IV appears similar to the basalt found in the northern tributary at about the same elevation. Both basalt flows seem to have followed pyroclastic activity leading to the deposition of coarsely bedded mudflows containing cinders and blocks along with grus and stream cobbles. However, the apparent total absence of basalt on the ridge between the two creeks is evidence that the two were erupted from separate centers, although both may have been active at about the same time. The dip of the North Fork lavas, conformable with the slope of the canyon wall, indicates that they were erupted locally and were not deposited as a "backwater" of some deep flow from the northern tributary. Both lavas may be correlative with the youngest lavas found in the bottom of the canyon of the North Fork east of the Independence Fault. Since those lavas were probably pre-Wisconsin in age, dating the basalts under the advance IV moraines could not be expected to give a useful upper limit to the Tioga stage.

In searching for the vent of the flow on the North Fork, cobbles of basalt were found in chutes leading to a small outcrop near the top of the ridge between the two creeks, at 2805 m (9200 ft) elevation. From its position alone, high on a thin ridge, it seems probably that this basalt is of great age. It must have been erupted before the deep canyons of the two creeks were cut, but its age and correlation with other basalt flows were not established. However, evidence of ancient volcanism within the North Fork drainage increases confidence in the hypothesis that the ridge-top basalts could have originated west of the Independence Fault.

If this high vent area were the source of the ridge-top basalt below,

then the elevation change of 550 m would be the sum of the actual vertical drop of the ancient lava flow and the subsequent tectonic offset along the Independence Fault. There is no way now to resolve these components. However, if the ancient North Fork had the same gradient across the range front that it has today (15°), then the total fall in the canyon was only 425 m. The remaining 125 m must include the height of the vent above the ancient canyon floor, and would thus be an approximate upper limit to tectonic offset in the last 1.2 my. This speculative offset rate, < 0.1 mm/y, is comparable to the modern rate along the Independence Fault at Onion Valley.

Glaciation in the Northern Tributary to the North Fork

Glaciers arising in the cirque under the southeast face of Mt. Baxter descended the unnamed canyon below to a point near its confluence with the larger canyon of the North Fork of Oak Creek (Fig. 5-38). Because of extensive erosion and colluviation, it was not possible to identify moraines older than advance IV, but it is likely that during the Tahoe stage (advance II) the glacier could have merged with the main ice stream. It seems fairly certain that an early or mid-Wisconsin glacier reached at least to the basalt outcrops found at about the 2560 m (8400 ft) elevation. In addition to locally derived colluvium, the lavas are overlain by debris containing round granitic boulders and gabbro clasts from the mafic pluton to the west. Both are exotic; neither could have been transported by downslope movement alone. One possibility is that they were transported by a glacier older than advance IV and younger than the lavas. However, even if the boulders do reflect an early glacial history, a precise

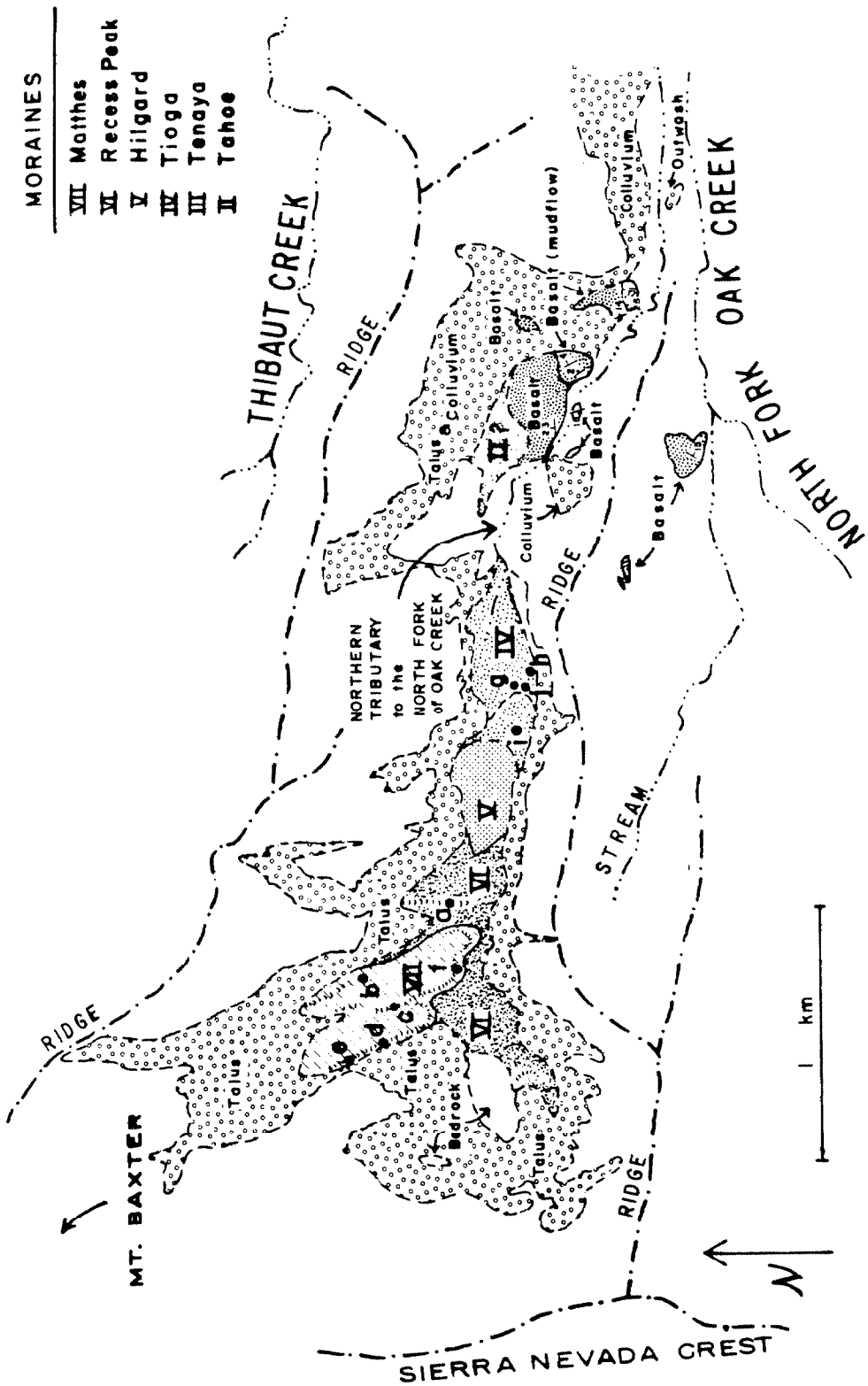

Fig. 5-38. Map of the Quaternary deposits along the unnamed northern tributary to the North Fork of Oak Creek. Sites where relative weathering data were gathered are shown. Map base is U.S. Geol. Survey aerial photograph GS-VDYM 2-192 (8-31-75), enlarged from a scale of ~ 1:80,000 to ~ 1:26,300.

radiometric age on the lava would be of little use in determining the glacial chronology, since the relative age of the glacial deposits is unknown.

The sides and top of the steep rock gorge upstream from the lava shows patches of glacial polish and striae. Fresh-looking cliffs on the south wall of the canyon above the gorge are found down to an elevation of about 2610 m (8560 ft). The snout of the glacier which left these traces must have reached downstream at least as far as the vent area.

The canyon above 2670 m (8800 ft) elevation is filled by a youthful "dump" moraine, probably belonging to advance IV on the Tioga stage. Such a moraine arises in steep terraine when the glacier ends in an ice fall rather than a well-defined and stable snout. The lateral moraines are poorly developed and merge with end moraines and ground till. Semi-quantitative weathering data gathered for this and younger moraines in the cirque itself are compared in Table 5-17. Neither the granodiorite weathering ratios nor the degree of boulder roundness or angularity showed any variation over the latest Pleistocene and Holocene moraines. Apparently insufficient time elapsed for weathering to modify these parameters. Interestingly, the ratio of granodiorite to aplitic boulders seemed to decrease with age. It is difficult to attribute this to weathering, because the other parameters (GWR and roundness) which should be more sensitive to light weathering showed no trends with age. Thus it seems most likely that variations in boulder composition, especially this close to the cirque, are best attributed to variations in provenance and mixing of debris from different glacierettes within the cirque itself.

Curry (1968, 1969) has experimented using the maximum size of

Table 5-17

Relative Age Data for Moraines on the Northern Tributary of the North Fork of Oak Creek.

Site[1]	Advance[2]	No. of Boulders[3]	GWR[4]	G/R[5]	Roundness[6]	Lichen Thalli Diameter[6] cm	Fraction of Boulders with Lichen[7]
e	VI-VII	-	-	-	-	-	0.15,0.50
d	VI-VII	-	-	-	-	1	0.35
c	VI-VII	-	-	-	-	0	0.20
b	VI-VII	100	4/96/0	100/0	1/70/28/1	0	0.10
f	VI-VII	-	-	-	-	-	0.45
a	VI	85	18/72/0	90/10	11/32/54/3	5	0.70
i	V	192	14/76/10	98/2	9/78/14/0	-	-
g	IV	120	4/90/6	81/19	9/38/53/0	-	0.80
j	IV	61	7/93/0	69/31	7/35/55/2	-	-
h	IV	38	5/89/6	68/32	6/29/57/9	-	-

[1] Sites are shown in Fig. 5-38.

[2] Glacial advances are those of Onion Valley. Advance VII corresponds to the Matthes neoglacial stage; VI to the Recess Peak stage; and V to the Hilgard stage. Advance IV is the Tioga stage of the Wisconsin glaciation, and advance II is the Tahoe stage.

[3] Number of boulders for the GWR measurements.

[4] Granodiorite weathering ratios. The percent of boulders in heavily weathered, lightly weathered, and unweathered categories is shown. See Ch. 2.

[5] Granodiorite/resistate boulder ratio, in percent. See Ch. 2.

[6] The percent of granodiorite boulders in four categories is shown. In order, the categories are: angular, sub-angular, sub-rounded, and rounded. See Ch. 2.

[7] Minimum diameter of the largest colonies of yellow-green lichen.

[8] Boulders with lichens of any species are counted.

yellow-green lichens (see Ch. 2) as an indicator not only of relative age, but also of absolute age in the Sierra Nevada. Variability of the parent rock type seemed to preclude effective use of lichenometry in the North Fork and its tributary. Lichen growth seemed to be controlled not only by rock type but by location with respect to sun and wind, depth of weathering of joints, and other factors. However, Table 5-17 shows that the percentage of boulders with lichens did seem to increase with the apparent age of the moraine.

Age assignments were thus based on lichen frequency and vegetative cover. The youngest moraines were thought to be somewhat older than the Matthes neoglacial advance (advance VII) of Onion Valley, because a fraction of the boulders had lichen growth. The youngest Matthes moraines in Onion Valley and elsewhere had no lichens at all. These moraines were mapped as intermediate in age between the Recess Peak (VI) and Matthes advances, because they could be distinguished from young neoglacial moraines (advance VI) at the mouth of the cirque. Forested moraines between the cirque moraines and the advance IV "dump" moraine were assumed to belong to the Hilgard neoglacial advance (V).

Absence of the youngest glaciers in the cirque under the high Mt. Baxter (4000 m elevation) is probably attributable to the southeast exposure and the relatively low elevation of 3400 m of the cirque. The cirque under the shaded north face of Mt. Baxter, 250 m higher, did have obvious Matthes glaciers.

Basalt flows in the northern tributary

The basalt flows at 2560 m (8400 ft) elevation were erupted before the earliest glaciation for which there is evidence in the northern

tributary to the North Fork. Moore (1963) and Darrow (1972) both regarded this vent as the source for the youngest lava flows east of the Independence Fault. These latter lavas predate the Wisconsin glaciation and have a tentative age of roughly 0.2 my (Ch. 4). Therefore the amount of post-eruption downcutting is of some interest as a guide to regional erosion rates.

Crudely bedded mudflow outcrops associated with the eruptions can be clearly seen to dip steeply both south and north (Fig. 5-38). A series of notched bedrock ribs shows the mudflows conformed to an ancient valley topography. The notches, now an estimated 25 m above the modern stream, delineate the stream channel floor of the ancient valley. Thus in the intervening years the stream has removed the basalt and cut at least 25 m through the old bedrock. This figure is a lower limit because the stream has been shifted south about 50 m, presumably by the lava. Thus the total amount of downcutting through bedrock could have been as much as 50 m, if the ancient southern valley wall had a slope of 30°. This implied rate, 0.13 to 0.25 mm/y, is equivalent to rates calculated east of the Independence Fault elsewhere in the North Fork drainage. If this equivalence could be confirmed it might indicate that incision is not being controlled by uplift along the range front itself.

The Upper Valley of the North Fork

West of the Tioga end moraines and below ~ 3170 m (10,400 ft) elevation lies the broad, open upper valley of the North Fork. Coalescing talus cones beneath the heavily fluted, 700-m-high valley walls blanket most of the valley floor and even control the course of the river. Throughout much of

this stretch the late-Wisconsin trim lines are about 150 m above the river, reflecting the depth of the glacier. In contrast, the depth of the tributary glacier was less than 75 m.

Rock glaciers in the three cirques of the North Fork were not visited. The most prominent, in the northern cirque beneath Diamond Peak (4000 m) has a convex surface and an oversteep snout. It appears from distant inspection to be active, or recently so. The U.S. Geological Survey topographic map (Mt. Pinchot Quadrangle, 1953) shows a pocket glacier on the north face of Diamond Peak. This glacier and the moraine below are included with the Matthes advance in this study.

The principal interest in the headwater region of the North Fork is in the old terrain deeply excavated by the modern cirques. The three cirques are decidedly different in this respect. The cirque northwest of Mt. Mary Austin is poorly developed, and a hanging glacier little more than 50 m deep cascaded north to join the larger trunk glacier. The floor of the short valley below the cirque is from 3660 m (12,000 ft) to 3780 m (12,400 ft) elevation. There is no headwall to the cirque; the arete has been reduced to a gentle ridge lower than the cirque cliffs to the west, and ice may have flowed equally north and south from the divide.

The cirque between Black Mt. and Diamond Peak has cut as much as 125 m into the old valley whose bottom was between 3535 m (11,600 ft) and 3610 m (11,850 ft) elevation. The nivated walls of the old valley dip gently (as little as 15° on Black Mt. and 6° on Diamond Peak). Despite this, there is no accumulated diamicton as in Sardine Canyon or on University Peak. At the eastern extremities of the old surface the fractured bedrock mantle has been swept clear by avalanches down the steeper fluted faces.

The northern cirque is the largest of the three. On its southern

side the ancient surface of Diamond Peak has been completely eliminated. Apparently the glaciers hugged the north face of Diamond Peak during the ice ages as well as now: on the northern side of the cirque (the crest of the Sierra Nevada) is a gentle divide above 3660 m (12,000 ft) elevation. This divide (Baxter Pass) seems to have been part of the same ancient valley system preserved in the other cirques. Its surface also has no accumulation of diamicton. Rock fragments reflect the local lithology only.

The divide has at least two trim lines cut into it. Both are virtually buried by colluvium today. The upper is about 125 m above the floor of the valley, and the other is perhaps 50 to 75 m lower. This lower line of cliffs plunges towards the valley floor downstream, and it appears to be the trace of a late Tioga or early Holocene (Hilgard ?) glacier, whose snout reached only to the confluence of the streams from the three cirques. The low lobe of debris under the talus cones of the north wall may be the moraine from this glacier. The absence of a larger moraine suggests that the duration of this advance was short.

An ancient trim line . . .

Both Matthes (1930) and Clark (1967) argue that glacier thickness near the cirque regions is independent of the length of the glacier or its thickness near its snout. Thus trim lines from different advances may converge to the same level upstream, unless the canyon has been more deeply eroded between advances.

The north face of Mt. Mary Austin has preserved on it a series of triangular facets whose apices may record an ancient trim line. If so, this trim line rose more steeply than the late-Wisconsin trim line. The two trim lines thus diverged upstream, in contradiction to the observations

of Matthes and Clark. Perhaps this is best explained if the upper trim line was cut into the walls of a valley steeper than the modern one. The line of apices has a gradient of 17°, compared to 11° defined by the modern trim line. This could well reflect a time when the valleys draining east from the Sierra upland had not yet cut headward to the modern divide. The two lines converge to within 125 m of each other 1.5 km west of the Independence Fault.

Summary

The North Fork of Oak Creek is near the southern edge of the Big Pine volcanic field. Basaltic lavas have been erupted into the drainage intermittently over at least the last 1.2 my. The oldest of these lavas now cap ridges 175 m above the modern stream. This relationship enables the calculation of an average incision rate of about 0.16 mm/y or more. This rate is a factor of two less than that observed at Coyote Creek in the Sierra Nevada near Bishop, California. The ancient lavas were apparently erupted into a channel of the North Fork already cut 200 m into a Pliocene erosion surface of the foothills, or at least into an embayment in the pediment. Younger lavas, as yet undated, are found on terraces and also underlying Tahoe glacial deposits. Dates on these lavas would provide upper limits to the age of the Tahoe glaciation and also would increase the accuracy of the estimated incision rate.

The 1.2-my-old lavas are found on the margins of the alluvial fan of the North fork, buried by a deeply weathered fanglomerate which is similar in appearance to those found locally on the fans of both Independence Creek and the South Fork of Oak Creek. Here the relationship with the underlying basalt provides an upper limit to the age of the

weathered debris. The late Pleistocene lavas are also exposed on the fan surface, partially buried by boulders. Dating of these lavas would help establish weathering rates for eastern Sierra Nevada fans. Accumulation rates of the North Fork fan at ~ 0.2 mm/y appears to be lower than the average Pliocene-Pleistocene rate, since to accumulate even the 278 m of fan penetrated by the Los Angeles Department of Water and Power well T.H.1 near Independence would take ~ 13 my, twice the age of the Owens Valley itself.

Pleistocene moraines of three ages were found in the canyon of the North Fork. The oldest and youngest were deposited during the Tahoe and Tioga stages (advances II and IV of Onion Valley). An intermediate moraine appears to grade into extensive terraces of glacial outwash. This outwash is probably mid-Wisconsin, and is assigned along with the moraine to the Tenaya stage (advance III). They could simply be early Tioga (advance IV) deposits, however.

The moraines and outwash do not appear to have been broken by the Independence Fault, which nevertheless has a 10-m-high scarp through debris skirts of the Sierra escarpment north of the glacial deposits. Only 6 km to the south, a scarp of the Independence Fault breaks latest-Pleistocene terraces; hence, activity on the range-front fault seems to be grossly episodic, with repeated events on the same short segment of the fault separated by long periods of quiesence.

Faulting and regional east-west tilting within the foothills appear to have been minimal during the last 1 my. Faulting, if any, has been located on the eastern margins of the foothill block or along the mid-valley fault zone.

5.5 THIBAUT AND BLACK CANYONS

At Baxter Pass the Sierra crest steps 2.5 km east. Thibaut and Black Canyons are the first canyons north of the jump in the crest. The offset crest continues north to Southfork Pass, in the Palisades (37°04.1'N, 118°27.1'W). This northern crest is in line with the massive isolated peaks east of the crest south of the North Fork of Oak Creek: (Mt. Mary Austin, Kearsarge Peak, Independence Peak, and Mt. Williamson) while the crest south of Baxter Pass is aligned with the east wall of Rae Lakes Basin and Crater Mt. The principal reason for the step in the crest may have been a congruent jump or bend in the range-front faults. Even cutting westward at the same rate as streams to the south, the streams of the eastern escarpment north of the step could not establish a watershed as far west. The effect of this could have been to diminish snowfall in eastern canyons north of Baxter Pass, since the drainages were farther into the rain shadow of the Sierra Nevada.

Perhaps because of diminished snowfall, Thibaut and Black Canyons were unable to support glaciers large enough to extend below 2749 m (9000 ft) and 2440 m (8000 ft) elevation, respectively. Thus the glaciers did not cross the range-front faults, which are at about 1770 m (5800 ft) elevation. For this region, neither canyon was studied in the field. Some features of the upper alluvial fans and the escarpment deserve mention, however.

Except for one small bedrock ridge, Thibaut Creek flows along the northern limit of the foothill block. Thibaut Creek shows no sign of right-lateral dislocation. The creek through McGann Springs, 0.5 km to the south, grades to the old pediment surface and does not seem to ever

have been throughgoing. Thus it could not have been an ancestral channel of Thibaut Creek, and there appears to be no evidence for horizontal displacement on the range-front faults.

Most of the alluvial fan of Thibaut Creek seems to be covered by debris and boulders of mid-Wisconsin age. At the narrow septum separating Thibaut from the creek to the north, this surface has been removed and older disintegrated boulders and grus are exposed. Thibaut Creek is incised deeply into this fan. The incision increases from zero at 118°15'W to 40 m at 1635 m (5360 ft) elevation. Just below the debris skirt flanking the range front, the incision has lessened to 25 m.

Neither the unnamed creek to the north nor Black Creek has cut a channel below about 1400 m (4600 ft) elevation. This is noteworthy because the creek of McGann Springs, which has a much smaller catchment, has incised the fan clear to its distal end below 1220 m (4000 ft) elevation. Possibly both the creek of McGann Springs and Thibaut Creek, situated at the northern edge of the foothill block, became incised in response to north-south warping or faulting upwards of the block with respect to the Owens Valley floor. Recent faulting is precluded by the absence of scarps on the ancient abandoned alluvial fan of the North Fork of Oak Creek. Response to the hypothesized warping continued at least into latest Pleistocene Epoch.

No fresh scarps on the range-front faults were found from the saddles south of Thibaut Creek to Grover Anton Spring. During the late afternoon, a scarp 0.8 km in length can be seen north of the spring, crossing the unnamed minor drainage south of Sawmill Canyon.

The bevelling of the Sierra escarpment is especially pronounced from Thibaut Creek to Sawmill Creek. Recognizable tiers of triangular facets

rise to above 3050 m (10,000 ft) elevation (e.g., Lookout Point) and to about 2560 m (8400 ft) elevation. The lower facets are steepened from 22° to 31° below about 1830 m (6000 ft) elevation.

Quaternary deposits of Thibaut and Black Canyons are shown in Plate I. These were mapped by photo-interpretation of black-and-white aerial photographs only. The fan of Thibaut Creek was traversed but not studied in detail. The fans from Thibaut Creek north to Sawmill Creek were not visited.

5.6 SAWMILL CANYON

Introduction

Sawmill Canyon is distinguished by an unusually complete sequence of glacial moraines. There are at least 13 recognizable crests. All of these are well west of the range front. That the older ones have been preserved at all results from the widening of the canyon at the confluence of two streams.

Sawmill Canyon has also been the locus of at least three and perhaps four volcanic eruptions. Basalt from one of these underlies the largest moraine, a prominent ridge of Tahoe till called the Hogsback which is easily visible from the floor of the Owen's Valley. Lava from this eruption flowed down the canyon at least to the range front, where it is found as much as 62 m above the modern stream. Only 0.5 km to the west, the lava flow is about 50 m thick. It is unlikely that such a thick flow would stop at the range front; yet the lava was not observed on the fan to the east. Its absence is probably best attributed to downfaulting and subsequent burial of the distal end of the flow. Pyroclastic debris and flow basalt west of the range front also cover an older pre-Wisconsin moraine. Thus radiometric dates for these lavas might provide age limits on two glacial advances, and also a minimum offset rate on the range-front fault.

Largely because of the opportunity to establish age limits for the moraines, Sawmill Canyon has been studied at least twice subsequent to the reconnaisance of Knopf (1918) and the mapping of the Mt. Pinchot quadrangle by Moore (1963). Both Knopf and Moore assigned the Hogsback and younger moraines to the Tioga stage, while they assigned the old moraine capped

by lava to the Tahoe stage. Dalrymple (1964) mapped the glacial moraines in greater detail than Moore, using semi-quantitative weathering criteria to distinguish deposits of different ages. Dalrymple assigned the old moraine capped by lava to a pre-Wisconsin glaciation, the Hogsback to the Tahoe stage, and younger moraines to the Tenaya and Tioga stages. Using K/Ar analysis, he determined a model age of 0.07 ± 0.09 (2σ) my for the interglacial basalt. As discussed in §4.3, this age is suspect because it is highly sensitive to the exact isotopic composition of non-radiogenic argon trapped in the lava upon cooling. The age is also uncertain because of possible contamination of the sample by incompletely degassed granitic xenoliths originally crystallized ~ 90 my ago (Dalrymple, 1964b). One of the goals of the present study was to remeasure this age using ^{40}Ar-^{39}Ar dating, which was expected to overcome the above problems (Ch. 4).

A recent study by Burke and Birkeland (1979) appears to contradict Dalrymple's interpretation of the glacial history, and instead supports the simpler interpretation of Knopf (1918) and Moore (1963). The actual age of the basalt analyzed by Dalrymple is a vital consideration in choosing between interpretations.

My reconnaisance of Sawmill Canyon showed that in addition to the dated basalt, a second and older basalt was overlain by the oldest moraine. Furthermore, as R.P. Sharp has pointed out (oral comm., 1978), the crest of the Hogsback is not uniform, but contains exceptionally fresh and bouldery regions alternating with patches of grusy boulders. This heterogeneity complicates the application of relative age dating techniques. Thus Sawmill Canyon was restudied to: (1) resolve the controversy concerning the relative ages of the moraines; (2) redate the interglacial basalt; (3) date for the first time the basalt under the oldest till; and (4)

compare this well-studied valley to others in the Mt. Pinchot quadrangle.

To this end a new approach to K/Ar dating was successfully developed and verified on the early Pleistocene ridge-top basalt of Oak Creek (Ch. 4). This approach exploited the presence of the same partially degassed granitic xenoliths which may increase the apparent K/Ar age. By dating the potassic xenocrysts, the fraction of ^{40}Ar which was radiogenic was increased, thus reducing the critical dependence on the isotopic composition of the trapped Ar. By using stepwise heating and ^{40}Ar - ^{39}Ar analysis instead of K/Ar analysis, it was possible to estimate the trapped Ar and K-derived Ar compositions during the same analysis. It also proved possible by stepwise heating to isolate Ar degassed from non-retentive reservoirs from Ar from retentive reservoirs. ^{40}Ar from non-retentive reservoirs, completely degassed during heating in the magma, consisted only of new ^{40}Ar created since cooling of the lava. Using this approach it was possible to obtain high-precision dates for the interglacial lava of 0.118 ± 0.007 my, and for the older lava of 0.46 ± 0.04 my (Ch. 4).

Because conventional relative dating techniques gave different results for different geologists, the acoustic wave speed technique of Crook and Kamb (1980) was tested for applicability to glacial moraines (Ch. 3). It was originally developed for terrace deposits. The results were remarkably good, and in two well-studied valleys in the central Sierra Nevada moraines were grouped correctly by this new approach. The goal of this effort was to apply the technique to the Sawmill Canyon moraines, and here too the technique appears to have been successful.

Discussion in this section is organized according to: (1) bedrock geology; (2) the glaciation of Sawmill Canyon; (3) relative dating of moraines; (4) geology of the fan head; and (5) incision and faulting rates.

Summary of Bedrock Geology (Moore, 1963)

Unlike the canyons to the south, Sawmill Canyon is cut into granitic plutons containing thin septa of metasedimentary rocks in the headwater region. Septa of meta-andesite and metarhyolite tuffs are found also, but not in the abundance characteristic of the canyons of Oak Creek.

The granitic rocks of the headwater region are granodiorites of the Tinemaha, McDoogle, and Mule Lake plutons. Most of the canyon (below Mule Lake) is in the lighter granodiorite or quartz monzonite of the Spook pluton. Basalts were erupted through the Spook pluton, both within the canyon and on the range front to the north of Sawmill Creek. As at the North Fork of Oak Creek, the basalt contains xenoliths of the country rock through which it erupted.

Glaciation in Sawmill Canyon

One of the best preserved Pleistocene moraine sequences of the study area is found in Sawmill Canyon, against the north wall of the main fork near Sawmill Meadow. Below the junction with a tributary canyon, Sawmill Canyon is widened. Here these moraines are free-standing, away from the canyon walls.

Four groups of moraines are readily recognized from morphologic criteria and from stratigraphic relationships with basalt flows and pyroclastic debris. These moraines appear to range from pre-Wisconsin to late-Wisconsin (Tioga stage), but different interpretations have been made. The ages assigned to these moraines in this study are compared to the age assignments of Dalrymple (1964) and Burke and Birkeland (1979) in Fig. 5-39. All three interpretations are similar in that the oldest

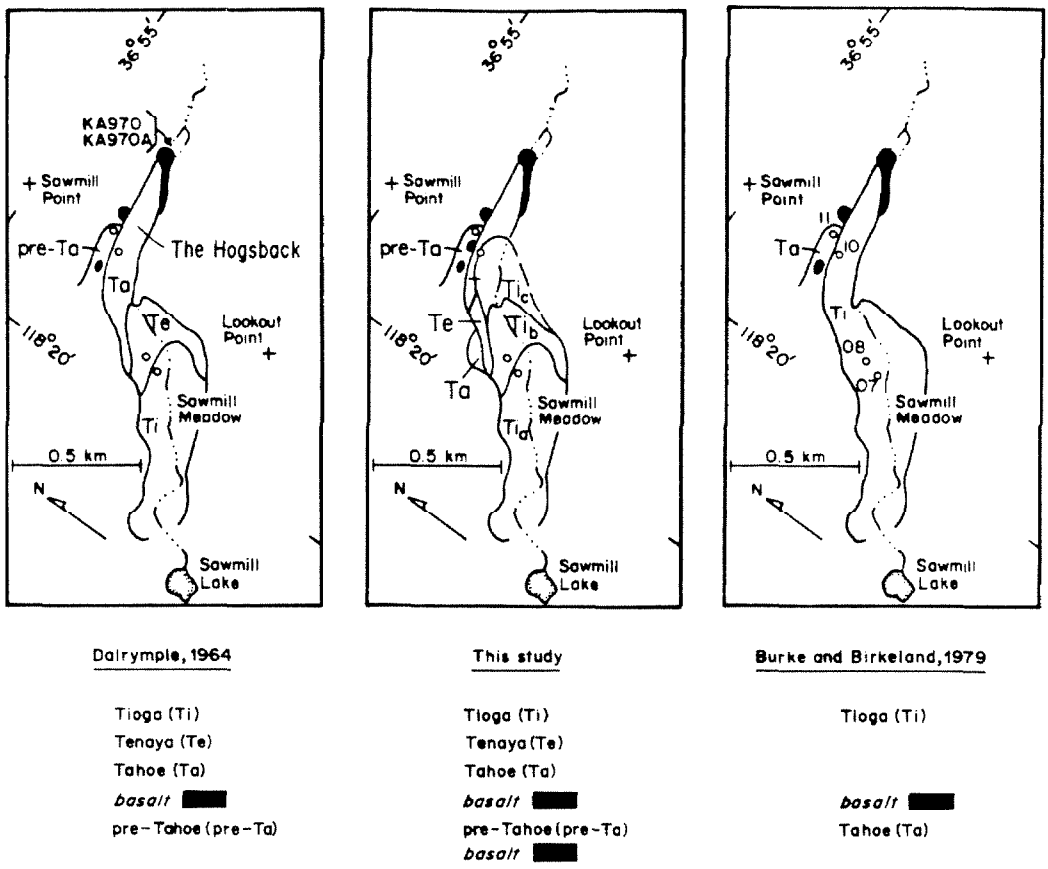

Fig. 5-39. Generalized maps of the Pleistocene moraines of Sawmill Canyon according to Dalrymple (1964), this study, and Burke and Birkeland (1979). Dalrymple used semi-quantitative weathering criteria to recognize three separate advances of post-basalt glaciers, which he correlated with the Tioga Tenaya, and Tahoe stages. His K/Ar dates of basalt samples KA970 and 970A gave a weighted average age of 70,000 ± 90,000 (2σ) y that was long regarded as an upper limit to the Tahoe stage. The northernmost moraine was thought to be pre-Wisconsin. Recently, Dalrymple, Burke, and Birkeland (1982) have redated the interglacial lava, finding an average age of only 53,000 ± 88,000 (2σ) y. Consistent with Burke and Birkeland (1979), they claim this to be a date for the Tahoe-Tioga interglacial period. Burke and Birkeland (1979), on the basis of intensive relative weathering studies of the four sites (7, 8, 10, and 11) shown on the map, concluded that all the Wisconsin moraines of Dalrymple were indistinguishable and were left during the Tioga stage. They considered the oldest moraines to be Tahoe. In the present study the basalts were redated using the ^{40}Ar–^{39}Ar technique. The oldest moraine was shown to be from ~ 460,000 y to 131,000 ± 10,000 (2σ) y in age, and was thus pre-Wisconsin. The younger moraines were found to be less than 118,000 ± 7000 (2σ) y old, within 2σ of the date of Dalrymple et al. (1982). Semi-quantitative studies and acoustic wave-speed studies showed the Hogsback, the Tahoe moraine of Dalrymple (1964), to be composite. Burke and Birkeland appeared to have chosen sites 7, 8, and 10 all in Tioga till; hence their results are consistent with those of this study, although their age assignments are not.

moraines are the northernmost or are found farthest down canyon (east). My interpretation is similar to that of Dalrymple, and is different from the simpler two-stage interpretation of Burke and Birkeland primarily in the age assignments of the two oldest moraines. It is these moraines that are interbedded with the lavas; thus the two different interpretations may be tested by radiometric dating.

In the discussion below, the glacial geology of Sawmill Canyon will be introduced without extensive justification of the age assignments of the Pleistocene moraines. In subsequent discussions, the age determinations by semi-quantitative relative weathering methods and by acoustic wave-speed measurements will be described. The relative ages will then be related to the absolute chronology according to ^{40}Ar-^{39}Ar dates of critical lava flows.

The age assignments of Dalrymple (1964) in Fig. 5-39 correspond to the four morphologic groups. The oldest group consists of a single broad and subdued left-lateral moraine. The central part of the moraine crest is buried by a thin deposit of pyroclastic cinders, bombs, and blocks of basalt. The size of the blocks (up to ~ 1 m) suggests that the vent area was nearby. The eastern end of the moraine was overrun by a basalt flow from the north wall of the canyon. No volcanic lapilli are found on any other moraines in Sawmill Canyon, although they are abundant on the canyon walls. Thus this moraine (advance I) alone predates the youngest volcanic activity within Sawmill Canyon. The ^{40}Ar-^{39}Ar date for a bomb atop the moraine was 131,000 ± 10,000 y.

On the south flank of the advance I moraine, eroded basalt is exposed on the Sawmill Pass Trail itself. A small outcrop is buried by the moraine. ^{40}Ar-^{39}Ar dates of this lava were 463,000 ± 40,000 y BP. Thus the age of the moraine, 130,000 y to 465,000 y, shows that it was emplaced

between the Sherwin and the Wisconsin glaciations. These age limits provide important constraints for dating by semi-quantitative or acoustic wave-speed methods.

The advance I moraine is buried at its western end by a 150-m-high complex of younger terminal moraines from the northern tributary. This complex also buries moraines of the second morphologic group, which includes the Hogsback. The Hogsback was assigned to the Tahoe stage by Dalrymple (Fig. 5-39). Its crest is 10 or 15 m higher than the crest of the pre-Wisconsin moraine. This difference may reflect extensive erosion of the older moraine prior to 131,000 y BP.

The Hogsback itself has been heavily modified by erosion. Ravines ~ 3 m deep have been cut into its northern flank. Sawmill Creek has undercut its southern flank, and in places the original moraine crest has been destroyed. No companion right-lateral moraine remains on the steep south wall of the canyon. Sawmill Creek has cut through ~ 15 m of quartz monzonite bedrock since the Hogsback was deposited.

The Hogsback is the largest moraine of Sawmill Canyon. It extends east from the rock rib separating the main fork from the smaller tributary to the north. At the base of the rib it merges with an older left-lateral moraine of similar weathering characteristics. The eastern end of the Hogsback, which must mark the approximate location of the glacier which created the moraine, is near the confluence of Sawmill Creek and its tributary at 1950 m (6400 ft) elevation.

At four locations below 2315 m (7600 ft) elevation the Hogsback can be seen to overlie basalt which has flowed down the canyon. The relationship is best exposed at the end of the moraine. From field relationships the basalt appears to be coeval with the lava atop the advance I moraine.

^{40}Ar-^{39}Ar ages giving a weighted average of 119,000 ± 9000 y were obtained for the lavas under the Hogsback, consistent with the above conclusion. An indistinguishable age of 118,000 ± 7000 y was obtained for an outcrop, probably of the same lava flow, farther down the canyon. These ages do not contradict the assignment by Burke and Birkeland (1979) of the Hogsback to the Tioga stage (Fig. 5-39), but they also permit its assignment to the Tahoe stage. In fact, the Hogsback appears to be a composite moraine with a massive Tahoe (advance II) core underlying thin layers of younger till.

From the bench mark (8152 ft) on the crest of the Hogsback, the Sawmill Pass trail traverses eight moraines before reaching Sawmill Meadow. These moraines form two groups. Both are characterized by fresh boulders and minimal erosion of the lateral moraines, which are preserved on both sides of Sawmill Creek. The moraines of the older group are completely breached, however, and no vestige of the terminal moraines remain. In contrast, the two youngest moraines are only slightly breached, their terminal moraines enclosing Sawmill Meadow. Stream incision within this youngest group does not exceed ~ 3 m. Dalrymple (1964) mapped the moraines of these two groups as Tenaya and Tioga, in the order discussed (Fig. 5-39). In the present study, as in Burke and Birkeland (1979) also, there seemed little justification based on weathering data for assigning the older group to a separate stage, and most of the moraines were assigned to the Tioga stage (advance IV). However, the outermost moraine of the two groups did appear to be distinctly more weathered and was assigned to the Tenaya stage (advance III) in this study.

Sawmill Meadow, just below 2560 m (8400 ft) elevation, is a recently filled lake and is similar to the meadow of upper Onion Valley. The

steep slopes to the west are covered by till of indistinct morphology, probably dumped by a rapidly retreating glacier. The lakes above the steep bedrock step west of Sawmill Meadow (Mule Lake and Sawmill Lake, at 3050 m or 10,000 ft elevation) are not yet filled. The glaciers of the early Holocene glaciation (Hilgard advance, or advance V of Onion Valley) appear to have terminated on the bedrock step.

Above Sawmill Lake are the cirques of the headwaters of Sawmill Creek. This region was extensively glaciated during the late Holocene Recess Peak advance (VI). Small moraines of the most recent advance (Matthes or VII) are found in the largest cirque, under the north face of Mt. Baxter. A smaller cirque filled with fresh and bouldery moraines, probably of advance VI, is found south of Sawmill Lake. This tributary glacier was fed by ice and snow from an unusual flat and nivated remnant of an ancient surface at about 3630 m (11,900 ft) elevation. The bedrock surface is covered by a diamicton like that of University Peak.

A transfluent tributary to the Sawmill glacier arose under the north face of Acrodeetes Peak, 0.6 km west of the Sierra crest. Fresh trim lines show that the late Pleistocene (or even Holocene) glaciers bifurcated, with one branch crossing the crest at the pass 1.1 km northwest of Mt. Baxter. Trim lines show that the smooth, rounded ridge on the divide north of this pass protruded about 100 m above these latest glaciers. This ridge once was the western wall of a broad valley draining northwest across the present crest from Mt. Baxter. The floor of this ancient valley, now Sawmill Pass, has been plucked to a depth of 115 m by the glaciers of Sawmill Canyon cutting westward. Capture of the headwaters of this drainage doubled the catchment of the Sawmill glaciers.

Capture appears to have occurred a considerable time ago. The smooth

features and subdued trim lines at Sawmill Pass contrast markedly with the fresh cliffs in the recently occupied pass to the south. While weathering conditions on the Sierra crest are probably quite different from those 1200 m lower in the canyons and fans of the range front, the absence of cavernous or disintegrated boulders or bedrock does suggest that capture could have occurred as recently as the Tahoe glaciation.

The marked morphologic similarity of the ancient valley at Sawmill Pass and upper Sardine Canyon strengthens the hypothesis that upper Sardine Canyon was cut by ancient glaciers.

Other ancient surfaces are preserved near Sawmill Pass. The most notable of these, 0.4 km south of the pass at an elevation of about 3630 m (11,900 ft), is a plateau which appears to have once been part of the ancient valley of Sawmill pass. This plateau is covered by till and has been incised as much as 170 m by more recent glaciers.

Colosseum Mt., north of Sawmill Pass, also is an ancient relict surface. This nivated surface was not visited. While from aerial photographs an accumulation of diamicton can be seen on the summit ridge, most of the surface is only thinly mantled by debris which, from its distinctive lithologies, was clearly derived by in situ processes. Other mantled surfaces may be seen at the summit of Mt. Baxter and on the ridge south of Woods Lake. Neither was visited.

Glaciation in the northern tributary to Sawmill Creek

The northern tributary was glaciated repeatedly down to at least 2440 m (8000 ft) elevation. This is about 370 m higher than the eastern end of the Hogsback. The difference probably reflects the smaller catchment of the tributary. Moraines ranged in age from early Wisconsin

(advance II) to neoglacial (advance VI), but the neoglacial moraines appear to have halted above 2895 m (9500 ft) elevation and were not found in the complex of overlapping Wisconsin terminal moraines.

The earliest moraines are largely buried by a succession of more recent ones. They reveal their presence only by the frequent disintegrated boulders found low on the terminal complex. The great bulk of the complex contains relatively unweathered boulders and lies buried beneath small unbreached moraines above 2560 m (8400 ft) elevation. Into this mass of till have been cut deep ravines, some of whose heads have been buried by the youngest moraines above. Thus at least glacial stades may be recorded here. The oldest was assigned to advance II; the others appeared to be of advance IV. A more thorough study of this complex might have identified moraines of advance III also, but no evidence of these was found.

The valley west of the terminal moraine complex contains abundant ground till and fragmentary lateral moraines. Polished bedrock knobs are littered with erratic boulders. Interestingly, the major neoglacial moraines and rock glaciers are found not under the Sierra crest but under the ridge between Sawmill Creek and its tributary. Even the cliffs of the cirque are subdued, especially on the northern side. Much of this should probably be attributed to the apparent lack of glaciers during the most recent neoglacial advances. In the adjacent Division Canyon to the north the same bedrock supports steep cliffs, apparently freshened by extensive neoglacial moraines. Closely spaced joints in the tributary to Sawmill Canyon may also have contributed to the subdued terraine.

Despite the poorly developed cirque morphology, the late Pleistocene glaciers were at least 125 m deep only 1.1 km from the divide. These glaciers deepened an old valley whose sloping sides are still preserved

on the modern ridges. On the south no diamicton was found, and the old bedrock surface has been modified only by infrequent avalanche chutes. On the forested north wall the surface may be deeply mantled by soil. It was not visited.

The ridge separating the drainage of Sawmill Creek and Division Creek preserves on its north side also a relict surface equivalent to the one of the Sawmill tributary. This surface extends along the ridge nearly 2.5 km from the crest. Farther east, it has been heavily eroded. Even here, bedrock ribs between gullies are congruent with the old surface and appear to have been little modified. This illustrates that a relict surface may be reconstructed in some instances from the profiles of ribs between avalanche chutes or ravines, even when most of the surface itself has not been preserved.

Relative dating of the moraines of Sawmill Canyon

The Pleistocene moraines of Sawmill Canyon were readily divided into four groups according to the morphologic criteria and stratigraphic relationships with basalt flows discussed above. However, just because these groups of moraines are morphologically distinct does not necessarily require that they be of grossly different ages. Indeed, the morphologic groups do not appear to be related in a straightforward way to different age groups, based on relative weathering data. Burke and Birkeland (1979), for instance, found little difference in a broad spectrum of parameters among moraines of the three "youngest" morphologic groups, and they concluded that the groups of moraines were simply left by different advances of the Tioga glaciation. A point central to the present study is that the morphologic groups were misleading because key moraines, especially the

Hogsback, contained till of strikingly different degrees of weathering. This most likely resulted from overlapping deposition of till on the same moraine during successive glaciations. In the discussion below, the relative weathering data gathered for the four groups of moraines are presented to justify the complicated age assignments of the present study. Extensive use is made of acoustic wave-speed data.

The principal focus of disagreement in Sawmill Canyon is the age of the Hogsback. R.P. Sharp (oral comm., 1978) has remarked on the variable character of the moraine crest near the Sawmill Pass trail, and herein lies the source of the confusion.

The Hogsback is not a single moraine. A few meters north of the bench mark on its higher crest may be seen a lower but distinct second crest (Fig. 5-40). To the east this secondary crest becomes less obvious; it appears to be buried by the larger moraine.

East of the bend in Sawmill Creek at 2385 m (7830 ft) elevation, the southern side of the Hogsback is steep (33°) and fluted. It is being undercut at its base by Sawmill Creek, resulting in sliding of till downslope. This process seems to have resulted in at least parts of the original crest of the moraine being eroded, with displacement northward of the apparent crest. Certainly the sharp-crested Hogsback is atypical among moraines of Tahoe age elsewhere in the Sierra. That the original crest has been destroyed is undeniable a few meters east of bench mark 8152. Here accelerated sapping is promoted by a spring or seep near the base of the moraine. A broad scoop in the flank of the moraine - - actually the headwall scarp of numerous land slides - - has left a scallop in the apparent crest of the Hogsback. To the west of this feature the moraine crest is quite bouldery, and appears to be quite young. Boulders

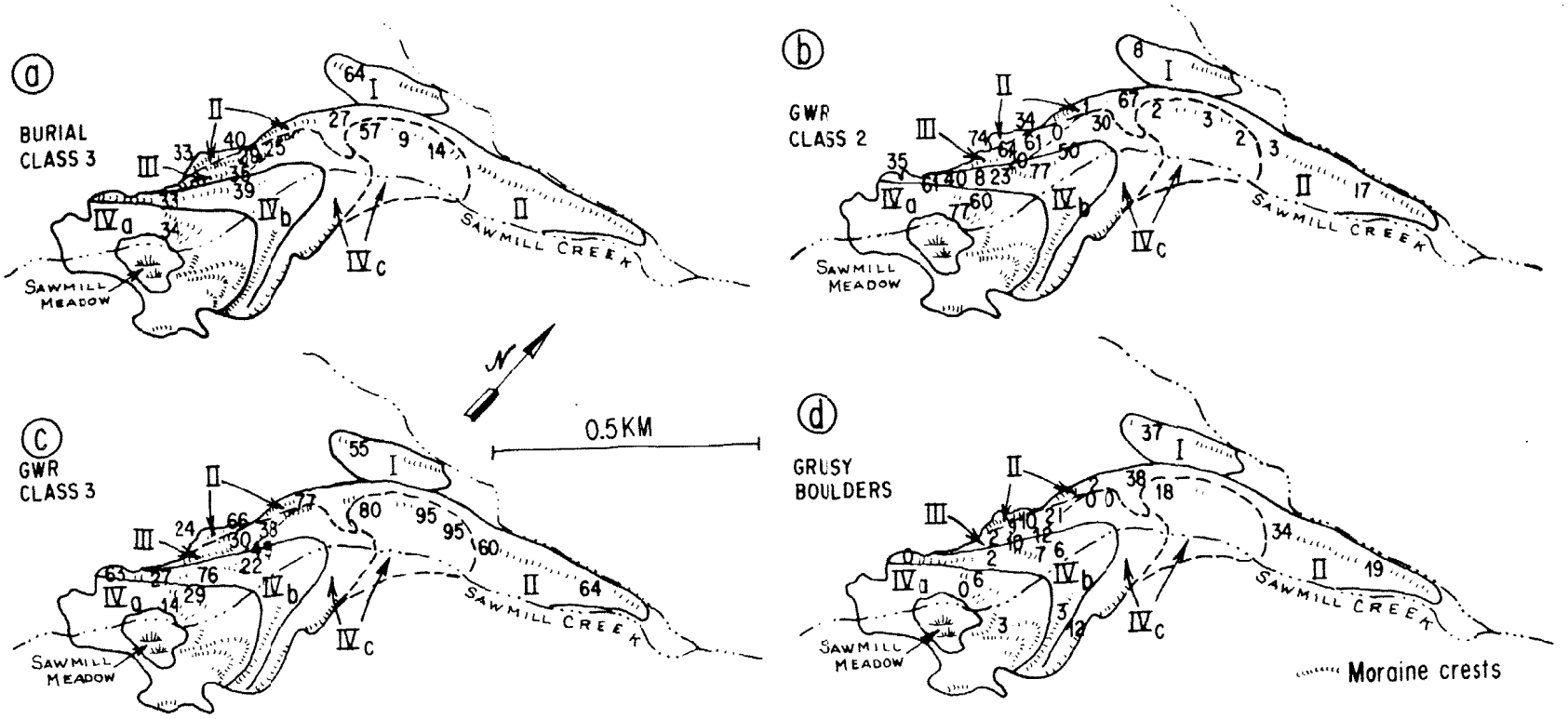

Fig. 5-40. Selected semi-quantitative weathering measurements for the Pleistocene moraines of Sawmill Canyon. Advances are identified by Roman numerals I (pre-Tahoe), II (Tahoe), III (Tenaya), and IV (Tioga). Subscripted a, b, and c refer to successively older moraines of the same stage. Four parameters are shown: a) the percent of boulders exposed on the surface which protrude only a quarter of their diameter (buried class 3); (b) the percent of boulders which are lightly weathered (GWR class 2); (c) the percent of boulders which are heavily weathered but which are not disintegrating (GWR class 3); and (d) the percent of boulders which are grusy.

with patches of glacially polished surface are common. No disintegrated or covernous boulders typical of Tahoe moraines elesewhere are seen. In fact, from this site alone the Hogsback would have to be considered younger than many of the moraines nested inside it.

However, the crest above the spring contains an unmistakably different assemblage of weathered boulders. The frequency of boulders was greatly reduced. Most boulders were grusy and even oxidized. The degree of weathering was characteristic of older moraines and, from this site alone, few would hesitate to assign the Hogsback to an earlier advance than the nested moraines.

The Hogsback thus appears to have at least two ages of till. This is not necessarily surprising. At many locations throughout the Sierra (e.g., at Bloody Canyon; Sharp and Birman, 1963) nested moraines are found in which the younger moraines are little more than thin veneers of till resting on the inner flanks of older moraines. At the Hogsback, a younger moraine appears to have overtopped the massive older one. Such a relationship is also seen at Green Creek in the northern Sierra (Sharp, 1972; Ch. 3, this study). The older till appears on the apparent crest where erosion has stripped the moraine of its young veneer or where the younger till was especially thin.

With this model in mind, the crests of each moraine were walked and examined for their full lengths. Semi-quantitative weathering data were gathered at numerous sites on these moraines. Some of these data are shown in Fig. 5-40. The first map (a) shows the percent of boulders that are deeply buried, such that only one quarter or less is exposed. In the youngest advance IV (Tioga) moraines, about one third of the boulders are deeply buried. In the advance I moraine this has increased to 64%.

However, for the advance II and III moraines, the number is the same as for the advance IV moraines. This parameter appears to be of little use in discriminating among the moraines of the Wisconsin glaciation, but it can be concluded that the period between advances I and II may have been long compared to the period from advances II to IV. Thus the interval from advance I to advance II may have significantly exceeded ~ 40,000 y.

It should be noted that the fraction of deeply buried boulders on the Hogsback east of the bench mark varies considerably and appears to be quite low. This probably reflects undercutting of the crest by Sawmill Creek.

Figure 5-40b shows that the fraction of lightly weathered boulders tends to decrease with the assigned age, from ~ 70% in the late Tioga moraines to 8% in the advance I moraine. Again, however, the sites on the Hogsback itself gave erratic results. To what this should be attributed is unclear, but the high scatter in values does emphasize the need for caution in interpreting the results.

Figure 5-40c shows the distribution of heavily weathered boulders, exclusive of grusy ones. This parameter increases from ~ 20% to 55% from the youngest advance IV moraines to the advance I moraine. The contrast in this parameter is reduced because heavily weathered boulders have been removed from the count if they were grusy. Thus the percent of boulders which are "heavily weathered" tends to stabilize with age, at least until there are no more "class 2" boulders to replenish "class 3". This apparently explains the anomalous values on the Hogsback east of the bench mark. Nevertheless, the moraine here assigned to the early advance IV appears to be more similiar to advance II moraines than to the younger advance IV moraines.

Figure 5-40d shows the distribution of grusy boulders. This appeared to be the most reliable of the semi-quantitative indicators of relative

age, no doubt in part because it is one of the least subjective. This parameter increased systematically from ~ 4% (advance IV) to 37% (advance I). The overridden crest of the advance II Hogsback east of the bench mark is clearly defined; it was largely the absence of disintegrating boulders which led to the interpretations of the Hogsback as a composite moraine.

It should be noted that weathering on the advance I moraine may not be directly comparable to weathering on the younger moraines, because the advance I moraine was buried by a layer of hot pyroclastic debris. The actual effect is uncertain, but at least the possibility exists that the relative age deduced from weathering data may be excessive.

Table 5-18 summarizes the weathering data presented in Fig. 5-40. The first two parameters tend to support the interpretation of Knopf (1918), Moore (1963), and Burke and Birkeland (1979) - - that there were only two distinct glacial advances, and that all moraines except the outer were of the same age. On the other hand, the abundance of heavily weathered boulders shows that, while there may have been only two distinct clusters, the advance II Hogsback should have been grouped with the pre-Wisconsin moraine. Finally, the abundance of grusy boulders suggests that there are four distinct age groups of moraines, as Dalrymple (1964) contended.

Because of the variability in the semi-quantitative data, the apparently unusually complicated history of the Hogsback, and the importance of Sawmill Canyon to understanding the glacial history of the Sierra Nevada, acoustic wave-speed data were also gathered to provide a more reliable basis for relative age determinations.

Acoustic wave-speed data . . .

Acoustic wave-speed data were gathered in large part to reduce the

Table 5-18

Summary of Selected Semi-Quantitative Weathering Data for Sawmill Canyon

Advance	Deeply Buried Boulders[2]	Lightly Weathered Boulders[3]	Heavily Weathered Boulders[4]	Grusy Boulders[5]
IV (Tioga)	32 ± 16	35 ± 29	46 ± 33	4 ± 6
III (Tenaya)	30 ± 5	40 ± 29	39 ± 10	11 ± 6
II (Tahoe)	33 ± 7	33 ± 32	62 ± 26	23 ± 16
I (pre-Tahoe)	64	8	55	37

---

[1] Advances of Onion Valley. Conventional equivalents are shown in parentheses. Data collection sites are indicated in Fig. 5-41.

[2] Percent of boulders in Boulder relief class 3 (Ch. 2). Errors are 1σ.

[3] Percent of GWR class 2 (Ch. 2). Errors are 1σ.

[4] GWR class 3 minus grusy boulders (Ch. 2). Errors are 1σ.

[5] GWR classes 4 and 5 (Ch. 2). Errors are 1σ.

potential for subjectivity which is unavoidable in conventional semi-quantitative relative age dating. The possibility of determining absolute age limits on two glacial advances by radiometrically dating the intercalated basalts justified this considerable effort. Speeds through 752 boulders distributed over 25 sites (Fig. 5-41) were measured. Summary data for the 30 measurements at each site are found in Table 5-19.

Wave speeds (V_p) ranged from 1.07 km/s (advance I) to 1.81 km/s (advance IV). Standard deviations ranged from 0.27 km/s to 0.52 km/s. One site (e) had an anomalously low $\overline{V_p}$ compared to adjacent sites. Talus falling onto the moraine, possibly during Holocene glaciations when snow filled the fosse separating the moraine from the canyon cliffs, may have been responsible. Talus measured at a nearby site (d) had a virtually identical $\overline{V_p}$.

The reduction in V_p through boulders with the passage of time may vary with the composition of the boulders. In Sawmill Canyon three granitic plutons contributed rock to moraines, but one of these, the Spook pluton, has two distinct facies. Another pluton (the Mule Lake pluton) crops out only on the south side of the canyon and thus contributed few boulders to the left-lateral moraines studied by the acoustic wave method. Both the Spook and Mule Lake plutons contain granodiorite and quartz monzonite. The third rock type, the dark granodiorite of the McDoogle pluton, crops out west of Mule Lake but is found on both sides of the canyon. No effort was made to measure boulders from only one pluton. Thus if the weathering rates of the various rock types are sufficiently different, distributions of acoustic wave speeds might be multimodal, or might become so as the moraine weathers. In acoustic wave-speed studies this possibility is guarded against by testing

Table 5-19

Acoustic Wave-Speed Data for Moraines of Sawmill Canyon

Site[1]	Age (Dalrymple, 1964)	Age (Burke and Birkeland, 1979)	Advance[2]	No. of Boulders	$\overline{V_p}$[3] km/s	s[4] km/s	D_{max}[5]	C[6] %
a	Tioga	Tioga	IVa	30	1.603	0.274	0.150	93
b	Tioga	"	IVa	30	1.771	0.443	0.098	36
c	Tenaya	"	IVb	30	1.728	0.363	0.099	38
d*	–	–	Holocene	31	1.560	0.427	0.106	50
e†	Tenaya	"	IVb	30	1.563	0.334	0.089	22
f	"	"	IVb	30	1.788	0.397	0.127	79
g	"	"	IVb	30	1.740	0.449	0.105	45
h	"	"	IVb	30	1.805	0.359	0.152	94
i	"	"	IIIa	30	1.632	0.453	0.134	85
j	"	"	IIIa	30	1.694	0.612	0.181	>99
k	Tahoe	"	IIIb	30	1.585	0.468	0.126	77
l	"	"	IIIb	30	1.598	0.385	0.072	6
m	"	"	IIIb	31	1.624	0.576	0.173	>99
n	"	"	IVc	30	1.817	0.397	0.111	57
o	"	"	IVc	30	1.707	0.431	0.097	33
p	"	"	IIa	30	1.466	0.376	0.131	82
q	"	"	IVc	30	1.698	0.468	0.115	61
r	"	"	IVc	30	1.768	0.323	0.104	44
s	"	"	IVc	30	1.669	0.307	0.136	85
t	"	"	IIa	30	1.509	0.322	0.112	57
u	"	"	IIa	30	1.512	0.357	0.117	64
v	–	–	IIa	30	1.516	0.494	0.077	8
w	–	–	IIb	30	1.524	0.430	0.128	80
x	Tahoe	"	IIb	30	1.547	0.344	0.105	45
y	pre-Tahoe	Tahoe	I	30	1.068	0.371	0.086	18

[1] Site locations are shown in Fig. 5-41
* Talus
† Possibly contaminated by talus

[2] Glacial advances I-IV are the Pleistocene advances recognized in Onion Valley. In order of decreasing age, IV corresponds to the Tioga stage, III to the Tenaya stage, and II to the Tahoe stage. I is a pre-Wisconsin advance. The lower case letters a, b, and c denote different groups of moraines within those assigned to each advance.

[3] $\overline{V_p}$ is the mean acoustic wave speed.

[4] s is the standard deviation of the distribution of V_p.

[5] D_{max} is the statistic from the one-sample Kolmogorov-Smirnov test, for normality of the sampled population of V_p.

[6] C is the confidence that the population of all V_p was not normally distributed.

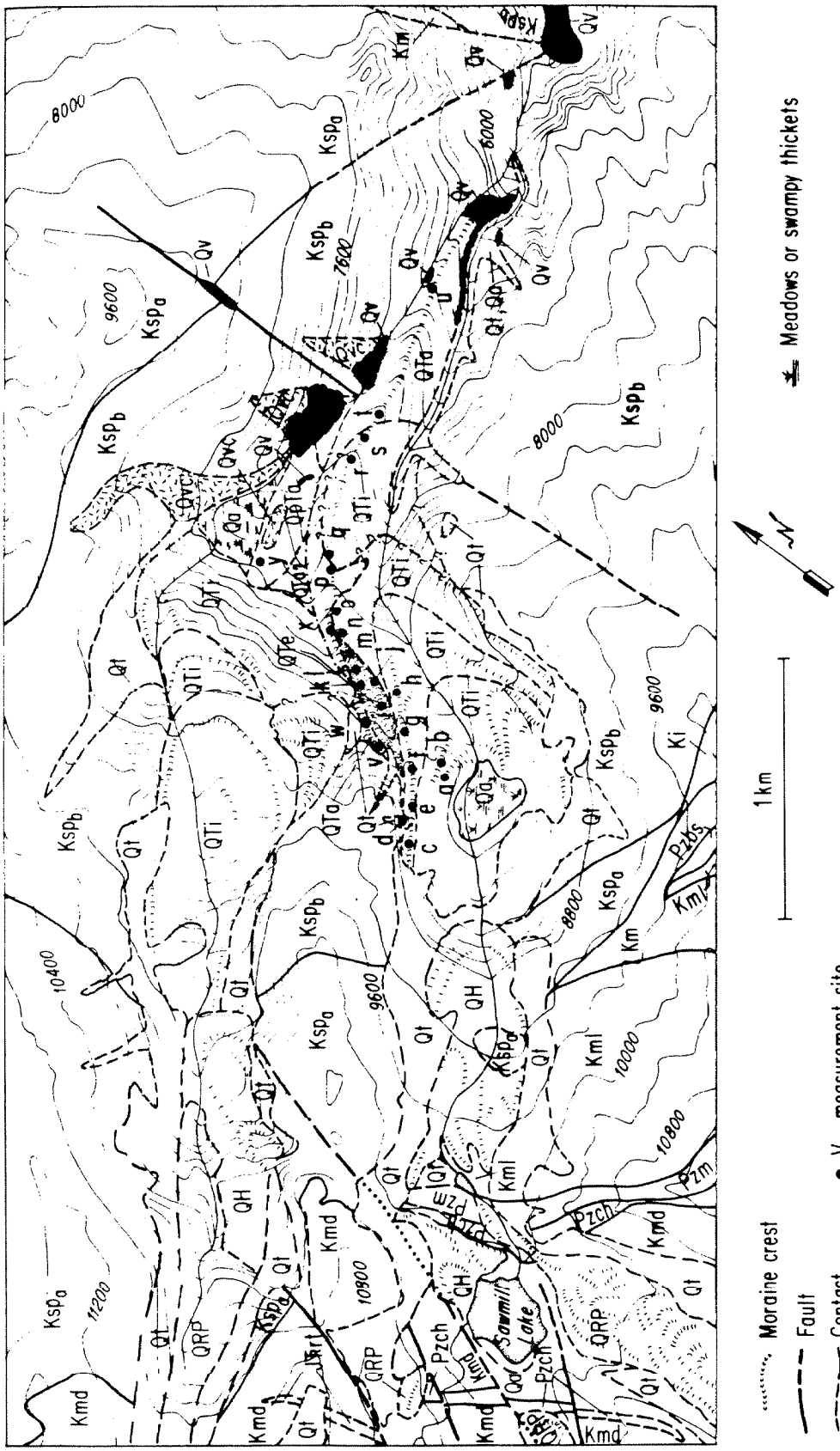

Fig. 5-41. Geologic map of Sawmill Canyon, showing the V_p measurement sites. The bedrock geology follows Moore (1963). See the next page for an explanation.

Fig. 5-41. Sawmill Canyon: V_p measurement sites and geology (continued).

The Quaternary deposits shown were mapped in the course of the present study:

Qa ..... Pleistocene or Holocene alluvium.
Qt ..... Pleistocene or Holocene talus.
QTi ..... Tioga moraines (advance IV).
QTe ..... Tenaya moraines (advance III).
QTa ..... Tahoe moraines (advance II).
QpTa ..... Pre-Wisconsin moraines (advance I).
Qvc ..... Pleistocene volcanic cinders.
Qv ..... Pleistocene basalt flows.

The bedrock geology follows Moore (1963):

Ksp_a; Ksp_b .. Cretaceous Spook pluton; granodiorite and quartz monzonite - - a) dark colored facies, b) light-colored prophyritic facies.
Kml ..... Cretaceous Mule Lake pluton; porphyritic granodiorite.
Ki ..... Cretaceous Independence pluton; alaskitic quartz monzonite.
Km ..... Cretaceous mafic plutonic rock.
J$\overline{\text{R}}$rt ..... Jurassic-Triassic metarhyolitic tuffs.
J$\overline{\text{R}}$a ..... Jurassic-Triassic meta-andesite.
Pzch ..... Paleozoic calc-hornfels
Pzm ..... Paleozoic marble
Pzbs ..... Paleozoic biotite schist

distributions from each site for normality, and by testing the distribution of the test statistics against random expectation (Ch. 3). Although four sites appear to represent non-normal populations at > 90% confidence (Table 5-19), out of 25 sites two or three are expected to be this deviant. Fig. 5-42 compares the cumulative distribution of confidences of normality for the 25 sites to the distribution expected if the populations were truly normal. The heavy solid line is this ideal distribution (for an infinite number of sites). The light solid and dashed lines parallel to the ideal distribution delineate the region within which 95% or 90% (respectively) of the distributions for groups of 25 sites will range, if the sampled populations were normal. The actual distribution for the sites in Sawmill Canyon was well within these limits, and it may be concluded that the populations of wave speeds which were sampled were nomally distributed. This conclusion permits the use of Student's t-test to discriminate the sampled populations, as discussed in Ch. 3.

In Fig. 5-43 the mean speeds for each site are grouped according to the moraine age assignments of (1) Burke and Birkeland (1979), (2) Dalrymple (1964), and (3) this study. The vertical spacing of the groups is arbitrary. In the third presentation (this study) sites within the two youngest groups (advances III and IV, or the Tenaya and Tioga stages) have been subdivided by individual moraine.

In each organization, $\overline{V_p}$ for site y on the outermost moraine is clearly less than $\overline{V_p}$ for the next youngest groups. Sites on the Tioga moraines of Burke and Birkeland show a considerable range of mean speeds: 1.65 ± 0.11 (1σ) km/s for 23 sites. According to the central limit theorem, the parent population of V_p for Tioga moraines should have a standard deviation $\sigma = 0.11\sqrt{23}$ or 0.52 km/s. However, only one site

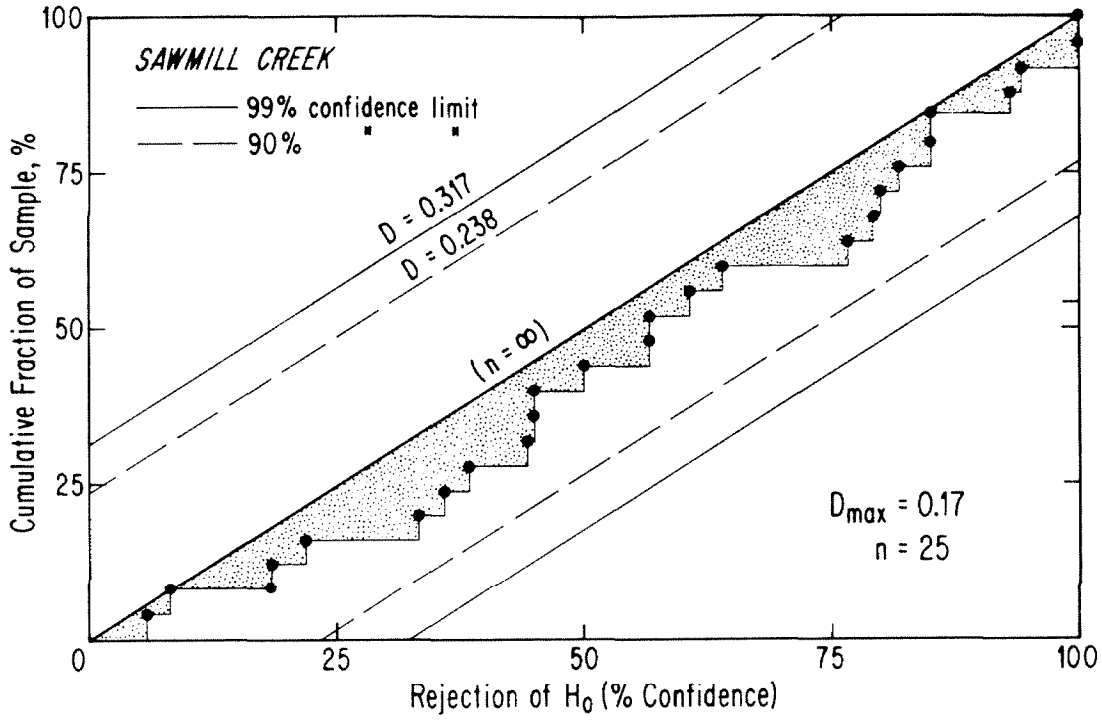

Fig. 5-42. The cumulative distribution of the confidence with which H_o may be rejected, for each site where acoustic wave speeds were measured. H_o is the hypothesis that the V_p data are a sample of a normally distributed population. The cumulative distribution lies well within the range of values anticipated for 90% of all samples; thus it appears that the parent populations were normal.

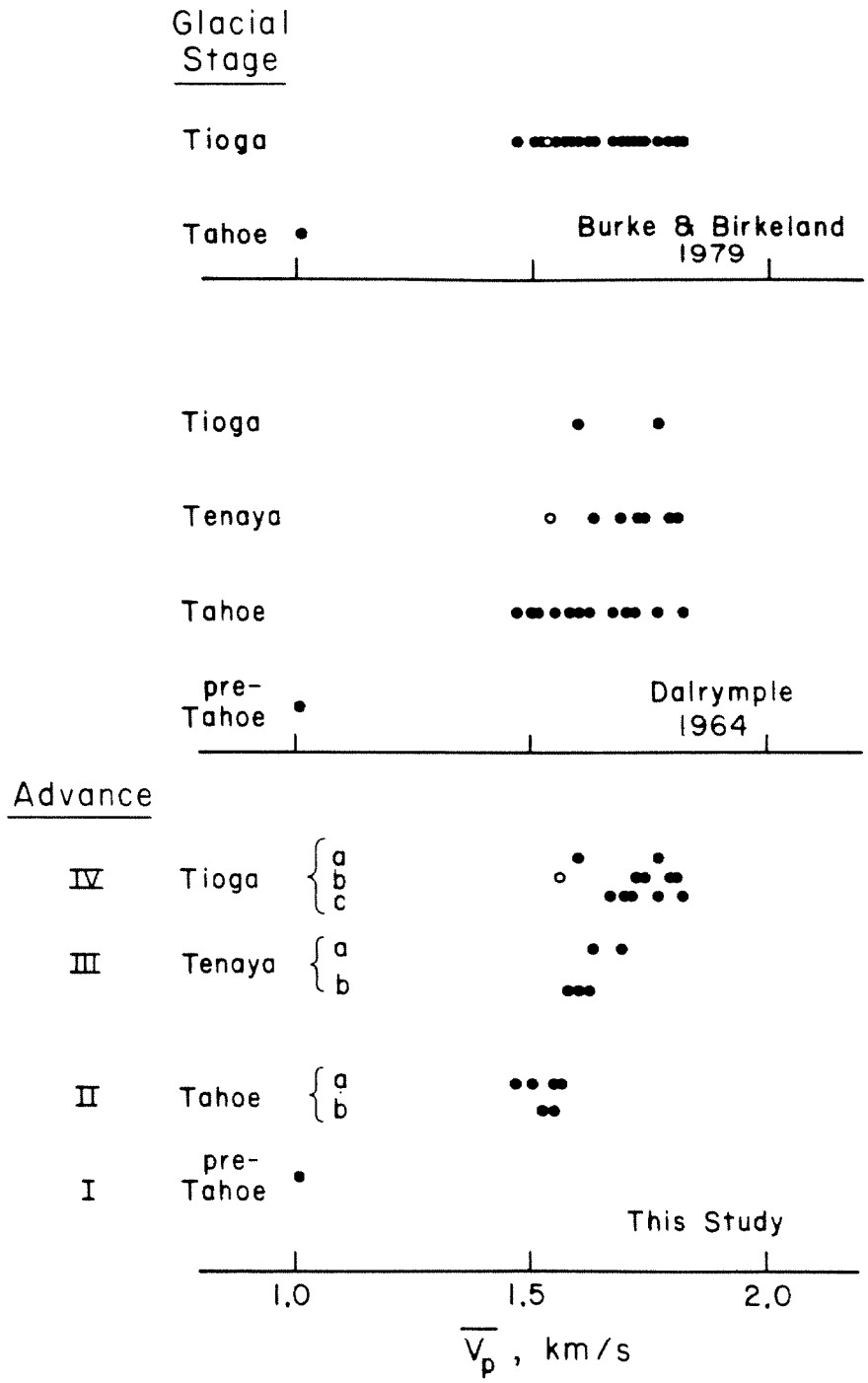

Fig. 5-43. $\overline{V_p}$ for sites in Sawmill Canyon partitioned by age according to different studies (see Fig. 5-39). The ordinate scale is arbitrary but is arranged in order of decreasing age. Data for the Tahoe and Tioga stages of Burke and Birkeland are clearly separable, but the excessive scatter of $\overline{V_p}$ values for the "Tioga" sites shows that more than one population was sampled, probably reflecting a variety of ages of till. Partitioning the data according to Dalrymple does not significantly modify this conclusion. Partitioning according to this study results in a clear trend towards increasing $\overline{V_p}$ with decreasing age. $\overline{V_p}$ for moraines of different stages are statistically separable. The open circle marks a site which may have been contaminated by rockfall.

has a standard deviation as large as that, and the mean of all the standard deviations for the group is only 0.44 km/s. This probably indicates that more than one population was sampled, and it appears that the assignment of the same age to the three youngest morphologic groups was not justified.

Grouping the $\overline{V_p}$ for sites according to the age assignments of Dalrymple (1964) shows that the younger moraines (Tioga and Tenaya stages) tend to have fewer low values than the Hogsback (Tahoe stage). However, the highest values of $\overline{V_p}$ are about 1.8 km/s for each age group. The absence of a strong trend in $\overline{V_p}$ with the assigned ages may be taken as evidence that Dalrymple's age assignments were not correct, or that there really was no significant age difference between the Hogsback and the youngest Tioga-stage moraines. Further consideration shows this latter possibility is not the case.

Analysis of variance using Fisher's method of randomization (see Ch. 3) shows that Dalrymple's post-Tahoe moraines appeared to be homogeneous (hypothesis H_o, that they were, could be rejected with only 77% confidence). On the other hand, the Hogsback seemed to be distinctly heterogeneous - H_o could be rejected with 99.8% confidence. Thus the apparent lack of a consistent increase in $\overline{V_p}$ with increasing age in Dalrymple's Wisconsin moraines could have resulted from the presence of a veneer of young till (high $\overline{V_p}$) on the Hogsback, as deduced in this study from the distribution of grusy boulders.

If the Hogsback is partitioned according to relative ages indicated by the semi-quantitative data, there are at least two ages of till (advance II, and advances III and IV combined). Using Fisher's method of randomization as before, we see that both groups are probably homogeneous (H_o can be rejected with only 15% and 62% confidence, respectively). Furthermore,

Student's t-test applied to the distributions of $\overline{V_p}$ shows that these groups are different, with more than 99% confidence. Thus the semi-quantitative analysis was correct; the Hogsback is a composite moraine.

Close inspection of the Hogsback crest east and west of the trail crossing near the bench mark (8152 ft) shows that there is good reason to assign different ages to those regions. However, neither can be assigned to advance II. It may be that the older till was left during advance III. The most impressive changes in the degree of weathering of the tills are: 1) the decrease in the number of boulders from east to west across the trail; (2) the strong increase in the amount of clay at 30-cm depth; and (3) the increase in the abundance of disintegrating boulders, from 0% to 9% (Fig. 5-40d). Thus the apparent age of the Hogsback crest actually decreases across from west to east (down-canyon) across the trail. This unusual occurrence is best explained by an advance IV glacier pushing over a composite advance II and advance III moraine, but not actually overriding the crest west of the trail.

Student's t-test shows that the $\overline{V_p}$ data support this complex interpretation (Table 5-20). The sites assigned to advances III and IV are shown to be different with more than 90% confidence. All other pairs of groups are different with more than 99% confidence.

If the $\overline{V_p}$ data for all sites in Sawmill Canyon are regrouped according to the age assignments of this study, a consistent decrease in $\overline{V_p}$ with age is seen (Fig. 5-43). The trend is even seen among moraines of the same advance. However, the changes in $\overline{V_p}$ among moraines assigned to the same stage are not statistically significant. Analysis of variance by Fisher's method of randomization, for instance, shows that sites from groups b and c of the advance IV (Tioga) moraines are homogeneous, with only a 44%

Table 5-20

Student's t-Test Applied to $\overline{\overline{V_p}}$ Data for Sites on the Hogsback

Advances	Degrees of Freedom *	t**	C_2†, %
IV - III (Tioga-Tenaya)	6	2.04	91
IV - II (Tioga-Tahoe)	7	6.65	>99
III- II (Tenaya-Tahoe)	5	4.29	>99
(IV, III) - II (post-Tahoe - Tahoe)	10	4.04	>99

* $n_1 + n_2 - 2$, where n_1 and n_2 are the numbers of site is the two groups (in order of listing).

** $$t = \left[\frac{n_1 + n_2 - 2}{n_1 + n_2} \quad \frac{n_1\, n_2}{(n_1-1)\, s_1^2 + (n_2-1)\, s_2^2}\right]^{1/2} \left(\overline{\overline{V_{p_1}}} - \overline{\overline{V_{p_2}}}\right)$$

where s_1, s_2, and $\overline{\overline{V_{p_1}}}$, $\overline{\overline{V_{p_2}}}$ are the standard deviations of the distributions of mean speeds, and the grand mean speeds of the two groups (in order of listing).

† Confidence with which H_o (the hypothesis that the sites were samples of the same population of $\overline{V_p}$) may be rejected (two-tailed test).

probability that they could have been samples of different populations; sites from the two advance III (Tenaya) moraines are heterogeneous with only 6% confidence; and sites from the three advance II (Tahoe) moraines are heterogeneous with only 2% confidence.

Table 5-21 shows the results of t-tests comparing the different groups. None of the adjacent moraines of advance III (Tenaya stage) or advance IV (Tioga stage) were separable. However, the advance III veneer on the Hogsback and the advance II till of the Hogsback were readily separated by Student's t-test on $\overline{\overline{V_p}}$; the test on $\overline{V_p}$ was less certain, but still indicated that advance II was more weathered than $\overline{V_p}$ with more than 90% confidence. In contrast, tests on data grouped by glacial stage, rather than by individual moraine, showed that advances II, III, and IV were separable with more than 95% confidence.

Thus the general scheme of age assignments deduced from semi-quantitative weathering measurements in this study appears to be supported by the acoustic wave-speed data. The critical conclusions are: 1) at least four ages of moraines are present in Sawmill Canyon; (2) the difference in wave speeds, and hence in age, between advance I and advance II is much greater than the difference between advances II and III or even advances II and IV; (3) the differences in wave speeds between adjacent moraines do not appear to be significant for moraines of the same stage, but are marginally significant for adjacent moraines of different stages. This final point suggests that the times between glaciations were somewhat greater than the times between stades during the last 0.1 my. The period between advances I and II was significantly longer.

Table 5-21

Student's t-Test Applied to V_p Data for Sites in Sawmill Canyon

	Distributions of $\overline{V_p}$				Distributions of V_p			
Advances[1]	Degrees of Freedom[2]	t[3]	C_1[4],%	C_2[5],%	Degrees of Freedom	t[7]	C_1[4],%	C_2[5],%
IV_b* - IV_c	7	0.49	-	-	-	-	-	-
IV_c - III_a	-	-	-	-	208	1.04	85	70
III_a-III_b	-	-	-	-	148	0.73	77	53
III_b-II_a	5	4.29	>99	>99	208	1.69	95	91
$IV_{b,c}$-$III_{a,b}$	13	2.77	99	98	449	2.42	99	98
$III_{a,b}$-$II_{a,b}$	9	2.46	98	96	329	2.37	99	98

* Site e has been excluded

1 Advances II–IV are those of Onion Valley, probably corresponding to the Tahoe, Tenaya, and Tioga stages (Wisconsin glaciation). Subscripted letters a, b, and c denote moraines within stages, in order of increasing age.

2 $n_1 + n_2 - 2$, where n_1 and n_2 are the numbers of site is the two groups (in order of listing).

3 $$t = \left[\frac{n_1 + n_2 - 2}{n_1 + n_2} \quad \frac{n_1\, n_2}{(n_1-1)\, s_1^2 + (n_2-1)\, s_2^2}\right]^{1/2} \left[\overline{\overline{V_{p_1}}} - \overline{\overline{V_{p_2}}}\right]$$

are the standard deviations of the means and $\overline{\overline{V_{p_1}}}$ and $\overline{\overline{V_{p_2}}}$ are the grand means for the two groups, in the order listed.

4 C_1 is the confidence with which H_1 ($\overline{\overline{V_{p_1}}} > \overline{\overline{V_{p_2}}}$, or $\overline{V_{p_1}} > \overline{V_{p_2}}$) may be rejected (one-tailed test).

5 C_2 is the confidence with which H_o (groups are the same) may be rejected (two-tailed test).

6 $N_1 + n_2 - 2$, where n_1 and n_2 are the numbers of measurements (V_p) in each group.

7 $$t = \left[\frac{n_1 + n_2 - 2}{n_1 + n_2} \quad \frac{n_1\, n_2}{(n_1-1)\, s_1^2 + (n_2-1)\, s_2^2}\right]^{1/2} \left[\overline{V_{p_1}} - \overline{V_{p_2}}\right]$$, where

s_1 and s_2 are the standard deviations of the distributions of V_p, and $\overline{V_{p_1}}$ and $\overline{V_{p_2}}$ are the means of the two groups, in the order listed.

Calibration of relative ages by dated interbedded lava . . .

The decrease of V_p may be a logarithmic function of age (Ch. 3). In Sawmill Canyon there is little case-hardening of boulder surfaces, so this relationship may obtain until a significant number of boulders are removed from the population by granular disintegration. In Fig. 5-44, conventional estimates of the ages of the Wisconsin glaciations, values of $\overline{V_p}$ for groups of sites, and age constraints from radiometric dates on interbedded lavas are shown.

Three different $\overline{V_p}$-age lines are shown in Fig. 5-44. The actual line for Sawmill Canyon must lie between the limits shown by lines A and C. Line A is constrained by the lower age limit for the advance I moraine (131,000 y) and by the age of the last glaciers of the Tioga stage (here taken as 11,500 y for moraine IV_b). Were line A the correct one, all moraines younger than the Hogsback of advance II would belong to the Tioga stage; however, an age of 28,500 y for advance II would be indicated. This would place advance II in an interglacial period.

Line C is constrained by the upper age limits of advances II and I provided by the radiometric ages of the interbedded basalts. Because the lava underlying the Hogsback was erupted before the Wisconsin Searles Lake formed 90,000 y ago (Smith, 1979), it may be an excessive age for advance II. Line C places advance III during the Tahoe stage, and advance IV during the Tahoe-Tenaya interglacial period. Thus neither limiting line appears to be realistic.

Line B lies between limits A and C and was chosen to place the ages of all moraines within conventional stages. If this line is correct, then advance I is nearly 0.5 my old, advance II correlates with the late Tahoe stage (~ 35,000 to ~ 45,000 y BP), and advances IV_b and IV_c were

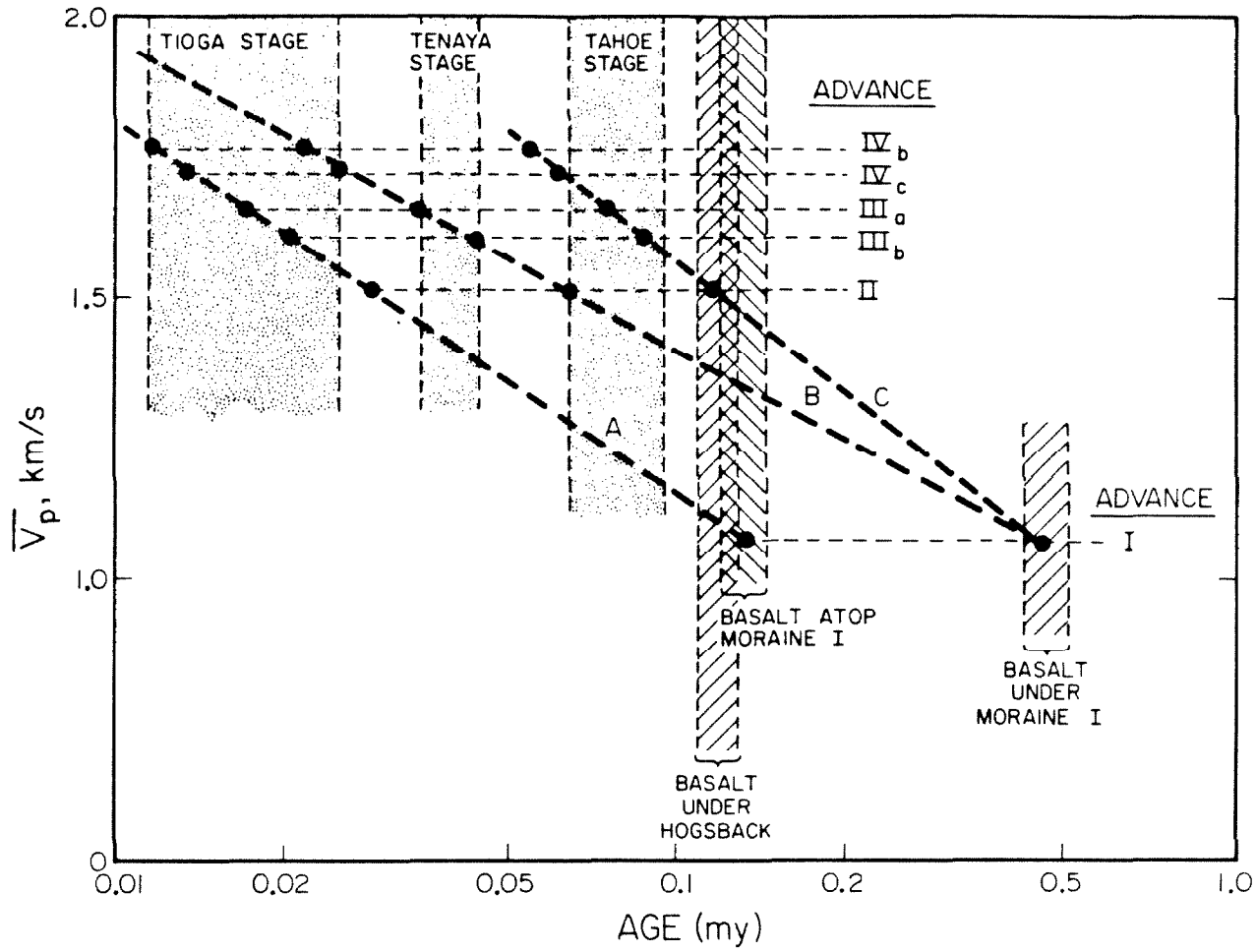

Fig. 5-44. $\overline{V_p}$ versus the age of glacial advances in Sawmill Canyon. If $\overline{V_p}$ decreases in proportion to the logarithim of the age of the till, then the age of an unknown moraine may be estimated provided the ages of two or more measured tills are known independently. Here three possibilities are shown. Ages are constrained by three radiometric dates on basalts interbedded with the older moraines. Line A was chosen by taking the age of the youngest moraines to be 11,500 y, near the end of the Tioga stage, and by taking the age of moraine I to be its lower limit. Line C was chosen by taking the ages of moraines I and II to be their upper limits. Since it is implausible that advance IV is not the Tioga stage, lines A and C were probably limits to the correct line. Line B is one line within these limits which gives reasonable ages for all the moraines.

were deposited during the early Tioga stage (~ 21,500 to ~ 25,000 y BP). Thus the V_p data together with the radiometric constraints on ages permit, but do not compel, the age assignments of this study.

Two points must be considered in interpreting Fig. 5-44. First, $\overline{V_p}$ for advance IV_a clearly plots belows any of the $\overline{V_p}$-age lines. The reason for this is unknown. From geological evidence it is clear that advance IV_a dates from the end of the Tioga stage at the latest. Three possibilities are suggested: 1) sites a and b were on a terminal moraine, which may have a different provenance from the lateral moraines, so that the V_p data need not be directly comparable; (2) as Birman (1964) argued, terminal moraines may weather faster than lateral moraines; and (3) advance IV_a may actually correlate with the Hilgard neoglacial advances. Birman (1964) found that Hilgard till appeared more weathered than late Tioga till. He attributed this to intensive weathering during the warm early Holocene Epoch. The solution to this problem is not central to understanding the critical Wisconsin-age glacial history in Sawmill Canyon, however.

The second point is of more importance. Because of burial of moraine I by hot pyroclastic debris, the state of weathering of the boulders now exposed on the moraine crest may have been altered. Presumably, heating the boulders would enhance weathering processes. However, burial would probably retard them, and the net effect is unknown, but if it were significant then it would change the limits A and C in Fig. 5-44. Because the pyroclastic ejecta blanket apparently was thin, and because no obvious baked zone was observed underlying it, it seems likely that effects of both heating and burial were minimal.

Summary of findings from relative dating . . .

The Hogsback appears to be a composite moraine containing till of at least two and probably three ages. Based on the prevalence of disintegrated boulders, it is best to assign the old core of the Hogsback to advance II, or the Tahoe stage. The immense bulk of this moraine is consistent with this assignment, if the relative sizes of moraines are similar over the Sierra (cf. Blackwelder, 1931). The outermost moraine must therefore be from either an early Tahoe or a pre-Tahoe advance. From the advanced state of decomposition of many of its boulders it could correlate with advance I of Onion Valley. Radiometric dating of lavas overlying the moraines showed it to be pre-Wisconsin. However, even in the absence of that constraint, the large difference in acoustic wave speeds compared to the Tahoe moraine would require this moraine to be regarded as pre-Wisconsin. The two other ages of till on the Hogsback were probably deposited during the Tenaya and Tioga stages (advances III and IV).

Moraines upstream from the Hogsback were divided into two groups morphologically. The youngest group (advance IVa) was clearly correlated with the late Tioga stage. However, weathering characteristics for most of the moraines in both groups were similar, and the moraines were regarded as different stades of the Tioga glaciation (IV). The outermost moraine appeared to be more weathered, and was assigned to the Tenaya stage (advance III). The question of whether this moraine belongs to a distinct stage or was just left by an early Tioga glacier cannot be answered, but because it could be statistically distinguished from the oldest advance IV moraine, and because adjacent advance IV moraines could not be, it is regarded in this study as belonging to a separate stage.

Basalts interbedded with the older moraines provided some chronologic

constraints to the assigned ages. The oldest moraine was bracketed by lavas dated at 131,000 y BP and 463,000 y BP and therefore predated the Wisconsin glaciation. This contradicts Burke and Birkeland (1979), who assigned it to the Tahoe stage (early Wisconsin). The Hogsback was constrained to be no more than 120,000 y BP by radiometric dates on underlying lavas. This permits its assignment to the Tahoe stage.

The radiometric ages and the V_p measurements are compatible with the assignment of advances II, III, and IV to the Tahoe, Tenaya, and Tioga stages, respectively. V_p data demonstrate that these advances are statistically separable, and hence have significantly different ages. However, this does not require that the advances belong to different stages; different advances within a long stage may be differently weathered also. In this study, stage boundaries were defined by adjacent moraines which were statistically separable.

Evidence of Ancient Glaciations from the Bedrock Ribs of Sawmill Canyon

Knopf (1918) felt that the lower reaches of Sawmill Canyon, below the Hogsback, were an excellent example of an unglaciated valley characterized by a V-shaped profile and a winding stream. The example is all the better because of the dramatic contrast with the glaciated valley upstream. Dalrymple (1964) agreed, raising the question of whether or not the southern Sierra Nevada had ever experienced a more extensive glaciation than that responsible for the Hogsback. Dalrymple felt that the Hogsback was of Tahoe age and interpreted his K/Ar dates of the subjacent basalt to mean that the moraine was less than 0.1 my old. In the northern and central Sierra Nevada, Wisconsin glaciers were dwarfed by the earlier

glaciers of the Sherwin glaciation. Dalrymple questioned whether the evidence of ancient extensive glaciations at Sawmill Canyon was removed by erosion, or whether because of climatic or tectonic changes the ancient glaciers did not form in the southern Sierra Nevada. He favored the latter explanation, suggesting that possibly the southern Sierra were uplifted later in the Pleistocene Epoch than the range farther north.

Evidence of ancient glaciation high in the Sierra Nevada has generally been obscured by the repeated late Pleistocene glaciers. Although the relict surfaces near the crest in Sawmill Canyon were not strongly modified by the glaciers at the end of the Pleistocene Epoch, it has not been shown that they were created before the early Wisconsin glaciers. Thus it appears that Dalrymple's argument is hard to test. However, indirect evidence of ancient glaciation may be preserved in the bedrock ribs of the steep south wall of Sawmill Canyon east of the Hogsback. These ribs have consistent profiles which seem to reflect the ancient valley floor and walls. As seen in Fig. 5-45, these profiles do not show the straight sides of the classical V-shaped canyon above the modern gorge of Sawmill Creek. Instead they suggest that the ancient valley may have had a concave cross section. Furthermore, there seems to have been more than one stage of erosion. Three stages are suggested by the segmented ribs mapped in Fig. 5-46. Three segments may also be recognized at different points along the south wall below Sawmill Meadow. These are marked by changes of slope in the topographic map 210 m, 290 m, and 340 m above the modern stream near its confluence with its northern tributary. These points rise westward at gradients of 15°, less steeply the ridge above (24°) but comparable to the modern stream (Fig. 5-46b). The consistent pattern lends credence to the interpretation of ribs as relicts of ancient valley floors and walls. The longitudinal

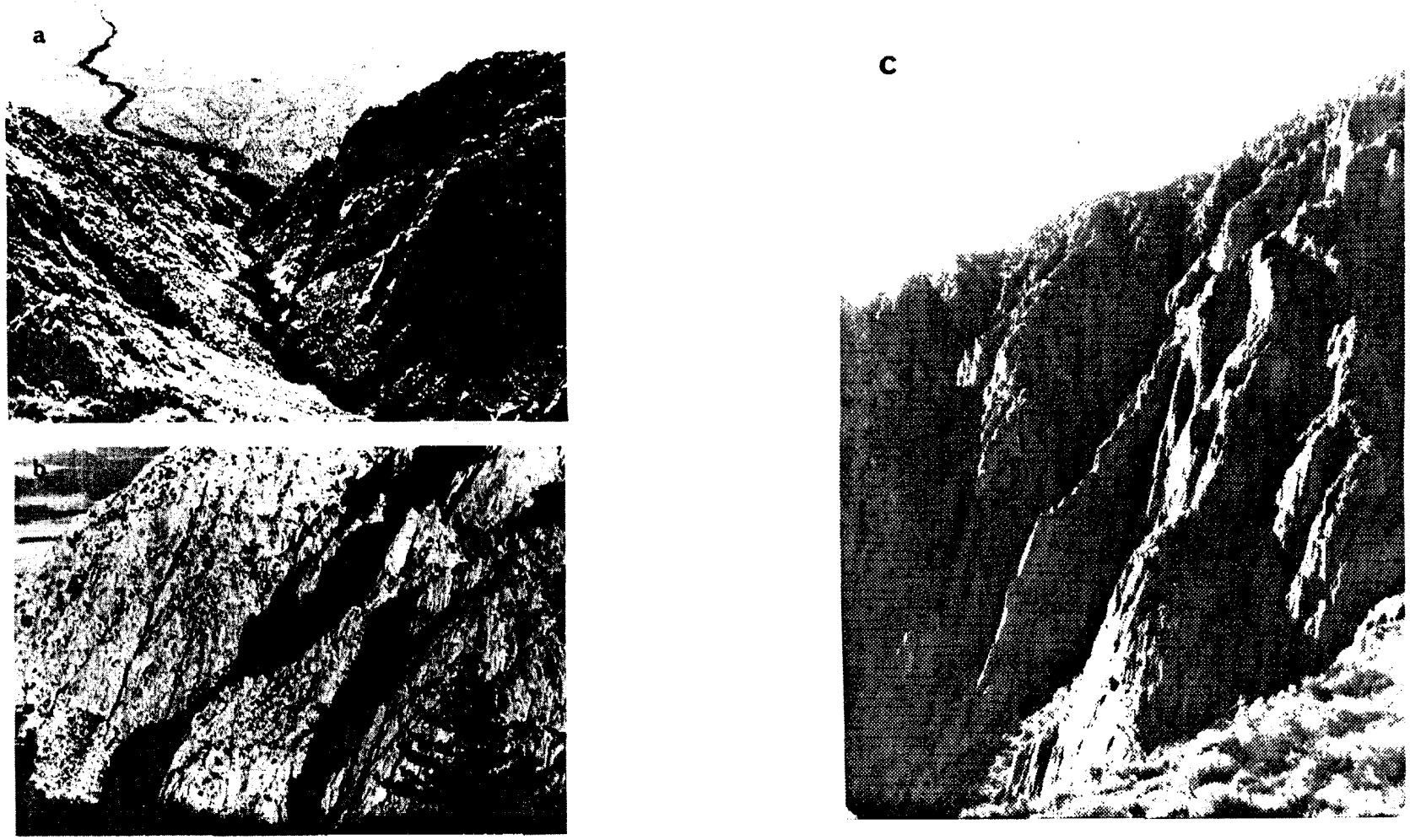

Fig. 5-45. Photographs of Sawmill Canyon. (a) The lower reaches of the canyon, viewed looking east towards the Owens Valley from the north ridge at about 2195 m elevation. The head of the alluvial fan is 1.5 km distant and 730 m lower than the camera. This part of the canyon was not glaciated during the late Pleistocene Epoch. Note the distinct breaks in slope on ribs within the canyon south of the creek, ~ 250 m above the creek. The ribs below the major break in slope are shown silhouetted at sunset in (b). These show that the gorge consists of two sections: a steep inner gorge and a zone in which the ribs have concave profiles. (c) Detail of the ribs viewed from the Hogsback looking south. It is possible that the consistent concave profiles above the lowest segment reflect the cross section of an ancient glaciated valley.

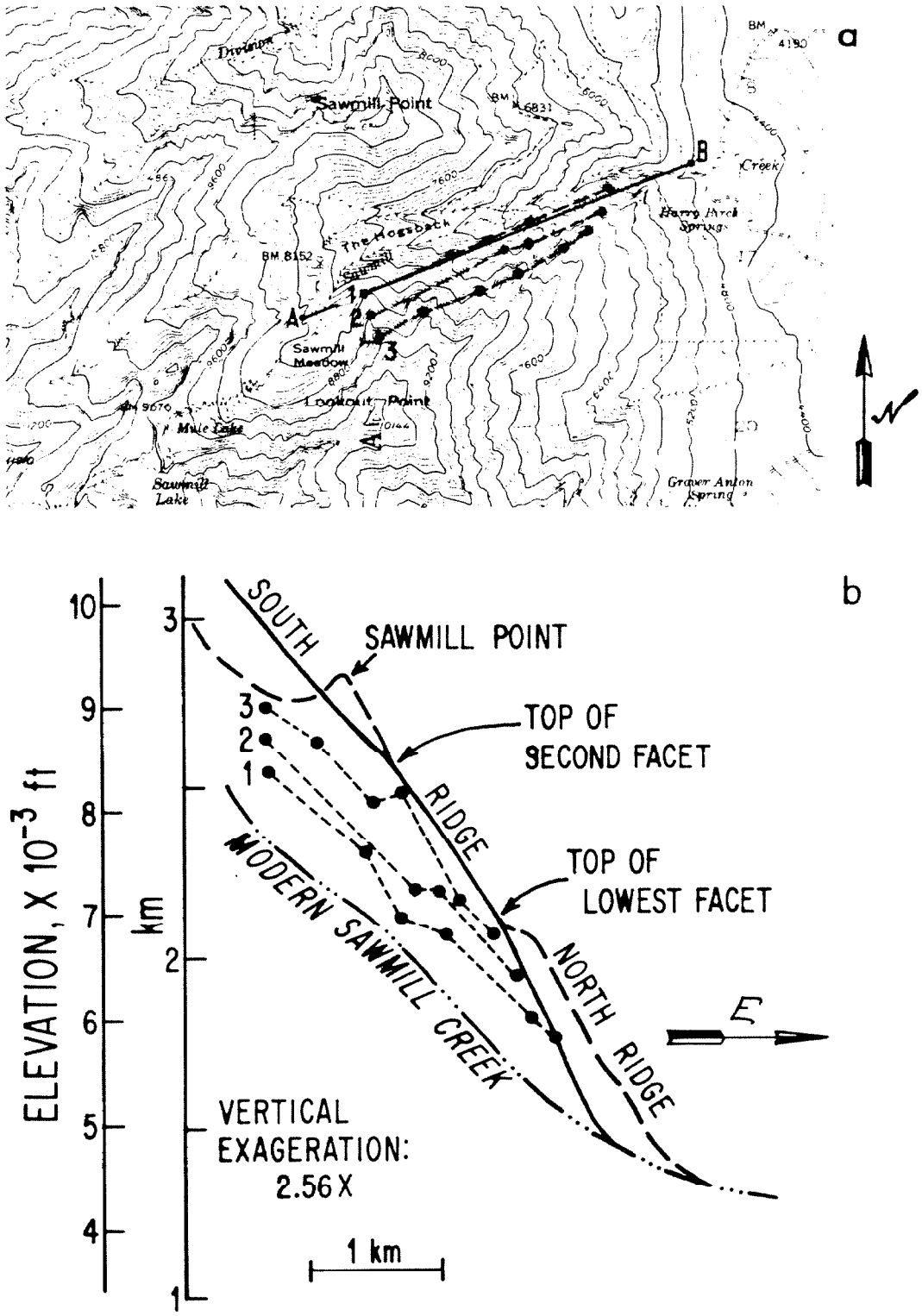

Fig. 5-46. Three zones of aligned breaks in slope are found on the south wall of Sawmill Canyon. See next page for explanation.

Fig. 5-46 (continued)

Three zones of aligned breaks in slope are found on the south wall of Sawmill Canyon. a) Topographic map showing points where ribs of the south wall showed breaks in slope. (b) Profiles of the three lines of breaks in slope of Sawmill Canyon are contrasted to the modern escarpment and to the modern Sawmill Creek. Profiles were projected onto line A-B in the map (a). The systematic trend in the elevation of the points and the similar elevation differences between points on the same ribs argue that the breaks in slope may be significant. The profiles are similar to the modern stream profile, but intersect the escarpment well above the modern fan. They may reflect the walls of the ancient canyon before Owens Valley was down-faulted as much as it is today. Topographic data are from U.S. Geol. Survey, Mt. Pinchot Quadrangle (1953), at a scale of 1:62,500 and with contour intervals of 80 ft.

profiles intersect the escarpment at angles of about 5°, well above the modern stream. This is especially clear for the profile of the lowest surface. It is evidence that the range front has experienced vertical displacements since each canyon level was cut. If the canyon levels resulted from episodic erosion in the absence of tectonic displacement, they would converge to the modern stream at the mouth of the canyon.

South of Sawmill Creek, the escarpment itself clearly shows evidence of at least two major rejuvenations. Projections of bevels to the range-front faults show that offset during the older episode totaled ~ 410 m and during the younger episode ~ 200 m, measured from the present stream at the range front. In contrast, the total offset has amounted to about 2500 m. The three ancient canyon levels were all cut during the final episode. On the bevelled northeast slope of Sawmill Point two distinct breaks in slope can be seen. These are at ~ 2440 m (8000 ft) and ~ 2070 m (6800 ft) elevation. They thus have the same elevation difference as breaks in slope on the escarpment south of Sawmill Creek, but are 125 m lower.

Lower Sawmill Canyon is developed in well-jointed quartz monzonite. The major joint plane is steeply dipping, and undoubtedly joints control the location and angle of the steep sections of the complex rib profiles. The gradational reduction of slope cannot be explained by joint control, however, and the profiles may be best interpreted as relict sections of ancient valley floors. The smooth surfaces and the concave profiles point to ancient glacial abrasion.

A Late-Pleistocene Incision Rate for Sawmill Creek

Two observations in Sawmill Canyon permit the exploitation of the

radiometric dates to yield upper and lower limits to the rate of downcutting by Sawmill Creek. First, Sawmill Creek appear to have cut through roughly 15 m of quartz monzonite bedrock since the eruption of the extensive intracanyon lava flow ~ 120,000 years ago. This gives a downcutting rate of roughly 0.125 mm/y, but this value must be a lower limit because Sawmill Creek also had to cut through the overlying lava.

The second observation was that the 465,000-y-old lava now crops out ~ 85 m above Sawmill Creek. This gives a downcutting rate of 0.16 mm/y, but this rate must be an upper limit because the outcrop was not necessarily at the bottom of the canyon when the lava was erupted.

Thus the late-Pleistocene downcutting rate of Sawmill Creek probably was between 0.125 mm/y and 0.16 mm/y. This is less than half of the upper limit of the incision rate estimated for Coyote Creek (<0.33 mm/y; cf. Bateman, 1965).

The Alluvial Fan of Sawmill Creek and an Offset Rate Along the Range-Front Fault

At 1465 m (4800 ft) elevation, Sawmill Creek exits from the range front to flow through the head of an alluvial fan in a channel incised about 25 m. The amount of incision lessens rapidly down the fan. The incised alluvial fan appears to grade to point near the top of the 0.12-my-old intracanyon basalt flow. An isolated outcrop of basalt, apparently a remnant of the same lava flow, is found on the north canyon wall, 62 m above the modern Sawmill Creek at the range front. The range front is marked by aligned springs and cinder cones, apparently developed along a fault. Cinders from these vents overlie the eroded remnants of the 0.12-my-old basalt flow. Thus the volcanic activity along the range front

postdated the intracanyon eruptions. Stream-worn pebbles are also found atop the basalt outcrop at the range front. After the basalt choked the canyon bottom, Sawmill Creek was forced to flow on top of the lava for a time.

Of critical interest is the observation that the first cinder cone north of Sawmill Creek overlies the ancient fan surface. This can be seen from the concentration of large boulders exposed on the cinder - covered north wall of the stream channel, below a line connecting the highest patches of fanglomerate ~ 44 m above Sawmill Creek at the range front and the fan surface just east of the cinder cone. These boulders are almost certainly exposed in situ. The alternative explanation, that they were deposited in a buttress unconformity with the cinder cone, is unattractive because the cinders are easily eroded. Some of the boulders are grusy. It seems unlikely that they would remain on such an unstable base long enough to disintegrate. The old fanglomerate is best exposed in a roadcut next to the gauging station 350 m east of the Sawmill Pass trail head. Boulders are heavily weathered and the matrix is rich in clay. Thus an old fan seems to have graded to the top of the intra-canyon basalt flows, probably before the eruptions of cinder cones along the range-front faults. The presence of basalt cobbles in the fanglomerate clearly shows that it postdates the 120,000-y-old lava flows. The volume and degree of weathering of the fanglomerate would be appropriate for Tahoe till. Thus the cinder cones may postdate some of the Tahoe glaciers and are thus less than ~ 90,000 y old. On the other hand, volcanic lapilli are conspicuously missing from the Tahoe fan south of Sawmill Creek. This is only 200 m from the nearest cinder cone north of the creek, and only 500 m from the nearest cone to the south. Thus it appears likely that the lapilli

were buried by the aggrading fan. This indicates that the cinder cones predate the incision of the fan and are thus older than the mid-Wisconsin glaciers, or older than ~ 45,000 y.

Apparently the incision and erosion of the intracanyon flows did not occur until well after the Tahoe glaciation began. When it did occur, it was probably hastened by the extraordinary volume of water pouring from retreating glaciers. The discrepancy (~ 18 m) between the height of the Tahoe fan and the basalt flow at the range front could have resulted in two ways: (1) the fan once graded to the top of the flow, and the discrepancy was caused by offset along the range-front fault, or (2) the fan graded to a knick point or series of knick points migrating west from the range front.

By mid-Wisconsin time incision of the intracanyon lava flows was complete. The Tahoe fan head was incised to a depth of 35 m or more, and a fill terrace 9 m above the modern stream was constructed. At an elevation of 1360 m (4460 ft) the fill terrace intersected the Tahoe fan surface; east of this point the fan surface is covered by the younger fanglomerate. No distinct fan of latest Tioga or neoglacial debris was constructed, perhaps because the moraines upstream were left largely intact.

The late-Pleistocene offset rate on the range-front fault

The most significant result from study of the fan head was a limit to the late-Pleistocene offset rate along the range-front fault. The intracanyon lava flow is not seen east of the range front, even though the stream has incised deeply into the cinder cone and fan below. It is unlikely that the flow was eroded from the fan surface because that process should leave scattered remnants. There are thus two possibilities: (1) the lava is buried in the fan below the modern stream, or (2) the

lava extended only a short distance down the fan north of Sawmill Creek. In the first case, the vertical displacement of the lava flow would best be explained by normal faulting on the range-front fault. In the second case, the outcrops could be buried by cinders from the vent north of the creek. However, it seems unlikely that the lava flow, probably more than 30 m thick at the range front, would not flow a considerable distance down the fan. Thus the first explanation is preferred. This model implies that there has been a total of > 62 m of vertical offset during the last 120,000 y, giving an average offset rate of > 0.5 mm/y. This rate is nearly twice the rate (<0.3 mm/y) of stream incision estimated at Coyote Creek (near Bishop, California) and three times the limit estimated for Sawmill Canyon. However, the elevation of the Tahoe fan head imposes an upper limit of 18 m of offset since the fan was incised, probably before the mid-Wisconsin glaciation. Thus the 18 m of offset probably took from 45,000 to ~ 90,000 y. This implies an upper limit of from 0.2 to 0.4 mm/y for offset during the late Wisconsin glaciation, which in turn requires the rate before and perhaps during the early Wisconsin glaciation to be more than 0.6 to 1.5 mm/y. Rapid faulting may thus have been episodic and followed or accompanied the volcanic eruptions, subsiding after a few tens of thousands of years.

It may be argued that the lava outcrop 62 m above Sawmill Creek at the range front was extruded from the adjacent cinder cone rather than from the vents in the canyon. If this was the case then its age could be as much as a factor of two or three less than 120,000 y. Because stream-worn cobbles were found atop the lava flow, it clearly dates from before the incision of the Tahoe fan, when Sawmill Canyon at the range front was filled either with lava or fanglomerate. However, the validity of the

average offset rate (>0.5 mm/y) depends on whether the intracanyon flow ever crossed the range front. Regardless of the origin of the isolated outcrop of lava, this much seems certain. The isolated outcrop serves mainly to provide an estimate of the offset. If the lava flow were from the cinder cone and if it rested mainly on the fan, then the actual fault offset might be more than measured, but 0.5 mm/y would still be a valid lower limit. If the flow rested on the intracanyon lava, then the measured offset might be fractionally too large. The error would be small however, since the heights above Sawmill Creek of the intracanyon flow and the range-front outcrop are about the same. I conclude that 0.5 mm/y is probably a valid limit for late-Pleistocene offset on the range-front fault at Sawmill Canyon.

5.7 DIVISION AND ARMSTRONG CANYONS

North of Sawmill Point the Sierra escarpment recedes ~ 3.5 km west and the elevation at the fan head increases to ~ 1830 m (6000 ft). The character of the escarpment changes as well. Instead of rising in a single sweep, it is broken by benches which themselves are highly faulted. These benches may be higher analogs of the foothill block to the south.

Perhaps in part because of the absence of transfluent tributaries, glaciers in Division and Armstrong Canyons were smaller than in adjacent canyons. As a consequence, runoff during glacial retreats was probably smaller also, and unusually complete sequences of moraines are preserved in the northern of the two canyons of Division Creek and in Armstrong Canyon. Armstrong Canyon was chosen for study, because access (from Scotty Spring) was superior. Armstrong Canyon was also chosen to provide relative age dating control for Goodale Canyon, the next canyon to the north.

Summary of Bedrock Geology (Moore, 1963)

Division Creek is cut primarily into the granodiorite or quartz monzonite of the Spook Pluton. In Armstrong Canyon the Spook pluton is exposed only for 1.5 km along the southern wall. Most of the upper canyon is in the porphyritic granodiorite of the Mule Lake pluton. Thus the rock types but not their abundances are similar to those of Sawmill Canyon. The lower reaches of Armstrong Canyon consist of the mafic pluton.

Moraines of Armstrong Canyon

All the moraines of Armstrong Canyon below 2500 m (8200 ft) elevation

were assigned to the Tioga glaciation by Moore (1963). However, weathering characteristics clearly varied among the four distinct moraines within this this part of the canyon, and appeared to justify a subdivision of the moraines by age.

In this study, the moraines below the cirque of Armstrong Canyon were divided into five groups (Fig. 5-47). The lowest was found at 2145 m (7040 ft) elevation. It was a short 100-m section of a left-lateral moraine largely buried by younger till. The soil appeared redder than in the younger moraine and boulders were oxidized and grusy. No volcanic ejecta were found on the moraine. This moraine is at least of Tahoe age, but is best matched by the pre-Tahoe moraines of Onion Valley and Sawmill Canyon. It was assigned to advance I.

The next group of moraines extends up to about 2165 m (7100 ft) elevation. The left-lateral moraines and outwash are cut by deep ravines which are buried above 2165 m elevation. The outwash grades to the fan head and merges with outwash and the right-lateral moraine of Goodale Creek east of the range-front. The outwash overlies basalt flows and the cinder cone south of Armstrong Creek. The right-lateral moraine was largely eroded. Boulders were heavily weathered with cavernous surfaces, but the distinctive oxidized and grusy boulders of the older moraine were not found. Boulders preserving original abraded surface were rare also. This group appeared to correlate with advance II of Onion Valley (Tahoe stage).

Above 2165 m (7100 ft) elevation moraines were found on both sides of Armstrong Creek. Bedrock knobs protruded through the right-lateral moraine, which appeared to have been extensively eroded. Despite this, the terminal moraine was not completely breached. Thus morphologically this group is distinctly younger than advance II. Although occasional

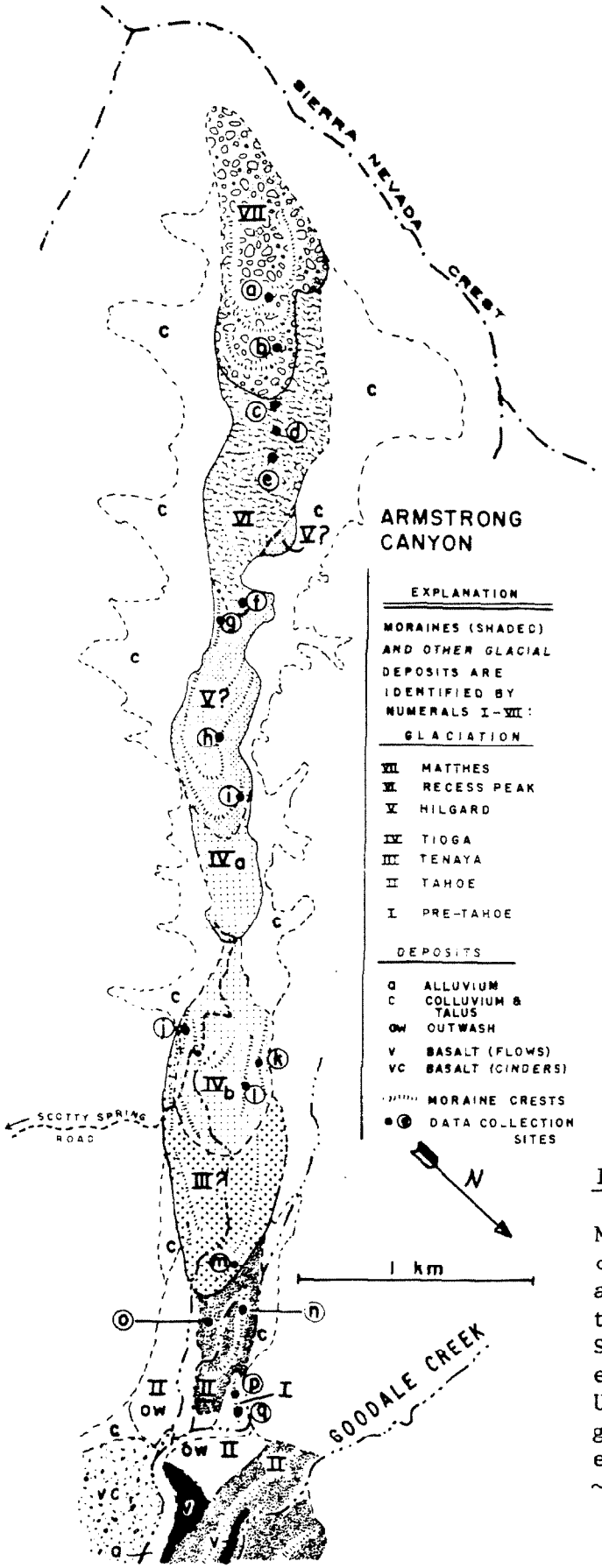

Fig. 5-47. Quaternary deposits in Armstrong Canyon. Moraines are numbered I-VII in order of decreasing age. Probable equivalents in the conventional glacial sequence for the Sierra Nevada are given in the explanation. The map base is U.S. Geol. Survey aerial photograph GS-VDYM 2-222 (8-31-75), enlarged from a scale of ~ 1:80,000.

grusy boulders were seen, in general the till appeared less weathered than in the two lower groups. In this study, this group was assigned to advance III, but the distinction from the younger moraine upstream was not profound, and the group could date from early advance IV.

The fourth group of moraines was found above 2345 m (7700 ft) elevation. These moraines enclosed the sage flats at the end of the road from Scotty Spring at 2535 m (8320 ft) elevation. The moraines of this group were quite youthful in general appearance. The thick terminal moraine has not yet been deeply breached by the intermittent Armstrong Creek, which percolates through the porous fill behind the moraine, emerging at about 2390 m (7850 ft) elevation from the base of the moraine in a large spring. This group was assigned to advance IV (Tioga stage).

At 2585 m (8480 ft), an enormous forested terminal moraine buries the sage flats behind the end moraines of the fourth group. The moraine has not been modified by stream erosion; Armstrong Creek is completely subsurface above the sage flat. Despite the clearly youthful character of the moraines, a few grusy boulders were found on its surface and in road cuts. At least the terminal moraine of this group is certainly of Tioga age (advance IV). However, the thick sequence of moraines (like that of the tributary to Sawmill Creek) may actually be composed of different layers of till, and the uppermost moraines may be neoglacial. These moraines were characterized by piles of boulders without large amounts of interstitial material. Boulder burial or relief ratios ranged from 0/0/100 (no burial) to 15/50/35 (15% of the boulders exposed on the surface were deeply buried), whereas on the moraines below the sage flat (fourth group) ratios of 33/33/33 were common. I suspect that the small, fresh-appearing moraines atop the complex of moraines of the fifth group date from advance V, the Hilgard neoglaciation.

Above 2925 m (9600 ft) elevation and in the cirque of Armstrong Canyon, there appear to be least two sets of young neoglacial moraines. These are probably the equivalent of the Recess Peak (advance VI) and Matthes (advance VII) glaciations.

Till of advance VI was well consolidated and 75% or more of the boulders were covered with brown lichens. Yellow-green lichens exceeded 20 cm in diameter. Sedges were common, but the moraines were unforested. The till was generally deposited in low hummocks and disconnected ridges, and it appeared that much of it originated from the shady south wall of the canyon.

Till of advance VII was restricted to the steep-sided rock glacier above 3170 m (10,400 ft) elevation in the cirque. Angular boulders on this unconsolidated moraine were unstable and rolled easily. There was no soil, vegetation, or lichens on the surface of the rock glacier. The lower reaches and snout of the rock glacier, however, were more stable and supported scattered sedges and lichens. The colonies of yellow-green lichens attained a size of 2 cm, which would correspond roughly to an age of 300 y at Mammoth Lakes, California (Curry, 1968).

Relative dating techniques were sufficiently powerful that progressive differences from moraine to moraine could be noticed within the young neoglacial till.

This raises the possibility that the three neoglacial advances generally recognized in the Sierra might be systematically subdivided, as Curry (1968) has reported doing in the Mammoth Lake region. No effort was made to do so for this study.

Granodiorite Weathering Ratios in Armstrong Canyon

To discriminate among tills of the different groups of moraines, semi-quantitative weathering data were gathered at 62 locations in Armstrong Canyon. Granodiorite weathering ratios were the most useful. These data are given in Table 5-22 and plotted on a three-component diagram in Fig. 5-48. GWR values for neoglacial moraines showed a strong trend towards fewer fresh (class 1) boulders with increasing age. The three neoglacial advances were readily separated.

Moraines older than advance VI had few class 1 boulders, and in Fig. 5-48 they plotted along the line: (class 2) + (class 3) = 1. The Pleistocene moraines showed a clear tendency towards more heavily weathered or grusy boulders with increasing age. However, from advance V to advance IV moraines showed a perplexing tendency towards fewer heavily weathered boulders with age. One site ("g") may have been anomalous because its boulders were derived in part from outcrops of Spook pluton quartz monzonite on the south wall instead of the more common Mule Lake porphyritic granodiorite, but the trend was apparently real. Perhaps this corresponds to the "reversed" weathering noted by Birman (1964), in which Hilgard till appeared more weathered than the older Tioga till.

Although mean values of GWR gathered at several locations on each Pleistocene moraine showed progressively more heavily weathered boulders with increasing age, the clusters of individual values overlapped considerably. Site "m", on the "advance III" moraine, could not be distinguished from the advance IV sites. On the other hand, the advance II group was distinct from all younger moraines, and advance I was clearly older than advance II. Site "q" on the advance I moraine probably plots anomalously close to site "n" (advance II) because data were gathered close to the

Table 5-22

GWR Data for Moraines in Armstrong Canyon

a) Individual Sites

Sites[1]	Advance[2]	No. of Boulders	GWR[3]
a-1	VII	50	4/6/90
a-2	VII	50	2/6/92
b-1	VII	56	11/21/68
b-2	VII	50	4/12/84
c	VI	65	29/23/48
d-1	VI	64	20/27/53
d-2	VI	50	26/32/42
d-3	VI	52	19/29/52
e-1	VI	50	20/30/50
e-2	VI	50	20/30/50
e-3	VI	51	18/27/55
e-4	VI	52	23/23/54
f-1	V	61	41/39/20
f-2	V	61	38/41/21
f-3	V	52	33/40/27
f-4	V	50	34/36/30
g-1	V	56	71/23/5
g-2	V	50	50/40/10
g-3	V	50	60/38/2
g-4	V	50	40/58/2
h-1	V	50	28/54/18
h-2	V	50	22/58/20
i-1	V	50	28/68/4
1-2	V	50	12/76/12
i-3	V	50	8/80/12
j-1	IV	51	37/57/6
j-2	IV	54	28/70/2
j-3	IV	46	39/59/2
j-4	IV	50	30/70/0
k-1	IV	51	31/69/0
k-2	IV	52	21/77/2
k-3	IV	52	15/77/8
1-1	IV	58	33/66/2
1-2	IV	58	34/66/0
1-3	IV	60	43/57/0
1-4	IV	47	45/53/2
k-1	IV	47	43/51/6
k-2	IV	51	45/49/6
k-3	IV	53	47/47/6
k-4	IV	49	43/55/2
k-5	IV	50	36/64/0
m-1	III?	47	47/49/4
m-2	III?	49	39/59/2
m-3	III?	50	38/60/2

Table 5-22a (continued)

Sites[1]	Advance[2]	No. of Boulders	GWR[3]
m-4	III?	50	28/70/2
m-5	III?	55	49/46/5
n-1	II	55	73/24/4
n-2	II	51	71/29/0
n-3	II	56	64/32/4
n-4	II	50	48/52/0
o-1	II	50	60/40/0
0-2	II	51	47/47/6
0-3	II	52	54/46/0
0-4	II	54	54/43/4
0-5	II	51	59/39/2
p-1	I	54	70/28/2
p-2	I	54	74/26/0
q-1	I	50	70/30/0
q-2	I	50	70/24/6
q-3	I	50	66/30/4
q-4	I	50	60/32/2
q-5	I	50	62/38/0

b) Groups

Sites[1]	Advance[2]	No. of Boulders	GWR[3]
a	VII	100	3/ 6/91
b	VII	106	8/17/75
c	VI	65	29/23/48
d	VI	166	22/29/49
e	VI	203	20/28/52
f	V	224	37/39/24
q (R)	V	206	56/39/5
h	V	100	25/56/19
i	V	155	15/75/10
j (R)	IV	356	29/69/3
k	IV	219	39/60/1
l	IV	250	43/53/4
m	III?	301	39/58/3
n	II	212	64/34/2
o	II	258	55/43/2
p	I	108	72/27/1
q	I	250	67/31/2

Table 5-22 (continued)

[1] Sites within groups are contiguous. Group locations are shown in Fig. 5-48. "R" denotes groups on right-lateral moraines.

[2] Advances are those of Onion Valley. Advances VII, VI, and V probably correspond to the neoglacial Matthes, Recess Peak, and Hilgard stages. Advances IV, III, and II are probably the Tioga, Tenaya, and Tahoe stages. Advance I is pre-Wisconsin.

[3] Granodiorite Weathering Ratios: listed in order are the percent of boulders in classes 3 (heavily weathered), 2 (lightly weathered), and 1 (fresh).

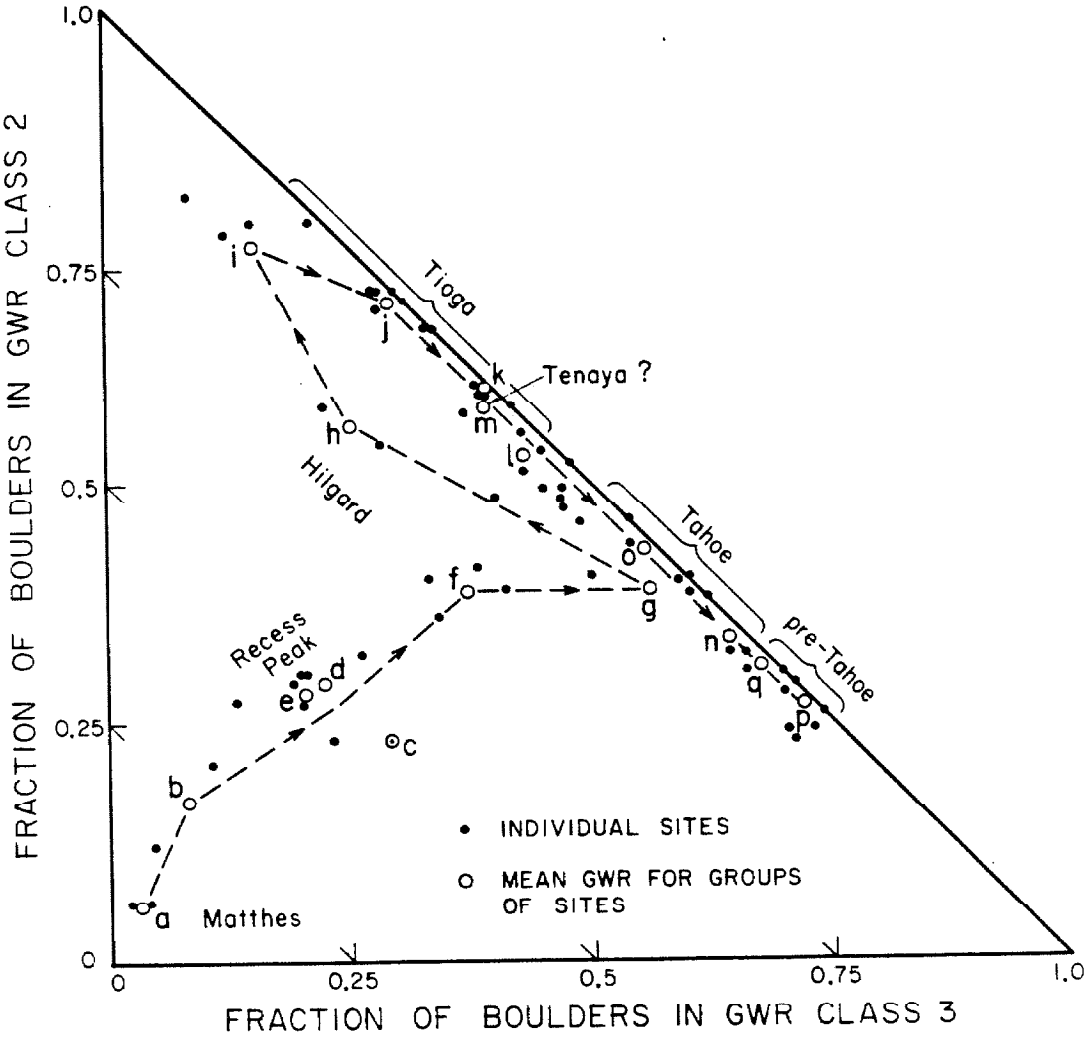

Fig. 5-48. Variation diagram for GWR data for moraines of Armstrong Canyon. The fraction of heavily weathered boulders (class 3) and lightly weathered boulders (class 2) are plotted on the abscissa and ordinate, respectively. Data for individual sites on the same moraine crest define clusters, but clusters for adjacent moraines generally overlap. Mean values of GWR for groups of sites on the same moraines define an evolution trajectory. The youngest neoglacial moraines consist dominantly of fresh (class 1) boulders. Class 1 has been largely depleted even in latest Pleistocene moraines. Remarkably, Tioga moraines have a lower proportion of class 3 boulders than the early Holocene Hilgard moraines. This cannot be explained by weathering. See text for discussion. Pleistocene moraines show an obvious trend towards a higher fraction of heavily weathered boulders with increasing age.

contact with the higher advance II moraine, and there was some possibility of contamination by the younger boulders. Sites of advance I showed a tendency to look older with with distance from the younger moraine.

It was concluded that the basic age assignments in Armstrong Canyon were warranted by the GWR data, except that advance III (Tenaya stage) could well have been simply an early advance IV (Tioga stage). The critical age assignment, advance II (Tahoe stage), appeared to be justified. This moraine was coeval with the moraine overlying the basalt flows at the range front along Goodale Creek.

Basalt Flows Near Armstrong Canyon

There has been an enormous outpouring of basalt from vents along the range-front faults from Sawmill Canyon to Armstrong Canyon (Moore, 1963; Darrow, 1972; Knopf, 1918). These are partly buried by fan deposits and glacial outwash of advance II (Tahoe stage). About 1.5 km northwest of the Division Creek powerhouse the pre-eruption fan surface is exposed. This surface, which was not visited, appears redder and less bouldery than the younger fan in natural color 1:16,000 scale aerial photographs. Perhaps some of the reddish color is due to a mixture of cinders with the fanglomerate. The relationship shows that the lava flows are probably pre-Tahoe in age.

Truncated Spurs Near Armstrong Canyon

Three triangular facets below ~ 3170 m (10,400 ft) elevation can be seen near Spook Canyon (Plate II). The apices are about 365 m below the end of the ridge separating Armstrong Canyon from Division Canyon. This ridge may in turn mark the higher apex of an older facet.

Four apices may be seen within the northern Division Canyon at about 3290 m (10,800 ft) elevation. Two of these are fairly obvious on both aerial photographs and on the topographic map; the other two are subtle even on the photographs. The significance of these facets is difficult to assess. The line of apices rises westward at only 5°. The face of the spur above the bench north of Spook Canyon is somewhat oversteepened for a height of ~ 150 m. This probably resulted from the latest offset between the main Sierra block and the bench. The bench does not contain any alluvial or fan deposits.

5.8 GOODALE CANYON

At Goodale Creek the alluvial fan heads are sufficiently elevated 1950 m (6400 ft) that Wisconsin glacial moraines cross the range-front fault. The extent of the glaciers was no doubt the greater because the catchment consisted of three large tributary canyons. The lowest moraines, probably of advance II (Tahoe stage), overlie a 25-m-thick sequence of olivine basalt flows (Fig. 5-49), and outwash of the same age overtopped other flows lower on the fan. The moraines may also have predated the cinder cones at the range front. This is indicated by the absence of volcanic bombs and lapilli on the moraines, despite their presence on the adjacent slopes north of Goodale Creek. The potential for obtaining an absolute age limit to a late Pleistocene glacial advance was the principal motivation for studying Goodale Canyon. The necessary date for the lava flow has not yet been obtained.

Summary of Bedrock Geology (Moore, 1963)

The upper reaches and cirques of Goodale Canyon are developed in quartz monzonite of the Siberian pluton. Only along the southern tributary does the Mule Lake pluton crop out. Part of the headwall of the middle tributary canyon consists of biotite schist, which is also found in the northern canyon. Striped Mtn. at the head of the northern canyon, is composed of a dark granodiorite or quartz diorite shot through with lighter granitic dikes. The lower portions of Goodale Canyon are cut through the mafic pluton.

Fig. 5-49. At Goodale Creek a left-lateral moraine of advance II (Tahoe stage) overlies basalt flows (left). The cinder cone (right) also predates the moraines but the light-colored deposits overlying it are colluvium from the escarpment rather than the moraine itself. View is to the north. The saddle west of the cinder cone is about 50 m above Goodale Creek.

At the mouth of Goodale Canyon a spectacular line of nine basaltic cinder cones occurs along the range-front faults. A thick series of basalt flows on either side of Goodale Creek underlie moraines of the late Pleistocene glaciers. Bedrock east of the fault is not exposed.

The bench south of Goodale and Armstrong Canyons, like Shingle Mill Bench to the north, seems to have been formed by antithetic normal faults dipping west into the main range-front fault. Similar antithetic faults were mapped by Moore south of Sawmill Canyon, although no bench is found there. This type of bench contrasts with the foothill block, which is usually characterized by normal faulting with the east side down.

Moraines of Goodale Canyon

Figure 5-50 shows the Quaternary deposits of Goodale Canyon and a generalized map of the maximum advances of the Wisconsin and younger glaciers. The trunk glaciers which extended east across the range front formed at the confluence of the middle and northern forks of Goodale Creek. Here the glaciers from the two cirques on the Sierra crest cascaded 600 m in enormous icefalls to their junction. The volume of the trunk glacier was probably increased but little by a third tributary, plunging ~ 300 m down the southern wall of Goodale Canyon from a hanging canyon 1 km farther east. The depth of the trunk glacier 1.5 km west of the range front was about 150 m. Despite this, the glacier extended beyond the range front onto the alluvial fans only ~ 0.5 km.

Only the oldest preserved moraine actually crosses the range front. The Holocene neoglacial advances appeared to have reached the icefalls from the cirques, but not to have reformed as a trunk glacier in the main canyon. The later Holocene glaciers were confined to the cirques

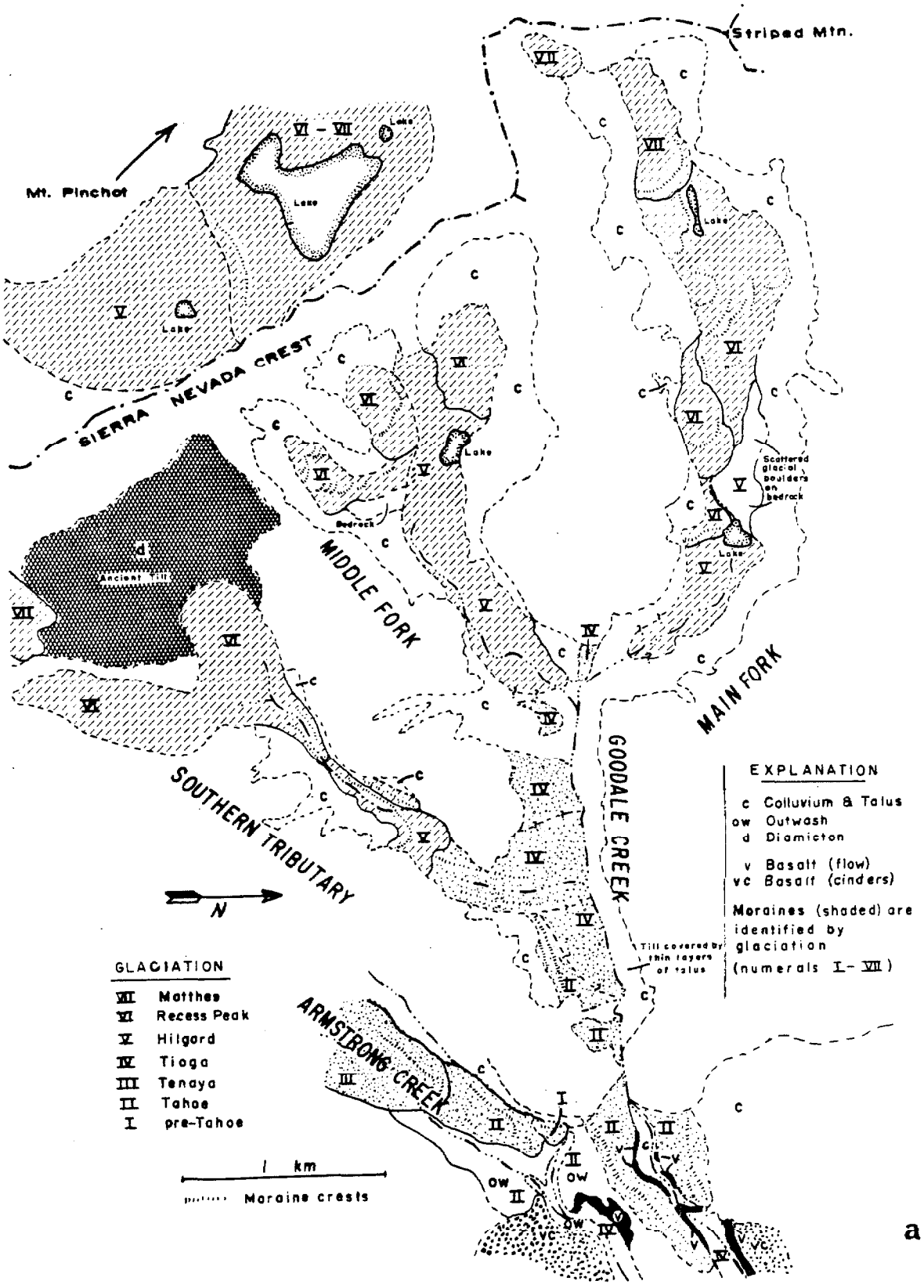

Fig. 5-50. Quaternary geology in Goodale Canyon. (a) Detailed map of Quaternary deposits.

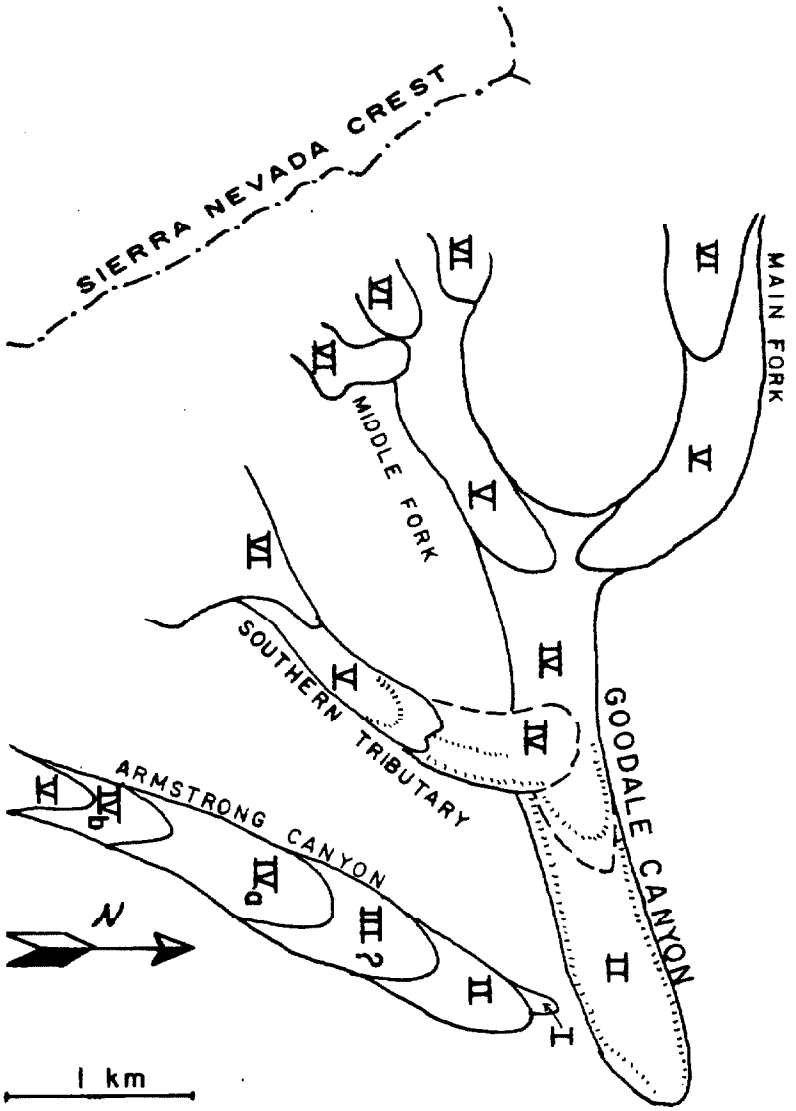

b

Fig. 5-50 (continued). Quaternary geology in Goodale Canyon. (b) Generalized map showing the maximum advances of the late Quaternary glaciers. The map base is U.S. Geol. Survey aerial photograph GS-VDYM 2-222 (8-31-75). Scale is variable because of foreshortening.

themselves.

The sequence of moraines in Goodale Canyon is not well preserved. The left-lateral moraines within the canyon west of the range front remain as only a thin veneer of till against the canyon wall. The right-lateral moraines are better preserved, and two parallel crests were found below the confluence with the southern tributary. No massive Tioga-stage terminals such as were found in most other canyons were observed. The reason for this in unclear.

Moore (1963) assigned the moraines east of the range front, like those of Armstrong Canyon, to the Tioga stage. Were this correct, it would mean that evidence of the Tahoe glaciers was absent, although this is the case in no other canyon.

Relative weathering data do suggest that the lowest moraines appear younger than most Tahoe moraines. The GWR for 52 boulders measured the same day as the Armstrong Canyon moraines was only 46/50/4. This could indicate a Tioga or Tenaya age if the weathering rates for the boulders were the same, but does not exclude a Tahoe age. However, there are several reasons for believing that the GWR underestimated the actual age. First, numerous heavily weathered boulders with case-hardened surfaces and as much as 15 cm of weathering relief were observed. This is uncharacteristic of Tioga moraines. Second, Goodale Creek has undercut both lateral moraines. This process tends to expose relatively unweathered boulders at the "crest". Third, the right-lateral moraine grades into the outwash plain from Armstrong Canyon which dated from advance II (Tahoe stage). Fourth, Goodale Creek has cut deeply into bedrock just west of the range front. Incision since the Tioga stage is typically only four or five meters, yet Goodale Creek was was incised perhaps 25 m. For these reasons, the lowest moraines of

Goodale Canyon were assigned to advance II in this study.

Two additional factors must be noted. First, till from the southern tributary appears to have reworked a large amount of older diamicton, possibly introducing a bias to the weathering data for the right-lateral moraines. The extent of the bias is uncertain, but because much of the reworked material was extremely fine, the actual effect on the GWR could be minimal. On the other hand, the introduction of even a few cavernous boulders to a moraine would possibly affect the conclusions drawn from relative dating techniques. Second, the basalt flow underlying the moraines at the range front has not yet been completely incised by Goodale Creek, and a waterfall is found within the basalt a few hundred meters east of the range front. Because the basalt elsewhere appears to be rapidly eroded by undercutting, this could be an indication of youth of the lava flow. This possibly makes this lava especially attractive for dating; it could provide a close upper limit for the age of the range-front moraines.

Each of the two factors discussed above suggests that the moraines may be younger than thought in this study. Because of the dearth of moraines preserved in Goodale Canyon, the GWR data cannot be placed in context and the extent of the bias cannot be assessed. Relative weathering data are thus unreliable for moraines of the trunk glaciers. The rate of incision of basalt was not determined, and complicating factors such as burial by glacial outwash may have lowered the rate anyway. Thus, the radiometric age of the lava would be the best clue to the age of the overlying moraines.

Above two waterfalls at 2070 m (6800 ft) elevation the character of Goodale Canyon (Fig. 5-51) is markedly different. Incision by the creek

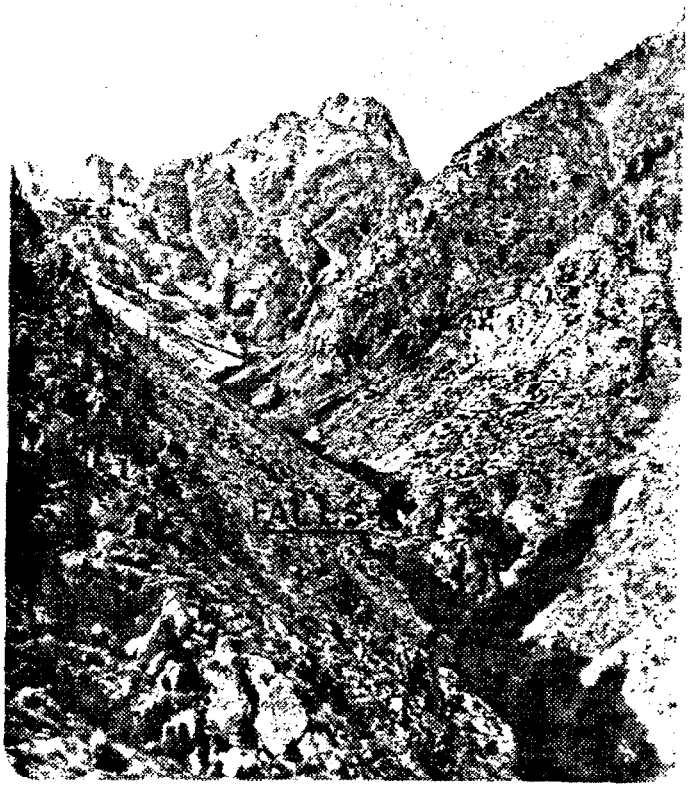

Fig. 5-51. Goodale Canyon from the range front. View is to the west. An eroded right-lateral moraine lies against the cliffs of the south wall of the canyon; moraines have largely been removed on the north side although till is abundant. Above the bedrock steps and waterfalls (foreground) Goodale Creek is incised less than 2 m into the valley floor. Although no prominent moraines were found, this must last have been glaciated during the Tioga stage.

is reduced to ~ 6 m at the top of the upper falls, and farther upstream the incision is nil. These falls may mark the lower limit of the latest Pleistocene glaciers. Certainly the Tioga glaciers reached below the confluence of the main and middle forks, for the patches of till remaining on the south wall of the canyon west of the southern tributary are distinctly fresher than the till near the range front.

Low and indistinct moraines are found at the base of the steep bedrock steps on both the main and middle forks above their confluence. These may be Tioga recessional moraines or Hilgard terminal moraines (advance V). Their general size is typical of advance V moraines elsewhere in the study area, and they are assigned to advance V. The unsedimented lakes at the top of each step were certainly covered by the advance V glaciers, which thus cascaded over the bedrock steps.

The Cirques of Goodale Canyon

Each of the three major cirques of Goodale Creek has an interesting feature which warrants a brief discussion. The northern cirque (main fork) is cut into the southeast face of Striped Mtn., whose summit (~ 4000 m or 13,120 ft) is an old erosion surface. East of Striped Mtn., Goodale Mtn. is flanked on the southeast by a 1.5-km-long rib whose 0.4-km-wide top is also part of an old surface (3410 - 3720 m or 11,200 - 12,000 ft elevation). Cut into this surface between Striped Mtn. and Goodale Mtn. is a remnant of a 0.75-km-wide U-shaped trough which is now the pass from Goodale Canyon to Taboose Canyon. This remnant stands now ~ 180 m above both the floor of the Goodale Canyon cirque and the broad valley to the north which contains Taboose Pass, on the Sierra crest. Apparently

the vicinity of Goodale Mtn. was once a gentle upland surface of considerable extent. Relief on this surface was perhaps 300 m. From the distinctive profile of the pass between Goodale Mtn. and Striped Mtn., this ancient surface appears to have been incised by glaciated valleys. The orientation of this pass and the presence of a high ridge 1 km to the south shows that the ancient glacier must have flowed northwest. It probably was a tributary to the ancient South Fork of the Kings River, which drains west. At that time, Goodale Mtn. was probably on the Sierra crest. This drainage has since been captured by Goodale Creek, probably as a consequence of its increased competence after the major uplift of the Sierra Nevada relative to Owens Valley. The middle fork of the Goodale glacier was actively working westward through another relict surface below Mt. Pinchot. This large plateau (~ 1 km^2) is only about 25 m below the present crest. It supports three small glaciers today, on the northeast face of Mt. Pinchot. The headwall of the Goodale cirque has cut sufficiently far into the plateau that recent moraines have been undercut and are exposed on the crest itself (Fig. 5-52). Undoubtedly, some ice from this plateau fed the glaciers to the east, although most joined the Woods Creek glacier west of the crest. This plateau is at about the same elevation as the sub-summit surface to the north, and they may have once been continuous. It may be an analog for the smaller remnant surface of University Peak.

The southern tributary of Goodale Creek was glaciated, but not as heavily as the northern ones. The southern tributary heads in two fresh cirques cut into a higher bench or ancient cirque ~ 170 m higher than that of middle fork. As seen from the north, the bedrock floor of this bench has a concave east-west profile and is buried by up to 50 m of

Fig. 5-52. The crest of the Sierra Nevada west of the middle fork of Goodale Creek, showing thin neoglacial moraines capping bedrock. View is to the north. The till is less than ~ 5 m thick on the crest. The contact between bedrock and till is sharp.

drift and ground till (Fig. 5-53). This diamicton is unusual because in the fresh exposure it has a large component of clay and very fine particles and relatively few boulders. Soil from the surface of the deposit is less rich in clay, and clay coatings on rock grains and pebbles are less well developed. Perhaps this reflects recent reworking of the surface layers. The age of the diamicton is uncertain, but the unusual abundance of clay suggests that it is at least pre-Wisconsin. Late Pleistocene and Holocene glaciers have reworked this ancient till, and some moraines below the recent cirques consist almost entirely of silt and clay. Relative dating is thus problematical.

Offset Across the Range-Front Fault

No scarps were found on the advance II (Tahoe) moraines that straddled the range-front or on the alluvial fans or debris skirts nearby. It is possible that hitherto unrecognized faults exist along the easternmost outcrops of bedrock, at about 2195 m (7200 ft) elevation on each moraine crest. Small scarps might be undetected in such a location, but activity should be reflected in a discontinuity in the height of the moraine crests across the range front. It was not possible to measure total offset of the moraine crests across this zone because the moraines to the west were severely eroded by Goodale Creek, and the original crests have been removed. By eye it appears that possible offset has been limited to a few meters. Furthermore, no scarps are seen across the moraines and outwash in Armstrong Canyon, although these would be on strike. Thus it seems that there has been little activity on the range-front faults at the mouth of Goodale Canyon at least since the end of the Tahoe stage, about 65,000 y ago.

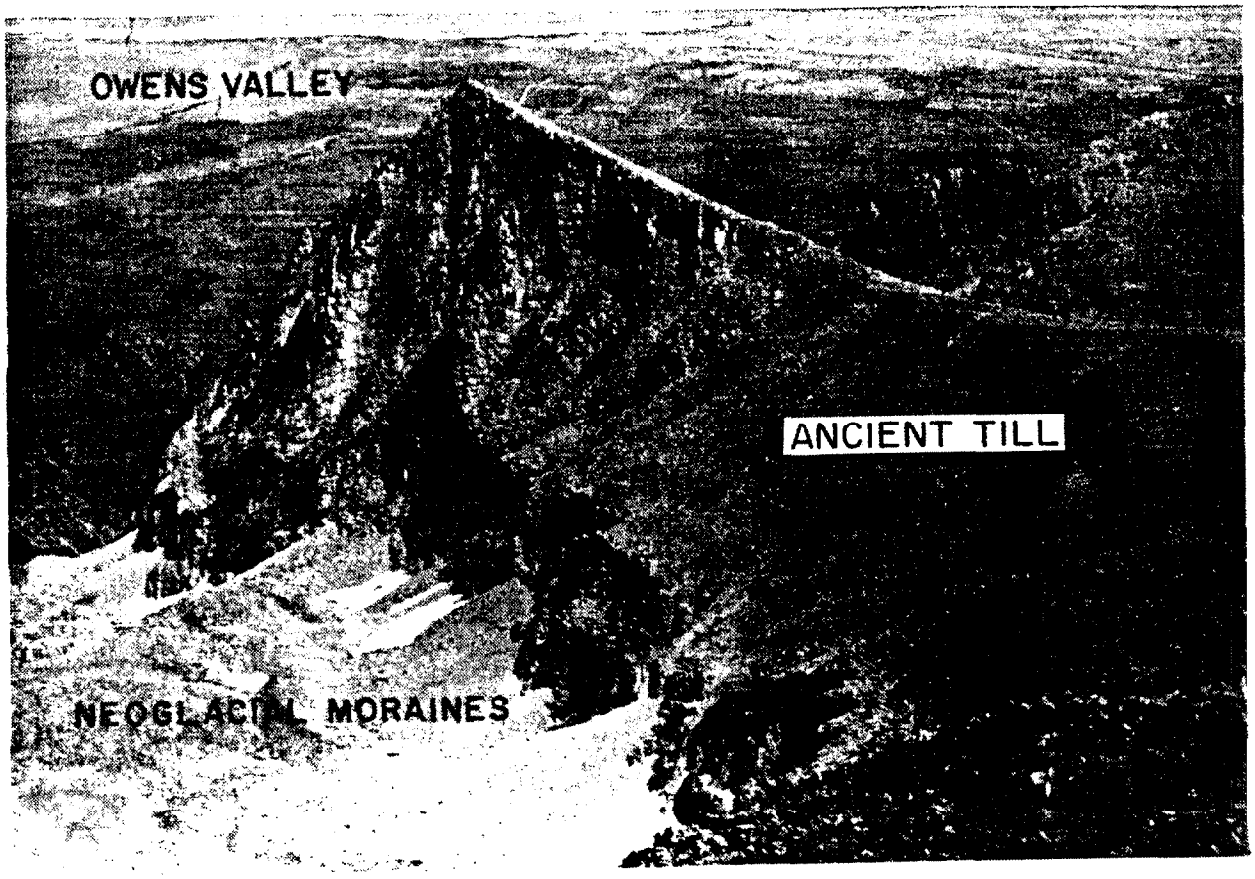

Fig. 5-53. Ancient diamicton rich in clay is exposed on the south wall of the middle cirque of Goodale Canyon. The top of the diamicton is ~ 170 m above the neoglacial moraines of the cirque. The diamicton is probably a weathered till. The view is from the Sierra crest looking east. The cinder cones at the mouth of Goodale Canyon are seen in the background.

5.9 TABOOSE CANYON

The cirques of the Taboose glaciers have been cut into the headwaters of the South Fork of the Kings River. Consequently, Taboose Pass is not a small col on a steep ridge, but is on the broad floor of the old valley. Taboose Pass is one of only two passes (the other is Piute Pass) lower than 3500 m (11,500 ft) elevation from Cottonwood Basin in the southern Sierra to Pine Creek, north of Bishop. At least the Wisconsin glaciers flowed east and west from the ice cap filling the pass.

Moraines from the Pleistocene glaciers are found in the main canyon and across the range front. Unlike Goodale Canyon, the terminal moraines of the Tioga glaciers are large and well preserved. Like Goodale Canyon, the Tahoe moraines at the range front do not seem to have been faulted. However, pre-Wisconsin moraines may have been offset vertically as much as 42 m.

Summary of Bedrock Geology (Moore, 1963; Bateman, 1965)

Taboose Canyon is developed almost entirely in granitic rocks. Three plutons are found: the Red Mountain Creek pluton (alaskitic quartz monzonite), the Goodale pluton (quartz-poor quartz monzonite), and the Taboose pluton (quartz-monzonite). Although basaltic cinder cones are found both north and south of Taboose Creek on the fans of Owens Valley, no record of volcanic activity is seen at the mouth of the canyon.

Between Taboose and Goodale Canyons lies a prominent forested bedrock bench (Shingle Mill Bench). This appears to be similar to the smaller bench south of Armstrong Canyon. Both appear to have resulted from normal offset on parallel low-angle (~ 30°) west-dipping faults.

Moraines in Taboose Canyon

Based on morphology there are four groups of Pleistocene moraines preserved in Taboose Canyon. Two of these cross the range front. The two sets of nested lateral moraines on either side of Taboose Creek at the head of the fan appear to be of pre-Wisconsin and Tahoe ages (advance II) and were so mapped by Bateman (1965). The distribution of the groups of moraines is shown in Fig. 5-54.

The outer moraines are smooth and rounded. Although the outer right-lateral moraine extends as far east as the inner one, the left-lateral moraine is truncated only ~ 200 m east of the range front, and appears to be cut off by the inner moraine. This implies a considerable age difference; the outer moraines were already widely breached when the inner moraines were deposited.

Boulders on the outer moraine are case-hardened or grusy, and few in number. The crest is littered with grus. The inner moraine is also characterized by heavily weathered boulders with disintegrating and oxidized surfaces. Weathering along joint has excavated to a depth of 35 cm. However, weathering does not seem as thorough as on the outer moraines.

The inner right-lateral moraine has an unusually sharp and narrow crest as a consequence of continuing erosion by Taboose Creek along its base. The locally bouldery crest is seemingly less weathered than its left-lateral counterpart. Perhaps this is due to the undercutting of the moraine and consequent removal of weathered till and exposure of fresh till on the retreating "crest". However, the bouldery till of the crest extends only about 8 m down the southern flank of the moraine. Lower,

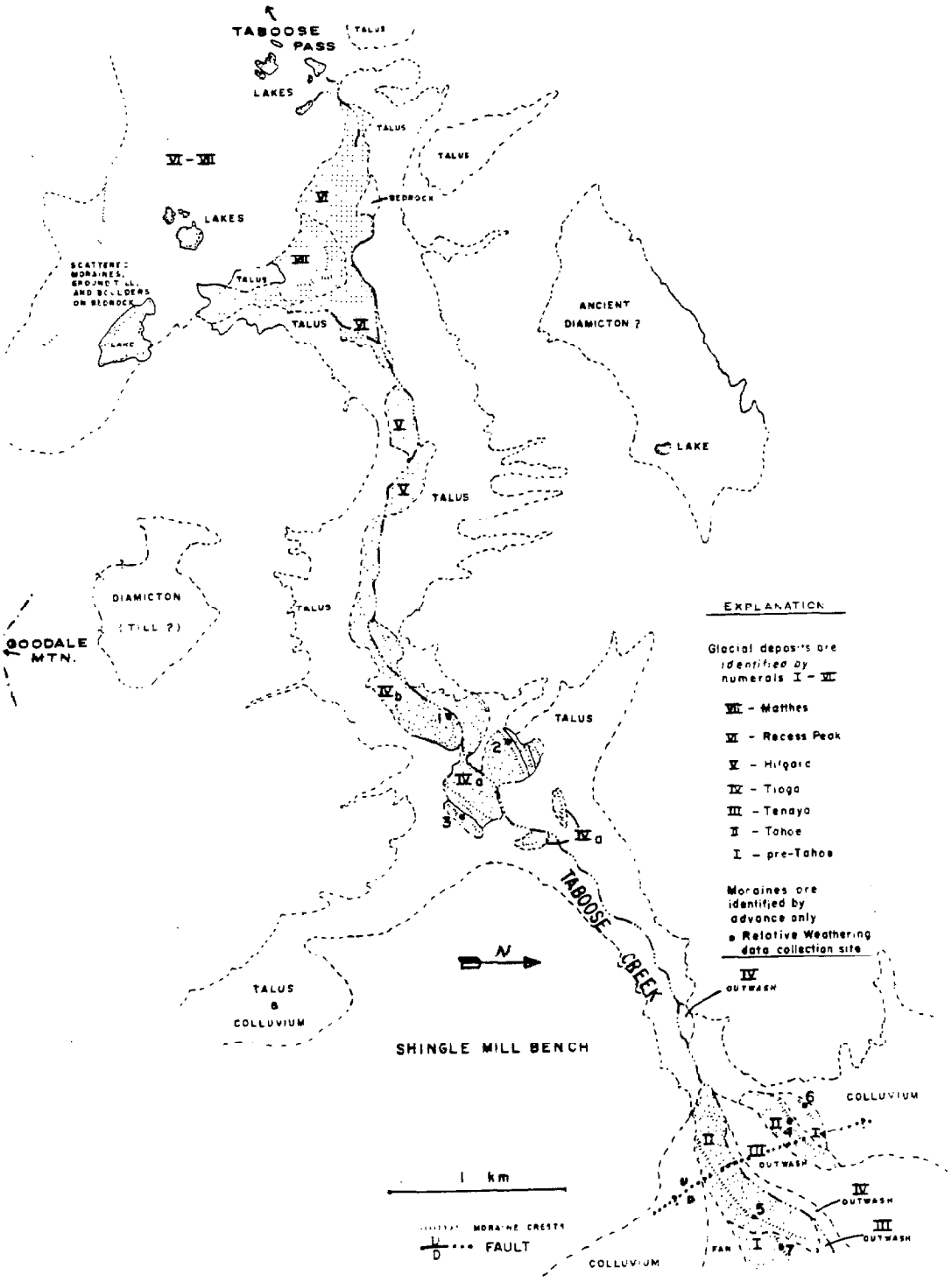

Fig. 5-54. Quaternary deposits of Taboose Creek. The map base is U.S. Geol. Survey aerial photograph GS-VDYM 2-222 (8-31-75). Scale is variable because of foreshortening.

the moraine consists of fine-grained particles and rock fragments. Whether this is slope wash or till weathered in situ is not clear, but the sharp boundary suggests the latter explanation. Compound moraines with analagous contacts were seen at Bloody Canyon and Green Creek (Ch. 3). If the moraine is compound, then its crest and eroded inner flank may date from a late glacier of advance II or even from advance III, which is otherwise unrepresented at Taboose Creek.

The inner moraines were assigned to advance II. The degree of weathering, especially on the left-lateral moraine, would permit assignment to no younger stage. The outer moraines probably correlate best with advance I of Onion Valley or Sawmill Canyon. The original morphology of the moraines is too well preserved for a moraine of the Sherwin glaciation.

Basalt cobbles about 15 cm in diameter were found on the left-lateral moraine of advance I and on the younger outwash, but not on the moraine of advance II. No smaller fragments were found. These could be airfall; however, in light of the Indian settlement on Taboose Creek and the prevalence of obsidian chips in the vicinity of the cobbles, another possibility is that they were carried to their locations.

The two other groups of moraines are found west of the range front, near the 2440 m (8000 ft) level of Taboose Creek. Terminal moraines of the lower group have been completely removed. Only fragments of the lateral moraines have been preserved on the canyon walls. In contrast, the terminal moraines of the higher group are only partly breached. To the west, Taboose Creek flows within 2 m of the glaciated floor of the canyon. Although this group is clearly from advance IV, lateral moraines are only poorly preserved.

Despite the strong differences in the degree of erosion of the

moraines of these two groups, weathering characteristics were similar, and there was insufficient justification to assign them to different glacial stages. Thus both are regarded as moraines of advance IV, the Tioga stage.

Above 2800 m (9200 ft) elevation, Taboose Creek rises over a steep bedrock step 250 m to meadows below Taboose Pass. Above the bedrock step are found small neoglacial moraines. Glaciers of advance V may have advanced to the bedrock step, but the more recent advances were confined to the cirque below the pass and to the upland surface of the pass itself.

Transfluent glaciers

During the late Quaternary Period, glaciers forming near Taboose Pass flowed both west down the Kings River, and east down Taboose Canyon. Because of the large area of well exposed polished bedrock near the pass, the topographic divide during glaciations could be determined from the orientation of glacial striae. Because winter storms are from the Pacific, a strong precipitation gradient occurs across the Sierra Nevada (cf. Curry, 1968), and the crest of the glaciers may have been some distance west of the bedrock crest.

A map of the orientation of glacial striae is shown in Fig. 5-55. The direction of the glaciers was determined from the orientation of crescentic gouges and chattermarks (Matthes, 1960). Clearly the divide for the glaciers was no more than ~ 250 m west of the bedrock crest.

Relative weathering data

Limited semi-quantitative weathering data were gathered from the Pleistocene moraines of Taboose Canyon. The chief goal was to establish

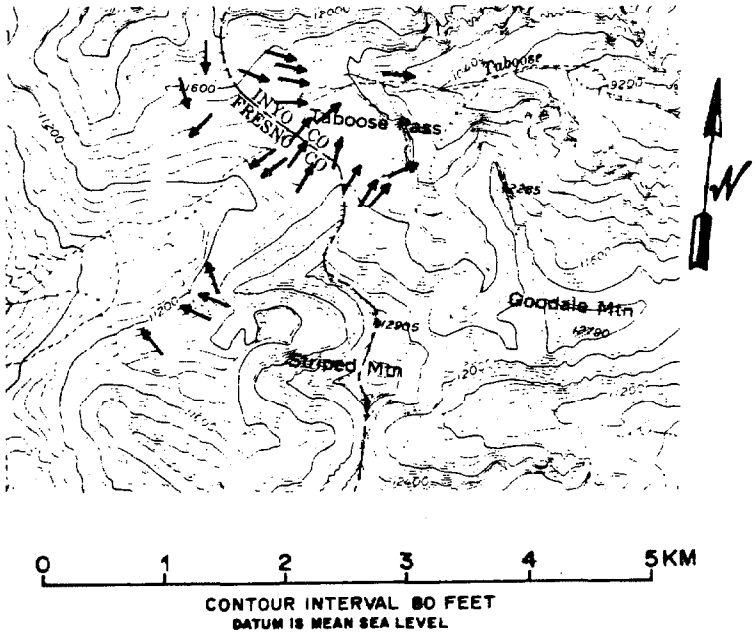

Fig. 5-55. Direction of flow of late Pleistocene or Holocene glaciers near Taboose Pass, inferred from glacial striae and the orientation of crescentic gouges. The ice divide was no more than 250 m west of Taboose Pass. Map base is U.S. Geol. Survey Mt. Pinchot Quadrangle (1953).

if there were weathering differences between the two groups of moraines, and between the two groups east of the range front.

The data are summarized in Table 5-23. Sites where data were gathered are shown in Fig. 5-54. The GWR data show the normal tendency towards large fractions of weathered boulders in the older tills. The two young groups of moraines, advances IVa and IVb, were inseparable. In part this may have been because the only moraine crests of advance IVb were found near or on the terminal moraine. As Birman (1964) noted, boulders in terminal moraines may be more heavily weathered than on the lateral moraines. Thus, the apparent contrast between advances IVa and IVb is probably less than it should be. The GWR data gathered did not permit the distinction between moraines of advance I and II. This was because virtually all the boulders fell in the "heavily" weathered category. Inspection showed that the degree of case-hardening, granular disintegration, oxidation, and the depth of weathering along joints all were greater for the advance I moraines, but these data were not gathered quantitatively. Site 5, on the right-lateral moraine of advance II, probably had an exceptionally small number of boulders exposed, and site 6 on the left-lateral moraine was probably exceptionally bouldery.

Faulting on the Range Front

As at Goodale Creek, the advance II moraines across the range front do not appear to have been faulted. Springs on the left-lateral moraine probably reflect the proximity of bedrock, but this may be a consequence of erosion along the flank of the moraine and not of recent faulting.

The pre-Wisconsin moraines of advance I appeared to have been faulted,

Table 5-23

Relative Weathering Data for Pleistocene Moraines of Taboose Canyon

a) Individual determinations of GWR

Site[1]	Advance[2]	No. of Boulders	GWR[3]
1-a	IVb	50	2/96/4
1-b	IVb	50	6/92/2
1-c	IVb	50	8/88/4
1-d	IVb	50	6/92/2
2-a	IVa	54	9/85/6
2-b	IVa	50	2/98/0
2-c	IVa	64	6/24/20
2-d	IVa	60	4/90/6
2-e	IVa	62	24/69/7
3-a	IVa	64	9/63/28
3-b	IVa	50	0/94/6
3-c	IVa	58	2/69/10
3-d	IVa	51	2/88/10
3-e	IVa	55	4/87/9
3-f	IVa	58	0/69/31
4-a	IVa	53	9/74/17
4-b	IVa	50	2/88/10
4-c	IVa	52	4/73/23
4-d	IVa	51	2/75/24
4-e	IVa	51	6/88/6
4-f	IVa	57	12/70/18
5-a	II	51	69/26/6
5-b	II	50	86/14/0
5-c	II	50	68/30/2
5-d	II	51	88/10/2
5-e	II	50	88/12/0
5-f	II	50	84/14/2
6	II	98	76/18/6
7	I	136	88/ 9/3

Table 5-23 (continued)

b) Mean values of GWR and other data

Site[1]	Advance[2]	No. of Boulders[4]	GWR[3]	BR[5]	BFC[6]
1	IVb	200	6/91/3	-	-
2	IVa	270	10/83/8	10/30/60	1.28
3	IVa	336	6/77/16	-	-
4	IVa	314	6/78/16	-	1.38
5	II	302	81/18/2	48/41/10	0.26
6	II	98	76/18/6	15/13/72	1.63
7	I	136	88/ 9/3	31/33/36	0.98

---

[1] Locations are shown in Fig. 5-54.

[2] Glacial advances I-IV are those of Onion Valley, in order of decreasing age. They correspond to: (I) a pre-Wisconsin glaciation; (II) Tahoe stage; (III) Tenaya stage; and (IV) Tioga stage.

[3] Granodiorite Weathering Ratio. The percent of heavily weathered, lightly weathered, and fresh boulders (see Ch. 2).

[4] Number of boulders counted for GWR.

[5] Boulder burial on relief on the surface. The percent of largely buried, partly buried, and exposed boulders (see Ch. 2).

[6] Boulder Frequency Count . The number of boulders per m^2.

although the evidence was indirect. No scarp was found, but the crest of the right-lateral moraine I was 17 m lower than the crest of the younger moraine II 60 m to the north. Clark (1972) has argued that elsewhere in the eastern Sierra Nevada such displacements may be due to downfaulting of the older moraine. At Taboose Creek, a paradox is presented by the left-lateral moraines: the crest of the older moraine (I) was 19 m higher than the crest of moraine II. However, the left-lateral moraine I was preserved only close to the range front, while the right-lateral moraine was found only 250 m or more east of the range front, where it emerged from the outer flank of the higher moraine II. A height difference of 36 m between lateral moraines of the same age is too great to be readily explained by irregular glacial deposition, and it seems probable that normal faulting was responsible. If this is correct, the fault must lie east of the remnant of the left-lateral moraine I and west of the remnant of the right-lateral moraine. The left-lateral moraine II is lower than the older moraine either because the snout of the advance II glacier did not extend as far from the range front as the earlier glaciers of advance I, so the moraines were near the terminus, or because erosion lowered the bed of Taboose Canyon ~ 19 m between advances I and II. This probably implies an interval of at least several tens of thousands of years. Downfaulting of 36 m between advances I and II would have produced the relationships observed today. If this did happen, offset on the same fault has not recurred since the advance II moraines were deposited. Thus, as at Sawmill and Goodale Creeks, faulting at Taboose Creek may be grossly episodic, with long quiet periods separating periods of activity.

The Age of Volcanism at Taboose Creek

The cinder cones nearest Taboose Creek were found 2 km to the southeast. Red Mountain, a 170-m-high cinder cone, rises from the alluvial fan 5.5 km to the northeast. Basalt flows were found on the fan downhill from both vents.

No volcanic cinders were found on the moraines of advance II. However, absence of lapilli this far from the vents is not conclusive evidence that volcanic activity predated advance II. Basalt cobbles were found on the younger outwash just east of the left-lateral moraine, as well as on the pre-Wisconsin moraine, but as mentioned above, these may have been carried there by Indians.

Some of the lava flows south of Taboose Creek appear to have been partly buried by fanglomerates of late- and mid-Wisconsin age. This would indicate an age in excess of perhaps 40,000 y. Radiometric dating of the basalt gave an apparent age of 70,000 ± 80,000 (2σ) y (Ch. 4). Bateman (1965) argued that Red Mountain also predated deposition of the upper layers of the Red Mountain Creek fan. He felt that an age of several tens of thousands of years was indicated also.

Darrow (1972) noted fresh-appearing lavas south of Taboose Creek, and argued that these were the youngest in the vicinity. Some of these could possibly be latest Pleistocene or even younger.

Shingle Mill Bench

If Taboose Canyon was host to early Pleistocene glaciations, no direct evidence is preserved in the canyon or on the alluvial fans. Taboose Creek has cut ~ 490 m through benches on the range front. At the erosion

rate at Coyote Creek, this would have taken 1.4 my. If at one time Taboose Creek debouched onto these benches, then ancient moraines might be found there. However, on Shingle Mill Bench (south of Taboose Creek) no such deposits were found. Thus if ancient glaciations did occur, there may already have been a deep gorge cut through the benches such that the glaciers did not overflow onto the benches.

This situation is analogous to that of Sawmill Canyon, where Dalrymple (1964) argued that there were no early Pleistocene glaciers. However, Bateman (1965) has reported Sherwin till at Tinemaha Creek, only 5 km north of Taboose Creek. Thus it is hard to invoke differential displacement or climatic boundaries as a mechanism to explain the apparent absence of ancient glaciers in Taboose Canyon. It is probable that any evidence has simply been eroded.

5.10 SUMMARY AND CONCLUSIONS

The Quaternary geology in the study area was naturally divisible into three categories: (1) construction of the alluvial fans east of the range front; (2) glacial geology and geomorphology of the canyons draining eastward from the Sierra crest; and (3) tectonic processes along the range front. Additionally, scattered relicts of the pre-uplift terraine gave clues to the nature of the Sierra Nevada before the Quaternary Period.

Alluvial Fans

Alluvial fans in the study area extend about 9 km east from the base of the Sierra escarpment to their distal ends in alluvium from the Owens River. Consistently, the fan heads have been incised as much as 20 m, and aggradation since the latest Pleistocene Epoch has occurred some distance from the range front. Incision appears to have begun during the middle of the Wisconsin glaciation, and deposition on the fan heads seems to generally date from the beginning of the Wisconsin glaciation (Tahoe stage). This pattern has also been reported by Lubetkin (1980) for the Lone Pine Creek fan. The volume of fanglomerate deposited during the Wisconsin glaciation seems to have declined in the later glacial advances. Perhaps this reflects the deep weathering and the large amount of easily eroded material in the mountain canyons at the end of the Sangamon interglacial stage. During subsequent short interstadial periods, such a large quantity of debris was not produced.

Aggradation of the alluvial fans since the Sangamon interglacial

period has not been great. Heavily weathered pre-Wisconsin fanglomerate was found in hollows sheltered from deposition, less than 10 m below the Wisconsin fan surface. Ancient fan surfaces were also exposed on the lateral margins of some fans. At the North Fork of Oak Creek such fanglomerate was found overlying a basalt that was probably 1.1 my old, and aggradation throughout much of the Pleistocene Epoch appears to have been no more than a few tens of meters. Yet from the depth of wells and from seismic exploration data, the total thickness of the fans must exceed 275 m. It must be concluded that the fans aggraded more rapidly soon after subsidence of the Owens Valley began, perhaps 6 my ago, and that the rate has slowed during the Quaternary Period. Alternatively, this could be in response to increased subsidence of the Owens Valley east of the mid-valley fault zone during the Pleistocene Epoch, so that for a time most debris was simply shuttled across the fans and deposited in the forming graben. At the present strain rate of 2.2 mm/y (Savage et al., 1975), all 1100 m of bedrock relief on the mid-valley fault zone near Independence could have been produced in the last 0.5 my. Late Pleistocene aggradation rates estimated for the Independence Creek and Oak Creek fans were 0.1 - 0.2 mm/y.

Glacial Geology and Geomorphology

Pleistocene glaciations

Typically, a single pre-Wisconsin glaciation and multiple Wisconsin advances were recognized in the study area. The pre-Wisconsin moraines were characterized by a well preserved form and heavily weathered till. The morainal form suggested that these tills postdated the Sherwin

glaciation. Radiometric dating of interbedded lavas at Sawmill Canyon confirmed this assessment, showing that the glaciation occurred sometime between 131,000 and 463,000 y ago. Acoustic wave speeds through boulders exposed on the moraine crests suggested that the actual age was closer to the upper (older) limit. At Independence Creek, acoustic wave-speed data again suggested that the oldest glaciation (advance I) predated the Wisconsin glaciation by a considerable amount.

Acoustic wave-speed data presumably reflect to some extent climate-controlled weathering rates, which probably differ during interglacial and glacial periods. Such complexities cannot now be accommodated in estimating ages from these data, and the model ages are therefore suspect. Thus it is not possible to ascertain whether the various moraines assigned to advance I are from the same or different pre-Wisconsin glaciations.

Moraines of the Sherwin glaciation were found nowhere in the study area, but Bateman (1965) recognized them as far south as Tinemaha Creek, only 5 km to the north. Both Bateman (1965) and Fleisher (1967) mapped extensive Sherwin moraines in the foothills at Big Pine Creek, 12 km farther north. It seems unlikely that extensive glaciers extending below the range front at Big Pine Creek could have developed without contemporary glaciers in similar environments a few km away. Hence it seems probable that the Sherwin moraines were eroded from the much steeper canyon walls in the study area. Sherwin glaciers may never have extended below the foothills to the fans near Oak Creek, or may not have pushed below the range front at Sawmill Creek. Sherwin-age till may have been reworked or deposited directly on the fan heads within the foothills, but these have largely been eroded now. The presence of resistant boulders

with parallel grooves and arcuate gouges in patches of ancient diamicton within the foothills supports this possibility.

Moraines of the Wisconsin glaciers were found in each canyon studied. The oldest moraines were heavily eroded and were covered by clay-rich till containing numerous grusy boulders or boulders with case-hardened surfaces. These moraines were assigned to advance II (Tahoe stage) and were easily distinguished from the younger Wisconsin moraines.

The youngest moraines were only lightly eroded. Terminal moraines were breached, but were generally not completely eroded. Lakes were generally not developed behind the terminal moraines, but where they were, they have been filled and are now meadows. Streams have cut only shallow channels upstream from the terminal moraines, which were assigned to advance IV (Tioga stage). Tills contained numerous boulders on which original glacially abraded surfaces were preserved. Virtually no disintegrating clasts were found. Soil development was minimal.

In most valleys more than one moraine shared the weathering characteristics of the youngest moraine. These were apparently created during the same stage. In some canyons, other moraines of intermediate character between Tioga and Tahoe moraines were recognized. These were assigned to the Tenaya stage (advance III). However, in the best preserved sequences of moraines, those of the Tenaya stage were only marginally separable from adjacent moraines of the Tioga stage. The pattern seemed to indicate more or less continuous glacial advances and retreats since mid-Wisconsin time. Thus Burke and Birkeland (1979) could be justified in regarding the Wisconsin glaciation as consisting of only two stages. At stake is the significance of the interstadial periods: did the glaciers retreat to

the cirques or disappear completely; was the duration of the retreat sufficient to merit recognition; and can the moraines of one advance be distinguished from those of other advances? Certainly relative dating of individual moraines from poorly preserved sequences is incapable of addressing the first two points. My study shows that adjacent moraines of the same stage may often be distinguished, but suggests that correlation of moraines from valley to valley is less certain.

Even recognition of Tahoe moraines among different valleys is not always straightforward. In particular, there seems to be a tendency among researchers to overestimate the age of moraines in the study area from the degree of weathering. Perhaps this is because most researchers have gained their initial experience conducting studies north of Owens Valley or west of the Sierra Crest. In these regions, Tahoe moraines appear to be more heavily weathered than those on the margins of the Owens Valley (e.g., Green Creek, Ch. 3; Sharp, 1972; Burke and Birkeland, 1979). Perhaps this may be attributed to the lesser rainfall in Owens Valley. Colman and Pierce (1981) found weathering rind thickness on volcanic clasts of the same age to be proportional to rainfall. Burke and Birkeland (1979) have estimated the mean annual precipitation of Sawmill Canyon to be 35 cm, compared to 45 cm at Bloody Canyon and 40 cm at Green Creek. Curiously, though, two studies in the Sierra Nevada which have addressed the issue of variation in weathering parameters with elevation failed to detect trends (Birman, 1964; Fleisher, 1967). Because of the decrease in rainfall from west to east across the Sierra Nevada, parallel to topographic gradient, these studies would seem to contradict the subsequent findings of Colman and Pierce (1981). This important question is thus

unresolved.

Acoustic wave speeds through weathered clasts in Pleistocene moraines showed a pronounced decrease with age. Unlike the pattern observed farther north at Green Creek, where the formation of case-hardened surfaces caused an increase in wave speeds for very old moraines, the decrease, at least at Sawmill Creek, appeared to be simply proportional to the logarithm of the age. The standard deviation for samples of boulders did not vary strongly as a function of age. Measurement of acoustic wave speeds proved to be a powerful relative dating technique which permitted statistical discrimination of moraines of different stages, and perhaps even of moraines of different advances in the same stage.

Holocene Glaciations

Three neoglaciations were recognized in the study area. These were distinguished by weathering characteristics, vegetative cover, and moraine morphology. The Holocene glaciations, identified in order of decreasing age, were labelled as advances V, VI, and VII in Onion Valley. These probably corresponded to the Hilgard, Recess Peak, and Matthes glaciations of Birman (1964), respectively.

Moraines of advance V were generally quite small, and were not recognized in canyons where steep terrain made construction and preservation difficult. Lakes impounded behind moraines or tarns in terrain last covered by the Hilgard glaciers were clear and generally were sedimented only near inlets, although exceptions were observed. In Onion Valley, filled lakes seemed to be located at junctions of streams, so that they received sediment from two or more sources. Stream incision through Hilgard terminal moraines was only one or two meters. Moraines were

typically forested. Generally, weathering of exposed boulders was indistinguishable from weathering in Tioga moraines. Only in Armstrong Canyon was the "weathering reversal" of Birman (1964), in which Hilgard moraines had fewer fresh boulders than Tioga moraines, suspected. In part, this could be due to poor exposure. In Onion Valley, acoustic wave speeds were generally higher for boulders in Hilgard moraines, contrary to the expectation for more highly weathered boulders. However, the standard deviation was also higher, and this may reflect a greater proportion of weathered boulders mixed with quite fresh ones. Acoustic wave speeds were measured for too few neoglacial moraines to permit generalization, but the absence of a "weathering reversal" in the acoustic wave-speed data may illustrate a strength of relative dating by this method: V_p may have a simpler time dependence than conventional measures of weathering, such as the granodiorite weathering ratio. Perhaps this is because for young boulders V_p is reduced by diurnal thermal cycling and microfracturing, independent of chemical weathering, as suggested in Ch. 3.

Recess Peak moraines were found in or just below cirques. Stream erosion was minimal. Till of this age was well consolidated, and boulders did not roll underfoot. Lichens were found on most rocks, with colonies of yellow-green lichens as large as 25 cm. Sedges were common, but trees were rare. The contrast in vegetation with the older moraines was thus marked.

Boulder weathering data were of little practical use in distinguishing Recess Peak from Hilgard moraines because of the obvious differences in vegetation. Nevertheless, a greater number of unweathered boulders were found in Recess Peak moraines. The contrast may have been the greater because of the unusual number of heavily weathered boulders in Hilgard

moraines (Birman, 1964). Acoustic wave speeds for the young neoglacial moraines were greater than for the Hilgard moraines. The standard deviation was also larger than that for the Hilgard moraines. The increase in standard deviation was not due to Birman's "weathering reversal" alone, but to some other factor such as distance of transport.

Matthes moraines were restricted to cirques beneath the highest peaks. There has been virtually no stream erosion, even in favorable locations. Moraines were unstable and supported virtually no vegetation. They are generally active or at least ice-cored rock glaciers today. Although most boulders are unweathered, none has an abraded surface, because of the short transport distance.

In several locations neoglacial moraines of intermediate characteristics were observed. For instance, in the main fork of Independence Creek and in Armstrong Canyon, relatively stable Matthes moraines with 2-cm-diameter yellow-green lichens were found. The lichens indicate an age of several hundred years (Curry, 1968). Thus as suggested by Curry, three discrete neoglacial advances may be too simple an interpretation of Holocene glaciation.

Maximum extent of glaciers in the study area

Table 5-24 lists the elevations of the snouts of glaciers of different advances in the study area and in canyons elsewhere in the eastern Sierra Nevada. Where terminal moraines have been eroded, the elevation of the stream between the lowest preserved lateral moraines is shown. Only the pre-Wisconsin and Tahoe moraines breached the range front. The lowest moraines were observed at Independence Creek, the southernmost part of the study area, at an elevation of 1890 m (6200 ft). No trends in

Table 5-24

Minimum Elevations of Glaciers in the Study Area and Other Selected Canyons of the Eastern Sierra Nevada

Canyon	Latitude at Canyon Mouth	Glaciation (Elevation of Glacier Snout in Meters) I pre-Wisconsin	II Tahoe	III Tenaya	IV Tioga	V Hilgard	VI Recess Peak	VII Matthes	Unspecified Wisconsin
Green[1] *	38°10'10"	2195††	2070	2135	2170	-	-	-	-
Bloody Canyon[2] *	37°54'19"	2135	2220	2245	2325	-	-	-	-
McGee[3]	37°34'52"	-	-	2135	-	-	-	-	-
Pine †	37°24'52"	-	-	-	-	-	-	-	1525
Big Pine[4]	37° 9'28"	-	1525	-	-	-	-	-	-
Taboose*	37° 0'19"	<2010	2010	-	2255	2805	3050	3290	-
Goodale*	36°57'38"	-	1950	-	2135	2620	3230	3475	-
Armstrong*	36°57'25"	<2075	2080	2170	2375	2805	3050	3170	-
Division †	36°55'04"	-	-	-	-	-	-	-	2440
Sawmill*	36°54'43"	<2225††	2050	<2375††	2195	2595	3080	3415	-
Sawmill tributary*	36°54'37"	-	-	-	2440	2901	-	-	-
Black †	36°52'27"	-	-	-	-	-	-	-	2315
Thibaut †	36°51'28"	-	-	-	-	-	-	-	2805
North Fork Oak tributary*	36°51' 2"	-	-	-	2535	2955	3110	-	-
North Fork Oak*	36°50'39"	-	<2010	2135	2375	2805?	3290	3535	-
South Fork Oak*	36°48'50"	<2075	2135	-	2220	2620	3290	3385	-
Sardine*	36°48'29"	-	<2120	2170	2610	-	-	-	-
Onion Valley*	36°47'14"	<1890	<1940	2145	2540	2750	3215	3355	-
Lone Pine †	36°35'35"	-	-	-	-	-	-	-	2100
Cottonwood Basin †	36°27'50"	-	-	-	-	-	-	-	2835

* This study
† Moraines identified from aerial photographs or topographic maps
[1] Sharp, 1972
[2] Sharp and Birman, 1963
[3] Clark and Gillespie, 1981
[4] Bateman, 1965

†† Only a small segment of the moraine was preserved

elevation with latitude were observed, and comparable moraines as far north as Green Creek attained a similar elevation. South of the study area there has been no careful inspection of moraines on the range front, but the lowest Pleistocene moraines visible on aerial photographs are at comparable elevations. Only from Lone Pine Creek south to Cottonwood Basin, the southernmost glaciated canyon of the Sierra Escarpment, did the elevation of the glacier snouts rise.

The Wisconsin glaciers of the Tahoe stage descended to about the same elevations as the pre-Wisconsin glaciers of advance I. The lowest moraines in the study area were found from 1940 m to 2135 m elevation. Again, there were no systematic trends with latitude.

The younger Wisconsin glaciers generally left well preserved moraines, and the snout elevations could therefore be accurately estimated. Where well preserved Tenaya moraines were found, the glacier snouts appear to have reached down to 2135 m - 2170 m elevation in the study area. Farther north, Tenaya glaciers descended to 2135 m - 2245 m elevation.

Tioga moraines descended to a wider range of elevations, from 2135 m to 2610 m. Some of this scatter may have resulted from misidentification of Tenaya moraines, and the highest snout - - in Sardine Canyon - - was anomalous, probably because of the small size of the canyon. Nevertheless, even the canyons with the best preserved Tioga moraines - - Taboose Creek, Armstrong Creek, the North and South Forks of Oak Creek, and Independence Creek - - showed large differences in the snout elevations. Perhaps this was due to the tendency of the late Wisconsin moraines to end in the steepest sections of the canyons. Tioga moraines in the northern Sierra descended to elevations of 2170 m - 2325 m. Thus late Wisconsin moraines, like their predecessors, showed no trends in elevation with latitude.

Neoglacial moraines were found only at high elevations. Hilgard glaciers descended to elevations from 2590 m to 2805 m. As for Tioga moraines, the variability probably was due to the steep terrain. Moraines of the Recess Peak and Matthes advances were found only near the Sierra crest, descending to elevations of 3050 m - 3290 m and 3170 m - 3535 m, respectively.

Ancient Surfaces

Throughout the study area remnants of ancient erosion surfaces were preserved. These could be grouped into three classes by elevation and by relation to the modern topography. The highest remnants were found only on peaks, such as Mt. Baxter (4000 m), Striped Mtn. (3933 m), or Mt. Gould (3964 m). These relict erosion surfaces were as much as 600 m above the modern cirques. None bore an ancient diamicton; instead frost-shattered bedrock lay under a thin layer of rubble derived in situ.

On ridges and high passes were the second group of relict surfaces. These were typified by the northeast ridge of University Peak, the upper reaches of Sardine Canyon, and the pass from Goodale Canyon to Taboose Canyon. The elevation was about 3650 m, and these surfaces were generally about 300 m above the modern cirques. More extensive than the oldest surfaces, these remnants were clearly related but not necessarily conformable to the present topography. They supported thick, weathered diamictons which may have been glacial in origin.

Neither of the two old groups of erosion surfaces was heavily glaciated during the late Pleistocene. The third group of surfaces conformed closely to the modern topography. The surfaces were at roughly 3500 m elevation, no more than 150 m above the modern cirques. Taboose

Pass and Sawmill Pass were typical members. The southern cirque of Goodale Canyon probably belongs with this group. These surfaces were clearly sculpted glacially, but not recently. The age of the glaciers which were responsible could not be determined, but they were probably pre-Wisconsin. The glaciers need not be as old as the erosion surface they modified. The surfaces, especially that at Taboose Pass, were probably glaciated repeatedly, even during the Holocene Epoch, but the recent glaciers have had little effect on the topography.

The three groups of surfaces have obvious parallels in the erosion surfaces of Matthes (1960, 1950) in the San Joaquin Basin to the north and in the Kern Basin to the south. In the terminology of the Kern Basin, the surfaces identified in this study probably correspond to the Whitney or Cirque Peak erosion surface, to the Boreal Plateau erosion surface, and to the Chagoopa Plateau erosion surface, respectively. Matthes thought that the Chagoopa plateau surface predated the last uplift of the Sierra, and was created during the Pliocene Epoch. Glaciation of this surface must have postdated at least the beginning of the Plio-Pleistocene uplift, but was probably early Pleistocene in age. If it was younger, stream erosion would already have incised the valleys of the Pliocene surface, and the subsequent glaciers would have created U-shaped troughs within the broad valleys instead of modifying the valleys themselves. A younger generation of glaciers has done just that in the late Pleistocene Epoch. This is especially obvious in the headwaters of the south fork of the Kings River, west of Taboose Pass.

Matthes (1960) felt that the Boreal Pleateau erosion surface was created during the Miocene Epoch. This age appears to be excessive for the equivalent surfaces of University Peak and Sardine Canyon; these

probably formed after the Owens Valley began subsiding, perhaps 6 my ago (Giovannetti, 1979; Bacon et al., 1979). If the diamictons on these surfaces were actually till, then a second and older ancient glaciation may be indicated. However, as Huber (1981) points out, because of the rapid uplift of the central Sierra Nevada during the Pleistocene Epoch, it is unlikely that the mountains (at least at latitude 37°30') were high enough to support glaciers before the end of the Pliocene Epoch or even later. Glaciation of the old surfaces in the southern Sierra appears to contradict that conclusion. Either the southern Sierra attained roughly their present elevation before the central Sierra (cf. Crough and Thompson, 1977), or glaciation occurred well after the old surfaces were formed. Because at least two episodes of erosion are involved, it is difficult to see how the Goodale - Taboose col could have been glacially cut after the Taboose Pass (Chagoopa ?) erosion surface had formed.

Wahrhaftig (1965) argues that the erosion surfaces of Matthes can be explained by continuous rather than episodic erosion in granitic terrane, and that correlation of such surfaces may be spurious. If this is true, then the correlation of the erosion surfaces identified in this study with those of Matthes may have no validity, but the local relationships are are still significant.

Inconsistent degrees of weathering of the old diamicton

The diamictons on the remnant erosion surfaces on the northeast ridge of University Peak, in Sardine Canyon, and on the southern cirque of Goodale Creek were similar. In each case the transition from bedrock or shattered bedrock to the overlying debris was abrupt. This thick diamicton differed from the thin layers of rubble described by Matthes

(1950, 1933) in the high fraction of small particles of a wide spectrum of sizes, from silt to coarse sand and pebbles. Especially the diamicton in Goodale Canyon appeared to be a till. However, the weathering characteristics of the University Peak diamicton appeared to be inconsistent with its relative age deduced from correlation with the erosion surfaces of Matthes (1950, 1960). The problem was that although boulders were oxidized and disintegrating, the soil itself had little clay, and pebbles and sand grains had only a light coating of clay. In contrast, tills of advance I were heavily laden with clay. Furthermore, the diamictons of Sardine and Goodale Canyons were strongly weathered, especially at a depth of several meters. Perhaps the answer may be found in the Goodale Canyon remnant: the upper layers of the diamicton on this surface were clay-deficient, just as at University Peak. The removal of clay from the surface of the diamicton may accompany nivation (cf. Matthes, 1900), possibly through percolation of snow melt.

Erosion surfaces at the range front . . .

Erosion surfaces found on the foothills at the range front dated from 1.2 my BP and earlier. Assuming constant erosion rates, the highest surface may have been formed during the Pliocene Epoch, and may thus correlate with the Chagoopa erosion surface of Matthes.

At least two other lower surfaces could be recognized in the foothills between the forks of Oak Creek. These are roughly 180 m and 275 m lower than the upper surface. Their origin is uncertain: they may have been cut after the highest surface as the Owens Valley subsided during the Pleistocene Epoch, or they may be part of the highest erosion surface offset by faulting. A fourth erosion surface capped by lava 1.2 my ago

was certainly cut into the older surfaces. It conceivably could have graded to the lowest of the three surfaces discussed above.

Weathered diamictons were found scattered throughout the foothills. Only one of these, near the mouth of the South Fork of Oak Creek, was on the highest erosion surface. This deposit, which contained metavolcanic clasts which may have been glacially abraded, could have been deposited long after the surface was formed. Other deposits were fanglomerates which were stranded by faulting along the range front or by subsidence of the graben in the central Owens Valley and incision of the foothills.

Volcanic Activity

The study area included the southern part of the Big Pine volcanic field. Basaltic lavas appear to have been erupted periodically throughout most of the Pleistocene Epoch. The earliest lavas were found at the North Fork of Oak Creek and on Sawmill Point. Moore (1963) thought that the basaltic dikes on Sawmill Point may have been emplaced late in the Pliocene Epoch, but these have not been dated. The early lavas in the foothills around the North Fork of Oak Creek were dated at about 1.1 my and 1.2 my for the present study (Ch. 4).

The most complete record of volcanism in the study area was at the North Fork. In addition to the ancient ridge-top lavas, other basalts were found on terraces 52 m above the modern stream and possibly also on terraces 37 m above the stream. These were not dated, yet younger lavas were found underlying Tahoe moraines and younger Wisconsin moraines, only a few meters above the modern stream. A tentative date on one of these was roughly 0.2 my. Thus perhaps four or five eruptions have occurred

during the last 1.2 my.

At Sawmill Canyon, there appear to have been at least three major eruptions during the Pleistocene Epoch. Two of these were from vents well west of the range-front faults. These were dated for this study at ~ 0.46 my and 0.12 my. A later cycle of eruptions along the range-front fault was responsible for the cinder cones on either side of the mouth of Sawmill Creek. This event was not dated, but probably occurred after the Tahoe stage of the Wisconsin glaciation and before the Tenaya or Tioga stages. Its age is thus estimated to be about 0.05 my.

North of Sawmill Creek, volcanism was restricted to the range front or Owens Valley, and was probably roughly contemporaneous with the range-front eruptions at Sawmill Canyon. The most significant date would be of the lavas at the mouth of Goodale Creek, for these would provide an upper limit to the age of the Tahoe stage of glaciation.

Nowhere in the study area was there clear evidence of volcanic activity more recent than the middle of the Wisconsin glaciation. The youngest lavas were found on the Taboose Creek fan; these could even be Holocene, based on their evident lack of weathering, but there is no direct evidence to support this contention.

Faulting

The range-front fault

The most important fault in the study area was the Independence Fault, along which as much as half of the subsidence of the Owens Valley has occurred. This fault was located at the base of the range front, between the Sierra Nevada and the foothills. About 1800 m of

offset (east side down) has occurred here since the Owens Valley began forming, probably in the Pliocene Epoch about 6 my ago. The average offset rate is thus ~ 0.36 mm/y, but this has probably not been constant throughout that time.

Young scarps on the Independence Fault were found from Independence Creek to Charlie Canyon, north of the North Fork, and between Black and Sawmill Canyons. Faulting at the mouth of Sawmill Creek itself was inferred from the truncation of 0.12-my-old intracanyon lava flows at the range front. North of Sawmill Canyon the fault itself is probably discontinuous. Minor scarps near the range front were found on the cinder cones north of Goodale Creek, on Shingle Mill Beach, and north of the study area near Red Mountain Creek. Faulting was inferred at Taboose Creek from discordant heights of moraine crests.

Only at Independence Creek did the scarp cross enough deposits of different and known ages to establish an offset rate. Here faulting has extended into the Holocene Epoch. The best estimate for the late Pleistocene offset rate was 0.12 mm/y. Assuming the worst conceivable errors in relative dating, this rate was still less than 0.2 mm/y - - well under the average for the Quaternary Period of ~ 0.36 mm/y.

Elsewhere on the range-front faults, Holocene scarps were noted only south of Sawmill Creek and near Shingle Mill Bench. From Sardine Creek to Thibaut Creek, and from Armstrong Creek north to Taboose Creek, even early Wisconsin moraines were apparently unbroken by faulting. Thus adjacent sections of the range-front faults have had different levels of activity for periods of 65,000 y or more.

If the truncated intracanyon lava flow at Sawmill Creek truly reflects range-front faulting, then an average late Pleistocene offset

rate of 0.5 mm/y is implied. This is considerably greater than at Independence, only 14 km to the south. Thus the rate of faulting seems to be variable over short distances, and differences seem to be maintained for periods of time as long as 0.12 my. In fact, the offset of the Tahoe fan deposits suggest that the faulting rate at Sawmill Creek was much higher from 0.12 my to ~ 0.065 my ago than from 0.065 my ago to the present. This same pattern was observed at Taboose Creek, where moraines of advance I were offset 36 m but Tahoe moraines were unfaulted. Thus at any given time, different segments of the range-front faults are active, and the active segments appear to change their levels of activity on a time scale of tens of thousands of years.

Other fault zones

Given the tectonic environment of the Owens Valley, it is reasonable to suspect that a fault zone parallel and intermediate to the Independence Fault and the Owens Valley fault zone (east of Independence) might bound the foothills found from Symmes Creek on the south to Black Creek on the north. This may be the case, but there is no evidence of any faulting of the fan surfaces which must cross the suspected fault. Thus there seems to have been little or no activity in the past 50,000 y or so. Although normal faults within the foothill block do appear to have been active during the past 1.2 my, the total proven offset along them in that time is not more than a few tens of meters. It is possible that the stepped character of the foothills is due to faulting, although other explanations are possible. If faulting is responsible, total offset on the order of 600 m may have occurred during the Quaternary Period - - an order of magnitude less than on the range-front faults. Again, faults within the

foothill block were not observed to have offset Wisconsin or Holocene fans, outwash, or terraces, (except at the South Fork of Oak Creek), so that recent activity has been minimal.

Comparison of faulting rates to those elsewhere in the eastern Sierra

From Mt. Tom to Olancha Peak, a distance of 150 km, the Sierra escarpment is about the same height as in the study area. If the depression of Owens Valley began at about the same time over its whole length, then offset rates on the range-front faults must be comparable - - from 0.6 mm/y to 0.36 mm/y, depending on when subsidence began (3 to 6 my ago; cf. Huber, 1981; Giovannetti, 1979). The other major zone of faulting in the western half of the Owens Valley, the mid-valley fault zone, has experienced total vertical offset (east side down) of less than 1100 m near Independence, increasing to 2440 m south of Lone Pine (Pakiser et al., 1964). Bedrock relief across the fault is masked by deep alluvium. Savage et al. (1975) have geodetically determined a modern strain rate of 2.2 mm/y which seems to be localized on the Owens Valley fault zone. This rate, an order of magnitude greater than the modern rate on the range-front fault, could account for the entire bedrock offset within the last million years or so. Thus either the mid-valley faults are younger than the range-front faults, or the strain rate of Savage et al. (1975) is significantly greater than the long-term average.

Offset rates for the eastern Sierra Nevada have also been determined north of the Owens Valley, around Long Valley and Mammoth Lakes. According to Huber (1981), the gross offset rate across the eastern side of the Sierra near Deadman Summit (north of Mammoth Lakes) has been about ~ 0.37 mm/y during the Pleistocene Epoch. Bailey et al. (1976) have determined

a vertical offset rate of ~ 0.4 mm/y for the Hartley Springs Fault, also near Mammoth Lakes, during the last 0.7 my. Rinehart and Ross (1964) found Tioga moraines at McGee Creek were broken by the Hilton Creek Fault. The offset of 25 m implies a late Quaternary offset rate greater than 1.0 mm/y. Clark and Gillespie (1981) measured the offset on progressively older moraines and found that this rate roughly applied throughout the entire Wisconsin glaciation. Late Pleistocene offset rates on the Sierra escarpment near Independence, then, were generally less than those near Mammoth.

The Sierra escarpment

Throughout the study area prominent triangular facets or truncated ridges of the escarpment on the east side of the Sierra Nevada were identified. As shown in Plate II, there were generally two rows of facets, with apices at different elevations. Locally, smaller facets could be seen near the base of the escarpment, but the range front was dominated by the two giant bevels defined by the larger facets.

Although the elevation of the apices was quite variable, the height of the facets was relatively constant. The upper zone was typically about 950 m high; the lower was about 750 m high. The slope of the upper bevel at ~ 22° was noticeably less than the slope of the lower bevel, at ~ 25° or more. These zones of facets ridges suggest that vertical offset across the range front was grossly episodic, with most of the displacement occurring in two periods separated by a long hiatus. Faulting rates during the active periods must have been significantly higher than today, or else the full 1700-m offset could not have been achieved in the 6 my or less since the Owens Valley began subsiding. Thus we may be in a second hiatus in faulting today, with most displacement currently

occurring in the mid-valley fault zone.

The elevation of the top of the higher bevel in the escarpment does not vary with the elevation of the Sierra crest, which is fairly constant throughout the study area. The elevation difference varies from essentially zero to as much as 685 m. Low-angle ridges connect the apices of the higher zone facets to the peaks of the Sierra Crest. The average gradient of these high ridges is less than 10°, but especially around Sawmill Creek, they have peaks which themselves are as high as the Sierra crest. The impression given is that before the inception of rapid faulting along the range front, the Sierra crest was a broad upland of perhaps only a few hundred meters relief. The site of the Owens Valley may well have already been a shallow depression at that time.

Erosion Rates

Erosion rates near Mammoth Lakes of 0.3 - 0.6 mm/y are inferred from the downcutting of McGee Creek ~ 850 m since the McGee glaciation (cf. Blackwelder, 1931; Christensen, 1966). The range reflects uncertainties in the age of the glaciation. Till of the McGee glaciation is generally thought to be 2.0 - 2.6 my old (cf. Curry, 1968), but Huber (1981) has argued that it may be as young as 1.5 my. Rates of 0.15 - 0.33 mm/y are inferred from the downcutting of Coyote Creek 240 m since the Sherwin glaciation (Bateman, 1965).

Erosion rates in the study area were at least 0.16 mm/y within the foothills at Oak Creek, and 0.13 - 0.16 mm/y within the Sierra Nevada at Sawmill Creek. These consistent rates on either side of the range-front fault argue that the base level of the streams draining the escarpment may have been controlled by down-faulting along the mid-valley fault

zone. The erosion rates are close to the lower limit of the estimate at Coyote Creek. The Coyote Creek rate could be higher than rates for the escarpment in general because of local deformation during the Pleistocene (cf. Bateman, 1965). Although the upper limit at Coyote Creek is compatible with the lower limit at McGee Creek, it is clear that erosion at McGee has been considerably faster than in the study area.

Geologic History

The geologic history of the study area presented below is a synthesis of the conclusions of this study and of other studies of adjacent areas as discussed above. The history is given in an assertive format, although the chronology is still uncertain. The reconstruction especially of the Tertiary and early Pleistocene history is speculative.

During the Miocene and early Pliocene Epochs the Sierra Nevada was a broad upwarp of a few hundred meters relief (Matthes, 1950). Even then, older erosion surfaces were preserved on ridges and peaks. Uplift accelerated throughout the Pliocene Epoch (Huber, 1981), and about 6 my ago the axis or eastern flank of the upwarp began subsiding (Bacon et al., 1979) along northwest-southeast normal faults. The zone of subsidence was already a valley when rapid faulting began (Matthes, 1950). Low-gradient streams incised the forming escarpment, defining much of the modern drainage pattern. Among these streams were Sardine Creek and Independence Creeks. Their ancient valley walls and floors are now seen on University Peak and in upper Sardine Canyon. Although only a 1-km segment of the ancient Sardine Canyon is preserved today, the ancient stream appears to have been graded to the base of the upper bevel of the escarpment. Some

of these valleys may have been glaciated, and were filled with diamictons as much as 20 m thick. The pass from Goodale to Taboose Canyon, which dates from this period, clearly was glaciated. Thus glaciation in the southeastern Sierra Nevada may have occurred by the time the Owens Valley had subsided to only half of its present depth. This is much earlier than previously recognized, but the actual age is only conjectual. If subsidence began 6 my ago (Giovannetti, 1979) and proceeded at a constant rate, glaciation must have occurred roughly 3 my ago, at the end of the Pliocene Epoch. This is about the age of the earliest glaciations suspected in the Sierra Nevada (Curry, 1966, 1971). At the time of this early glaciation, the Sierra must already have achieved most of its present height (cf. Huber, 1981). Thus tectonic activity during much of the Pleistocene has involved the subsidence of the Owens Valley rather than uplift of the Sierra Nevada. This pattern of uplift contrasts with that deduced by Huber (1981) for the Mammoth Lakes - San Joaquin River region. Huber (1981) saw evidence for accelerated uplift throughout the Pleistocene Epoch, with the Sierra Nevada becoming high enough to host glaciers only after ~ 1.5 my ago. Perhaps, as Crough and Thompson (1977) argued, uplift was earlier in the southern Sierra.

Although the Sierra Nevada was elevated to much of its present height by the late Pliocene Epoch, uplift continued throughout the Pleistocene. The erosion surface of Taboose Pass was cut at this time. If this surface can be correlated with the Chagoopa erosion surface of Matthes (1950), then this surface may be Plio-Pleistocene rather than Pliocene, as Matthes (1950) claimed. If, as Wahrhaftig (1965) claimed, such correlations are not possible, the evidence of ancient glaciations still has a local validity.

The erosion surface of Taboose Pass was also glaciated, prior to the final cycle of uplift and stream incision. The timing of these events is unknown, but by roughly 0.5 my ago the canyons of the escarpment had been cut down to essentially their modern levels, as shown by the presence of lava and till of about this age in Sawmill Canyon. The four or more major glaciations leaving the moraines found in the study area occurred after this time. An early glacier of this series advanced shortly after 460,000 years ago but well before 131,000 years ago, as determined by ^{40}Ar-^{39}Ar dating of interbedded lavas. The largest of these late Pleistocene glaciations advanced during the early Wisconsin or Tahoe stage, after the eruption of basaltic lava 120,000 years ago in Sawmill Canyon. Three of four advances occurred after the Tahoe glaciation. These are probably stades of the Tioga glaciation. The first of these appeared to be separated from the others by a longer interstadial period. This may be the Tenaya glaciation of Sharp and Birman (1963) and Birman (1964). During the Holocene Epoch small glaciers advanced short distances from the Sierra crest three or more times.

The Foothills

The position of the foothill block with respect to the Sierra upland at the time the uppermost surface of the foothills near Oak Creek was cut is uncertain, as is the age of the surface. Matthes (1950) felt that the similar erosion surface of the Alabama Hills was cut before subsidence of of the Owens Valley began. However, this surface could just as well have been part of the Owens Valley floor as part of the Sierra upland. By 1.2 my ago the foothill block had already been incised, probably as a consequence of subsidence along the mid-valley fault zone. Basalt erupted

repeatedly from vents on the range-front fault and within the range. This lava filled the canyons cut through the highest erosion surface. Incision of bedrock has been negligible during the last 0.1 my or so, and aggrading fans have penetrated the foothills to the range front itself. Partly, this may have resulted from large amounts of debris eroded early in the Wisconsin glaciation. Most fans were incised later in the Wisconsin glaciation. At least one earlier period of aggradation is indicated by thick fanglomerates atop the 1.2-my-old basalt and elsewhere in the foothills. Surprisingly, contemporaneous fan surfaces are still exposed in protected locations east of the foothills.

The range front

Faulting on the range front is now erratic and may have slowed considerably during the Pleistocene Epoch. In some canyons, even Tahoe moraines, older than ~ 65,000 y, are unfaulted while in adjacent valleys coeval moraines are vertically offset several meters. At the modern faulting rate at Independence Creek of <0.2 mm/y, the Sierra escarpment would have required more than 11 my to form, more than twice the age of the Owens Valley (Giovanneti, 1979). The lower facets would represent more than 5 my. Even at 0.5 mm/y, the highest faulting rate inferred for the range-front fault in the study area, the lower facets represent about 2 my.

If the geodetic strain rates of Savage et al. (1975) for the mid-valley fault zone represent an average rate for the Pleistocene Epoch, then the entire bedrock displacement along the mid-valley faults could have occurred in the last million years. It is possible that these faults became active only then. Transferral of much of the displacement

from the Independence Fault to a newer Owens Valley fault at that time is consistent with reduced faulting rates along the range front in the late Pleistocene Epoch.

References Cited

Bacon, C.R., Giovannetti, D.M. Duffield, W.A., and Dalrymple, G.B., 1979, New constraints on the age of the Coso Formation, Inyo, County, California, [abs]: Geol. Soc. America Abstracts with Programs, 11, No. 3, p. 67.

Bailey, R.A., Dalrymple, G.B., and Lanphere, M.A., 1976, Volcanism, structure, and geochronology of Long Valley caldera, Mono County, California: Jour. Geophys. Research 81, 725-744.

Bateman, P.C., 1965, Geology and Tungsten Mineralization of the Bishop District, California: U.S. Geol. Survey, Prof. Paper 470, 208 p.

Beaty, C.B., 1970, Age and estimated rate of accumulation of an alluvial fan, White Mountains, California, USA: Am. Jour. Sci. 268, 50-77.

Birman, J.H., 1964, Glacial geology across the crest of the Sierra Nevada, California: Geol. Soc. America Spec. Paper 75, 80 p.

Blackwelder, E., 1931, Pleistocene glaciation in the Sierra Nevada and Basin Ranges: Geol. Soc. America Bull. 42, 865-891.

Burke, R.M., and Birkeland, P.W., 1979, Reevaluation of multiparameter relative dating techniques and their application to the glacial sequence along the eastern escarpment of the Sierra Nevada, California: Quaternary Research 11, 21-51.

Christensen, M.N., 1966, Late Cenozoic crustal movements in the Sierra Nevada of California: Geol. Soc. America Bull. 77, 163-182.

Clark, M.M., 1967, Pleistocene Glaciation of the Drainage of the West Walker River, Sierra Nevada, California: Ph.D. thesis, Stanford University; University Microfilms, Inc., No. 68-0401, Ann Arbor, MI, 130 p.

Clark, M.M., 1972, Range-front faulting: Cause of anomalous relations among moraines of the eastern slope of the Sierra Nevada, California: Geol. Soc. America Abstracts with Programs, 4, p 137.

Clark, M.M., and Gillespie, A.R., 1981, Record of late Quaternary faulting along the Hilton Creek Fault in the Sierra Nevada, California [abs]: Earthquake Notes, Seismological Soc. America, v. 52, no. 1, p. 46.

Colman, S.M., and Pierce, K.L., 1981, Weathering Rinds on Andesitic and Basaltic Stones as a Quaternary Age Indicator, Western United States: U.S. Geol. Survey Prof. Paper 1210, 56 p.

Crook, R. and Kamb, B., 1980, A new method of alluvial age dating based on progressive weathering, with application to the time-history of fault activity in Southern California: Final Rept., U.S. Geol. Survey Contract No. 14-08-001-17760, 41 p.

Crough, S.T., and Thompson, G.A., 1977, Upper mantle origin of Sierra Nevada uplift: Geology 5, 396-399.

Curry, R.R., 1966, Glaciation about 3,000,000 years ago in the Sierra Nevada, California: Science 154, 770-771.

Curry, R.R., 1968, Quaternary Climatic and Glacial History of the Sierra Nevada, California: Ph.D. thesis, Univ. California, Berkeley; University Microfilms, Inc., No. 68-13896, Ann Arbor, MI, 204 p.

Curry, R.R., 1969, Holocene Climatic and Glacial History of the Central Sierra Nevada, California: in Schumm, S.A. and Bradley, W.C. (eds.), United States Contributions to Quaternary Research: Geol. Soc. America Spec. Paper No. 123, 1-47.

Curry, R.R., 1971, Glacial and Pleistocene History of the Mammoth Lakes Sierra, California - A Geologic Guidebook: Univ. Montana, Dept. of Geology, Missoula, Mont., Geol. Serial Publication 11, 49 p.

Dalrymple, G.B., 1964, Potassium-argon dates of three Pleistocene interglacial basalt flows from the Sierra Nevada, California: Geol. Soc. America Bull. 75, 753-758.

Dalrymple, G.B., 1964b, Argon retention in a granitic xenolith from a Pleistocene basalt, Sierra Nevada, California: Nature 201, 282.

Dalrymple, G.B., Burke, R.M., and Birkeland, P.W., 1982, Note concerning K-Ar dating of a basalt flow from the Tahoe-Tioga interglaciation, Sawmill Canyon, Sierra Nevada, California: Quaternary Research, in press.

Darrow, A.C., 1972, Origin of the Basalts of the Big Pine Volcanic Field, California: unpublished MS thesis, University of California, Santa Barbara, 61 p.

Davis, W.M., 1938, Sheetfloods and Streamfloods: Geol. Soc. America Bull. 49, 1337-1416.

Embleton, C., and King, C.A.M., 1975, Glacial Geomorphology, John Wiley and Sons, New York, p. 262 (573 p.)

Fleisher, P.J., 1967, Glacial Geology of the Big Pine Drainage, Sierra Nevada, California: Ph.D. thesis, Washington State University; University Microfilms Inc., Ann Arbor, MI 68-695, 128 p.

Flint, R.F., 1971, Glacial and Quaternary Geology: John Wiley and Sons, New York, 892 p.

Giovannetti, D.M., 1979, Volcanism and sedimentation associated with the formation of southern Owens Valley, California [abs]: Geol. Soc. America Abstracts with Programs, 11, No. 3, 79.

Gutenberg, B., Wood, H.O., and Buwalda, J.P., 1932, Experiments testing seismographic methods for determining crustal structure: Seismo. Soc. America Bull. 22, 185-246.

Hooke, R. leB, 1972, Geomorphic evidence for late-Wisconsin and Holocene tectonic deformation, Death Valley, California: Geol. Soc. America Bull. 83, 2073-2098.

Huber, N.K., 1981, Amount and Timing of Late Cenozoic Uplift and Tilt of the Sierra Nevada, California - Evidence from the Upper San Joaquin Basin: U.S. Geol. Soc. Prof. Paper 1197, 28 p.

Janda, R.J., 1966, Pleistocene History and Hydrology of the San Joaquin River, California: Ph.D. thesis, Univ. California, Berkeley; University Microfilms, Inc., No. 67-5086, Ann Arbor MI., 425 p.

Kane, M.F., and Pakiser, L.C., 1961, Geophysical study of subsurface structure in California: Geophysics 26, 12-26.

Knopf, A., 1918, A Geologic Reconnaissance of the Inyo Range and Eastern Slope of the Southern Sierra Nevada, California, with a Section on the Stratigraphy of the Inyo Range, by Edwin Kirk: U. S. Geol. Survey Prof. Paper 110, 130 p.

Los Angeles Dept. Water and Power (1978), Draft Environmental Impact Rept. on Increased Pumping of the Owens Valley Groundwater Basin, Los Angeles, Calif.

Lubetkin, L.K. (1980), Late Quaternary Activity Along the Lone Pine Fault, Owens Valley Fault Zone, California: unpublished MS thesis, Stanford University, Stanford, Calif., 85 p.

Mabbut, J.A., 1977, Desert Landforms: MIT Press, Cambridge, MASS, 340 p.

Matthes, F.E., 1900, Glacial sculpture of the Big Horn Mountains, Wyoming: U.S. Geol. Survey Ann. Rept. 21, part 2, 171-190.

Matthes, F.E., 1930, Geologic History of the Yosemite Valley: U.S. Geol. Survey Prof. Paper 160, 137 p.

Matthes, F.E., 1933, The little "lost valley" on Shepherd's Crest: reprinted from Sierra Club Bull., 1933, p. 68-80, in Fryxell, F., 1962, Francois Matthes and the Marks of Time: Sierra Club, San Francisco, p. 109-121.

Matthes, F.E., 1936, Avalanche sculpture in the Sierra Nevada: Trans. Mtg. Int'l Comm. Snow and Glaciers, Edinburgh, Sept. 1936, Int'l Assoc. Hydrology Bull. 23, 631-637; reprinted in Fryxell, F., 1962, Francois Matthes and the Marks of Time: Sierra Club, San Francisco, 189 p.

Matthes, F.E., (Fryxell, F., ed.),1950, Sequoia National Park, Univ. California Press, Berkeley, 136 p.

Matthes, F.E., 1960, Reconnaissance of the Geomorphology and Glacial Geology of the San Joaquin Basin, Sierra Nevada, California: U.S. Geol. Survey Prof. Paper 329, 62 p.

Mayo, E.B., 1941, Deformation in the interval Mt. Lyell-Mt. Whitney, California: Geol. Soc. America Bull. 52, 1001-1084.

McCulloch, D.S., 1963, Late Cenozoic Erosional History of Huerfano Park, Colorado: Ph.D. thesis, Univ. Michigan; University Microfilms, Inc., No. 63-6922, Ann Arbor, MI., 158 p.

Moore, J.G., 1963, Geology of the Mount Pinchot Quadrangle, Southern Sierra Nevada, California: U.S. Geol. Survey Bull. 1130, 152 p.

Moore, J.G., 1981, Geologic map of the Mount Whitney Quadrangle, Inyo and Tulare Counties, California: U.S. Geol. Survey Map GQ-1545.

Moore, J.G. and Hopson, C.A., 1961, The Independence dike swarm in eastern California: Am. Jour. Sci. 259, 241-259.

Moore, J.G., and Dodge, F.C.W., 1980, Late Cenozoic volcanic rocks of the southern Sierra Nevada, California: I, Geology and petrology: Geol. Soc. America Bull. 91 part II, 1995-2038.

Pakiser, L.C., 1960, Transcurrent faulting and volcanism in Owens Valley: Geol. Soc. America Bull. 71, 153-160.

Pakiser, L.C., Kane, M.F., and Jackson, W.H., 1964, Structural Geology and Volcanism of Owens Valley Region, California - a Geophysical Study: U.S. Geol. Survey Prof. Paper 438, 68 p.

Richardson, L.K., 1975, Geology of the Alabama Hills: unpublished MS thesis, Univ. Nevada, Reno, Nevada.

Rinehart, C.D., and Ross, D.C., 1964, Geology and Mineral Deposits of the Mount Morrison Quadrangle, Sierra Nevada, California: U.S. Geol. Survey Prof. Paper 385, 106 p.

Ross, D.C., 1962, Correlation of Granitic Plutons Across Faulted Owens Valley, California: U.S. Geol. Survey Prof. Paper 450-D, 86-88.

Ross, D.C., 1965, Geology of the Independence Quadrangle, Inyo County, California: U.S. Geol. Survey Bull. 1181-O, 64 p.

Savage, J.C., Church, J.P., and Prescott, W.H., 1975, Geodetic measurement of deformation in Owens Valley, California: Seismo. Soc. America Bull. 65, 865-874.

Sharp, R.P., 1968, Sherwin Till-Bishop Tuff relationship, Sierra Nevada, California: Geol. Soc. America Bull. 79, 351-364.

Sharp, R.P., 1969, Semiquantitative differentiation of glacial moraines near Convict Lake, Sierra Nevada, California: Jour. Geology 77, 68-91.

Sharp, R.P., 1972, Pleistocene glaciation, Bridgeport Basin, California: Geol. Soc. America Bull. 83, 2233-2260.

Sharp, R.P., and Birman, J.H., 1963, Additions to the classical sequence of Pleistocene glaciations, Sierra Nevada, California: Geol. Soc. America Bull. 74, 1079-1086.

Smith, G.I., 1979, Subsurface Stratigraphy and Geochemistry of Late Quaternary Evaporites, Searles Lake, California: U.S. Geol. Survey Prof. Paper 1043, 130 p.

Wahrhaftig, C., 1965, Stepped topography of the southern Sierra Nevada, California: Geol. Soc. America Bull. 76, 1165-1189.

Wallace, R.E., 1977, Profiles and ages of young fault scarps, north-central Nevada: Geol. Soc. America Bull. 88, 1267-1281.

APPENDIX 5-A: PLATES I AND II

Plate I: Map of the Quaternary Geology from Onion Valley North to Taboose Canyon, and from U.S. Highway 395 West to the Crest of the Sierra Nevada

Deposits were divided into four categories: tills, glacial outwash, other diamictons, and lavas. The tills are correlated with conventional Sierra glaciations except for pTa, which is uncertain. The Tenaya glaciation may be an early stade of the younger Tioga glaciation, but is mapped separately in this study. The oldest, pre-Tahoe tills may be from more than one glaciation, but all are probably post-Sherwin. No Sherwin till was recognized. Correlation to the glacial advances I - VII of Onion Valley may be found in Table 5-10.

Tenaya and Tahoe boulder trains and outwash ("Teow", "Taow") were common. Correlation to the specific glaciation was based on spatial relationships primarily, and on weathering characteristics also.

The youngest fans ("yf") are coeval with or postdate the Tenaya outwash; the old fans ("of") appear to be coeval with the Tahoe outwash. Remnants of ancient fans are clearly pre-Wisconsin but the age relationship with the pre-Wisconsin moraines was not established.

Alluvium, talus, and colluvium were also mapped. "Talus" consisted of rockfall and scree, protalus ramparts, and minor debris flows. Most talus was Holocene or latest Pleistocene in age. In older, well stabilized talus cones slopewash has been appreciable; such deposits were mapped as "colluvium". Colluvial deposits thus bracket a considerable period of time. Undoubtedly some of the colluvial aprons and debris skirts along the Sierra escarpment began developing early in the Pleistocene Epoch, though many are still active today.

Ancient diamictons were also mapped. These were of uncertain age, but most were probably deposited in the Pliocene or early Pleistocene Epochs. Diamictons at the range front were probably fanglomerates. Those near the Sierra crest probably have a different origin, most likely arising from nivation or glacial or periglacial processes. It is unlikely that they developed by in situ weathering.

Lavas in the study area were olivine basalts (Moore, 1963; Darrow, 1972). These are divided into five broad age groups, but members of the same group are not necessarily coeval. The oldest group ("v_1") may be late Pliocene in age (Moore, 1963). Dikes of this group are found along Division Creek at the range front. Lavas of the second group ("v_2") were found on ridges in the foothills. Some of these were dated at ~1.2 my (Ch. 4). These lavas underlie both diamictons (df) and ancient fanglomerates (vof), providing an upper age limit for at least some members of these units. Lavas of the third group ("v_3") were found within stream canyons but well above the modern streams. At Sawmill Canyon, one of these lavas was dated at ~0.46 my. Lavas of group for ("v_4") were found near the bottoms of canyons, sometimes underneath Tahoe moraines or outwash. Dates appeared to be around 0.1 my. Lavas of the youngest group ("v_5") were found along the range-front faults and on the alluvial fans. The cinder cones from this group appear fresh upon first inspection, but probably date from between the Tahoe and Tioga glaciations. However, near Taboose Creek some flows may well be Holocene in age.

Thibaut, Black, and Division Canyons were not visited. Undifferentiated ("u") talus and till (largely neoglacial or Tioga) were mapped using aerial photographs. Regions west of the Sierra Nevada crest were mapped in the same way. Faults that were found only in bedrock and were not related to

Quaternary deposits were not mapped in Plate I, but most be found in Moore (1963).

Plate II: The Apices of Facets on Truncated Ridges on the Eastern Escarpment of the Sierra Nevada

Plate IIa is a map showing prominent topographic features in the study area. The truncated ridges and zones of facets were identified by inspection in the field and by inspection of oblique and normal aerial photographs. The Sierra escarpment appears to consist of two parallel zones of facets, characterized by different slopes. The slopes in the lower and steeper zone are typically about 29°; those in the upper zone are about 24°.

Plate IIb shows as a profile the relation of the escarpment to the Sierra crest. The crest is of roughly constant elevation, but the escarpment elevation varies considerably. The two lines of apices maintain roughly constant spacing. The elevation of the apices appears to correlate primarily with the distance of the escarpment east of the crest. This pattern could have been produced by two episodes of offset of an east-dipping surface along a sinuous fault.

CHAPTER 6

CONCLUSIONS

The significant achievements and conclusions of this study are listed below.

Geology

- The Quaternary geology in eight canyons of the Sierra escarpment from latitude 36°45'N to 37°00'N was studied and mapped. Two other canyons in the central Sierra were studied to test relative dating techniques and to provide a basis for the comparison of the results of this study to those of other published studies.
- Holocene glaciers left moraines near the crest of the Sierra Nevada. There were at least three distinct advances.
- Pleistocene moraines of several glaciations were found in most canyons. As many as three different stades of the Tioga glaciations were found, but these had only marginally different weathering characteristics and could not be correlated from canyon to canyon. Moraines thought to be from the Tenaya glaciation were more distinct, but probably not sufficiently so to prove that the Tenaya glaciation was not just an early stade of the Tioga glaciation. The Tahoe moraines were distinct from the younger moraines, and from the weathering differences the interglacial period following the Tahoe glaciation appeared to be longer than the subsequent ones.

  Also recognized in four canyons were pre-Tahoe moraines. From their state of preservation and weathering these appeared to be post-Sherwin, but they were not necessarily all of the same age. These

early glaciers were about the same length as the later Tahoe glaciers. All the moraines in the study area were deposited after the canyons were cut to approximately their present depth.

- In the central Sierra, the Tenaya glaciation appear to be distinct from the Tioga and Tahoe glaciations. At Bloody Canyon, two stades of the Tahoe glaciations were resolved, and two glaciations predating the Mono Basin glaciation were identified. At Green Creek two distinct stades of the Tioga glaciation were recognized.
- ^{40}Ar-^{39}Ar dating of lavas interbedded with tills in Sawmill Canyon established 118,000 ± 7000 y as the upper limit to the Tahoe stage and 131,000 ± 10,000 y and 463,000 ± 40,000 y as limits to one of the pre-Tahoe stages. Acoustic wave speeds through boulders in the tills indicated that the age of the pre-Tahoe glaciation in Sawmill Canyon was closer to the upper (older) limit.
- Deeply weathered diamictons were found on ancient erosion surfaces. These surfaces are generally preserved as ridges as much as 250 m above the modern canyons. In at least one instance the diamicton appeared to be till, but generally this was not established. Sections of ancient valleys were U-shaped, suggesting that ancient glaciations were found in the southern Sierra Nevada. These must have been at least as old as the Sherwin stage.
- The foothills east of the Sierra escarpment from Symmes Creek north to Thibaut Creek were found to have two or more erosion surfaces. The highest of these was cut significantly more than 1.2 my ago. A diamicton found on this surface contained metavolcanic boulders with parallel gouges which appeared to have been caused by glacial abrasion. This diamicton could have been till or outwash, or simply fanglomerate

containing reworked glacial drift. It may have been deposited long after the erosion surface was cut.

A lower erosion surface was capped by basalt flows dated at 1.18 ± 0.05 my and 1.13 ± 0.07 my by ^{40}Ar–^{39}Ar analysis. The older flow was capped by 25 m or more of fan deposits.

° Stream incision of 125 m through the bedrock under the 1.2-my-old lava indicates an erosion rate of 0.16 mm/y or more. Rates of 0.13–0.16 mm/y were found in Sawmill Canyon west of the range front. These rates are as much as a factor of three lower than rates reported along the Sierra escarpment to the north.

° Faulting along the range-front fault (Independence Fault) has been erratic in the past ~ 0.15 my or more. At Taboose Creek, Tahoe moraines did not appear to be offset at all. At Goodale Canyon Tahoe moraines were unfaulted, while at Sawmill Canyon a basalt flow may have been offset more than 62 m in 0.12 my. At the South Fork of Oak Creek, Tahoe moraines were unbroken although old scarps could be seen on adjacent hillsides. The best preserved record of faulting, at Independence Creek, was a series of progressively offset moraines and outwash deposits indicating a fault rate for the past 65,000 y of about 0.1 mm/y and not more than 0.2 mm/y. In general, offset rates on the Independence Fault for the past 65,000 y seem to be less than the average rate since faulting began (perhaps about 6 my ago).

° No fault scarps were found on alluvial fans between the range front and the Owens Valley fault zone, except within the foothills. Therefore there seems to have been no faulting there for the last ~ 50,000 y and subsidence of the Owens Valley is probably occurring only on the

Independence (range-front) and the Owens Valley (mid-valley) faults.

- Extensive volcanism seems to have begun at least 1.2 my ago. Repeated eruptions of basalt occurred up until perhaps 50,000 y ago, and minor eruptions may have occurred more recently.
- Alluvial fans appear to have aggraded early in the Wisconsin glaciation. Much of the present fan surfaces dates from the end of this cycle in mid-Wisconsin time. During the late Wisconsin glacial advances deposition on the fans has been minimal. The fan heads have been incised. Older pre-Wisconsin fan deposits can be found in areas sheltered from recent depositions. Fan aggradation rates in the late Pleistocene Epoch may be about 0.1 - 0.2 mm/y.
- The escarpment of the Sierra Nevada shows two zones of facetted ridges, defining bevels of roughly 950 m (upper) and 750 m (lower). Ridges from the apices of the upper zone of facets to the Sierra Crest define a third surface. These three features appear to record the gross characteristics of the subsidence of the Owens Valley. During the early stages of subsidence the Owens Valley was a shallow graben on the east of the Sierra crest. Rapid faulting occurred in two major episodes separated by a significant hiatus. Alternatively, if offset during the second episode were more rapid, the hiatus is not required.

Techniques

To assist in the correlation of stratigraphic units and in understanding the chronology of tectonic and climatic events in the Sierra Nevada, two new techniques for the dating of late Pleistocene deposits and lavas were developed or refined. The first technique relied on

the speed of acoustic waves through clasts from a deposit as a means of correlating physically separated terraces or moraines, and of determining the relative ages of such deposits. The second technique used ^{40}Ar–^{39}Ar analysis of granitic inclusions found in lavas to date the eruption and cooling of the lava.

- The speed of acoustic waves through weathered granodiorite or quartz monzonite boulders from moraine crests was shown to decrease monotonically with age, unless the surfaces of the boulders were case-hardened. Samples of wave speeds formed a quantitative statistical basis for relative dating. If the ages of two or more moraines are known a priori, approximate absolute ages of other moraines of the same valley may be interpolated. The wave speed seems to decrease with the logarithm of the age; the accuracy of the inferred moraine age depends on how well this relationship is obeyed.
- Precise and accurate dating of K-poor basic lavas by ^{40}Ar–^{39}Ar analysis of K-rich granitic xenoliths was demonstrated for Pleistocene basalts. This approach can be successful even if the ancient xenoliths retain a fraction of their radiogenic ^{40}Ar created between their original crystallization and their degassing in the magma during eruption. Ages of lava flows as young as 120,000 y were measured with precisions approaching those obtained in dating young sanidine crystals by the conventional K/Ar method. This innovation is significant because it extends our ability to determine the age of late Pleistocene volcanic eruptions when conventional K/Ar dating fails because of (1) insufficient K, (2) non-atmospheric isotopic compositions of Ar trapped in the lava upon crystallization, or (3) excess ^{40}Ar contributed by ancient K-rich xenocrysts degassing in the magma.

PLATE I: QUATERNARY GEOLOGY

Gillespie, A.R., 1982,

Quaternary Glaciation and Tectonism in the Southeastern Sierra Nevada, Inyo County, California

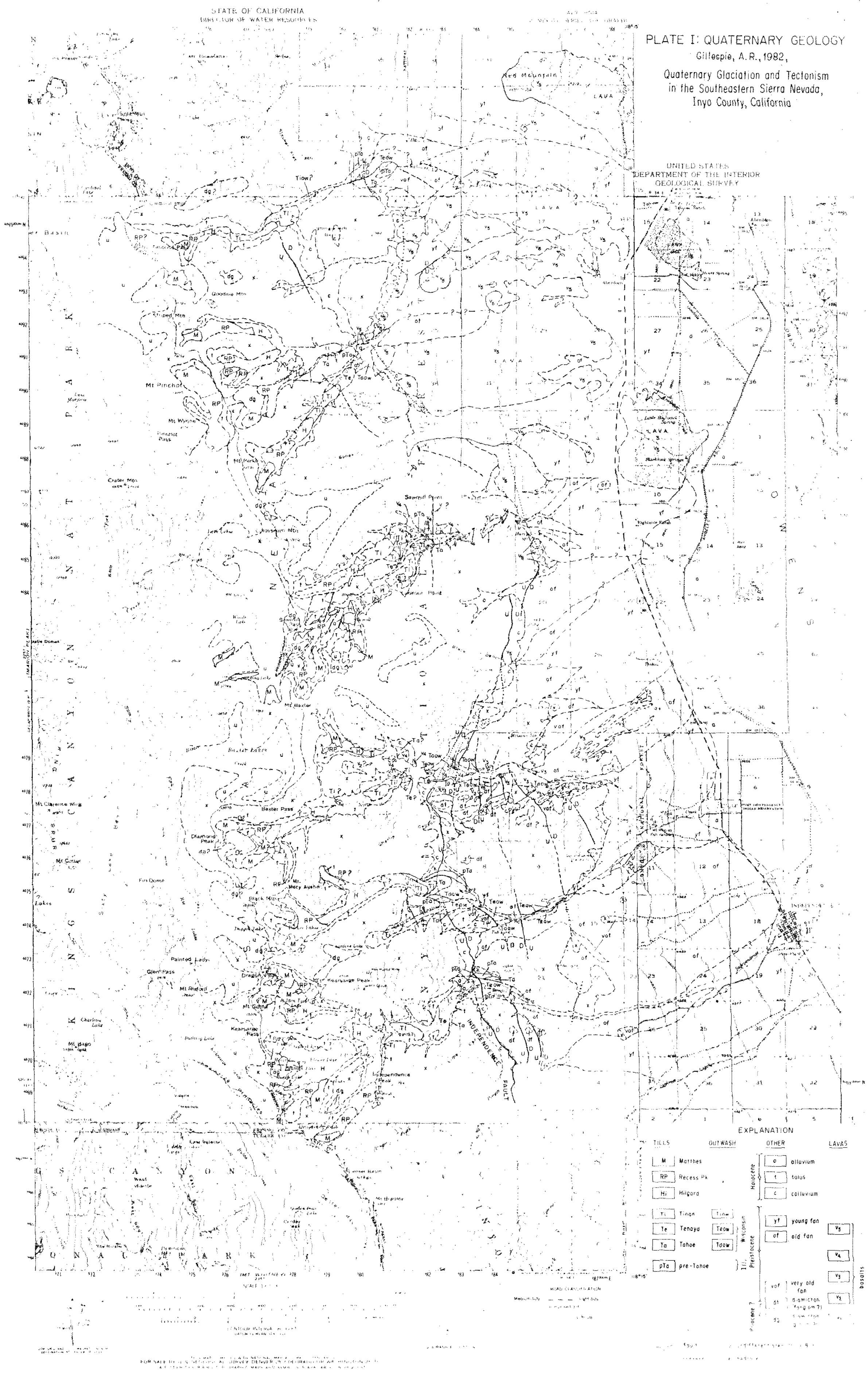

PLATE IIb

PROFILE OF THE SIERRA NEVADA

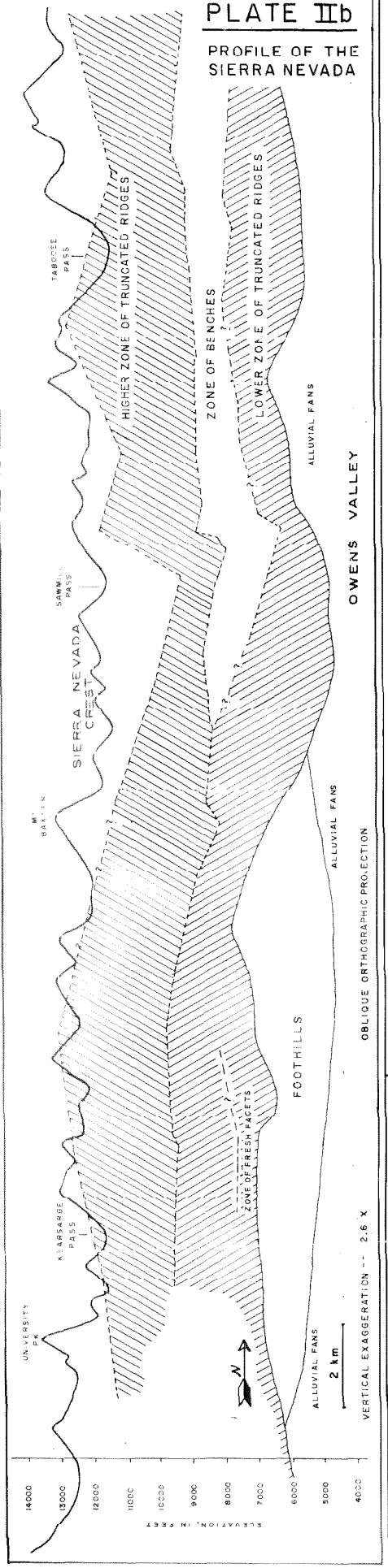

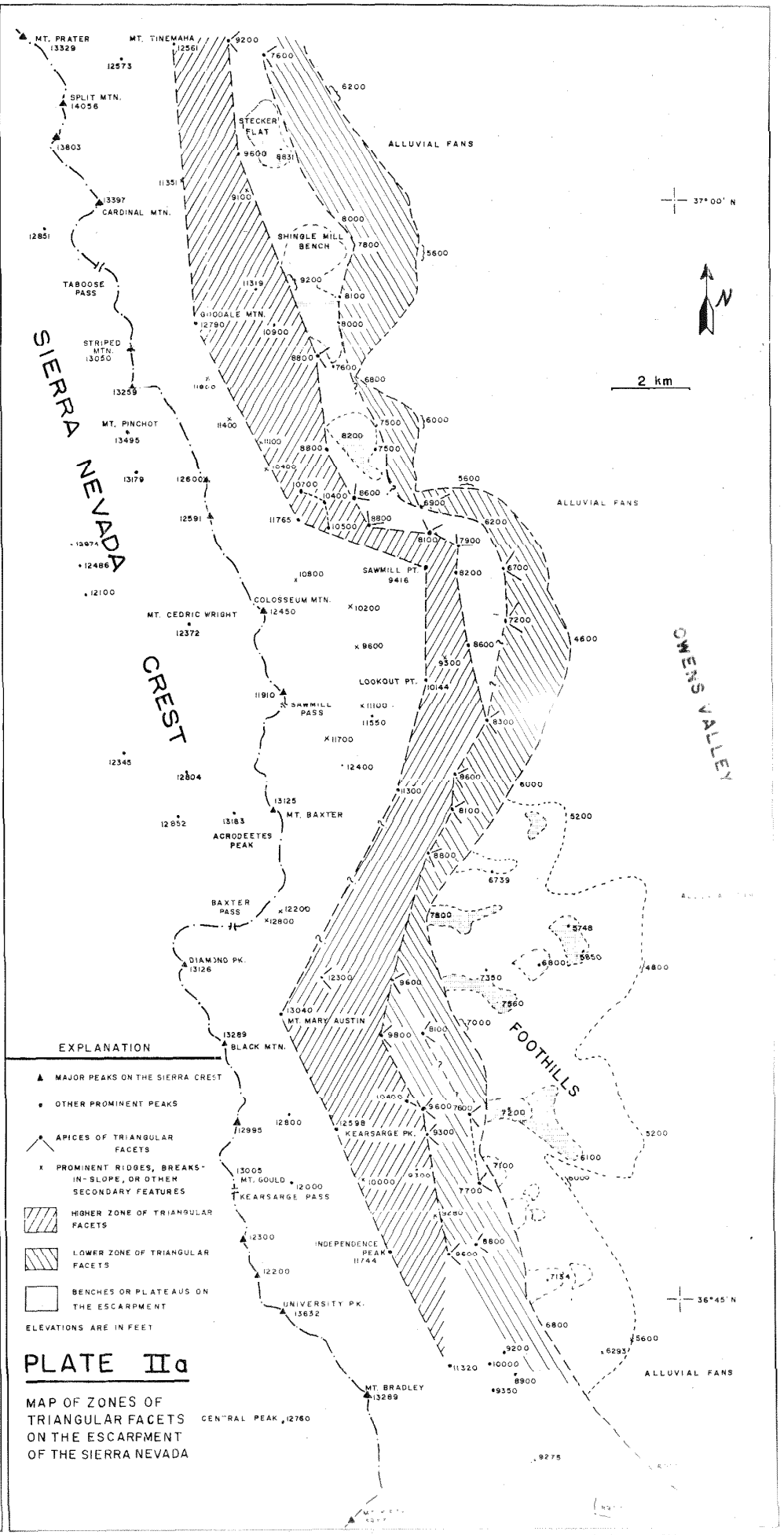

PLATE IIa

MAP OF ZONES OF TRIANGULAR FACETS ON THE ESCARPMENT OF THE SIERRA NEVADA